Targeted protein degradation for disruption of key proteins that overcome genomic instability in cancers: Wee1 and KIFC1

Marine Céline Aublette

A thesis submitted for the degree of Doctor of Philosophy in the Faculty of Health and Medicine at Lancaster University

August 2022

Declaration

I hereby declare that this thesis is my own work, except where otherwise stated, and has not been submitted for the award of a higher degree elsewhere.

Marine Aublette

Abstract

Targeted protein degradation, especially using proteolysis targeting chimeras (PROTACs), is rapidly emerging as an interesting tool to target and selectively degrade cancer driving proteins. PROTACs are bifunctional molecules composed of a target-protein ligand and a ubiquitin E3-ligase binder linked together. These form a ternary complex to degrade the target via the proteasome instead of inhibiting it. Because of the added complexity of PROTACs, they are typically found to exhibit enhanced selectivity for certain targets over others.

Current inhibitors for cancer therapy are typically not very selective towards their intended targets, especially protein kinases due to their conserved ATP-binding sites. Wee1 kinase has an important role in the cell cycle as it regulates the G_2/M checkpoint and is overexpressed in many cancers. It is an interesting target for which therapeutic intervention would be useful. The first chapter of results, Chapter 3, focuses on how I designed and synthesised Wee1 PROTACs using a potent but not very selective inhibitor (AZD1775) and two E3 ligase recruiters for von Hippel-Lindau (VHL) and Cereblon (CRBN), part of the Cullin-RING ubiquitin ligases.

A structure activity relationship of Wee1 PROTACs around the linker was generated and their potential cytotoxic activity assessed in cancer cells, as detailed in the next chapter, Chapter 4. I established the Wee1 degradation profiles of the two series of PROTACs recruiting CRBN or VHL toward different target kinases. A range of activities were observed depending on the recruited E3 ligase and the linker (length and nature). Wee1 was degraded selectively, bringing a promising tool to target kinases selectively for cancer treatments. A corresponding decrease in downstream phosphorylation of CDK1 was observed in multiple cell lines. The target engagement and the ternary complex formation were studied to validate the PROTAC mechanism of action.

The linker had a determining influence in the degradation which led to optimisation of the PROTACs, as discussed in Chapter 5. I show the synthesis of new PROTACs by removing an amide bond in the molecule and using different linkers. One PROTAC of each new series displayed significantly improved potency against Wee1.

In Chapter 6, I propose the generation of a new type of 3D linkers for bifunctional molecules using photochemistry: cubanes. With the hypothesis in mind that short linkers can block the conformation of the PROTAC to possibly favour ternary complex formation for further degradation, using 1,2- and 1,3-cubanes could become a key technology to use in the PROTAC field and medicinal chemistry in general. The 1,3-disubstituted cubane was successfully obtained at the required scale, although enabling selective functionalisation of the substituents required additional optimisation. The synthesis of a 1,2-disubstituted cubane was more challenging however the "almost cubane", before closing the last bond, was successfully obtained. Some additional synthetic effort to close the final bond of the cubane is needed to complete this work.

Finally, in Chapter 7, I show the design and synthesis of KIFC1 PROTACs. KIFC1 overexpression in cancers lead to multipolar mitosis and successful cancer cell proliferation. KIFC1 inhibitor AZ82 was selected and studied to find an attachment point, despite the lack of an available crystal structure. I synthesised the PROTACs using both CRBN and VHL recruiters and different alkyl linkers. After assessment in cancer cells, one PROTAC (MA185) recruiting CRBN successfully degraded KIFC1. MA185 is the first KIFC1 PROTAC to our knowledge, which opens up exciting prospects for future development as a cancer-selective treatment. MA185 exhibits enhanced cytotoxicity as compared with AZ82 inhibitor. The influence of this first KIFC1 PROTAC on the cell cycle is currently being investigated to better understand its mechanism of action, as well as the extent of this discovery.

Acknowledgements

First of all, I would like to express my deepest and sincere gratitude to my supervisor Dr. Morgan Gadd for his help, support and advice throughout my PhD. I was so fortunate to be supervised by someone who trusted me and enabled me to always do what was best for me, and learn continuously in all the fields I wanted. Thank you so much for everything.

I am also grateful to Dr. Sarah Allinson who took over my supervision towards the end of my PhD. I really appreciated the advice and comments on my thesis, as well as the valuable input into experimental ideas. I would also like to thanks Dr. Susannah Coote for enabling me to work for a few months on very exciting chemistry in her lab, and for including me so well. I learned so much.

A huge thank you to Dr. Michael Coogan for his support and advice in chemistry. Many thanks to Dr. Nikki Copeland for his comments during lab meetings and to Dr. Andrew Fielding for his guidance, ideas and the collaboration on the KIFC1 project.

Thank you to Dr. Amanda Thomaz for working with me on such an exciting project, and for all the experiments we worked on together to move forward with it.

I would also like to thank all my fellow post-graduate research students for making the department a friendly and positive environment to work in and for their support through these four years. I would particularly like to thank Dimitra for being a great friend every day, and always make me feel good, and Lauryn for being my bench mate, and for laughing with me in the lab. Many thanks to Kim, James and Jack for creating a little running club with me, which was so important for stress relief. Outside of the work bubble, I would like to thank by best friends Eloïse and Rémi for supporting me every day no matter where I am in the world, and my friends in Lancaster, Rob and Luke.

Table of Contents

viii

List of Figures

Chapter 1

Chapter 3

Chapter 4

Chapter 5

Chapter 9

List of Tables

Chapter 1

Chapter 2

Chapter 3

Chapter 4

Chapter 5

Chapter 6

Chapter 7

List of schemes

Chapter 1

Chapter 3

Chapter 7

Abbreviations

3D: 3 dimensional

APC/C: Anaphase-promoting complex/cyclosome

ABPP: Activity-based protein profiling

AcCl: Acetyl chloride

ADMET: absorption, distribution, metabolism, excretion and toxicity

AIBN: Azobisisobutyronitrile

AKT: Protein kinase B

ALPHA: amplified luminescent proximity homogeneous assays

Amp: Ampicillin

AMPK: AMP-activated protein kinase

Aq.: Aqueous

ATM: Ataxia telangiectasia-mutated kinase

ATP: Adenosine triphosphate

ATR: Ataxia telangiectasia and Rad3-related kinase

AUTAC: Autophagy targeting chimaera

B-Me: Betamercaptoethanol

BRD: Bromodomain

BSA: Bovine serum albumin

CDK: Cyclin-dependent kinase

CDS: Coding sequence

Chl: Chloramphenicol

cIAP: Cellular Inhibitor of Apoptosis

CRBN: Cereblon

CRL: Cullin ring ligase

DABSO: 1,4-Diazabicyclo [2.2.2]octane bis (sulfur dioxide)

DAPI: 4',6-Diamidino-2-phenylindole

DCC: *N,N'*-Dicyclohexylcarbodiimide

DCM: Dichloromethane

DEACM: [7-(Diethylamino)coumarin-4-yl]methyl

DIAD: Diisopropyl azodicarboxylate

DIBAL-H: Diisobutylaluminium hydride

DIPEA: *N,N*-Diisopropylethylamine

DMA: *N,N*-Dimethylacetamide

DMAP: 4-Dimethylaminopyridine

DMEM: Dulbecco's Modified Eagle Medium

DMF: Dimethylformamide

DMNB: Dimethoxy-2-nitrobenzyl

DMPK: Drug metabolism and pharmacokinetics

DMSO: Dimethylsufoxide

DNA: Deoxyribonucleic Acid

dNTP: Deoxynucleotide Triphosphates

DPPA: Diphenylphosphoryl azide

DTT: Dithiothreitol

DUBTAC: Deubiquitinase targeting chimera

EDTA: Ethylenediaminetetraacetic acid

EGFR: Epidermal growth factor receptor

Eq.: Equivalent

ER: Estrogen receptor

ERK: Extracellular signal-regulated kinase

ESCRTs: Endosomal sorting complexes required for transport

F: Phenylalanine

FBS: Foetal bovine serum

FT: Flow through

FVP: Flash vacuum pyrolysis

Fwd: Forward

HATU: (1-[Bis(dimethylamino)methylene]-1H-1,2,3-triazolo[4,5-b]pyridinium 3-oxide hexafluorophosphate

HEPES: *N*-2-hydroxyethylpiperazine-N-2-ethane sulfonic acid

Hg: Mercury

HIF: Hypoxia-inducible factor

IC_{50}: Half maximal inhibitory concentration

IMiDs: Immunomodulatory drugs

IPTG: Isopropyl β-D-1-thiogalactopyranoside

IR: Infrared

ITC: Isothermal Titration Calorimetry

JAK: Janus kinase

Kan: Kanamycin

Kb: Kilobase

KEAP1: Kelch-like ECH-associated protein-1

KIFC1: Kinesin-like protein

L: Leucine

LB: Lysogeny broth

LTR: Lysosome-targeting receptors

Lys: Lysine

LYTAC: Lysosome targeting chimera

m.p.: Melting point

MAPK: Mitogen-activated protein kinase

mCPBA: Meta-chloroperoxybenzoic acid

MDM2: Mouse double minute 2

MetAP: Methionine aminopeptidase

MQW: Milli-Q water

MS: Mass spectrometry

MT: Microtubule

NBS: *N*-Bromosuccinimide

Ncd: Nonclaret disjunctional protein

NMR: Nuclear magnetic resonance

Ni: Nickel

Ni-NTA: Nickel - nitrilotriacetic acid

NVOC: *o*-Nitroveratryloxycarbonyl (4,5-dimethoxy-2-nitrobenzyloxycarbonyl)

PBS: Phosphate buffered saline

PCA: Photocycloaddition

PCM: Pericentriolar material

Pd: Palladium

PFA: Paraformaldehyde

PHICS: Phosphorylation-inducing small chimeric molecules

PhoRC: Phosphatase recruiting chimaera

PHOTAC: Photochemically targeting chimaera

PI: Propidium iodide

PK: Pharmacokinetics

PKC: Protein kinase C

PLK: Polo-like kinase

POM: Pomalidomide

PP1: Protein-phosphatase 1

PPI: Protein-protein interaction

PROTAC: Proteolysis targeting chimaera

PS: Penicillin-Streptomycin

PTAD: 4-Phenyl-1,2,4-triazoline-3,5-dione

PTM: Post translational modification

Quant.: Quantitative

Rev: Reverse

RIBOTAC: Ribonuclease targeting chimaera

RIPK2: Receptor-interacting serine/threonine-protein kinase 2

RNA: Ribonucleic acid

RNase: Ribonuclease

ROI: Region of interest

Rpm: Revolutions per minute

RPMI medium: Roswell Park Memorial Institute Medium

SAR: Structure activity relationship

SARM: Non-steroidal androgen receptor

SCF: Skp1–Cullin–F-box-protein

SDS: Sodium Dodecyl Sulphate

SDS-PAGE: Sodium Dodecyl Sulphate-Polyacrylamide Gel Electrophoresis

SKP: S-phase kinase-associated protein

SM: Starting material

SPR: Surface Plasmon Resonance

Strep: Streptomycin

TAE: Tris-acetate-EDTA

TBS: Tris-buffered saline

TBST: Tris-buffered saline Tween-20

^{t}Bu: *Tert*-Butyl

^{t}BuOH: *Tert*-Butyl alcohol

^{t}BuOK: Potassium *tert*-butoxide

TCEP: Tris(2-carboxyethyl)phosphine

TEMED: *N,N,N',N'*- Tetramethylethylenediamine

TFA: Trifluoroacetic acid

THF: Tetrahydrofuran

TLC: Thin layer chromatography

TMSOT$_f$: Trimethylsilyl trifluoromethanesulfonate

TPD: Targeted protein degradation

TPS: Targeted protein stabilization

TR-FRET: Time-resolved fluorescence energy transfer

Tyr: Tyrosine

Ub: Ubiquitin

UPS: Ubiquitin-proteasome system

VBC: Complex of VHL, Elongin B and Elongin C

VHL: Von Hippel-Lindau

v/v: Volume per volume

wt: Wild type

w/v: Weight per volume

Y: Tyrosine

Zn: Zinc

1 Introduction

1.1 Ubiquitination and consequences

1.1.1 Ubiquitin

Ubiquitin is a 76-amino-acid protein present in eukaryotic cells and is important in the regulation of cellular functions (Hershko *et al.*, 1998). One of the most important roles of ubiquitin is in the ubiquitin-proteasome system, most commonly called UPS. Here, polyubiquitin chains are used as a marker for degradation of proteins by the proteasome (Zheng *et al.*, 2017).

The process of ubiquitination modifies a substrate protein as a result of an enzyme cascade with three key enzymes: E1, E2 and E3 (Figure 1.1) (Hershko *et al.*, 1992). The E1 (activating) enzyme activates the ubiquitin by forming a thioester with its own cysteine residue and the C-terminus of the ubiquitin. The ubiquitin is then transferred to a cysteine on the E2 (conjugating) enzyme, again attached via the C-terminus of the ubiquitin. The E3 (ligating) enzyme, or E3 ligase, then binds to both the ubiquitin-E2 intermediate and the protein substrate in order to transfer the ubiquitin from the intermediate to a lysine on the substrate (Berndsen *et al.*, 2014). An isopeptide bond is thus formed between the lysine of the substrate protein and the C-terminus of the ubiquitin.
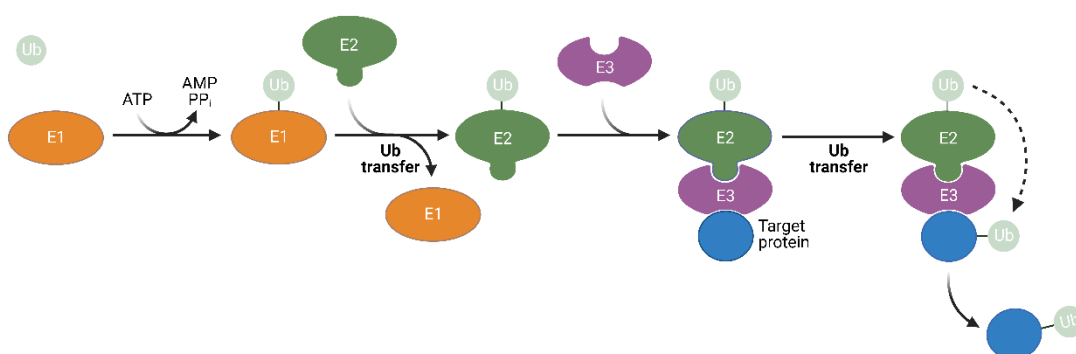
Figure 1.1: Ubiquitination enzymatic cascade (Using BioRender). Ub = Ubiquitin.

Further ubiquitination events can then occur to define the fate of the substrate protein. For degradation via the proteasome, a chain of ubiquitins is formed, with the C terminus of each new ubiquitin being attached to Lys48 of the previous. At least four ubiquitins are needed in the Lys48-linked chain for the substrate to be sent to the proteasome for degradation (Hershko *et al.*, 1992). After the initial (mono)ubiquitination, only the third step is changing, the ubiquitin is transferred onto one of the seven lysines or N terminus of the previous ubiquitin that has been attached. In this way, the various different possible polyubiquitin chains define different fates for the modified substrate protein (Finley *et al.*, 2012).

1.1.2 Consequences of ubiquitination

1.1.2.1 Change of protein function

Ubiquitins regulate a range of physiological processes, such as interactions of proteins with other macromolecules, proteins or the proteasome for instance (Akutsu *et al.*, 2016). Ubiquitination of a substrate can change the protein function and dictate its fate, which can have different consequences. The consequences of the modification are different depending on the number and structure of attached ubiquitins (Figure 1.2). For instance, mono-ubiquitination can act on functions such as DNA repair, transcription, endocytosis, membrane protein trafficking (Hochstrasser, 2009) and poly-ubiquitination on proteolysis. All these different consequences emphasise the importance of ubiquitination in cells. Seven lysines are available for ubiquitation: K6, K11, K27, K29, K33, K48 and K63, and are used differently depending on their physiological consequence (Akutsu *et al.*, 2016).
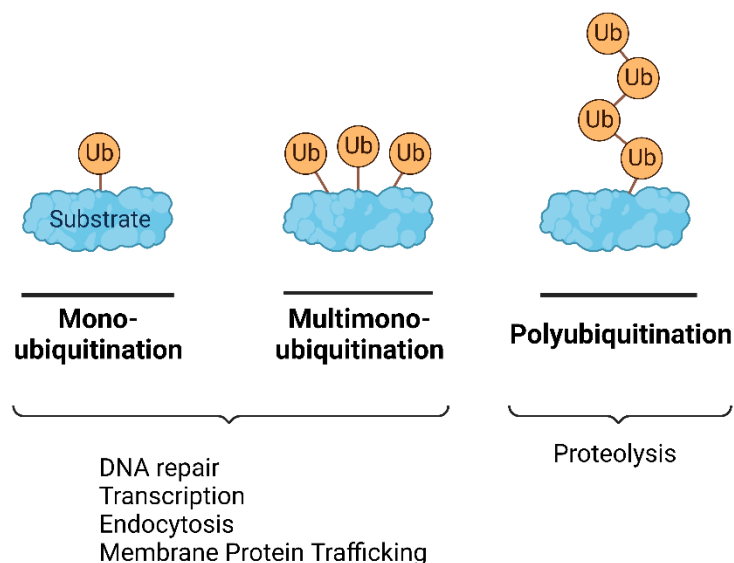
Figure 1.2: Mono and polyubiquitination to modify proteins functions (Using BioRender).

1.1.2.2 Lysosomal degradation

The lysosome is one of the main sites of degradation of cellular proteins (de Duve *et al.*, 1966) and is an essential organelle responsible of the turnover of plasma membrane proteins, such as receptors (Li *et al.*, 2015). Ubiquitination can be used to direct these receptors toward the lysosome for degradation by using the engagement with endosomal sorting complexes required for transport (ESCRTs). A single ubiquitin modification at one, or several different sites in proteins is enough to act as a signal for degradation (Clague *et al.*, 2010). The ubiquitin can be linked through one of the seven lysines, particularly Lys63 (K63) for lysosomal degradation (Kawadler *et al.*, 2006). For instance, this targets cell surface membrane proteins for lysosomal degradation in the early endosome (Mizuno *et al.*, 2011). Proteins such as Ste6p (yeast ABC transporter) (Galan *et al.*, 1997), TrkA (Geetha *et al.*, 2005) or MHC-1 (Duncan *et al.*, 2006) require mono or polyubiquitination at Lys63 for efficient endocytosis and further degradation by the lysosome. Lysosomal degradation was considered for a long time as the main degradation pathway, until the proteasome was discovered and further investigated.

1.1.2.3 Proteasomal degradation

In contrast with Lys63 ubiquitination for nonproteolytic function such as signal transduction, the Lys48-linked polyubiquitin chain works in concert with the proteasome (Hershko *et al.*, 1992). The proteasome, a multicatalytic enzyme complex, is responsible for degradation of proteins that are either not needed anymore, damaged, or misfolded (Ciechanover, 1994; Adams, 2003). The proteasome consists of a 20S core with 19S regulatory particles which cleave the ubiquitin from the substrate, and four rings. The two outer rings create a channel for proteins to enter and the two inner rings form the catalytic chamber with active enzymes for degradation (Adams, 2003). It recognises when a protein is marked with at least four Lys48-linked ubiquitins. The polyubiquitin chain allows the modified protein to enter the proteasome, where it is proteolytically cleaved into small peptides, or individual amino acids (Tanaka, 2009).

1.1.3 Use of the UPS to control degradation

Protein degradation is an essential part of our cellular network. Due to its ability to rapidly remove specific proteins, the UPS plays a role in controlling most cellular processes such as the cell cycle, cell division and the inflammatory response (Tanaka, 2009). This emphasises the interest in modulating natural proteasome degradation for treatments to target human diseases. As such, the proteasome has generated interest as a therapeutic tool for the past couple of decades. Proteasome inhibitors have been developed since the 1990s, such as bortezomib, carfilzomib and ixazomib (Manasanch *et al.*, 2017). These treatments were originally made to prevent cancer-related problems in protein regulation.

The drug thalidomide was first developed in the 1950s and subsequently developed a notorious reputation for causing severe birth defects (Ward, 1962). Just before the year 2000, thalidomide was found to have anti-angiogenic properties (D'Amato *et al.*, 1994) and immunomodulatory properties (Haslett *et al.*, 1998) which made it evolve into IMiDs (Immunomodulatory drugs). Chemists used thalidomide as a template to build compounds with increased immunological and anticancer properties, but trying to reduce

side effects (Bartlett *et al.*, 2004). About 10 years later, as the first IMiDs were officially approved following clinical trials, thalidomide was shown to bind to cereblon (CRBN) (Ito *et al.*, 2010; Lu *et al.*, 2014). The cereblon complex is a substrate recognition component of a cullin-RING-ubiquitin ligase (CRL) complex for cullin4 (CRL4^{CRBN}) that, like all CRL complexes, mediates ubiquitination and degradation by the proteasome. The IMiDs were found to be a type of molecular glue that modulates substrate recognition by the CRBN E3 ligase, causing it to polyubiquitinate and trigger the degradation of key neo-substrate proteins by the UPS.

More recently, using the same concept as IMiDs, but directly recruiting both partners (the E3 ligase and the substrate), a new technology based around the concept of proteolysis-targeting chimaera (PROTAC) has been developed (Sakamoto *et al.*, 2001, 2003) for targeted protein degradation (TPD), which hijacks the UPS to remove specific proteins and can be applied to many disease classes, in particular cancer, and will be described in Section 1.3. With these modern advances, ubiquitination, and more especially the recruitment of the proteasome system, has become a key tool for research and the treatment of diseases.

1.2 Biorecruters

Post-translational modifications are an important part of our proteome and regulate many pathways. In the last few years, targeting the ubiquitin system has become a key technology. PROTACs have been the most developed so far by recruiting an E3 ligase for ubiquitination and degradation by the proteasome. Most aspect of development are still empirical in the PROTAC technology (Kostic *et al.*, 2020) but the freedom around the E3 ligase recruitment shows that this part of the molecule could possibly recruit other biologies to bring things in a way they would not normally do. PROTACs generate post translational modifications (PTMs) by transferring ubiquitins to the target protein through a lysine residue. Because this PTM appears to be very useful, scientists decided to study other PTMs and see if they could also be used (Conway, 2020). The proteasome cannot be applied to all intracellular material so it would be beneficial to broaden the scope of targets and biologies.

Thus, other bio-recruiter protein-protein interaction (PPI) inducers such as LYTACs, PHOTACs, PhoRCs, DUBTACs, AUTACs, opto-TACs have been studied recently to use other biologies/regulatory pathways and brought a lot of new interesting perspectives for the protein degradation future: how to control degradation in the years to come and how to target the undruggable (Table 1.1).

Table 1.1: Table of emerging biorecruiters. Biorecruiters using different biologies and regulatory pathways to control degradation and target new tissues.

	Biorecruter for	**Biology used**
PROTAC	E3 ligase	Ubiquitination
PhoRC	Phosphatase	Dephosphorylation
LYTAC	LTR	Lysosome
DUBTAC	Deubiquitinase	Deubiquitination
AUTAC	S-guanylation	Autophagy
RIBOTAC	RNA	Ribonuclease
PHIC	Kinase	Phosphorylation
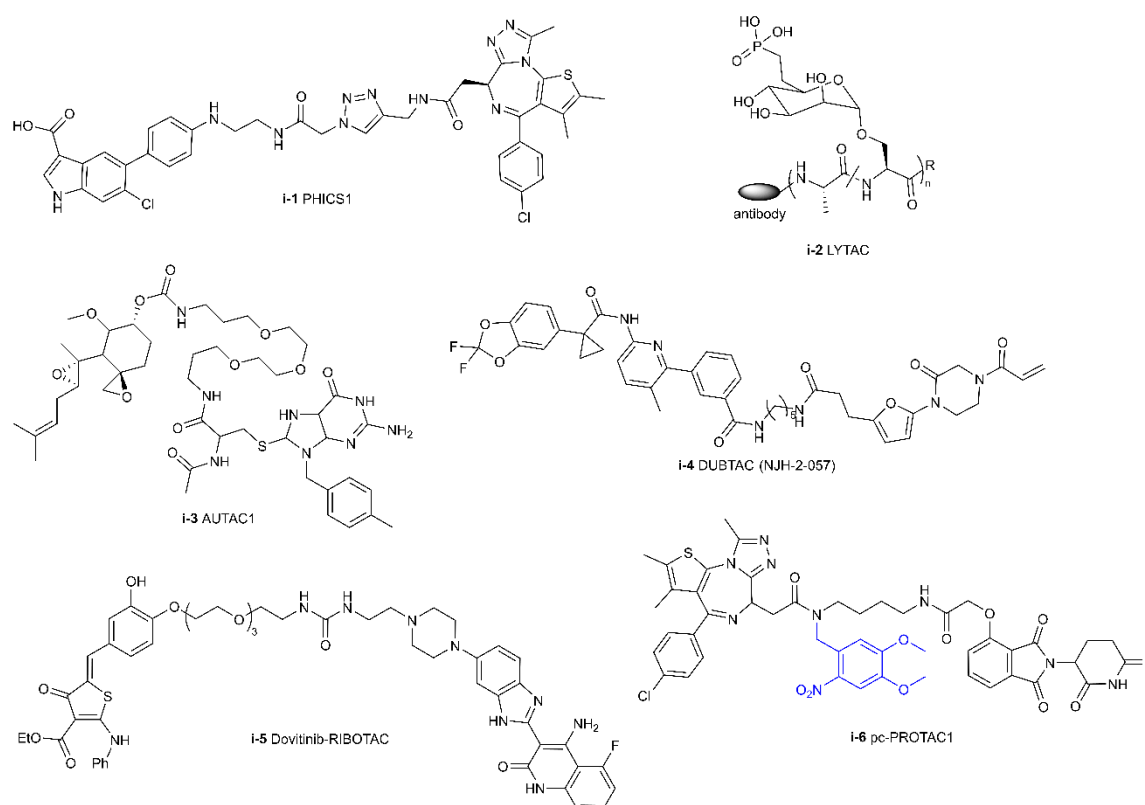
Figure 1.3: Examples of the different biorecruiters: PHICS1 recruiting BRD4 and AMPK, LYTAC with Poly(M6Pn-co-Ala) conjugated to an antibody, AUTAC1 targeting MetAP2, DUBTAC NJH-2-057 recruiting OTUB1 and CTFR, RIBOTAC targeting miR-21, and pc-PROTAC1 targeting BRD4.

1.2.1 PhoRCs and PHICS

Phosphorylation and dephosphorylation are involved in many regulatory pathways and thus present a major PTM to study (Nolen *et al.*, 2004). Yamazoe *et al*. showed proof of concept that a heterobifunctional molecule recruiting a phosphatase on one side and a target protein on the other side could lead to dephosphorylation (Yamazoe *et al.*, 2020) of the target protein. The recruitment of protein-phosphatase 1 (PP1) to AKT (protein kinase B) and EGFR (epidermal growth factor receptor) by a bifunctional molecule resulted in the dephosphorylation of both target proteins. Such molecules are called phosphatase recruiting chimaeras (PhoRCs) and use protein phosphatases as a biorecruiter. While much work is required to improve the properties of these molecules,

phosphorylation/dephosphorylation biology could be readily exploited as an important advance in the chimeric molecules field.

Extending this concept, phosphorylation-inducing chimeric small molecules (PHICS) are bifunctional molecules recruiting a kinase and a target protein in order to phosphorylate the protein that is not usually targeted by the kinase (Siriwardena *et al.*, 2020). The authors created PHICS that could phosphorylate BRD4 with AMP-activated protein kinase (AMPK) and protein kinase C (PKC) (using JQ1 as the BRD4 recruiter and the modified PF-06409577 for AMPK or 9-(4-aminomethylbenzyloxy)-substituted benzolactam for PKC) and selected PHICS1 (Figure 1.3) and PHICS2 as the best molecules for each series, respectively. A hook effect (binary complex formation instead of ternary complex formation, see Section 1.3.3) was observed at high concentrations and linker length was shown to be important too, similarly to PROTACs. Phosphorylation is involved in many pathways and can change a protein function, structure and interaction. As such, the exploitation of this PTM will be very advantageous.

1.2.2 LYTAC

Lysosome-targeting chimaeras (LYTAC) also appeared recently (Banik *et al.*, 2020). Unlike PROTACs, LYTACs target extracellular and membrane-associated proteins, also involved in many cancers and diseases (Banik *et al.*, 2020). This bifunctional molecule aims to transport a protein to the lysosome for lysosomal degradation, which is an interesting biology to use, by targeting the lysosome-targeting receptors (LTRs) on the cell surface and an extracellular protein of interest. For this proof of concept, they developed a LYTAC warhead for the LTR CI-M6PR as a shuttling receptor linked to an antibody (Figure 1.3). Targeting extracellular proteins will be very worthwhile investigating further because shuttling receptors can be specific to certain tissues and thus bring targeted tissue specificity (Ahn *et al.*, 2021).

1.2.3 AUTAC

Autophagy-targeting chimaeras (AUTACs) (Takahashi *et al.*, 2019) aim to degrade proteins that cannot be degraded by the proteasome with PROTACs using another

intracellular degradation pathway known as autophagy. Autophagy is a process used for degradation of cellular proteins by the lysosome which has recently appeared to be usable to manipulate autophagy in cancers (Towers *et al.*, 2016). Takahashi *et al*. first verified that EFGP autophagy was promoted by S-guanylation and that S-guanylation was a tag triggering cargo-selective autophagy using a HaloTag. They then used a guanine tag and a specific protein binder for their bifunctional molecule to design and synthesise a few AUTACs (using *p*-fluorobenzylguanine (FBnG) ligand as a guanine tag linked to the target binder with a PEG linker). They prepared two AUTACs, AUTAC1 targeting MetAP2 and AUTAC2 targeting FKBP12. Both AUTAC1 and AUTAC2 removed the target (Figure 1.3). They also prepared AUTAC3 using JQ1 to target BRD4, which only showed a small decrease due to the target's nuclear localisation, as the lysosome is not available to degrade nuclear proteins. Selective autophagy and controlled S-guanylation could become a significant tool in the targeted protein degradation arena.

1.2.4 DUBTAC

PROTACs induce protein ubiquitination for further degradation by the proteasome in order to remove an unwanted protein. However, some cancer and diseases are driven by active ubiquitination and degradation. Thus, using targeted protein stabilization (TPS) instead of TPD could also be useful. The Nomura group recently developed a deubiquitinase-targeting chimaera (DUBTAC) (Henning *et al.*, 2021). They discovered a covalent recruiter for OTUB1 deubiquitinase and managed to stabilise human cystic fibrosis mutant protein CFTR with DUBTAC NJH-02-057 (Figure 1.3). Mutation of CFTR is responsible for most cases of cystic fibrosis by degrading the CFTR proteins that have not matured beyond the endoplasmic reticulum (Ward *et al.*, 1995). Thus, stabilising proteins instead of degrading them using a bifunctional molecule could become a very useful tool for some diseases.

1.2.5 RIBOTAC

Ribonuclease targeting chimaera (RIBOTAC), for targeted RNA degradation, has also emerged as another modality in the field. A group showed proof of concept of recruiting

RNA by repurposing a PROTAC (Cao *et al.*, 2021) into a RIBOTAC targeting pre-miR-21 and activating ribonuclease L (RNase L) to cleave the target (Figure 1.3) (Zhang *et al.*, 2021). The VHL-recruiting part of the original PROTAC was replace by a recruiter of RNase L to induce RNA catalytic degradation. Selectivity towards the target was significantly improved which widened the scope of targeted protein degradation by using other biomolecules such as RNA comparing to proteins with PROTACs.

1.2.6 To go even further: control degradation

In order to make protein degradation even more specific, over the last few years, efforts have been made to control protein degradation using light. This can be done with either photo-caged PROTACs (pc-PROTACs) or photoswitchable PROTACs (photoPROTACs). pc-PROTACs only become active upon irradiation with light, which removes a blocking group to release the PROTAC and enable controlled degradation. The caging group must block the interaction of the PROTAC with the protein (either target protein or E3 ligase protein) and must be easily removed with light. For instance, Xue *et al.* showed that the 4,5-dimethoxy-2-nitrobenzyl (DMNB) group (Xue *et al.*, 2019) could be used and removed with 365 nm irradiation to target BRD$_4$ with pc-PROTAC1 (Figure 1.3). Naro *et al.* used [7-(diethylamino)coumarin-4-yl]methyl (DEACM) group (Hamerla *et al.*, 2020) that can be removed at the same wavelength (Naro *et al.*, 2020). Liu *et al.* published what they called an opto-PROTAC, also a caged PROTAC, with a o-nitroveratryloxycarbonyl (NVOC) group on the pomalidomide which can only recruit CRBN after being removed with light (J. Liu *et al.*, 2020).

On the other hand, photoPROTACs, as shown in Pfaff *et al.* paper (Pfaff *et al.*, 2019) present a linker (ortho-F4-azobenzene) that changes in length upon exposure to light, where the *cis* conformation is inactive and *trans* is active. Moreover, in comparison to pc-PROTACs, the control of photoPROTACs is reversible, and each state is stable, so it does not require a constant irradiation. Reynders *et al.* published a PHOTAC (Photochemically targeting chimaera) with an azobenzene photoswitch on the E3 ligase ligand that can be activated with light (blue-violet (380 to 440 nm)) (Reynders *et al.*, 2020) to adopt the active *cis* form. Without light, it goes back to the inactive *trans* conformation.

These new light technologies could help explore different signalling pathways (Figure 1.3). They appear through different forms as they can be inside the PROTAC or on the PROTAC, they can be reversible or irreversible. Possible uncontrollable degradation that could be caused by the release of a normal PROTAC could become controllable with this type of technology. Similarly, by bringing precision in the therapeutic release, it could improve drug toxicity profiles.

1.2.7 Perspectives

Over the last few years, targeted protein degradation has become one of the hottest topics, with PROTACs being the most developed field so far, as will be detailed in the next section. The PROTAC principle is now being used to develop other technologies using different biologies, as the same concept that degradation can be controlled using chimeric molecules has been applied to many other machineries. Indeed, recent advances in the field show that new signalling pathways are now being explored with technologies such as LYTACs, DUBTACs as PhoTAC as described above. What started with utilising E3 ligase recruiters for PROTACs has now become a very diverse array of ideas of what could become a biorecruiter as it aims to recruit a variety of biologies offering forward-looking perspectives.

1.3 PROTACs

1.3.1 Mechanism of PROTAC activity

PROTACs are bifunctional molecules composed of a target protein ligand and an E3 ligase ligand, joined by a flexible linker (Figure 1.4). The PROTAC brings the target protein close enough to the E3 ligase in order to form a ternary complex, the most important step in the PROTAC mechanism (Schneekloth *et al.*, 2004). This proximity causes the target protein to become polyubiquitinated by the activity of the E3 ligase in the same way as the native substrate would. The target protein is subsequently recognised and degraded by the proteasome into small peptides and individual amino acids that are not offensive for the body anymore. Furthermore, the PROTAC is released and can be reused to ubiquitinate another target protein, enabling it to act catalytically (Bondeson *et al.*, 2015).
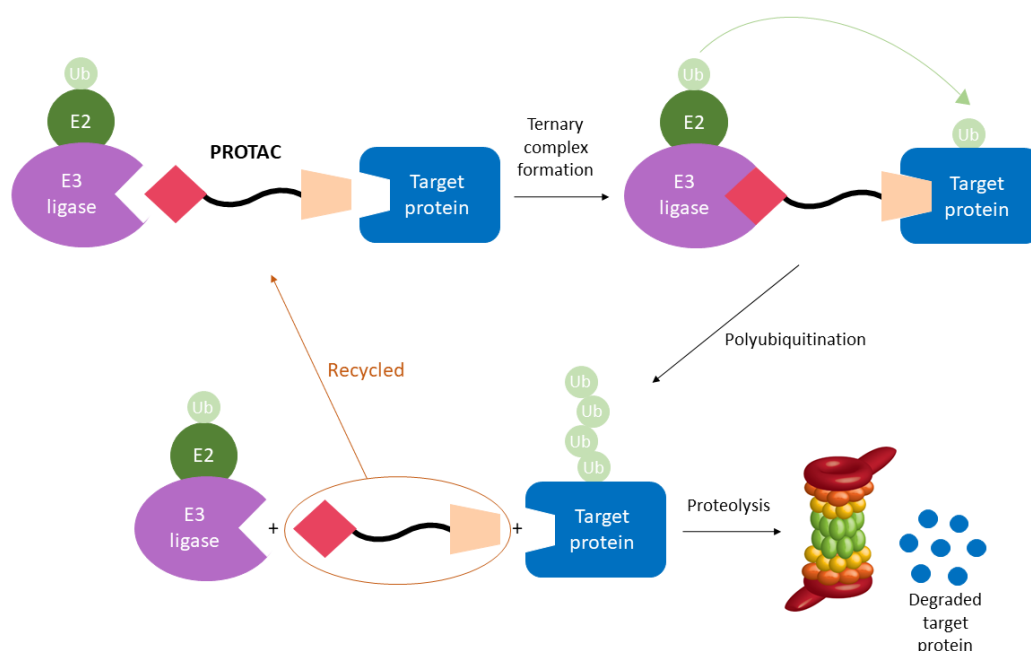
Figure 1.4: PROTAC mechanism of action.

1.3.2 PROTAC history

The first PROTAC developed less than 20 years ago by Crews, Sakamoto and Deshaies was a peptide-based molecule called Protac-1 (Figure 1.5). Protac-1 is comprised of ovalicin recruiting the target protein MetAP-2 and the IκBα peptide recruiting the SCFβ-TrCP E3 ligase (Sakamoto *et al.*, 2001). SCF, or Skp Cullin F-box, was at the time one of the most well characterised E3 ubiquitin ligases, playing an important role in marking regulatory proteins for degradation by the proteasome (Deshaies, 1999). Protac-1 was developed, synthesised and tested, showing proof of concept that targeted protein degradation could be useful in the future as a therapeutic tool to selectively eliminate proteins responsible for diseases. However, Protac-1 also showed poor cell penetration, indicating the requirement of significant development of greater drug-like properties in future PROTAC molecules (Sakamoto *et al.*, 2001). Following this work, the same group showed degradation of the human estrogen receptor with another PROTAC, demonstrating the applicability of targeted protein degradation to a wide range of potential targets (Sakamoto *et al.*, 2003).

i-7
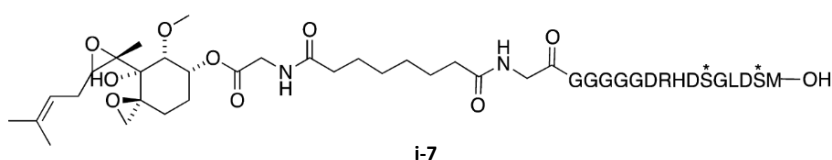
Figure 1.5: Protac-1: first PROTAC developed.

Further efforts were made to address the cell penetration problem by changing the E3 ligase ligand to target another E3 ligase, which showed the possibility to design cell permeable PROTACs (Schneekloth *et al.*, 2004). A seven amino acid sequence capable of recognising the VHL (von Hippel–Lindau protein) E3 ligase (part of the CRL2^{VHL} complex) was utilised in the new PROTACs with better cell penetration properties. However, further work was required on the E3 ligase ligand to improve the degradation activity as well as on the E3 ligase choice.

Even though the first generation of PROTACs, utilising peptides, demonstrated proof of concept for the approach, improvements were required to make more drug-like PROTACs. Therefore, attention started to turn to replacing the peptide ligands that were used in the first PROTACs with small molecule E3 ligase ligands. Peptide-based PROTACs have a high molecular weight, many peptide bonds and poor cell penetration (Lai *et al.*, 2017). Over the following decade, four main E3 ubiquitin ligases emerged as promising tools for targeted protein degradation: mouse double minute 2 (MDM2), cellular inhibitor of apoptosis protein-1 (cIAP1), von Hippel–Lindau protein (VHL) and cereblon (CRBN), all of which now have very good ligands (Figure 1.6).
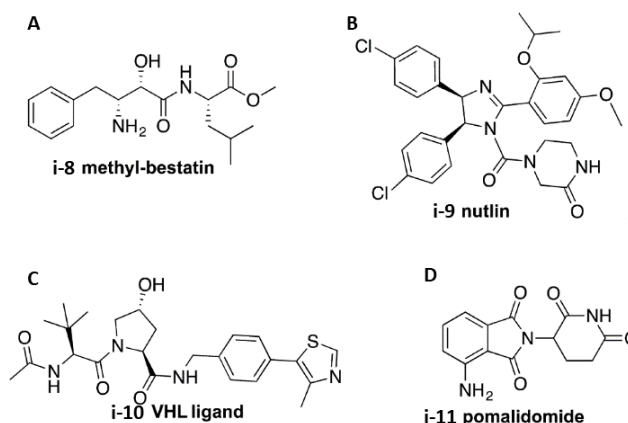
Figure 1.6: E3 ligase small molecule ligands. **A** is for cIAP1, **B** is for MDM2, **C** is for VHL and **D** is for CRBN.

The first all-small molecule PROTAC (PROTAC 14) using one of these small-molecule ligands was developed for degradation of the androgen receptor (Schneekloth *et al.*, 2008). This PROTAC used non-steroidal androgen receptor ligand (SARM) linked to the MDM2 ligand nutlin (Vassilev *et al.*, 2004) by a PEG linker. While this work proved the potential of smaller PROTAC molecules as therapeutics for targeted protein degradation, the compound was less efficient than the peptide-based PROTACs developed previously. Around same time, a PROTAC using the small molecule ligand methyl-bestatin (Umezawa *et al.*, 1976) recruiting the E3 ligase cIAP1 was developed to target the cellular retinoic acid binding proteins (CRABP-I and -II) (Itoh *et al.*, 2010). They showed proof of concept that cIAP can be recruited for proteasomal degradation. However, ligands for MDM2 (Schneekloth *et al.*, 2008) or cIAP E3 ligases (Itoh *et al.*, 2010) in PROTACs did not lead to very good potency. More recently, idasanutlin (RG7388) was also used instead of Nutlin in PROTACs (Hines *et al.*, 2019) and LCL161 was used to recruit cIAP instead of methyl-bestatin (Ohoka *et al.*, 2019). Nevertheless, within the space of a few years of nutlin's initial use in PROTACs, smaller and more drug-like E3 ligase ligands were discovered, which could recruit Cereblon (CRBN; a part of CRL4^{CRBN}) with pomalidomide (Ito *et al.*, 2010) and von Hippel-Lindau (VHL; a part of CRL2^{VHL}) (Buckley *et al.*, 2012). These are now the most commonly used E3 ligases in the field.

1.3.2.1 VHL E3 ligase

The von Hippel-Lindau protein (VHL) is part of an E3 ligase complex that ubiquitinates the hypoxia-inducible factor alphas (HIF1-α, HIF2-α, HIF3-α) in normoxia for degradation by the proteasome (Cockman *et al.*, 2000). VHL is part of the Cullin 2 (CRL2) complex (Sarikas *et al.*, 2011) which interacts with VHL, Elongin B, Elongin C and Rbx 1 (Kibel *et al.*, 1995; Nguyen *et al.*, 2015). The interaction between VHL and HIF1α presented an interest in the treatment of anaemia so scientists tried to design an inhibitor for it. Inhibition of the interaction was first illustrated by a peptide inhibitor (Willam *et al.*, 2002) and then by a small molecule mimicking the binding mode of HIF1α (Buckley *et al.*, 2012). This small molecule was composed of a hydroxyproline as a base and is attached to a methyl-isoxazole (Scheme 1.1).
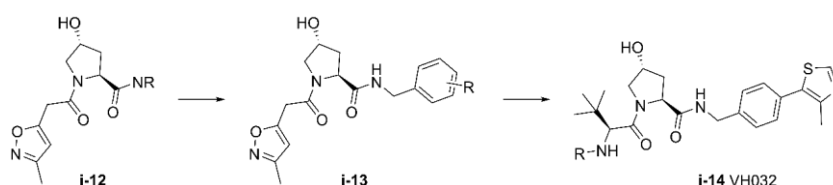
Scheme 1.1: Design of the VHL recruiter leading to VH032.

They then showed that introducing a benzyl group with a para substitution could improve affinity (Buckley *et al.*, 2012) and another isoxazole at the para substitution would give the best compound. Their co-crystal structure (RCSB PDB 1LM8) showed the important interactions created between VHL and the inhibitor binding at the HIF1α binding site. Two years later, a *tert*-butyl group on one side of the molecule and a methyl-thiazole on the other side were introduced (Galdeano *et al.*, 2014). This led to the compound VH032 (R = acetyl group) that is now used as the basis of a VHL-recruiting ligand in PROTACs (Scheme 1.1). VH032 was further optimised into VH298 where R is a cyanocyclopropyl group (Frost *et al*., 2016). Around the same time, the Ciulli and Crews groups took small molecule inhibitors they had developed against VHL (Buckley *et al.*, 2012; Galdeano *et al.*, 2014) and incorporated them into PROTACs targeting BET protein BRD4: MZ1 (Zengerle *et al.*, 2015), and receptor-interacting serine/threonine-protein kinase 2 (RIPK2) and estrogen-related receptor alpha (ERRα), respectively (Figure 1.7) (Bondeson *et al.*, 2015).
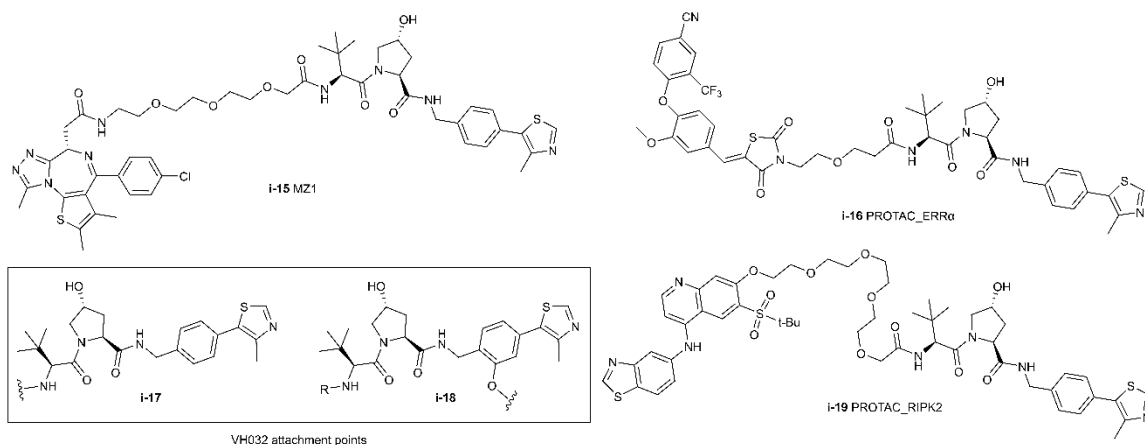
Figure 1.7: First PROTACs using VH032 to recruit VHL E3 ligase: MZ1, PROTAC_ERRα, PROTAC_RIPK2; and possible attachment points on VH032.

VH032 has two primarily utilised attachment points to recruit VHL, on the nitrogen of the *tert*-butyl side and on the benzyl ring (Maniaci *et al.*, 2017) (Figure 1.7). The first one is the most used but the second one was also used successfully in a PROTAC to create another generation of BRD7 and BRD9 degraders (VZ185) when studying the influence of the attachment point (Zoppi *et al.*, 2019), which was also used to degrade SMARCA2/4 (ACBI1) (Farnaby *et al.*, 2019) (Figure 1.8).
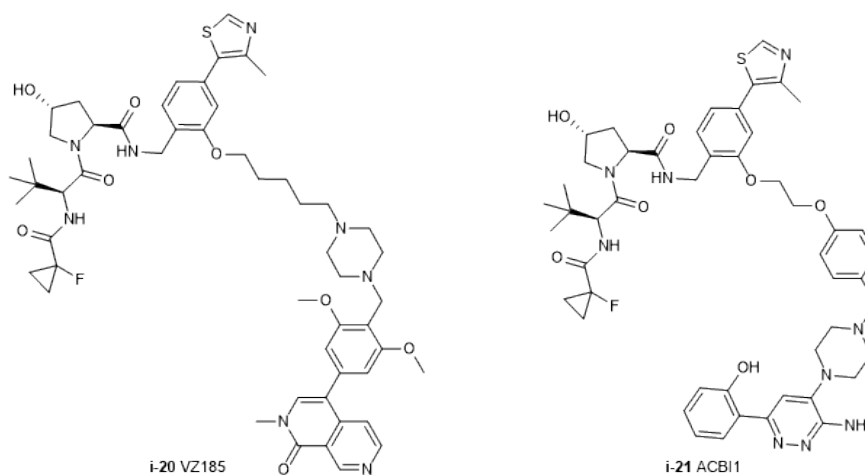
Figure 1.8: Examples of two PROTACs using VH101 as the VHL recruiter and the benzene for the linker attachment to target BRD4/9 with VZ185 and SMARCA2/4 with ACBI1.

1.3.2.2 CRBN E3 ligase

IMiDs, based on the molecule thalidomide, were shown to be anti-angiogenic and a T-cell co-stimulator, and started to be used as clinical lead compounds (Figure 1.9) (Lentzsch *et al.*, 2002; Bartlett *et al.*, 2004; LeBlanc *et al.*, 2004). As stated previously, about 10 years ago, the first IMiDs were officially approved and thalidomide was shown to bind to cereblon (Ito *et al.*, 2010; Lu *et al.*, 2014).
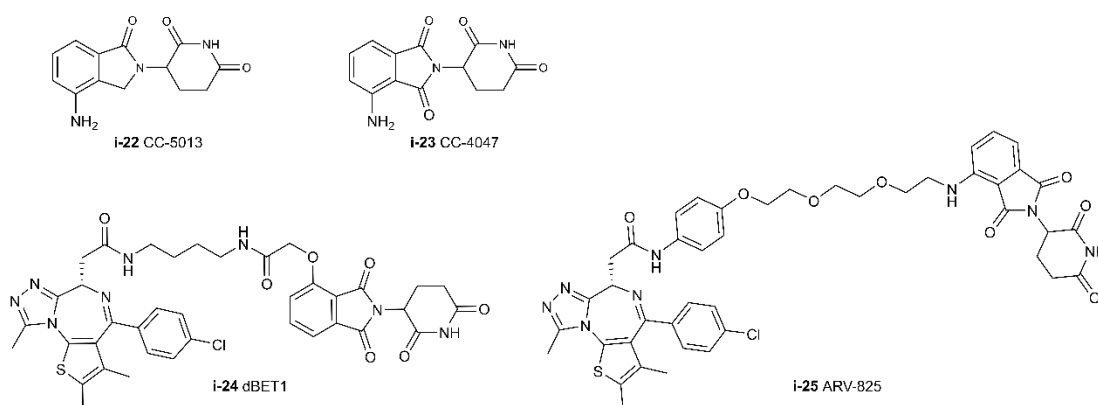
Figure 1.9: IMiDs clinical lead compounds CC-5013 and CC-4047 (anti-angiogenic).

This is when researchers started to use it to generate PROTACs. The first ones targeting the BET bromodomain with JQ1 linked to pomalidomide were generated independently in the Crews (ARV-825) and Bradner (dBET1) groups (Lu *et al.*, 2015; Winter *et al.*, 2015) and showed degradation of the target (Figure 1.9). Degrading BRD4 removed the protein from the cell, presenting advantages compared to a BRD4 inhibitor, which typically resulted in protein accumulation that led to a reduction in effectiveness (Lu *et al.*, 2015). Using IMiDs as E3 ligase binders was revealed to be a promising way to target proteins by degradation and PROTACs recruiting CRBN were found to be very potent and attractive.

For instance, two CRBN PROTACs have made very good advancement in clinical trial since 2019 and are now in Phase II: ARV-110 (Gao *et al.*, 2022) and ARV-471 (Hamilton *et al.*, 2022) targeting the androgen receptor and the estrogen receptor, respectively (Figure 1.10). The successful Phase I trials showed that PROTACs are safe in humans, have drug-like properties, and have a therapeutic effect against the target of interest, a milestone for the field.
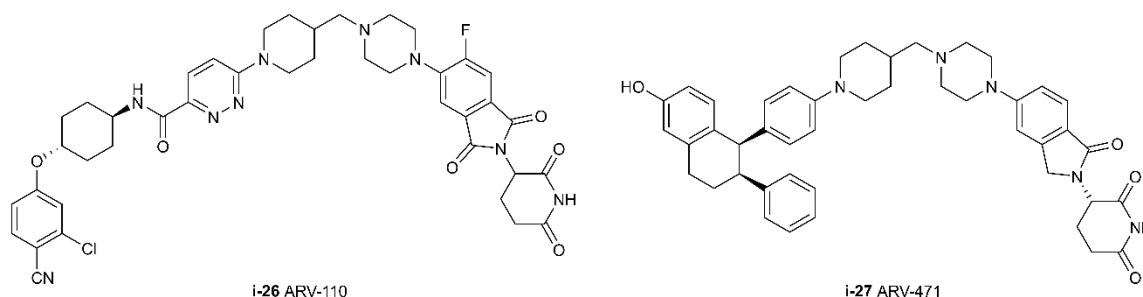
Figure 1.10: Structures of two PROTACs in clinical trials: ARV-110 (androgen receptor), ARV-471 (estrogen receptor).

1.3.2.3 Towards other E3 ligases

PROTACs containing either the CRBN or VHL ligands showed effective and prolonged degradation of their targets. They seem to be the most effective E3 ligase binders discovered at present. However, our genome encodes for over 600 E3 ubiquitin ligases, which offers many other possibilities to identify even better ligases and discover improved ligase-binding ligands in the future.

Recently, a few molecules appeared as new E3 ligases recruiters (Figure 1.11). A sulfonamide drug was shown to induce polyubiquitination and proteasomal degradation of the cancer target RBM39 by recruiting the DCAF15 E3 ligase with indisulam (Han *et al.*, 2017). Also recruiting DCAF15, other anticancer sulfonamides (E7820 and CQS) were shown to degrade the splicing factor CAPERα (Uehara *et al.*, 2017). These sulfonamide drugs seem to act like IMiDs, starting point of the commonly used CRBN recruiter. The use of DCAF15 recruited by an aryl sulfonamide was then confirmed in PROTAC DP1 (L. Li *et al.*, 2020). Furthermore, DCAF16 was recently shown to be engaged by electrophilic PROTACs (such as C-KB02-SLF) (X. Zhang *et al.*, 2019) that are capable of degrading their target. DCAF16 is localised in the nucleus, and thus only degrades nuclear proteins, which highlights the need to characterize E3 ligases depending on their location. A PROTAC was recently published recruiting Kelch-like ECH-associated protein-1 (KEAP1) using bardoxolone methyl (CDDO-Me) as a KEAP1 recruiter (Tong *et al.*, 2020). Recently, a covalent ligand screening helped discover a ligand for RNF4 E3 ligase that could be used to make a recruiter to use for targeted protein degradation (Ward *et al.*, 2019). Another

discovery using activity-based protein profiling (ABPP) chemoproteomic platforms showed that the natural product nimbolide can be used to recruit RNF14 E3 ligase and could potentially be used in PROTACs (Spradlin *et al.*, 2019). Alongside ligands for the RNF4 and RNF114 E3 ligases, the use of these new E3 ligases in PROTAC technology is promising and keeps rising.
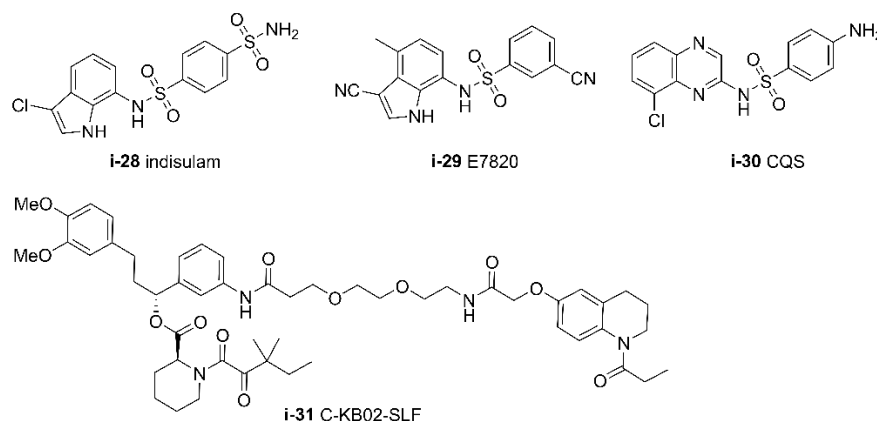
Figure 1.11: DCAF15 recruiters indisulam, E7820 and CQS, and DCAF15 electrophilic PROTAC C-KB02-SLF.

1.3.3 Ternary complex and cooperativity

Ternary complex formation is a determining step of PROTAC mechanism. Interactions between the target, the PROTAC and the E3 ligase are a critical step but had not been explained until Gadd and colleagues showed measurements of thermodynamic parameters of the complex formation in order to quantify the cooperativity of the complex for the first time (Gadd *et al.*, 2017).

The cooperativity of a ternary complex characterises how the three elements of the complex interact with each other in an interdependent manner (Figure 1.12). When the two proteins don't interact together there is no cooperativity. Cooperativity α is positive when α = K_d(binary)/K_d(ternary) > 1, which means that the ternary complex formation is favourable and additional interactions are formed, and negative when α = K_d(binary)/K_d(ternary) < 1, which means that the formation of ternary complex is diminished because of steric clashes or some other restrictions (Figure 1.12). As cooperativity can favour or disfavour ternary complex formation, it is thus a parameter

that could improve the potency of PROTACs and drive selectivity for some targets over others. The linker nature and length, as well as the recruited E3 ligase, have a direct influence on ternary complex formation and cooperativity.
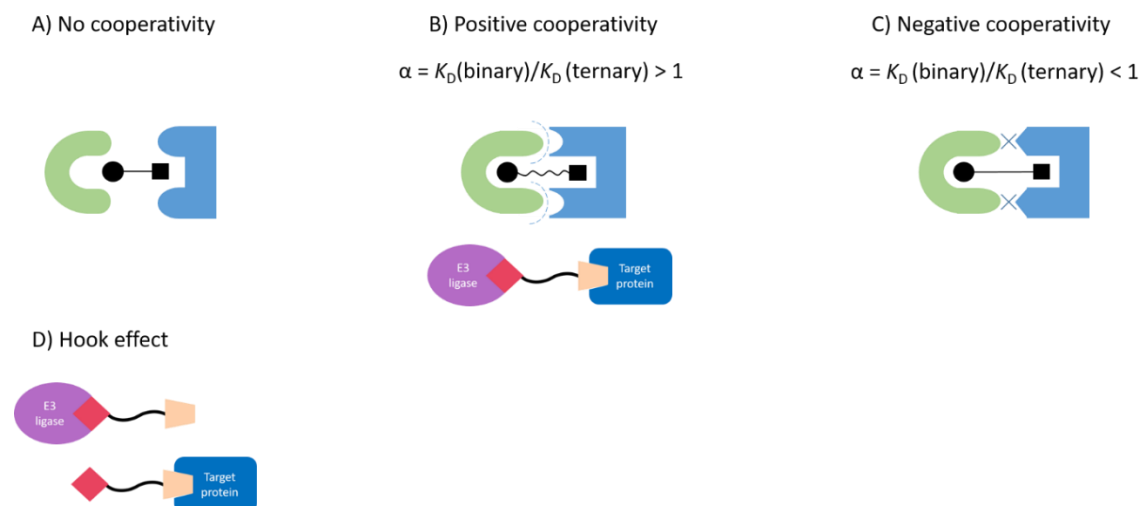
Figure 1.12: Different cooperativity of PROTACs. **A**) No cooperativity between the two proteins; **B**) Positive cooperativity between the two proteins creating PPIs; **C**) Negative cooperativity between the two proteins because of steric clashes; **D**) Hook effect only forming binary complex between the PROTAC and one of the proteins.

Alongside cooperativity, the hook or prozone effect is a feature of ternary complex formation. The hook effect is a consequence of an excess of the bridging molecule (in this case PROTAC) competing with productive ternary complexes to make unproductive binary complexess (Figure 1.12 D) (Roy *et al.*, 2017). In this scenario, the PROTAC will cause self-inhibition of its degradation activity, and thus act more like an inhibitor than a degrader. Cooperativity can have a significant effect on this phenomenon, as positive cooperativity promotes ternary complex formation, and thus will act against the hook effect (Douglass Jr *et al.*, 2013).

Gadd *et al.* published the first crystal structure of PROTAC MZ1 in complex with BRD4 bromodomain 2 and VHL E3 ligase (Figure 1.13) (Gadd *et al.*, 2017), which allowed an explanation and rationalisation of how PPIs and cooperativity lead to selectivity. Isothermal titration calorimetry (ITC) was used to study the thermodynamic of PROTAC complex formation. To avoid the hook effect, they focused on the ternary complex by

titrating the two proteins alone against the PROTAC and also titrating a protein against the binary complex already formed between the PROTAC and the other protein, in order to understand the impact of cooperativity. By using the binding information of the crystal structure of MZ1 in BRD4 and VHL, they were able to design a new BRD4-selective PROTAC, AT1 (Figure 1.13).

i-**32** MZ1   i-**33** AT1
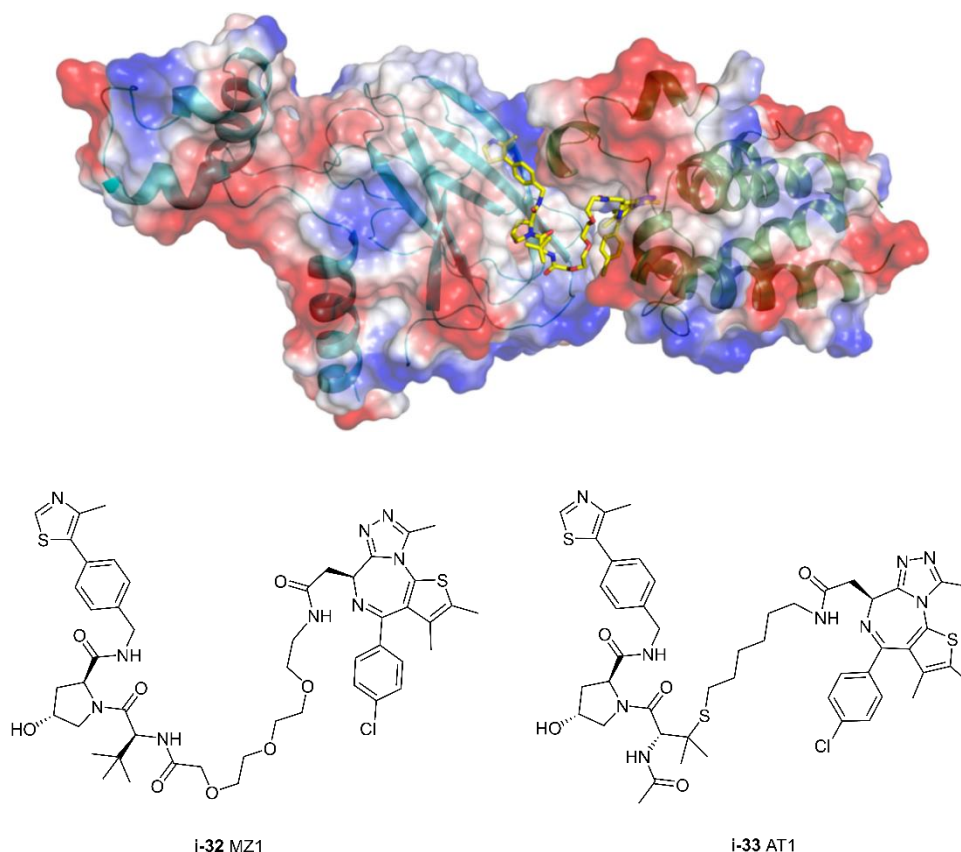
Figure 1.13: Ternary complex of between VHL protein (left), PROTAC MZ1 and BRD4[BD2] protein (right) (PDB 5T35); and structures of PROTACs MZ1 and AT1.

Another group also tried to gain insight toward rationalisation of target recruitment and selectivity looking at ternary complex formation. They confirmed that the modulation of the PROTAC to create PPIs between the target protein (BRD4) and the E3 ligase (CRBN) could result in different low-energy binding conformations depending on the linker length (Nowak *et al.*, 2018). They also highlighted that selectivity could be achieved without very tight binding or positive cooperativity. The Ciulli's group had similarly showed that a more potent inhibitor for the BET domain could lead to negative cooperativity and less potency than a less potent inhibitor which was inducing positive cooperativity (Chan *et al.*, 2018).

These findings revealed the potential of PROTACs to induce new PPIs as a new class of drugs to modulate protein activity as well as the complexity of ternary complex formation which is a balance between potency and interactions to create the more favourable ternary complex for degradation.

1.3.4 PROTAC advantages

As described previously, PROTACs create a ternary complex between the target protein and the E3 ubiquitin ligase. Small molecule inhibitors typically bind into well-defined but often highly conserved pockets that are critical to the protein's function, such as enzyme active sites. As PROTAC activity relies on the formation of a ternary complex alone, PROTAC molecules do not have to act as competitor or bind in an active site. Thus, they can target what usual inhibitors cannot. PROTACs have the potential to create novel protein-protein and protein-ligand interactions to stabilize the ternary complex. These induced ternary complex interactions can thus inform, facilitate and drive PROTAC development and they can be exploited for enhanced potency, efficacy and selectivity in targeted protein degradation (Gadd *et al.*, 2017; Y. Zhang *et al.*, 2019). By degrading the protein instead of inhibiting it, a PROTAC could help with drug resistance as it removes the target completely (Neklesa *et al.*, 2017). Also, PROTACs can be reused in multiple cycles and function in a catalytic way, which could help with lowering dosages and reducing drug toxicity (Bondeson *et al.*, 2015). Their limitations at the moment come from their high molecular weights, pharmacokinetic (PK) and ADMET (absorption, distribution, metabolism, excretion and toxicity) properties (Deshaies, 2015).

1.3.5 PROTAC design

Making a PROTAC is a challenging and long process as every part of the molecule can influence its efficacy (Burslem *et al.*, 2020). Indeed, it depends on the recruited E3 ligase, on the target ligand, but also on the linker, as its length, nature, flexibility, attachment point and the way it binds, have a direct impact on the created PPIs (Chamberlain, 2018). Thus, it is important to consider all the three parts of the molecule during PROTAC design efforts. At the moment, most understanding is empirical (Kostic *et al.*, 2020) and findings

on ligands and linkers are specific to individual targets. Varying the two warheads of the PROTAC as well as the linker is a starting point and strategy in PROTAC design (Lai and Crews, 2016) that could lead rapidly to an efficient molecule.

The first step in PROTAC design is the selection of a target. The target commonly has an inhibitor or binding molecule, and a co-crystal structure of the inhibitor into the protein of interest. By looking at X-ray structures, the best attachment point for the inhibitor can be found by looking at solvent exposed areas and determining which type and length of linker to use (Huang *et al.*, 2018). Then, the E3 ligase is selected, often VHL or CRBN. Finally, a relevant ligand for that E3 ligase can be attached via a variety of linkers.

In the initial efforts at developing PROTACs, the linker was just used to link the two ligands together and the main effort focused on the two warheads. It was soon appreciated, however, that the nature of the linker, the attachment site (Cyrus *et al.*, 2010) and the length could have an important impact on the degradation of the target. The first linker study (Cyrus *et al.*, 2011), using the estrogen receptor as a target, examined the effects of different lengths of alkyl linkers on PROTAC activity. While this investigation showed that using a sixteen-atom linker yielded the best degradation and the importance of the linker length in PROTAC design, the optimal linker would vary on a case-by-case basis, as it will depend on the selected target and the E3 ubiquitin ligase. Furthermore, recent work has shown not only how the linker gives mobility to the proteins so that the PROTAC can adopt the best conformation to create PPIs with each other, but also that the linker itself can fold into secondary structures that enable favourable ternary complex formation, and thus improve stability (Gadd *et al.*, 2017). In this way, linkers are very influential, but due to our limited knowledge, it is not possible to rationally optimise the linker without already having structural information of the target ternary complex (Cyrus *et al.*, 2010, 2011; Troup *et al.*, 2020; Zagidullin *et al.*, 2020; Bemis *et al.*, 2021).

1.3.6 Towards new type of linkers

Linkers were shown to be an important part of the molecule that influences degradation and thus play an important role in PROTACs design (Cyrus *et al.*, 2010, 2011). The structure-activity relationship (SAR) around the linker for multiple projects has shown

different degradation profiles depending on the type and length of linkers but not much attention was brought to them as mostly alkyl and PEG linkers were used. However, to work on PROTAC optimisation and molecule conformation, it is now important to work on the design of new linkers (Troup *et al.*, 2020). More rigid and less polar linkers would be useful to improve drug metabolism and pharmacokinetics (DMPK) properties of PROTACs in the future (Troup *et al.*, 2020). Both the manner of attachment as well as the length of the linker have major influence, as previously discussed. Moreover, crystal structures have brought insights on how the linker can influence the shape of the molecule to adopt the best conformation for forming the ternary complex (Gadd *et al.*, 2017). Engineering new types of linkers would thus provide a greater diversity of properties that can be imbued in this key component of the PROTAC (Cyrus *et al.*, 2010, 2011; Troup *et al.*, 2020; Zagidullin *et al.*, 2020; Bemis *et al.*, 2021). As a matter of fact, while some linkers bring flexibility, others can result in rigidity (Troup *et al.*, 2020; Zagidullin *et al.*, 2020) and act as a conformational lock.

Cubanes have recently been explored at potential building blocks in medicinal chemistry (Reekie *et al.*, 2019). Cubanes are considered to be bioisosteres of the benzene ring (Eaton, 1992). While markedly different molecules, they also present a number of similar properties relevant to biological contexts. The former is saturated whereas the latter is unsaturated. One is three-dimensional, potentially allowing access to new areas of chemical space, and the other is flat. However, the distance of the cubane diagonal and that of the benzene ring are similar, 2.72 vs. 2.79 Å, respectively (Figure 1.14) (Yildirim *et al.*, 1998). Cubanes are biologically stable as they are saturated compounds, so their use could be beneficial compared to the unsaturated benzene that can be subject to more metabolic activity such as the oxidation of a C-H bond by the cytochrome P450 superfamily for instance (Chalmers *et al.*, 2016).
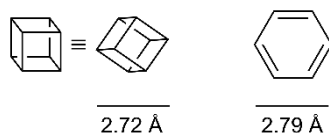
Figure 1.14: Comparison of the structures of cubane and benzene.

The challenging synthesis of cubanes comes mainly from the fact that they present a high strain energy. Two main C-C-C angles exist in molecules: 120° for sp^2 carbons and 109.5° for sp^3 carbons. With a C-C-C angle of 90°, cubanes have a positive heat of formation (endothermic) and before they were first synthesised (Eaton *et al.*, 1964), it was considered unbelievable that such a structure could hold together. The cubane 3D arrangement can be interesting in bioactive molecules interacting with proteins comparing to benzene for instance. Cubanes have eight corners, so can bear up to eight different substituents. The different attachment points on this 3D structure could allow various attachments in medicinal chemistry. By using two different corners of the cubane: 1 and 2, or 1 and 3, or 1 and 4 to attach parts of molecules, the cubane could be used to lock the full molecule in different specific conformations depending on the needs of the molecule. Thus, developing their synthesis could be useful to use in PROTACs and will be explored in Chapter 6.

1.4 Cell cycle as a target for cancer therapy

Cancer cells commonly have defects in their regulatory pathways that can generate limitless replication, invasion of tissues, responsivity to growth regulators for instance, all hallmarks of cancers that can be targeted for treatments (Hanahan, 2022). There are currently different therapies for cancers: chemotherapy (Kanzawa *et al.*, 2004; Amaravadi *et al.*, 2007), radiotherapy (Paglin *et al.*, 2001; Yao *et al.*, 2003), surgeries, and targeted therapies for instance. Chemotherapy uses DNA-damaging agents. It is known to be invasive as it can also damage healthy cells. Radiotherapy or radiation therapy uses high dose of radiation to kill cancer cells and decrease tumour size. This damages the DNA of cancer cells beyond repair with the radiation, which cause the cells to die. Targeted therapy is used to target proteins involved in the fast growth, division and spread of cancer cells. Many of the proteins targeted for cancer therapies are involved in the cell cycle (Suski *et al.*, 2021) and especially in checkpoints, such as the G_2/M with Wee1, or mitosis, with KIFC1, as cancers often carry genomic instabilities that make them susceptible at these checkpoints. Such treatments are useful because they mainly affect cells that are dividing or replicating i.e. cancer cells comparing to healthy cells which do not go through the cell cycle as much.

1.4.1 Cell cycle as a target

The cell cycle is the most important process in our body as it regulates how our cells grow and divide to stay healthy. Proteins are constantly being created, regulated and degraded in order to control where, when and what cells and their contents have to do. When DNA is damaged, cell cycle checkpoints can arrest the cell cycle and allow time for damaged DNA to repair in order to keep our genome intact (Hartwell *et al.*, 1989). There are two main checkpoints, occurring at the ends of the G_1 and G_2 phases: G_1/S and G_2/M checkpoints, respectively. They are regulated by many different proteins, some of which have been correlated with cancer when overexpressed, such as Wee1 that will be developed in this thesis (Do *et al.*, 2013).

Some cancers can develop resistance to the DNA-damaging therapies that have successfully treated them, causing a relapse of disease (L.-Y. Li *et al.*, 2020). This resistance is caused by the overexpression of some proteins regulating the checkpoints as they can stop cells from dividing and provide the time necessary for DNA to be repaired from DNA damaging agents. This is the case of Wee1 protein, a protein kinase overexpressed in many cancers which plays a regulatory role at the G_2/M checkpoint, which potential will be developed in this thesis. As such, the efficiency of DNA damaging agents is greatly reduced when cells are blocked by these checkpoints. Designing a drug to abrogate these checkpoints would thus enhance the efficacy of DNA-damaging therapies leading to mitotic lethality (L.-Y. Li *et al.*, 2020).

Another important part of the cell cycle is mitosis, during which a cell divides into two identical daughter cells in order to pass the same genetic information. This is the driving process of cell reproduction. Abnormalities during mitosis can lead to genetic defects as cell division must maintain the genome and same number of chromosomes to be distributed to the daughters cells. Many proteins are involved in mitosis and overexpression of certain proteins has been correlated with cancer because of their malfunction and disruption of normal/regulated cell division. Mitosis comprises prophase (chromosome formation with two chromatids attached at the centromere), metaphase (microtubules pull chromosomes which align in the middle of the cell on the metaphase

plate, this corresponds of the splitting of the two centrosomes (Vasquez-Limeta *et al.*, 2021)), anaphase (fibres pull the chromosomes toward the poles of the cell), telophase (the chromosomes at the poles come together as a mass and the nuclear envelope starts forming around it). KICF1 protein, a motor kinase, plays an important role in centrosome clustering in cancer cells with centrosome amplification (more than two centrosomes) (Cai *et al.*, 2010). KIFC1 has been observed as overexpressed in cancers, preventing aneuploidy and cell death by clustering more than two centrosomes into the normal two poles of the cell, thus leading to cancer cells survival (Anderhub *et al.*, 2012). The potential of KIFC1 as a target for cancer therapy will be developed in this thesis.

1.4.2 Target pathways for cancer therapies

1.4.2.1 Kinase inhibition

Kinases are essential enzymes that add a phosphate group to another protein with ATP as a source and kinase signal transduction cascades regulate most cellular pathways, such as cell division and cell growth. Kinases are thus important and essential to the cells in our body. There are many protein kinases, with approximately 500 protein kinases identified in the human genome (Ardito *et al.*, 2017). However, due to their important regulatory functions, protein kinases are also responsible for many malfunctions in diseases and especially cancers as they control many key processes and pathways. In cancers, mutations lead to dysregulation of signalling pathways such as MAPK/ERK, which is one of the most critical pathways in such diseases and is a key therapeutic target (Figure 1.15) (Burotto *et al.*, 2014). This pathway is fundamental for cells as it controls their growth, differentiation, apoptosis and proliferation (Zhang *et al.*, 2002; Dhillon *et al.*, 2007). A small GTPase activates a MAP3K, the MAP3K activates a MAP2K which activates a MAP kinase (MAPK) as shown below (Figure 1.15). MAPK pathway was also correlated with the phosphorylation and activation of p53 in response to DNA damage (Gen Sheng Wu, 2004). Thus, Ras mutations as an important role in the MAPK pathway by either leading to cell cycle arrest and apoptosis or to cell survival following p53 mutation.

In particular, Ras GTPase proteins play an important role in a variety of cancers. Growth factors activate Ras which in turn activates Raf kinase by phosphorylation. Then, Raf kinase phosphorylates and activates MEK. MEK phosphorylates and activates extracellular signal-regulated kinase 1/2 (ERK1/2), a group of MAPK (Dhillon *et al.*, 2007) (Figure 1.15).
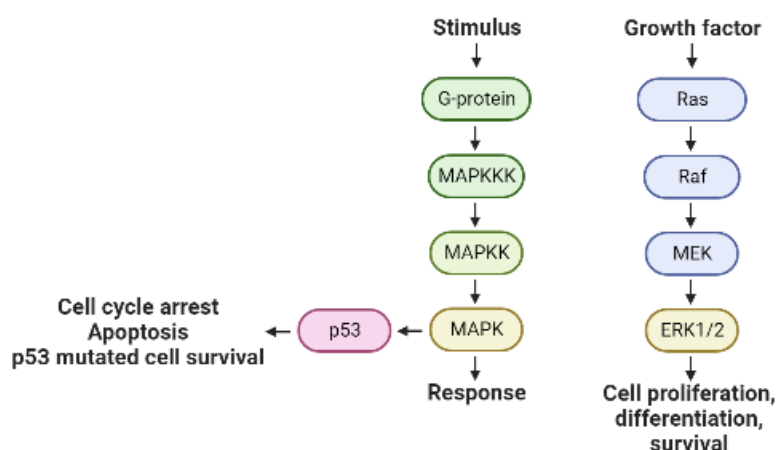
Figure 1.15: MAPK signalling pathway organisation.

Dysregulation in this pathway occurs in around one third of human cancers and the implication of kinases in such diseases make them a good target for research and treatments (Dhillon *et al.*, 2007). The very first drugs targeting protein kinases were ATP competitors such as isoquinoline and naphthalene sulphonamides, which were shown to reduce kinase activity (Hidaka *et al.*, 1984). Since the initial discovery of these basic inhibitors, the targeting of protein kinases has become a very attractive topic and constitutes roughly 20% of drug development activity (Santos *et al.*, 2016). Over the past 10 years, a lot of progress has been made towards the discovery of kinase inhibitors in oncology as well as autoimmune diseases for instance. New kinase targets are being explored such as CDK7/8/12 and 13 for transcriptional kinases and TAM kinases for the immuno-regulatory kinases (Ferguson *et al.*). Improvement in the selectivity analysis of kinase inhibitors also helps with the development. Due to their similarities, kinases are very challenging to target selectively (Ferguson *et al.*).

1.4.2.2 ATR inhibition

Ataxia telangiectasia and Rad3-related kinase (ATR) is part of the DNA-damage response (DDR) machinery. ATR is stimulated when DNA is damaged in order to repair it and maintain integrity of the genome. Cancer cells often present genomic instability, which is maintained when the DDR mechanism has dysfunctions (Barnieh *et al.*, 2021). ATM (a p53 activator) and p53 (induces apoptosis and cell arrest when DNA damage or oncogenic activity are detected (Li *et al.*, 2012)) are key regulators of the DDR and tumours rely a lot on pathways likes ATR (Jackson *et al.*, 2009) to survive (Figure 1.16). ATR is mainly activated in the present of single stranded DNA. Tumour cells were shown to be sensitive to ATR inhibition, which became a good target for therapies (Karnitz *et al.*, 2015; Weber *et al.*, 2015). Recently two potent and selective ATR inhibitors have entered clinical trials AZD6738 (Jones *et al.*, 2013) and VX-970 (Hall *et al.*, 2014) in monotherapies or paired with chemotherapies.
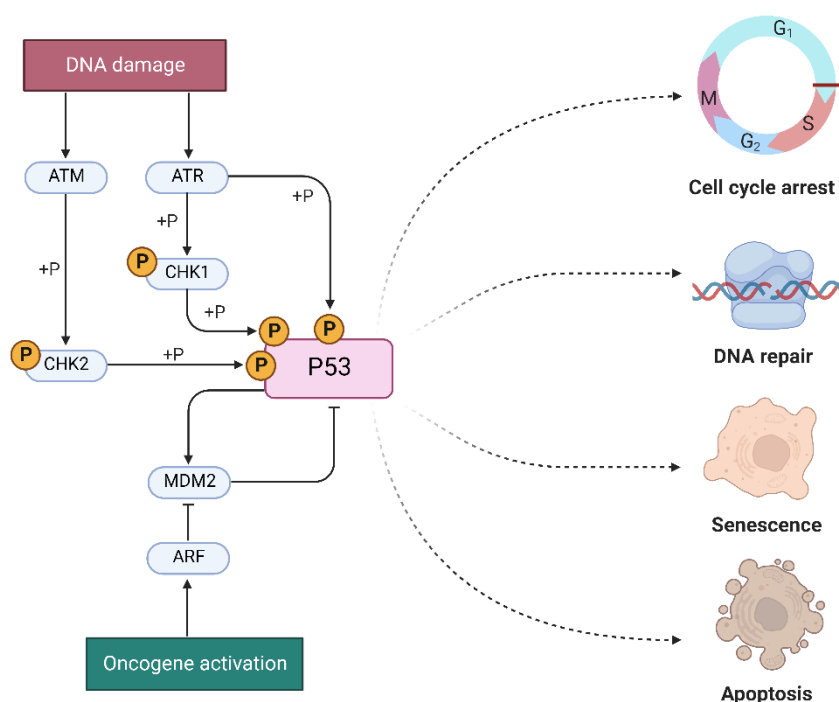
Figure 1.16: Illustration of the activation of the ATM and ATR pathway by DNA damage or oncogenes (Using BioRender).

Inhibition of important pathways such as ATR that are involved in the cell cycle and are critical for tumour proliferation, have become very attractive targets for inhibition and cancer therapies. CHK1 and Wee1, both downstream effectors of the ATR pathway and DNA-damage response, have recently brought a lot of interest as targets and Wee1 will be developed in this thesis.

2 Materials and methods

2.1 Materials

Chemicals for biological work were purchased from Sigma Aldrich and Thermo Fisher Scientific, or as otherwise specified. All tissue culture media, FBS, PS and Trypsin were obtained from Gibco. Cell culture flasks and cell culture dishes were from Corning incorporated.

2.2 Buffer and solutions

All buffers and solutions were prepared using ultrapure water filtered (MQW) in the Milli-Q Integral Water Purification System.

Agar plating medium: 1% (w/v) Tryptone, 0.5% (w/v) NaCl, 0.5% (w/v) yeast extract, 1.5% (w/v) agar in MQW.

Agarose gel medium: 1.5% (w/v) agarose in TAE buffer with 1:10000 SYBR Safe.

Blocking Solution: 5% (w/v) Skim Milk Powder in TBST or 5% (w/v) BSA in TBST.

Coomassie Brillant blue destain solution: 40% (v/v) methanol, 10% (v/v) acetic acid, 50% (v/v) MQW.

Coomassie Brillant blue stain solution: 0.1% (w/v) Coomassie R-250, 40% (v/v) ethanol, 10% (v/v) acetic acid, 50% (v/v) MQW.

Crystal violet solution: 0.5% (w/v) Crystal Violet in MQW.

Hot Lysis Buffer (Laemmli buffer): 50 mM Tris-Cl, 2% (w/v) SDS, 10% (v/v) Glycerol, pH 6.8 in MQW.

LB medium: 1% (w/v) Tryptone, 0.5% (w/v) NaCl, 0.5% (w/v) yeast extract in MQW.

Loading buffer for SDS PAGE gels: 1 M DTT, 1% (w/v) bromophenol blue in MQW.

20× Coomassie blue: 0.4% (w/v) Coomassie G-250 in MQW.

1× Native PAGE blue running buffer (1 L): 10% (v/v) 10× running buffer, 5% (v/v) 20x Coomassie in MQW.

6× Native PAGE loading buffer: 40% (w/v) sucrose, 187.5 mM Tris pH 8.8, 60 mM DTT in MQW.

10× Native page running buffer (1 L): ~pH 8.3, 250 mM Tris-Cl, 1.92 M Glycine in MQW.

4% PFA: Prepared from 16% paraformaldehyde ampoule (methanol free, Agar Scientific AGR1026) and diluted by four.

Resolving gel Tris buffer: 1.5 M Tris-Cl, pH 8.8 in MQW.

Solution for antibodies dilution: 5% (w/v) BSA, 0.05% (w/v) NaN_3 in 1× TBST.

Stacking gel Tris buffer: 0.5 M Tris-Cl, pH 6.8 in MQW.

50× TAE buffer: 2 M Tris-Cl, 1 M acetic acid, 0.05 M EDTA (pH 8) in MQW.

10× TBS: 50 mM Tris-Cl, 150 mM NaCl, pH 7.5 in MQW.

TBST: 10% (v/v) 10× TBS, 0.1% (v/v) Tween-20.

10× Tris-glycine Running Buffer: 250 mM Tris, 1.92 M glycine, 1% (w/v) SDS, pH 8.3 in MQW.

2.3 Polyacrylamide gels preparation

Polyacrylamide gels were prepared with or without SDS using the conditions indicated in Table 2.1. The glass plates and combs were used from the Bio-Rad Mini-Protean system. The resolving gel was prepared, poured and left to set for ~ 15 min after adding a layer of ethanol. Once set, ethanol was removed and the stacking gel was prepared and poured. The comb was placed and the gel was allowed to set for another 15 min. Once set, the comb was removed and the gels were ready to use or stored at 4 °C until use. PageRuler™ Plus Prestained Protein Ladder (Thermo Fisher Scientific, 26619) was used to run the gels.

Table 2.1: Composition of polyacrylamide gels used for Western blotting, protein expression analysis and native PAGE experiments.

Gel	Resolving SDS PAGE (20 mL)	Resolving SDS PAGE (20 mL)	Resolving native PAGE (20 mL)	Resolving native PAGE (20 mL)	Stacking SDS PAGE (5 mL)	Stacking native PAGE (5 mL)
Percentage	10%	14%	10%	7.75%	4%	4%
MQW	9.7 mL	7.7 mL	9.9 mL	12.37	3.17 mL	3.67 mL
Resolving Tris buffer	5 mL	5 mL	5 mL	5 mL	-	-
Stacking Tris buffer	-	-	-	-	1.25 mL	1.25 mL
Acrylamide (40%)	5 mL	7 mL	5 mL	2.56 mL	0.5 mL	0.5 mL
SDS (10%)	200 µL	200 µL	-	-	50 µL	-
APS (10%)	100 µL	100 µL	100 µL	100 µL	25 µL	25 µL
TEMED	20 µL	20 µL	20 µL	20 µL	5 µL	5 µL

2.4   Cell culture and routine passaging

Human HeLa S3, MCF7, BT549 and MDA-MB-231 cells were purchased from the ATCC and were cultured in Dulbecco's modified eagle's medium (DMEM) with 10% (v/v) of fetal bovine serum (FBS), 4 mM L-glutamine, 25 mM D-glucose, 1 mM sodium pyruvate, and 1% (v/v) penicillin/streptomycin (PS) (100 units penicillin and 10 µg streptomycin/mL) at 37 °C and 5% CO_2. PC3 and LNCaP cells were purchased from the ECACC and were cultured in RPMI 1640 with 10% (v/v) of fetal bovine serum (FBS), 2 mM L-glutamine, 11 mM D-

glucose, and 1% (v/v) penicillin/streptomycin (PS) (100 units penicillin and 10 μg streptomycin/mL) at 37 °C and 5% CO_2.

Cell lines were cultured for no more than twenty passages from the purchased stock. For the passages, the media were removed from the flask. Cells were then washed twice with PBS and incubated for 5 min with trypsin at 37 °C. Media were added to the detached cells to resuspend the cells and dilute the cells to divide them in the appropriate number of new flasks/plates after cell counting using an haemocytometer (Counting chamber, Hawksley, AC1000), a trypan blue solution in a 1:1 ratio (v/v) of trypan blue and sample (0.4% solution, Fluka, 93595) and a microscope (World Precision Instruments PIM-III).

2.5 Cell proliferation assay using MTS

MCF7, BT549, PC3, LNCaP and MDA-MB-231 cells were plated in a 96-well plate at a density of respectively 4×10^3, 7×10^3, 2×10^3, 2×10^3, 2×10^3 cells per well and incubated overnight at 37 °C (See Section 2.4). The cells were then treated in a dose-dependent manner from 0 to 20 μM with the indicated compound in 100 μl of media and incubated at 37 °C for 72 h. 20 μL of CellTiter 96® AQ$_{ueous}$ One Solution Cell Proliferation Assay (MTS) (Promega) reagent was added to each well and the plate incubated at 37 °C for 1 to 3 h. Formazan product was measured by absorbance at 490 nm using a Wallac 1420 Victor^2 multilabel counter (PerkinElmer) as an indicator of cellular proliferation. The data were processed using non-linear regression to a dose-response logistic function in OriginPro 2019b (OriginLab) or GraphPad Prism 9.2.0.

2.6 Cell treatments for immunoblotting

Cells were split and seeded (See Section 2.4) the day before treatment in 6-well plates at 0.3×10^6 cells per well in 2 mL of media in each well, except for BT549 cell where 0.4×10^6 cells per well was needed. The next day, cells were treated with PROTAC solutions or the DMSO control (0.1% v/v) at 37 °C and 5% CO_2, for the time and at the concentration indicated, before harvesting.

For co-treatment with mechanistic inhibitors for the Wee1 project, MLN4924 (1 μM) (Selleckchem), MG132 (20 μM) (Tocris), pomalidomide (10 μM) (Selleckchem), VH298 (100 μM) (Sigma Aldrich), or AZD1775 (1 μM) (Cayman Chemical) was added into the desired wells two hours prior to PROTAC treatment. Cells had a final concentration of DMSO of 0.1% (v/v). Plates were incubated for a further 5 h at 37 °C and 5% CO_2 before harvesting.

For co-treatment with mechanistic inhibitors for the KIFC1 project, MLN4924 (3 μM), MG132 (40 μM), pomalidomide (10 μM) or AZ82 (1 μM) (Sigma Aldrich) was added into the desired wells three hours prior to PROTAC treatment. Cells had a final concentration of DMSO of 0.1% (v/v). Plates were incubated for another 20 h at 37 °C and 5% CO_2 before harvesting.

2.7   Immunoblotting

After the treatment and incubation, cells were washed twice with PBS and lysed with 120 μL of Laemmli lysis buffer at 105 °C. The wells were then scraped to harvest the lysates, which were heated for a further 10 minutes at 105 °C and vortexed every two minutes to generate whole cell extracts. Protein concentrations in the samples were determined using a Pierce BCA Protein Assay Kit (Thermo Fisher Scientific) following the manufacturer's protocol, using one-in-five dilutions for each sample. Protein concentrations were measured with the BCA method applet on a NanoDrop 2000c at a wavelength of 562 nm (Thermo Fisher Scientific).

Between 20 and 50 μg total protein was mixed with 0.1 volumes of loading buffer (See Section 2.2.) and heated at 100 °C for five minutes before loading and running them on SDS-PAGE (10% or 14%) prepared in house (Section 2.3). Gels were transferred to a nitrocellulose membrane using Trans-Blot Turbo RTA Transfer Kit (BioRad) on a Trans-Blot Turbo (transfer system) (BioRad). The membrane was blocked at room temperature for 2 h with 5% skimmed milk (w/v) or 5% bovine serum albumin (BSA) (w/v) in TBST and washed three times with TBST. The membrane was then incubated overnight at 4 °C with the indicated primary antibody. Primary antibodies were made up in 0.05% NaN_3 (w/v) and 5% BSA (w/v) in TBST and used at the concentrations indicated in Table 2.2.

For chemiluminescent detection, the membrane was washed three times with TBST before the corresponding secondary antibodies were used against each primary antibody for 2 h at room temperature three times more diluted than the primary antibody concentration (Table 2.2). Signals were detected with the ChemiDoc MP Imaging System (Bio-Rad) using Clarity Western ECL Substrate (BioRad) or Clarity Max Western ECL Substrate (BioRad). The results were then analysed with Image Lab software 6.0.1.

For fluorescent detection, fluorescently-labelled secondary antibodies were used. The membrane was washed three times with TBST, incubated for 2 h at room temperature with the appropriate secondary antibody (Table 2.2), washed three times with TBST and once with PBS. Signals were then detected using LICOR Odyssey Fc. Image Studio software was used to quantify the bands. Wee1, pCDK1(Y15) and KIFC1 were reported as a ratio of the protein band and the loading control band (β-actin or GAPDH). They were then normalised to the 0.1% DMSO control sample.

Table 2.2: Table of antibody details and their usage concentrations.

Antibody	Supplier	Catalogue	Dilution	Species
Wee1	Abcam	ab137377	1:1,000	Rabbit
MAP3K4	Abcam	ab186125	1:1,000	Rabbit
PLK1	Abcam	ab17057	1:500	Mouse
JAK2	Abcam	ab108596	1:1,000	Rabbit
β-actin	Abcam	ab8227	1:10,000	Rabbit
CDK1	Cell Signaling Technology	#9116	1:1,000	Mouse
pCDK1	Cell Signaling Technology	#9111	1:1,000	Rabbit
PLK3	Cell Signaling Technology	#4896	1:500	Rabbit
PLK2	Protein tech	15956-1-AP	1:500	Rabbit
KIFC1	Abcam	ab172620	1:5,000	Rabbit
Tubulin	Sigma Aldrich	T6199	1:10,000	Mouse
GAPDH	Abcam	ab181602	1:10,000	Rabbit
Anti-Mouse	Cell Signaling Technology	#7076	-	-
Anti-Rabbit	Cell Signaling Technology	#7074	-	-
IRDye® 680RD Donkey anti-Rabbit	LI-COR	926-68073	1:10,000	-
IRDye® 800CW Donkey anti-Mouse	LI-COR	926-32212	1:10,000	-

2.8 Flow cytometry

Plates were seeded on day 1 (See Section 2.4). On day 2, cells were treated with the PROTAC, the inhibitor or DMSO (0.1% v/v DMSO) and incubated for 24 h at 37 °C. On day 3, the media were removed from the flask, the cells were washed twice with PBS and trypsinised for 5 min at 37 °C. The cells were then resuspended up to 1 mL of media and transferred in a microcentrifuge tube to count the cells. The cells were kept on ice for the next steps. Cells were centrifuged for 3 min at 1.5 rpm. The media was removed gently to not disturb the pellet. The pellet was washed with 500 μL of PBS, centrifuged for 3 min and the PBS was removed gently. The pellet was resuspended in ice cold 100% ethanol (500 μL) by adding ethanol dropwise and vortexing slowly, and finally the microcentrifuge tube was vortexed at high speed after full addition. The samples were left in the −20 °C freezer for 2 h and centrifuged for 5 min. The ethanol was removed gently and 250 μl of FxCycle PI (RNase Staining Solution) (ThermoFisher Scientific, F10797) was added. The microcentrifuge tube was vortexed, covered from light and incubated at 4 °C for 30 min before running the samples.

Data was acquired using the CytoFLEX (Beckman) Flow Cytometer. Data were analysed using CytExpert software after collecting 20,000 events per sample. It was manually analysed and cells were gated with PE width versus area to remove doublets and SSC versus FSC for size and complexity.

2.9 IF - Immunofluorescence (Confocal microscopy, Image J)

MDA-MB-231 wt cells were plated on day 1 in a 24-well glass bottom plate (3 sets of staining): 25000 cells/well in DMEM supplemented with 10% (v/v) FBS and 1% (v/v) PS (500 μL/well) (See Section 2.4). The cells were then treated with the PROTAC, the inhibitor or the DMSO (0.1% DMSO) and incubated for 24 h. On day 3, the cells were fixed and then stained with primary antibodies: Pericentrin, Centrin and Tubulin at a concentration of 1:1000 (Table 2.3). Secondary antibodies were used as indicated in Table 2.4.

Table 2.3: Table of primary antibodies for IF staining.

Antibody	Supplier	Catalogue	Dilution	Species
Tubulin	Millipore	MAB1864	1:1,000	Rat
Centrin	Millipore	04-1624	1:1,000	Mouse
Pericentrin	Abcam	ab4448	1:1,000	Rabbit

Table 2.4: Table of secondary antibodies for IF staining.

Antibody	Supplier	Catalogue	Dilution	Raised in	Tag
Tubulin	Invitrogen	A32732	1:500	Goat	Alexa-Fluor Plus 555nm
Centrin	Invitrogen	A32723	1:500	Goat	Alexa-Fluor Plus 488nm
Pericentrin	Invitrogen	A21247	1:500	Goat	Alexa-Fluor 647nm

To fix the cells, the media were removed from the wells and cells were washed twice with 1 mL of PBS. ~2 mL of ice-cold methanol was added to fix and permeabilize the cells and the plate was incubated for 15 min at –20 °C. The ethanol was then removed, and each well was washed with 1 mL of PBS. The plate was stored in the fridge until it was stained.

To stain the cells, the PBS was removed and 1 mL of 5% (v/v) goat serum was added to each well for 30 min at room temperature (r.t.) to block. The serum was then removed and 800 µL primary antibody mix was added to each well and incubated for 2 h at r.t.. The antibody mix was removed and the wells were washed three times with PBS and once for 5 min. 400 µL of secondary antibody mix was then added to each well and incubated for 1 h at r.t. in the dark. The secondary antibody mix was removed and the wells were

washed three times with PBS and once for 5 min. DAPI was added at 1 µg/mL in PBS for 10 min, removed and washed once with PBS. Plates were stored at 4 °C until ready for imaging.

A Zeiss-LSM880-Airyscan confocal microscope and Zen software were used to image the immunofluorescence of stained cells on glass-bottomed 24-well plates, using a 20× objective dry lenses (Plan-Apochromat 20×/0.8 M27), taking 2×2 tiled images and 5 fields of view for each well. Images were analysed in FIJI software (2.3.0). Mitotic cells were identified using the merged images and marked as regions of interest (ROI). The ROIs were saved as an overlay to further identify mitotic phenotypes.

2.10 Clonogenic assay

24-well plates were seeded on day 1 with 25000 cells per well into 500 µL of media (DMEM full medium (MDA-MB-231) or RPMI full medium (BT549)). On day 2, the cells were treated at the required concentration with the PROTAC, the inhibitor or DMSO to 0.1% (v/v) DMSO. On day 3, after 24 h treatment, the media was removed and the cells were washed once with PBS (200 µL), and trypsin-EDTA (200 µL) was added. The plate was incubated 5 min in the cell incubator at 37 °C. The cells were then transferred to a microcentrifuge tube to a final volume of 1 mL and cells were counted. 6-well plates were reseeded with 2000 cells/well (BT549) and 500 cells/well (MDA-MB-231) in three replicates for each condition. The media was changed every three days until imaging (after 7-10 days). On the day of imaging, the cells were fixed and stained. The media was removed and the cells were washed twice with PBS (2 and 1 mL). 1 mL of 4% PFA was then added and left for 15 min. The PFA was removed and 1 mL of crystal violet solution was added per well. The plate was incubated for 30 min and the crystal violet was removed. The wells were finally washed with PBS (2 × 1 mL) and left to dry. The colonies were then quantified using the plugin ColonieArea in ImageJ (Guzmán *et al.*, 2014).

2.11 Cloning

Primers were designed by looking at the DNA template sequence needed and by using XhoI (CTCGAG) and NdeI (CATATG) restriction enzymes cutting sites to allow further insertion in pET28a (Table 2.5). Primers were ordered from Sigma-Aldrich.

Table 2.5: Primers used for cloning Wee1 into the pET28a vector. Restriction sites underlined.

CDS		Primer
Wee1	Forward	5' GCG<u>CATATG</u>AAAAGCCGCTATACCAC 3'
	Reverse	5' GCG<u>CTCGAG</u>TCATTACTATTTACGGCTTGCGCTCAG 3'

2.12 Agarose gel

To prepare 1-1.5% (w/v) agarose gels, the required amount of agarose was measured and resuspended in TAE. The suspension was microwaved until the agarose was fully dissolved. Agarose was then cooled to around 50 °C and poured in the gel tray and SYBR Safe DNA gel stain (Invitrogen, S22102) was added (1:1000). The combs were placed and the gel was allowed to set. Once set, the gel was placed in the electrophoresis unit (Bio-Rad). Loading buffer (Gel Loading Dye Purple 6×, New England Biolabs, B7024S) was added to the DNA samples and the samples were loaded in the gels. Quick-Load® 1 kb Plus DNA Ladder (NEB, N0469S) was used to provide standard markers. The gel was run in TAE buffer at 100 V for around 1 h. The gel was visualised using the Chemidoc UV transilluminator function.

2.13 Polymerase chain reaction

Polymerase chain reaction (PCR) was used to amplify DNA fragments. PCR reactions were prepared in 0.2 mL PCR tubes (Table 2.6) and were placed in the PCR machine (Mastercycler Personal, Eppendorf) for the designated reaction cycle (Table 2.7).

Reactions were checked by running an agarose gel (Section 2.12). PCR reaction concentration was measured using NanoDrop Spectrophotometer (Thermo Fisher Scientific – Nucleic acid). The PCR product was then ethanol precipitated by adding 0.1 volumes of 3M NaOAc and 2 volumes of chilled absolute ethanol to the PCR product. The solution was centrifuged at 4 °C for 30 min at 14,000 rpm. The liquid was then removed carefully and the pellet was stored at −20 °C until use. Or, where permissible, the PCR product was also used directly for the restriction digest without ethanol precipitation.

Table 2.6: Composition of the PCR reactions. Different percentage of DMSO were used.

Percentage of DMSO	0%	5%	10%
5X HF buffer	10 µL	10 µL	10 µL
DMSO	0 µL	2.5 µL	5 µL
dNTPs	1.25 µL	1.25 µL	1.25 µL
10 ng/µL template	1 µL	1 µL	1 µL
20 µM Fwd primer	1 µL	1 µL	1 µL
20 µM Rev primer	1 µL	1 µL	1 µL
MQW	35.25 µL	32.75 µL	30.25 µL
Phusion (2 U/µL)	0.5 µL	0.5 µL	0.5 µL

Table 2.7: Temperature cycling profile for PCR reactions.

Stage	Temperature (°C)	Time (min)	Number of cycles
Initial denaturation	95	5	1
Denaturation	95	1	25
Annealing	51-54	1	
Extension	72	10	
Final elongation	71	30	1

2.14 Restriction digest

Restriction enzymes were purchased from New England Biolabs. The PCR products and pET28a vector were digested with XhoI and NdeI enzymes. Reactions were prepared in microcentrifuge tubes as indicated in Table 2.8, and they were placed in a water bath at 37 °C for 90 min. 1 U of rSAP was added to pET28a and it was incubated for a further 45 min. Reactions were placed in the heat block at 65 °C for 5 min to stop the reaction and inactivate the enzymes. DNA was then purified using centrifugation and the Gene JET PCR Purification Kit (Thermo Fisher Scientific). The final 50 µL of elution buffer containing the DNA were kept and stored at –20 °C. Samples concentrations were measured using the Nanodrop.

Table 2.8: Conditions for the restriction digest reactions.

For 30 µL	Insert NX (Ethanol precipitated)	Insert NX	pET28a NX
10x Cutsmart	3 µL	3 µL	3 µL
PCR product	pellet	20 µL	-
pET28a (~130 ng/µL)	-	-	10 µL
MQW	25 µL	5 µL	15 µL
NdeI (20 U/µL)	1 µL	1 µL	1 µL
XhoI (20 U/µL)	1 µL		1 µL

2.15 Ligation of DNA

The digested insert was then ligated into pET28a vector (pET28a map in appendix 1). The reactions were prepared following conditions (Table 2.9), placed on ice and allowed to warm to room temperature overnight or directly incubated at room temperature for 3 h. Ligations were checked by doing a diagnostic digest on the transformant (Sections 2.16 and 2.17).

Table 2.9: Conditions for ligation reactions between the insert and the plasmid.

For 10 µL	Control (µL)	Ligation (µL)
Insert NX (~60 ng/µL) (3x more than plasmid)	-	2
pET28a NX (~20 ng/µL)	2	2
10x ligase buffer	1	1
T4 DNA ligase (400 cohesive end U/µL)	0.5	0.5
MQW	6.5	4.5

2.16 Transformation

Frozen aliquots of Turbo cells (New England Biolabs), Rosetta2 (DE3) pLysS and BL21 (DE3) were available in the lab.

Transformation in turbo cells: Aliquots (50 µL each) of Turbo cells were allowed to thaw on ice. ~100 ng of plasmid DNA from the ligation reaction was added to 50 µL of competent cells in a microcentrifuge tube.

Transformation in Rosetta 2 (DE3) pLysS/BL21 (DE3) cells: Aliquots of competent cells were allowed to thaw on ice. 100 ng of purified plasmid DNA (~1 µL) was added directly to 50 µL of competent cells in a microcentrifuge tube.

The microcentifuge tube was left on ice for 10 min, heat shocked for 45 seconds at 42 °C and put back on ice. 300 µL of LB were added to the microcentrifuge tube and the tube was incubated in a water bath at 37 °C for 1.5 h. The transformation reaction was then plated on LB agar containing the appropriate antibiotic (Table 2.10; Table 2.11) and the plate left overnight in the incubator at 37 °C (~16 h). A growth control and a positive control were done every time.

Single colonies were picked for overnight growth in 10 mL LB with the appropriate antibiotic (10 µL) (Table 2.10; Table 2.11) and incubated overnight in the incubator shaker at 37 °C. In the morning, the tube was centrifuged for 10 min and the plasmid was purified from the pellet using QIAprep spin Miniprep Kit (QIAGEN). The concentration was determined using the NanoDrop Spectrophotometer 2000c.

Table 2.10: Table of antibiotics and their concentrations.

Antibiotic	Concentration (µg/mL)
Kanamycin	100
Ampicillin	33
Streptomycin	25
Chloramphenicol	33

Table 2.11: Antibiotic resistance of the competent cells and plasmids.

	Antibiotic resistance
Turbo cells	None
BL21 (DE3) cells	None
Rosetta 2 (DE3) pLysS cells	Chloramphenicol
pET28a plasmid	Kanamycin
pIVM02 plasmid	Ampicillin
pIVM26 plasmid	Streptomycin

2.17 Diagnostic digest

A restriction digest was then performed on a colony for the ligation transformant to check that it contained insert of the correct size using XhoI and another enzyme ApaI (GGGCCC). Samples were prepared following conditions in Table 2.12 and incubated at 37 °C for 1.5 h. An agarose gel was then run to verify that the ligation worked. Cut pET28a was also run on the gel to compare the size.

Table 2.12: Conditions for the diagnostic digest.

	Sample (30 µL)
Cutsmart 10x	3 µL
Construct (~300 ng/µL)	5 µL
XhoI (20 U/µL)	1 µL
ApaI (20 U/µL)	1 µL
MQW	20 µL

2.18 Protein expression

2.18.1 Protein staining

In order to visualise the proteins on SDS gels (Section 2.3), gels were stained with the Coomassie Stain solution. The gels were first fixed for 15 min in Destain solution and then gels were immersed in the Stain solution and left for one hour on the rocker. Gels were subsequently destained in Destain solution. The Destain solution was left overnight or changed until the background of the gel was fully destained. The gels were imaged on a Chemidoc system (BioRad) using Image Lab software 6.0.1.

2.18.2 Wee1 protein expression

Human protein Wee1 (UniProt accession number: P30291). Details of the sequence and properties can be found in Appendix 2.

Wee1 (291-575) was transformed and expressed in Rosetta 2 (DE3) pLysS in 6 × 1 L of LB with Kan (100 µg/mL) and Chl (30 µg/mL) in overnight cultures to an OD of 0.05 and incubated with shaking at 37 °C for 5 h. When the $OD_{600\ nm}$ was ~0.8, temperature was dropped to 20 °C. It was induced with 0.1 mM IPTG and shaken for 16 h at 20 °C. Cells were harvested by centrifugation. Harvested pelleted cells were resuspended in 100 mL of lysis buffer (50 mM Na Phosphate pH 8.0, 300 mM NaCl, 10 mM imidazole, 0.03% Triton x100, 5 mM B-ME with 0.1 mg/mL lysozyme, and 10 µg/mL DNAseI). Cells were then lysed five times at 4 °C (ice bath) by sonication and centrifuged in a JA25.50 rotor at 14,000 rpm for 40 minutes at 4 °C. The clear supernatant was loaded into a 50 mL superloop and purified on an AKTA system using HisTrap FF (GE healthcare) and an imidazole gradient (50 mM Tris pH 8.0, 300 mM NaCl, 0-250 mM imidazole, 0.03% Triton ×100 and 5 mM B-ME). HisTrap FF is a Ni-NTA column to purify His-Tag Wee1. It was then dialysed overnight at 4 °C (50 mM Tris pH 8.5, 50 mM NaCl, 1 mM DTT), and was further purified using anion exchange column Uno Q-1 (BioRad) with a NaCl gradient (20 mM HEPES, pH 7, 0-500 mM NaCl, 1 mM DTT). Finally, the complex was purified using a size-exclusion column Superdex 75 HiLoad 16/600 (GE Heathcare) (20mM Tris, pH 8.5, 150 mM NaCl, 1mM DTT). Pure fractions were combined, concentrated to 9.6 mg/mL, aliquoted in 100 µL aliquots in microcentrifuge tubes, snap frozen and stored at –80 °C until use. The Wee1 band was analysed by 10% SDS PAGE gel (Sections 2.3 and 2.18.1) to verify the purity.

2.18.3 VBC protein expression

Human proteins VHL (UniProt accession number: P40337), Elongin C (Q15369), and Elongin B (Q15370). Details of the sequence and properties can be found in Appendix 3.

The VBC construct was a gift from Alessio Ciulli's lab (University of Dundee). VHL was cloned into pIVM02, and Elongin B and Elongin C were cloned into pIVM26. N-terminally

His$_6$-tagged VHL (54–213), Elongin C (17–112) and Elongin B (1–104) were co-transformed and co-expressed in Escherichia *coli* Rosetta 2 (DE3) pLysS in 6 × 1 L of LB with Amp (100 µg/mL), Strep (50 µg/mL), Chl (30 µg/mL) in overnight cultures to an OD of 0.05 and incubated with shaking at 37 °C for 5 h. When the OD$_{600\ nm}$ was ~0.8, temperature was dropped to 24 °C. It was induced with 0.3 mM IPTG and shaken for 16 h at 24 °C. Cells were harvested by centrifugation. Harvested pelleted cells were resuspended in 80 mL of lysis buffer (50mM HEPES, pH 7, 500mM NaCl, 20mM imidazole, 5mM B-ME with lysozyme, DNAse and IPTG). Cells were then lysed five times at 4 °C by sonication and centrifuged in a JA25.50 rotor at 14,000 rpm for 40 minutes at 4 °C. The clear supernatant was loaded into a 50 mL superloop and purified on an AKTA system using HisTrap FF (GE healthcare) and an imidazole gradient (from 20 to 500 mM). The fractions with the protein complex were incubated overnight with TEV (1:1 w/w) to cleave the His-tag in a dialysis buffer (50 mM HEPES, pH 7, 500 mM NaCl, 20 mM imidazole, 5 mM B-ME). After cleavage, the protein complex was purified again using the AKTA system with a HisTrap FF is a Ni-NTA column. The flow through containing the cleaved complex was recovered, dialysed twice for 1.5 h each time (20 mM HEPES, 1 mM DTT, pH 7), and the complex was further purified using anion exchange column Uno Q-1 (BioRad) with a NaCl gradient (20 mM HEPES, pH 7, 0-500 mM NaCl, 1 mM DTT). Finally, the complex was purified using a size-exclusion column Superdex 75 HiLoad 16/600 (GE Healthcare) (20 mM HEPES, pH 7, 150 mM NaCl, 1mM DTT). Pure fractions were combined, concentrated to 8.50 mg/mL, aliquoted in 100 µL volumes into microcentrifuge tubes, snap frozen and stored at –80 °C until use. The VBC bands were analysed by 15% SDS PAGE gel to verify the purity (Sections 2.3 and 2.18.1).

2.19 Native PAGE

10% (for blue native PAGE) or 7.5% (for standard native PAGE) gels were prepared following Section 2.3 (Table 2.1). The samples were prepared by pipetting the correct volumes of the two proteins (n = 0.29 nM for one equivalent) and the PROTAC into 0.5 mL microcentrifuge tubes. The solutions were mixed by pipetting up and down carefully to mix without making bubbles and incubated 1 h at 4 °C. 1/6 volume of the 6× loading sucrose solution was added to each sample in the microcentrifuge tubes and mixed

carefully. The gel box was set and the gel was loaded with the samples and run in 1× native PAGE running buffer: blue or clear. Clear native PAGE was run for ~1 h at 150 V at r.t. and ~1.5 h in the cold room for blue native PAGE. Gels were then stained for 1 h in Coomassie stain and destained overnight in the destain solution.

2.20 Isothermal titration calorimetry (ITC)

Proteins (Wee1 and VBC) were dialysed overnight (50 mM Hepes, 150 mM NaCl, pH 7.5). Titrations were performed on an ITC200 MICROCAL PEAQ-ITC (Malvern). The titrations were performed with the protein in the syringe and ligand in the cell, or the binary complex (Protein+ligand) in the cell and the other protein in the syringe. It consisted of 18 injections of 2 µL protein solution (50 HEPES, 150 mM NaCl, 1 mM TCEP, 0.2% v/v DMSO, pH 7.5) at a rate of 0.5 µL/s at 150 s time intervals. An initial injection of protein (0.4 µl) was made and discarded during data analysis. All experiments were performed at 25 °C, whilst stirring at 750 rpm. PROTACs were diluted from a 10 mM DMSO stock solution to 20 µM in buffer containing 50 mM HEPES, 150 mM NaCl, 1 mM TCEP, pH 7.5. The final DMSO concentration was 0.6%, except for experiments with PROTAC MA199, for which 2% was used. Protein VBC (200 µM, in the syringe) was titrated into the PROTAC or PROTAC-Wee1 binary complex (20 µM, in the cell). The data were fitted to a single-binding-site model to obtain the stoichiometry n, the dissociation constant K_d and the enthalpy of binding ΔH using the MicroCal PEAQ-ITC Malvern software provided by the manufacturer. The reported values are the mean ± s.e.m. from independent measurements (n = 2).

2.21 Crystallography

Wee1 protein was cleaved using thrombin (Novagen, Thrombin, restriction Grade, 69671) for 2 h incubation and purified using Ni-NTA column. VBC, Wee1 and the PROTAC were mixed as a 1:1:1 stoichiometric ratio and the ternary complex was purified by size-exclusion chromatography (20 mM Tris, 150 mM NaCl, 0.5 mM TCEP, pH 8) and diluted to obtain a final concentration of 5 mg/ml. Drops of the ternary complex were mixed in a 1:1 ratio (1.5 µL + 1.5 µL) with solutions from multiple kits (Molecular Dimensions:

Structure screens 1 and 2; PACT PREMIER MD1-29; ProPlex) in the hanging-drop vapor diffusion format in 24-well plates and incubated at room temperature. Four trays were set manually for each screen composed of 96 conditions to obtain a total of 768 different conditions. Drops were monitored with a microscope (LEICA M80, Leica) with a polarising filter to look for crystals.

For crystal analysis, a crystal was flash frozen and mounted on the 4-circle Kappa precision goniometer data were acquired using a Rigaku Oxford Diffraction SuperNova diffractometer, an Atlas S2 135 mm CCD Area Detector, and a copper microfocus X-ray source. Default screening settings were used for collecting the test images.

2.22 Chemistry

2.22.1 Reagents, solvents and analysis

Reagents and solvents were obtained at reagent/ACS grade from Fluorochem, Sigma Aldrich, Acros Organics, Fisher Scientific, Alfa Aesar and VWR Chemicals. For reactions conducted under an inert atmosphere, glassware was oven dried overnight and cooled under argon. The photoreactions were performed at wavelengths 254 and 300 nm, at a standard temperature (fan cooling) in a Rayonet RPR-100 Photoreactor irradiating. Reactions were monitored by TLC and ^{1}H NMR spectroscopy. TLC was conducted using Merck Millipore aluminium TLC silica gel 60 F254 plates, and analysed under UV light (254 nm) as well as staining with potassium permanganate, MOLY, bromocresol green or *p*-anisaldehyde. Purifications via flash column chromatography were conducted on silica gel from Fisher Scientific or VWR (60 Å particle size, 40-63 microns). NMR data was obtained using a Bruker AVANCE III 400 instrument. ^{1}H NMR data were obtained at 400 MHz and ^{13}C NMR data were obtained at 101 MHz at 298 K. Chemical shifts (δ) were referenced to residual solvent signals (CDCl$_3$: 7.26 and 77.16 ppm for ^{1}H NMR and ^{13}C NMR, respectively. d_6-DMSO: 2.50 and 39.52 ppm for ^{1}H NMR and ^{13}C NMR, respectively. MeOD: 3.34 and 49.86 for ^{1}H NMR and ^{13}C NMR, respectively. d_3-Acetonitrile: 1.96 and 118.26 + 1.79 ppm for ^{1}H NMR and ^{13}C NMR, respectively). The assignment of the ^{1}H and ^{13}C NMR signals was supported by 2D-NMR (COSY, HSQC, HMBC), DOSY and DEPT-135

data using TopSpin (3.6.1) or MestReNova softwares. In the cubane Chapter 6, the atom numbering in compounds is given for ease for assigning NMR data, but does not necessarily correspond to IUPAC nomenclature. Infrared spectra were recorded using an Agilent Technologies Cary 630 FTIR spectrometer. Mass spectrometry (MS) data were recorded using electron spray ionisation (ESI) or chemical ionization (APCI) on a Shimadzu LCMS-IT-TOF mass spectrometer. Purity assessment of the compound was done using a Shimadzu NexeraX2 UHPLC instrument. Separation was performing using a Shimadzu Shimpack XR-ODS III column (1.6 µm, 2.0×50 mm) with gradient elution using ultrapure water (0.1% formic acid, v/v, Mobile A) and acetonitrile (0.1% formic acid, v/v, Mobile B). Chromatograms were analysed, and results obtained using 254 nm wavelength using the LabSolutions software.

2.22.2 General procedures

2.22.2.1 General procedure A for HATU-mediated amide coupling

The deprotected amine TFA salt (0.20 mmol, 1.0 eq.) was dissolved in N,N-dimethylformamide (DMF) (2 mL). The carboxylic acid (0.20 mmol, 1.0 eq.) was then added to the solution, followed by hexafluorophosphate azabenzotriazole tetramethyl uronium (HATU) (0.22 mmol, 1.1 eq.) and N,N-diisopropylethylamine (DIPEA) (0.80 mmol, 4.0 eq,). The reaction mixture was then stirred at room temperature for 18 h before water (5 mL) was added. The mixture was then extracted with dichloromethane (DCM) (3 × 10 mL, dried over anhydrous sodium sulfate (Na_2SO_4) and concentrated under reduced pressure to afford the crude product, which was purified by flash column chromatography (eluent specified for each procedure).

2.22.2.2 General procedure B for nucleophilic aromatic substitution

2-(2,6-Dioxopiperidin-3-yl)-4-fluoroisoindoline-1,3-dione **24** (0.20 mmol, 1.0 eq.) was dissolved in N,N-dimethylacetamide (1 mL). DIPEA (0.40 mmol, 2.0 eq.) was added, followed by the amine (0.22 mmol, 1.1 eq.) (Nowak *et al.*, 2018). The reaction mixture was then heated to 90 °C for 18 hours and monitored using TLC analysis. After completion, the reaction was cooled to room temperature and partitioned between ethyl

acetate (10 mL) and water (10 mL). The organic layer was washed with brine (3 × 10 mL), dried over Na_2SO_4 and concentrated under reduced pressure to afford the crude product, which was purified by flash column chromatography (eluent specified for each procedure).

2.22.2.3   General procedure C nucleophilic substitution

The amine (0.20 mmol, 1.0 eq.) was dissolved in DMF (1 mL). Bromo-compound (0.22 mmol, 1.1 eq.) was added, followed by potassium carbonate (K_2CO_3) (0.40 mmol, 2.0 eq.). The reaction was heated to 60 °C for 6 h. After completion of the reaction, water (5 mL) was added and the reaction was extracted with EtOAc (3 x 10 mL), washed with brine (5 mL), dried over Na_2SO_4 and concentrated under reduced pressure to afford the crude product, which was purified by flash column chromatography (eluent specified for each procedure).

2.22.2.4   General procedure D for Boc deprotection

The Boc-protected compound (0.20 mmol, 1.0 eq.) was dissolved in DCM (1 mL), and trifluoroacetic acid (TFA) (1 mL) was added slowly in a 1:1 (v/v) ratio. The reaction mixture was then stirred at room temperature for 1 h before being evaporated to dryness. The product was used in the next step without further purification.

2.22.2.5   General procedure E for the Curtius reaction

The starting material featuring a carboxylic acid (0.30 mmol, 1.0 eq.) was added to an oven-dried vial under argon followed by dry *tert*-butanol (2 mL), dry Et_3N (0.30 mmol, 1.0 eq.) and diphenylphosphoryl azide (0.30 mmol, 1.0 eq.) (Nicolaou *et al.*, 2016). The vial was sealed and heated to reflux overnight. After full consumption of the starting material (followed by TLC analysis), the reaction was allowed to cool to room temperature and concentrated. The residue was dissolved in EtOAc (10 mL), washed with brine (3 × 5 mL), dried over Na_2SO_4 and concentrated under reduced pressure to give the crude product, which was purified by flash column chromatography (eluent specified for each procedure).

2.22.2.6 General procedure F for the Diels-Alder of 161 with different dienophiles

The starting material **161** (0.20 mmol, 1.00 eq.) was dissolved in dry toluene (3 mL) under argon and the dienophile (0.24 mmol, 1.20 eq.) was added (Grange *et al.*, 2010). The mixture was stirred at the indicated temperature for the indicated time. ^{1}H NMR spectroscopy and TLC were used to follow the conversion of the starting material into the product. The reaction mixture was concentrated and purified by flash column chromatography (eluent specified for each procedure).

2.22.2.7 General procedure G for [2+2] photoreaction between two alkenes

The starting material was dissolved in dry acetone under argon (C = 10 mM) in a dry phototube. The solution was degassed for 15 min with argon, then irradiated at 300 nm. Full conversion was observed by ^{1}H NMR with solvent suppression. The reaction was concentrated and the crude product was purified by column chromatography (eluent specified for each procedure).

2.22.2.8 X-ray diffraction analysis

Single crystals were obtained following details in for each compound. A suitable crystal was selected and mounted on a Mitegen loop using Paratone-N oil on a SuperNova, Dual, Cu at zero, AtlasS2 diffractometer. The crystal was kept at the indicated temperature in Table 2.13 during data collection. Using Olex2 [1], the structure was solved with the SHELXT [2] structure solution program using Intrinsic Phasing and refined with the SHELXL [3] refinement package using Least Squares minimisation. Figures were prepared using Mercury 4.1.0.

Table 2.13: Table of temperatures to keep the crystal during data collection.

Compound	Temperature for data collection (K)
120	100.00(10)
121	99.99(10)
123	220.00(10)
167	120.00(10)

1. Dolomanov, O.V., Bourhis, L.J., Gildea, R.J, Howard, J.A.K. & Puschmann, H. (2009), J. Appl. Cryst. 42, 339-341.
2. Sheldrick, G.M. (2015). Acta Cryst. A71, 3-8.
3. Sheldrick, G.M. (2015). Acta Cryst. C71, 3-8.

3 Design and synthesis of Wee1 PROTACs

3.1 Introduction

3.1.1 Wee1 kinase: role in cell cycle

Cells are dependent on cell-cycle checkpoints to repair DNA and maintain genome integrity (Chen *et al.*, 2012). In cancer cells, p53 is often mutated, leading to a deficient G_1/S checkpoint (Do *et al.*, 2013) which means these cells are reliant on the G_2/M checkpoint to repair their DNA prior to cell division in order to produce viable daughter cells (Do *et al.*, 2013). Wee1 is a serine/threonine kinase-family member that plays an important role in regulating the G_2/M checkpoint (Figure 3.1).
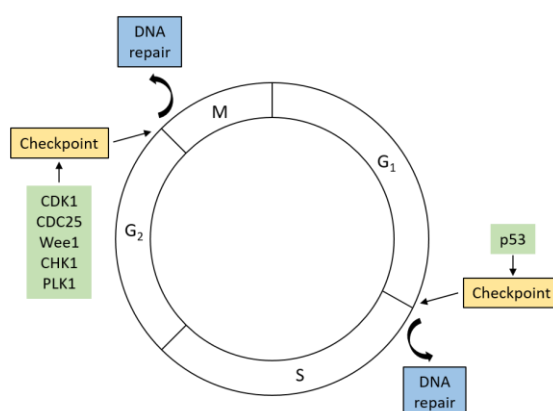
Figure 3.1: Cell cycle regulated by cyclin dependent kinases through two main cell cycle checkpoints: G_1/S and G_2/M.

When DNA is damaged, an ATR and CHK1-driven signalling cascade results in Wee1 phosphorylating CDK1 (CDC2) at Tyr15 to inactivate the CDK-Cyclin B complex and thus arrest entry into mitosis, which allows time for DNA repair (Figure 3.2) (Matheson, Backos, *et al.*, 2016). When DNA is repaired, PLK1 (a Polo-like kinase, part of the serine/threonine protein kinases subfamily (Zhu *et al.*, 2016)) phosphorylates Wee1 to inhibit and degrade it via the proteasome. PLK1 also activates the protein phosphatase CDC25C by phosphorylation which then dephosphorylates and activates CDK1, enabling it to bind to cyclin B and leading to entry into mitosis.
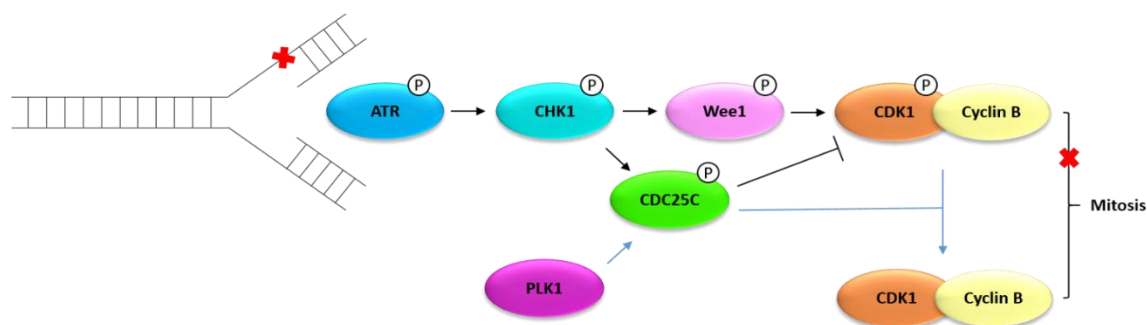
Figure 3.2: Activation of Wee1 at the G_2/M checkpoint inactivates the CDK1/Cyclin B complex to allow time for DNA repair before entry into mitosis.

Wee1 is overexpressed in many cancers, and has been correlated with poor disease-free survival for cancer patients (Matheson, Backos, *et al.*, 2016). Thus, inhibition of Wee1 is likely to be an effective strategy for therapeutic intervention as it results in abrogation of the G_2/M DNA repair checkpoint and could lead to mitotic lethality in cancer cells (Szmyd *et al.*, 2019).

3.1.2 Wee1 and inhibitors

Due to its involvement in the G_2/M checkpoint and overexpression in many cancers, Wee1 is an interesting target for therapies (See Section 1.4). Due to their conserved ATP-binding sites, kinases are hard to target selectively and few Wee1 inhibitors have been developed.

The first small molecule inhibitor for Wee1 was a pyridopyrimidine (PD0166285) (Wang *et al.*, 2001) and was shown to abrogate the G_2/M checkpoint leading to a premature mitosis for cancers deficient in p53 (Figure 3.3). Even though being potent towards Wee1 (IC_{50} = 24 nM), PD0166285 was not very selective and targeted other proteins including CHK1 (IC_{50} = 3.4 µM), MYT1 (IC_{50} = 72 nM), c-Src as well as some growth factor receptors. A less potent but more selective Wee1 inhibitor (IC_{50} = 97 nM) was identified later through high-throughput screening: a pyrrolocarbazole (PD0407824) (Palmer *et al.*, 2006), and had less activity against c-Src (IC_{50} > 50 µM) compared to PD0166285 (Figure 3.3). However, this did not progress into *in vivo* studies. Further screening lead to

AZD1775 (Hirai *et al.*, 2009), a potent Wee1 inhibitor (IC$_{50}$ = 5.2 nM) currently undergoing clinical trials (Figure 3.3).
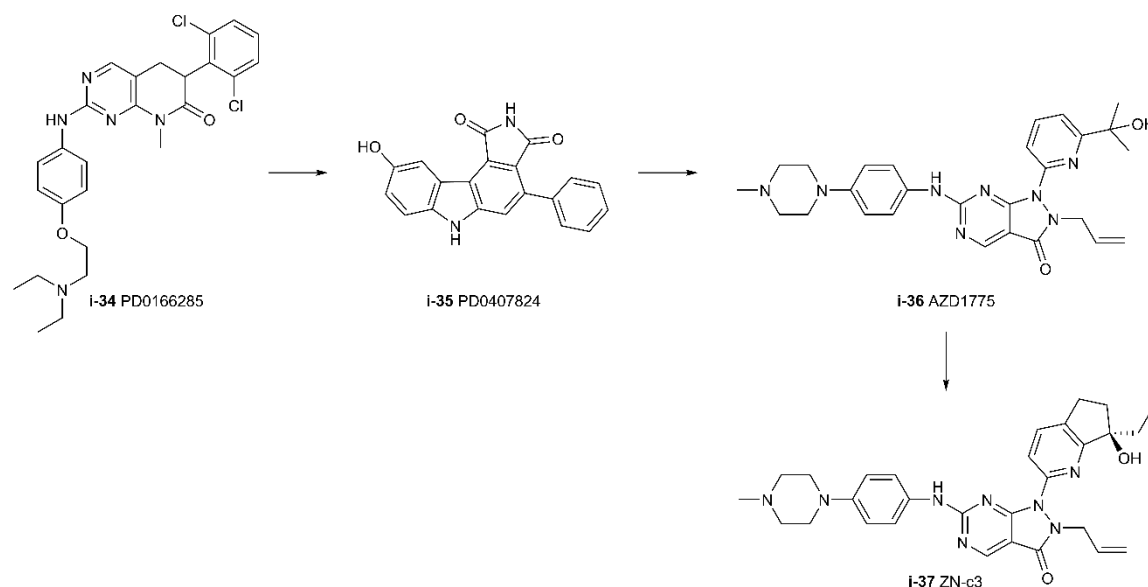
Figure 3.3: Evolution of Wee1 inhibitor: from PD0166285 to PD0166285 to AZD1775 to ZN-c3.

More recently, toward the end of the project, a more potent inhibitor ZN-c3 (Wee1 IC$_{50}$ = 3.9 nM) was published and is undergoing Phase II of clinical trial (Huang *et al.*, 2021). ZN-c3 was developed from AZD1775 that presents tolerability issues in clinical trial likely due to its selectivity problems. Huang *et al.* found that the ethyl group on the right side of the molecule helped with potency, polarity, and intrinsic clearances as well as the tertiary alcohol helping with interactions. ZN-c3 showed improved potency and selectivity over AZD1775 IC$_{50}$(PLK1) = 227 nM, IC$_{50}$(PLK2) = 40 nM, IC$_{50}$(PLK3) = 70 nM, IC$_{50}$(YSK4) = 59 nM) (Huang *et al.*, 2021).

3.1.2.1 AZD1775 inhibitor

AZD1775/MK1775/adavosertib is the first selective inhibitor towards Wee1. AZD1775 acts as an ATP competitor and inhibits the phosphorylation of CDK1 at Tyr15 by Wee1 (Hirai *et al.*, 2009), leading to the abrogation of the G$_2$/M checkpoint. AZD1775 is the most selective inhibitor to date towards Wee1, leading to apoptosis when used in combination with DNA-damaging agents to treat p53-inactive cells. AZD1775 is currently undergoing Phase I (Do *et al.*, 2015; Mendez *et al.*, 2018; Cole *et al.*, 2020; Kato *et al.*,

2020; Kong *et al.*, 2020) and Phase II (Moore *et al.*, 2015; Leijen *et al.*, 2016; Gray *et al.*, 2017) clinical trials in combination with a number of other treatments, including chemotherapies and radiotherapies. AZD1775 has also been used for Wee1 inhibition as a single agent in numerous disease contexts such as ovarian cancer (Zhang *et al.*, 2017), sarcoma (Kreahling *et al.*, 2012), and laryngeal squamous cell carcinoma (Yuan *et al.*, 2018).

3.1.2.2 AZD1775 selectivity issues

Additional AZD1775 targets have recently been identified, including some inhibited with similar potency to Wee1, such as PLK1 (Wright *et al.*, 2017). PLK1 inhibition has an important role in regulating Wee1's activity (3.1.1), and as such, the efficacy of AZD1775 cannot solely be considered as a result of selectivity against Wee1. Thus, all studies using AZD1775 as a probe for Wee1 have to be considered carefully. Moreover, kinome profiling has revealed a number of other kinases targeted by AZD1775, including Wee2, PLK2, PLK3, JAK2, JAK3 (Table 3.1) (Zhu *et al.*, 2017). All of these proteins have important regulatory roles in key cellular processes, so it is important to improve selectivity. For instance, PLK2 is another key regulator of the cell cycle, DNA damage response pathway and neurological activity (Kim *et al.*, 2015; Shan *et al.*, 2015). The Janus Kinase (JAK) such as JAK2 and JAK3, nonreceptor tyrosine kinases, have an important role in the immune system (Ghoreschi *et al.*, 2011; Forster *et al.*, 2016). As AZD1775 is being clinically developed to work in combination with other treatments to increase their effectiveness, inhibiting so many targets beyond Wee1 may not yield the desired outcome, or worse multiply the number of potential side effects of the treatment.

Table 3.1: Kinome profiling results of AZD1775 (500 nM single concentration) determined by Discoverx Corp.

Gene Symbol	Activity remaining (% of control)
YSK4	0
WEE2	0.25
WEE1	0.3
PLK1	0.35
JAK3	0.45
PLK2	0.6
PLK3	1.3
GAK	2
JAK2	6.1
ABL1	10

3.1.3 Design of Wee1 PROTACs

AZD1775 is the perfect candidate to use to generate PROTAC molecules targeting Wee1. In particular, the opportunity to increase selectivity for Wee1 through the recruitment of ternary complexes makes this target promising. Previous studies have shown how selective degraders can be made starting from a less selective inhibitor as the target-binding ligand (Zengerle *et al.*, 2015; Bondeson *et al.*, 2018). The synthesis of AZD1775, first elucidated in a patent, has been reproduced by a few different groups (Matheson, Venkataraman, *et al.*, 2016; Wright *et al.*, 2017). In particular, Wright and colleagues generated an analogue for covalent linkages that retains Wee1-binding activity (Matheson, Venkataraman, *et al.*, 2016; Wright *et al.*, 2017).

The co-crystal structure of AZD1775 in Wee1 shows that the methyl group of the piperazine is solvent exposed and can be used as the attachment point for linkers and E3 to generate Wee1-targeting PROTACs (Zhu *et al.*, 2017) (Figure 3.4). VHL and CRBN, both part of the cullin-RING ligase (CRL) family, have been exploited successfully in the design of protein degraders showing potent and sustained target degradation (Bondeson *et al.*, 2015; Lu *et al.*, 2015; Winter *et al.*, 2015; Zengerle *et al.*, 2015). They are to date the most common E3 ligases used in PROTACs design and are thus the two best candidates to start with and link to Wee1 inhibitor AZD1775 using different types and lengths of linkers to create an SAR.
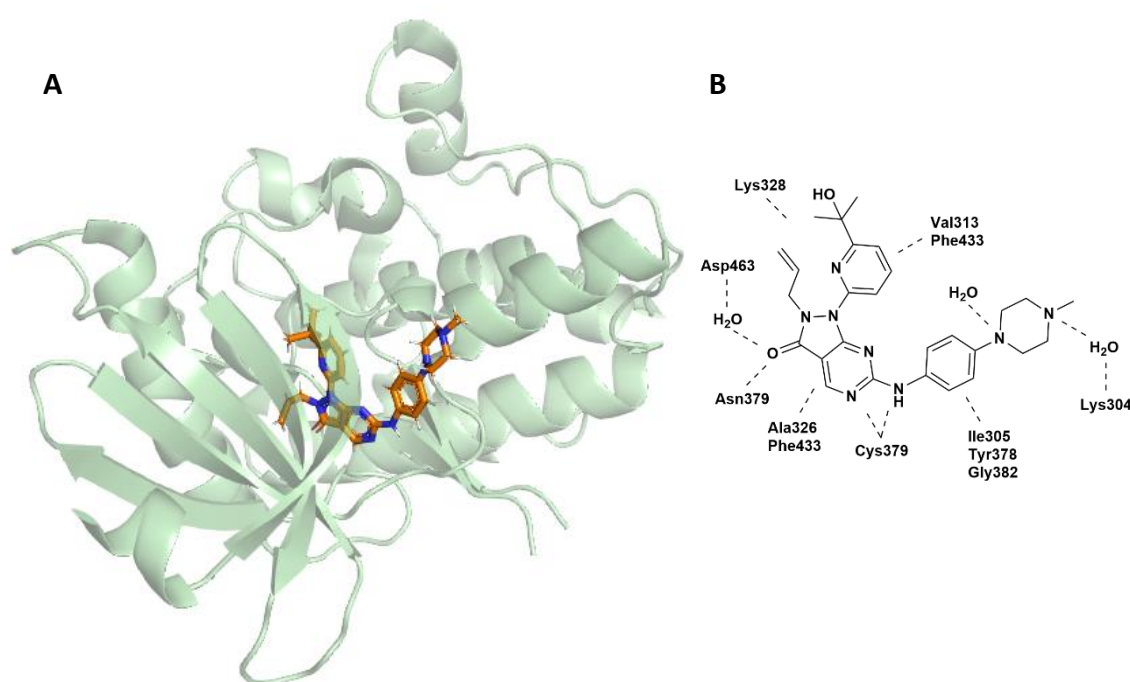
Figure 3.4: Co-crystal structure of AZD1775 in Wee1 protein (PDB 5V5Y). **A**) Structure of AZD1775 in the ATP-binding pocket of Wee1. **B**) Interactions of AZD1775 with Wee1 ATP-site.

In their study to discover ZN-c3, Huang *et al.* compared the main kinases inhibited by the pyrazolopyrimidinone scaffold such as Wee1, PLK, YSK4 by superimposing them to find a possible explanation for selectivity improvement (Huang *et al.*, 2021). Their analysis revealed that Wee1 ATP binding pocket had more space at the entrance of the pocket in the solvent-exposed region, and in the G-loop. Therefore, they used this information and

built their chemistry around making new ligand-protein interactions with Tyr378 in the hinge binding region and Phe310 in the G-loop.

Thus, two series of Wee1 PROTACs recruiting either CRBN or VHL E3 ligases were synthesised using different type of linkers, such as alkyl or polyethylene glycol, and different lengths: short, intermediate and long (Figure 3.5). These PROTACs were then assessed in cancer cells to study the influence of the linker and E3 ligase on Wee1 degradation and modulation.
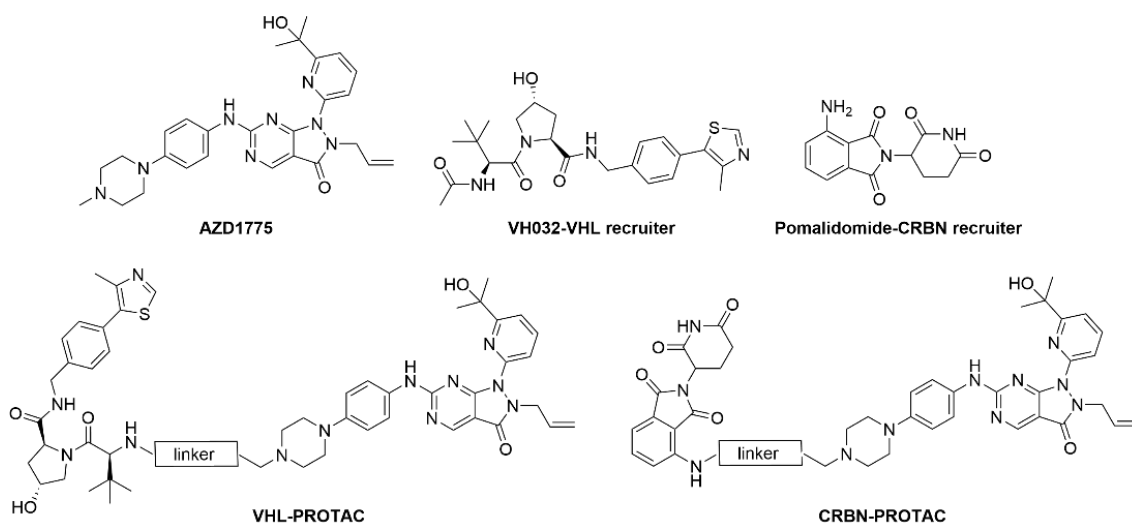
Figure 3.5: AZD1775 Wee1 inhibitor, and the two E3 ligase ligands, VH032 (VHL) and pomalidomide (CRBN). The two PROTAC series: VHL-PROTAC and CRBN-PROTAC, using AZD1775 inhibitor linked to either E3 ligase ligand (VHL or CRBN).

3.2   Aims and objectives

The aim of this chapter is to synthesise PROTAC molecules from AZD1775 inhibitor by linking it to two E3 ligase ligands recruiting VHL and CRBN with different types of linkers (nature and length) to create an SAR around the linker and E3 ligase. These molecules will allow the study of Wee1 degradation in terms of its activity and selectivity in cancer cells.

3.3 Results and discussion

3.3.1 Synthesis of AZD1775 analogue

AZD1775 analogue was synthesised following the synthetic approach in the literature (Scheme 3.1; Scheme 3.3) (Matheson, Venkataraman, *et al.*, 2016; Wright *et al.*, 2017). For intermediate **10** of AZD1775 analogue, being expensive and to enable access to it on a multi-gram scale, its synthesis following the literature was attempted. *Tert*-butylcarbazide **1** was protected following the reaction with phthalic anhydride **2** to give carbamate nitrogen **3** in 87% yield, which was then functionalized with allyl bromide to afford **4** in 95% yield. Methyl hydrazine was then used to remove the phthalamide protecting group to give *tert*-butyl allylcarbazide **5** in 85% yield.
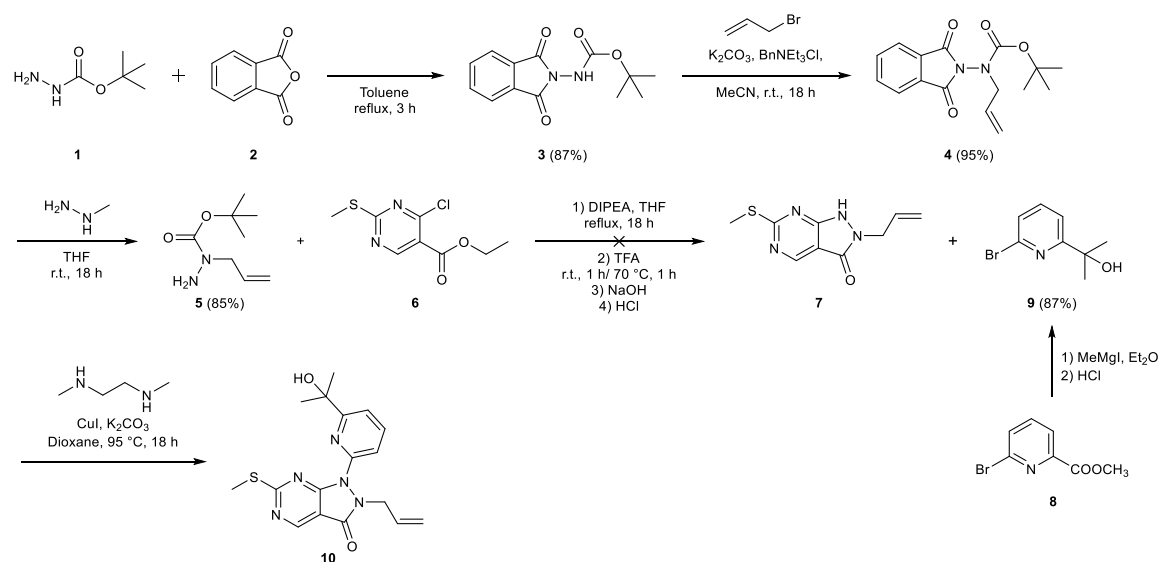
Scheme 3.1: Attempt to prepare intermediate **10** for AZD1775 analogue synthesis.

However, obtaining **7** was more challenging. The conditions from the literature did not give the expected compound. As a matter of fact, the NMR did not show the cyclised product **7**. To interrogate the problems with this part of the synthesis, step 1) was repeated on a small scale to see if the coupling between **5** and **6** was working correctly and NMR analysis showed that this was the case (Scheme 3.2). The product from this coupling **7a** was then used to repeat step 2), which is a Boc deprotection using trifluoroacetic acid. NMR revealed that the Boc protecting group was removed as

anticipated and gave **7b**. The Boc deprotected compound was then reacted with sodium hydroxide as a base in step 3) to hydrolyse the ester into a carboxylic acid **7c**. However, the extraction with a mixture of chloroform and isopropanol after neutralisation did not seem to extract anything as nothing was recovered in the organic layer. If the hydrolysis had been successful then, the compound was still in the aqueous layer. So an NMR of the concentrated aqueous layer was recorded in D_2O in order to see if it was the case, the peaks for $-CH_2-CH_3$ seemed to disappear, but it is a possibility that they are just hidden under the solvent peak.
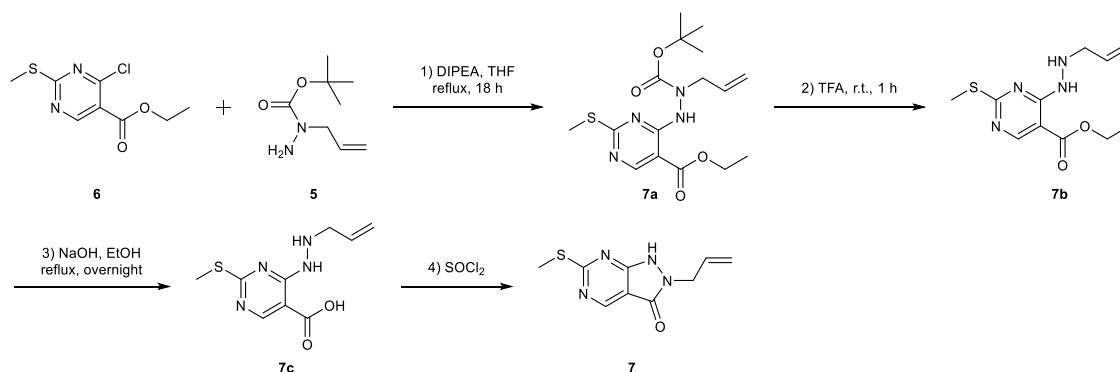
Scheme 3.2: Troubleshooting of the synthesis to give compound **7**.

The product was impossible to extract from the aqueous layer so it was concentrated in order to remove the water, but the assumed compound is mixed with all the sodium hydroxide salt. Being a test reaction on a small scale, it was decided to try to add thionyl chloride ($SOCl_2$) directly to the salt/assumed compound instead of hydrochloric acid (HCl) which did not work in the first attempt. The acyl chloride should react with the amine to create a cyclic amide bond for **7**. An NMR in D_2O did not indicate a difference between the assumed compound and the cyclised compound as it is not possible to see the proton of N-H in this solvent. An infrared analysis was performed, and it seemed that it could have worked as the C=O stretch was observable around 1636 cm^{-1} which is lower than for the carboxylic acid. Unfortunately, it is still not clear if the product has formed as it was not possible to extract it nor to use it to pursue the reaction further. In order to move on from this reaction after multiple attempt to optimise the synthesis, intermediate **10** was purchased from Fluorochem.

Separately, **11** was first attached to linker *tert*-butyl 4-bromobutanoate by nucleophilic substitution and further reduced with hydrogen and palladium on carbon to afford aniline **12** in excellent yield (93%) after two steps (Scheme 3.3) (Matheson, Venkataraman, *et al.*, 2016; Wright *et al.*, 2017). It was then attached to commercially available **10** following sulfur oxidation and then nucleophilic aromatic substitution to afford AZD1775 analogue ester in good yield (74%), which was deprotected using formic acid to obtain carboxylic acid AZD1775 analogue **13** in quantitative yield. This facilitates the attachment by amide coupling to any linker and E3 ligase building blocks with an available amine.
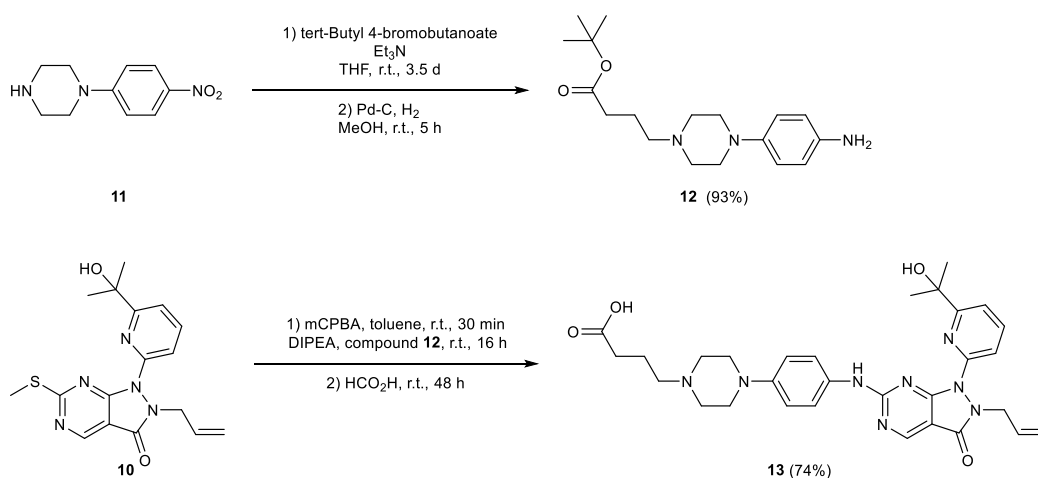
Scheme 3.3: Synthesis of AZD1775 analogue **13**.

3.3.2 Design and synthesis of Wee1 PROTACs for the VHL-series

3.3.2.1 Synthesis of the VHL ligand

The VHL recruiting ligand building block **18** was then prepared following the literature (Scheme 3.4) (Galdeano *et al.*, 2014). **14** and **15** were coupled together using Pd(OAc)$_2$ in DMAc and the nitrile was reduced with sodium borohydride into an amine to afford **16**. Amine **16** was then attached to Boc-hydroxyproline by HATU-mediated amide coupling to give **17**, which was Boc deprotected and linked to Boc-L-*tert*-leucine by HATU-mediated amide coupling to obtain the VHL building block, **18**. **18** was then deprotected to obtain an amine and allow attachment to different linkers (with varying length and nature) with a carboxylic acid group, as well as the AZD1775 analogue **13**.
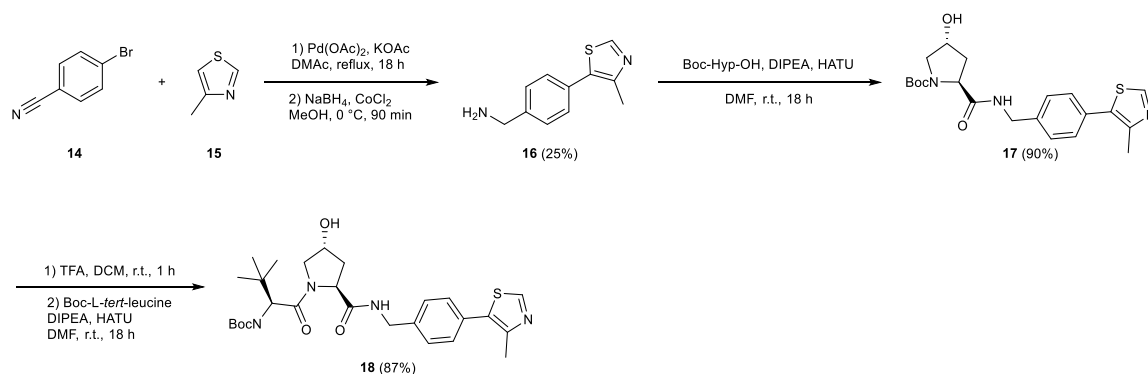
Scheme 3.4: Synthesis of the VHL ligand **18**.

3.3.2.2 Synthesis of Wee1 PROTACs recruiting VHL E3 ligase

To introduce different linkers, VH032 **18** was deprotected and attached to four alkyl linkers with three L_a, five L_b, seven L_c and ten L_d carbons by HATU-mediated amide coupling to give **20a**, **20b**, **20c** and **20d** in 53-84% yield, respectively. It was also attached to two polyethylene glycol linkers: PEG3 L_e and PEG4 L_f, to give molecules **20e** and **20f** in 26 and 43% yield, respectively. These compounds were then used to synthesise the final PROTACs. VH032 building block **18** was used directly for coupling to AZD1775 analogue **13** to give **19 (MA055)** in 61% yield (Scheme 3.5).
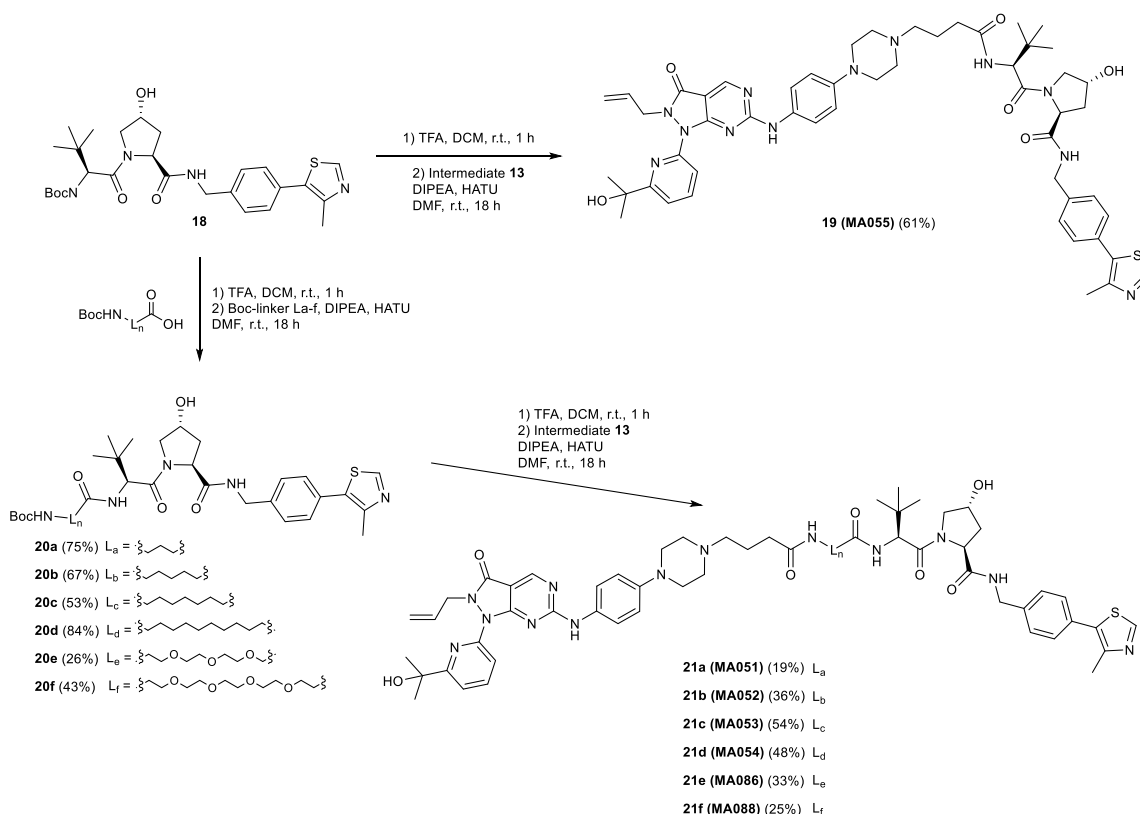
Scheme 3.5: VHL-based Wee1 degrader synthetic approaches.

The VH032 and linker molecules **20a-20f** were Boc deprotected and then linked to AZD1775 analogue **13** by HATU-mediated amide coupling to give PROTACs **21a (MA051)**, **21b (MA052)**, **21c (MA053)**, **21d (MA054)**, **21e (MA086)** and **21f (MA088)** in 19-54% yield, respectively (Scheme 3.5). These seven PROTACs comprise the VHL library. **MA055** possesses the shortest linker and **MA088** the longest to study the influence of the linker's length. Alkyl linkers **L$_{a-d}$** and PEG linkers **L$_{e-f}$** are compared to investigate the importance of the linker's nature.

3.3.3 Design and synthesis of Wee1 PROTACs for the CRBN-series

3.3.3.1 Synthesis of the CRBN ligand

First, the CRBN recruiter pomalidomide was prepared by coupling **22** to **23** to give **24** in 75% yield following the procedure in the literature (Scheme 3.6) (Au - Lindner *et al.*, 2019). Pomalidomide **24** was then attached to different type of linkers by nucleophilic aromatic substitution: two alkyl linkers of two **L$_g$** and six **L$_h$** carbons to give molecules **25a**

and **25b** in 41 and 53% yield, respectively. It was attached in the same way to five PEG linkers (PEG1 **Lᵢ**, PEG2 **Lⱼ**, PEG3 **Lₖ**, PEG4 **Lₗ** and PEG5 **Lₘ**) to give compounds **25c**, **25d**, **25e**, **25f** and **25g** respectively, in 19-47% yield, respectively (Scheme 3.7).
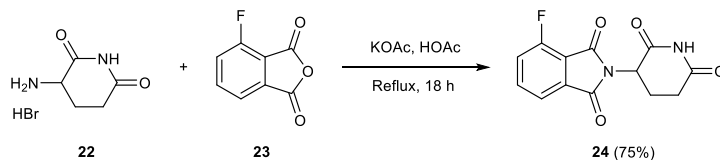
Scheme 3.6: CRBN recruiter **24** synthesis.

The pomalidomide with the two-carbon linker **25a** was Boc deprotected and coupled by HATU-mediated amide coupling to linkers **Lₐ**, **L_b**, **L_c**, **L_d**, **L_e** and **L_f** with three, five, seven and ten carbons, PEG3 and PEG4, respectively to obtain six molecules with longer linkers: **27a-f** in 29-70% yield, respectively (Scheme 3.8).

3.3.3.2 Synthesis of Wee1 PROTACs recruiting CRBN E3 ligase

All the pomalidomide-linker building blocks **25a-g** and **27a-f** were finally Boc deprotected to obtain an amine and enable attachment to the carboxylic acid of AZD1775 analogue **13** by HATU-mediated amide coupling (Scheme 3.7; Scheme 3.8) to afford PROTACs **26a (MA049)**, **26b (MA048)**, **26c (MA072)**, **26d (MA071)**, **26e (MA073)**, **26f (MA074)**, **26g (MA076)**, **28a (TH013)**, **28b (TH011)**, **28c (TH014)**, **28d (TH012)**, **28e (MA093)**, **28f (MA081)** in 6-47% yield respectively. The CRBN library is composed of thirteen PROTACs to have a variety of linkers. The final step (last amide coupling) of the PROTACs using the initials "TH" were synthesised with the assistance of Tom Harrison.
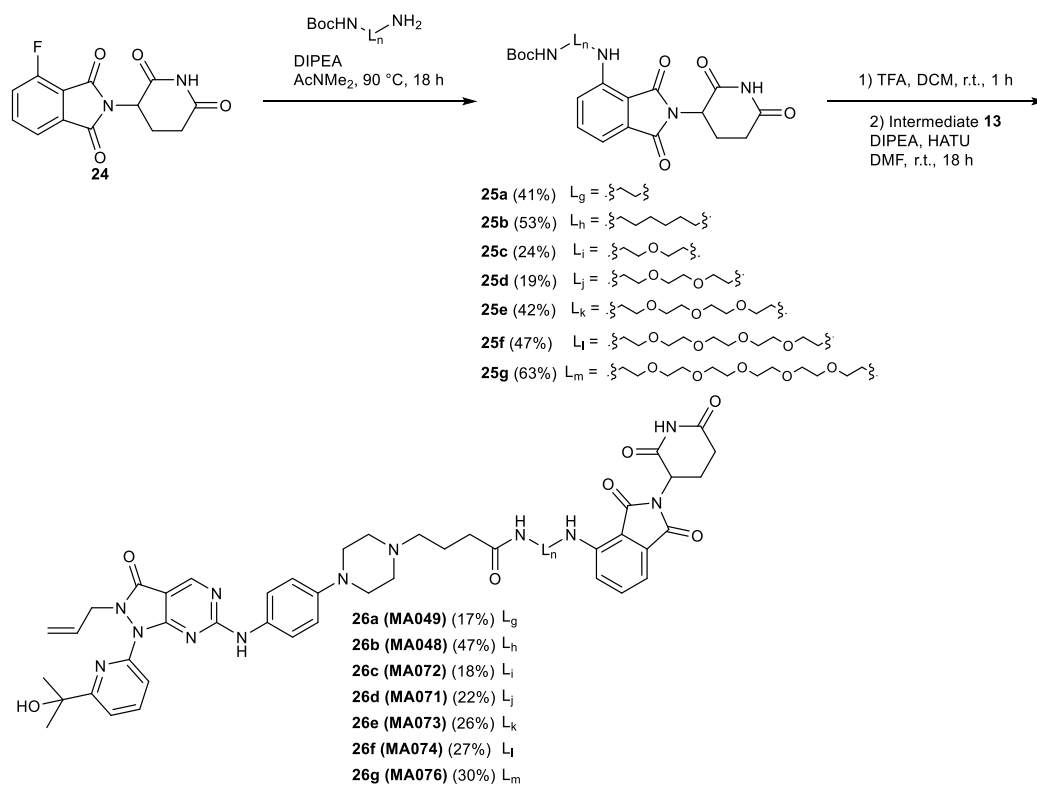
Scheme 3.7: CRBN-based Wee1 degraders synthetic approaches.
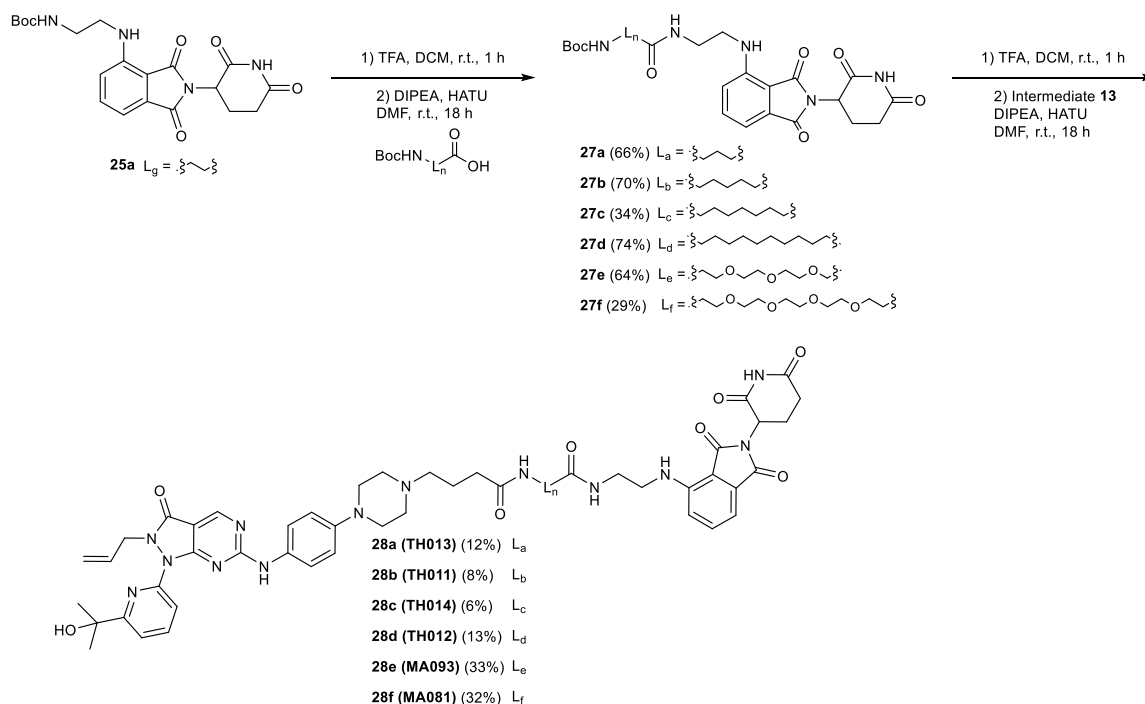
Scheme 3.8: CRBN-based Wee1 degraders synthesis using **25a** and adding another linker (**L$_{a-f}$**).

3.3.4 Synthesis of negative control PROTACs

3.3.4.1 Negative control PROTACs for the VHL-series

In order to verify the target engagement of the best PROTACs of the CRBN- and VHL-series, two negative control PROTACs were synthesised for each series. Details of the PROTAC assessment and selection are in Chapter 4. For the VHL-series, the negative control is reached by changing the configuration of the hydroxyl group of VH032. In the active PROTAC, the hydroxyl group is *trans* whereas in the negative control it is *cis*. Changing the configuration prevents its binding to the VHL protein. Thus, the PROTAC cannot recruit the E3 ligase and cannot induce degradation. **30** was synthesized in the same way as **18** but using Boc-*cis*-Hyp-OH (Frost *et al.*, 2016) in 63% yield. **30** was deprotected and attached directly to AZD1775 analogue **13** by HATU-mediated amide coupling to give **31 (negMA055)** in 22% yield. Alternatively, it was attached to the ten-carbon alkyl linker **L$_d$** to give **32** first, and then deprotected to be coupled to AZD1775 analogue **13** and give **33** (**negMA054)** in 14% yield (Scheme 3.9). The two VHL negative control PROTACs **negMA055** and **negMA054** are the negative epimers of PROTACs **MA055** and **MA054**, respectively.
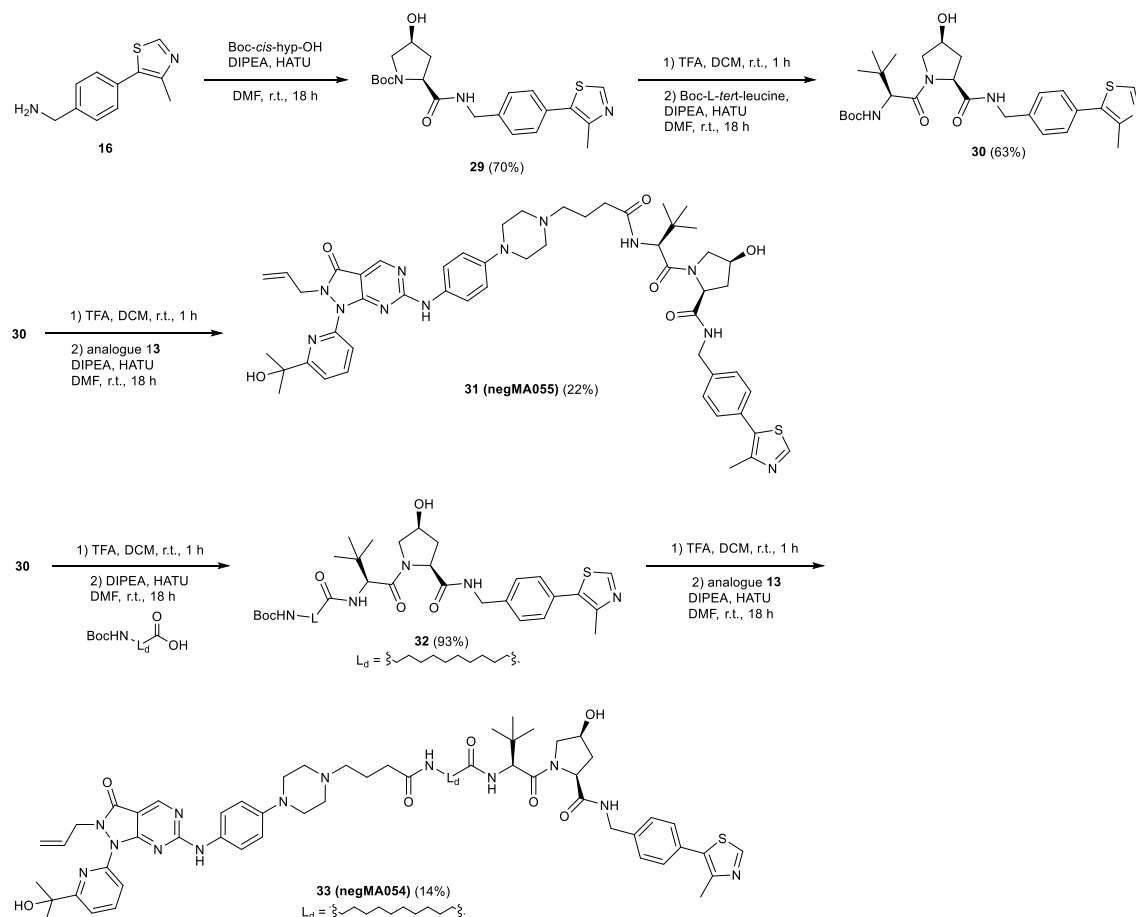
Scheme 3.9: Negative control PROTACs synthesis for VHL-based PROTACs.

3.3.4.2 Negative control PROTACs for the CRBN-series

In a similar way, to prevent the binding of the recruiter pomalidomide to the E3 ligase CRBN, the nitrogen of the glutarimide ring of pomalidomide **24** was methylated using iodomethane in 75% yield (Scheme 3.10). The new building block **34** was then linked to two linkers **Lh** and **Lj** through nucleophilic aromatic substitution to afford **35a** and **35b** in 36 and 34% yield respectively. They were then Boc deprotected and coupled to AZD1775 analogue **13** by HATU-mediated amide coupling to give PROTACs **36a (negMA048)** and **36b (negMA071)** in 23 and 11% yield, respectively (Scheme 3.10). The two VHL negative control PROTACs **negMA0071** and **negMA048** correspond to the PROTACs **MA071** and **MA048**, respectively.
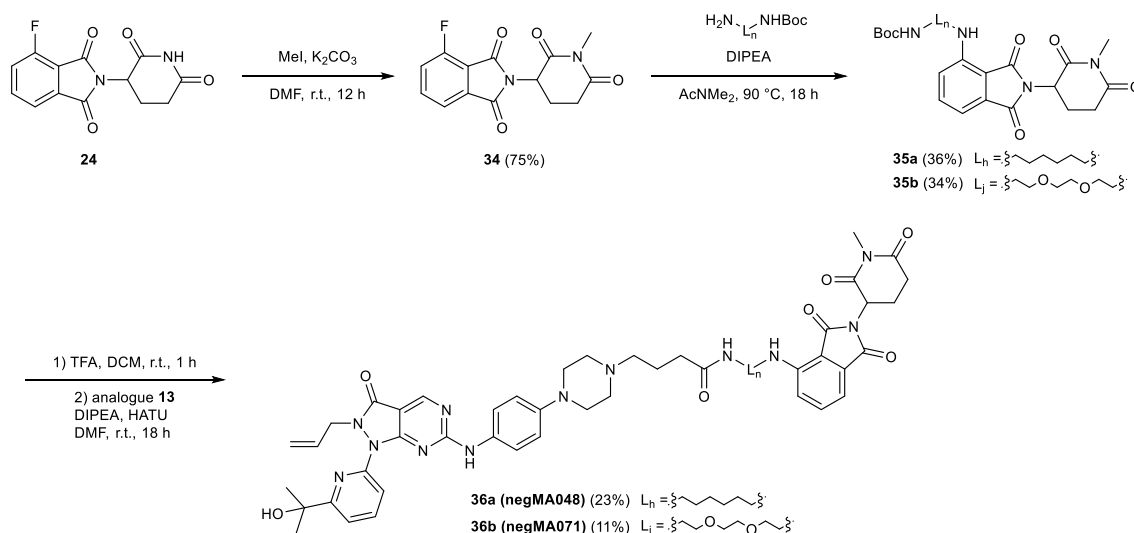
Scheme 3.10: Negative control PROTACs synthesis for CRBN-based PROTACs.

3.4 Experimental

General procedures are detailed in the Materials and methods Chapter 2 Section 2.22.2.

3.4.1 Synthesis of AZD1775 analogue

***Tert*-Butyl (1,3-dioxoisoindolin-2-yl)carbamate (3)** (Matheson *et al.*, 2016)
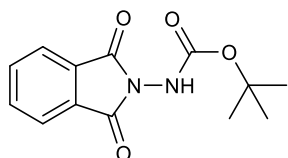
To a solution of phthalic anhydride **2** (8.0 g, 54.0 mmol, 1.0 eq.) in toluene (130 mL) was added *tert*-butyl carbazate **1** (7.5 g, 56.7 mmol, 1.1 eq.) portionwise. The resultant suspension was then heated under reflux conditions (110 °C) with a Dean-Stark appartus. After 18 h, the TLC analysis showed full conversion of the starting material, so it was cooled to room temperature and the white precipitate formed in solution was removed by filtration. This precipitate was washed with hexanes and dried under vacuum to give the desired product **3** (12.2 g, 46.7 mmol, 87%) as a white crystalline solid.

TLC: R_f = 0.05 (1:1 Hexane/EtOAc); UV.

^{1}H-NMR (400 MHz, d_6-DMSO): δ (ppm) = 9.86 (s, 1H), 8.00-7.91 (m, 4H), 1.45 (s, 9H).

IR (ATR): ν (cm^{-1}) = 3310, 2970, 1794 (s, C=O), 1730 (s, C=O), 1610 (s, C=O), 1485.

Spectral data matched those reported in the literature.

Tert-Butyl allyl(1,3-dioxoisoindolin-2-yl)carbamate (4) (Matheson _et al._, 2016)
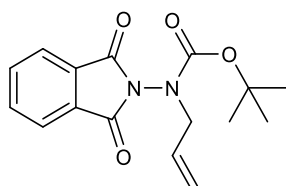
To a suspension of carbamate **3** (12.20 g, 46.6 mmol, 1.0 eq.) in acetonitrile (100 mL) were added sequentially: potassium carbonate (12.2 g, 88.5 mmol, 1.9 eq.), benzyltriethylammonium chloride (1.1 g, 4.7 mmol, 0.1 eq.) and allyl bromide (6.04 mL, 69.90 mmol, 1.5 eq.). The reaction mixture was then stirred at room temperature for 18 h and followed my TLC analysis. When the starting material was used, water (100 mL) was added to quench the reaction. The organic extract was dried over MgSO$_4$ and evaporated to dryness. The resulting pale-yellow wet solid was cooled to 5 °C and then triturated with hexanes. The precipitate was filtered and washed with hexanes to afford the desired product **4** (13.4 g, 44.3 mmol, 95%) as a white crystalline solid.

TLC: R_f = 0.10 (4:1 Hexane/EtOAc); UV.

^{1}H-NMR (400 MHz, d_6-DMSO): δ (ppm) = 8.02-7.92 (m, 4H), 5.94-5.76 (m, 1H), 5.27 (dd, 1H, J = 17.1, 0.9 Hz), 5.17-5.10 (m, 1H), 4.19 (d, 2H, J = 17.1 Hz), 1.27 (s, 9H).

IR (ATR): ν (cm^{-1}) = 2981, 2930, 1794 (s, C=O), 1717 (s, C=O), 1645 (s, C=O).

Spectral data matched those reported in the literature.

***Tert*-Butyl 1-allylhydrazine-1-carboxylate (5)** (Matheson *et al.*, 2016)
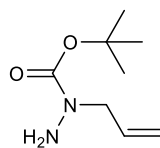
Phthalamide **4** (13.4 g, 44.3 mmol, 1.0 eq.) was dissolved in THF (90 mL) and the solution was cooled in an ice bath. Methylhydrazine (2.7 mL, 54.4 mmol, 1.2 eq.) was added and the reaction mixture was allowed to warm to room temperature and was then stirred for 18 h. The obtained white suspension was filtered, and the filtrate was concentrated in vacuo. A mixture of Hexanes:EtOAc (3:1) was added to form a precipitate that was removed via filtration. This process was repeated two more times, and the final filtrate was concentrated to give the desired compound **5** (6.5 g, 37.8 mmol, 85%) as a pale-yellow oil.

TLC: R_f = 0.05 (1:1 Hexane/EtOAc); UV.

^{1}H-NMR (400 MHz, d_6-DMSO): δ (ppm) = 5.86-5.73 (m, 1H), 5.13-5.09 (m, 1H), 5.09-5.05 (m, 1H), 4.47 (s, 2H), 3.85 (dt, 2H, J = 5.5, 1.5 Hz), 1.40 (s, 9H).

IR (ATR): v (cm^{-1}) = 3330, 2979, 2930, 1690 (s, C=O).

Spectral data matched those reported in the literature.

2-(6-Bromopyridin-2-yl)propan-2-ol (9) (Matheson *et al.*, 2016)
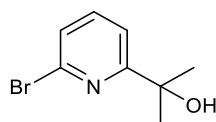
A solution of methyl 6-bromopyridine-2-carboxylate **8** (2.6 g, 12.0 mmol, 1.0 eq.) was prepared in dry Et$_2$O (75 mL) under N$_2$ and methyl magnesium bromide (3 M in Et$_2$O, 9.0 mL, 27.0 mmol, 2.3 eq.) was added. After stirring the reaction mixture at room temperature for five minutes, the reaction was quenched with 1 M HCl (50 mL) and

extracted three times with EtOAc (50 mL). The combined organic layer was washed with saturated. $NaHCO_3$ solution (50 mL) and then with brine (30 mL), dried ($MgSO_4$) and concentrated in vacuo. The desired product **9** (2.2 g, 10.2 mmol, 87%) was obtained as a yellow oil and was used without further purification.

TLC: R_f = 0.80 (1:1 Hexane/EtOAc); UV.

^{1}H-NMR (400 MHz, d_6-DMSO): δ (ppm) = 7.74-7.65 (m, 2H), 7.44 (dd, 1H, J = 7.5, 1.1 Hz), 5.31 (s, 1H), 1.42 (s, 6H).

Spectral data matched those reported in the literature.

Tert-Butyl 4-[4-(4-aminophenyl)piperazin-1-yl]butanoate (12)
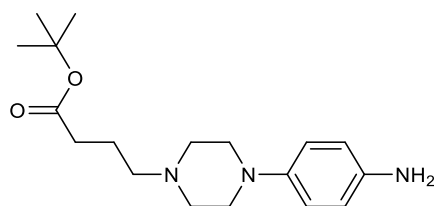
Triethylamine (2.6 mL, 18.6 mmol, 1.1 eq.) was added to a solution of 4-nitrophenylpiperazine **11** (3.5 g, 16.9 mmol, 1.0 eq.) in THF (40 mL), followed by *tert*-butyl 4-bromobutanoate (3.3 g, 18.6 mmol, 1.1 eq.). The reaction mixture was stirred at room temperature for 3.5 days, after which the solvent was evaporated under reduced pressure. Water (20 mL) was then added to the residue and a yellow precipitate was obtained. The solid was filtered and washed with water (2 × 5 mL) and then recrystallized using DCM/hexane mixture to give the product yellow solid. The crude product was used in the next step without further purification. A solution of the intermediate (1.5 g, 4.3 mmol, 1.0 eq.) in dry MeOH (40 mL) was purged with argon, and 5% Pd-C (170 mg) was added under inert atmosphere. Argon was removed under vacuum and the mixture was purged with hydrogen using a hydrogen balloon. The hydrogenation reaction was stirred for 5 h. The crude reaction mixture was filtered using a pad of celite, washed with

methanol, and the filtrate was evaporated to obtain **12** (1.3 g, 4.1 mmol, 93%) as a sticky brown oil which was used in the next step without further purification.

TLC: R_f = 0.20 (1:1 hexane/EtOAc); UV.

^{1}H-NMR (400 MHz, CDCl$_3$): δ (ppm) = 6.82 (d, 2H, J = 8.8 Hz), 6.66 (d, 2H, J = 8.8 Hz), 3.19 (br t, 4H, J = 4.9 Hz), 2.84 (br t, 4H, J = 4.9 Hz), 2.63 (br t, 2H, J = 7.8 Hz), 2.31 (br t, 2H, J = 7.2 Hz), 1.88-1.97 (m, 2H), 1.45 (s, 9H).

Spectral data matched those reported in the literature.

4-{4-[4-({1-[6-(2-Hydroxypropan-2-yl)pyridin-2-yl]-3-oxo-2-(prop-2-en-1-yl)-1H,2H,3H-pyrazolo[3,4-d]pyrimidin-6-yl}amino)phenyl]piperazin-1-yl}butanoic acid (13)
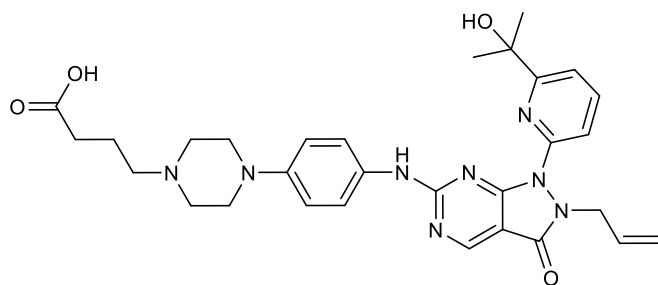
Meta-chloroperoxybenzoic acid (1.3 mmol, 1.0 eq.) was added to a solution of **10** (1.3 mmol, 1.3 eq.) in toluene. The reaction mixture was stirred for 30 min at room temperature, and diisopropylethylamine (5.0 mmol, 4.0 eq.) and aniline **12** (1.5 mmol, 1.2 eq.) were added. The mixture was then stirred overnight before adding saturated Na$_2$CO$_3$ (20 mL), and subsequently extracted with EtOAc (100 mL). The organic phase was washed with brine, dried over Na$_2$SO$_4$, filtered and concentrated. The crude product was then purified by column chromatography on silica gel using a gradient of 0-5% of MeOH in DCM to give Boc-AZD1775 analogue (583 mg, 1.0 mmol, 74%) as an orange solid.

TLC: R_f = 0.40 (5:95 MeOH/DCM); UV.

^{1}H-NMR (400 MHz, CDCl$_3$): δ (ppm) = 8.81 (s, 1H), 7.87 (t, 1H, J = 7.9 Hz), 7.77 (dd, 1H, J = 8.0, 0.7 Hz), 7.47 (d, 2H, J = 8.8 Hz), 7.36 (dd, 1H, J = 7.6, 0.7 Hz), 6.94 (d, 2H, J = 8.8 Hz),

5.77 – 5.65 (m, 1H), 5.06 (dd, 1H, *J* = 10.2, 1.1 Hz), 4.95 (dd, 1H, *J* = 17.1, 1.1 Hz), 4.76 (d, 2H, *J* = 6.2 Hz), 3.22 (br t, 4H, *J* = 4.8 Hz), 2.66 (br t, 4H, *J* = 4.8 Hz), 2.46 (t, 2H, *J* = 7.5 Hz), 2.31 (t, 2H, *J* = 7.4 Hz), 1.93-1.79 (m, 2H), 1.60 (s, 6H), 1.48 (s, 9H).

IR (ATR): v (cm^{-1}) = 3409, 2958, 2875, 2820, 1692, 1670, 1608.

Formic acid (10 mL) was added to Boc-AZD1775 analogue (200 mg, 0.3 mmol, 1.0 eq.) and the reaction mixture was stirred at r.t. for 48 h. It was then diluted with water and extracted three times with EtOAc (3 × 10 mL), dried over Na_2SO_4 and concentrated under reduced pressure to give AZD1775 analogue **13** as a yellow solid which was used without further purification (quantitative).

HRMS (ESI): *m/z* calculated for: $C_{30}H_{36}N_8O_4$ [M+H]$^+$, 573.2932, found: 573.2921.

3.4.2 Synthesis of the VHL ligand

(4-(4-Methylthiazol-5-yl)phenyl)methanamine (16) (Roger *et al.*, 2009)
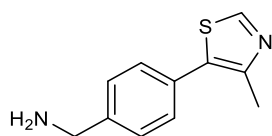
4-bromobenzonitrile **14** (5.0 g, 27.5 mmol, 1.0 eq) and palladium (II) acetate (8.0 mg, 10 mol %) were dissolved in DMAc (27.5 mL). 4-methylthiazole **15** (5.5 g, 54.9 mmol, 2.0 eq.) and potassium acetate (9.0 g, 54.9 mmol, 3.3 eq.) were added to the suspension under nitrogen. The mixture was then heated to 150 °C and stirred for 18 h before being cooled to room temperature. The reaction was then partitioned between water (110 mL) and EtOAc (100 mL), extracted with EtOAc (2 × 100 mL). The combined organic layers were washed with water (2 × 100 mL), dried (MgSO$_4$) and concentrated in vacuo to give the cyano derivative (4.7 g, 23.3 mmol, 85%) as a beige solid which was used without further purification.

A solution of cyano derivative (4.7 g, 23.5 mmol, 1.0 eq.) in methanol (220 mL) was cooled at 0 °C in an ice bath. CoCl$_2$ (4.5 g, 35.5 mmol, 1.5 eq.) was then added to the reaction mixture, followed by the addition of NaBH$_4$ (4.4 g, 117.5 mmol, 5.0 eq.) portionwise

(Buckley *et al.*, 2012). The mixture was stirred at r.t. for 90 min before being quenched with a solution of ammonium hydroxide and water. The reaction mixture was then extracted six times with chloroform, dried (Na_2SO_4) and concentrated in vacuo to give a brown residue. The crude product was purified by column chromatography on silica gel using a gradient of 10-30 % of 0.5M NH_3 MeOH in DCM to afford **16** (1.4 g, 6.7 mmol, 29%) as a yellow oil.

TLC: R_f = 0.10 (1:9 0.5 M NH_3 in MeOH/DCM); UV.

^{1}H-NMR (400 MHz, $CDCl_3$): δ (ppm) = 8.69 (s, 1H), 7.46-7.38 (m, 4H), 3.94 (s, 2H), 2.55 (s, 3H).

^{13}C-NMR (101 MHz, $CDCl_3$): δ (ppm) = 152.8, 149.0, 143.6, 133.4, 131.4, 130.5, 129.1, 46.4, 15.8.

Spectral data matched those reported in the literature.

(2*S*,4*R*)-*Tert*-Butyl-4-hydroxy-2-((4-(4-methylthiazol-5-yl)benzyl)carbamoyl)pyrrolidine-1- carboxylate (17) (Galdeano *et al.*, 2014)
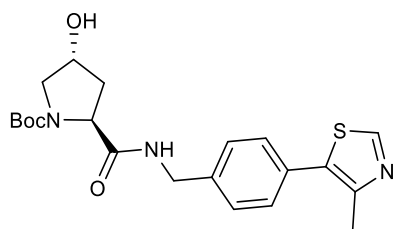
Boc-Hyp-OH (736 mg, 3.2 mmol, 1.0 eq.) was attached to (4-(4-methylthiazol-5-yl)phenyl)methanamine **16** (650 mg, 3.2 mmol, 1.0 eq.) by HATU-mediated amide coupling following general procedure **A**. The crude product was purified by column chromatography on silica gel using 0-10% MeOH in DCM to afford **17** (1.2 g, 2.8 mmol, 90%) as a yellow oil.

TLC: R_f = 0.85 (1:9 MeOH/DCM); UV.

^{1}H-NMR (400 MHz, CDCl₃): δ (ppm) = 8.66 (s, 1H), 7.39-7.29 (m, 4H), 4.60-4.26 (m, 4H), 3.66-3.45 (m, 2H), 2.48 (s, 3H), 2.35 (br s, 1H), 2.11 (br s, 1H), 1.41 and 1.31 (s, 9H).

^{13}C-NMR (101 MHz, CDCl₃): δ (ppm) = 173.0, 151.9, 148.3, 139.9, 129.3, 129.2, 127.2, 126.6, 79.0, 68.3, 60.1, 59.4, 55.3, 49.0, 38.6, 28.3, 14.4.

Spectral data matched those reported in the literature.

Tert-Butyl((_S_)-1-((2_S_,4_R_)-4-hydroxy-2-((4-(4-methylthiazol-5-yl)benzyl)carbamoyl) pyrrolidin-1-yl)-3,3-dimethyl-1-oxobutan-2-yl)carbamate (18) (Galdeano *et al.*, 2014)
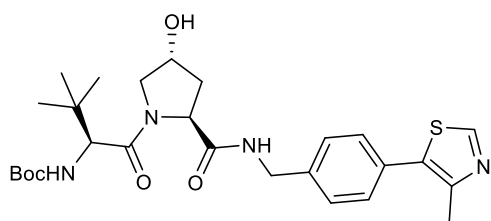
Intermediate **17** (400 mg, 0.70 mmol, 1.0 eq.) was Boc deprotected following general procedure **D**. It was then reacted to Boc-L-*tert*-leucine (169 mg, 0.70 mmol, 1.0 eq.) by HATU-mediated amide coupling following general procedure **A**. The crude product was purified by column chromatography on silica gel using 0-7% MeOH in DCM to afford the VHL ligand **18** (323 mg, 0.610 mmol, 87%) as a yellow solid.

TLC: R_f = 0.75 (7:93 MeOH/DCM); UV.

^{1}H-NMR (400 MHz, CDCl₃): δ (ppm) = 8.70 (s, 1H), 7.60 (br t, 1H, J = 5.8 Hz), 7.34-7.29 (m, 4H), 5.30 (d, 1H, J = 9.2 Hz), 4.70 (t, 1H, J = 7.9 Hz), 4.56-4.46 (m, 2H), 4.31 (dd, 1H, J = 15.1, 5.3 Hz), 4.19 (d, 1H, J = 9.3 Hz), 3.97 (d, 1H, J = 11.1 Hz), 3.63 (dd, 1H, J = 11.1, 3.3 Hz), 2.48 (s, 3H), 2.44-2.34 (m, 1H), 2.16-2.06 (m, 1H), 1.39 (s, 9H), 0.93 (s, 9H).

^{13}C-NMR (101 MHz, CDCl₃): δ (ppm) = 172.2, 171.2, 156.2, 150.7, 148.0, 138.3, 131.9, 130.5, 129.4, 127.8, 80.3, 70.0, 58.9, 58.8, 56.7, 43.1, 36.4, 35.3, 28.3, 26.5, 15.8.

IR (ATR): ν (cm^{-1}) = 3298, 2963, 1675 (s, C=O), 1627 (C=O), 1258.

HRMS (ESI): *m/z* calculated for: $C_{27}H_{38}N_4O_5SNa$ [M+Na]$^+$, 553.2455, found: 553.2458.

Spectral data matched those reported in the literature.

3.4.3 VHL ligand coupling to linkers

Compounds **20a-f** were prepared by deprotecting **18** following general procedure **D** and linking to linker **L$_{a-f}$** by HATU-mediated amide coupling following general procedure **A**.

***Tert*-Butyl N-(3-{[(2*S*)-1-[(2*S*,4*R*)-4-hydroxy-2-({[4-(4-methyl-1,3-thiazol-5-yl)phenyl]methyl}carbamoyl)pyrrolidin-1-yl]-3,3-dimethyl-1-oxobutan-2-yl]carbamoyl}propyl)carbamate (20a)**
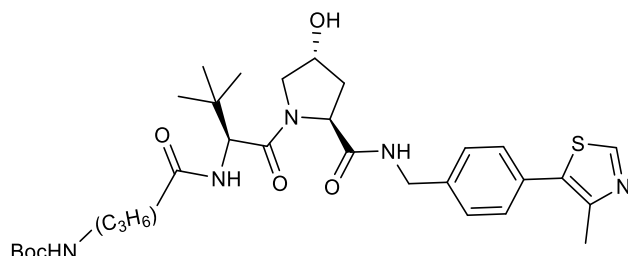
The crude product was purified by column chromatography on silica gel using 5% MeOH in DCM to afford the product **20a** (70 mg, 0.11 mmol, 75%) as a yellow solid.

TLC: R_f = 0.75 (1:9 MeOH/DCM); UV.

^{1}H-NMR (400 MHz, CDCl$_3$): δ (ppm) = δ 8.67 (s, 1H), 7.62 (br t, 1H, *J* = 6.0 Hz), 7.39-7.31 (m, 4H), 7.21 (br d, 1H, *J* = 7.8 Hz), 5.07 (br s, 1H) 4.69 (t, 1H, *J* = 7.9 Hz), 4.60-4.44 (m, 3H), 4.33 (dd, 1H, *J* = 14.9, 5.4 Hz), 4.06 (d, 1H, *J* = 11.1 Hz), 3.64 (dd, 1H, *J* = 11.1, 2.6 Hz), 3.18-3.03 (m, 2H), 2.50 (s, 3H), 2.42-2.28 (m, 1H), 2.26-2.10 (m, 3H), 1.72 (p, 2H, *J* = 6.8 Hz), 1.40 (s, 9H), 0.97 (s, 9H).

^{13}C-NMR (101 MHz, CDCl$_3$): δ (ppm) = 173.6, 171.7, 171.3, 162.7, 156.6, 150.4, 148.3, 138.3, 131.7, 130.7, 129.4, 128.0, 79.4, 70.1, 58.8, 58.1, 56.9, 43.1, 39.6, 36.5, 35.0, 33.1, 28.4, 26.4, 16.0.

IR (ATR): ν (cm^{-1}) = 3285, 3062, 2953, 1664, 1623, 1198.

HRMS (ESI): *m/z* calculated for: $C_{26}H_{37}N_5O_4S$ [M+H]$^+$, 516.2639, found: 516.2619.

Tert-Butyl N-(5-{[(2S)-1-[(2S,4R)-4-hydroxy-2-({[4-(4-methyl-1,3-thiazol-5-yl)phenyl]methyl}carbamoyl)pyrrolidin-1-yl]-3,3-dimethyl-1-oxobutan-2-yl]carbamoyl}pentyl)carbamate (20b)
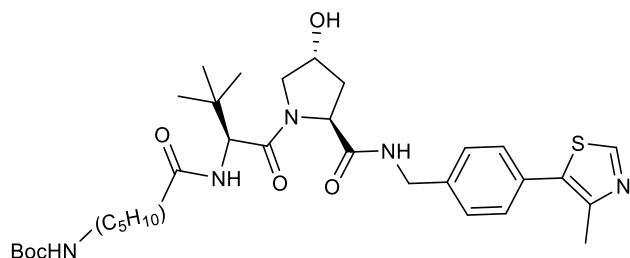
The crude product was purified by column chromatography on silica gel using 5% MeOH in DCM to afford the product **20b** (73 mg, 0.11 mmol, 67%) as a yellow solid.

TLC: R_f = 0.40 (5:95 MeOH/DCM); UV.

^{1}H-NMR (400 MHz, CDCl$_3$): δ (ppm) = 8.68 (s, 1H), 7.48 (br s, 1H), 7.40-7.30 (m, 4H), 6.55 (d, 1H, *J* = 8.0 Hz), 4.87 (br s, 1H), 4.66 (t, 1H, *J* = 8.0 Hz), 4.59-4.46 (m, 3H), 4.34 (dd, 1H, *J* = 5.1, 5.4 Hz), 4.03 (d, 1H, *J* = 11.2 Hz), 3.74-3.59 (m, 1H), 3.10-2.99 (m, 2H), 2.49 (s, 3H), 2.41-2.29 (m, 1H), 2.26-2.11 (m, 3H), 1.59 (p, 2H, *J* = 19.9 Hz), 1.50-1.34 (m, 11H), 1.33-1.20 (m, 2H), 0.94 (s, 9H).

^{13}C-NMR (101 MHz, CDCl$_3$): δ (ppm) = 174.0, 171.6, 171.3, 162.8, 156.5, 148.3, 138.3, 131.8, 130.7, 129.4, 128.0, 79.2, 69.9, 58.9, 57.5, 57.0, 43.2, 43.1, 40.3, 36.3, 36.2, 29.5, 28.4, 26.4, 26.2, 25.2, 15.9.

IR (ATR): ν (cm^{-1}) = 3278, 3060, 2940, 2871, 1668, 1623, 1198.

HRMS (ESI): *m/z* calculated for: $C_{28}H_{41}N_5O_4S$ [M-Boc+H]$^+$, 544.2952, found: 544.2946.

***Tert*-Butyl N-(7-{[(2*S*)-1-[(2*S*,4*R*)-4-hydroxy-2-({[4-(4-methyl-1,3-thiazol-5-yl)phenyl]methyl}carbamoyl)pyrrolidin-1-yl]-3,3-dimethyl-1-oxobutan-2-yl]carbamoyl}heptyl)carbamate (20c)**
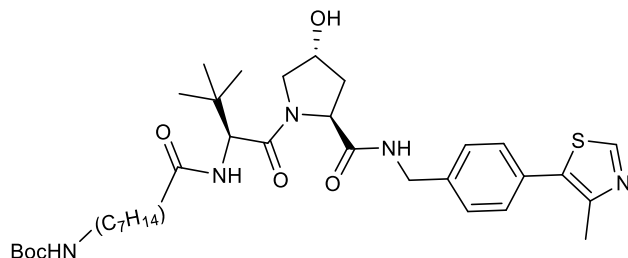
The crude product was purified by column chromatography on silica gel using 5% MeOH in DCM to afford the product **20c** (60 mg, 0.09 mmol, 53%) as a yellow solid.

TLC: R_f = 0.40 (5:95 MeOH/DCM); UV.

^{1}H-NMR (400 MHz, CDCl$_3$): δ (ppm) = 8.67 (s, 1H), 7.49 (br s, 1H), 7.38-7.30 (m, 4H), 6.42 (br d, 1H, *J* = 8.0 Hz), 4.72 (br s, 1H), 4.67 (t, 1H, *J* = 8.0 Hz), 4.55 (d, 1H, *J* = 8.7 Hz), 4.54-4.47 (m, 2H), 4.34 (dd, 1H, *J* = 15.1, 5.5 Hz), 4.02 (d, 1H, *J* = 11.2 Hz), 3.64 (dd, 1H, *J* = 11.2, 3.4 Hz), 3.09-3.00 (m, 2H), 2.49 (s, 3H), 2.43-2.32 (m, 1H), 2.22-2.08 (m, 3H), 1.61-1.51 (m, 2H), 1.45-1.34 (m, 11H), 1.33-.120 (br s, 6H), 0.94 (s, 9H).

^{13}C-NMR (101 MHz, CDCl$_3$): δ (ppm) = 173.7, 171.6, 171.2, 162.7, 156.1, 148.3, 138.3, 131.7, 130.7, 129.4, 128.0, 79.0, 69.9, 66.9, 58.8, 57.4, 56.8, 43.1, 40.5, 36.3, 35.3, 29.8, 28.9, 28.8, 28.4, 26.5, 26.4, 25.4, 16.0.

IR (ATR): v (cm^{-1}) = 3285, 3069, 2935, 2862, 1664, 1623, 1198.

HRMS (ESI): *m/z* calculated for: C$_{30}$H$_{45}$N$_5$O$_4$S [M-Boc+H]$^+$, 572.3265, found: 572.3247.

Tert-Butyl N-(10-{[(2S)-1-[(2S,4R)-4-hydroxy-2-({[4-(4-methyl-1,3-thiazol-5-yl)phenyl]methyl}carbamoyl)pyrrolidin-1-yl]-3,3-dimethyl-1-oxobutan-2-yl]carbamoyl}decyl)carbamate (20d)
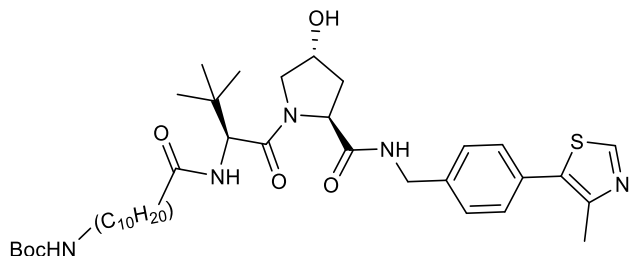
The crude product was purified by column chromatography on silica gel using 5% MeOH in DCM to afford the product **20d** (78 mg, 0.11 mmol, 84%) as a yellow solid.

TLC: R_f = 0.30 (5:95 MeOH/DCM); UV.

^{1}H-NMR (400 MHz, CDCl$_3$): δ (ppm) = 8.66 (s, 1H), 7.47 (br t, 1H, J = 5.9 Hz), 7.35-7.29 (m, 4H), 7.40 (br d, 1H, J = 8.4 Hz), 4.69 (br s, 1H), 4.65 (t, 1H, J = 7.9 Hz), 4.54 (d, 1H, J = 9.0 Hz), 4.52-4.45 (m, 2H), 4.31 (dd, 1H, J = 15.1, 5.4 Hz), 3.98 (d, 1H, J = 11.0 Hz), 3.63 (dd, 1H, J = 11.0, 3.8 Hz), 3.09-2.99 (m, 2H), 2.47 (s, 3H), 2.41-2.32 (m, 1H), 2.17-2.08 (m, 3H), 1.60-1.49 (m, 2H), 1.43-1.37 (m, 11H), 1.27-1.18 (m, 12H), 0.92 (s, 9H).

^{13}C-NMR (101 MHz, CDCl$_3$): δ (ppm) = 173.6, 171.6, 171.1, 162.7, 156.0, 150.4, 148.3, 138.2, 131.6, 130.7, 129.4, 128.0, 78.9, 69.9, 58.8, 57.3, 56.7, 43.1, 43.1, 40.6, 36.4, 36.3, 35.0, 30.0, 29.4, 29.3, 29.2, 28.4, 26.7, 26.4, 25.6, 16.0.

IR (ATR): v (cm^{-1}) = 3285, 3069, 2933, 2862, 1664, 1623, 1198.

***Tert*-Butyl N-(2-{2-[2-({[(2*S*)-1-[(2*S*,4*R*)-4-hydroxy-2-({[4-(4-methyl-1,3-thiazol-5-yl)phenyl]methyl}carbamoyl)pyrrolidin-1-yl]-3,3-dimethyl-1-oxobutan-2-yl]carbamoyl}methoxy)ethoxy]ethoxy}ethyl)carbamate (20e)**

The crude product was purified by column chromatography on silica gel using 5% MeOH in DCM to afford the product **20e** (22 mg, 0.03 mmol, 26%) as a yellow solid.

TLC: R_f = 0.60 (1:9 MeOH/DCM); UV.

^{1}H-NMR (400 MHz, CDCl$_3$): δ (ppm) = 8.69 (s, 1H), 7.46 (br s, 1H), 7.38-7.29 (m, 4H), 5.16 (br s, 1H), 5.72 (t, 1H, *J* = 7.8 Hz), 4.60-4.47 (m, 3H), 4.34 (dd, 1H, *J* = 14.8, 4.7 Hz), 4.06-3.96 (m, 3H), 3.76-3.55 (m, 9H), 3.50 (t, 2H, *J* = 5.3 Hz), 3.32-3.22 (m, 2H), 2.51 (s, 3H), 2.48-2.39 (m, 1H), 2.20-2.07 (m, 1H), 1.42 (s, 9H), 0.96 (s, 9H).

^{13}C-NMR (101 MHz, CDCl$_3$): δ (ppm) = 171.1, 170.8, 170.4, 156.1, 150.5, 148.3, 138.3, 130.8, 129.4, 128.1, 120.2, 79.3, 70.1, 70.6, 70.4, 70.3, 70.2, 70.1, 58.7, 58.2, 57.0, 56.8, 43.2, 40.4, 36.2, 35.2, 28.4, 26.4, 16.0.

IR (ATR): ν (cm^{-1}) = 3285, 3069, 2924, 2862, 1669, 1628, 1200.

HRMS (ESI): *m/z* calculated for: C$_{30}$H$_{45}$N$_5$O$_7$S [M-Boc+H]$^+$, 620.3112, found: 620.3111.

***Tert*-Butyl N-(14-{[(2*S*)-1-[(2*S*,4*R*)-4-hydroxy-2-({[4-(4-methyl-1,3-thiazol-5-yl)phenyl]methyl}carbamoyl)pyrrolidin-1-yl]-3,3-dimethyl-1-oxobutan-2-yl]carbamoyl}-3,6,9,12-tetraoxatetradecan-1-yl)carbamate (20f)**
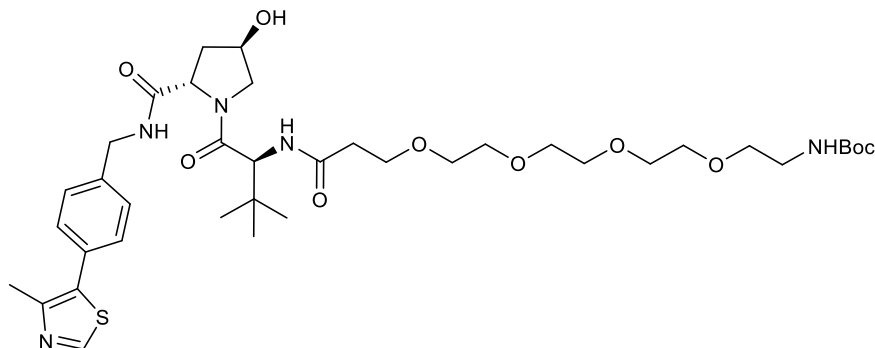
The crude product was purified by column chromatography on silica gel using 5% MeOH in DCM to afford the product **20f** (43 mg, 0.06 mmol, 43%) as a yellow solid.

TLC: R_f = 0.55 (1:9 MeOH/DCM); UV.

^{1}H-NMR (400 MHz, CDCl$_3$): δ (ppm) = 8.68 (s, 1H), 7.48 (br s, 1H), 7.37-7.31 (m, 4H), 7.04 (br d, 1H, *J* = 6.9 Hz), 5.18 (br s, 1H), 4.69 (t, 1H, *J* = 7.9 Hz), 4.57-4.47 (m, 3H), 4.34 (dd, 1H, *J* = 15.02, 5.4 Hz), 4.02 (d, 1H, *J* = 11.0 Hz), 3.70 (t, 2H, *J* = 5.7 Hz), 3.67-3.57 (m, 13H), 3.56-3.48 (m, 2H), 3.35-3.23 (m, 2H), 2.52-2.45 (m, 5H), 2.45-2.36 (m, 1H), 2.18-2.09 (m, 1H), 1.42 (s, 9H), 0.95 (s, 9H).

^{13}C-NMR (101 MHz, CDCl$_3$): δ (ppm) = 172.1, 171.5, 171.1, 156.3, 150.3, 148.4, 138.3, 131.6, 129.4, 128.0, 120.5, 79.2, 70.5, 70.4, 70.3, 70.3, 70.0, 67.1, 60.4, 58.7, 57.7, 56.7, 43.1, 40.3, 36.6, 36.3, 35.1, 28.4, 26.4, 16.0.

IR (ATR): ν (cm^{-1}) = 3202, 3073, 2961, 1675, 1634, 1202.

3.4.4 Wee1 PROTACs recruiting VHL

(2S,4R)-4-Hydroxy-1-[(2S)-2-(4-{4-[4-({1-[6-(2-hydroxypropan-2-yl)pyridin-2-yl]-3-oxo-2-(prop-2-en-1-yl)-1H,2H,3H-pyrazolo[3,4-d]pyrimidin-6-yl}amino)phenyl]piperazin-1-yl}butanamido)-3,3-dimethylbutanoyl]-N-{[4-(4-methyl-1,3-thiazol-5-yl)phenyl]methyl}pyrrolidine-2-carboxamide (19 – MA055)
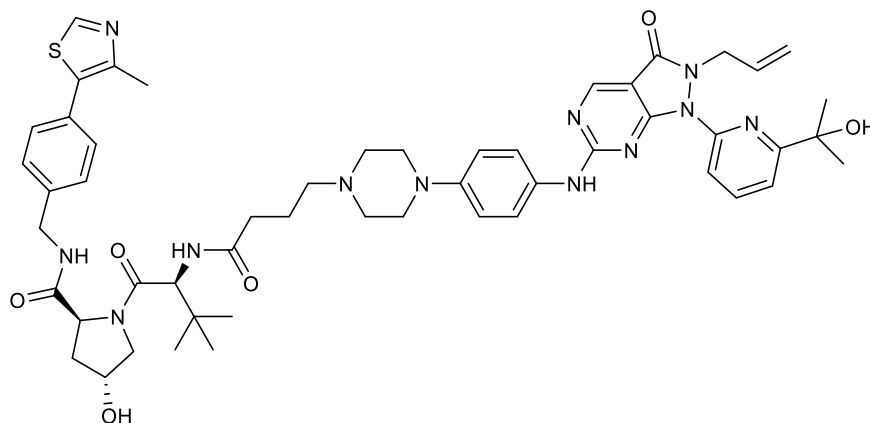
19 (MA055) was prepared following general procedure **D** to deprotect **18** (13.4 mg, 0.03 mmol, 1.0 eq.) and then general procedure **A** for HATU-mediated amide coupling to AZD1775 analogue **13** (17 mg, 0.03 mmol, 1.0 eq.). The crude product was purified by column chromatography on silica gel using 5% MeOH in DCM to afford the product **19** (15 mg, 0.02 mmol, 61%) as a yellow solid.

TLC: R_f = 0.20 (1:9 MeOH/DCM); UV.

^{1}H-NMR (400 MHz, CDCl$_3$): δ (ppm) = 8.79 (s, 1H), 8.64 (s, 1H), 7.86 (t, 1H, J = 7.9 Hz), 7.70 (d, 1H, J = 7.9 Hz), 7.45 (br d, 2H, J = 8.3 Hz), 7.39-3.30 (m, 6H), 6.90-6.73 (m, 3H), 5.73-5.62 (m, 1H), 5.05 (d, 1H, J = 10.4 Hz), 4.94 (dd, 1H, J = 17.1, 1.1 Hz), 4.76-4.66 (m, 3H), 4.59-4.48 (m, 3H), 4.31 (dd, 1H, J = 15.0, 5.1 Hz), 4.08 (d, 1H, J = 11.4 Hz), 3.62 (dd, 1H, J = 11.4, 3.1 Hz), 3.19 (br s, 4H), 2,71 (br s, 4H), 2.60-2.37 (m, 7H), 2.32-2.24 (m, 2H), 2.19-2.11 (m, 1H), 1.86-1.78 (m, 2H), 1.57 (s, 6H), 0.96 (s, 9H).

IR (ATR): ν (cm^{-1}) = 3397, 3290, 2955, 1654, 1619, 1533.

HRMS (ESI): m/z calculated for: C$_{52}$H$_{64}$N$_{12}$O$_6$S [M+H]$^+$, 985.4845, found: 985.4872.

HPLC: 95.3% purity, t_R = 8.61 min.

21a-f were prepared following general procedure **D** to deprotect **20a-f** and then general procedure **A** for HATU-mediated amide coupling with AZD1775 analogue **13**.

(2S,4R)-4-Hydroxy-1-[(2S)-2-[4-(4-{4-[4-({1-[6-(2-hydroxypropan-2-yl)pyridin-2-yl]-3-oxo-2-(prop-2-en-1-yl)-1H,2H,3H-pyrazolo[3,4-d]pyrimidin-6-yl}amino)phenyl]piperazin-1-yl}butanamido)butanamido]-3,3-dimethylbutanoyl]-N-{[4-(4-methyl-1,3-thiazol-5-yl)phenyl]methyl}pyrrolidine-2-carboxamide (21a – MA051)
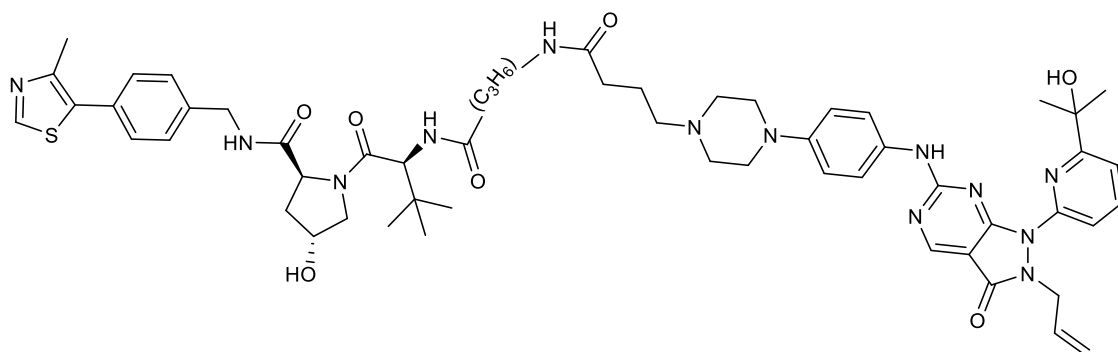
The crude product was purified by column chromatography on silica gel using 5% MeOH in DCM to afford the product **21a** (4.7 mg, 0.01 mmol, 19%) as a yellow solid.

TLC: R_f = 0.20 (1:9 MeOH/DCM); UV.

^{1}H-NMR (400 MHz, CDCl$_3$): δ (ppm) = 8.82 (s, 1H), 8.66 (s, 1H), 7.86 (t, 1H, J = 7.9 Hz), 7.72 (dd, 1H, J = 7.9, 0.7 Hz), 7.51-7.44 (m, 3H), 7.39-7.30 (m, 5H), 6.95-6.78 (m, 4H), 5.75-5.64 (m, 1H), 5.04 (dd, 1H, J = 10.3, 1.1 Hz), 4.93 (dd, 1H, J = 17.1, 1.3 Hz), 4.79-4.70 (m, 3H), 4.61-4.48 (m, 3H), 4.33 (dd, 1H, J = 15.1, 5.2 Hz), 4.10 (d, 1H, J = 10.9 Hz), 3.61 (dd, 1H, J = 11.2, 3.3 Hz), 3.31-3.14 (m, 6H), 2.89 (br s, 4H), 2.78-2.64 (m, 2H), 2.52-2.42 (m, 4H), 2.34-2.29 (m, 2H), 2.29-2.19 (m, 2H), 1.98-1.86 (m, 4H), 1.80-1.66 (m, 1H), 1.59 (s, 6H), 0.98 (s, 9H), 0.91-0.81 (m, 1H).

IR (ATR): ν (cm^{-1}) = 3304, 2963, 2927, 1671, 1619, 1200.

HRMS (ESI): m/z calculated for: C$_{56}$H$_{71}$N$_{13}$O$_7$S [M+H]$^+$, 1070.5393, found: 1070.5414.

HPLC: 92.8% purity, t_R = 8.54 min.

(2S,4R)-4-Hydroxy-1-[(2S)-2-[6-(4-{4-[4-({1-[6-(2-hydroxypropan-2-yl)pyridin-2-yl]-3-oxo-2-(prop-2-en-1-yl)-1H,2H,3H-pyrazolo[3,4-d]pyrimidin-6-yl}amino)phenyl]piperazin-1-yl}butanamido)hexanamido]-3,3-dimethylbutanoyl]-N-{[4-(4-methyl-1,3-thiazol-5-yl)phenyl]methyl}pyrrolidine-2-carboxamide (21b – MA052)
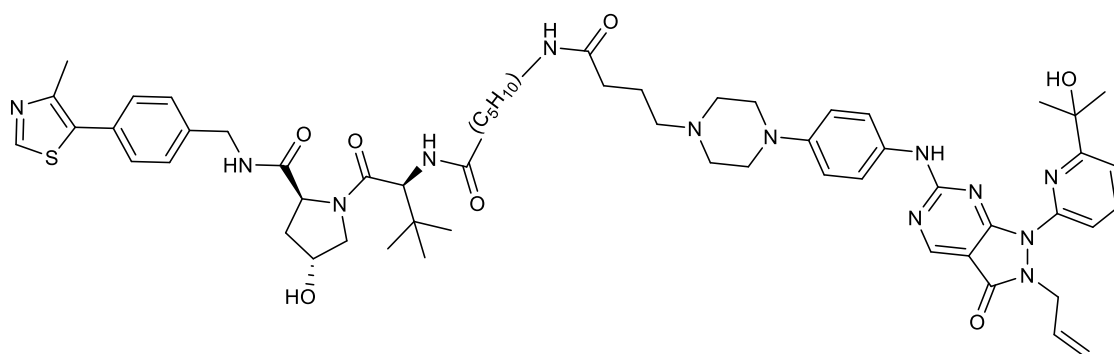
The crude product was purified by column chromatography on silica gel using 5% MeOH in DCM to afford the product **21b** (9.0 mg, 0.01 mmol, 36%) as a yellow solid.

TLC: R_f = 0.20 (1:9 MeOH/DCM); UV.

^{1}H-NMR (400 MHz, CDCl$_3$): δ (ppm) = 8.80 (s, 1H), 8.74 (s, 1H), 7.93 (t, 1H, *J* = 7.9 Hz), 7.71 (dd, 1H, *J* = 7.9, 0.5 Hz), 7.57 (br d, 2H, *J* = 8.7 Hz), 7.48 (br t, 1H, *J* = 5.9 Hz), 7.44 (d, 1H, *J* = 7.9 Hz), 7.40-7.34 (m, 4H), 7.20 (br t, 1H, *J* = 5.5 Hz), 6.94-6.88 (m, 3H), 5.77-5.64 (m, 1H), 5.07 (dd, 1H, *J* = 10.3, 1.1 Hz), 4.94 (dd, 1H, *J* = 17.1, 1.3 Hz), 4.76 (d, 2H, *J* = 6.2 Hz), 4.72 (t, 1H, *J* = 8.3 Hz), 4.68-4.57 (m, 2H), 4.58 (s, 1H), 4.35 (dd, 1H, *J* = 15.1, 5.3 Hz), 4.11 (d, 1H, *J* = 12.5 Hz), 3.47 (br s, 4H), 3.35 (br s, 4H), 3.27-3.19 (m, 2H), 3.18-3.11 (m, 2H), 3.11-3.05 (m, 1H), 2.52 (s, 3H), 2.48-2.40 (m, 2H), 2.40-2.20 (m, 4H), 2.13 (m, 2H), 1.74-1.62 (m, 1H), 1.62 (s, 6H), 1.48-1.42 (m, 4H), 1.36-1.27 (m, 2H), 1.00 (s, 9H).

IR (ATR): ν (cm^{-1}) = 3278, 2955, 2926, 2855, 1689, 1617, 1200.

HRMS (ESI): *m/z* calculated for: C$_{58}$H$_{75}$N$_{13}$O$_7$S [M+H]$^+$, 1098.5706, found: 1098.5689.

HPLC: 95.1% purity, t_R = 8.73 min.

(2S,4R)-4-Hydroxy-1-[(2S)-2-[8-(4-{4-[4-({1-[6-(2-hydroxypropan-2-yl)pyridin-2-yl]-3-oxo-2-(prop-2-en-1-yl)-1H,2H,3H-pyrazolo[3,4-d]pyrimidin-6-yl}amino)phenyl]piperazin-1-yl}butanamido)octanamido]-3,3-dimethylbutanoyl]-N-{[4-(4-methyl-1,3-thiazol-5-yl)phenyl]methyl}pyrrolidine-2-carboxamide (21c – MA053)
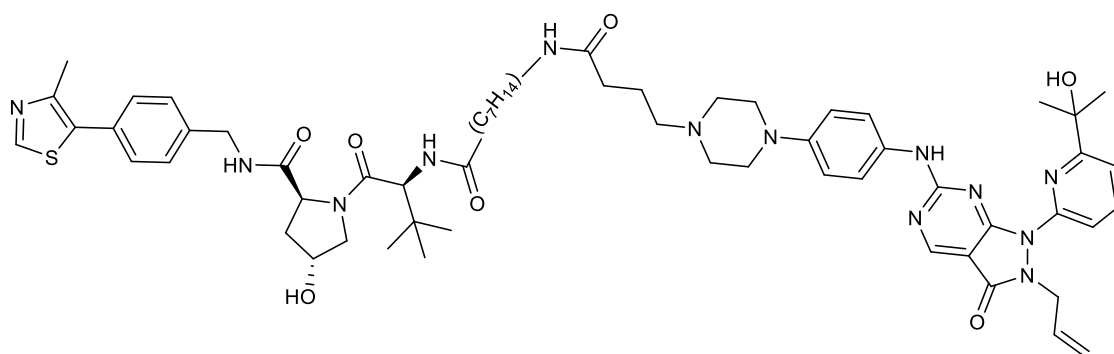
The crude product was purified by column chromatography on silica gel using 5% MeOH in DCM to afford the product **21c** (13 mg, 0.01 mmol, 54%) as a yellow solid.

TLC: R_f = 0.20 (1:9 MeOH/DCM); UV.

^{1}H-NMR (400 MHz, CDCl$_3$): δ (ppm) = 8.81 (s, 1H), 8.69 (s, 1H), 7.90 (t, 1H, J = 7.7 Hz), 7.72 (d, 1H, J = 8.0 Hz), 7.57-7.48 (m, 3H), 7.44-7.32 (m, 5H), 6.94-6.82 (m, 2H), 6.49 (d, 1H, J = 8.8 Hz), 5.76-5.64 (m, 1H), 5.05 (d, 1H, J = 10.1 Hz), 4.94 (d, 1H, J = 17.2 Hz), 4.78-4.66 (m, 3H), 4.63-4.53 (m, 2H), 4.34 (dd, 1H, J = 15.2, 5.1 Hz), 4.07 (d, 1H, J = 12.0 Hz), 3.47-3.32 (m, 4H), 3.20 (br s, 4H), 3.01 (br s, 2H), 2.51 (s, 3H), 2.37 (br s, 2H), 2.23-2.14 (m, 2H), 2.13-1.54 (m, 1H), 1.60 (s, 6H), 1.49-1.44 (m, 8H), 1.30-1.24 (m, 6H), 0.97 (br s, 6H).

IR (ATR): v (cm^{-1}) = 3295, 2959, 2926, 1669, 1619.

HRMS (ESI): m/z calculated for: C$_{55}$H$_{80}$N$_{15}$O$_9$S [M+NH$_4$]$^+$, 1126.5979, found: 1126.6074.

HPLC: 90.8% purity, t_R = 8.65 min.

(2*S*,4*R*)-4-Hydroxy-1-[(2*S*)-2-[11-(4-{4-[4-({1-[6-(2-hydroxypropan-2-yl)pyridin-2-yl]-3-oxo-2-(prop-2-en-1-yl)-1H,2H,3H-pyrazolo[3,4-d]pyrimidin-6-yl}amino)phenyl]piperazin-1-yl}butanamido)undecanamido]-3,3-dimethylbutanoyl]-N-{[4-(4-methyl-1,3-thiazol-5-yl)phenyl]methyl}pyrrolidine-2-carboxamide (21d – MA054)
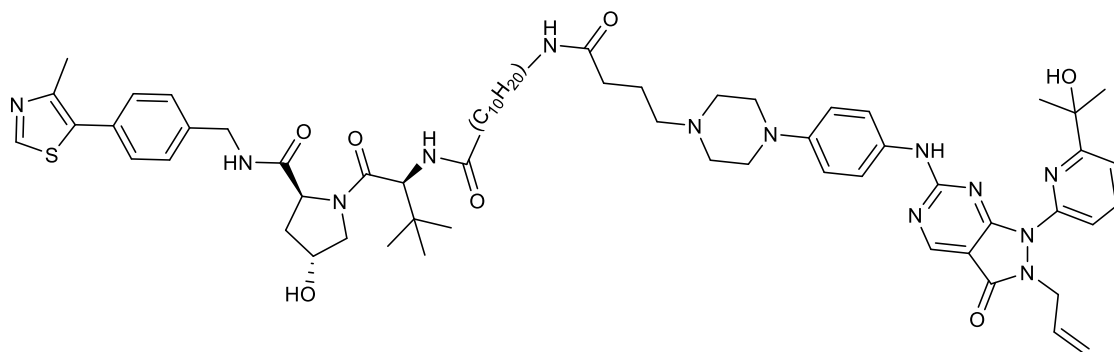
The crude product was purified by column chromatography on silica gel using 5% MeOH in DCM to afford the product **21d** (12 mg, 0.01 mmol, 48%) as a yellow solid.

TLC: R_f = 0.20 (1:9 MeOH/DCM); UV.

^{1}H-NMR (400 MHz, CDCl$_3$): δ (ppm) = 8.80 (s, 1H), 8.66 (s, 1H), 7.85 (t, 1H, *J* = 8.0 Hz), 7.72 (d, 1H, *J* = 8.0 Hz), 7.54-7.43 (m, 3H), 7.38-7.31 (m, 5H), 6.89 (d, 2H, *J* = 8.9 Hz), 6.60-6.52 (m, 1H), 6.31 (d, 1H, *J* = 8.7 Hz), 5.73-5.63 (m, 1H), 5.05 (d, 1H, *J* = 10.9, 1.1 Hz), 4.94 (d, 1H, *J* = 17.1, 1.1 Hz), 4.77-4.68 (m, 2H), 4.61-4.51 (m, 3H), 4.31 (dd, 1H, *J* = 15.1, 5.2 Hz), 4.07 (d, 1H, *J* = 11.4 Hz), 3.64-3.59 (m, 1H), 3.36-3.28 (m, 4H), 3.24-3.17 (m, 2H), 2.91 (br s, 4H), 2.81-2.71 (m, 2H), 2.53-2.45 (m, 4H), 2.35 (t, 2H, *J* = 6.7 Hz), 2.19-2.10 (m, 3H), 2.04-1.95 (m, 2H), 1.58 (s, 6H), 1.53-1.43 (m, 4H), 1.35-1.17 (m, 12H), 0.93 (s, 9H).

IR (ATR): ν (cm^{-1}) = 3281, 2924, 2853, 1669, 1617, 1198.

HRMS (ESI): *m/z* calculated for: C$_{63}$H$_{85}$N$_{13}$O$_7$S [M+H]$^+$, 1168.6488, found: 1168.6500.

HPLC: 94.8% purity, t$_R$ = 9.64 min.

(2*S*,4*R*)-4-Hydroxy-1-[(2*S*)-2-[2-(2-{2-[2-(4-{4-[4-({1-[6-(2-hydroxypropan-2-yl)pyridin-2-yl]-3-oxo-2-(prop-2-en-1-yl)-1H,2H,3H-pyrazolo[3,4-d]pyrimidin-6-yl}amino)phenyl]piperazin-1-yl}butanamido)ethoxy]ethoxy}ethoxy)acetamido]-3,3-dimethylbutanoyl]-N-{[4-(4-methyl-1,3-thiazol-5-yl)phenyl]methyl}pyrrolidine-2-carboxamide (21e – MA086)

The crude product was purified by column chromatography on silica gel using 5% MeOH in DCM to afford the product **21e** (8.2 mg, 0.01 mmol, 33%) as a yellow solid.

TLC: R_f = 0.10 (1:9 MeOH/DCM); UV.

^{1}H-NMR (400 MHz, CDCl$_3$): δ (ppm) = 8.84 (s, 1H), 8.69 (s, 1H), 7.89 (t, 1H, *J* = 8.0 Hz), 7.75 (dd, 1H, *J* = 8.0, 0.5 Hz), 7.54 (br s, 1H), 7.50 (d, 2H, *J* = 9.0 Hz), 7.39-7.34 (m, 6H), 6.92 (d, 2H, *J* = 9.0 Hz), 5.77-5.66 (m, 1H), 5.06 (dd, 1H, *J* = 10.4, 1.2 Hz), 5.96 (dd, 1H, *J* = 17.1, 1.4 Hz), 4.80-4.70 (m, 3H), 4.65-4.53 (m, 3H), 4.35 (dd, 1H, *J* = 15.0, 5.3 Hz), 4.11-4.00 (m, 4H), 3.74-3.60 (m, 10H), 3.57-3.52 (m, 2H), 3.47-3.38 (m, 2H), 3.25 (br s, 4H), 2.78 (br s, 4H), 2.54-2.50 (m, 4H), 2.49-2.44 (m, 1H), 2.32 (br t, 2H, *J* = 6.9 Hz), 2.24-2.15 (m, 1H), 1.96-1.87 (m, 2H), 1.61 (s, 6H), 1.01 (s, 9H).

IR (ATR): ν (cm^{-1}) = 3377, 3000, 2926, 1650, 1619, 1533.

HRMS (ESI): *m/z* calculated for: C$_{60}$H$_{79}$N$_{13}$O$_{10}$S [M+H]$^+$, 1174.5866, found: 1174.5844.

HPLC: 91.5% purity, t_R = 8.65 min.

(2S,4R)-4-Hydroxy-1-[(2S)-2-[1-(4-{4-[4-({1-[6-(2-hydroxypropan-2-yl)pyridin-2-yl]-3-oxo-2-(prop-2-en-1-yl)-1H,2H,3H-pyrazolo[3,4-d]pyrimidin-6-yl}amino)phenyl]piperazin-1-yl}butanamido)-3,6,9,12-tetraoxapentadecan-15-amido]-3,3-dimethylbutanoyl]-N-{[4-(4-methyl-1,3-thiazol-5-yl)phenyl]methyl}pyrrolidine-2-carboxamide (21f – MA088)
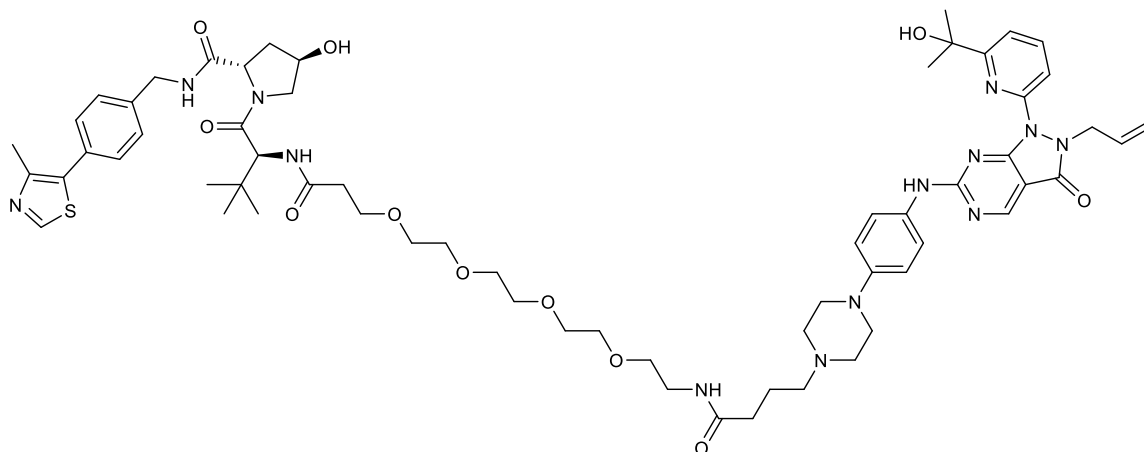
The crude product was purified by column chromatography on silica gel using 5% MeOH in DCM to afford the product **21f** (6.4 mg, 0.01 mmol, 25%) as a yellow solid.

TLC: R_f = 0.10 (1:9 MeOH/DCM); UV.

^{1}H-NMR (400 MHz, CDCl$_3$): δ (ppm) = 8.84 (s, 1H), 8.68 (s, 1H), 7.89 (t, 1H, J = 7.9 Hz), 7.75 (dd, 1H, J = 8.0, 0.6 Hz), 7.55-7.43 (m, 3H), 7.39-7.34 (m, 5H), 7.05 (br s, 1H), 6.92 (d, 2H, J = 9.0 Hz), 5.77-5.66 (m, 1H), 5.06 (dd, 1H, J = 10.2, 1.1 Hz), 4.95 (dd, 1H, J = 17.1, 1.1 Hz), 4.78-4.71 (m, 3H), 4.60 (dd, 1H, J = 15.0, 6.6 Hz), 4.56-4.49 (m, 2H), 4.35 (dd, 1H, J = 15.0, 5.2 Hz), 4.11 (d, 1H, J = 11.4 Hz), 4.05 (br s, 1H), 3.72 (t, 2H, J = 5.3 Hz), 3.69-3.55 (m, 15H), 3.50-3.40 (m, 2H), 3.24 (br s, 4H), 2.76 (br s, 4H), 2.62-2.54 (m, 2H), 2.54-2.50 (m, 4H), 2.51-2.41 (m, 1H), 2.32 (t, 2H, J = 7.1 Hz), 2.24-2.16 (m, 1H), 1.5-1.86 (m, 4H), 1.61 (s, 6H), 0.98 (s, 9H).

IR (ATR): ν (cm^{-1}) = 3399, 2957, 2931, 1654, 1916, 1533.

HRMS (ESI): *m/z* calculated for: C$_{63}$H$_{85}$N$_{13}$O$_{11}$S [M+H]$^+$, 1232.6285, found: 1232.6296.

HPLC: 93.2% purity, t_R = 8.64 min.

3.4.5 Synthesis of the CRBN ligand

2-(2,6-Dioxo-3-piperidinyl)-4-fluoro-1H-isoindole-1,3(2H)-dione (24) (Au - Lindner *et al.*, 2019)
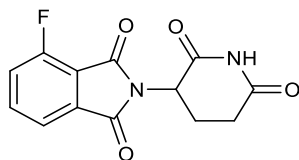
4-Fluoro-2-benzofuran-1,3-dione **23** (2.5 g, 15 mmol, 1.0 eq) and 3-Amino-2,6-piperidindionhydrobromide salt **22** (3.1 g, 15 mmol, 1.0 eq) were dissolved in AcOH (50 mL). Potassium acetate (4.9 g, 50 mmol, 3.3 eq) was then added to the reaction mixture and it was heated to 90 °C with a condenser for 18 h. The mixture was cooled to r.t. and the solvent was evaporated. The residue was resuspended in water (5 mL) and filtered to afford a dark grey crude. The crude product was then purified by column chromatography on silica gel with a gradient of 5-10% of MeOH in DCM to give a beige solid **24** (3.10 g, 10.5 mmol, 75%).

TLC: R_f = 0.80 (1:9 MeOH/DCM); UV.

^{1}H-NMR (400 MHz, d_6-DMSO): δ (ppm) = 8.01 (br s, 1H), 7.83-7.77 (m, 1H), 7.71 (d, 1H, J = 7.0 Hz), 7.44 (td, 1H, J = 8.6, 0.8 Hz), 4.98 (dd, 1H, J = 12.4, 5.3 Hz), 2.98-2.70 (m, 3H), 2.22-2.13 (m, 1H).

^{13}C-NMR (101 MHz, CDCl$_3$): δ (ppm) = 173.2, 170.1, 166.6, 166.6, 164.4, 158.6, 156.0, 138.6, 138.5, 133.9, 123.6, 123.4, 120.5, 120.5, 117.6, 117.4, 49.5, 31.4, 22.3.

IR (ATR): ν (cm^{-1}) = 3190, 3091, 2883, 1712 (s, C=O), 1697 (s, C=O).

Spectral data matched those reported in the literature.

3.4.6 CRBN ligand coupling to linkers

25a-g were prepared following general procedure **B** for nucleophilic aromatic substitution from fluoro-substituted thalidomide **24** and linkers **L$_{g-m}$**.

Tert-Butyl N-(2-{[2-(2,6-dioxopiperidin-3-yl)-1,3-dioxo-2,3-dihydro-1H-isoindol-4-yl]amino}ethyl)carbamate (25a)
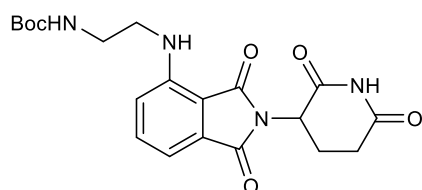
The crude product was purified by column chromatography on silica gel using 5% MeOH in DCM to afford the product **25a** (934 mg, 2.20 mmol, 41%) as a green solid.
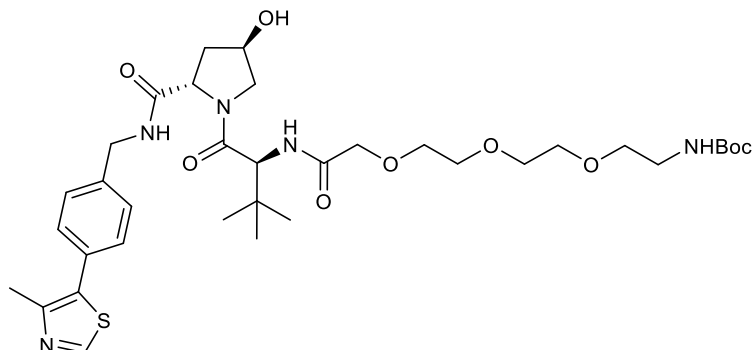
TLC: R_f = 0.60 (5:95 MeOH/DCM); UV.

^{1}H-NMR (400 MHz, CDCl$_3$): δ (ppm) = 7.99 (br s, 1H), 7.53 (dd, 1H, J = 8.5, 7.1 Hz), 7.15 (d, 1H, J = 7.1 Hz), 7.01 (d, 1H, J = 8.5 Hz), 6.42 (br s, 1H), 4.94 (dd, 1H, J = 12.3, 5.4 Hz), 4.83 (br s, 1H), 3.50-3.44 (m, 2H), 3.42-3.35 (m, 2H), 2.92-2.70 (m, 3H), 2.18-2.12 (m, 1H), 1.47 (s, 9H).

^{13}C-NMR (101 MHz, CDCl$_3$): δ (ppm) = 171.1, 169.4, 168.3, 167.5, 156.5, 146.9, 136.3, 132.5, 116.7, 111.9, 110.3, 79.8, 48.9, 42.5, 40.1, 31.4, 28.4, 28.2, 22.8.

IR (ATR): ν (cm^{-1}) = 3401 (w, N-H), 3365, 3205, 2960, 2920, 1712, 1694, 1681.

HRMS (ESI): m/z calculated for: C$_{20}$H$_{24}$N$_4$O$_6$Na [M+Na]$^+$, 439.1588, found: 439.1594.

Tert-Butyl N-(6-{[2-(2,6-dioxopiperidin-3-yl)-1,3-dioxo-2,3-dihydro-1H-isoindol-4-yl]amino}hexyl)carbamate (25b)
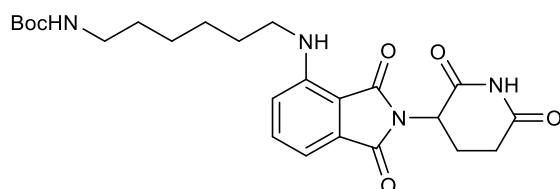
The crude product was purified by column chromatography on silica gel using 3% MeOH in DCM to afford the product **25b** (180 mg, 0.38 mmol, 53%) as a green solid.

TLC: R_f = 0.65 (5:95 MeOH/DCM); UV.

^{1}H-NMR (400 MHz, CDCl$_3$): δ (ppm) = 8.35 (br s, 1H), 7.49 (dd, 1H, J = 8.3, 7.4 Hz), 7.09 (d, 1H, J = 7.3 Hz), 6.88 (d, 1H, J = 8.4 Hz), 6.24 (br t, 1H, J =5.5 Hz), 4.93 (dd, 1H, J = 12.0, 5.4 Hz), 4.57 (br s, 1H), 3.32-3.22 (m, 2H), 3.18-3.06 (m, 2H), 2.94-2.67 (m, 3H), 2.16-2.09 (m, 1H), 1.67 (p, 2H, J = 7.1 Hz), 1.56-1.31 (m, 15H).

^{13}C-NMR (101 MHz, CDCl$_3$): δ (ppm) = 171.1, 169.5, 168.4, 167.6, 147.0, 136.1, 132.5, 116.6, 111.4, 109.9, 48.9, 42.6, 40.4, 31.6, 31.4, 30.0, 29.2, 28.4, 26.6, 26.5, 22.8, 22.7.

IR (ATR): ν (cm^{-1}) = 3386 (w, N-H), 3199, 3091, 2927, 2857, 1686.

HRMS (ESI): m/z calculated for: C$_{24}$H$_{32}$N$_4$O$_6$Na [M+Na]$^+$, 495.2214, found: 495.2207.

Tert-Butyl N-[2-(2-{[2-(2,6-dioxopiperidin-3-yl)-1,3-dioxo-2,3-dihydro-1H-isoindol-4-yl]amino}ethoxy)ethyl]carbamate (25c)
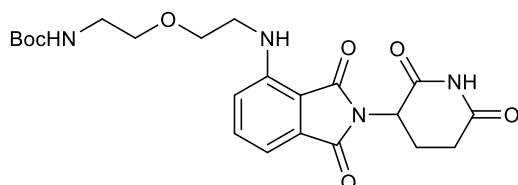
The crude product was purified by column chromatography on silica gel using 3% MeOH in DCM to afford the product **25c** (40 mg, 0.09 mmol, 24%) as a green solid.

TLC: R_f = 0.60 (5:95 MeOH/DCM); UV.

^{1}H-NMR (400 MHz, CDCl$_3$): δ (ppm) = 8.70 (s, 1H), 7.49 (dd, 1H, J = 8.4, 7.2 Hz), 7.10 (d, 1H, J = 7.2 Hz), 6.92 (d, 1H, J = 8.4 Hz), 6.51 (br t, 1H, J = 5.6 Hz), 5.05 (t, 1H, J = 5.5 Hz), 4.93 (dd, 1H, J = 15.3, 5.3 Hz), 3.69 (t, 2H, J = 5.3 Hz), 3.55 (t, 2H, J = 3.5 Hz), 3.49-3.42 (m, 2H), 3.36-3.29 (m, 2H), 2.90-2.71 (m, 3H), 2.19-2.09 (m, 1H), 1.42 (s, 9H).

^{13}C-NMR (101 MHz, CDCl$_3$): δ (ppm) = 171.4, 169.4, 168.6, 167.6, 156.0, 146.8, 136.1, 132.5, 116.8, 111.7, 110.4, 79.2, 70.3, 69.3, 48.9, 42.2, 40.4, 31.4, 28.4, 22.7.

IR (ATR): ν (cm^{-1}) = 3380, 3109, 2920, 2853, 1694, 1625.

HRMS (ESI): *m/z* calculated for: C$_{17}$H$_{20}$N$_4$O$_5$ [M-Boc+H]$^+$, 361.1506, found: 361.1500.

Tert-Butyl N-{2-[2-(2-{[2-(2,6-dioxopiperidin-3-yl)-1,3-dioxo-2,3-dihydro-1H-isoindol-4-yl]amino}ethoxy)ethoxy]ethyl}carbamate (25d)
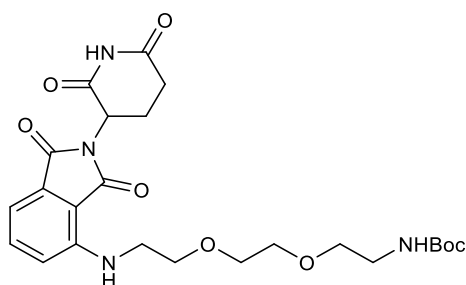
The crude product was purified by column chromatography on silica gel using 5% MeOH in DCM to afford the product **25d** (35 mg, 0.07 mmol, 19%) as a green solid.

TLC: R_f = 0.55 (5:95 MeOH/DCM); UV.

^{1}H-NMR (400 MHz, CDCl$_3$): δ (ppm) = 8.94 (s, 1H), 7.47 (dd, 1H, *J* = 8.4, 7.2 Hz), 7.08 (d, 1H, *J* = 7.2 Hz), 6.90 (d, 1H, *J* = 8.4 Hz), 6.50 (t, 1H, *J* = 5.3 Hz), 5.09 (br s, 1H), 4.95-4.84 (m, 1H), 3.71 (t, 2H, *J* = 5.4 Hz), 3.66-3.62 (m, 4H), 3.57-3.52 (m, 2H), 3.49-3.43 (m, 2H), 3.34-3.27 (m, 2H), 2.88-2.70 (m, 3H), 2.14-2.08 (m, 1H), 1.41 (s, 9H).

^{13}C-NMR (101 MHz, CDCl$_3$): δ (ppm) = 171.5, 169.3, 168.7, 167.6, 156.1, 146.8, 136.0, 13.5, 116.7, 111.6, 110.4, 79.2, 70.7, 70.3, 70.1, 68.4, 48.9, 42.3, 40.4, 31.4, 28.4, 22.8.

IR (ATR): ν (cm^{-1}) = 3285, 3106, 2972, 2868, 1690, 1623.

HRMS (ESI): *m/z* calculated for: C$_{24}$H$_{32}$N$_4$O$_8$ [M+H]$^+$, 527.2112, found: 527.2113.

Tert-Butyl N-(2-{2-[2-(2-{[2-(2,6-dioxopiperidin-3-yl)-1,3-dioxo-2,3-dihydro-1H-isoindol-4-yl]amino}ethoxy)ethoxy]ethoxy}ethyl)carbamate (25e)
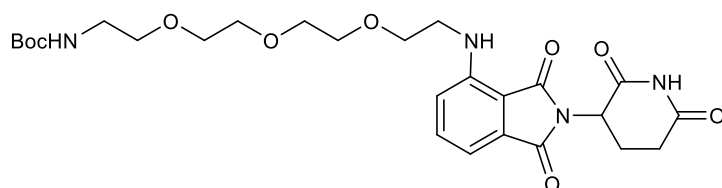
The crude product was purified by column chromatography on silica gel using 5% MeOH in DCM to afford the product **25e** (57 mg, 0.10 mmol, 42%) as a green solid.

TLC: R_f = 0.50 (5:95 MeOH/DCM); UV.

^{1}H-NMR (400 MHz, CDCl$_3$): δ (ppm) = 9.13 (s, 1H), 7.44 (dd, 1H, J = 8.4, 7.2 Hz), 7.04 (d, 1H, J = 7.2 Hz), 6.88 (d, 1H, J = 8.4 Hz), 6.45 (br t, 1H, J = 5.5 Hz), 5.12 (br t, 1H, J = 5.3 Hz), 4.89 (dd, 1H, J = 15.2, 5.3 Hz), 3.70-3.66 (m, 2H), 3.65-3.62 (m, 4H), 3.61-3.58 (m, 2H), 3.58-3.54 (m, 2H), 3.52-3.47 (m, 2H), 3.46-3.40 (m, 2H), 3.29-3.22 (m, 2H), 2.85-2.68 (m, 3H), 2.10-2.06 (m, 1H), 1.39 (s, 9H).

^{13}C-NMR (101 MHz, CDCl$_3$): δ (ppm) = 171.6, 169.3, 168.7, 167.6, 156.0, 146.8, 136.0, 132.5, 116.7, 111.5, 110.3, 79.1, 70.7, 70.5, 70.2, 70.1, 69.5, 48.9, 42.3, 40.3, 31.4, 28.4, 22.7.

IR (ATR): ν (cm^{-1}) = 3384, 3104, 2922, 2868, 1695, 1625.

HRMS (ESI): *m/z* calculated for: C$_{21}$H$_{28}$N$_4$O$_7$ [M-Boc+H]$^+$, 449.2031, found: 449.2053.

***Tert*-Butyl N-(14-{[2-(2,6-dioxopiperidin-3-yl)-1,3-dioxo-2,3-dihydro-1H-isoindol-4-yl]amino}-3,6,9,12-tetraoxatetradecan-1-yl)carbamate (25f)**
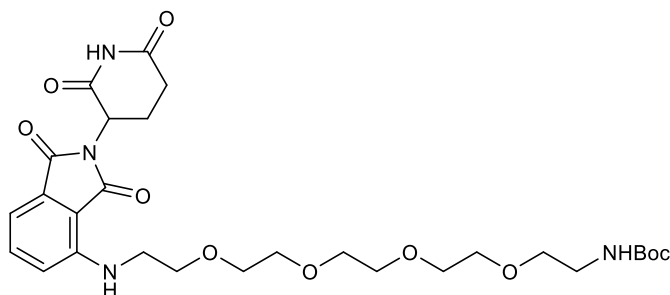
The crude product was purified by column chromatography on silica gel using 5% MeOH in DCM to afford the product **25f** (70 mg, 0.12 mmol, 47%) as a green solid.

TLC: R_f = 0.55 (5:95 MeOH/DCM); UV.

^{1}H-NMR (400 MHz, CDCl$_3$): δ (ppm) = 8.86 (s, 1H), 7.47 (dd, 1H, J = 8.5, 7.1 Hz), 7.07 (d, 1H, J = 7.14 Hz), 6.91 (d, 1H, J = 8.5 Hz), 6.48 (br t, 1H, J = 5.4 Hz), 5.14 (br s, 1H), 4.91 (dd, 1H, J = 15.1, 5.5 Hz), 3.70 (t, 2H, J = 5.4 Hz), 3.67-3.58 (m, 12H), 3.52 (t, 2H, J = 5.1 Hz), 3.48-3.42 (m, 2H), 3.32-3.24 (m, 2H), 2.89-2.69 (m, 3H), 2.13-2.07 (m, 1H), 1.42 (s, 9H).

^{13}C-NMR (101 MHz, CDCl$_3$): δ (ppm) = 171.5, 169.3, 168.6, 167.6, 156.0, 146.8, 136.0, 132.5, 116.8, 111.6, 110.3, 79.1, 70.7, 70.6, 70.6, 70.4, 69.5, 48.9, 42.4, 40.3, 31.4, 28.4, 22.8.

IR (ATR): ν (cm^{-1}) = 3397, 3106, 3084, 2873, 1690, 1671, 1625.

HRMS (ESI): *m/z* calculated for: C$_{23}$H$_{32}$N$_4$O$_8$ [M-Boc+H]$^+$, 493.2291, found: 492.2281.

Tert-Butyl N-(17-{[2-(2,6-dioxopiperidin-3-yl)-1,3-dioxo-2,3-dihydro-1H-isoindol-4-yl]amino}-3,6,9,12,15-pentaoxaheptadecan-1-yl)carbamate (25g)
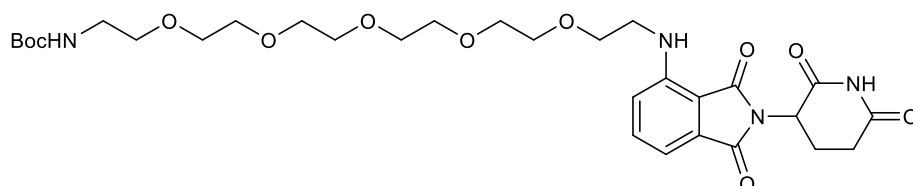
The crude product was purified by column chromatography on silica gel using 5% MeOH in DCM to afford the product **25g** (57 mg, 0.09 mmol, 63%) as a green solid.

TLC: R_f = 0.50 (5:95 MeOH/DCM); UV.

^{1}H-NMR (400 MHz, CDCl$_3$): δ (ppm) = 8.71 (s, 1H), 7.48 (dd, 1H, J = 8.5, 7.1 Hz), 7.09 (d, 1H, J = 7.1 Hz), 6.92 (d, 1H, J = 8.52 Hz), 6.48 (br s, 1H), 5.12 (br s, 1H), 4.92 (dd, 1H, J = 12.1, 5.5 Hz), 3.72 (t, 2H, J = 5.4 Hz), 3.68-3.64 (m, 12H), 3.63-3.52 (m, 4H), 3.53 (t, 2H, J = 5.1 Hz), 3.49-3.43 (m, 2H), 3.33-3.26 (m, 2H), 2.89-2.68 (m, 3H), 2.14-2.08 (m, 1H), 1.44 (s, 9H).

^{13}C-NMR (101 MHz, CDCl$_3$): δ (ppm) = 171.3, 169.3, 168.5, 167.6, 156.0, 146.8, 136.0, 132.5, 116.8, 111.6, 110.3, 79.1, 70.7, 70.6, 70.6, 70.5, 70.4, 70.2, 69.5, 48.9, 42.4, 40.3, 31.4, 28.4, 22.9.

IR (ATR): ν (cm^{-1}) = 3388, 3091, 2873, 1694, 1623.

HRMS (ESI): m/z calculated for: C$_{25}$H$_{36}$N$_4$O$_9$ [M-Boc+H]$^+$, 537.2555, found: 537.2636.

Compounds **27a-f** were prepared following general procedure **D** for Boc deprotection of **25a** and then general procedure **A** for HATU-mediated amide coupling to attach them to alkyl linkers **L$_{a-d}$** and PEG linkers **L$_{e-f}$**.

***Tert*-Butyl N-{3-[(2-{[2-(2,6-dioxopiperidin-3-yl)-1,3-dioxo-2,3-dihydro-1H-isoindol-4-yl]amino}ethyl)carbamoyl]propyl}carbamate (27a)**
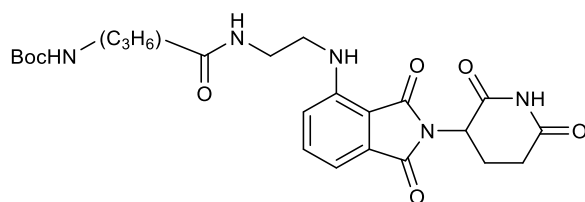
The crude product was purified by column chromatography on silica gel using 5% MeOH in DCM to afford the product **27a** (45 mg, 0.09 mmol, 66%) as a green solid.

TLC: R_f = 0.60 (5:95 MeOH/DCM); UV.

^{1}H-NMR (400 MHz, CDCl$_3$): δ (ppm) = 9.00 (s, 1H), 7.52-7.46 (m, 1H), 7.09 (d, 1H, *J* = 7.1 Hz), 6.98 (d, 1H, *J* = 8.5 Hz), 6.95 (br s, 1H), 6.44 (br s, 1H), 4.99-4.91 (m, 1H), 3.51-3.40 (m, 4H), 3.18-3.05 (m, 2H), 2.87-2.69 (m, 3H), 2.20 (t, 2H, *J* = 7.2 Hz), 2.18-2.16 (m, 2H), 2.14-2.08 (m, 1H), 1.77 (p, 2H, *J* = 6.9 Hz), 1.42 (s, 9H).

^{13}C-NMR (101 MHz, CDCl$_3$): δ (ppm) = 173.6, 171.7, 169.4, 169.1, 167.6, 156.6, 146.8, 136.3, 132.5, 116.9, 111.8, 110.2, 79.4, 53.5, 42.1, 38.9, 33.4, 31.4, 30.9, 28.4, 26.3, 22.8.

IR (ATR): ν (cm^{-1}) = 3370, 2970, 2910, 1699, 1624.

***Tert*-Butyl N-{5-[(2-{[2-(2,6-dioxopiperidin-3-yl)-1,3-dioxo-2,3-dihydro-1H-isoindol-4-yl]amino}ethyl)carbamoyl]pentyl}carbamate (27b)**
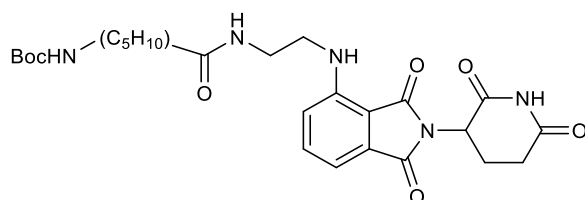
The crude product was purified by column chromatography on silica gel using 5% MeOH in DCM to afford the product **27b** (51 mg, 0.09 mmol, 70%) as a green solid.
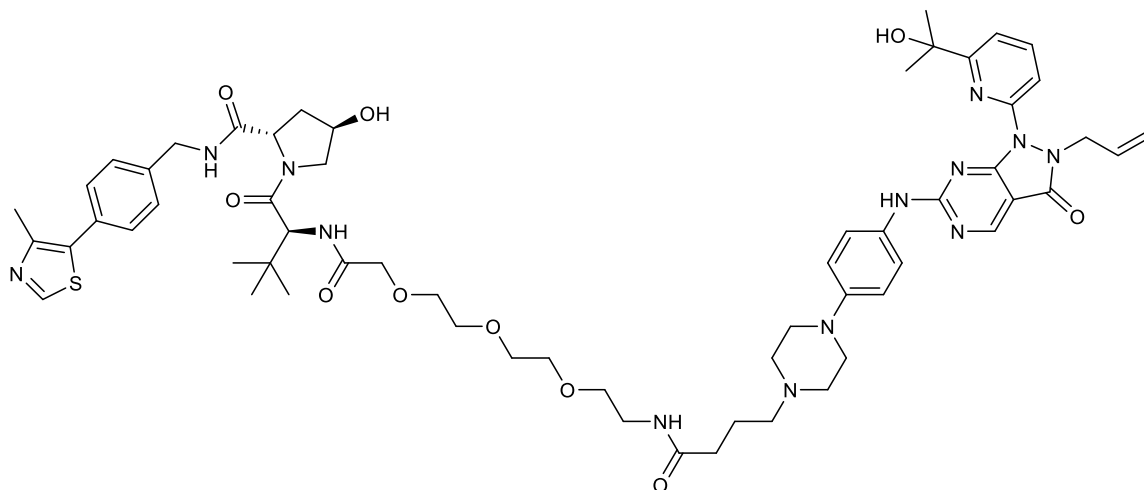
TLC: R_f = 0.55 (5:95 MeOH/DCM); UV.

^{1}H-NMR (400 MHz, CDCl$_3$): δ (ppm) = δ 8.84 (s, 1H), 7.53-7.48 (m, 1H), 7.13-7.09 (m, 1H), 6.99 (d, 1H, J = 8.6 Hz), 6.44-6.30 (m, 2H), 4.98-4.91 (m, 1H), 4.71 (br s, 1H), 3.53-3.40 (m, 4H), 3.13-3.02 (m, 2H), 2.79-2.73 (m, 1H), 2.17 (t, 1H, J = 7.3 Hz), 1.62 (p, 2H, J = 7.3 Hz), 1.47-1.40 (m, 11H), 1.36-1.27 (m, 2H).

IR (ATR): v (cm^{-1}) = 3375, 2965, 2920, 1690, 1623.

Tert-Butyl N-{7-[(2-{[2-(2,6-dioxopiperidin-3-yl)-1,3-dioxo-2,3-dihydro-1H-isoindol-4-yl]amino}ethyl)carbamoyl]heptyl}carbamate (27c)

The crude product was purified by column chromatography on silica gel using 5% MeOH in DCM to afford the product **27c** (26 mg, 0.05 mmol, 34%) as a green solid.

TLC: R_f = 0.55 (5:95 MeOH/DCM); UV.

^{1}H-NMR (400 MHz, CDCl$_3$): δ (ppm) = 8.83 (br s, 1H), 7.50 (dd, 1H, J = 8.5, 7.2 Hz), 7.11 (d, 1H, J = 7.2 Hz), 7.00 (d, 1H, J = 8.5 Hz), 6.48-6.30 (m, 2H), 4.97-4.91 (m, 1H), 4.63 (br s, 1H), 3.46 (br s, 4H), 3.14-3.00 (m, 2H), 2.92-2.73 (m, 3H), 2.17-2.08 (m, 3H), 1.59 (p, 2H, J = 7.6 Hz), 1.44 (s, 13H), 1.30-1.26 (m, 4H).

^{13}C-NMR (101 MHz, CDCl$_3$): δ (ppm) = 174.1, 171.5, 169.5, 168.9, 167.6, 146.8, 136.8, 132.4, 116.8, 111.9, 110.2, 79.1, 48.9, 42.1, 40.5, 39.1, 36.4, 31.5, 29.9, 29.1, 28.8, 28.5, 26.5, 25.5, 22.7.

IR (ATR): v (cm^{-1}) = 3375, 2980, 2920, 1695, 1630.

Tert-Butyl N-{10-[(2-{[2-(2,6-dioxopiperidin-3-yl)-1,3-dioxo-2,3-dihydro-1H-isoindol-4-yl]amino}ethyl)carbamoyl]decyl}carbamate (27d)
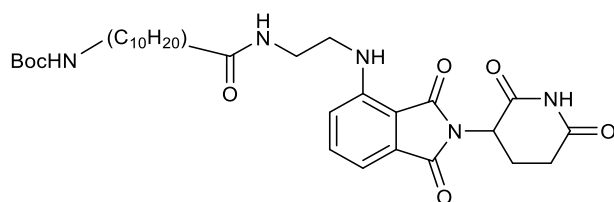
The crude product was purified by column chromatography on silica gel using 5% MeOH in DCM to afford the product **27d** (62 mg, 0.10 mmol, 74%) as a green solid.

TLC: R_f = 0.55 (5:95 MeOH/DCM); UV.

^{1}H-NMR (400 MHz, CDCl$_3$): δ (ppm) = 9.43 (s, 1H), 7.41 (dd, 1H, J = 8.5, 7.2 Hz), 6.99 (d, 1H, J = 7.2 Hz), 6.95 (d, 1H, J = 8.5 Hz), 6.82 (br s, 1H), 6.37 (br s, 1H), 4.89-4.82 (m, 1H), 4.74 (br t, 1H, J = 7.2 Hz), 3.42-3.34 (m, 4H), 3.05-2.95 (m, 2H), 2.73-2.65 (m, 1H), 2.08 (t, 2H, J = 7.6 Hz), 2.06-2.00 (m, 1H), 1.51 (p, 2H, J = 7.6 Hz), 1.42-1.32 (m, 4H), 1.36 (s, 9H), 1.24-1.12 (m, 12H).

IR (ATR): ν (cm^{-1}) = 3370, 2970, 2910, 1695, 1620.

Tert-Butyl N-[2-(2-{[(2-{[2-(2,6-dioxopiperidin-3-yl)-1,3-dioxo-2,3-dihydro-1H-isoindol-4-yl]amino}ethyl)carbamoyl]methoxy}ethoxy)ethyl]carbamate (27e)

The crude product was purified by column chromatography on silica gel using 5% MeOH in DCM to afford the product **27e** (43 mg, 0.08 mmol, 64%) as a green solid.

TLC: R_f = 0.65 (1:9 MeOH/DCM); UV.

^{1}H-NMR (400 MHz, CDCl$_3$): δ (ppm) = 8.74 (s, 1H), 7.51 (dd, 1H, J = 8.4, 7.2 Hz), 7.38 (br s, 1H), 7.10 (d, 1H, J = 7.2 Hz), 7.01 (d, 1H, J = 8.4 Hz), 6.47 (br t, 1H, J = 5.7 Hz), 5.03 (br s, 1H), 4.94 (dd, 1H, J = 11.9, 5.4 Hz), 4.00 (s, 2H), 3.61 (s, 4H), 3.58-3.47 (m, 6H), 3.32-3.24 (m, 2H), 2.91-2.72 (m, 3H), 2.16-2.10 (m, 1H), 1.43 (s, 9H).

^{13}C-NMR (101 MHz, CDCl$_3$): δ (ppm) = 171.5, 170.9, 169.4, 167.6, 156.1, 146.7, 136.3, 132.5, 116.8, 111.9, 110.3, 79.5, 70.8, 70.4, 70.2, 69.9, 48.9, 41.9, 40.3, 38.4, 31.4, 28.4, 22.7.

IR (ATR): ν (cm^{-1}) = 3370, 2972, 2915, 1690, 1625.

HRMS (ESI): *m/z* calculated for: C$_{21}$H$_{27}$N$_5$O$_7$ [M-Boc+H]$^+$, 462.1983, found: 462.1987

Tert-Butyl N-{2-[2-(2-{[(2-{[2-(2,6-dioxopiperidin-3-yl)-1,3-dioxo-2,3-dihydro-1H-isoindol-4-yl]amino}ethyl)carbamoyl]methoxy}ethoxy)ethoxy]ethyl}carbamate (27f)

The crude product was purified using 5% MeOH in DCM to afford the product **27f** (14 mg, 0.04 mmol, 29%) as a green solid.

TLC: R_f = 0.60 (1:9 MeOH/DCM); UV.

^{1}H-NMR (400 MHz, CDCl$_3$): δ (ppm) = 8.57 (s, 1H), 7.55 (br s, 1H), 7.51 (m, 2H, J = 8.5, 7.2 Hz), 7.11 (d, 1H, J = 7.2 Hz), 7.02 (d, 1H, J = 8.52 Hz), 6.49 (br s, 1H), 5.14 (br s, 1H), 4.93 (dd, 1H, J = 11.9, 5.4 Hz), 4.05-4.00 (m, 2H), 3.66-3.62 (m, 4H), 3.62-3.57 (m, 4H), 3.57-3.48 (m, 6H), 3.30 (br s, 2H), 2.93-2.69 (m, 3H), 2.17-2.09 (m, 1H), 1.44 (s, 9H).

^{13}C-NMR (101 MHz, CDCl$_3$): δ (ppm) = 171.3, 171.1, 169.3, 167.6, 156.1, 146.7, 132.5, 116.7, 111.8, 110.3, 79.4, 70.9, 70.3, 70.2, 70.1, 70.1, 48.9, 41.9, 38.4, 31.4, 28.4, 22.8.

IR (ATR): ν (cm^{-1}) = 3375, 2974, 2918, 1692, 1623.

HRMS (ESI): *m/z* calculated for: C$_{28}$H$_{39}$N$_5$O$_{10}$Na [M+Na]$^+$, 628.2589, found: 628.2581.

3.4.7 Wee1 PROTACs recruiting CRBN

26a-g were prepared following general procedure **D** to deprotect **25a-g** and then general procedure **A** for HATU-mediated amide coupling to attach them to AZD1775 analogue **13**.

N-(2-{[2-(2,6-Dioxopiperidin-3-yl)-1,3-dioxo-2,3-dihydro-1H-isoindol-4-yl]amino}ethyl)-4-{4-[4-({1-[6-(2-hydroxypropan-2-yl)pyridin-2-yl]-3-oxo-2-(prop-2-en-1-yl)-1H,2H,3H-pyrazolo[3,4-d]pyrimidin-6-yl}amino)phenyl]piperazin-1-yl}butanamide (26a – MA049)
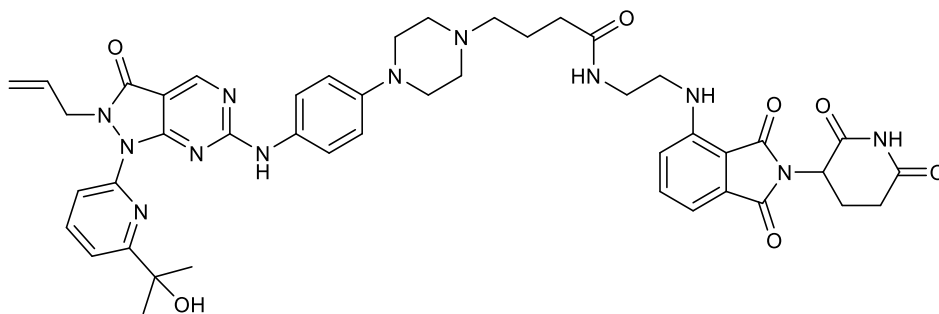
The crude product was purified by column chromatography on silica gel using 5% MeOH in DCM to afford the product **26a** (3.5 mg, 0.01 mmol, 17%) as a green solid.

TLC: R_f = 0.10 (1:9 MeOH/DCM); UV.

^{1}H-NMR (400 MHz, CDCl$_3$): δ (ppm) = 8.84 (s, 1H), 7.91 (t, 1H, *J* = 7.9 Hz), 7.72 (d, 1H, *J* = 7.9 Hz), 7.54 (t, 1H, *J* = 7.9 Hz), 7.47 (br d, 1H, *J* = 8.9 Hz), 7.40 (d, 1H, *J* = 7.7 Hz), 7.16 (d, 1H, *J* = 7.0 Hz), 7.00 (d,1H, *J* = 8.7 Hz), 6.84 (br d, 2H, *J* = 8.9 Hz), 6.58 (br s, 1H), 5.80-5.68 (m, 1H), 5.11-5.07 (m, 1H), 5.02-4.91 (m, 2H), 4.75 (d, 2H, *J* = 6.2 Hz), 3.99 (s, 1H), 3.63-3.51 (m, 4H), 3.36 (s, 1H), 2.93-2.63 (m, 7H), 2.57-2.34 (m, 2H), 2.20-2.04 (m, 3H), 1.62 (s, 6H), 1.32-1.25 (m, 2H).

IR (ATR): v (cm^{-1}) = 3383, 3296, 2926, 2851, 1695, 1625, 1617.

HRMS (ESI): *m/z* calculated for: C$_{45}$H$_{50}$N$_{12}$O$_7$ [M+H]$^+$, 871.3998, found: 871.3993.

HPLC: 96.3% purity, t$_R$ = 8.24 min.

N-(6-{[2-(2,6-Dioxopiperidin-3-yl)-1,3-dioxo-2,3-dihydro-1H-isoindol-4-yl]amino}hexyl)-4-{4-[4-({1-[6-(2-hydroxypropan-2-yl)pyridin-2-yl]-3-oxo-2-(prop-2-en-1-yl)-1H,2H,3H-pyrazolo[3,4-d]pyrimidin-6-yl}amino)phenyl]piperazin-1-yl}butanamide (26b – MA048)

The crude product was purified by column chromatography on silica gel using 5% MeOH in DCM to afford the product **26b** (12 mg, 0.01 mmol, 47%) as a green solid.

TLC: *R*$_f$ = 0.10 (1:9 MeOH/DCM); UV.

^{1}H-NMR (400 MHz, CDCl$_3$): δ (ppm) = 8.85 (s, 1H), 7.89 (t, 1H, *J* = 7.9 Hz), 7.75 (dd, 1H, *J* = 8.0, 0.5 Hz), 7.55-7.43 (m, 3H), 7.38 (dd, 1H, *J* = 7.7, 0.5 Hz), 7.10 (d, 1H, *J* = 6.9 Hz), 7.93-7.86 (m, 3H), 7.55 (br s, 1H), 6.23 (t, 1H, *J* = 5.5 Hz), 5.78-5.65 (m, 1H), 5.06 (dd, 1H, *J* = 10.2, 1.2 Hz), 4.99-4.90 (m, 2H), 4.75 (d, 2H, *J* = 6.2 Hz), 3.41-3.32 (m, 4H), 3.31-3.23 (m, 4H), 2.94 (br s, 4H), 2.91-2.71 (m, 5H), 2.39 (t, 2H, *J* = 6.7 Hz), 2.19-2.11 (m, 1H), 2.06-1.98 (m, 2H), 1.71-1.63 (m, 2H), 1.61 (s, 6H), 1.58-1.52 (m, 2H), 1.46-1.36 (m, 4H).

IR (ATR): v (cm^{-1}) = 3378, 3071, 2929, 2855, 1694, 1620, 1604.

HRMS (ESI): *m/z* calculated for: C$_{49}$H$_{58}$N$_{12}$O$_7$ [M+H]$^+$, 927.4624, found: 927.4616.

HPLC: 97.2% purity, t_R = 9.08 min.

N-[2-(2-{[2-(2,6-Dioxopiperidin-3-yl)-1,3-dioxo-2,3-dihydro-1H-isoindol-4-yl]amino}ethoxy)ethyl]-4-{4-[4-({1-[6-(2-hydroxypropan-2-yl)pyridin-2-yl]-3-oxo-2-(prop-2-en-1-yl)-1H,2H,3H-pyrazolo[3,4-d]pyrimidin-6-yl}amino)phenyl]piperazin-1-yl}butanamide (26c – MA072)

The crude product was purified by column chromatography on silica gel using 5% MeOH in DCM to afford the product **26c** (4.5 mg, 0.01 mmol, 18%) as a green solid.

TLC: R_f = 0.10 (1:9 MeOH/DCM); UV.

^{1}H-NMR (400 MHz, CDCl$_3$): δ (ppm) = 8.84 (s, 1H), 7.90 (t, 1H, J = 7.9 Hz), 7.76 (d, 1H, J = 8.2, 0.5 Hz), 7.54 (dd, J = 8.3, 7.3 Hz, 1H), 7.47 (d, 2H, J = 8.8 Hz), 7.37 (dd, 1H, J = 8.3, 7.3 Hz), 7.16 (d, 1H, J = 7.3 Hz), 6.96-6.87 (m, 3H), 6.80 (br t, 1H, J = 5.6 Hz), 6.73 (br t, 1H, J = 4.8 Hz), 5.77-5.66 (m, 1H), 5.06 (dd, 1H, J = 10.2, 1.1 Hz), 4.99-4.88 (m, 2H), 4.76 (d, 2H, J = 6.1 Hz), 3.83-3.67 (m, 4H), 3.59 (td, 1H, J = 8.9, 2.3 Hz), 3.48-3.40 (m, 2H), 3.39-3.21 (m, 5H), 2.93-2.64 (m, 8H), 2.63-2.52 (m, 1H), 2.34 (t, 2H, J = 7.6 Hz), 2.18-2.11 (m, 1H), 2.01-1.92 (m 2H), 1.61 (s, 6H).

IR (ATR): ν (cm^{-1}) = 3386, 3230, 2920, 2870, 1690, 1670, 1625.

HRMS (ESI): m/z calculated for: C$_{47}$H$_{54}$N$_{12}$O$_8$ [M+H]$^+$, 915.4260, found: 915.4290.

HPLC: 93.4% purity, t_R = 8.44 min.

N-{2-[2-(2-{[2-(2,6-Dioxopiperidin-3-yl)-1,3-dioxo-2,3-dihydro-1H-isoindol-4-yl]amino}ethoxy)ethoxy]ethyl}-4-{4-[4-({1-[6-(2-hydroxypropan-2-yl)pyridin-2-yl]-3-oxo-2-(prop-2-en-1-yl)-1H,2H,3H-pyrazolo[3,4-d]pyrimidin-6-yl}amino)phenyl]piperazin-1-yl}butanamide (26d – MA071)
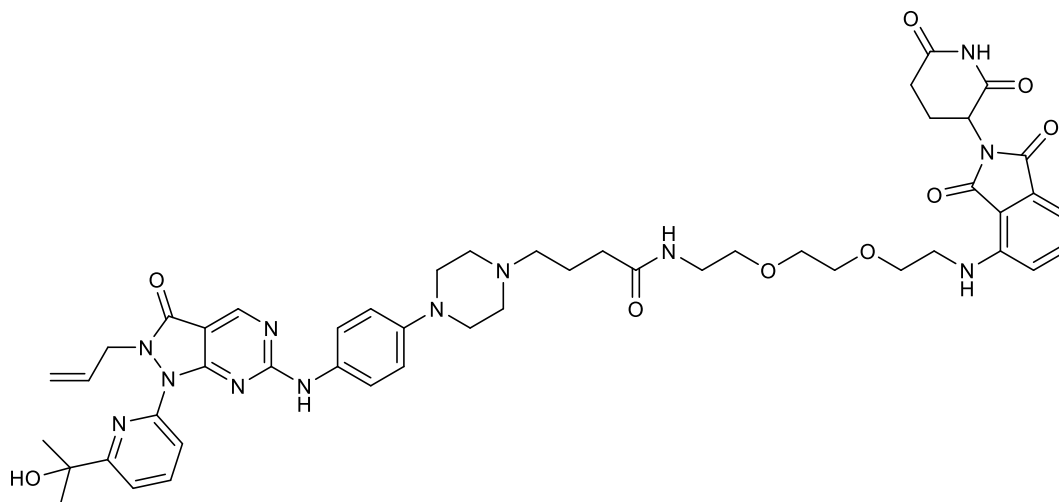
The crude product was purified by column chromatography on silica gel using 5% MeOH in DCM to afford the product **26d** (9.1 mg, 0.01 mmol, 22%) as a green solid.

TLC: R_f = 0.10 (1:9 MeOH/DCM); UV.

^{1}H-NMR (400 MHz, CDCl$_3$): δ (ppm) = 8.81 (s, 1H), 8.01 (t, 1H, J = 7.8 Hz), 7.78 (d, 1H, J = 7.8 Hz), 7.66 (dd, 1H, J = 7.8, 0.6 Hz), 7.59 (d, 2H, J = 9.1 Hz), 7.53 (dd, 1H, J = 8.5, 7.1 Hz), 7.09-7.03 (m, 2H), 6.99 (d, 2H, J = 9.1 Hz), 5.79-5.67 (m, 1H), 5.09-5.02 (m, 2H), 4.96-4.89 (m, 1H), 4.83 (d, 2H, J = 6.1 Hz), 3.74 (t, 2H, J = 5.2 Hz), 3.70-3.65 (m, 4H), 3.59 (t, 2H, J = 5.4 Hz), 3.49 (t, 2H, J = 5.2 Hz), 3.43-3.35 (m, 6H), 3.32-3.26 (br s, 4H), 3.09 (t, 2H, J = 7.0 Hz), 2.88-2.65 (m, 3H), 2.42 (t, 2H, J = 7.0 Hz), 2.15-2.06 (m, 1H), 2.01 (p, 2H, J = 7.0 Hz), 1.59 (s, 6H).

IR (ATR): ν (cm^{-1}) = 3380, 3310, 3230, 2920, 2870, 1697, 1670, 1624.

HRMS (ESI): m/z calculated for: C$_{49}$H$_{58}$N$_{12}$O$_9$ [M+H]$^+$, 959.4522, found: 959.4518.

HPLC: 95.3% purity, t_R = 8.48 min.

N-(2-{2-[2-(2-{[2-(2,6-Dioxopiperidin-3-yl)-1,3-dioxo-2,3-dihydro-1H-isoindol-4-yl]amino}ethoxy)ethoxy]ethoxy}ethyl)-4-{4-[4-({1-[6-(2-hydroxypropan-2-yl)pyridin-2-yl]-3-oxo-2-(prop-2-en-1-yl)-1H,2H,3H-pyrazolo[3,4-d]pyrimidin-6-yl}amino)phenyl]piperazin-1-yl}butanamide (26e – MA073)

The crude product was purified by column chromatography on silica gel using 5% MeOH in DCM to afford the product **26e** (6.4 mg, 0.01 mmol, 26%) as a green solid.

TLC: R_f = 0.10 (1:9 MeOH/DCM); UV.

^{1}H-NMR (400 MHz, CDCl$_3$): δ (ppm) = 8.86 (s, 1H), 7.89 (t, 1H, J = 7.9 Hz), 7.76 (dd, 1H, J = 7.9, 0.5 Hz), 7.52-7.47 (m, 3H), 7.37 (dd, 1H, J = 7.9, 0.5 Hz), 7.12 (d, 1H, J = 7.1 Hz), 6.93-6.89 (m, 3H), 6.77 (br s, 1H), 6.50 (t, 1H, J = 5.5 Hz), 5.78-5.66 (m, 1H), 5.06 (dd, 1H, J = 10.2, 1.1 Hz), 4.99-4.91 (m, 2H), 4.76 (d, 2H, J = 6.2 Hz), 4.02 (s, 1H), 3.78-3.71 (t, 2H, J = 5.3 Hz), 3.70-3.67 (m, 4H), 3.67-3.61 (m, 6H), 3.58 (t, 2H, J = 5.3 Hz), 3.49-3.43 (m, 4H), 3.31 (br s, 4H), 2.93-2.73 (m, 7H), 2.34 (t, 2H, J = 6.9 Hz), 2.17-2.09 (m, 1H), 2.02-1.94 (m, 2H), 1.61 (s, 6H).

IR (ATR): ν (cm^{-1}) = 3300, 3230, 2920, 2885, 1695, 1626.

HRMS (ESI): m/z calculated for: C$_{51}$H$_{62}$N$_{12}$O$_{10}$ [M+H]$^+$, 1003.4785, found: 1003.4760.

HPLC: 95.6% purity, t_R = 8.53 min.

N-(14-{[2-(2,6-Dioxopiperidin-3-yl)-1,3-dioxo-2,3-dihydro-1H-isoindol-4-yl]amino}-3,6,9,12-tetraoxatetradecan-1-yl)-4-{4-[4-({1-[6-(2-hydroxypropan-2-yl)pyridin-2-yl]-3-oxo-2-(prop-2-en-1-yl)-1H,2H,3H-pyrazolo[3,4-d]pyrimidin-6-yl}amino)phenyl]piperazin-1-yl}butanamide (26f – MA074)
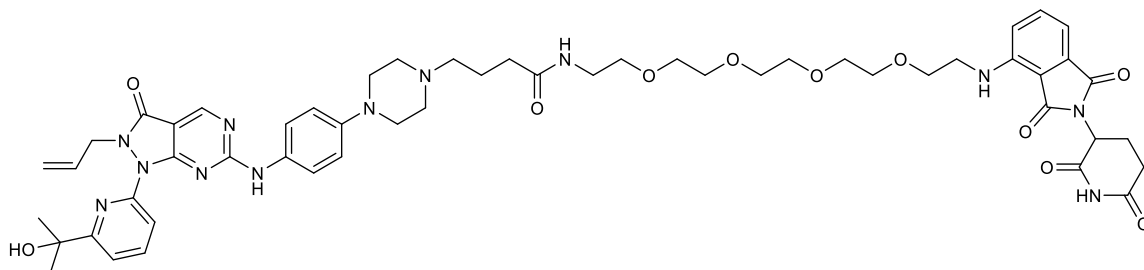
The crude product was purified by column chromatography on silica gel using 5% MeOH in DCM to afford the product **26f** (6.7 mg, 0.01 mmol, 27%) as a green solid.

TLC: R_f = 0.10 (1:9 MeOH/DCM); UV.

^{1}H-NMR (400 MHz, CDCl$_3$): δ (ppm) = 8.86 (s, 1H), 7.90 (t, J = 7.9 Hz, 1H), 7.75 (dd, J = 7.9, 0.3 Hz, 1H), 7.54-7.47 (m, 3H), 7.38 (dd, J = 7.6, 0.3 Hz, 1H), 7.12 (d, J = 7.1 Hz, 1H), 7.05-6.88 (m, 4H), 6.52 (t, J = 5.6 Hz, 1H), 5.78-5.66 (m, 1H), 5.06 (dd, J = 10.2, 1.1 Hz, 1H), 4.99-4.91 (m, 2H), 4.78 (d, J = 6.0 Hz, 2H), 4.02 (s, 1H), 3.74 (t, J = 5.3 Hz, 2H), 3.71-3.63 (m, 14H), 3.60 (t, J = 5.0 Hz, 2H), 3.49-3.44 (m, 4H), 3.36 (br s, 2H), 2.99-2.70 (m, 7H), 2.37 (t, J = 6.7 Hz, 2H), 2.17-2.10 (m, 1H), 1.96-2.05 (m, 2H), 1.60 (s, 6H).

IR (ATR): ν (cm^{-1}) = 3386, 3280, 3215, 2920, 2870, 1700, 1620.

HRMS (ESI): m/z calculated for: C$_{53}$H$_{66}$N$_{12}$O$_{11}$ [M+H]$^+$, 1047.5047, found: 1047.5068.

HPLC: 95.8% purity, t_R = 8.53 min.

N-(17-{[2-(2,6-Dioxopiperidin-3-yl)-1,3-dioxo-2,3-dihydro-1H-isoindol-4-yl]amino}-3,6,9,12,15-pentaoxaheptadecan-1-yl)-4-{4-[4-({1-[6-(2-hydroxypropan-2-yl)pyridin-2-yl]-3-oxo-2-(prop-2-en-1-yl)-1H,2H,3H-pyrazolo[3,4-d]pyrimidin-6-yl}amino)phenyl]piperazin-1-yl}butanamide (26g – MA076)

The crude product was purified by column chromatography on silica gel using 5% MeOH in DCM to afford the product **26g** (7.4 mg, 0.01 mmol, 30%) as a green solid.

TLC: R_f = 0.10 (1:9 MeOH/DCM); UV.

^{1}H-NMR (400 MHz, CDCl$_3$): δ (ppm) = 8.87 (s, 1H), 7.89 (t, 1H, J = 7.8 Hz), 7.77 (dd, 1H, J = 8.2, 0.5 Hz), 7.53-7.47 (m, 3H), 7.37 (dd, 1H, J = 7.8, 0.6 Hz), 7.12 (dd, 1H, J = 7.1, 0.4 Hz), 6.96-6.89 (m, 3H), 6.78 (br s, 1H), 6.52 (br t, 1H, J = 5.6 Hz), 5.78-5.66 (m, 1H), 5.06 (dd, 1H, J = 10.1, 1.2 Hz), 4.99-4.90 (m, 2H), 4.76 (d, 2H, J = 6.2 Hz), 3.99 (s, 1H), 3.73 (t, 2H, J = 5.3 Hz), 3.71-3.60 (m, 16H), 3.58 (t, 2H, J = 5.1 Hz), 3.50-3.43 (m, 4H), 3.26 (br s, 4H), 2.92-2.70 (m, 7H), 2.57 (br s, 2H), 2.32 (t, 2H, J = 6.8 Hz), 2.18-2.09 (m, 1H), 2.01-1.88 (m, 2H), 1.61 (s, 6H).

IR (ATR): ν (cm^{-1}) = 3296, 3237, 2920, 2871, 1697, 1623.

HRMS (ESI): *m/z* calculated for: C$_{55}$H$_{70}$N$_{12}$O$_{12}$ [M+H]$^+$, 1091.5309, found: 1091.5329.

HPLC: 92.9% purity, t_R = 8.64 min.

28a-f were prepared following general procedure **D** to deprotect **27a-f** and then general procedure **A** for HATU-mediated amide coupling to attach them to AZD1775 analogue **13**.

N-(2-{[2-(2,6-Dioxopiperidin-3-yl)-1,3-dioxo-2,3-dihydro-1H-isoindol-4-yl]amino}ethyl)-4-(4-{4-[4-({1-[6-(2-hydroxypropan-2-yl)pyridin-2-yl]-3-oxo-2-(prop-2-en-1-yl)-1H,2H,3H-pyrazolo[3,4-d]pyrimidin-6-yl}amino)phenyl]piperazin-1-yl}butanamido)butanamide (28a – TH013)
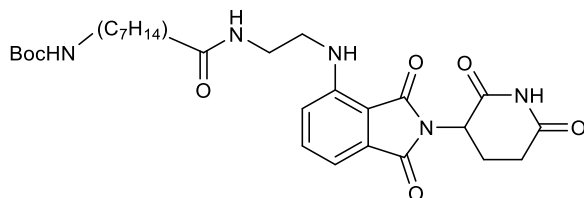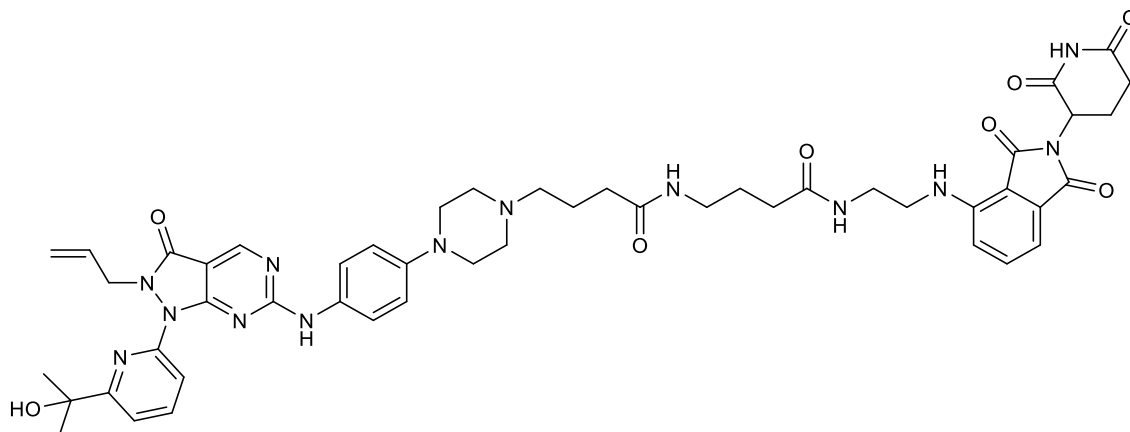

The crude product was purified by column chromatography on silica gel using 5% MeOH in DCM to afford the product **28a** (3.1 mg, 0.01 mmol, 12%) as a green solid.

TLC: R_f = 0.20 (1:9 MeOH/DCM); UV.

^{1}H NMR (400 MHz, d_3-Acetonitrile): δ (ppm) 8.74 (s, 1H), 8.28 (br s, 1H), 7.98 (t, 1H, J = 7.9 Hz), 7.75 (d, 1H, J = 8.3 Hz), 7.58-7.51 (m, 4H), 7.09 (d, 1H, J = 8.7 Hz), 7.04 (dd, 1H, J = 7.2, 0.5 Hz), 6.98-6.94 (m, 2H), 6.56-6.49 (m, 1H), 5.78-5.67 (m, 1H), 5.02 (dd, 1H, J = 10.3, 1.3 Hz), 4.98-4.88 (m, 2H), 4.72 (dt, 2H, J = 6.0, 1.3 Hz), 3.44-3.36 (m, 4H), 3.25 (br s, 4H), 2.80-2.68 (m, 7H), 2.59 (br s, 2H), 2.15-2.11 (m, 1H), 1.90-1.82 (m, 3H), 1.76-1.67 (m, 2H), 1.54 (s, 6H), 1.34-1.27 (m, 4H), 0.93-0.87 (m, 1H).

IR (ATR): ν (cm^{-1}) = 3287, 2824, 2855, 1695, 1653, 1620.

HRMS (ESI): m/z calculated for: $C_{49}H_{57}N_{13}O_8$ [M+H]$^+$, 956.4526, found: 956.4530.

HPLC: 91.1% purity, t_R = 8.09 min.

N-(2-{[2-(2,6-Dioxopiperidin-3-yl)-1,3-dioxo-2,3-dihydro-1H-isoindol-4-yl]amino}ethyl)-6-(4-{4-[4-({1-[6-(2-hydroxypropan-2-yl)pyridin-2-yl]-3-oxo-2-(prop-2-en-1-yl)-1H,2H,3H-pyrazolo[3,4-d]pyrimidin-6-yl}amino)phenyl]piperazin-1-yl}butanamido)hexanamide (28b – TH011)
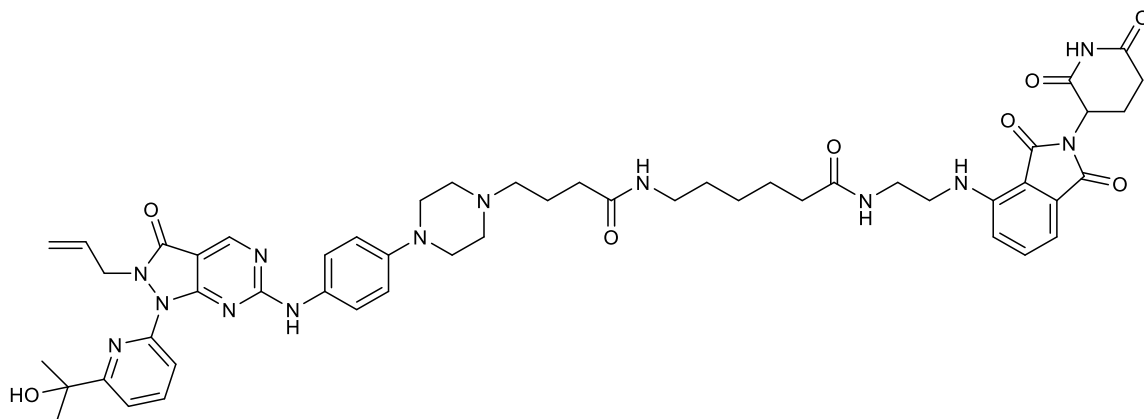
The crude product was purified by column chromatography on silica gel using 5% MeOH in DCM to afford the product **28b** (2.0 mg, 0.01 mmol, 8%) as a green solid.
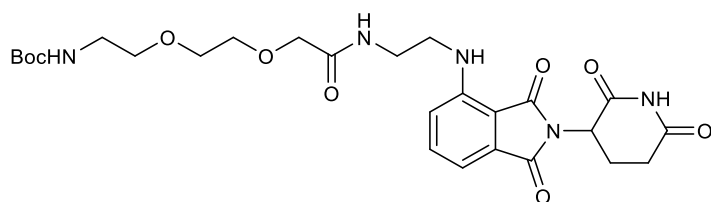
TLC: R_f = 0.20 (1:9 MeOH/DCM); UV.

^{1}H NMR (400 MHz, d_3-Acetonitrile): δ (ppm) = 9.12 (s, 1H), 8.76 (s, 1H), 8.32 (s, 1H), 7.98 (t, 1H, J = 7.9 Hz), 7.74 (d, 1H, J = 7.9 Hz), 7.61-7.50 (m, 4H), 7.08-6.99 (m, 4H), 6.63-6.55 (m, 1H), 6.51-6.42 (m, 1H), 5.79-5.67 (m, 1H), 5.03 (dd, 1H, J = 10.3, 1.2 Hz), 4.99-4.88 (m, 2H), 4.73 (dt, 2H, J = 6.0, 1.3 Hz), 3.42-3.35 (m, 6H), 3.08 (br s, 4H), 2.80-2.63 (m, 3H), 2.54-2.46 (m, 2H), 2.12-2.08 (m, 5H), 1.61-1.55 (m, 2H), 1.54 (s, 6H), 1.52-1.43 (m, 4H), 1.34-1.25 (m, 6H).

IR (ATR): v (cm^{-1}) = 3281, 2824, 2855, 1695, 1620.

HRMS (ESI): m/z calculated for: $C_{51}H_{61}N_{11}O_8$ [M+H]$^+$, 984.4839, found: 984.4815.

HPLC: 93.4% purity, t_R = 8.28 min.

N-(2-{[2-(2,6-Dioxopiperidin-3-yl)-1,3-dioxo-2,3-dihydro-1H-isoindol-4-yl]amino}ethyl)-8-(4-{4-[4-({1-[6-(2-hydroxypropan-2-yl)pyridin-2-yl]-3-oxo-2-(prop-2-en-1-yl)-1H,2H,3H-pyrazolo[3,4-d]pyrimidin-6-yl}amino)phenyl]piperazin-1-yl}butanamido)octanamide (28c – TH014)
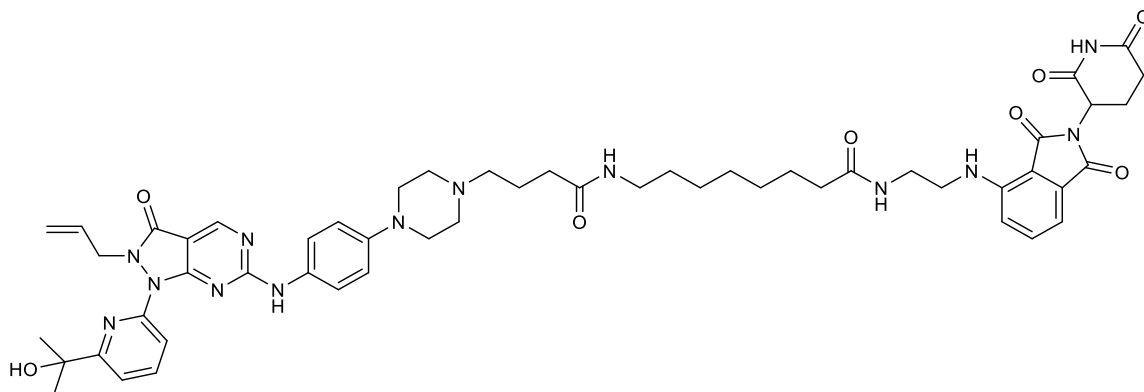
The crude product was purified by column chromatography on silica gel using 5% MeOH in DCM to afford the product **28c** (1.6 mg, 0.01 mmol, 6%) as a green solid.

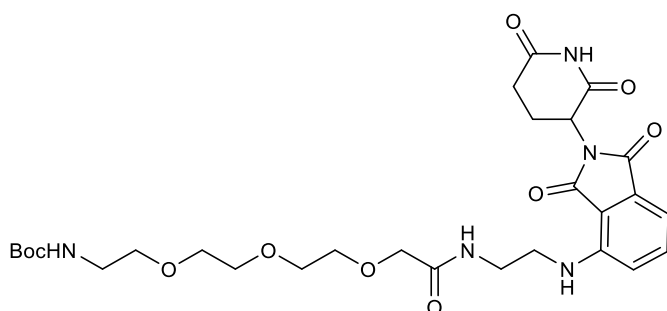TLC: R_f = 0.20 (1:9 MeOH/DCM); UV.

^{1}H NMR (400 MHz, MeOD): δ (ppm) = 8.80 (s, 1H), 8.00 (t, 1H, J = 8.0 Hz), 7.81-7.76 (m, 1H), 7.65 (dd, 1H, J = 7.7, 0.6 Hz), 7.59-7.50 (m, 3H), 7.10 (d, 1H, J = 8.5 Hz), 7.05 (d, 1H, J = 7.1 Hz), 7.02-6.94 (m, 2H), 5.79-5.66 (m, 1H), 5.09-5.02 (m, 2H), 4.96-4.89 (m, 1H), 4.84-4.80 (m, 2H), 3.87-3.39 (m, 4H), 3.24 (br s, 4H), 3.19-3.15 (m, 2H), 2.88-2.68 (m, 7H), 2.56 (br s, 2H), 2.28 (t, 2H, J = 7.1 Hz), 2.22-2.15 (m, 2H), 2.14-2.06 (m, 1H), 1.93-1.85 (m, 2H), 1.59 (s, 6H), 1.55-1.41 (m, 4H), 1.37-1.34 (m, 2H), 1.35-1.30 (m, 6H).

IR (ATR): ν (cm^{-1}) = 3375, 2926, 2855, 1697, 1619.

HRMS (ESI): m/z calculated for: $C_{55}H_{65}N_{13}O_8$ [M+H]$^+$, 1012.5152, found: 1012.5125.

HPLC: 93.7% purity, t_R = 8.62 min.

N-(2-{[2-(2,6-Dioxopiperidin-3-yl)-1,3-dioxo-2,3-dihydro-1H-isoindol-4-yl]amino}ethyl)-11-(4-{4-[4-({1-[6-(2-hydroxypropan-2-yl)pyridin-2-yl]-3-oxo-2-(prop-2-en-1-yl)-1H,2H,3H-pyrazolo[3,4-dpyrimidin-6-yl}amino)phenyl]piperazin-1-yl}butanamido)undecanamide (28d – TH012)
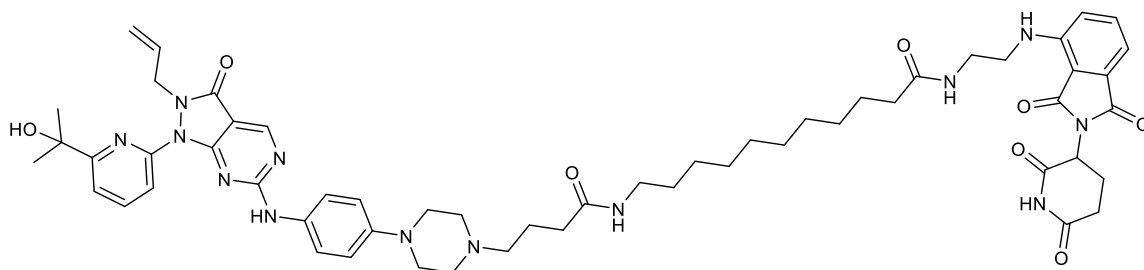
The crude product was purified by column chromatography on silica gel using 5% MeOH in DCM to afford the product **28d** (3.2 mg, 0.01 mmol, 13%) as a green solid.

TLC: R_f = 0.20 (1:9 MeOH/DCM); UV.

^{1}H-NMR (400 MHz, CDCl$_3$): δ (ppm) = 9.07 (s, 1H), 8.76 (s, 1H), 8.41 (s, 1H), 7.98 (t, 1H, J = 7.9 Hz), 7.75 (d, 1H, J = 7.9, 0.5 Hz), 7.62-7.58 (m, 2H), 7.58-7.50 (m, 2H), 7.08-6.98 (m, 5H), 6.61-6.55 (m, 1H), 6.51-6.45 (m, 1H), 5.78-5.66 (m, 1H), 5.02 (dd, 1H, J = 10.4, 1.3 Hz), 4.98-4.88 (m, 2H), 4.73 (dt, 2H, J = 6.0, 1.3 Hz), 3.41-3.36 (m, 4H), 3.22-3.14 (m, 4H), 3.14-3.07 (m, 2H), 2.81-2.64 (m, 3H), 2.56-2.49 (m, 2H), 2.11-2.05 (m, 5H), 1.55 (s, 6H), 1.53-1.43 (m, 6H), 1.32-1.21 (m, 16H).

IR (ATR): ν (cm^{-1}) = 3280, 2926, 2853, 1695, 1693.

HRMS (ESI): m/z calculated for: C$_{51}$H$_{62}$N$_{12}$O$_{10}$ [M+H]$^+$, 1054.5621, found: 1054.5640.

HPLC: 92.8% purity, t_R = 9.29 min.

N-[2-(2-{[(2-{[2-(2,6-Dioxopiperidin-3-yl)-1,3-dioxo-2,3-dihydro-1H-isoindol-4-yl]amino}ethyl)carbamoyl]methoxy}ethoxy)ethyl]-4-{4-[4-({1-[6-(2-hydroxypropan-2-yl)pyridin-2-yl]-3-oxo-2-(prop-2-en-1-yl)-1H,2H,3H-pyrazolo[3,4-d]pyrimidin-6-yl}amino)phenyl]piperazin-1-yl}butanamide (28e – MA093)
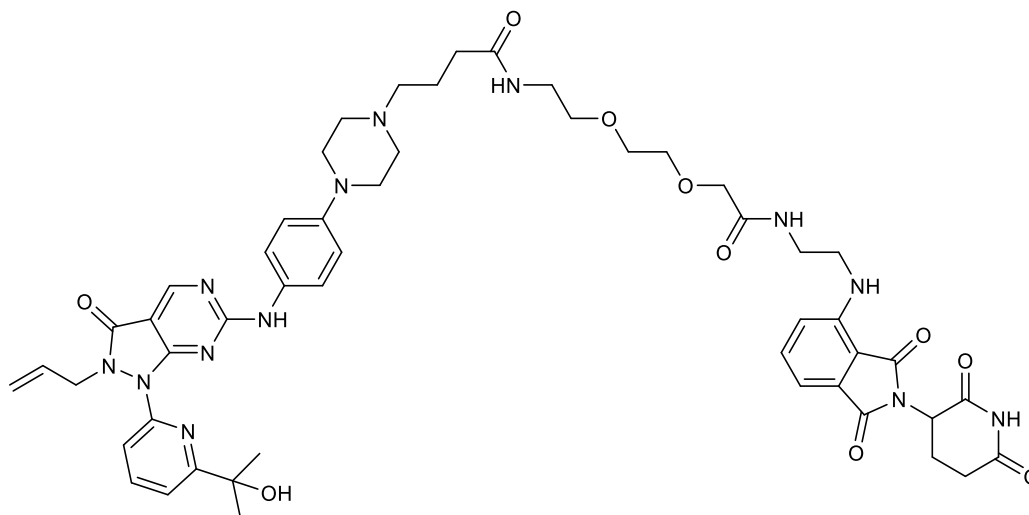
The crude product was purified by column chromatography on silica gel using 5% MeOH in DCM to afford the product **28e** (7.3 mg, 0.01 mmol, 33%) as a green solid.

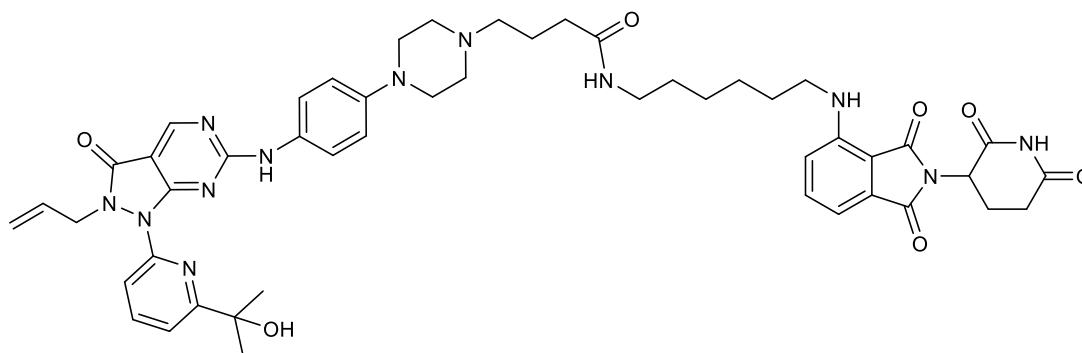TLC: R_f = 0.25 (1:9 MeOH/DCM); UV.

^{1}H-NMR (400 MHz, CDCl$_3$): δ (ppm) = 8.86 (s, 1H), 7.89 (t, 1H, J = 7.9 Hz), 7.16 (dd, 1H, J = 8.1, 0.6 Hz), 7.55-7.46 (m, 3H), 7.37 (dd, 1H, J = 7.6, 0.6 Hz), 7.3-7.30 (m, 1H), 7.13 (d, 1H, J = 6.9 Hz), 6.99 (d, 1H, J = 8.6 Hz), 6.91 (d, 2H, J = 8.9 Hz), 6.61 (br s, 1H), 6.46 (br t, 1H, J = 5.4 Hz), 5.78-5.67 (m, 1H), 5.06 (dd, 1H, J = 10.2, 1.1 Hz), 4.99-4.92 (m, 2H), 4.76 (d, 2H, J = 6.2 Hz), 4.03-3.88 (m, 2H), 3.65-3.62 (m, 4H), 3.62-3.47 (m, 6H), 3.47-3.41 (m, 2H), 3.27-3.19 (m, 4H), 2.91-2.67 (m, 7H), 2.59-2.50 (m, 2H), 2.30 (t, 2H, J = 7.3 Hz), 2.18-2.11 (m, 1H), 1.95-1.87 (m, 2H), 1.61 (s, 6H).

IR (ATR): ν (cm^{-1}) = 3310, 3230, 2900, 2865, 1695, 1624.

HRMS (ESI): m/z calculated for: C$_{51}$H$_{61}$N$_{13}$O$_{10}$ [M+H]$^+$, 1016.4737, found: 1016.4719.

N-{2-[2-(2-{[(2-{[2-(2,6-Dioxopiperidin-3-yl)-1,3-dioxo-2,3-dihydro-1H-isoindol-4-yl]amino}ethyl)carbamoyl]methoxy}ethoxy)ethoxy]ethyl}-4-{4-[4-({1-[6-(2-hydroxypropan-2-y)pyridin-2-yl]-3-oxo-2-(prop-2-en-1-yl)-1H,2H,3H-pyrazolo[3,4-d]pyrimidin-6-yl}amino)phenyl]piperazin-1-yl}butanamide (28f – MA081)

The crude product was purified by column chromatography on silica gel using 5% MeOH in DCM to afford the product **28f** (7.1 mg, 0.01 mmol, 32%) as a green solid.
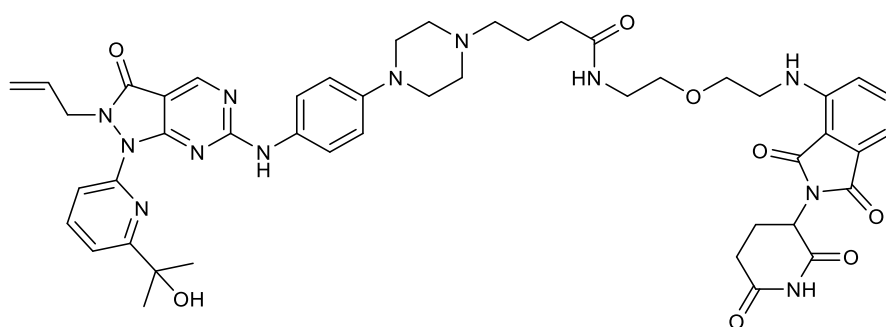
TLC: R_f = 0.20 (1:9 MeOH/DCM); UV.

^{1}H-NMR (400 MHz, CDCl$_3$): δ (ppm) = 8.84 (s, 1H), 7.87 (t, 1H, *J* = 7.9 Hz), 7.73 (d, 1H, *J* = 7.9 Hz), 7.55-7.44 (m, 5H), 7.35 (dd, 1H, *J* = 7.7, 0.5 Hz), 7.11 (d, 1H, *J* = 7.1 Hz), 7.01 (d, 1H, *J* = 8.5 Hz), 6.91-6.87 (m, 2H), 6.46-6.40 (m, 1H), 5.76-5.64 (m, 1H), 5.04 (dd, 1H, *J* = 10.2, 1.1 Hz), 4.97-4.88 (m, 2H), 4.74 (d, 2H, *J* = 6.1 Hz), 4.03-4.00 (m, 2H), 3.97 (s, 1H), 3.79 (t, 1H, *J* = 5.1 Hz), 3.67-3.60 (m, 4H), 3.60-3.58 (m, 4H), 3.57-3.52 (m, 2H), 3.46-3.42 (m, 2H), 3.39-3.32 (m, 2H), 3.30-3.20 (m, 2H), 3.09-3.01 (m, 2H), 2.95-2.85 (m, 4H), 2.80-2.70 (m, 3H), 2.36-2.26 (m, 2H), 2.16-2.09 (m, 1H), 1.59 (s, 6H), 1.31-1.22 (m, 4H), 0.90-0.80 (m, 2H).

IR (ATR): v (cm^{-1}) = 3330, 2927, 1697, 1654, 1671, 1619.

HRMS (ESI): *m/z* calculated for: C$_{53}$H$_{65}$N$_{13}$O$_{11}$ [M+H]$^+$, 1060.4999, found: 1060.4970.

HPLC: 93.6% purity, t_R = 8.18 min.

3.4.8 Wee1 negative control PROTACs recruiting VHL

Tert-Butyl-((*S*)-1-((2*S*,4*S*)-4-hydroxy-2-((4-(4-methylthiazol-5-yl)benzyl)carbamoyl) pyrrolidin-1-yl)-3,3-dimethyl-1-oxobutan-2-yl)carbamate (30) (Frost *et al.*, 2016)
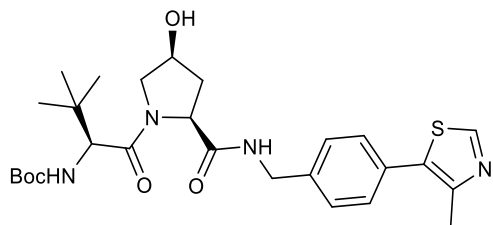
30 was synthesised using the same protocol than for molecule **18** by replacing Boc-*trans*-hyp-OH by Boc-*cis*-hyp-OH, starting from molecule **16**. The crude product was purified by column chromatography on silica gel using 3% MeOH in DCM to afford the product **30** (40 mg, 0.08 mmol, 63%) as a yellow solid.

TLC: R_f = 0.60 (5:95 MeOH/DCM); UV.

^{1}H-NMR (400 MHz, CDCl$_3$): δ (ppm) = 8.68 (s, 1H), 7.58 (br s, 1H), 7.38-7.30 (m, 4H), 5.11 (d, 1H, *J* = 9.2 Hz), 4.75 (d, 1H, *J* = 7.9 Hz), 4.65-4.61 (m, 1H), 4.46 (s, 1H), 4.28 (dd, 1H, *J* = 15.1, 5.3 Hz), 4.17 (d, 1H, *J* = 9.3 Hz), 3.90-3.75 (m, 2H), 2.50 (s, 3H), 2.38-2.34 (m, 1H), 2.22-2.16 (m, 1H), 1.4 (s, 9H), 0.89 (s, 9H).

IR (ATR): ν (cm^{-1}) = 3300, 2985, 1670, 1630, 1250.

Spectral data matched those reported in the literature.

(2*S*,4*S*)-4-Hydroxy-1-[(2*S*)-2-(4-{4-[4-({1-[6-(2-hydroxypropan-2-yl)pyridin-2-yl]-3-oxo-2-(prop-2-en-1-yl)-1H,2H,3H-pyrazolo[3,4-d]pyrimidin-6-yl}amino)phenyl]piperazin-1-yl}butanamido)-3,3-dimethylbutanoyl]-N-{[4-(4-methyl-1,3-thiazol-5-yl)phenyl]methyl}pyrrolidine-2-carboxamide (31 – negMA055)
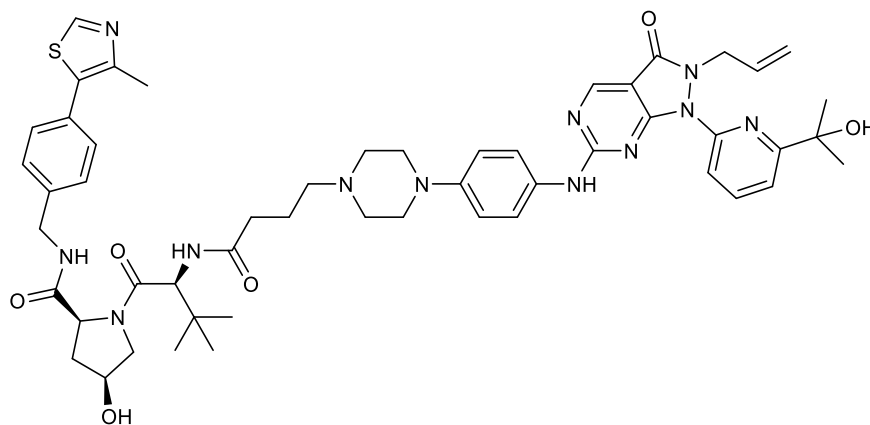
Negative control PROTAC **31 (negMA055)** was prepared following general procedure **D** to deprotect **30** and then general procedure **A** for HATU-mediated amide coupling to attach it to AZD1775 analogue **13.** The crude product was purified by column chromatography on silica gel using 5% MeOH in DCM to afford the product **31** (5.4 mg, 0.01 mmol, 22%) as a yellow solid.
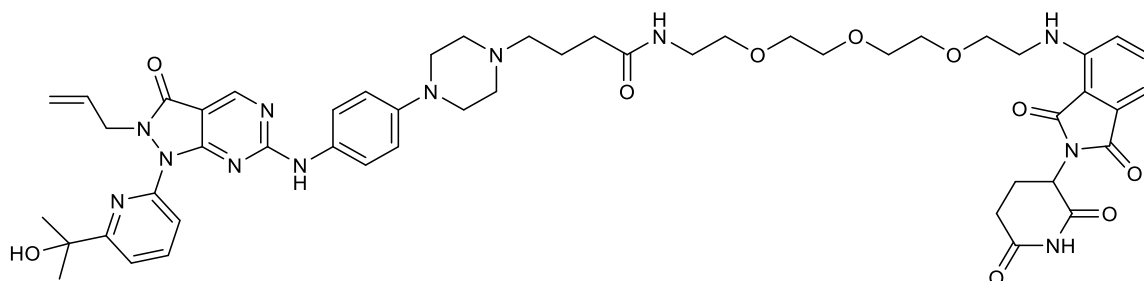
TLC: R_f = 0.20 (1:9 MeOH/DCM); UV.

^{1}H-NMR (400 MHz, CDCl$_3$): δ (ppm) = 8.83 (s, 1H), 8.67 (s, 1H), 7.87 (t, 1H, *J* = 8.0 Hz), 7.73 (dd, 1H, *J* = 8.0, 0.7 Hz), 7.50-7.43 (m, 3H), 7.39-7.32 (m, 6H), 6.93-6.88 (m, 2H), 5.75-5.64 (m, 1H), 5.51 (d, 1H, *J* = 9.4 Hz), 5.04 (dd, 1H, *J* = 10.2, 1.1 Hz), 4.94 (dd, 1H, *J* = 17.1, 1.1 Hz), 4.76-4.69 (m, 3H), 4.68-4.62 (dd, 1H, *J* = 15.0, 7.2 Hz), 4.52 (d, 1H, *J* = 9.0 Hz), 4.49-4.43 (m, 1H), 4.30 (dd, 1H, *J* = 15.0, 5.0 Hz), 3.99-3.89 (m, 1H), 3.80 (d, 1H, *J* = 10.9 Hz), 3.26 (br s, 4H), 2.87-2.56 (m, 6H), 2.51 (s, 3H), 2,42-2.30 (m, 2H), 1.96-1.88 (m, 2H), 1.58 (s, 6H), 0.92 (s, 9H).

IR (ATR): v (cm^{-1}) = 3296, 2927, 2855, 1653, 1621, 1534.

HRMS (ESI): *m/z* calculated for: C$_{52}$H$_{64}$N$_{12}$O$_6$S [M+H]$^+$, 985.4865, found: 985.4863.

***Tert*-Butyl N-(10-{[(2*S*)-1-[(2*S*,4*S*)-4-hydroxy-2-({[4-(4-methyl-1,3-thiazol-5-yl)phenyl]methyl}carbamoyl)pyrrolidin-1-yl]-3,3-dimethyl-1-oxobutan-2-yl]carbamoyl}decyl)carbamate (32)**
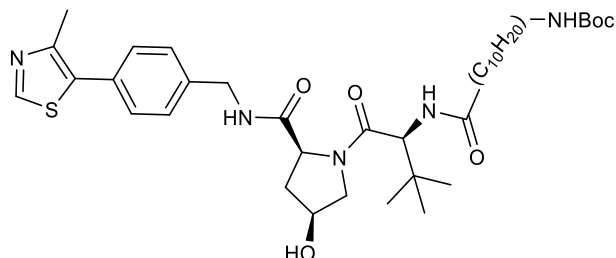
32 was prepared following general procedure **D** to deprotect **30** and then general procedure **A** for HATU-mediated amide coupling to attach it to linker **L$_d$**. The crude product was purified by column chromatography on silica gel using 3% MeOH in DCM to afford the product **32** (55 mg, 0.08 mmol, 93%) as a yellow solid.

TLC: R_f = 0.25 (5:95 MeOH/DCM); UV.

^{1}H-NMR (400 MHz, CDCl$_3$): δ (ppm) = 8.60 (s, 1H), 7.98-7.88 (m, 4H), 7.83 (br t, 1H, *J* = 6.1 Hz), 6.25 (d, 1H, *J* = 9.0 Hz), 4.60 (dd, 1H, *J* = 8.1, 1.7 Hz), 4.53 (dd, 1H, *J* = 13.8, 6.9 Hz), 4.47 (d, 1H, *J* = 9.0 Hz), 4.35 (br s, 1H), 4.22 (dd, 1H, *J* = 15.2, 5.2 Hz), 3.87-3.72 (m, 2H), 3.03-2.96 (m, 2H), 2.41 (s, 3H), 2.19-2.05 (m, 4H), 1.56-1.44 (m, 2H), 1.39-1.32 (m, 10H), 1.22-1.13 (m, 13H), 0.85 (s, 9H).

IR (ATR): ν (cm^{-1}) = 3290, 3070, 2930, 2862, 1667, 1623, 1200.

(2*S*,4*S*)-4-Hydroxy-1-[(2*S*)-2-[11-(4-{4-[4-({1-[6-(2-hydroxypropan-2-yl)pyridin-2-yl]-3-oxo-2-(prop-2-en-1-yl)-1H,2H,3H-pyrazolo[3,4-d]pyrimidin-6-yl}amino)phenyl]piperazin-1-yl}butanamido)undecanamido]-3,3-dimethylbutanoyl]-N-{[4-(4-methyl-1,3-thiazol-5-yl)phenyl]methyl}pyrrolidine-2-carboxamide (33 – negMA054)
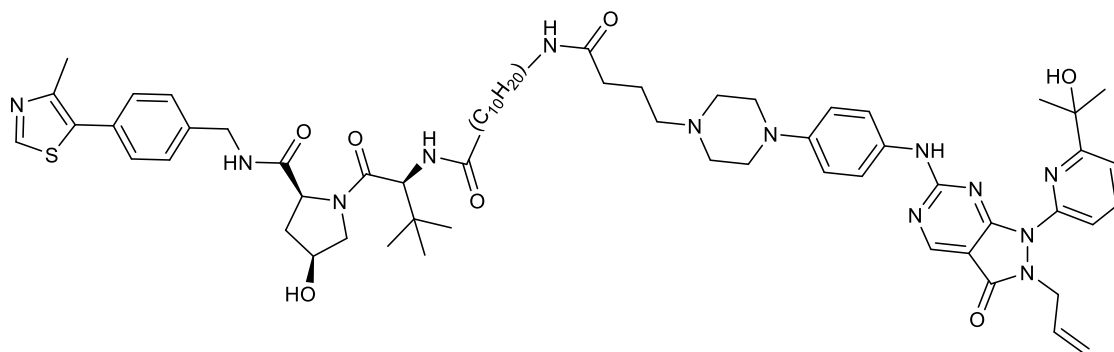
33 (negMA054) was prepared following general procedure **D** to deprotect **32** and then general procedure **A** for HATU-mediated amide coupling to attach it to AZD1775 analogue **13**. The crude product was purified by column chromatography on silica gel using 5% MeOH in DCM to afford the product **33** (4 mg, 0.01 mmol, 14%) as a yellow solid.
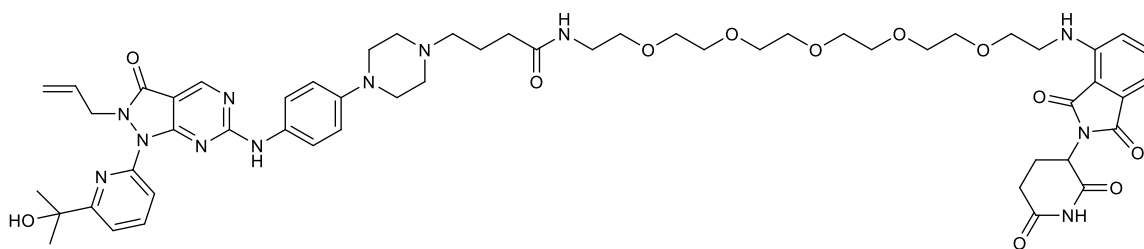
TLC: R_f = 0.20 (1:9 MeOH/DCM); UV.

^{1}H-NMR (400 MHz, CDCl$_3$): δ (ppm) = 8.80 (s, 1H), 8.67 (s, 1H), 7.86 (t, 1H, *J* = 7.9 Hz), 7.72 (d, 1H, *J* = 8.0 Hz), 7.50 (br d, 1H, *J* = 9.0 Hz), 7.38-7.33 (m, 5H), 6.93-6.86 (m, 2H), 6.17 (br s, 1H), 5.99 (d, 1H, *J* = 9.0 Hz), 5.75-5.57 (m, 2H), 5.04 (dd, 1H, *J* = 10.3, 1.1 Hz), 4.93 (dd, 1H, *J* = 17.1, 1.1 Hz), 4.76-4.70 (m, 4H), 4.54 (d, 1H, *J* = 9.1 Hz), 4.47 (br s, 1H), 4.27 (dd, 1H, *J* = 14.9, 4.8 Hz), 3.99-3.89 (m, 2H), 3.84 (d, 1H, *J* = 10.9 Hz), 3.31-3.18 (m, 6H), 2.86-2.56 (m, 5H), 2.55-2.45 (m, 4H), 2.49 (s, 3H), 2.37-2.28 (m, 3H), 2.24-2.13 (m, 2H), 2.12-2.05 (m, 2H), 1.98-1.90 (m, 2H), 1.58 (s, 6H), 1.52-1.44 (m, 2H), 1.30-1.19 (m, 15H), 0.93 (s, 9H).

IR (ATR): ν (cm^{-1}) = 3289, 2924, 2855, 1640, 1619, 1533.

HRMS (ESI): *m/z* calculated for: C$_{63}$H$_{85}$N$_{13}$O$_7$S [M+H]$^+$, 1168.6488, found: 1168.6500.

3.4.9 Wee1 negative control PROTACs recruiting CRBN

4-Fluoro-2-(1-methyl-2,6-dioxo-3-piperidyl)isoindoline-1,3-dione (34) (Nowak *et al.*, 2018)
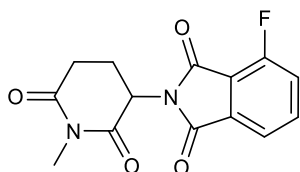
Fluoro-substituted thalidomide **24** was dissolved in DMF (3 mL) and K_2CO_3 was added (99.5 mg, 0.72 mmol, 2.0 eq.). MeI (34 µL, 0.05 mmol, 1.5 eq.) was then added dropwise to the reaction mixture before being stirred at room temperature for 12 h. The reaction was diluted with EtOAc and washed with water. The aqueous layer was then extracted with EtOAc (3 × 10 mL). The combined organics layers were washed with brine (10 mL) and dried over Na_2SO_4 before being concentrated in vacuo. The crude product was then purified using column chromatography on silica gel using a gradient of 0-10% of MeOH in DCM to afford the product **34** (78 mg, 0.54 mmol, 75 %) as yellow solid.

TLC: R_f = 0.30 (1:9 MeOH/DCM); UV.

^{1}H-NMR (400 MHz, $CDCl_3$): δ (ppm) = δ 7.79-7.74 (m, 1H), 7.71 (d, 1H, *J* = 7.1 Hz), 7.43 (td, 1H, *J* = 8.5, 0.9 Hz), 5.01-4.95 (m, 1H), 3.21 (s, 3H), 3.05-2.70 (m, 3H), 2.16-2.09 (m, 1H).

^{13}C-NMR (101 MHz, $CDCl_3$): δ (ppm) = 171.0, 168.4, 159.0, 137.1, 137.0, 132.0, 122.7, 120.0, 108.7, 50.2, 31.9, 27.3, 21.9.

IR (ATR): ν (cm^{-1}) = 1957, 2905, 1710, 1675, 1608.

Spectral data matched those reported in the literature.

Molecules **35a** and **35b** were prepared following general procedure **B** for nucleophilic aromatic substitution with linkers **L$_h$** and **L$_j$**.

***Tert*-Butyl N-(6-{[2-(1-methyl-2,6-dioxopiperidin-3-yl)-1,3-dioxo-2,3-dihydro-1H-isoindol-4-yl]amino}hexyl)carbamate (35a)**
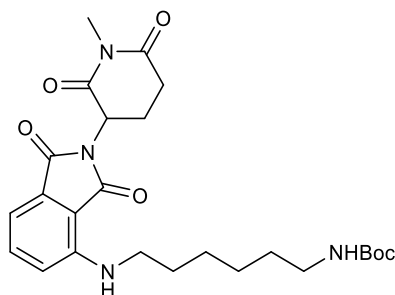
The crude product was purified by column chromatography on silica gel using 5% MeOH in DCM to afford the product **35a** (56 mg, 0.11 mmol, 36%) as a green solid.

TLC: R_f = 0.40 (1:9 MeOH/DCM); UV.

^{1}H-NMR (400 MHz, CDCl$_3$): δ (ppm) = 7.48 (dd, 1H, J = 8.4, 7.2 Hz), 7.07 (d, 1H, J = 7.2 Hz), 6.86 (d, 1H, J = 8.4 Hz), 6.21 (br t, 1H, J = 5.4 Hz), 4.93-4.87 (m, 1H), 4.53 (br s, 1H), 3.27-3.22 (m, 2H), 3.20 (s, 3H), 3.13-3.07 (m, 2H), 2.98-2.94 (m, 1H), 2.80-2.71 (m, 2H), 2.12-2.08 (m, 1H), 1.69-1.61 (m, 2H), 1.52-1.32 (m, 15H).

IR (ATR): ν (cm^{-1}) = 2950, 2900, 1700, 1675, 1607.

***Tert*-Butyl N-{2-[2-(2-{[2-(1-methyl-2,6-dioxopiperidin-3-yl)-1,3-dioxo-2,3-dihydro-1H-isoindol-4-yl]amino}ethoxy)ethoxy]ethyl}carbamate (35b)**
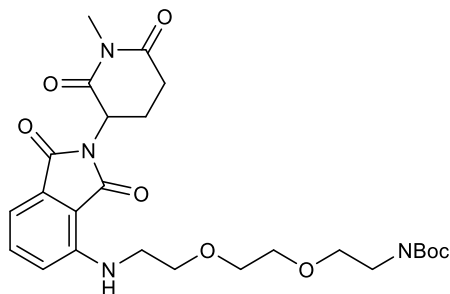
The crude product was purified by column chromatography on silica gel using 5% MeOH in DCM to afford the product **35b** (60 mg, 0.12 mmol, 34%) as a green solid.

TLC: R$_f$ = 0.40 (1:9 MeOH/DCM); UV.

^{1}H-NMR (400 MHz, CDCl$_3$): δ (ppm) = 7.49 (dd, 1H, J = 8.4, 7.2 Hz), 7.10 (d, 1H, J = 7.2 Hz), 6.91 (d, 1H, J = 8.4 Hz), 6.50 (br s, 1H), 5.04 (br s, 1H), 4.96-4.86 (m, 1H), 3.72 (t, 2H, J = 5.3 Hz), 3.67-3.61 (m, 4H), 3.57-3.52 (m, 2H), 3.50-3.44 (m, 2H), 3.34-3.27 (m, 2H), 3.20 (s, 3H), 2.99-2.92 (m, 1H), 2.81-2.70 (m, 2H), 2.11-2.05 (m, 1H), 1.42 (s, 9H).

IR (ATR): v (cm^{-1}) = 2970, 2908, 1701, 1678, 1604.

36a (negMA048) and **36b (negMA071)** were prepared following general procedure **D** and then general procedure **A** for HATU-mediated amide coupling to AZD1775 analogue **13** using **35a** and **35b** respectively**.**

4-{4-[4-({1-[6-(2-Hydroxypropan-2-yl)pyridin-2-yl]-3-oxo-2-(prop-2-en-1-yl)-1H,2H,3H-pyrazolo[3,4-d]pyrimidin-6-yl}amino)phenyl]piperazin-1-yl}-N-(6-{[2-(1-methyl-2,6-dioxopiperidin-3-yl)-1,3-dioxo-2,3-dihydro-1H-isoindol-4-yl]amino}hexyl)butanamide (36a – negMA048)
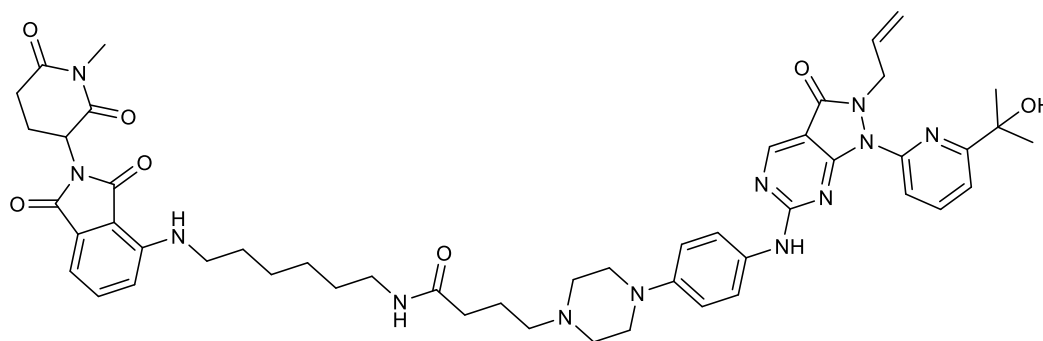
The crude product was purified by column chromatography on silica gel using 7% MeOH in DCM to afford the product **36a** (6.5 mg, 0.01 mmol, 23%) as a green solid.

TLC: R_f = 0.20 (1:9 MeOH/DCM); UV.

^{1}H-NMR (400 MHz, CDCl$_3$): δ (ppm) = 8.82 (s, 1H), 7.93 (t, 1H, J = 7.8 Hz), 7.71 (d, 1H, J = 8.1 Hz), 7.60-7.44 (m, 4H), 7.39 (d, 1H, J = 7.8 Hz), 7.04 (d, 1H, J = 7.1 Hz), 6.92-6.85 (m, 3H), 6.56 (br s, 1H), 6.19 (br t, 1H, J = 5.7 Hz), 5.75-5.64 (m, 1H), 5.04 (dd, 1H, J = 10.2, 1.1

Hz), 4.96-4.88 (m, 2H), 4.73 (d, 2H, J = 6.2 Hz), 4.00 (s, 1H), 3.72-3.27 (m, 7H), 3.27-3.21 (m, 5H), 3.19 (s, 3H), 3.18-3.13 (m, 2H), 2.97-2.93 (m, 1H), 2.78-2.71 (m, 2H), 2.67-2.60 (m, 2H), 2.11-2.06 (m, 1H), 2.03-1.96 (m, 2H), 1.68-1.60 (m, 2H), 1.59 (s, 6H), 1.57-1.51 (m, 2H), 1.46-1.34 (m, 4H).

IR (ATR): ν (cm^{-1}) = 3350, 2968, 1694, 1675.

HRMS (ESI): m/z calculated for: $C_{50}H_{60}N_{12}O_{7}$ [M+H]$^{+}$, 941.4781, found: 941.4779.

4-{4-[4-({1-[6-(2-Hydroxypropan-2-yl)pyridin-2-yl]-3-oxo-2-(prop-2-en-1-yl)-1H,2H,3H-pyrazolo[3,4-d]pyrimidin-6-yl}amino)phenyl]piperazin-1-yl}-N-{2-[2-(2-{[2-(1-methyl-2,6-dioxopiperidin-3-yl)-1,3-dioxo-2,3-dihydro-1H-isoindol-4-yl]amino}ethoxy)ethoxy]ethyl}butanamide (36b – negMA071)
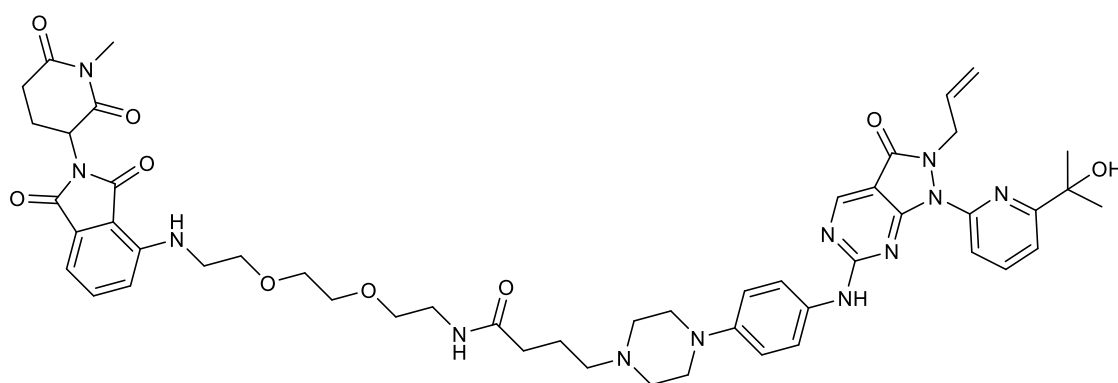
The crude product was purified by column chromatography on silica gel using 7% MeOH in DCM to afford the product **36b** (3.2 mg, 0.01 mmol, 11%) as a green solid. This PROTAC was prepared with the assistance of Lizzy Thorpe.

TLC: R_{f} = 0.15 (1:9 MeOH/DCM); UV.

^{1}H-NMR (400 MHz, CDCl$_{3}$): δ (ppm) = 8.82 (s, 1H), 7.94 (t, 1H, J = 7.8 Hz), 7.71 (d, 1H, J = 8.1 Hz), 7.53-7.48 (m, 3H), 7.39 (d, 1H, J = 7.8 Hz), 7.09 (d, 1H, J = 7.1 Hz), 6.98-6.88 (m, 4H), 6.51 (br t, 1H, J = 5.5 Hz), 5.75-5.64 (m, 1H), 5.04 (dd, 1H, J = 10.2, 1.1 Hz), 4.97-4.90 (m, 2H), 4.73 (d, 2H, J = 6.2 Hz), 4.02 (s, 1H), 3.75 (t, 2H, J = 5.3 Hz), 3.70-3.64 (m, 5H),

3.63-3.52 (m, 4H), 3.50-3.40 (m, 4H), 3.24-3.06 (m, 7H), 2.99-2.92 (m, 1H), 2.84-2.69 (m, 2H), 2.59-2.51 (m, 2H), 2.12-2.06 (m, 1H), 1.98-1.89 (m, 2H), 1.59 (s, 6H).

IR (ATR): v (cm^{-1}) = 3345, 2926, 1695, 1675.

HRMS (ESI): *m/z* calculated for: $C_{50}H_{60}N_{12}O_9$ [M+H]$^+$, 973.4679, found: 973.4671.

3.5   Conclusion

Two series of Wee1 PROTACs were synthesised using the most selective Wee1 inhibitor to date at the time of starting the project, AZD1775, and E3 ligase binders for VHL and CRBN. The use of non-selective inhibitors as target-binding moieties in PROTAC molecules can result in target selectivity beyond that of the original inhibitor (Zengerle *et al.*, 2015; Jiang *et al.*, 2019; Smith *et al.*, 2019). The Wee1 inhibitor AZD1775, while relatively selective for a kinase binder, exhibits off-target inhibition for a number of other kinases (Wright *et al.*, 2017; Zhu *et al.*, 2017). By modifying the E3-ligase binder and also the linker using different lengths and nature to create an SAR, this allows the investigation of Wee1 degradation and selectivity against other kinases in cancer cells in the next Chapter 4.

The AZD1775 analogue building block **13** was synthesised and functionalised to feature a carboxylic acid. The VHL recruiter VH032 **18** was synthesised to obtain a terminal amine. And the CRBN recruiter **24** was synthesised to enable nucleophilic aromatic substitution with an amine. Linkers were selected to feature either an amine or a carboxylic acid in order to attach them to the building blocks that were made through a series of Boc-deprotections and HATU-mediated amide coupling, or through nucleophilic aromatic substitution for the CRBN recruiter. This allowed the construction of a library of PROTACs by attaching these building blocks together. The final purifications were the hardest and most time-consuming steps. PROTACs are high molecular weight and polar molecules that are hard to purify with manual normal phase column chromatography (Hendrick *et al.*, 2022) and required multiple series of purifications to obtain a pure product which explains the low yields. The active PROTACs were obtain at high purity over at least 90% and 95% for the most interesting compounds for which multiple biological testing were required in this study.

Building a PROTAC library is a long process and the synthesis is time consuming. There are always more parameters to study such as different attachment points on the E3 ligase for instance as developed in the introduction (Section 1.3.2.1; Figure 1.7). However, the variety of linkers used for this study is a very good starting point, especially because it also allows the investigation of two different E3 ligases. In the future of PROTACs, it would be interesting to find a faster way to synthesize small library for PROTACs study. "Click chemistry" could be a fast and clean way to join the three parts of a PROTAC together (Wurz *et al.*, 2018; Zagidullin *et al.*, 2020). For instance, Wurz *et al.* linked a linker containing a terminal alkyne motif by "click chemistry" catalysed by $CuSO_4$ to the inhibitor containing an azide.

The Wee1 PROTACs and their negative controls can now be tested in cancer cells to study Wee1 degradation and selectivity. Commonly, PROTACs are assessed in relevant cell lines and analysed by Western blot using the target protein antibody to establish the degradation profile and the appropriate working concentration at different time points. Then, target engagement and E3 ligase recruitment can be verified using the negative control PROTACs, and by doing competition experiments with the target inhibitor and E3 ligase inhibitor. Cell proliferation assays can be performed to compare the IC_{50} of the PROTAC to the target inhibitor. To go even further in the assessment, ternary complex can be studied using different methods such as isothermal titration calorimetry (ITC), surface plasmon resonance (SPR) or crystallography for instance (Gadd *et al.*, 2017; Roy *et al.*, 2019). These allow to understand the binding of the proteins and the PROTAC together, and crystal structures can even give understanding in the linkers role to further improve the PROTACs. These techniques will be explored in the following chapter 4 to evaluate the Wee1 PROTACs.

4 Assessment of the first generation of Wee1 PROTACs

4.1 Introduction

To compare the efficacy of the recruited E3 ligase and the influence of the linker nature on Wee1 degradation activity, two different E3 ligase ligands as well as different types and lengths of linkers were used to synthesise PROTACs (See Chapter 3) to be assessed in cancer cells. Both components have been shown to have an important impact on PROTACs activity (Cyrus *et al.*, 2011; Lai, Toure, *et al.*, 2016). The ability of the PROTACs to degrade Wee1 as well as reduce levels of Tyr15 phosphorylation of CDK1 (pCDK1(Y15)), the key target of Wee1's kinase activity, were compared using Western blot to establish an SAR for different types and lengths of linkers using each of the E3 ligase binders. The selectivity, target recruitment and ternary complex formation were also investigated in cells and with purified proteins.

4.2 Aims and objectives

The first aim is to assess PROTACs in cancer cells and determine if the PROTACs induce Wee1 degradation.

The second aim is to compare the degradation profiles of the Wee1 PROTACs and confirm target engagement.

The third aim is to study ternary complex formation to better understand the mechanism of Wee1 PROTAC activity.

4.3 Results and discussion

4.3.1 Degradation assessment: dose response of the Wee1 PROTACs

To evaluate the Wee1 degradation profiles of the PROTACs, HeLa S3 cells were treated with different dosages of all the degraders from 10 µM to 1 nM for 4 h. Wee1,

pCDK1(Y15), CDK1 and β-actin, were probed by Western blot using the corresponding specific antibodies.

4.3.1.1 VHL-series of Wee1 PROTACs

Compound MA055 of the VHL-series successfully induced Wee1 degradation from 30 nM to 3 μM after 4 h incubation in HeLa S3 cells (Figure 4.1). Wee1 levels were largely restored at 10 μM MA055 as a consequence of self-inhibition of the compound, due to the hook effect generating unproductive binary over productive ternary complexes. Treatment with MA055 from 30 nM to 10 μM also resulted in decreased levels of pCDK1(Y15) as a downstream consequence of modulation of Wee1 activity. Degradation by the other VHL-based PROTACs of this series did not result in considerable Wee1 degradation after 4 h treatment. However, alkyl-linked compounds MA051, MA052, MA053 and MA054, reduced pCDK1(Y15) levels at higher concentrations, but not PEG-linked compounds MA086 and MA088 (Figure 4.1), likely due to a combination of limited degradation potency and also inhibition at higher concentrations of PROTAC.
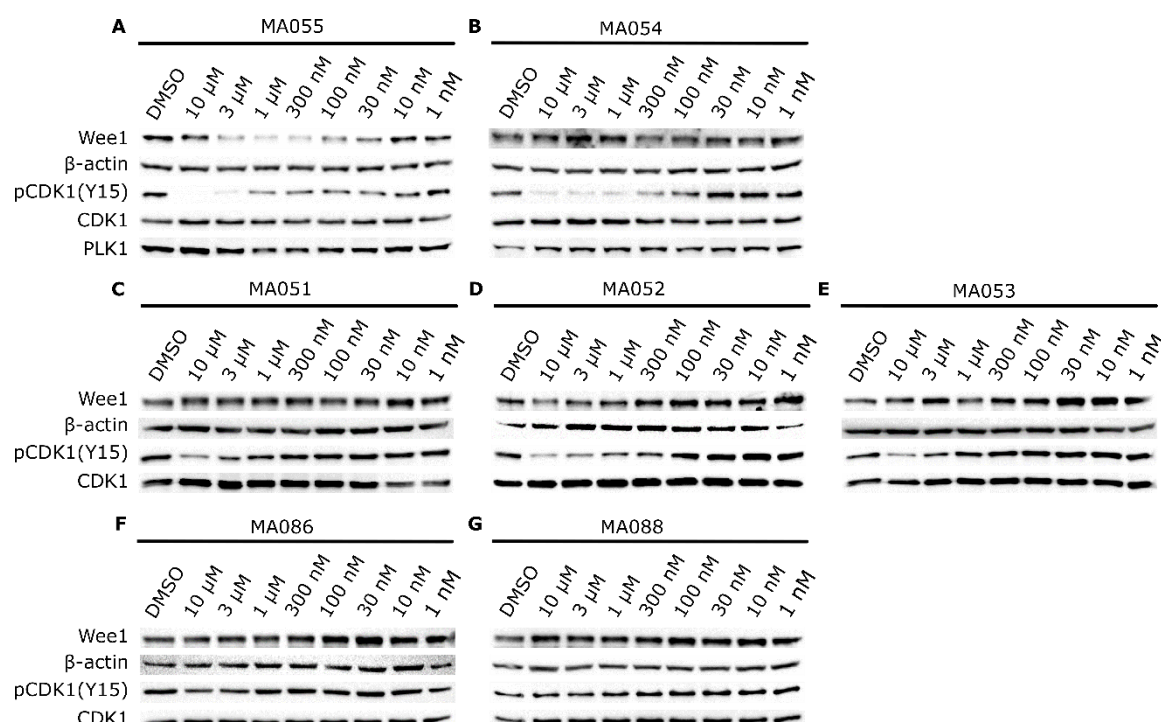
Figure 4.1: Degradation profiles of PROTACs recruiting the VHL E3 ubiquitin ligase. Western blots of HeLa S3 cells treated with different concentrations of PROTACs **A**) MA055, **B**) MA054, **C**) MA051, **D**) MA052, **E**) MA053, **F**) MA086, **G**) MA088 for 4 h. The membrane was blotted for Wee1, pCDK1(Y15), CDK1 and β-actin as the loading control, and additionally for PLK1 for PROTACs MA055 and MA054 (n = 2).

4.3.1.2 CRBN-series of Wee1 PROTACs

In the CRBN-series, the PROTACs MA049, MA048, MA072 and MA071 exhibited the greatest levels of Wee1 reduction over a range of concentrations, with Wee1 degradation observed from 30 nM to 10 μM of compound after 4 h treatment in HeLa S3 cells (Figure 4.2). They are the PROTACs with the shortest alkyl linkers of two and six carbons for MA049 and MA048, respectively, and the shortest PEG linkers with PEG1 and PEG2 for MA072 and MA071, respectively. pCDK1(Y15) levels were also decreased at treatments of 100 nM to 10 μM. PROTACs MA073, MA074, TH013 and TH012 induced degradation from ~100 nM to 10 μM, albeit less than that for MA049, MA048, MA072 and MA071. pCDK1(Y15) levels were also decreased from 300 nM to 10 μM for these. PROTACs MA076, MA093, MA081, TH014 and TH011 did not seem to degrade Wee1 at 4 h and subsequently only a slight decrease in pCDK1(Y15) at 3 and 10 μM was observed.
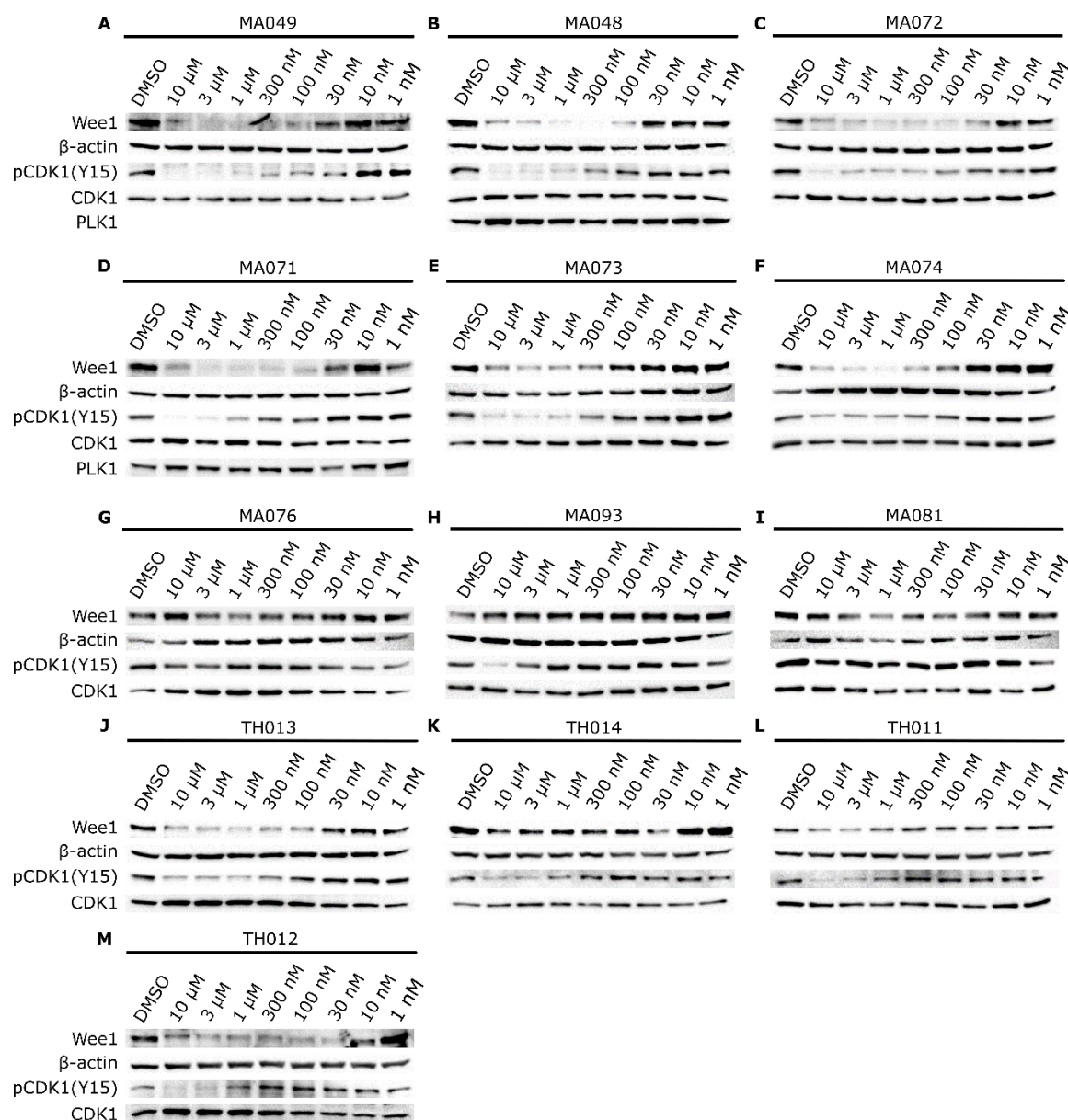
Figure 4.2: Degradation profiles of PROTACs recruiting the CRBN E3 ubiquitin ligase. Western blots of HeLa S3 cells treated with different concentrations of PROTACs **A**) MA049, **B**) MA048, **C**) MA072, **D**) MA071, **E**) MA073, **F**) MA074, **G**) MA076, **H**) MA093, **I**) MA081, **J**) TH013, **K**) TH014, **L**) TH011 and **M**) TH012 for 4 h. The membrane was blotted for Wee1, pCDK1(Y15), CDK1 and β-actin as the loading control, and additionally for PLK1 for PROTACs MA048 and MA071 (n = 2).

4.3.2 Comparison of all the PROTACs

After seeing successful Wee1 degradation and to compare all the PROTACs together, a single concentration of 1 μM was selected because all the successful PROTACs generally showed the greatest extent of degradation at this concentration. HeLa S3 cells were

treated for 24 h with 1 µM of each PROTAC. A wide range of Wee1 levels across compounds using both E3 ligase binders was observed suggesting that while both E3 ligases can form productive complexes with Wee1, different linkers result in different Wee1 degradation profiles and intensity (Figure 4.3; Table 4.1). Matching decreases in pCDK1(Y15) levels were also observed, indicating correlation with Wee1 degradation activity.
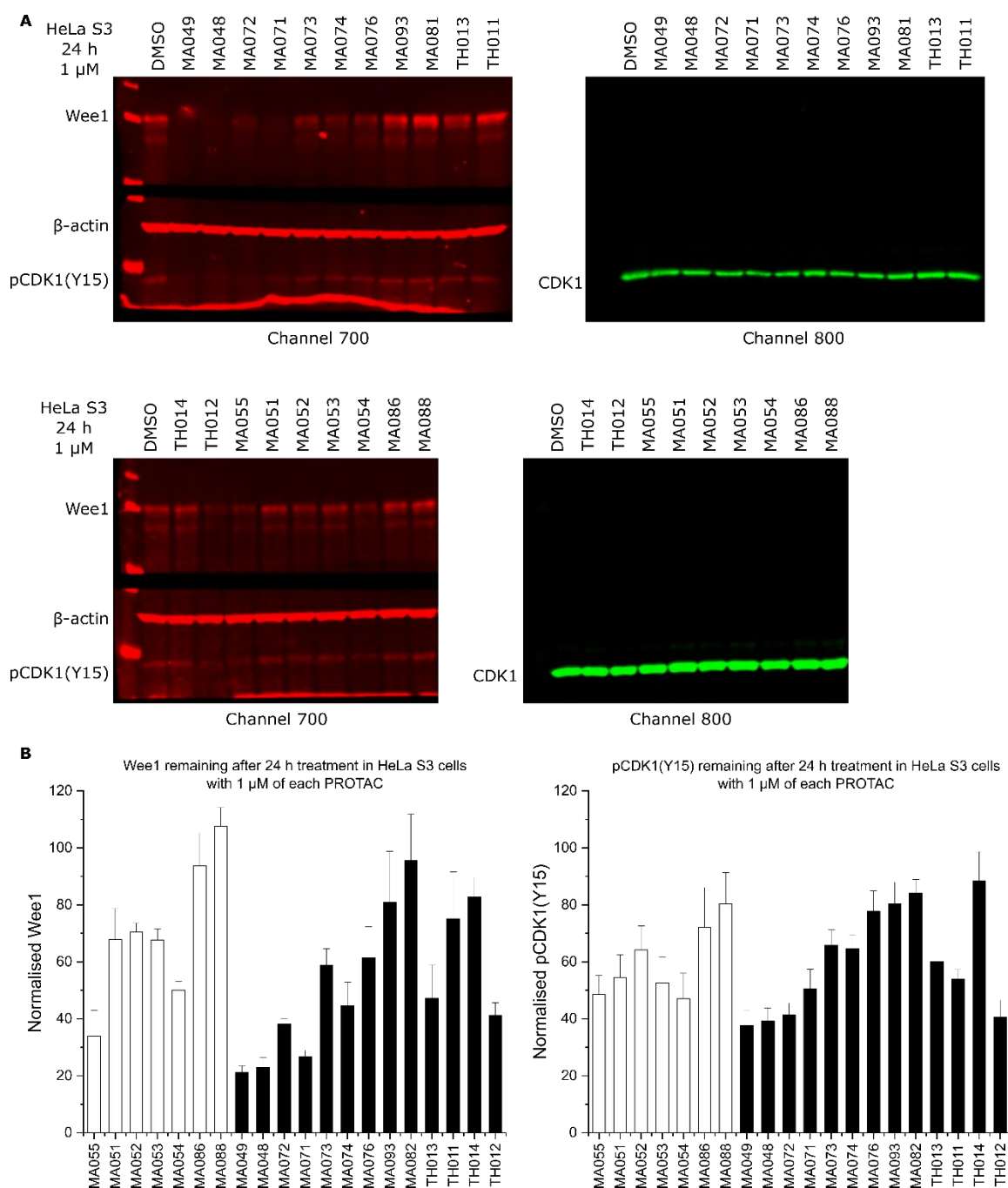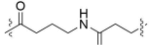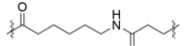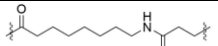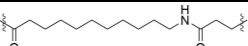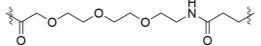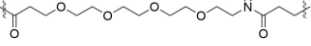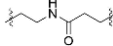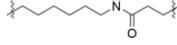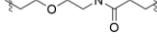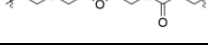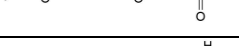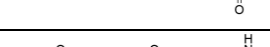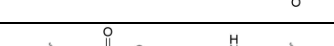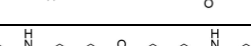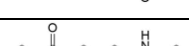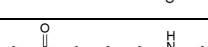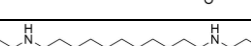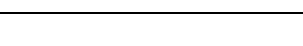
Figure 4.3: Screening of all the degraders. **A**) Western blot of HeLa S3 cells treated with 1 µM of the indicated PROTAC for 24 h. The membrane was blotted for Wee1, pCDK1(Y15), CDK1 and β-actin as the loading control. **B**) Wee1 and pCDK1(Y15) bands were quantified and normalised (n = 4 for Wee1 and for pCDK1(Y15)) for each PROTAC. The average of Wee1 and pCDK1(Y15) remaining is presented in Table 4.1. (VHL-based PROTACs in White, and CRBN-based PROTACs in Black).

Table 4.1: SAR of PROTACs recruiting two E3 ubiquitin ligases (VHL and CRBN) and using different linkers. Levels of Wee1 and pCDK1(Y15) are reported as the percentage of protein observed by Western blot following treatment of HeLa S3 cells with 1 µM of PROTAC for 24 h (n = 4) (Figure 4.3). The number of atoms for the linker length starts from the carbon linked to the piperazine on the AZD1775 to the carbonyl linked to VH032 for VHL and to the carbon attached to pomalidomide for CRBN.

PROTAC	Linker	E3 ligase	# of O and N atoms	Linker length	Wee1 24 h (%)	pCDK1(Y15) 24 h (%)
MA055		VHL	1	4	34 ± 9	49 ± 6
MA051			3	9	68 ± 11	55 ± 7
MA052			3	11	71 ± 3	64 ± 8
MA053			3	13	68 ± 4	53 ± 9
MA054			3	16	50 ± 3	47 ± 9
MA086			6	16	94 ± 12	72 ± 14
MA088			7	20	108 ± 7	80 ± 11
MA049		CRBN	2	7	21 ± 2	38 ± 5
MA048			2	11	23 ± 3	39 ± 5
MA072			3	10	38 ± 2	41 ± 4
MA071			4	13	27 ± 2	51 ± 7
MA073			5	16	59 ± 6	66 ± 5
MA074			6	19	45 ± 8	65 ± 5
MA076			7	22	51 ± 11	78 ± 7
MA093			6	16	81 ± 18	80 ± 8
MA081			7	19	96 ± 16	84 ± 5
TH013			4	12	47 ± 12	60 ± 4
TH011			4	14	75 ± 16	54 ± 3
TH014			4	16	83 ± 7	88 ± 10
TH012			4	19	41 ± 4	41 ± 6

4.3.2.1 VHL-series

After 24 h treatment with 1 μM of PROTAC in HeLa S3 cells, the five PROTACs of the VHL series featuring an alkyl linker (MA055, MA051, MA052, MA053, MA054) resulted in effective Wee1 degradation (Table 4.1), with MA055 (four-atom linker) and MA054 (16-atom linker) being the most efficient, removing about 65% and 50% of Wee1 protein, respectively. They consequently induced a decrease in pCDK1(Y15) levels, with only 50% remaining after 24 h. PROTACs MA051, MA052 and MA053, with intermediate linker lengths of 9-13 atoms, appeared to be less efficient, with ~70% of Wee1 remaining. The compounds with polyethylene glycol linkers MA086 and MA088, had even less effect on Wee1 degradation (0–6%) after 24 h treatment.

4.3.2.2 CRBN-series

Multiple PROTACs of the CRBN series induced strong Wee1 degradation following 24 h treatment in HeLa S3 cells with 1 μM of compound (Table 4.1). 21–38% of Wee1 and 38–51% of pCDK1(Y15) remained following treatment with MA049, MA048, MA072 and MA071, each featuring shorter linkers of 7–13 atoms. MA074 and TH012, each featuring longer linkers of nineteen atoms, also showed strong degradation at 24 h with 40-45% of Wee1 and 40–65% of pCDK1(Y15) remaining in each case. Overall, medium-length linker PROTACs with fourteen to sixteen atoms (MA073, TH014, TH011) seemed less potent for Wee1 degradation compared to the other PROTACs with similar linker's nature of shorter or longer length. Additionally, PROTACs with a long PEG linker and one more amide bond (MA093 and MA081) are poor degraders of Wee1.

Overall, observations at 24 h for both series of PROTACs were consistent with the dose-response profile of each PROTAC at 4 h. A recent paper tried to rationalised PROTAC design by suggesting that the linker length has an optimal zone in which PROTACs would result in the best degradation (Bemis *et al.*, 2021). Following the Wee1 PROTACs study, there seems to be at least two "zones" for the linker to facilitate degradation, as short and long linkers seem to be the best for the Wee1 PROTACs, while intermediate linkers were less efficient. This probably also indicates that different PROTACs form different

type of ternary complexes: favourable or not. Other parameters such as cellular permeability and efflux, protein expression levels, ubiquitination rate as well as other metabolic parameters of the PROTACs may play an important role in the degradation profile depending on the type and length of linker. Previous work has shown that cooperative stabilisation of PROTAC ternary complexes can result in both more (Farnaby *et al.*, 2019; Smith *et al.*, 2019) and less (Zorba *et al.*, 2018; Schiemer *et al.*, 2021) effective targeted protein degradation. Thus, enthalpy and entropy of the ternary complex are also important parameters to take into consideration. Longer linkers could help produce flexible ternary complex that adopt multiple conformations (Nowak *et al.*, 2018; Schiemer *et al.*, 2021).

4.3.3 Wee1 degradation over time

To verify that some PROTACs degrade Wee1 and others do not, and to investigate how fast Wee1 degradation is, time course experiments were performed. A PROTAC inducing Wee1 degradation and another PROTAC not showing degradation after 4 h or 24 h treatment were selected: MA055 and MA088 for the VHL-series, MA071 and MA093 for the CRBN series. Both MA055 and MA071 induced Wee1 degradation quickly, from 30 min and 1 h respectively to 48 h (Figure 4.4 A and D). The other two PROTACs MA088 and MA093 did not decrease Wee1 level from 15 min to 48 h treatment with 1 µM (Figure 4.4 C and F). To confirm that degradation was maintained, another PROTAC of each series was tested: MA054 for VHL and MA048 for CBRN, for 2 to 48 h (Figure 4.4 B and E). They also show degradation from the shorter time point of 2 h and up to 48 h. Wee1 levels for MA048 almost completely disappeared from 8 h. Thus, depending on the length and nature of the linker, some PROTACs are ineffective, but for potent PROTACs, degradation is quick and maintained over time. For the active PROTACs, pCDK1(Y15) levels seem to decrease before Wee1 levels, probably due to little inhibition of Wee1 at this concentration for the best PROTACs.
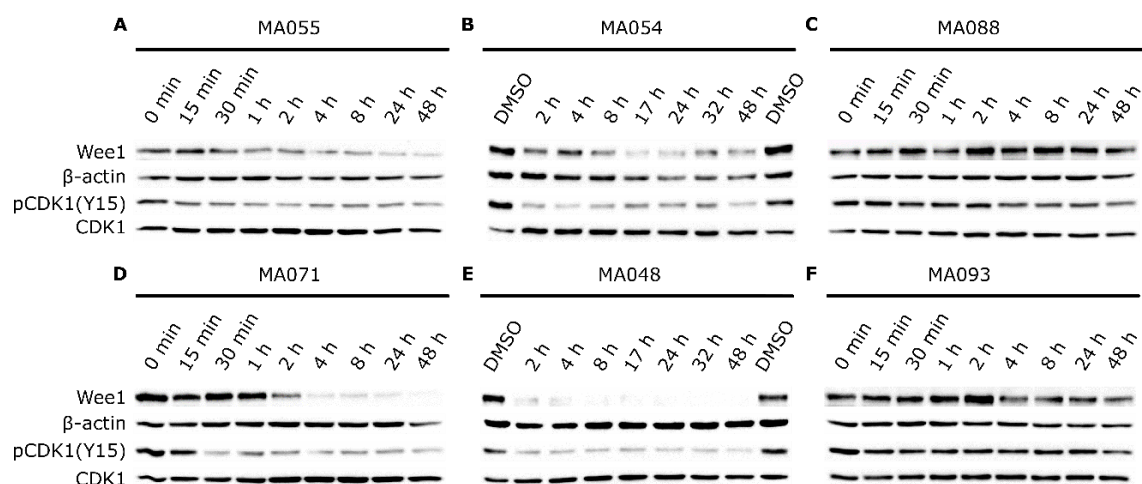
Figure 4.4: Wee1 degradation profile over time. Western blot analysis of time-dependant degradation of Wee1 in HeLa S3 cells treated with 1 µM of three VHL-PROTACs: **A**) MA055, **B**) MA054 and **C**) MA088, and three CRBN-PROTACs: **D**) MA071, **E**) MA048 and **F**) MA093, for the indicated times. The membrane was blotted for Wee1, pCDK1(Y15), CDK1 and β-actin as the loading control.

4.3.4 PROTAC selectivity

AZD1775 has been the most potent and selective Wee1 inhibitor in clinical development (Hirai *et al.*, 2009). However, AZD1775 has been found to inhibit a number of other kinase targets (Zhu *et al.*, 2017) (Chapter 3 Section 3.1.2.2). In designing Wee1 PROTAC molecules, the objective was to target Wee1 more selectively and avoid modulation of off-target kinases. Thus, selectivity was investigated using Western blot and commercially available antibodies for a number of previously identified off-target proteins of AZD1775, including PLK1, PLK2, PLK3, MAP3K4 and JAK2 (Zhu *et al.*, 2017). Efforts were focused on one PROTAC targeting each E3 ligase, MA055 for VHL and MA071 for CRBN, which were amongst the best degraders in their respective series. PROTACs MA055 and MA071 did not degrade PLK1 following treatment in HeLa S3 after 4 h (Figure 4.5). No decrease was observed in levels of PLK2, PLK3, MAP3K4 and JAK2 for the same treatment. Therefore, it indicates that the two series of Wee1 PROTACs are selective towards Wee1 for the tested kinases. Due to the dual inhibition and degradation at higher concentrations where the hook effect is observed, off target inhibition might be observed and could be explored by proteomics for instance.
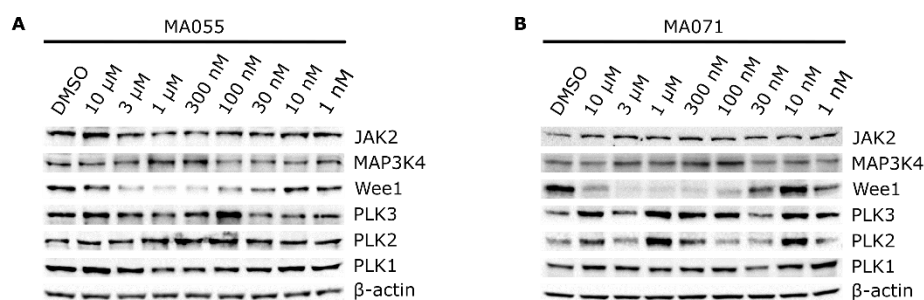
Figure 4.5: Assessment of PROTAC selectivity for AZD1775 targets. Western blot of HeLa S3 cells treated for 4 h with different concentrations of PROTACs **A**) MA055 recruiting VHL and **B**) MA071 recruiting CRBN. The membrane was blotted for JAK2, MAP3K4, Wee1, PLK3, PLK2, PLK1 and β-actin as the loading control (n = 2).

4.3.5 Target engagement

4.3.5.1 Negative controls

To validate the mechanistic activities of the PROTACs, corresponding negative control compounds for a few PROTACs were synthesised: including negMA055 and negMA054 for the VHL-series (containing *cis*-hydroxyproline), and negMA071 and negMA048 for the CRBN-series (containing an N-methylated glutarimide). These modifications to the E3 ligase-binding ligands prevent their respective E3 ligases from being recruited by the PROTAC, enabling assessment of the activities of the compounds in the absence of E3 ligase (Zengerle *et al.*, 2015; Lebraud *et al.*, 2016).

The four negative controls: negMA055, negMA054, negMA071 and negMA048, did not degrade Wee1 when treating HeLa S3 cells with a dose-response for 4 h (Figure 4.6 A, B, C and D). The four negative control PROTACs were found to inhibit Wee1 by showing some reduction in pCDK1(Y15) levels at the higher concentrations of 3 and 10 μM, following a 4 h treatment of HeLa S3 cells (Figure 4.6).

HeLa S3 cells were also treated with a range of doses of AZD1775 inhibitor. Wee1 levels stayed the same as the DMSO control at all the doses tested for 4 h (Figure 4.6 E). The inhibitory effect observed for the negative control compounds, by looking at pCDK1(Y15)

level, is lower than that of AZD1775 itself (Figure 4.6), likely due to the reduced cell penetration of the PROTACs and negative controls compared to the inhibitor.
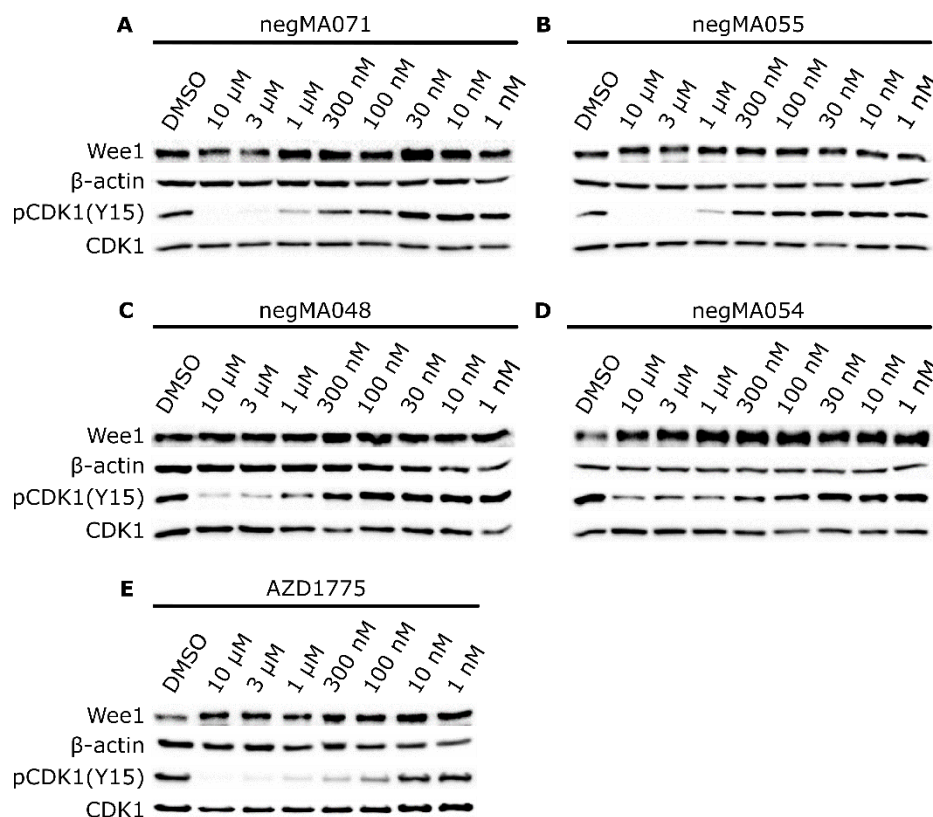
Figure 4.6: Negative controls and AZD1775 dose response in HeLa S3. Western blots of HeLa S3 cells treated for 4 h with different concentrations of **A**) negMA071, **B**) negMA055, **C**) negMA048, **D**) negMA054 and (**E**) AZD1775. The membrane was blotted for Wee1, pCDK1(Y15), CDK1 and β-actin as the loading control.

Neither negMA055 or negMA071 exhibited degradation of Wee1 in HeLa S3 cells at 24 h and up to 48 h (Figure 4.7), whereas the active PROTACs showed loss of Wee1 at these timepoints. Reduction in pCDK1(Y15) levels when treated with 1 µM for 24 and 48 h with negMA055 and negMA071 was observed (Figure 4.7). As these compounds cannot recruit the E3 ligase, they must form a binary complex with Wee1 and act as inhibitors rather than degraders in this instance. This demonstrated that the productive recruitment of VHL or CRBN is mandatory for Wee1 degradation. However, at higher concentrations of PROTAC, Wee1 activity is modulated by a combination of inhibition and degradation. MA071 showed a greater reduction in pCDK1(Y15) than negMA071, whereas for MA055, it is similar to negMA055. This indicated that the degradation activity of the CRBN-based

Wee1 PROTACs modulates Wee1 activity more effectively than the VHL-based Wee1
PROTACs.
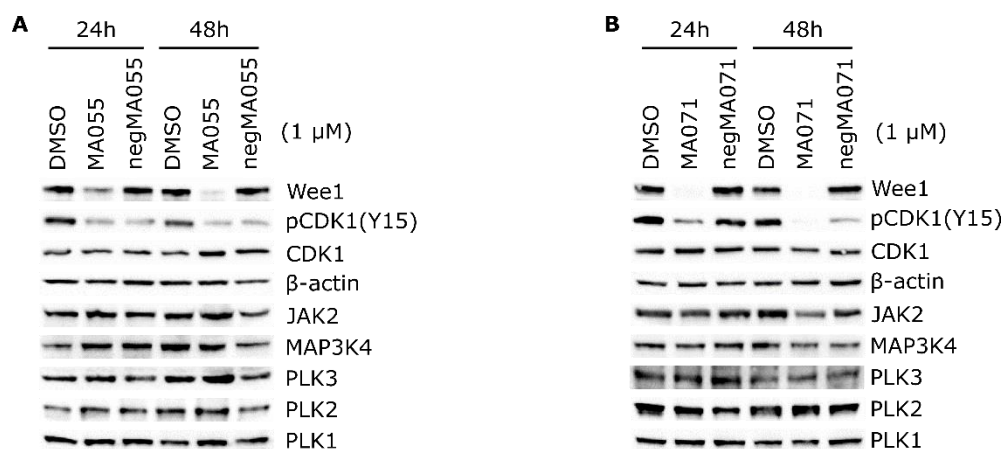
Figure 4.7: Assessment of PROTAC selectivity over 24 and 48 h. Western blot of HeLa S3 cells
treated with 0.1% DMSO, 1 µM of **A**) PROTAC MA055 and its negative control negMA055 or **B**)
PROTAC MA071 and its negative control negMA071, for 24 and 48 hours. The membrane was
blotted for Wee1, pCDK1(Y15), CDK1, JAK2, MAP3K4, PLK3, PLK2, PLK1, and β-actin as the loading
control (n = 2).

Furthermore, MA055 and MA071 significantly degraded Wee1 at 1 µM in HeLa S3 cells
for 24 h and 48 h, while the other kinases remained unaffected (Figure 4.7). Altogether,
these data indicate that the synthesised Wee1 PROTACs, using the non-selective Wee1
inhibitor AZD1775, have the desired selectivity and activity against Wee1 across multiple
time points.

4.3.5.2 Proteasome dependence and target engagement

To verify that the PROTACs are degraders dependent on the E3 ligase and proteasome
activity, their efficiency was compared in the presence and absence of proteasome and
E3 ligase inhibitors (Figure 4.8). Pre-treating HeLa S3 cells with proteasome inhibitor
MG132 (20 µM) for 2 h before adding the PROTAC for 5 h abrogated Wee1 degradation
by MA055 and MA071, indicating that the observed degradation is proteasome
dependent (Figure 4.8). Likewise, cells were pre-treated with MLN4924, an inhibitor of
neddylation of CRLs (Ceccarelli *et al.*, 2011), at 1 µM for 2 h. Wee1 degradation by MA055

and MA071 was similarly blocked corroborating the dependence of the PROTAC activity on the neddylation and activation of CRLs (CRL2^{VHL} and CRL4^{CRBN}, respectively).
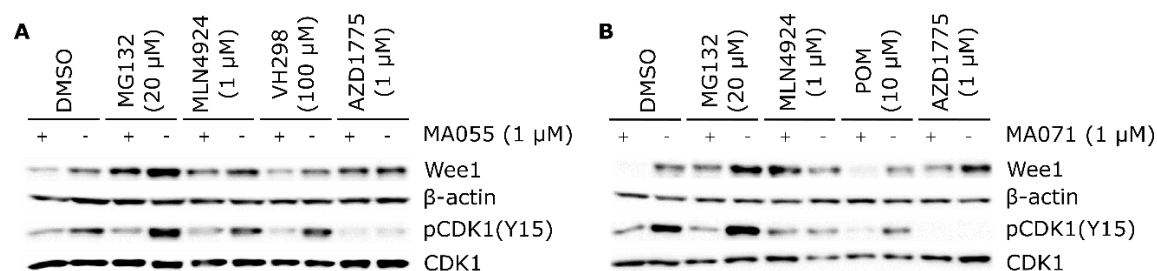
Figure 4.8: Assessment of Wee1 PROTACs target engagement. Inhibition of PROTAC mechanism for **A**) MA055 recruiting the VHL E3 ubiquitin ligase and **B**) MA071 recruiting the CRBN E3 ubiquitin ligase. HeLa S3 cells were pre-treated with DMSO, MG132 (20 µM), MLN4924 (1 µM), VH298 (100 µM) or pomalidomide (10 µM), and AZD1775 (1 µM) for 2 h prior to the addition of the indicated PROTAC (1 µM) for a further 5 h. The membrane was blotted for Wee1, pCDK1(Y15), CDK1 and β-actin as the loading control (n = 2).

Further pre-treatment of cells with inhibitors engaging the PROTAC-binding sites (target or E3 ligase) were investigated to confirm the essentiality of engaging both partner proteins for degradation. Pre-treatment with Wee1 inhibitor AZD1775 (1 µM) for 2 h and subsequent treatment with PROTACs MA055 and MA071 failed to degrade Wee1 (Figure 4.8). However, pCDK1(Y15) levels were decreased, correlating with AZD1775 inhibitory effect on Wee1 activity independently of degradation. In contrast, pre-treatment with VHL E3 ligase inhibitor VH298 (100 µM), prevented very little Wee1 degradation by MA055 (Figure 4.8 A). Similarly, pre-treatment with CRBN E3 ligase inhibitor pomalidomide (10 µM), only prevented some Wee1 degradation by MA071 (Figure 4.8 B). The abrogation of Wee1 degradation by AZD1775 was more profound than that of VH298 or pomalidomide, which did not completely recover Wee1 levels. This might be due to the high cellular concentration of E3 ligases in the cells which would require a more concentrated dose of E3 ligase inhibitor or maybe a longer pre-treatment with the inhibitor (Lu *et al.*, 2015). The lack of activity of the negative control PROTACs (negMA055 and negMA071) confirmed the essentiality of E3 ligase recruitment for their activity.

4.3.6 Activity of Wee1 PROTACs in different cancer cell lines

In a next step, it was critical to verify that the Wee1 degradation observed in HeLa S3 cells was reproducible in other cancer cell lines. Four cell lines were selected: prostate cancer cell lines PC3 and LNCaP, and breast cancer cell lines BT549 and MCF7, which are each p53 null/mutant and p53 wild type, respectively, for each tissue.
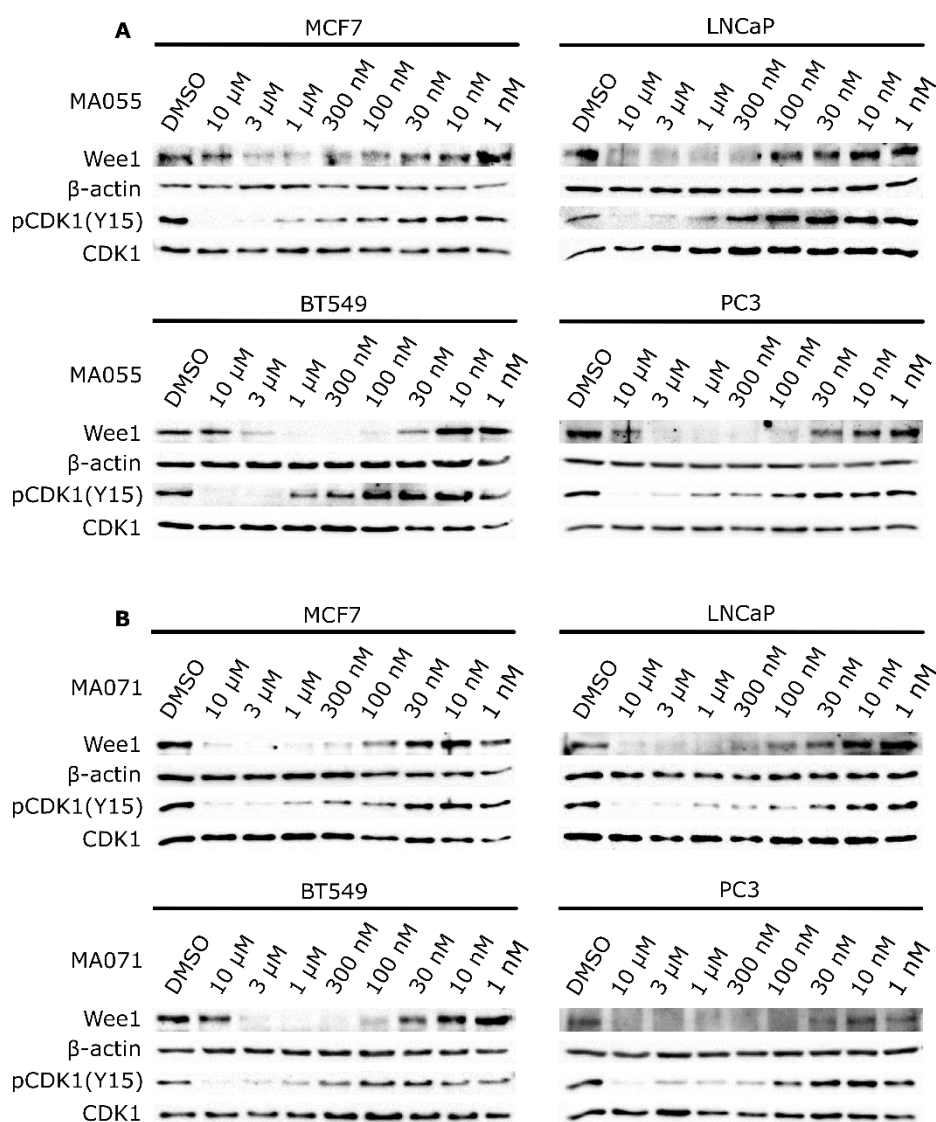
Figure 4.9: Dose response of Wee1 PROTACs in different cancer cell lines. Wee1 degradation profile of **A**) MA055 for VHL and **B**) MA071 for CRBN in a variety of cell lines: breast cancer with MCF7 (p53 wild-type) and BT549 (p53 mutant) and prostate cancer with LNCaP (p53 wild-type) and PC3 (p53 deficient), treated for 4 h. The membrane was blotted for Wee1, pCDK1(Y15), CDK1 and β-actin as the loading control.

Wee1 degradation and reduced pCDK1(Y15) levels were observed in all four cell lines following treatment with a PROTAC of each series: MA055 and MA071 (Figure 4.9). For both PROTACs, the Wee1 band largely disappears at 100 nM and above, in PC3 and BT549 cells, and at 300 nM or higher, in MCF7 and LNCaP cells. Degradation seemed less affected by the hook effect in MCF7 and LNCaP, and is more prominent in the treatments of HeLa S3, PC3 and BT549 cells. However, overall Wee1 degradation by the PROTACs is largely similar between the cancer cell lines utilising either VHL or CRBN E3 ligases.

4.3.7 Cell proliferation

After observing Wee1 degradation and reduction of pCDK1(Y15) levels in several cancer cell lines (Figure 4.9), the half-maximum response (IC_{50}) of the best PROTACs as agents of cell growth inhibition or cytotoxicity compared to their negative controls and the inhibitor AZD1775 was investigated using the MTS cell viability assay (Figure 4.10).
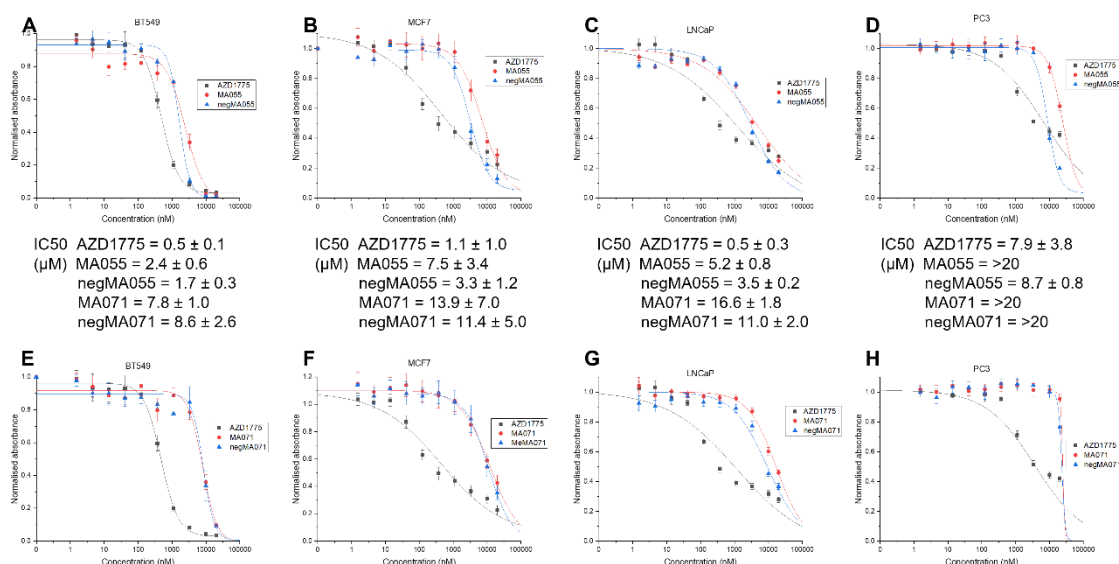
Figure 4.10: Cell proliferation inhibition of cancer cell lines by the PROTACs and control molecules. Superimpostion of cell proliferation assays normalised with DMSO for a PROTAC and its negative control for (**A**, **B**, **C** and **D**) the VHL-series and (**E**, **F**, **G** and **H**) CRBN-series in BT549, MCF7, LNCaP and PC3 cells treated for 72 h: MA055, negMA055, MA071, negMA071, and inhibitor AZD1775. IC$_{50}$ data are presented as mean ± s.d. of n = 4 biologically independent experiments.

MCF7, BT549, LNCaP and PC3 were treated for 72 h with varying doses of PROTACs MA055 and MA071, their negative controls (negMA055 and negMA071, respectively), and the inhibitor AZD1775 (Figure 4.10). BT549 cells were more sensitive to all tested compounds than MCF7 for the breast cancer cell lines, and LNCaP cells were more sensitive to all tested compounds than PC3 for the prostate cancer cell lines. MA055 exhibits similar IC$_{50}$ values (2.4 µM in BT549, 7.5 µM in MCF7, 5.2 µM in LNCaP, >20 µM in PC3) to its negative control negMA055 (1.7 µM in BT549, 3.3 µM in MCF7, 3.5 µM in LNCaP, 8.7 µM in PC3). MA071 also exhibits similar IC$_{50}$ values (7.9 µM in BT549, 13.9 µM in MCF7, 16.6 µM in LNCaP, >20 µM in PC3) to its negative control negMA071 (8.6 µM in BT549, 11.4 µM in MCF7, 11.0 µM in LNCaP, >20 µM in PC3), but these are higher than those for MA055.

To investigate the reasons for seemingly higher potency of MA055 compared to MA071, a 72-h treatment with 1 µM of the two PROTACs and their negative controls was done in

HeLa S3 cells to compare MA055 and MA071 degradation at this time point (in line with the incubation time of the cell proliferation assay). MA055 does not generate a more profound reduction in Wee1 (~50%) or pCDK1(Y15) levels than MA071 (~30%) after 72 h (Figure 4.11), consistent with earlier timepoints. Both PROTACs were found to be roughly an order of magnitude less potent than equivalent treatment with Wee1 inhibitor AZD1775 (IC_{50} values of 0.5 µM in BT549, 1.1 µM in MCF7, 0.5 µM in LNCaP, 7.9 µM in PC3).
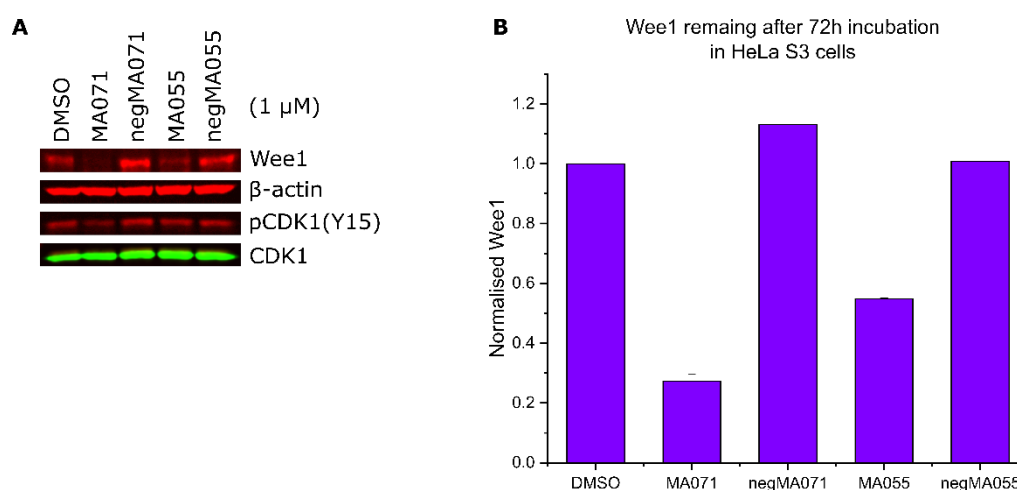
Figure 4.11: Degradation over 72 h for PROTACs MA055 and MA071, and their negative controls. **A**) Western blot of HeLa S3 cells treated with 1 µM of the indicated compounds for 72 h. The membrane was blotted for Wee1, pCDK1(Y15), CDK1 and β-actin as the loading control. **B**) Wee1 bands were quantified and normalised to the DMSO control sample for each compound (n = 2).

In order to confirm the results from the first cell proliferation assay experiment, other PROTACs were tested. BT549 cells seemed to be the more sensitive to Wee1 degradation and inhibition, so they were selected to test another PROTAC and negative control for each series: MA054 and negMA054 for the VHL-series, and MA048 and negMA048 for the CRBN-series. Results were similar to the other PROTACs tested previously (Figure 4.12). The PROTACs were less potent than AZD1775 inhibitor (IC_{50} values of 0.5 µM for AZD1775 comparing to 3.1 µM for MA054, 4.5 µM for negMA054, 1.0 µM for MA048 and 5.0 µM for negMA048).
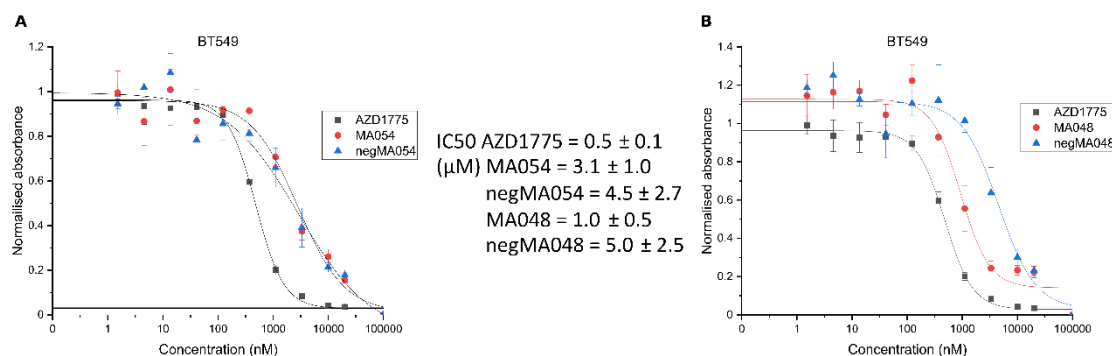
Figure 4.12: Cell proliferation inhibition of cancer cell lines by two other PROTACs. Superimpostion of cell proliferation assays normalised with DMSO for a PROTAC and its negative control for **A**) the VHL series and **B**) CRBN series in BT549 cells treated for 72 h: MA054, negMA054, MA048, negMA048, and inhibitor AZD1775. IC_{50} data are presented as mean ± s.d. of n = 4 biologically independent experiments.

Cell proliferation experiments revealed that even though the CRBN-PROTACs seem to be better Wee1 degraders than the VHL-PROTACs, our VHL-PROTACs were more cytotoxic, although these differences were only significant ($p < 0.05$) in BT549 and LNCaP cell lines. The negative controls exhibited similar effects on cell proliferation as their equivalent PROTACs so this may suggest that one or both of the E3 ligase-binding moieties has some non-specific activity mediated by another portion of the binder that could have had an impact on cell growth. Finally, the lack of efficacy of the PROTAC compounds on cell proliferation suggests the need to further optimise our PROTACs around either shorter or longer linker options, as was pursued by Li *et al.* for shorter linkers (Z. Li *et al.*, 2020).

4.3.8 Protein expression

The ternary complex formation between the target protein, the PROTAC and the E3 ligase is a determining step in PROTAC mechanism. Neo-interactions within the ternary complex between the E3 ligase and the target protein but also with the PROTAC are important and are a determining parameter for thermodynamic and kinetic favourability of ternary complex formation. They dictate the complex stability, cooperativity and life for efficient polyubiquitination. Thus, different methods were developed, and different techniques were used to try to gain insights into PPIs and ternary complex formation. Wee1 and VHL

proteins were expressed in E. *coli* cells as indicated in the Methods Chapter 2 (Section 2.18) in order to run experiments to look at the ternary complex. CRBN expression was attempted in Sf9 insect cells but was unfortunately unsuccessful even after optimisation and troubleshooting. The bacmids were obtained and the transfection in cells seemed to work, but the viral assay did not show any baculovirus content. Thus, the ternary complex experiments were done only for the Wee1:PROTAC:VHL system.

4.3.8.1 Wee1 subcloning, expression and purification

Wee1 template (291-575) (Sequence in Appendix 2) was amplified by PCR (Section 2.13) after designing primers (Section 2.11; Table 2.5) to be clone in frame with the His-tag in pET28a vector (map in Appendix 1). The three different conditions using different amounts of DMSO were successful (Figure 4.13 A). The PCR product and pET28a were then digested with XhoI and NdeI enzymes, and Wee1 was ligated into pET28a plasmid (Section 2.15). The ligation product was transformed in Turbo cells following the method in Section 2.16 to generate pWee1a (Section 2.16). Plasmids were isolated from colonies. Restriction digest using XhoI and ApaI enzymes (Figure 4.13 B; Section 2.14), as well as sequencing, were then performed to verify whether Wee1 insert had been successfully incorporated into the pET28a vector. These confirmed that the plasmid from the pWee1a clone contained the insert, and thus could be used for Wee1 expression.
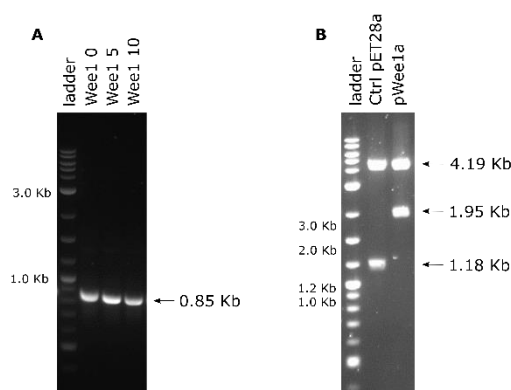
Figure 4.13: Analysis of Wee1 cloning. Agarose gels analysis of **A**) PCR products of Wee1 PCR cloning reactions with different percentages of DMSO (0, 5 and 10%) and **B**) restriction digest with XhoI and ApaI enzymes of plasmids pWee1a isolated from a clone following ligation and transformation. Kb = kilobase.

Wee1 construct was transformed in Rosetta cells for protein expression as described in Sections 2.16 and 2.18.2 (Zhu *et al.*, 2017). Wee1 protein was successfully induced as a Wee1 band appeared strongly post induction (Figure 4.14 A). The pellet was lysed and purified through a Ni-NTA affinity column due to the presence of the His-tag (Figure 4.14 A) to obtain Wee1 protein, and remove a lot of impurities. Ni-NTA is a nickel column composed of nickel coupled to nitrilotriacetic acid to purify His-Tag proteins based on the ionic interactions of the protein with the coupled metal. To obtain purer Wee1, Wee1 was then purified by an anion exchange column (Figure 4.14 B). At this point, it was recognised that the yield of Wee1 was unexpectedly high and saturated the Uno Q column, so it also came out in the flow through (FT). However, conveniently, the impurities largely bound to the column, meaning the Wee1 protein collected in the flow through was actually considerably purer than that which was eluted from the column normally. Finally, the protein was purified by size exclusion chromatography (Figure 4.14 C) to obtain Wee1 of sufficient purity to be used in subsequent assays.
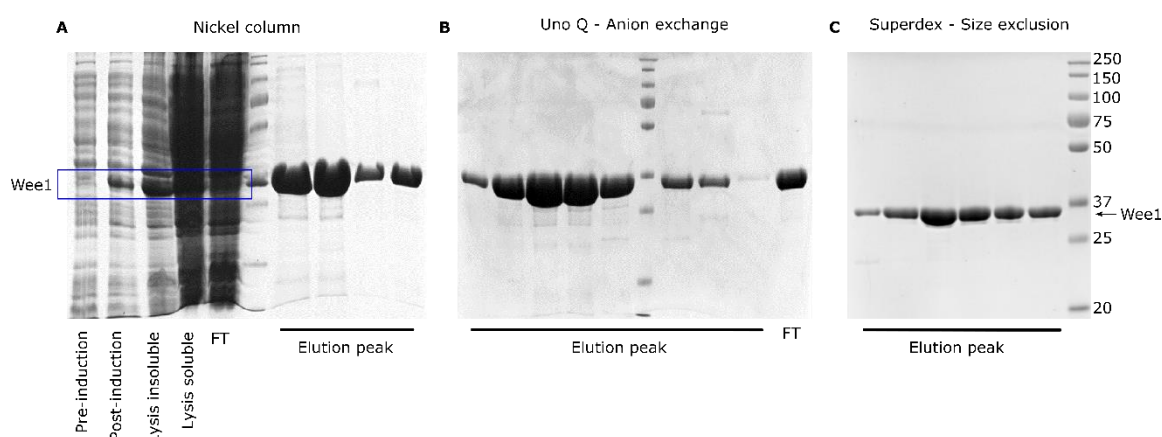
Figure 4.14: Analysis of Wee1 expression and purification. Coomassie-stained gel with **A)** Samples pre- and post-induction, samples from the soluble and insoluble fractions after lysis, and elution peak of the nickel purification with an imidazole gradient of 0 to 250 mM; **B)** elution peak of the anion exchange purification with a sodium chloride gradient of 0 to 500 mM; **C)** elution peak of the size exclusion chromatography purification. FT = flow though.

4.3.8.2 VBC expression and purification

His-tagged VBC (a heterotrimer of VHL (54–213), Elongin C (17–112) and Elongin B (1–104)) construct was transformed in BL21 (DE3) cells (Section 2.16) for protein expression as described in the method Section 2.18.3 (Galdeano *et al.*, 2014). The pellet was lysed and purified through a Ni-NTA column thank to the presence of the His-tag (Figure 4.15 A). N-terminal His-Tag was cleaved with TEV protease and purified by Ni-NTA column again to isolate the cleaved VBC and remove any possible leftover of His-Tag complex. As the VBC complex lacked a His-Tag at this point, the flow through was recovered (Figure 4.15 B). This was further purified by anion exchange column and finally by size-exclusion column chromatography to obtain pure VBC (Figure 4.15 B).
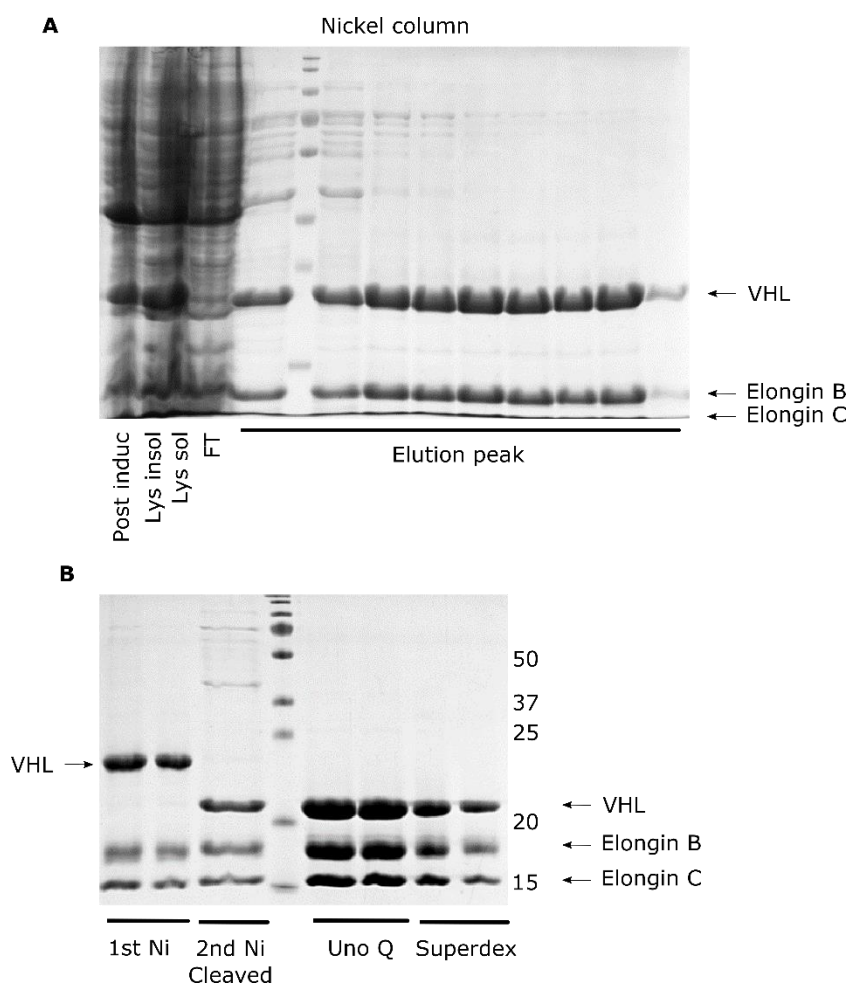
Figure 4.15: Analysis of VBC expression and purification. Coomassie-stained **A**) 10% SDS-PAGE gel of the nickel affinity column chromatography (Ni-NTA) with an imidazole gradient from 0 to 250 mM. **B**) 15% SDS-PAGE gel with the first Ni-NTA column fractions used as a reference, sample from the flow through of the second Ni-NTA column after His-Tag cleavage with TEV, anion exchange purification by Uno Q with a gradient of 0 to 500 mM NaCl, size exclusion purification with Superdex column.

4.3.9 Ternary complex evaluation

4.3.9.1 Size exclusion binding for ternary complex formation

In the first instance, to check easily the binding of the two proteins Wee1 and VHL in the presence of a PROTAC, samples were run on a size exclusion column (SEC) and compared to see if the ternary complex was observable. VBC and Wee1 were run alone, together (Wee1:VBC), and with PROTAC MA055 (Wee1:MA055:VBC) (Figure 4.16 A). Two peaks

were observed when the two proteins were run together (blue), corresponding to the same peak of the proteins when run alone. This showed that the proteins do not interact together. A new peak appeared (13.8 mL-yellow) for the ternary complex which is different from the Wee1 (15.8 mL-orange) and VBC (15.2 mL-grey) peaks. A gel was also run with a sample from each peak and confirmed the presence of both Wee1 and VBC in the new ternary complex peak (Figure 4.16 B). This suggests that the new peaks is for the ternary complex Wee1:MA055:VBC. The presence of the ternary complex under the new peak could further be confirmed using native MS.

A
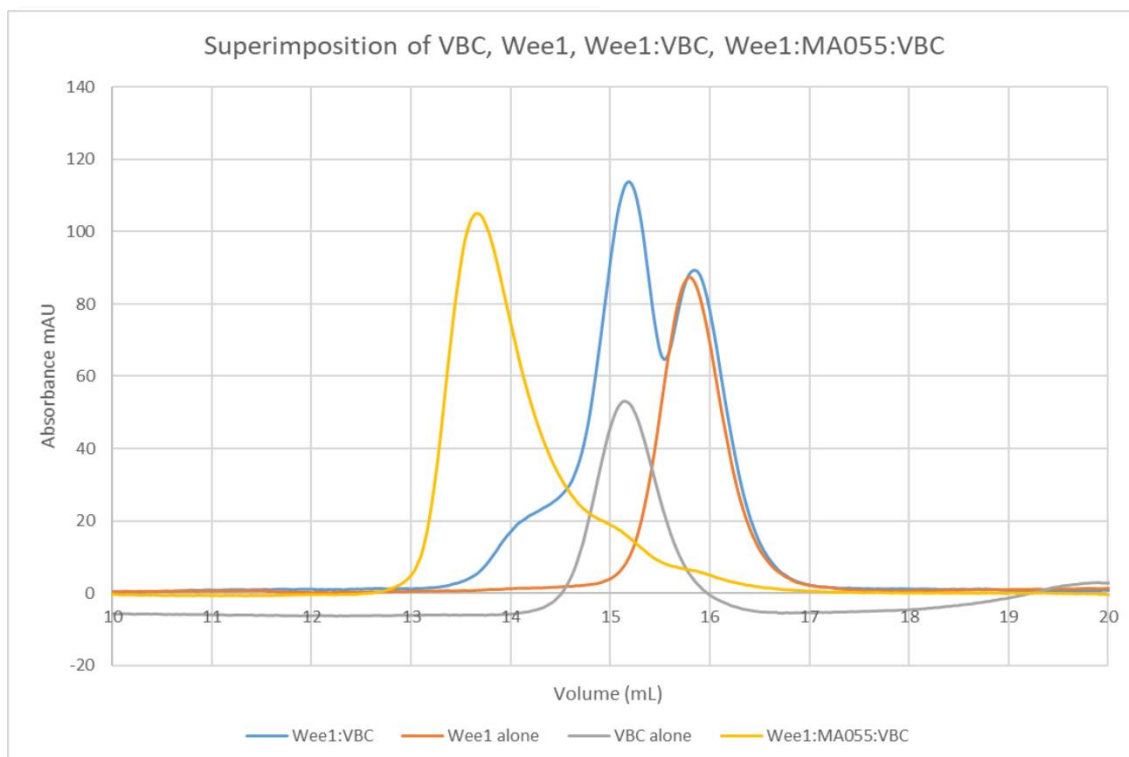
B
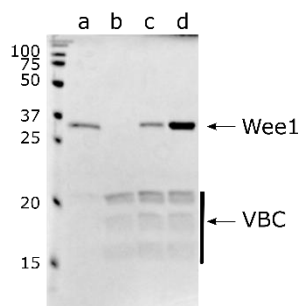
Figure 4.16: Ternary complex formation test by SEC. **A**) Superimposition of the chromatograms from size exclusion run with VBC alone (grey), Wee1 alone (Orange), the two proteins together Wee1:VBC (blue), and the ternary complex with PROTAC MA055 Wee1:MA055:VBC (yellow). **B**) Coomassie-stained gel of fractions from a) Wee1 peak, b) VBC peak, c) and d) Wee1:MA055:VBC peak collected from each different run. (2 nM of protein or compound in a 1:1 or 1:1:1 ratio were used and it was eluted with 20 mM Tris, 150 mM NaCl, 1 mM DTT, pH 8.4 on Superdex 200 10/300 column).

To confirm that the new peak was due to ternary complex formation and that both proteins interact together, a control experiment was performed using MA055 negative control: negMA055 (Figure 4.17-green). Two peaks were observed corresponding to VBC and Wee1 alone being similar to the run of the proteins ran together (blue). No peak was

observed for the ternary complex. This confirms that the negative control PROTAC does not allow ternary complex formation. Additionally, a competition experiment using Wee1 inhibitor AZD1775 was done by adding one equivalent of the inhibitor to the ternary complex: Wee1:MA055:VBC:AZD1775 (1:1:1:1 ratio) (Figure 4.17-red). Three peaks were observed for Wee1, VBC and the ternary complex showing that it was possible to disturb the ternary complex formation by preventing full binding of the two proteins Wee1 and VHL together. Furthermore, the ternary complex population seemed slightly lower than the binary peaks. This may suggest a slightly negative cooperativity as there is a ratio of 1:1 for AZD1775 and MA055 in the sample. Other experiments are needed to confirm this hypothesis.
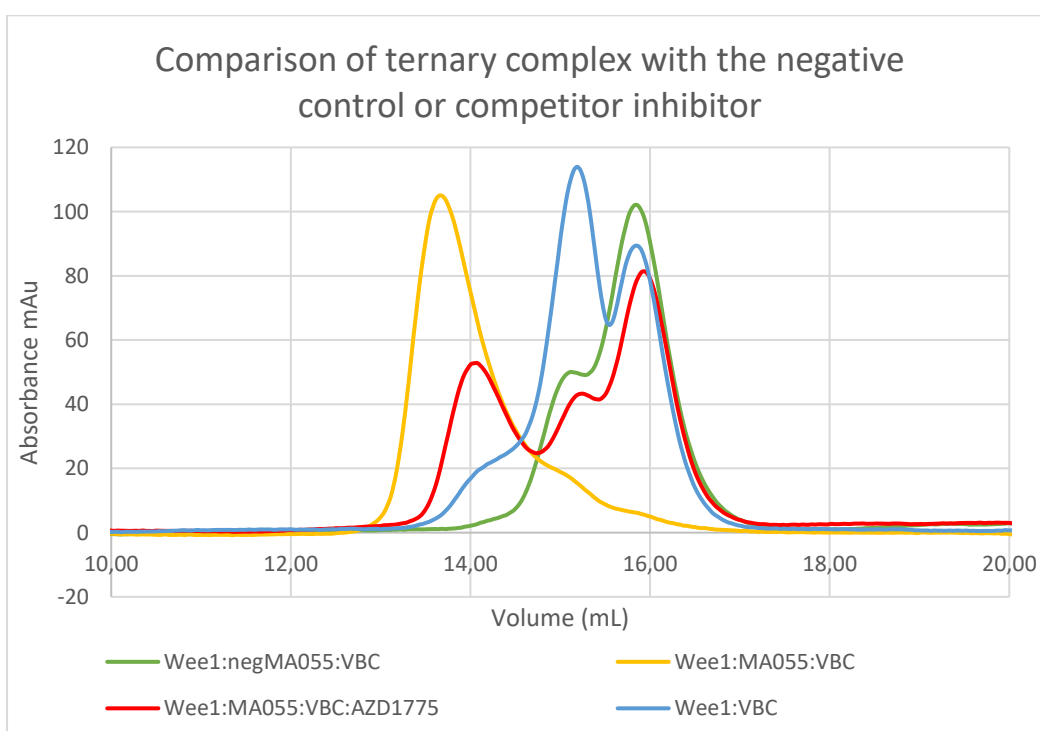
Figure 4.17: Ternary complex formation control and competition. Superimposition of the chromatograms from size exclusion chromatography of samples run with: the negative control Wee1:negMA055:VBC (green), the ternary complex with MA055 Wee1:MA055:VBC (yellow) and in competition with Wee1 inhibitor AZD1775 Wee1:MA055:VBC:AZD1775 (red) or the two proteins alone Wee1:VBC (blue).

4.3.9.2 Native PAGE

4.3.9.2.1   Optimisation and ternary complex formation

To further investigate ternary complex formation between Wee1 target protein, a PROTAC and the E3 ligase VHL, I developed a native PAGE approach to monitoring ternary complex formation. In contrast to SDS-PAGE, which uses a denaturing gel to separate molecules based exclusively on their molecular weight, non-denaturing gels in native PAGE are used to separate molecules based on their size, charge and shape under native conditions, which may allow the visualisation of ternary complex between the two proteins in the presence of a PROTAC. As this approach had not been utilised in a quantitative manner in the PROTAC field before, it could be an interesting method to develop and to assess PROTAC parameters of PROTAC ternary complex formation. Blue native PAGE uses negatively charged protein that are bound to the Coomassie dye to influence the shift of the proteins whereas clear native PAGE depends on the protein intrinsic charge (Wittig *et al.*, 2005). Thus, they could potentially be both interesting to use as they could separate the proteins differently.

Blue native PAGE and clear native PAGE were used in the first instance to see what could be observed and the conditions were subsequently optimised (concentration, gel percentage) (Section 2.19). 10% gels were used first to compare blue and clear native PAGE (Figure 4.18 A). A new band appeared when adding PROTAC MA055 to the two proteins Wee1 and VBC complex for both techniques, as shown by the arrow in Figure 4.18 A. However, the bands for the blue native PAGE gel were blurry, and the percentage acrylamide of the clear native PAGE gel was too high (Figure 4.18 A). Clear native PAGE was selected for subsequent experiments and the gel percentage was changed to 7.5% to test all the VHL-PROTACs and the two VHL-negPROTACs (Figure 4.18 B).
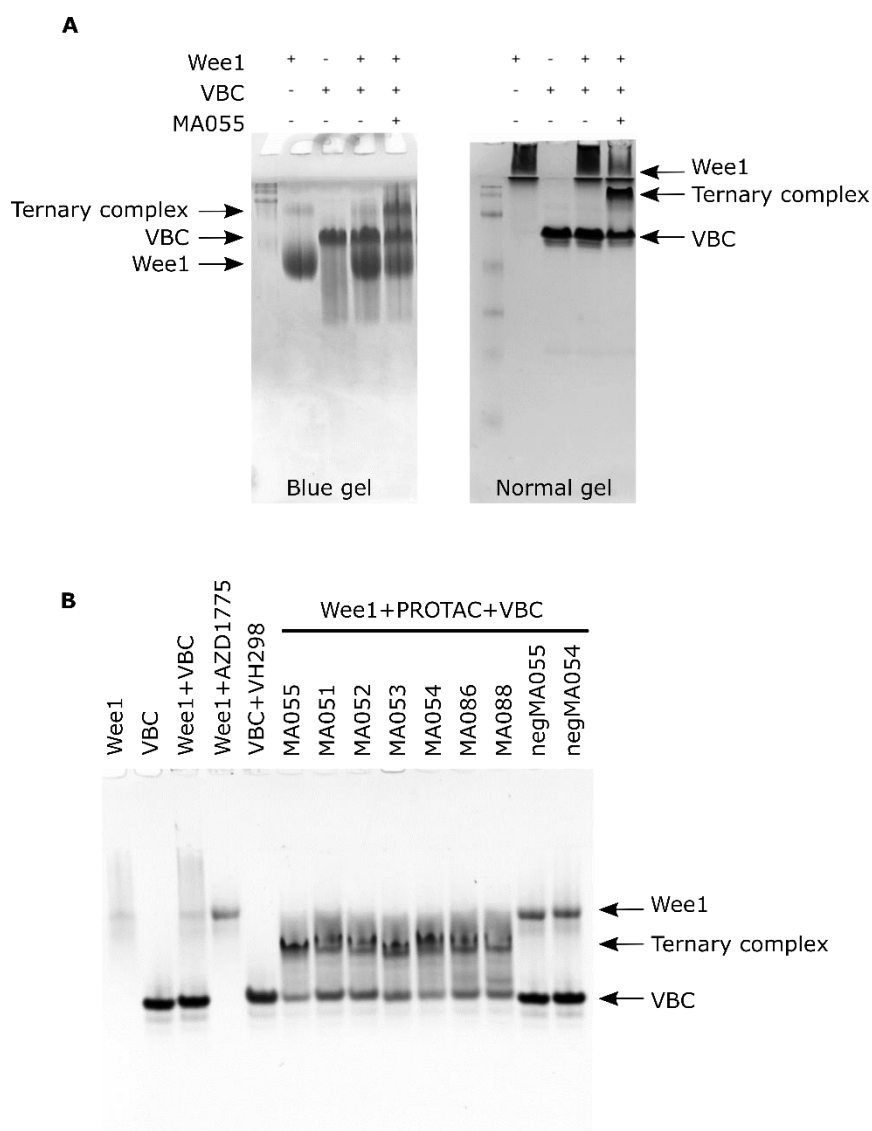
Figure 4.18: Ternary complex formation observed with native PAGE. **A**) Optimisation of the native PAGE gels and conditions by using blue native PAGE and clear native PAGE to look at the ternary complex. **B**) Comparison of all the VHL-PROTACs ternary complex formation using normal native PAGE. negMA055 and negMA054 were used as controls.

4.3.9.2.2   Competition experiments

After looking at ternary complex formation between Wee1, VBC and all the VHL-PROTACs, a competition experiment was designed to see if it was possible to stop ternary complex formation by adding the inhibitor of one of the two proteins as a binding competitor. AZD1775 was used to bind to Wee1 and VH298 was used to bind to VHL. 0.5 to 100 equivalents were used (Figure 4.19 A and B). Firstly, MA055 seemed to form a

stronger ternary complex as only the band of the ternary complex was visible (Figure 4.19 A), whereas leftovers of VBC and Wee1 were visible for MA054, when no inhibitor was added. By increasing the number of equivalents of both inhibitors, the VBC band intensity increased, suggesting a decrease in ternary complex for both PROTACs (Figure 4.19). Finally, even with 100 equivalents of ADZ1775 or VH298, the ternary complex was still present, indicating that it is probably strong and hard to break apart. The ternary complex seemed more sensitive to AZD1775, for which the VBC levels seemed to increase faster with the two PROTACs: MA055 and MA054, comparing to VH298 competition. A final experiment with more equivalents of AZD1775 (100 to 1000) showed that it was possible to break down the ternary complex a little bit more but it was not possible to fully prevent it (Figure 4.19 C). Above 1000 equivalents, it was precipitating. Overall this experiment suggests that depending on the PROTAC used, the ternary complex can have different strength and even with an excess of protein inhibitor, it is not possible to fully break it down suggesting strong PPIs between VBC and Wee1 or that new interactions might have formed in the ternary complex, making it impossible to disrupt by competitors for this experimental setup.
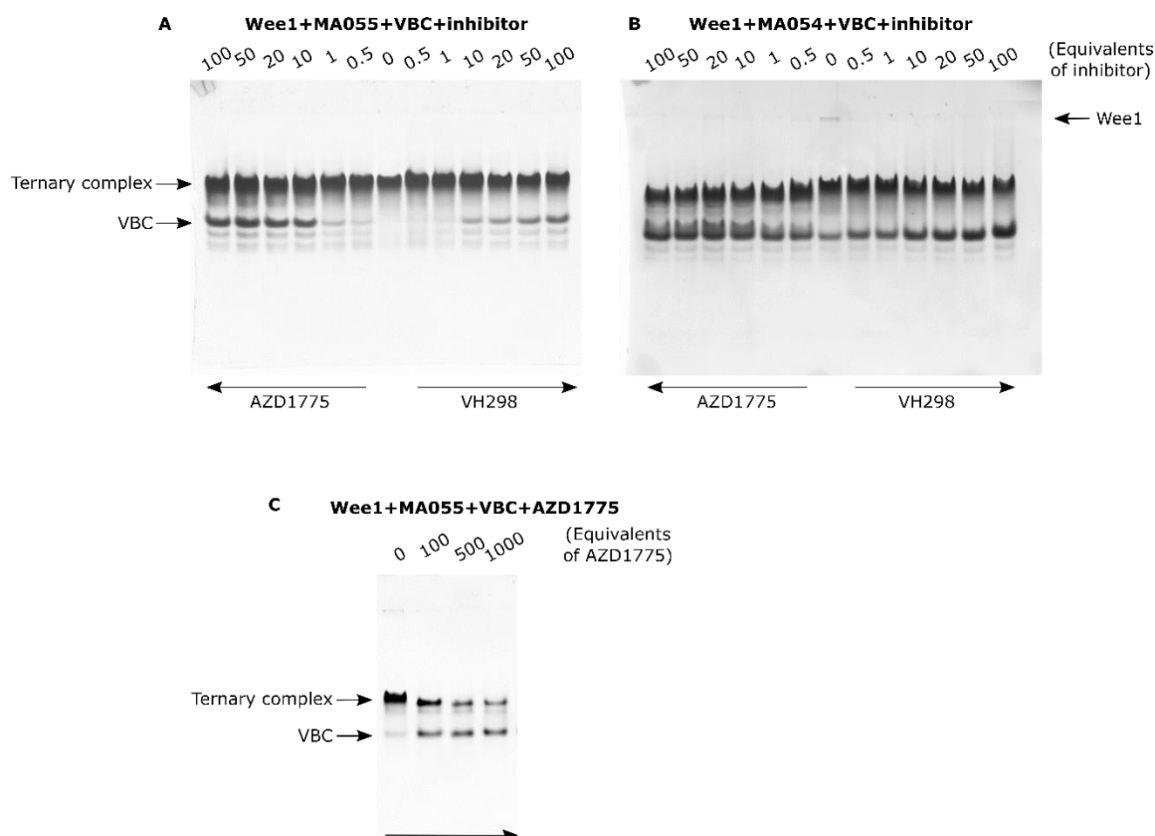
Figure 4.19: Native PAGE competition experiments. Native PAGE gels of the ternary complex with PROTACs **A**) MA055 and **B**) MA054, Wee1 and VBC proteins with the indicated number of equivalents of competitor inhibitors AZD1775 for Wee1 and VH298 for VBC. **C**) Gel of the ternary complex Wee1:MA055:VBC in competition with greater equivalents of AZD1775.

The SEC experiments showed in section 4.3.9.1 suggested that a 1:1 ratio of PROTAC to AZD1775 inhibitor could disrupt ternary complex formation significantly, whereas only a light band of binary complex is observed with the same 1:1 ratio in the native PAGE experiment. Native PAGE has not been previously used to study ternary complex formations. Difficulties to disrupt the ternary complex might come from the formation of new bonds between the two proteins under these conditions such as disulfide bonds, for which reducing conditions could potencially be studied. Other ionic interactions due to the pH, the pI of the proteins or the way that native PAGE separates proteins may also influence the ternary complex band in the gel. The maximum disruption seems to happen at 10 equivalents of AZD1775 and 100 equivalents of VH298 for MA055, and is similar for MA054 with a transition between 1 and 10 equivalents of AZD1775 and 50 and 100 equivalents of VH298. Binding assays and native PAGE experiments demonstrated

ternary complex formation for the system Wee1:PROTAC:VBC, and enabled the visualisation of the ternary complex in a qualitative way.

4.3.9.3 Ternary complex cooperativity - Isothermal titration calorimetry

After showing ternary complex formation, there was still a need to characterise the ternary complex not only qualitatively but also quantitatively. Isothermal titration calorimetry (ITC) is a technique that enables the calculation of binding constants between two partners, which can then be used to calculate cooperativity in order to study if ternary complex formation is involved.

Wee1 and VBC proteins were used to run ITC experiments to obtain binding constants for binary and ternary complexes between VBC and the PROTAC MA055, and between VBC and the binary complex MA055:Wee1. The protocol can be found in the Methods Section 2.20. Firstly, both inhibitors VH298 for VHL and AZD1775 for Wee1 were titrated into their respective protein to verify that that binding could be observed in the calorimeter and that the proteins were functional (Figure 4.20). Titration of VH298 into VBC was comparable to the published data (K_d = 90 ± 5 nM published data vs. K_d = 46 ± 9.2 nM in this study) (Frost *et al.*, 2016) as well as titration of AZD1775 into Wee1 (Zhu *et al.*, 2017). The transition for the titration of AZD1775 into Wee1 was very small but similar to the literature (K_d = 13.4 ± 1.2 nM) (Zhu *et al.*, 2017), however, a binding isotherm could not be adequately fitted to the data. The transition is very small with ~ 1 µcal/s, and there is the presence of spikes on the second part of the graph likely due to a little buffer mismatch (Figure 4.20 B). For this reason, the K_d was not determined for the experiment as it induced too much error in the calculation. These first experiments confirmed that ligand binding to both proteins could be observed in the calorimeter and affirmed that I could then continue with the PROTACs.

N(sites) = 0.688 ± 0.003
K_d (nM) = 46.0 ± 9.2
ΔH (cal/mol) = -7,570 ± 78
ΔS (cal/mol/deg) = 8.2

N(sites) = 0.676 ± 0.015
K_d (nM) = ND
ΔH (cal/mol) = -2,310 ± 186
ΔS (cal/mol/deg) = 47.3
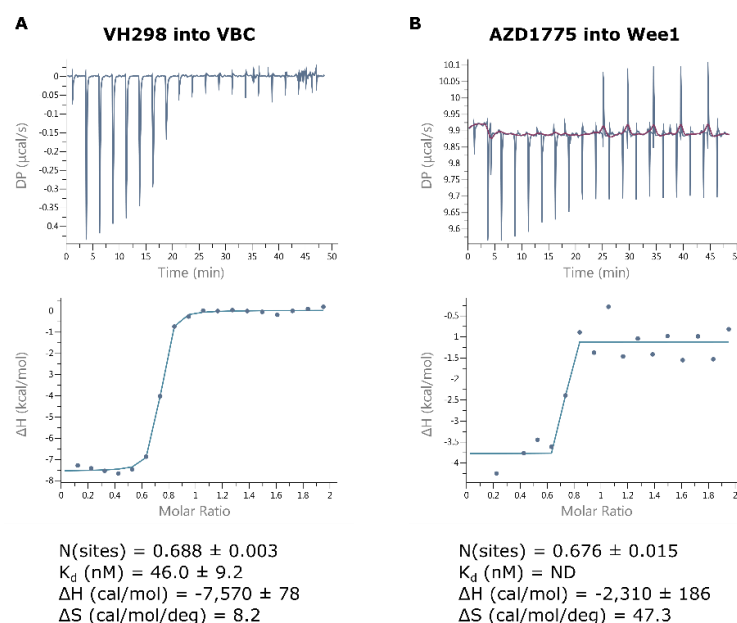
Figure 4.20: Test of the binding between the ligands (inhibitors) and their respective protein. ITC titrations of **A**) VH298 (300 µM) into VBC (30 µM) and **B**) AZD1775 (300 µM) into Wee1 (30 µM). Raw data (above) and fitted curve (below).

To assess ternary complex formation and cooperativity in ITC, it is possible to measure the binary and ternary complex binding constant. A protein is placed in the syringe and titrated into the PROTAC in the cell, by a series of injections releasing heat when the protein binds to the PROTAC. The heats are measured and allow determination of different parameters such as enthalpy (ΔH), entropy (ΔS) and binding affinity (K_d). For ternary complex formation, a protein is placed in the syringe, and is then titrated in the cell with the PROTAC and the other protein in binary complex. It was decided to titrate VBC (200 µM, in the syringe) into the PROTAC or binary complex PROTAC:Wee1 (20 µM, in the cell). The binary complex PROTAC:Wee1 was prepared in a 1:2 ratio in order to have the PROTAC fully into complex. This setup was chosen because Wee1 was observed to be more stable/less prone to aggregation at low concentration or when bound to one of its ligands, while VBC gave much stronger heats in response to binding its ligand than Wee1 did. Concentrations were decreased to 200/20 µM instead of 300/30 µM to use less sample and keep Wee1 concentrations as low as possible. A final test of titration of VBC into VH298 was performed (Figure 4.21 A), which correlated with the literature (K_d = 90 ± 5 nM published data vs. K_d = 38.8 ± 24.8 nM in this study) (Galdeano *et al.*, 2014;

Gadd *et al.*, 2017) and confirmed that changing the titrant and titrating solution was also effective, as well as using 200/20 µM for the sample.

N(sites) = 1.05 ± 0.01
K$_d$ (nM) = 38.8 ± 24.8
ΔH (cal/mol) = -6,180 ± 254
ΔS (cal/mol/deg) = 13.2

N(sites) = 0.554 ± 0.017
K$_d$ (nM) = 353 ± 131
ΔH (cal/mol) = -5,200 ± 265
ΔS (cal/mol/deg) = 11.3

N(sites) = 0.943 ± 0.022
K$_d$ (nM) = 191 ± 88
ΔH (cal/mol) = -6,075 ± 300
ΔS (cal/mol/deg) = 10.4
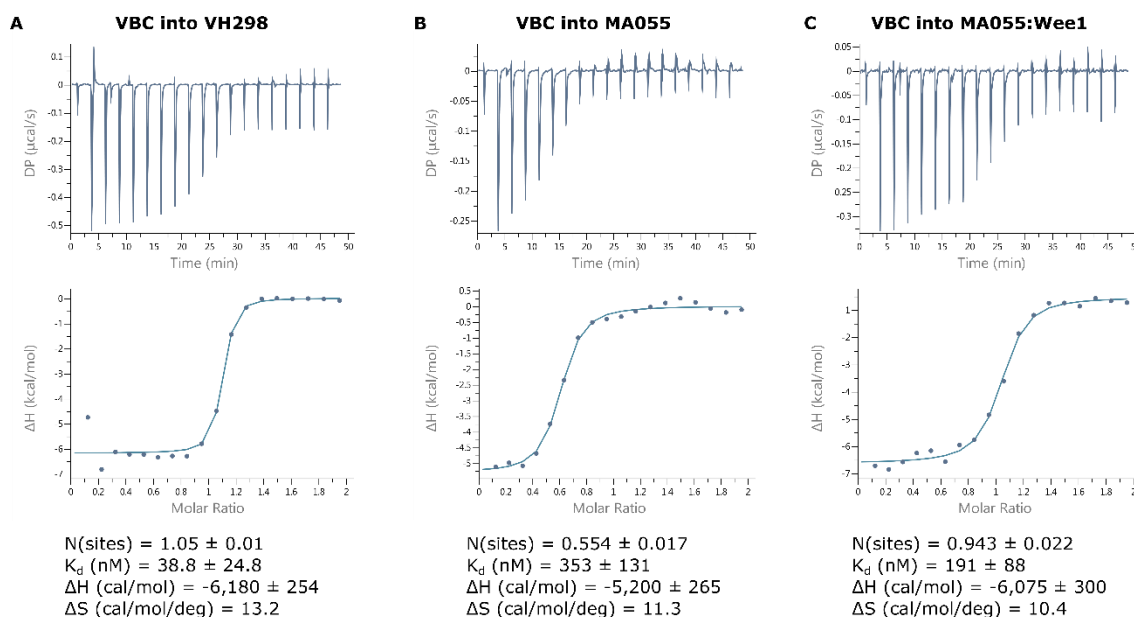
Figure 4.21: ITC titrations for ternary complex analysis. Raw data (above) and fitted curve (below) of the **A**) titration of VBC into VH298, titration of **B**) VBC into the PROTAC MA055 and **C**) VBC into Wee1:MA055. Experiments performed in duplicate (200/20 µM).

As MA055 is the most potent PROTAC of the VHL-series, it was chosen for use in the experiments. The binary complex binding constant was obtained from titration of VBC into the PROTAC: K_d(VBC:MA055) = 353 ± 131 nM, and then the ternary complex binding constant was obtained from titration of VBC into the binary complex Wee1:PROTAC: K_d(Wee1:MA055:VBC) = 191 ± 88 nM (Figure 4.21 B and C). It was then possible to calculate a cooperativity value for the ternary complex: α = K_d(VBC:MA055)/K_d(Wee1:MA055:VBC) = 1.9. Because of Covid-19 restrictions, I was not able to access the instrument sooner and as such I was not able to do ITC experiments for all the PROTACs. However, the cooperativity of Wee1:MA055:VBC ternary complex is 1.9 (>1), which suggests that ternary complex is favoured and could explain MA055's potency. However, more repeats as well as data with other PROTACs would be useful to study the cooperativity better. This could not be done due to covid restrictions and access to ITC facilities in Manchester.

4.3.9.4 Crystallography

To obtain more information about the ternary complex and the importance of the linker, crystal trays were set up with Wee1:MA055:VBC ternary complex using four different screens (768 conditions – details in Section 2.21). The Wee1 protein was cleaved using thrombin to use in the ternary complex for crystallography to avoid unwanted interactions from the tag. Wee1 was incubated with thrombin to remove the purification tag and run through a Ni-NTA affinity column to purify it from possible leftover of uncleaved Wee1 protein. The flow through was recovered (with the untagged protein) and used for the ternary complex formation.

The ternary complex was prepared and purified by size exclusion column to remove any excess of protein, and trays were prepared as described in Section 2.21. Two trays (using Structure screen 2 MD1-03 box 1) were set using 10 mg/mL of ternary complex but too much precipitation was observed in the drops. Thus, the concentration was decreased to 5 mg/mL of complex to set up new trays for the four selected screens (Molecular Dimensions: Structure screens 1 and 2, PACT PREMIER MD1-29, ProPlex). Crystals were found in one condition after 7 days incubation and kept growing for a few weeks (PACT PREMIER - 0.2 M NaF, 20% PEG 3350). A refinement tray was set by changing the PEG concentration (14-24%) from left to right and the pH from top to bottom (pH 7.5-8.5), keeping NaF concentration constant (0.2 M). Some crystals were formed and were analysed by X-ray crystallography. However, they appeared to be NaF salt crystals following a crush test and collection of single diffraction images (Figure 4.22; Section 2.21). Thus, no ternary complex crystal structure was obtained from these crystallisation experiments, even after a few months of incubation. Trying another screen could maybe be useful or trying other PROTACs in the ternary complex.
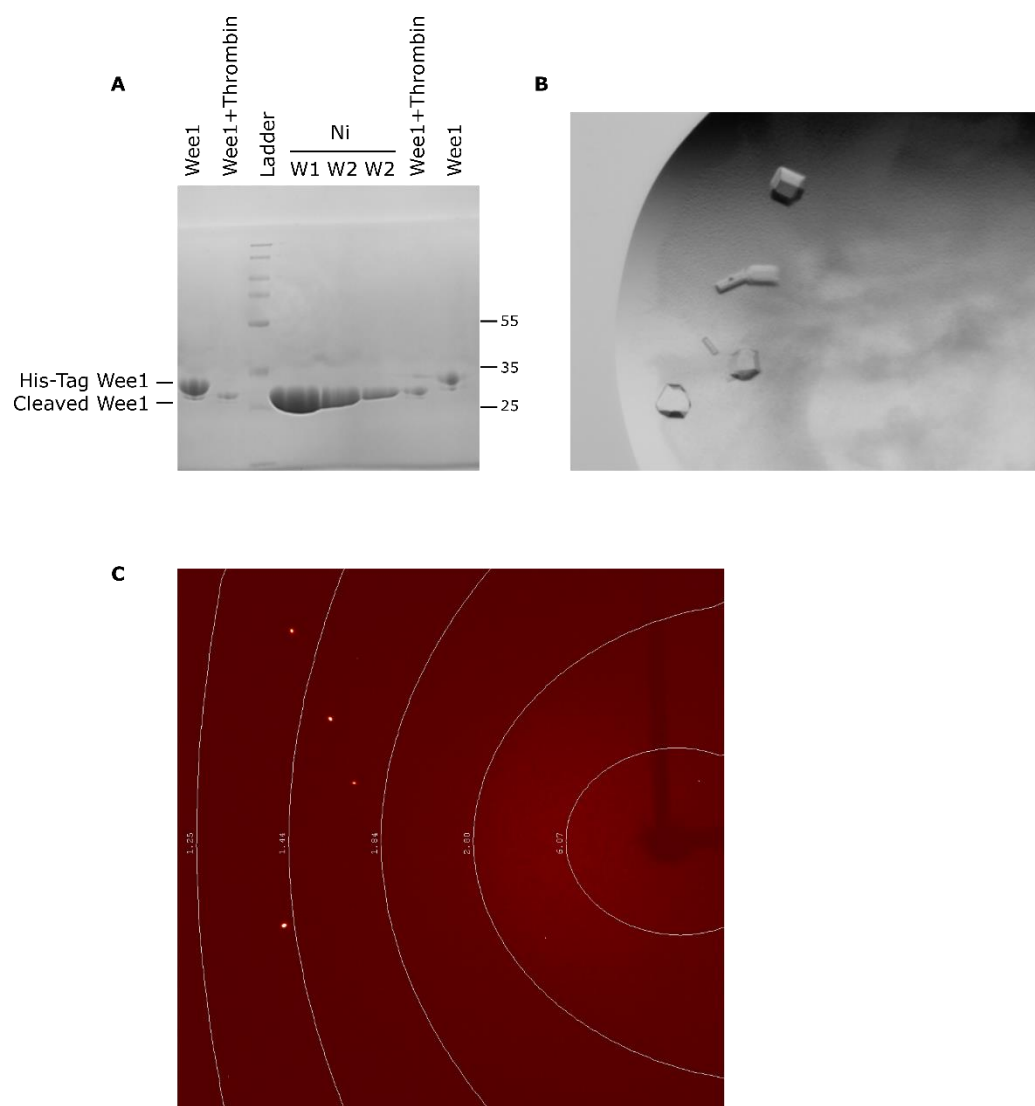
Figure 4.22: Attempt of ternary complex crystallography. **A**) Wee1 gel before and after thrombin cut. W1-W3 are the washes from the Ni-NTA affinity column to purify Wee1 after the thrombin cut. **B**) Picture of the salt crystals obtained with 0.2 M NaF and 20% PEG 3350 using a microscope with polarisator. **C**) Diffraction image of one crystal acquired with the CCD (charge-coupled device) detector.

4.4 Conclusion

An SAR of Wee1 PROTAC degraders was designed, synthesised and assessed in cancer cells. Using the Wee1-VHL or Wee1-CRBN pairs, I showed that both E3 ligases can be hijacked to induce productive and selective Wee1 ubiquitination and degradation, provided the right length and nature of linker. For both series, short and long linkers seemed more potent than intermediate length linkers. Short linkers (alkyl or PEG) could lock in a favourable conformation and thus reduce the enthalpic cost by decreasing the flexibility of the PROTAC, and longer linkers could allow freedom. However, medium linker might be too intermediate and not form ternary complexes easily. New interactions between protein-protein or protein-ligand are expected to decrease the entropy (Gadd *et al.*, 2017) so there is a balance between cooperativity, PPIs and PROTAC flexibility. Moreover, the number of amide bonds in the molecule seemed to decrease PROTAC degradation, as well as the nature of the linker, with PEG linkers being less efficient than alkyl linkers. It was hypothesised that when degradation was decreased due to the nature of the PROTAC that could be less cell penetrant or less stable in the cells and media.

The PROTACs also reduced pCDK1(Y15) levels, a key signifier that Wee1 activity had been modulated. However, in both cases the negative control PROTACs decreased pCDK1(Y15) levels, showing the dual inhibition/degradation at higher concentrations. The treatment of HeLa S3 cells at different time points resulted in selective Wee1 degradation over other off-targets of AZD1775 such as PLK1 (a crucial regulator of Wee1), PLK2, PLK3, JAK2, MAP3K4.

Cell growth experiments revealed that even though the CRBN-PROTACs are better degraders of Wee1 than the VHL-PROTACs, the VHL-PROTACs were a little bit more cytotoxic. PROTACs lack of efficacy compared to AZD1775 inhibitor suggests the need to further optimise Wee1 PROTACs and improve degradation activity.

Following the observations of this first SAR of Wee1 PROTACs recruiting either VHL or CRBN E3 ligases, it was interesting to see that the CRBN-series was overall more potent than the VHL-series and that the linker had a major influence on the degradation profiles (Figure 4.23). It would be useful to design a new generation of PROTACs to improve the

potency and possibly the cell penetration by removing an amide bond in the molecule for instance or methylating it. As the CRBN-series of PROTACs seemed to be most efficacious with shorter linkers, then exploring short, rigid linkers could be useful to verify that these linkers can lock the PROTAC conformation to recruit the two proteins favourably for potent degradation. I would be also useful to check the PROTACs cell penetration and solubility that are important parameters for degradation. For the VHL-series, shorter or long linkers with one less amide bond could be interesting to check our hypothesis about cell penetration and PROTACs conformation improving potency, given that the PROTACs with the greatest potency were those with the shortest and longest alkyl linkers. This will be developed in the next Chapter 5. Donovan *et al*. also observed a high tolerance in the variation of the linker's length for kinases to form productive ternary complex for degradation, which reflects the observations made for Wee1 PROTACs (Donovan *et al.*, 2020). As a matter of fact, a variety of linkers are efficient for both E3 ligases used, especially CRBN. They also identified Wee1 as a highly degradable kinase, which suggests that ternary complex with the PROTACs might not be the only factor influencing selectivity. Linker attachment and length, as well as target expression and location (Békés *et al*., 2022), can also be very influential as a lot of PROTACs they used in their study feature the same attachment on the nitrogen of pomalidomide, or the amine of VH032, as well as the benzene/piperazine motif of Wee1 inhibitor.
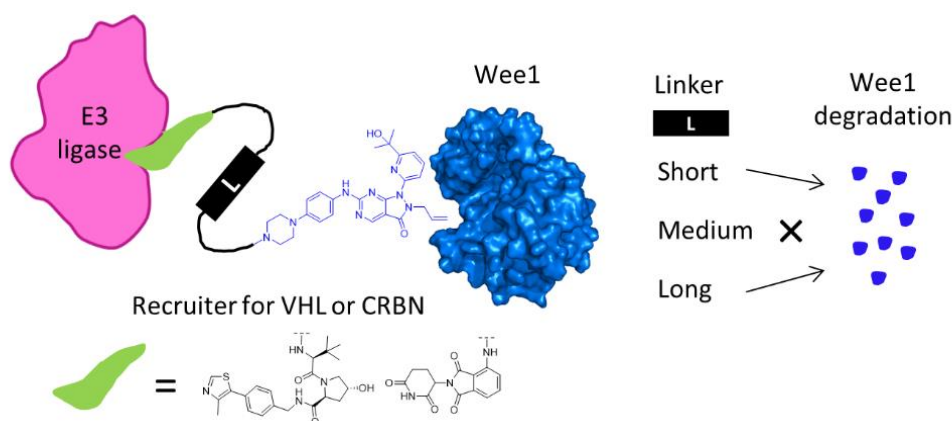
Figure 4.23: Summary of Wee1 degradation by PROTACs recruiting VHL or CRBN E3 ligases. Short and long linkers seem better than intermediate length linkers.

Finally, ternary complex formation was investigated qualitatively using proteins for the Wee1:PROTAC:VBC system for a binding assay with a size-exclusion column and by native PAGE experiment. These experiments suggest favourable ternary complex formation, though it was difficult to establish the strength of these complexes. ITC was used to quantify the ternary complex binding with PROTAC MA055 and suggested small positive cooperativity, confirming the observations made from the previous binding experiments.

Cooperativity governs formation of productive complexes that results in effective target degradation (Rodriguez-Rivera *et al.*, 2021). This could explain our observations, if Wee1 degradation and cooperativity are directly correlated, both shorter and longer linkers facilitate productive ternary complex formation through favourable and cooperative complex formation, while the intermediate length linkers due to steric clashed for instance, could be constrained from doing so. By offering an input in the transition states kinetics leading to productive ubiquitination of the target (Rodriguez-Rivera *et al.*, 2021), Rodriguez-Riviera and Levi suggest that cooperative ternary complex formation must balance the needs of effective induction of proximity between the components against overstabilisation of earlier energy states that are unproductive. This means that there should be a balance between the enthalpy of ternary complex formation and the entropy of the PROTAC rearrangement. In this case, intermediate length linkers may stabilise and lock the complexes in an unproductive form. The recent discovery of highly cooperative FAK PROTACs identified a series of FAK:PROTAC:E3 complexes, with longer and shorter linkers yielding stronger FAK degradation than intermediate ones, owing to their higher cooperativities (Law *et al.*, 2021). It was hypothesised that while both showed strong cooperativity, the shorter linker rigidity could be a key factor in the even more potent degradation, which is what also seems to happen with our Wee1 PROTACs.

5 Optimisation of Wee1 PROTACs

5.1 Introduction

After synthesising and testing a first generation of PROTACs targeting Wee1 kinase as described in Chapter 3 and Chapter 4, I was able to compare both series recruiting either VHL or CRBN E3 ligases with different type of the linker. Overall, the PROTAC series recruiting the CRBN E3 ligase was more potent than the series of PROTACs recruiting the VHL E3 ligase. Shorter and longer linkers seemed to induce better degradation, whereas intermediate length linkers induced little to no degradation. This could potentially be explained by the favourability of ternary complex formation for different linker lengths (Bemis *et al.*, 2021). Reducing hydrogen bonding atoms by reducing the number of amide bond appeared to improve PROTAC potency, likely due to cell penetration, and would be helpful to optimise the molecules with this in mind.

With these observations and hypotheses in mind, I worked on optimising Wee1 PROTAC synthetic route in order to improve PROTACs properties by removing an amide bond in the molecule, and tuning the length of the linker. This required the synthesis of a new AZD1775 building block. New short linkers such as propyl, but also linkers that could lock the PROTAC linker conformation by imbuing rigidity, such as benzyl and pyrrolidine were selected for the CRBN-series. This would allow the exploration of entropically locking the PROTAC conformation in ways that might favour ternary complex formation. These efforts were focused on using the CRBN E3 ligase, which seemed to be more potent for the first generation, and appeared to somewhat favour shorter linkers, with a study by Li *et al*. published during the project identifying ZNL-02-096, with a three-atom linker, as being a highly potent Wee1 degrading PROTAC (Z. Li *et al.*, 2020). Four new CRBN-PROTACs, including MA144, which is analogous to ZNL-02-096, and a negative control were designed and synthesised. The synthesis of new VHL-PROTACs was also attempted for which two long and three short alkyl linkers were selected. All new PROTACs were assessed in cells to look at their potency and to compare them to the first generation of PROTACs (Chapters 3 and 4), with the best PROTACs explored in more detail.

5.2 Aims and objectives

The first aim is to design and synthesise a second generation of PROTACs for both CRBN- and VHL-series to improve PROTAC potency, and study the influence of linker length and rigidity for both series, as well as the effect of losing an amide bond.
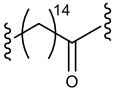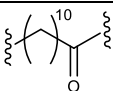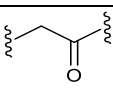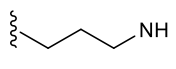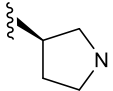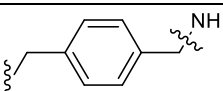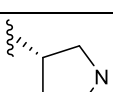
The second aim is to assess the PROTACs in cancer cells, and compare their potency to the PROTACs from the first generation.

5.3 Results and discussion

5.3.1 Synthesis of a second generation of Wee1 PROTACs

A new generation of Wee1 PROTACs was designed to improve PROTACs recruiting both VHL and CRBN E3 ligases (Table 5.1). Short and rigid linkers were selected for the CRBN-series. Short and long alkyl linkers were selected for the VHL-series.

Table 5.1: Focused SAR of Wee1 PROTACs to create a second generation recruiting two E3 ubiquitin ligases VHL and CRBN by changing the linker's length and type. The right side is attached directly to the E3 ligase recruiter: amine of VH032 with the carbonyl of the linker for the VHL-series or pomalidomide with the nitrogen atom of the linker directly attached to thalidomide, and the left side is attached to piperazine of AZD1775 analogue **40** as indicated in Scheme 5.2 and Scheme 5.6.

PROTAC	E3 ligase	Linker	Linker length
MA198	VHL		15
MA199			11
MA204			2
MA144	CRBN		3
MA159			3
MA162			6
MA165			3

5.3.1.1 Synthesis of the new AZD1775 building block

In order to create a new generation of PROTACs, a new AZD1775 building block **40** was synthesised, similar to the one of the first-generation **13** but with no linker attached (Scheme 5.1). Instead, it presents a free amine on the piperazine to allow direct nucleophilic substitution with a linker. This removes an amide bond in the molecule compared to the first generation and also allows the linker's length to be decreased more readily.
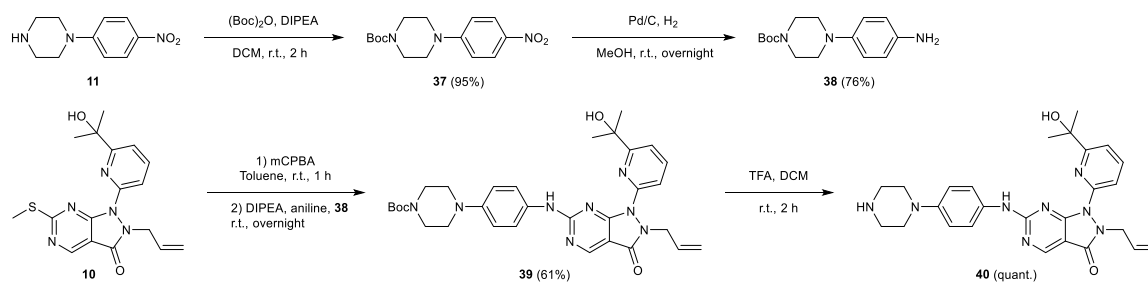
Scheme 5.1: Synthesis of AZD1775 building block **40** for the second generation of PROTACs.

In a first instance, the aniline was functionalised through two steps (Scheme 5.1). First, the amine of piperazine **11** was Boc protected in very good yield (95%) to avoid its reaction in the next step, and then the nitro group of **37** was reduced with Pd/C and H_2 to obtain amine **38** in 76% yield. **38** could then be coupled to the commercially available building block **10**. The sulfur of **10** was oxidised with mCPBA and aniline **38** was added by nucleophilic substitution to form **39** in 61% yield. The piperazine of **39** was then Boc deprotected to obtain an amine **40** in quantitative yield, that can then be attached to a linker to further synthesise the PROTAC molecules.

5.3.1.2 Synthesis of the second generation of Wee1 PROTACs for the CRBN-series

To create the new generation of Wee1 PROTACs recruiting CRBN (Scheme 5.2), four PROTACs were synthesised with new shorter linkers for the CRBN-series: a propyl, *R*-pyrrolidine, *S*-pyrrolidine, and benzyl (Scheme 5.3; Table 5.1).
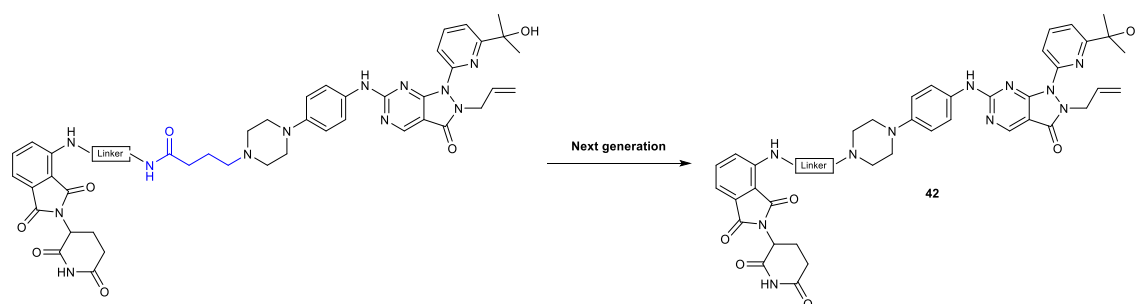
Scheme 5.2: Structures of the first and second generations of the CRBN-series of PROTACs targeting Wee1. The second generation was obtained by removing the amide bond and the three-carbon linker in blue.

The four linkers were attached to AZD1775 building block **40** by a nucleophilic substitution in the presence of a base to give **41a-d** in moderate yields: 34-92%. The building blocks of AZD1775 and linkers **41a-d** were then Boc deprotected to obtain an amine and attached to pomalidomide by nucleophilic aromatic substitution to give four PROTACs: **42a (MA144)**, **42b (MA162)**, **42c (MA165)** and **42d (MA159)** in low yields: 26-45%, respectively, due to the difficulties in purifying the PROTACs with manual normal phase column chromatography. Compounds were purified twice to be used for biological assays.
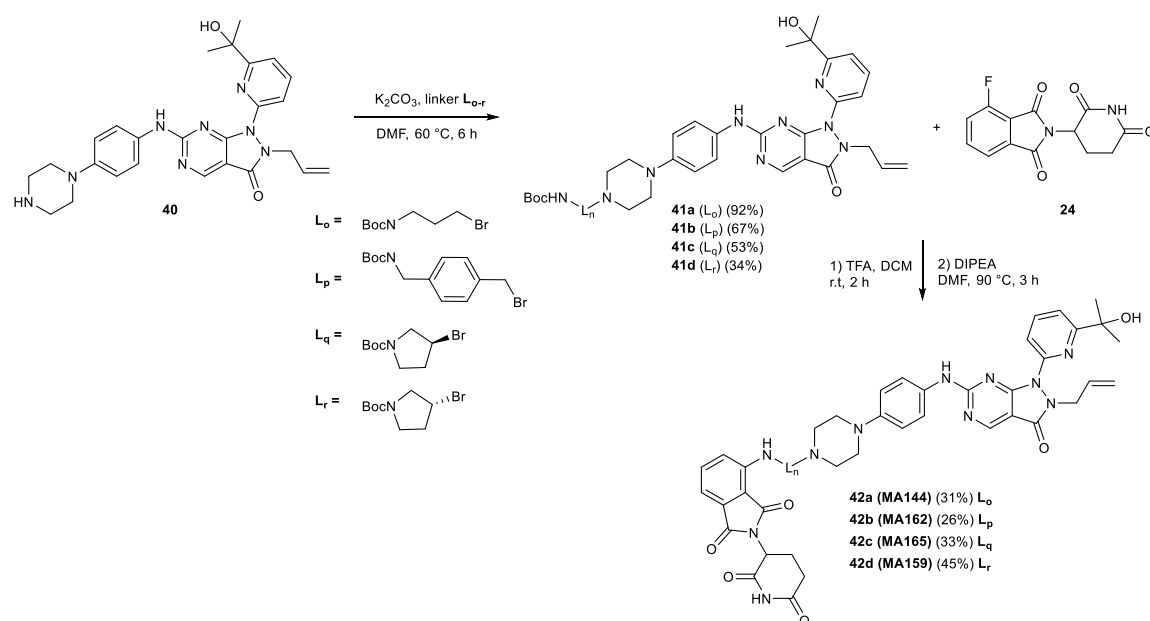
Scheme 5.3: Synthesis of the second generation of Wee1 PROTACs recruiting CRBN E3 ligase **MA144**, **MA162**, **MA165** and **MA159** where the nitrogen of the linker is the nitrogen of the pomalidomide.

The propyl linker L_o was chosen because it is short with only three carbons in the linker. The pyrrolidine linkers L_q and L_r were chosen because they copy the propyl linker with three carbons as shown in Scheme 5.4 but are restrained in fewer conformations by the additional methylene in the pyrrolidine ring. We hoped that this linker might lock the PROTAC molecule in a useful conformation that might favour ternary complex formation and thus improve degradation. Also, the stereocentre of the pyrrolidine allows two similar PROTACs to be made, but with a different orientation of AZD1775 building block, either at the front or at the back. The benzene linker L_p was chosen to bring length with

six atoms in the linker but rigidity with the ring. They are all shorter than the linkers used for the first generation of Wee1 PROTACs recruiting CRBN.
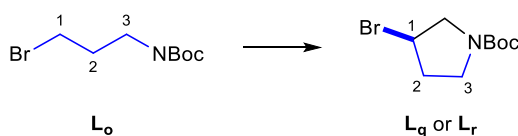
Scheme 5.4: Propyl vs pyrrolidine.

5.3.1.3 Attempt to synthesise a CRBN-PROTAC with a short and rigid linker

The synthesis of a very short and rigid PROTAC with an alkyne linker was then attempted (Scheme 5.5). 4-Iodo substituted analogue of pomalidomide **44** was first prepared from commercially available 3-iodophthalic anhydride **22** reacted by dehydrative condensation with 3-aminopiperidine-2,6-dione HBr salt **43** in 55% yield. Then, AZD1775 building block **40** was reacted with 3-bromoprop-1-yne by nucleophilic substitution under basic conditions to give **45** obtained in moderate yield (48%).
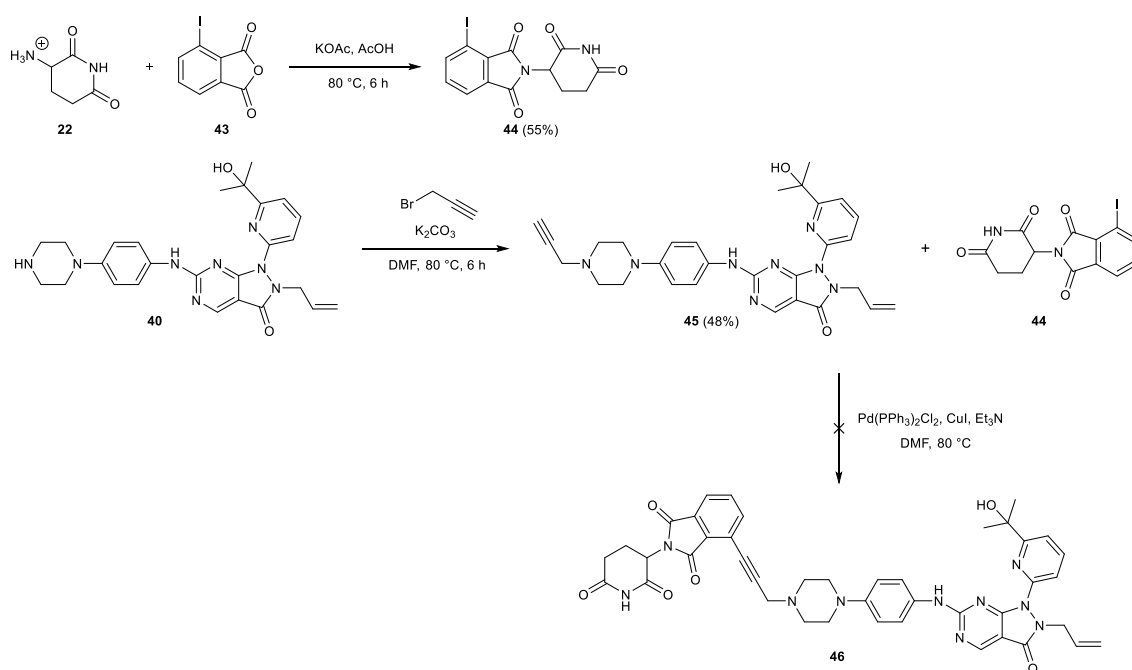
Scheme 5.5: Attempt to synthesise a Wee1 PROTAC recruiting CRBN using a short alkyne linker.

Afterwards, a Sonogashira coupling was attempted to attach **45**, with a terminal alkyne, to the aryl halide iodo-substituted pomalidomide **44**. Conditions were found in the

literature (Han *et al.*, 2019) for a similar example using a terminal alkyne and an iodo-substituted aryl halide. **44** and **45** were reacted with copper iodide, bis(triphenylphosphine)palladium chloride and triethylamine in dimethylformamide. However, the desired product **46** was not isolated. Different attempts with very dry conditions and freshly made compound **44** were made, but very small amounts of crude were recovered from the purification which was not enough to analyse (no LCMS was available) and conclude if it was the wanted product. Thus, the reaction was unsuccessful and it might be due to the degradation of **44**. Due to the lack of time to finish the project, no other conditions were attempted for this molecule. However, other catalyst or solvent could be attempted for the Sonogashira coupling, or the alkyne could be coupled to the Cereblon recruiter first and then attached to Wee1 recruiter.

5.3.1.4 Synthesis of the second generation of Wee1 PROTACs for the VHL-series

To create a new generation of Wee1 PROTACs recruiting VHL (Scheme 5.6), two PROTACs were synthesised for the VHL-series (Scheme 5.7; Table 5.1) where one amide bond was removed from the molecule to help with cell penetration.
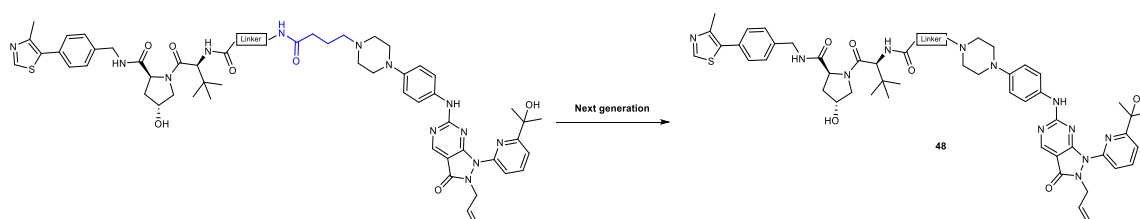
Scheme 5.6: Structures of the first and second generations of the VHL-series of PROTACs targeting Wee1. The second generation was obtained by removing the amide bond and the three carbons in blue.

Contrary to the second generation of the CRBN series, the E3 ligase ligand was attached first to the linker and then to the new AZD1775 building block **40**. The E3 ligase ligand was attempted first because the molecule is easier to purify than the AZD1775 building block and is also cheaper to synthesise.

In order to investigate our hypotheses from the first generation of Wee1 PROTACs, two long linkers of different length but same nature (alkyl) were used: ten and fourteen carbons were used (Scheme 5.7). After researching linkers, these were chosen because they were available commercially, and were interesting long alkyl chains which we knew were better than PEG for our system. The ten-carbon linker has a similar length as PROTAC MA052 of the first generation to compare an intermediate length with one less amide bond that could make the linker more flexible. The fourteen-carbon linker is close to MA054's longer length.

The selected alkyl linkers with ten or fourteen carbons were linked to the VHL ligand **18** by HATU-mediated amide coupling to obtain **47a** and **47b**, in 37 and 42% yield, respectively. Purification was difficult due to the presence of leftover linker, but **47a** and **47b** were obtained in moderate yields. They were then attached to AZD1775 building block **40** by nucleophilic substitution under basic conditions to afford the two PROTACs **48a** (**MA199** – eleven-atom linker) and **48b** (**MA198** – fifteen-atom linker) in low yields: 41 and 10%, respectively, due to difficulties to purify the compounds with normal phase column chromatography on silica gel. The PROTACs eluted at the same time as starting material **40** (AZD1775 building block). The E3 ligase ligands attached to the linker molecules **47a** and **47b** were added in a little excess to try and avoid it, which helped with the purification a little. Two column purifications were needed to obtain the pure product and use it in the next step. **48a** and **48b** were purified twice to obtain pure PROTACs for further biological testing.
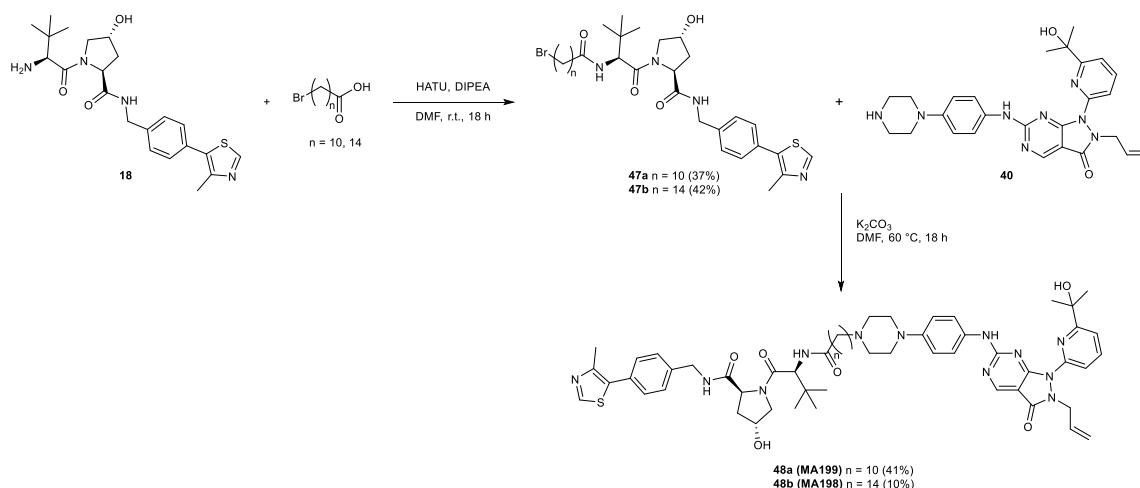
Scheme 5.7: Synthesis of the second generation of Wee1 PROTACs recruiting VHL E3 ligase.

Two other linkers with four- and seven-atom linkers were also attempted to be akin to the linker's length range of MA055 (four-atom linker) and MA051 (nine-atom linker) from the first generation (Scheme 5.8). However, the intermediates **47c** and **47d** were not isolated. Only the linker and the E3 ligase ligand were isolated after purification, but they were not attached together. The reactions were attempted multiple times unsuccessfully and were dropped because of time constraints.
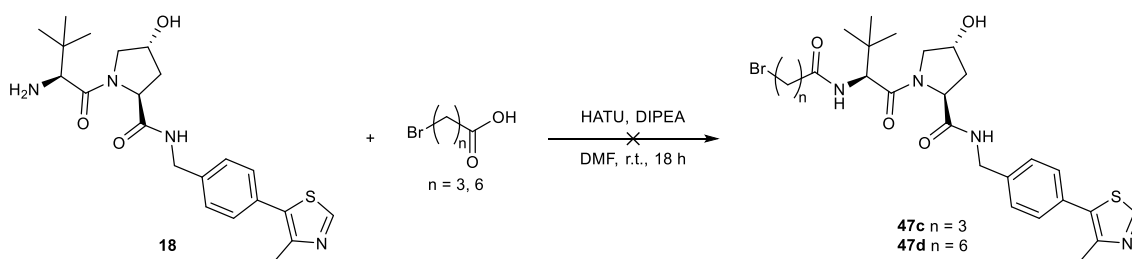
Scheme 5.8: Attempt to synthesise Wee1 PROTACs recruiting VHL with shorter linkers.

As previously highlighted, the number of amide bonds in the molecule seemed to play a role in the degradation potency, but the linker's length seemed to be even more impactful. MA055 of the first generation of VHL-PROTACs with the shortest alkyl linker and MA054 (sixteen-atom linker) with the longest were the most potent of the VHL-series. In order to verify if a very shorter acetyl linker (two-atom linker) (Scheme 5.9; Table 5.1) could lead to a potent PROTAC, another AZD1775 building block **51** was synthesised using a different aniline **49** finishing with an ester. Aniline **49** was added by

nucleophilic substitution to **10** after sulfur oxidation in low yield (7%) due to the stickiness of the aniline that had difficulties being in solution. The ester of **50** was then deprotected into a carboxylic acid **51** in quantitative yield. Finally, the carboxylic acid **51** was attached to the E3 ligase ligand **18** directly by HATU-mediated amide coupling to obtain **52** (**MA204** – two-atom linker) in 34% yield.
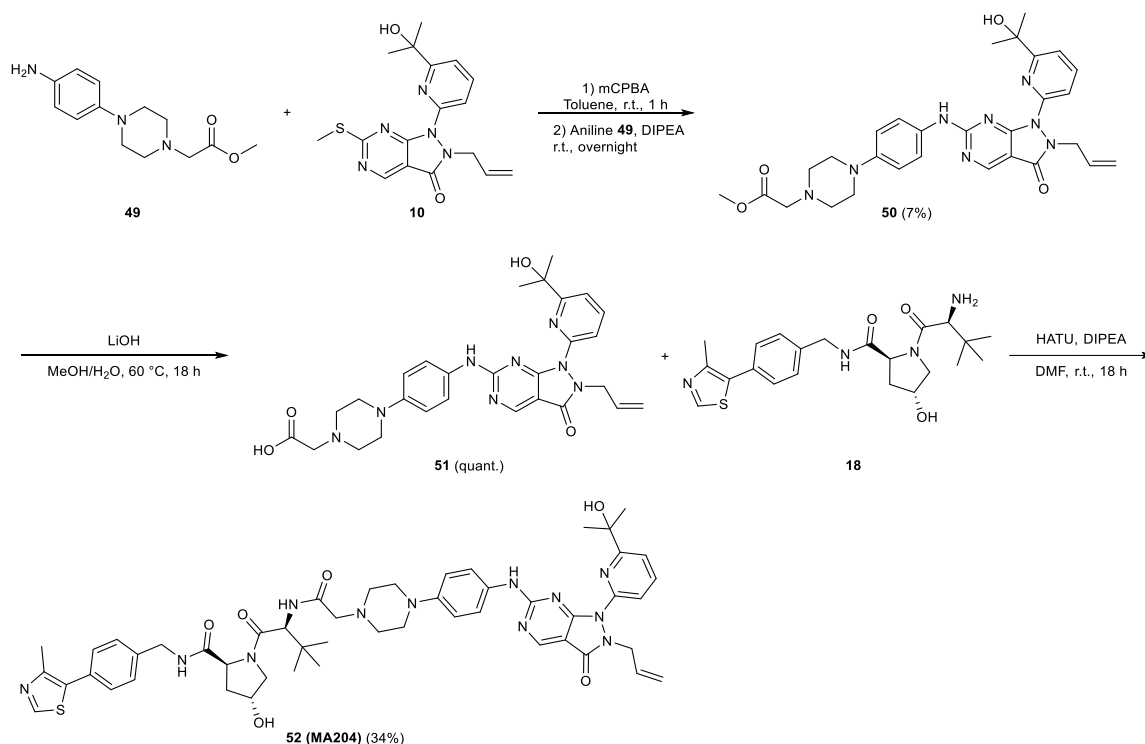
Scheme 5.9: Synthesis of **52** (**MA204**) with a very short linker.

5.3.2 Assessment of the second generation of Wee1 PROTACs

Four Wee1 PROTACs recruiting CRBN and three Wee1 PROTACs recruiting VHL have been successfully synthesised. The PROTACs were then tested in cancer cells in order to establish their degradation profiles and compare them to the PROTACs of the first generation to see if their biological properties have been improved (solubility and degradation activity).

For the purpose of keeping results consistent and comparable to the first generation of PROTACs, the new PROTACs were tested in HeLa S3 cells for 4 h with a dose response of compound from 1 nM to 10 µM. Cells were then lysed and protein levels were

investigated by Western blot to establish the SAR of the new generation of Wee1 PROTACs.

5.3.2.1 CRBN-series

PROTACs MA144, MA159 and MA162 of the CRBN-series successfully induced Wee1 degradation from 10 nM to 1 µM after 4 h treatment in HeLa S3 cells (Figure 5.1). After 4 hours incubation, MA144 almost completely removed Wee1 from 30 to 300 nM and thus seemed to be the more potent PROTAC out of the four new compounds of this series. MA165 seemed to show light degradation from 30 to 300 nM but Wee1 levels were not decreased as much as for the three other PROTACs for this incubation time. All four PROTACs induced decreased levels of pCDK1(Y15) as a downstream effect of Wee1 degradation: between 100 nM and 10 µM for MA144 and MA162, and between 300 nM and 10 µM for MA159 and MA165.
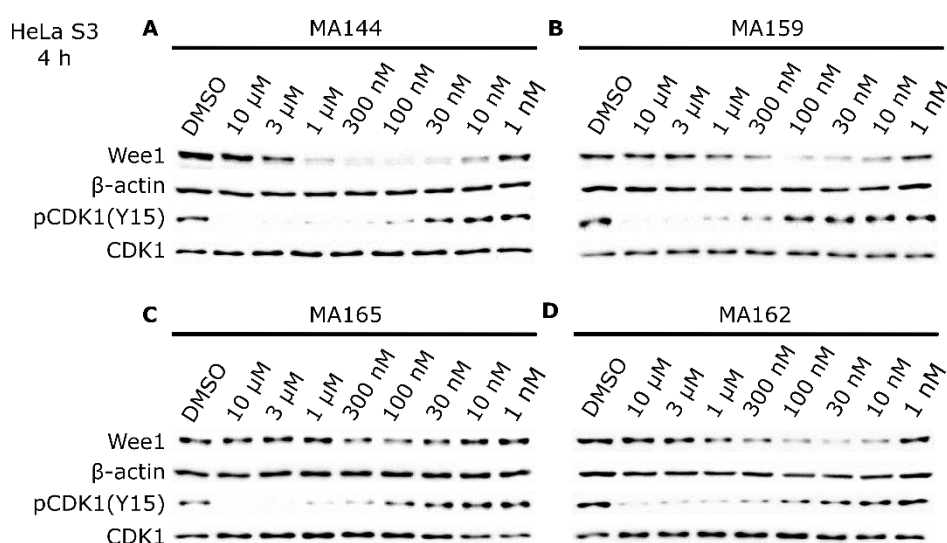
Figure 5.1: Evaluation of the second generation of CRBN-PROTACs. Western blots of HeLa S3 cells treated with a decreasing dose of **A**) MA144, **B**) MA159, **C**) MA165 and **D**) MA162 for 4 h. The membrane was blotted for Wee1, pCDK1(Y15), CDK1 and β-actin as the loading control (n = 2).

MA144 maximal degradation seemed to be reached at around 100 nM and exhibited some hook effect from 1 to 10 µM. Due to these observations, Wee1 degradation for MA144 up to 10 nM was more potent than the best PROTACs of the first generation of

Wee1 PROTACs recruiting the CRBN E3 ligase: MA048, MA071, MA072 and MA049. This will be investigated and developed later in section 5.3.2.5.

5.3.2.2 VHL-series

Compound MA199 of the VHL-series successfully induced Wee1 degradation from 10 nM to 10 µM after 4 h incubation in HeLa S3 cells (Figure 5.2). Levels of Wee1 were restored between 1 and 10 µM of MA199, a consequence of self-inhibition of the compound due to the hook effect generating unproductive binary over productive ternary complexes. The hook effect appeared stronger than the one of MA055 from the first generation. This could be explained by a higher cell penetration from MA199 which thus would be present in higher concentration in the cell. However, this would need to be validated using a cell penetration assay. The maximal degradation was reached between 100 and 300 nM suggesting that MA199 is more potent than the best PROTAC MA055 of the first generation for which maximum degradation was around 1 µM. Treatment with MA199 from 30 nM to 10 µM, also resulted in decreased levels of pCDK1(Y15) as a downstream effect. MA204 also induced Wee1 degradation from 100 nM to 10 µM with less hook effect as only a light band was visible at the higher concentration of 10 µM. The MA204 degradation profile looked similar to MA055. p(CDK1)Y15 levels were reduced for the same concentrations as Wee1 from 100 nM to 10 µM. Degradation by the other VHL-based PROTAC, MA198, did not result in Wee1 degradation after 4 hours treatment. pCDK1(Y15) levels were reduced at higher concentrations of 3 and 10 µM probably due to its inhibitory effect on Wee1 at high concentration, but likely not as a consequence of degradation.
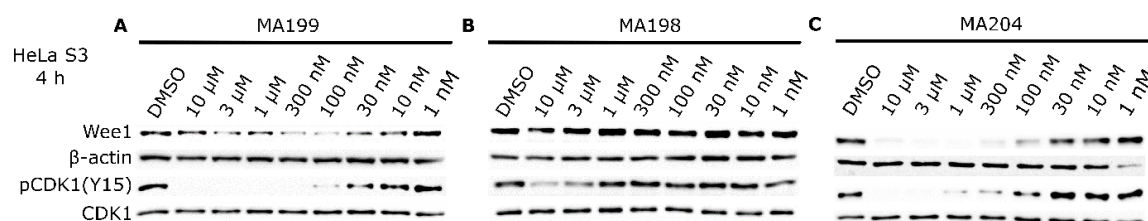
Figure 5.2: Evaluation of the second generation of VHL-PROTACs. Western blots of HeLa S3 cells treated with a different dosage of **A)** MA199, **B)** MA198 and **C)** MA204 for 4 h. The membrane was blotted with Wee1, pCDK1(Y15), CDK1 and β-actin as the loading control (n = 2).

Therefore, both series of the new generation of PROTACs trying to improve biological properties such as cell penetration as well as using very short or longer, and rigid linkers, showed Wee1 degradation after 4 hours treatment in HeLa S3 cells, except MA198 for the VHL-series. Two PROTACs seemed to induce stronger degradation than the PROTACs of the first generation of Wee1 PROTACs: MA144 of the CRBN-series and MA199 of the VHL-series. In order to investigate Wee1 degradation further, confirm the potency and compare the PROTACs together, other experiments with a single concentration of PROTAC and a longer incubation time were performed.

5.3.2.3 Comparison of the new PROTACs – screening of the second generation

To compare the new PROTACs degradation together, HeLa S3 cells were treated with a single concentration of 1 µM of the new Wee1 PROTACs: MA198 and MA199 for the VHL-series, and MA144, MA159, MA162 and MA165 for the CRBN-series for 24 h. Using Western blot and near infrared fluorescent imaging (LICOR), Wee1 and pCDK1(Y15) were quantified (n = 2) and plotted (Figure 5.3; Table 5.2).
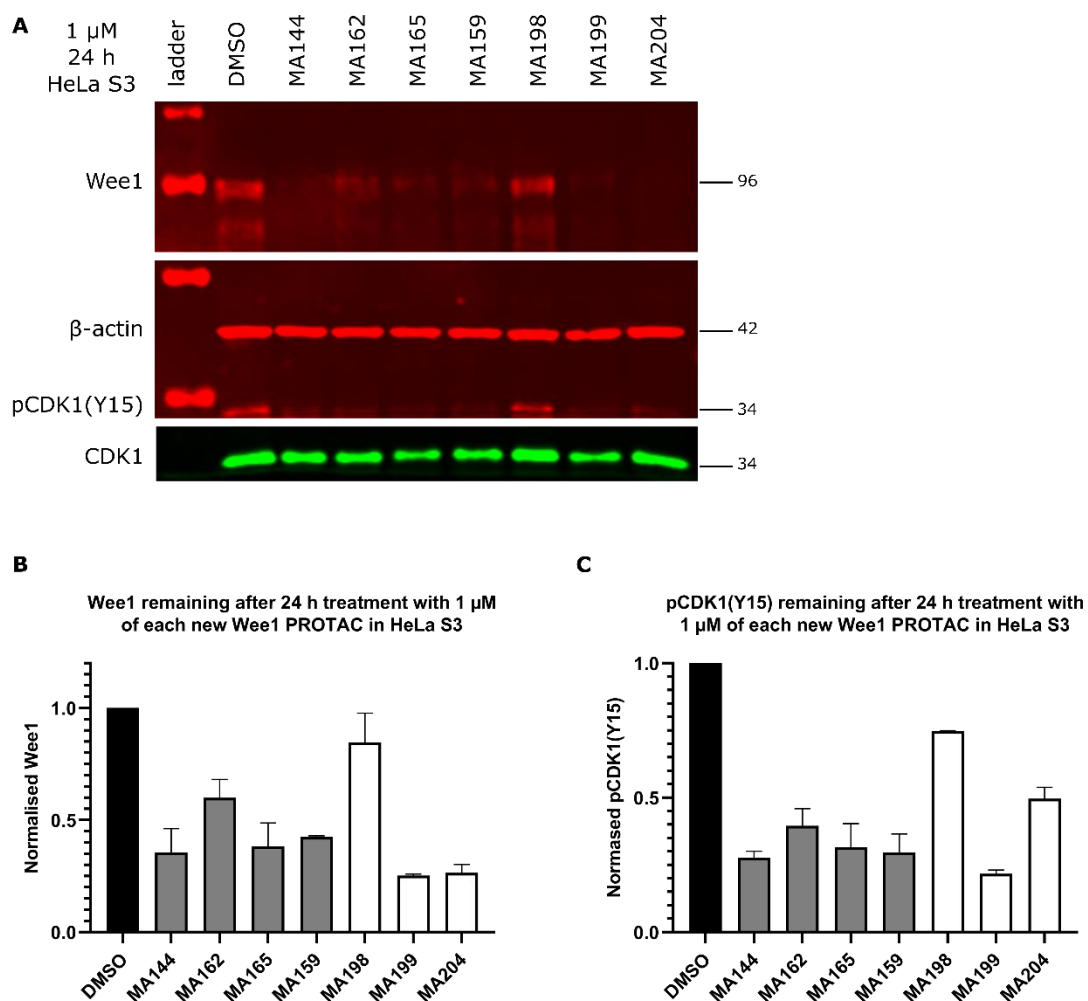
Figure 5.3: Screening of the new Wee1 PROTACs recruiting either the VHL or the CRBN E3 ligase. **A**) Western blot of HeLa S3 cells treated for 24 h with 1 μM of each PROTAC. Graph showing **B**) Wee1 and **C**) pCDK1(Y15) remaining: the CRBN-series in grey and the VHL-series in white.

Table 5.2: SAR of the second generation of Wee1 PROTACs. Table showing Wee1 degradation and pCDK1(Y15) percentage remaining after 24 h treatment. Wee1 and pCDK1(Y15) bands were quantified and normalised using β-actin as the loading control and the DMSO control as a reference for no drug treatment for each PROTAC (n = 2).

PROTAC		Wee1 degradation (%)	pCDK1 (Y15) remaining (%)
MA144	CRBN	64 ± 11	28 ± 3
MA162		40 ± 8	40 ± 6
MA165		62 ± 11	32 ± 9
MA159		58 ± 20	30 ± 7
MA198	VHL	15 ± 13	75 ± 1
MA199		75 ± 1	22 ± 2
MA204		74 ± 4	50 ± 4

After a 24-hour treatment with 1 µM of PROTAC, the four PROTACs recruiting the CRBN E3 ligase induced Wee1 degradation from 40 to 64%. MA144 seemed to be slightly better than the other CRBN-PROTACs at this concentration as it induced the strongest Wee1 degradation (64%) and the lowest pCDK1(Y15) level remaining (28%). It was shown above that MA144 exhibited the hook effect at this concentration. The other three PROTACs MA162, MA165 and MA159 also reduced pCDK1(Y15) levels, with 30 to 40% remaining. Similar degradation profiles for the PROTACs MA159 and MA162, both with a pyrrolidine linker, were observed. The slight change in orientation did not appear to have an influence on Wee1 degradation. When looking at this direct comparison of the CRBN-series at 1 µM, as well as the dose response for 4 h, MA144 was selected as the best compound from this series to undergo further investigation.

Out of the three PROTACs recruiting the VHL E3 ligase, two induced Wee1 degradation at 24 h (Figure 5.3; Table 5.2) in accordance with the 4 h dose response. MA199 and MA204 induced the same Wee1 degradation with 75 and 74% respectively after 24 h incubation with 1 µM. However, pCDK1(Y15) levels were less decreased with MA204, the shortest linker, with 50% remaining for MA204 compared to only 20% for MA199. MA199

previously showed hook effect at this concentration and the stronger downstream effect induced by PROTAC MA199 suggested that it is more potent. Thus, MA199 was selected for further investigation. MA198 did not induce significant Wee1 degradation, with a reduction of only 15%. This is also reflected in the pCDK1(Y15) level, with 75% remaining following treatment with MA198.

The 1 µM treatment had been selected to keep results consistent and allow direct comparison to the PROTACs of the first generation, however, a greater hook effect was observed for the best compounds of the new generation at this concentration. Thus, it does not fully reflect Wee1 degradation anymore for the most potent PROTACs such as MA144 and MA199. Therefore, the single treatment concentration needed to be decreased to conduct more experiments with the two best PROTACs.

5.3.2.4 Degradation over time for the best PROTACs

The new PROTACs of the second generation seemed more potent than the first generation when looking at the dose response in HeLa S3 cells at 4 h treatment. As a matter of fact, the DC_{50} seemed lower than for the first series and pCDK1(Y15) levels were effectively decreased at lower treatment concentrations, especially for MA144 (CRBN-series) and MA199 (VHL-series). They also both showed a considerable hook effect at the highest concentrations. Thus, the concentration of the single treatment was decreased in order to avoid the hook effect and have biological effects reflecting degradation as much as possible without the confounding effect of inhibition. As a consequence, cells were now treated with 300 nM of PROTAC, the concentration at which maximal degradation was reached for the best PROTACs.

Therefore, the selected best PROTACs of the new generation: MA199 for the VHL-series and MA144 for the CRBN-series were further investigated to verify Wee1 degradation after 24 and 48 hours of incubation in HeLa S3 at 300 nM using Western blotting and near infrared fluorescent imaging (LICOR) (Figure 5.4; Table 5.3).
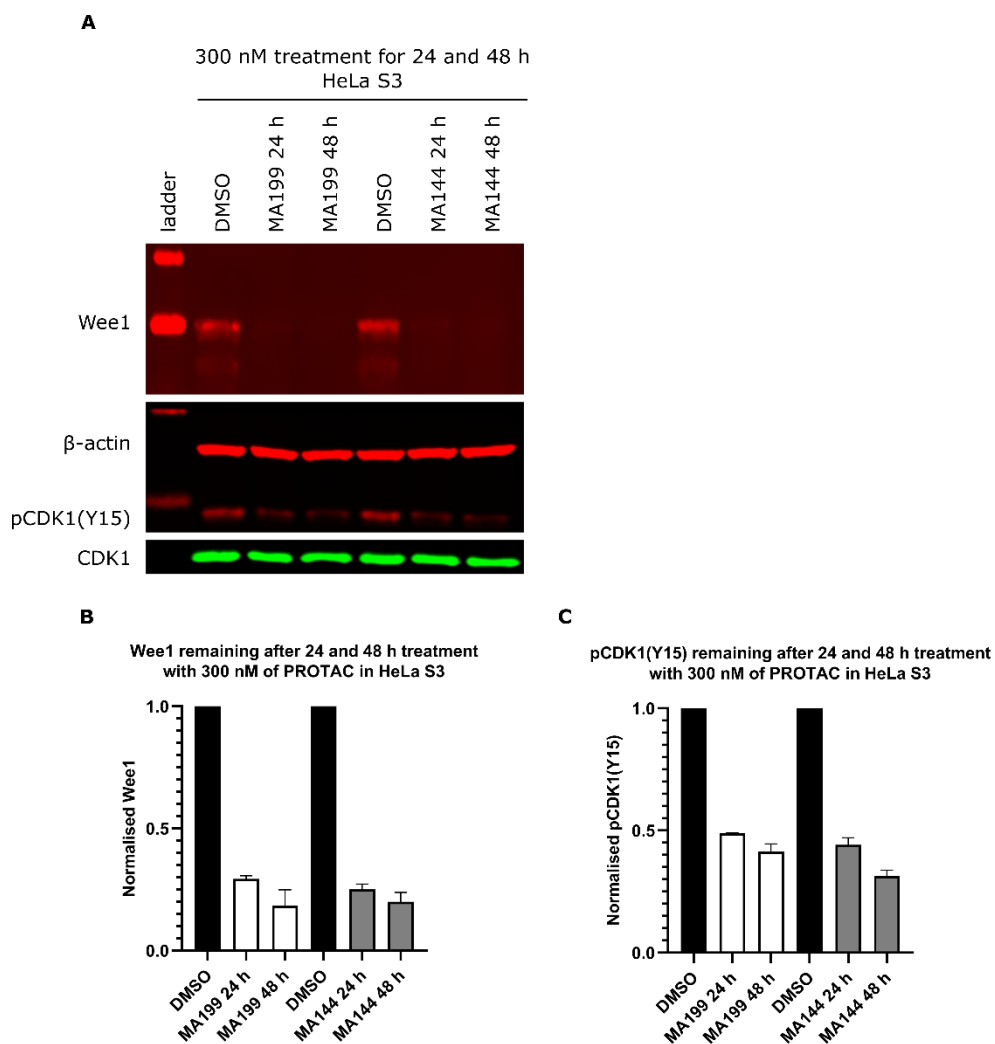
Figure 5.4: Comparison between MA199 and MA144, the most potent PROTACs of the second generation for the VHL- and CRBN-series, respectively. **A**) Western blot of HeLa S3 cells treated for 24 and 48 h with 300 nM of MA199 and MA144. Graph showing **B**) Wee1 and **C**) pCDK1(Y15) remaining: the VHL-series in white on the left and the CRBN-series in grey on the right (n = 2).

Table 5.3: Strong Wee1 degradation over time. Table showing Wee1 degradation and pCDK1(Y15) percentage remaining after 24 and 48 h treatment at 300 nM for MA199 and MA144. Wee1 and pCDK1(Y15) bands were quantified and normalised for each PROTAC (n = 2).

PROTAC	Wee1 degradation (%)	pCDK1(Y15) remaining (%)
MA199 24 h	71 ± 1	49 ± 0
MA199 48 h	82 ± 6	41 ± 3
MA144 24 h	75 ± 2	44 ± 3
MA144 48 h	80 ± 4	31 ± 2

Similar Wee1 levels for MA199 and MA144 were observed, with around 71 and 75% degradation respectively at 24 h and around 80% at 48 h for both. pCDK1(Y15) levels were also similar for both PROTACs, with 49% after 24 h and 41% after 48 h for MA199, and 44% after 24 h and 31% after 48 h for MA144. Furthermore, pCDK1(Y15) levels are higher than for the 1 µM treatment whereas Wee1 levels are lower, which suggests that the contribution of inhibition to pCDK1(Y15) levels is substantially reduced at the 300 nM treatment (Table 5.2; Table 5.3). Therefore, MA199 and MA144 induced potent Wee1 degradation after 24 h and 48 h at 300 nM.

5.3.2.5 Comparison of the best Wee1 PROTACs from the two generations

After comparing the new PROTACs together, I thought to compare the best compounds of the new generation directly to PROTACs of the first generation using the 300 nM of PROTACs for treatments. MA048, MA049, MA072 and MA071 were selected for the CRBN-series to compare with MA144, as they showed similar degradation profiles. MA055 and MA054 were chosen for the VHL-series to compare with MA199, as they were the most potent. Wee1 levels after 24 h treatment with these PROTACs were analysed and quantified (Figure 5.5).

Out of the three VHL-PROTACs tested, MA199 showed the most Wee1 degradation: 71%, whereas MA055 exhibited 41% and MA054 52%. This is also reflected on the pCDK1(Y15)

levels with 52% remaining for MA199, and 87 and 98% remaining for MA055 and MA054, respectively (Table 5.4). Thus, pCDK1(Y15) remaining was much lower for the new PROTAC, MA199.
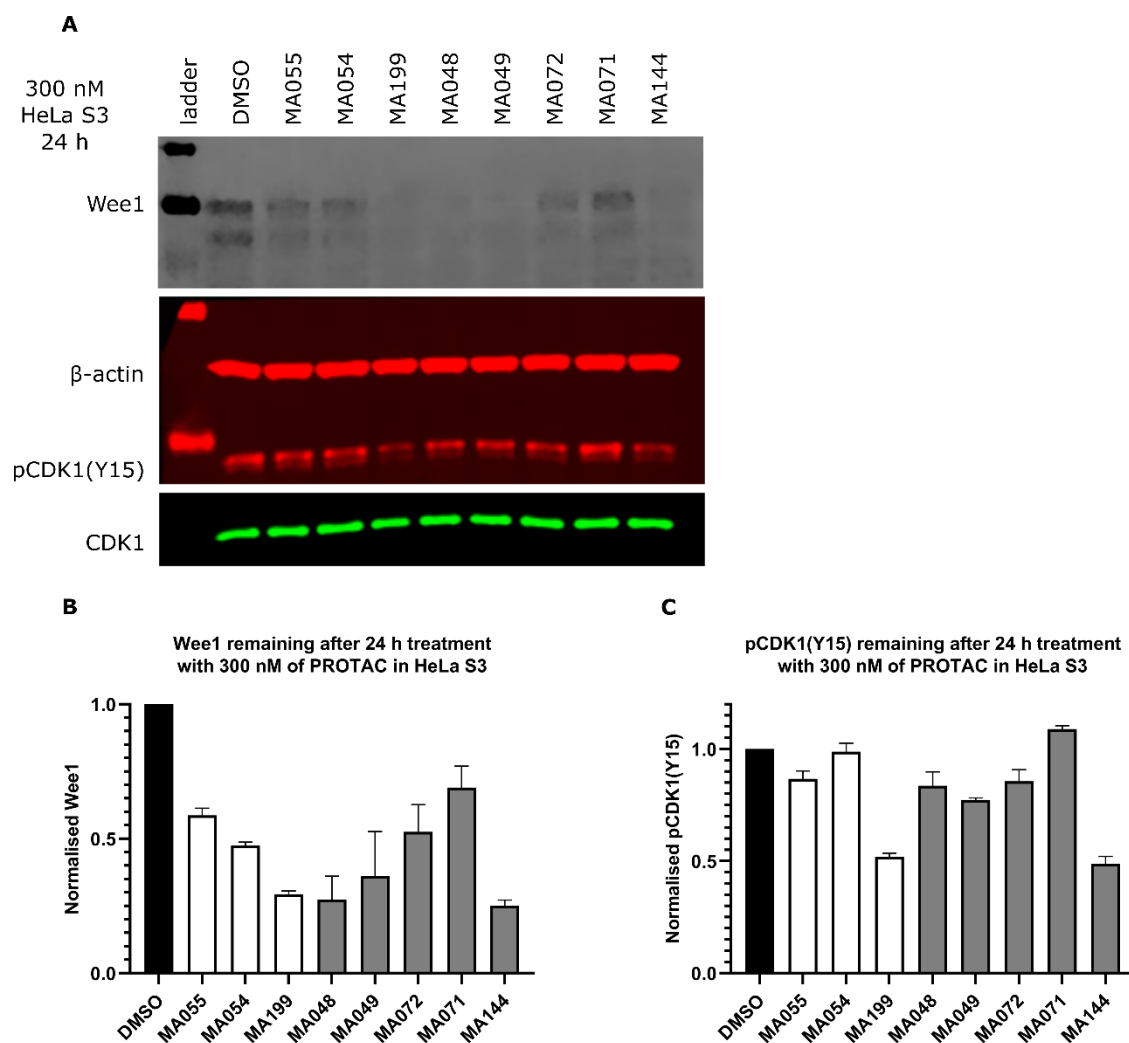
Figure 5.5: Comparison of the best PROTACs from the second generation to the best PROTACs from the first generation. **A**) Western blot of the indicated PROTACs after 24 h treatment with 300 nM in HeLa S3 cells. Wee1 and pCDK1(Y15) bands were quantified and normalised for each PROTAC (n = 2). **B**) Wee1 remaining and **C**) pCDK1(Y15) remaining were plotted.

Looking at the four PROTACs from the first generation (MA048, MA049, MA072 and MA072) and MA144 for the second generation of the CRBN-series, the new PROTAC MA144 appeared to be the best with 75% of Wee1 degradation after 24 h treatment with 300 nM of compound (Table 5.4). MA048 was close with 74%, followed by MA049 with

64% of Wee1 degradation. MA072 and MA071 induced less degradation at this concentration with 47 and 31%, respectively. pCDK1(Y15) levels followed Wee1 degradation pattern. Lower pCDK1(Y15) levels were observed for MA144 with 49% remaining. Whereas for the four PROTACs of the first generation, it was above 77%.

Table 5.4: Comparison of Wee1 and pCDK1(Y15) remaining for the best PROTACs of both generations. Wee1 and pCDK1(Y15) bands after 24 h treatment at 300 nM were quantified and normalised for each PROTAC (n = 2).

PROTAC	Wee1 remaining (%)	pCDK1(Y15) remaining (%)
MA055	59 ± 3	87 ± 4
MA054	48 ± 1	99 ± 4
MA199	29 ± 1	49 ± 2
MA048	26 ± 9	84 ± 6
MA049	36 ± 16	77 ± 1
MA071	53 ± 10	86 ± 5
MA071	69 ± 8	109 ± 2
MA144	25 ± 2	44 ± 3

This confirmed that the two new best PROTACs MA199 (VHL-series) and MA144 (CRBN-series) of the second generation were more potent than the best PROTACs of the first generation of Wee1 PROTACs for their equivalent E3 ligase series. They showed both stronger Wee1 degradation and lower levels of pCDK1(Y15), an indicator of Wee1 degradation downstream effect, confirming the improvement in the potency.

5.3.2.6 Selectivity

The best PROTACs of each series were blotted for the main AZD1775 off target kinase, PLK1 (Figure 5.6). PLK1 was not degraded after 4 h treatment in HeLa S3 cells at any of the concentrations of MA199 and MA144 tested. This showed that the second generations of PROTACs were also selective towards Wee1 over the other main kinase inhibited by AZD1775, PLK1. Other off-targets were not tested for the second generation

of PROTACs as the paper from Li *et al*. did a proteomics experiment on their equivalent of MA144 called ZLN-02-096 which showed selectivity for Wee1 (Li *et al*., 2020).
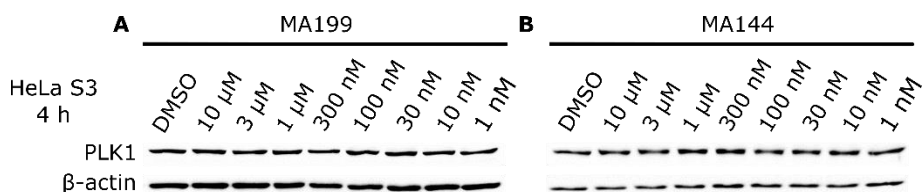
Figure 5.6: Selective Wee1 degradation with the two best PROTACs of each series MA199 (VHL) and MA144 (CRBN). Western blots of HeLa S3 cells treated for 4 h with different doses of **A**) MA199 and **B**) MA144. The membrane was blotted for PLK1 and β-actin as the loading control (n = 2).

5.3.2.7 Target engagement and negative control PROTAC

To verify the PROTAC target engagement on the E3 ligase side, a negative control PROTAC was synthesised for MA144, the most potent PROTAC of the second generation after 4 and 24 h treatment. The negative control **54** (negMA144) was synthesised by linking the building block AZD1775 attached to the propyl linker **41a** to the methylated pomalidomide **34** through nucleophilic aromatic substitution in low yield (36%) due to the challenging purification (Scheme 5.10).
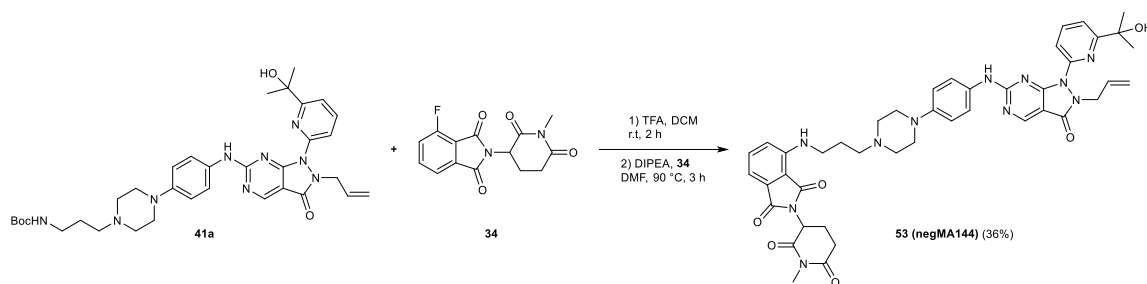
Scheme 5.10: Synthesis of **53** (**MA144**) negative control molecule, negMA144.

negMA144 was tested in HeLa S3 cells with the same dosages as the normal PROTACs (Figure 5.7). Western blot was used to look at Wee1 levels and no degradation was observed at 4 h. pCDK1(Y15) levels were decreased between 300 nM and 10 μM due to its inhibitory effect on Wee1 as the negative control can still recruit Wee1 protein on the AZD1775 side. As a consequence, PROTAC MA144 needs to recruit the E3 ligase for

degradation. Unfortunately, due to time constraints, it was not possible to generate a negative control PROTAC for MA199 of the second generation for the VHL-series.

Figure 5.7: Negative control PROTAC and E3 ligase engagement. **A**) Western blots of HeLa S3 cells treated for 4 h with a different dosage of negMA144: MA144 negative control PROTAC from the second generation of the CRBN-series. **B**) Structures of MA144 and negMA144.

5.3.2.8 Cell proliferation assay

After observing an improvement in Wee1 degradation for the second generation of PROTACs, the half-maximum response (IC_{50}) of the selected best PROTACs MA199 and MA144 in BT549 cells was investigated (Figure 5.8). BT549 cells were the most sensitive to Wee1 degradation during the evaluation of the first generation of PROTACs, so they were selected to carry out the cell proliferation assays. The IC_{50} of both MA199 (IC_{50} = 0.69) and MA144 (IC_{50} = 0.59) was improved compared to that of IC_{50} of MA055 (IC_{50} = 2.4) and MA071 (IC_{50} = 7.9) of the first generation for the VHL-series and the CRBN-series, respectively. They were also much more similar to AZD1775 IC_{50} of 0.49. This confirms that the best PROTACs of the second generation had improved cellular potencies compared to the first generation, and almost had the same influence on cell proliferation as Wee1 inhibitor AZD1775.
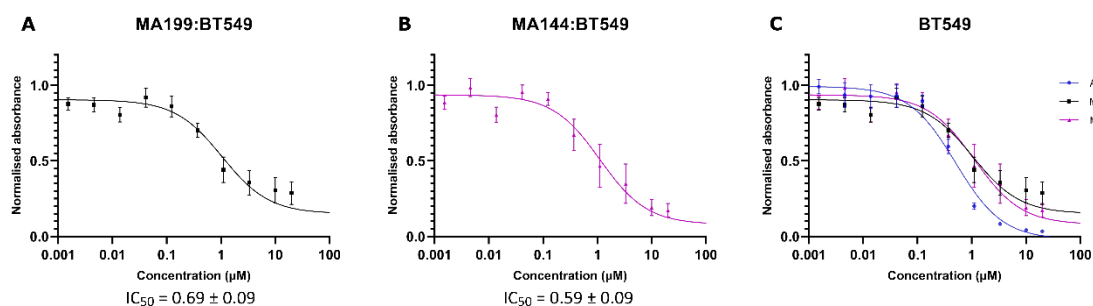
Figure 5.8: Cell proliferation inhibition of cancer cells by PROTACs MA199 and MA144. Cell proliferation assays normalised using the DMSO control for **A**) MA199 and **B**) MA144 in BT549 cells treated for 72 h. **C**) Superimposition of cell proliferation assays of the two PROTACs and AZD1775 inhibitor. Data are presented as mean ± s.d. of n = 4 biological independent experiments using GraphPad PRISM 9.2.0.

5.3.2.9 Ternary complex formation

In order to explain the improvement in potency from PROTAC MA199 of the VHL-series of the second generation of Wee1 PROTACs, the thermodynamics of ternary complex formation were investigated by ITC in solution. The same technique was used after optimisation for the first generation of PROTACs (Chapter 4, section 4.3.9.3). VBC was titrated into MA199, however very large heats of dilution were observed on every attempt, despite best efforts to reduce them. This generated unreliable data for both duplicates and gave a K_d(VBC:MA199) of 13 ± 3 µM due to the error generated (Figure 5.9 A). As buffer matching had been performed very carefully by dialysis and dilution with dialysis buffer, these heats of dilution could be explained by the fact that MA199 was not very soluble in the buffer used (50 mM HEPES, 150 mM NaCl, pH 7.5) and was dissolving in very small amounts as the volume of the solution increased with each titration. Even tiny amounts of dissolution will result in large enthalpic heats in an instrument as sensitive as the ITC. A higher percentage of DMSO (2% compared to 0.6% previously) in the sample was also attempted to improve the solubility of MA199, but it did not help to have a better binding curve. The binary complex Wee1:MA199 was then prepared with a 2:1 ratio to ensure that all of the PROTAC was bound to the protein to avoid any excess that could still bind VBC and interfere with the thermodynamic parameters of the ternary complex vs binary complex. The titration of VBC into the binary complex Wee1:MA199

was better quality and gave K_d(Wee1:MA199:VBC) = 61 ± 26 nM (Figure 5.9 B). The ternary complex binding constant was improved compared to MA055 (Chapter 4, section 4.3.9.3) with 191 ± 88 nM. Unfortunately, it was not possible to calculate the cooperativity due to the error in the K_d(VBC:MA199).
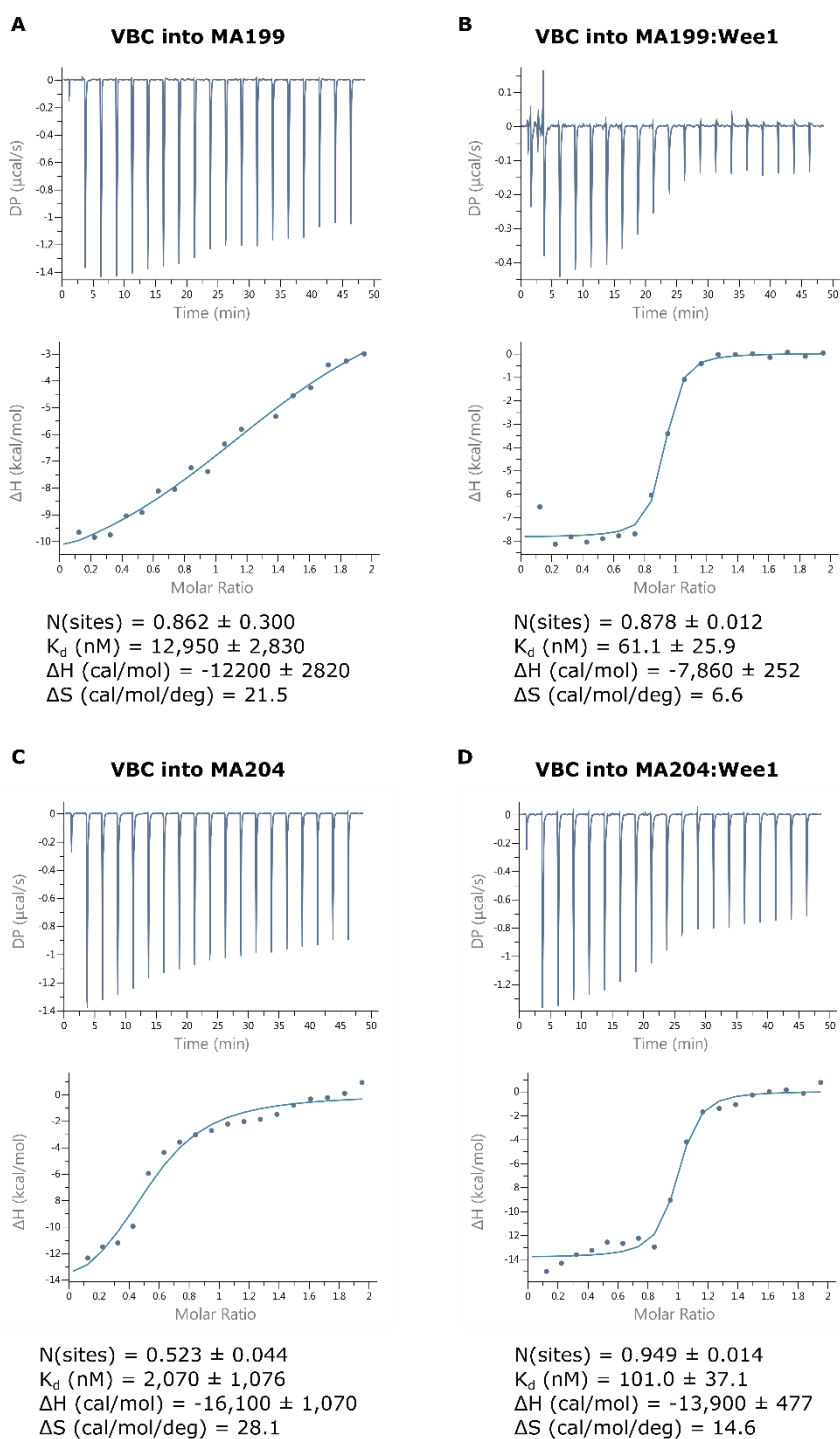
Figure 5.9: ITC titration for ternary complex analysis. Titration of **A)** VBC into MA199, **B)** VBC into Wee1:MA199, **C)** VBC into MA204 and **D)** VBC into Wee1:MA204 (200/20 µM, experiments done in duplicates for MA199, and once as a test for MA204).

As MA204 of the second generation of Wee1 PROTACs was of a similar potency as MA055 from the first generation, it was also used for ITC. The same problem as MA199 was

observed for the binary complex formation when titrating VBC into MA204 (Figure 5.9 C) and gave K_d(VBC:MA204) = 2 ± 1 µM. The ternary complex was once again better and gave K_d(Wee1:MA204:VBC) = 101 ± 37 nM. The cooperativity was not calculated because of the error in the binary complex constant. As the VHL-recruiting part of the PROTACs is similar for all the PROTACs of the VHL-series, we could hypothesise that they will all bind the same way to VHL and thus give very similar binary binding constants for the VBC:PROTAC complex. With this in mind, it is possible to at least compare their ternary complex binding constant in a qualitative way. K_d(Wee1:MA204:VBC) seemed similar to K_d(Wee1:MA055:VBC), if taking the error into consideration. This would correlate with the observations made by Western blot which showed a similar potency for MA055 of the first generation and MA204 of the second generation.

Due to time constraints, the ITC experiments could not be optimised further, but they suggest that MA199 ternary complex is the most favourable or locked in an energetically favourable ternary complex. It would be useful to also have binding constants for other PROTACs that do not degrade Wee1, such as MA198, to see if the lack of degradation is the result of lack of ternary complex formation. For these PROTACs, the cooperativity could be negative and thus be unfavourable for their ternary complex formation leading to successful degradation (Gadd *et al.*, 2017).

5.4 Experimental

General procedures are detailed in the Materials and methods Chapter 2 Section 2.22.2.

5.4.1 Synthesis of the new AZD1775 building block

***Tert*-Butyl 4-(4-nitrophenyl)piperazine-1-carboxylate (37)** (Mou *et al.*, 2015)
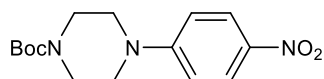
1-(4-nitrophenyl)piperazine **11** (500 mg, 2.4 mmol, 1.0 eq.) was dissolved in DCM (10 mL). DIPEA (0.84 mL, 4.8 mol, 2.0 eq.) was then added to the reaction mixture, followed by (Boc)$_2$O (1.05 g, 4.8 mmol, 2.0 eq.) portionwise. The mixture was then stirred at r.t. for

18 h. H_2O (10 mL) and DCM (10 mL) were added to the reaction, and the aqueous layer was extracted with DCM (15 mL). The combined organic layers were washed with saturated $NaHCO_3$, brine and dried over Na_2SO_4 before being concentrated in vacuo to afford the crude product **37** (700 mg, 2.3 mmol, 95%) as a yellow solid which was used without further purification.

TLC: R_f = 0.75 (1:1 EtOAc/Hexane); UV.

^{1}H-NMR (400 MHz, CDCl$_3$): δ (ppm) = 8.14 (dt, 2H, J = 9.5, 2.2 Hz), 6.82 (dt, 2H, J = 9.5, 2.2 Hz), 3.63-3.57 (m, 4H), 3.45-3.39 (m, 4H), 1.49 (s, 9H).

^{13}C-NMR (101 MHz, CDCl$_3$): δ (ppm) = 154.6, 138.8, 126.0, 112.9, 85.2, 80.4, 46.9, 28.4, 27.4.

IR (ATR): ν (cm^{-1}) = 2955, 2900, 2850, 2365, 1692.

Tert-Butyl 4-(4-aminophenyl)piperazine-1-carboxylate (38)
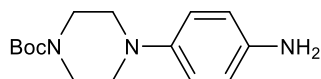
Tert-Butyl 4-(4-nitrophenyl)piperazine-1-carboxylate **37** (0.5 g, 1.6 mmol, 1.0 eq.) was resuspended in dry MeOH (20 mL) in a flask under nitrogen. Pd/C 5% (100 mg) was then added to the suspension. Nitrogen was removed from the flask with vacuum and the flask was filled with H_2 (balloon). The reaction was stirred overnight before being filtered through a pad of celite, washed with MeOH and concentrated in vacuo. The crude product was purified by flash column chromatography on silica gel with a gradient 0-100% EtOAc in Hexane to afford the product **38** (210 mg, 1.2 mmol, 76%) as a pink solid.

TLC: R_f = 0.20 (1:1 EtOAc/Hexane); UV.

^{1}H-NMR (400 MHz, CDCl$_3$): δ (ppm) = 6.83 (d, 2H, J = 8.8 Hz), 6.68 (d, 2H, J = 8.8 Hz), 3.65-3.38 (m, 6H), 3.03-2.93 (m, 4H), 1.50 (s, 9H).

IR (ATR): v (cm^{-1}) = 3430, 3015, 2952, 2915, 1680, 1607.

Tert-Butyl 4-[4-({1-[6-(2-hydroxypropan-2-yl)pyridin-2-yl]-3-oxo-2-(prop-2-en-1-yl)-1H,2H,3H-pyrazolo[3,4-d]pyrimidin-6-yl}amino)phenyl]piperazine-1-carboxylate (39)

(Matheson, Venkataraman, *et al.*, 2016)
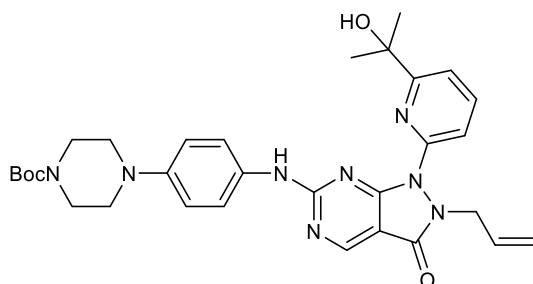
10 (300 mg, 0.8 mmol, 1.0 eq.) was resuspended in toluene (12 mL) and mCPBA (174 mg, 1.0 mmol, 1.2 eq.) was added. The mixture was stirred at room temperature for 1 h. Then, DIPEA (0.75 mL, 4.0 mmol, 5.0 eq.) was added, followed by aniline **38** (280 mg, 1.0 mmol, 1.2 eq.). The reaction mixture was stirred overnight. In the morning, saturated NaHCO$_3$ (30 mL) was added and it was extracted with EtOAc (3 × 30 mL), washed with brine (20 mL), dried over MgSO$_4$ and concentrated under reduced pressure to give the crude product. The crude product was purified by column chromatography on silica gel with 2% MeOH in DCM to give **39** (300 mg, 0.5 mmol, 61%) as a yellow solid.

TLC: R_f = 0.30 (5:95 MeOH/DCM); UV.

^{1}H-NMR (400 MHz, CDCl$_3$): δ (ppm) = 8.85 (s, 1H), 7.88 (t, 1H, *J* = 7.9 Hz), 7.76 (dd, 1H, *J* = 7.9, 0.8 Hz), 7.59-7.47 (m, 3H), 7.37 (dd, 1H, *J* = 7.6, 0.8 Hz), 6.95 (d, 2H, *J* = 9.0 Hz), 5.78-5.68 (m, 1H), 5.07 (dq, 1H, *J* =10.3, 1.3 Hz), 4.96 (dq, 1H, *J* = 17.1, 1.3 Hz), 4.76 (d, 2H, *J* = 6.3 Hz), 3.67-3.56 (m, 4H), 3.19-3.10 (m, 4H), 1.67-1.58 (m, 4H).

^{13}C-NMR (101 MHz, CDCl$_3$): δ (ppm) = 165.8, 162.2, 156.4, 154.7, 131.6, 119.1, 117.1, 116.2, 116.1, 80.0, 72.4, 49.8, 47.7, 30.6, 28.4.

IR (ATR): v (cm^{-1}) = 3380, 2974, 2930, 1725, 1682.

5.4.2 Synthesis of the second generation of CRBN-PROTACs

Tert-Butyl **N-(3-{4-[4-({1-[6-(2-hydroxypropan-2-yl)pyridin-2-yl]-3-oxo-2-(prop-2-en-1-yl)-1H,2H,3H-pyrazolo[3,4-d]pyrimidin-6-yl}amino)phenyl]piperazin-1-yl}propyl)carbamate (41a)**
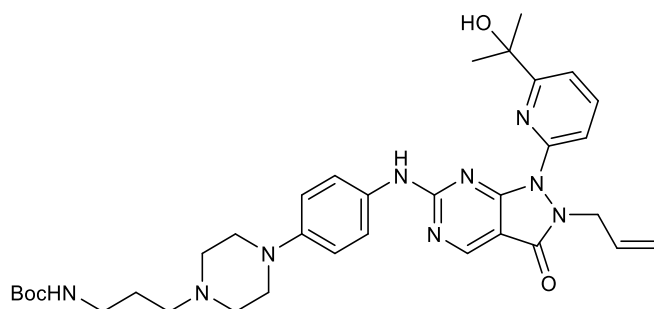
The new AZD1775 building block **40** was Boc deprotected following general procedure **D** and attached to linker **L₀** following general procedure **C** for nucleophilic substitution. The crude product was purified by column chromatography on silica gel using 1% MeOH in DCM to afford the product **41a** (22 mg, 0.03 mmol, 92%) as a yellow solid.

TLC: R_f = 0.30 (5:95 MeOH/DCM); UV.

^{1}H-NMR (400 MHz, CDCl$_3$): δ (ppm) = 8.84 (s, 1H), 7.87 (t, 1H, J = 7.9 Hz), 7.77 (d, 1H, J = 7.9 Hz), 7.48 (d, 2H, J = 8.7 Hz), 7.36 (dd, 1H, J = 7.6, 0.7 Hz), 6.94 (d, 2H, J = 9.3 Hz), 5.78-5.65 (m, 1H), 5.06 (dq, 1H, J = 10.3, 1.2 Hz), 4.96 (dq, 1H, J = 17.1, 1.2 Hz), 4.76 (d, 2H, J = 6.2 Hz), 3.99 (br s, 1H), 3.29-3.14 (m, 6H), 2.72-2.59 (m, 4H), 2.51 (t, 2H, J = 6.7 Hz), 1.74 (p, 2H, J = 6.7 Hz), 1.48 (s, 9H).

^{13}C-NMR (101 MHz, CDCl$_3$): δ (ppm) = 165.7, 162.3, 161.3, 156.3, 156.1, 148.2, 147.5, 138.8, 131.6, 119.0, 116.5, 116.2, 116.0, 72.4, 56.7, 53.4, 53.2, 49.6, 47.7, 39.8, 30.6, 28.5, 26.5.

IR (ATR): ν (cm^{-1}) = 3265, 2977, 2931, 1726, 1680.

N-{[4-(Bromomethyl)phenyl]methyl}-2,2-dimethylpropanamide (Lₚ) (Vassiliou *et al.,* 2007)
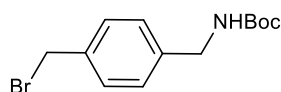
4-(Bromomethyl)benzylamine HBr salt (150 mg, 0.8 mmol, 1.0 eq.) was dissolved in H_2O and dioxane (1:1 (v/v), 6 mL). The solution was cooled to 0 °C with an ice bath and di-*tert*-butyl decarbonate (500 mg, 2.3 mmol, 3.0 eq.) was added. $NaHCO_3$ (126 mg, 1.5 mmol, 2.0 eq.) was then added to the mixture at 0°C and it was stirred at room temperature overnight. In the morning, H_2O (10 mL) was added and it was extracted with EtOAc (3 × 20 mL), dried over Na_2SO_4 and concentrated under reduced pressure to give the crude **Lₚ** as a white solid. The crude product was washed with hexane and dried under vacuum (215 mg, 0.5 mmol, 67%).

TLC: R_f = 0.20 (4:6 EtOAc/Hexane); UV.

^{1}H-NMR (400 MHz, CDCl$_3$): δ (ppm) = 7.40-7.35 (m, 2H), 7.30-7.26 (m, 2H), 4.86 (s, 1H), 4.51 (s, 2H), 4.33 (d, 2H, *J* = 5.7 Hz), 1.49 (s, 9H).

***Tert*-Butyl   N-{[4-({4-[4-({1-[6-(2-hydroxypropan-2-yl)pyridin-2-yl]-3-oxo-2-(prop-2-en-1-yl)-1H,2H,3H-pyrazolo[3,4-d]pyrimidin-6-yl}amino)phenyl]piperazin-1-yl}methyl)phenyl]methyl}carbamate (41b)**
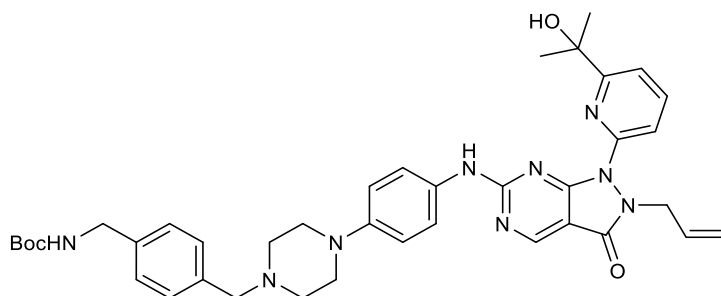
New AZD1775 building block **40** was Boc deprotected following general procedure **D** and was attached to linker **Lₚ** following general procedure **C** for nucleophilic substitution. The

crude product was purified by column chromatography on silica gel using 1% MeOH in DCM to afford the product **41b** (47 mg, 0.07 mmol, 67%) as a yellow solid.

TLC: R_f = 0.55 (1:9 MeOH/DCM); UV.

^{1}H-NMR (400 MHz, CDCl$_3$): δ (ppm) = 8.81 (s, 1H), 7.85 (t, 1H, J = 7.8 Hz), 7.75 (dd, 1H, J = 8.1, 0.7 Hz), 7.45 (d, 2H, J = 8.9 Hz), 7.37-7.30 (m, 3H), 7.26-7.23 (m, 2H), 6.91 (d, 2H, J = 8.9 Hz), 6.78-6.62 (m, 1H), 5.07-5.01 (m, 1H), 4.98-4.87 (m, 2H), 4.75 (d, 2H, J = 6.2 Hz), 4.32 (d, 2H, J = 5.7 Hz), 4.01 (br s, 1H), 3.58 (s, 2H), 3.25-3.13 (m, 4H), 2.70-2.53 (m, 4H), 1.59 (s, 6H), 1.49 (s, 9H).

IR (ATR): ν (cm^{-1}) = 3285, 2972, 2931, 1723, 1682.

Tert-Butyl (3*S*)-3-{4-[4-({1-[6-(2-hydroxypropan-2-yl)pyridin-2-yl]-3-oxo-2-(prop-2-en-1-yl)-1H,2H,3H-pyrazolo[3,4-d]pyrimidin-6-yl}amino)phenyl]piperazin-1-yl}pyrrolidine-1-carboxylate (41c)

New AZD1775 building block **40** was Boc deprotected following general procedure **D** and was attached to pyrrolidine **L$_q$** following general procedure **C** for nucleophilic substitution. The crude product was purified by column chromatography on silica gel using 1% MeOH in DCM to afford the product **41c** (35 mg, 0.05 mmol, 53%) as a yellow solid.

TLC: R_f = 0.53 (1:9 MeOH/DCM); UV.

^{1}H-NMR (400 MHz, CDCl$_3$): δ (ppm) = 8.87-8.81 (m, 1H), 7.90-7.84 (m, 1H), 7.56-7.46 (m, 2H), 7.40-7.34 (m, 1H), 6.96-6.90 (m, 2H), 5.76-5.65 (m, 1H), 5.08-5.03 (m, 1H), 4.99-4.90 (m, 1H), 4.75 (d, 2H, *J* = 6.1 Hz), 4.02 (s, 1H), 3.72-3.51 (m, 2H), 3.54-3.41 (m, 4H), 3.30-3.14 (m, 4H), 2.27-2.10 (m, 1H), 2.01-2.74 (m, 4H), 1.60 (s, 6H), 1.47 (s, 9H).

IR (ATR): ν (cm^{-1}) = 3275, 2977, 2935, 1726, 1687.

Tert-Butyl (3*R*)-3-{4-[4-({1-[6-(2-hydroxypropan-2-yl)pyridin-2-yl]-3-oxo-2-(prop-2-en-1-yl)-1H,2H,3H-pyrazolo[3,4-d]pyrimidin-6-yl}amino)phenyl]piperazin-1-yl}pyrrolidine-1-carboxylate (41d)

New AZD1775 building block **40** was Boc deprotected following general procedure **D** and was attached to pyrrolidine **L$_r$** following general procedure **C** for nucleophilic substitution. The crude product was purified by column chromatography on silica gel using 1% MeOH in DCM to afford the product **41d** (10 mg, 0.02 mmol, 34%) as a yellow solid.

TLC: R_f = 0.55 (1:9 MeOH/DCM); UV.

^{1}H-NMR (400 MHz, CDCl$_3$): δ (ppm) = 8.84 (s, 1H), 7.90-7.83 (m, 1H), 7.75 (d, 1H, *J* = 8.5 Hz), 7.54-7.46 (m, 2H), 7.39-7.35 (m, 1H), 6.93 (d, 2H, *J* = 9.0 Hz), 5.78-5.63 (m, 1H), 5.08-5.00 (m, 1H), 4.99-4.89 (m, 1H), 4.75 (d, 2H, *J* = 6.1 Hz), 4.02 (s, 1H), 3.85-3.39 (m, 7H), 3.35-3.07 (m, 6H), 2.20-2.03 (m, 1H), 1.60 (s, 6H), 1.52-1.46 (m, 10H).

IR (ATR): ν (cm^{-1}) = 3255, 2970, 2931, 1725, 1679.

41a-b were Boc deprotected following general procedure **D** and attached to pomalidomide **24** by nucleophilic aromatic substitution following general procedure **B** to give **42a-b**.

2-(2,6-Dioxopiperidin-3-yl)-4-[(3-{4-[4-({1-[6-(2-hydroxypropan-2-yl)pyridin-2-yl]-3-oxo-2-(prop-2-en-1-yl)-1H,2H,3H-pyrazolo[3,4-d]pyrimidin-6-yl}amino)phenyl]piperazin-1-yl}propyl)amino]-2,3-dihydro-1H-isoindole-1,3-dione (42a – MA144)
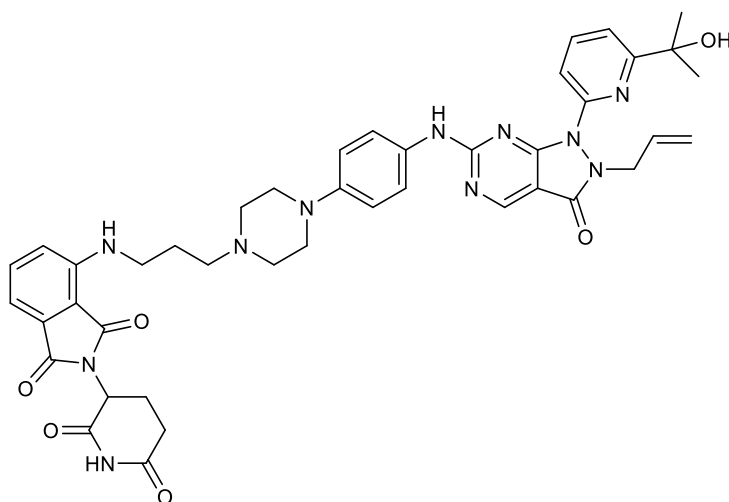
The crude product was purified by column chromatography on silica gel using 5% MeOH in DCM to afford the product **42a** (11 mg, 0.01 mmol, 31%) as a green solid.

TLC: R_f = 0.50 (1:9 MeOH/DCM); UV.

^{1}H-NMR (400 MHz, CDCl$_3$): δ (ppm) = 8.86 (s, 1H), 8.37 (s, 1H), 7.88 (t, 1H, J = 7.9 Hz), 7.76 (d, 1H), 7.56-7.44 (m, 3H), 7.36 (d, 1H, J = 7.4 Hz), 7.11 (d, 1H, J = 7.1 Hz), 6.99-6.78 (m, 4H), 5.80-5.68 (m, 1H), 5.09-5.03 (m, 1H), 5.00-4.82 (m, 2H), 4.75 (d, 2H, J = 6.1 Hz), 3.99 (s, 1H), 3.50-3.11 (m, 6H), 2.89-2.49 (m, 7H), 2.13-2.04 (m, 1H), 2.03-1.88 (m, 2H), 1.74-1.65 (m, 8H).

IR (ATR): ν (cm^{-1}) = 3404, 2968, 1681, 1619, 1405, 1120.

HRMS (ESI): m/z calculated for: C$_{42}$H$_{45}$N$_{11}$O$_6$ [M+H]$^+$, 800.3627, found: 800.3606.

HPLC: 95.0% purity, 8.32 min.

2-(2,6-Dioxopiperidin-3-yl)-4-({[4-({4-[4-({1-[6-(2-hydroxypropan-2-yl)pyridin-2-yl]-3-oxo-2-(prop-2-en-1-yl)-1H,2H,3H-pyrazolo[3,4-d]pyrimidin-6-yl}amino)phenyl]piperazin-1-yl}methyl)phenyl]methyl}amino)-2,3-dihydro-1H-isoindole-1,3-dione (42b – MA162)
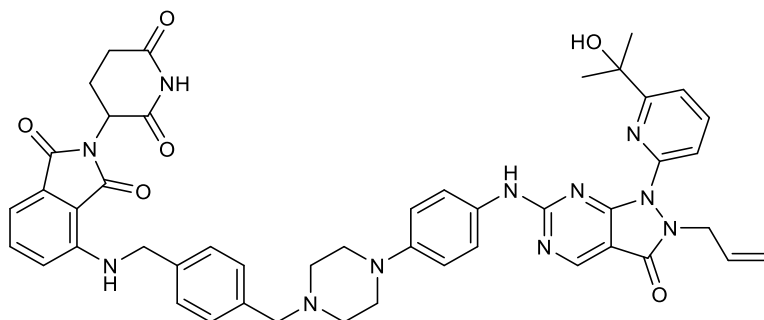
The crude product was purified by column chromatography on silica gel using 5% MeOH in DCM to afford the product **42b** (10 mg, 0.01 mmol, 26%) as a green solid.

TLC: R_f = 0.55 (1:9 MeOH/DCM); UV.

^{1}H-NMR (400 MHz, CDCl$_3$): δ (ppm) = 8.85 (s, 1H), 8.77 (s, 1H), 7.87 (t, 1H, J = 7.9 Hz), 7.76 (d, 1H, J = 7.9 Hz), 7.52-7.44 (m, 3H), 7.42-7.31 (m, 4H), 7.15 (d, 1H, J = 7.0 Hz), 6.96-6.86 (m, 3H), 6.70 (br t, 1H, J = 5.8 Hz), 5.77-5.65 (m, 1H), 5.08-5.02 (m, 1H), 4.98-4.90 (m, 2H), 4.75 (d, 2H, J = 6.1 Hz), 4.52 (d, 2H, J = 5.8 Hz), 3.99 (s, 1H), 3.69-3.58 (m, 2H), 3.31-3.15 (m, 4H), 2.93-2.62 (m, 7H), 2.21-2.12 (m, 1H), 1.60 (s, 6H).

IR (ATR): ν (cm^{-1}) = 3377, 2944, 1684, 1619, 1407, 1120.

HRMS (ESI): m/z calculated for: C$_{47}$H$_{47}$N$_{11}$O$_6$ [M+H]$^+$, 862.3784, found: 862.3756.

2-(2,6-Dioxopiperidin-3-yl)-4-[(3S)-3-{4-[4-({1-[6-(2-hydroxypropan-2-yl)pyridin-2-yl]-

3-oxo-2-(prop-2-en-1-yl)-1H,2H,3H-pyrazolo[3,4-d]pyrimidin-6-

yl}amino)phenyl]piperazin-1-yl}pyrrolidin-1-yl]-2,3-dihydro-1H-isoindole-1,3-dione

(42c – MA165)

The crude product was purified by column chromatography on silica gel using 5% MeOH in DCM to afford the product **42c** (12 mg, 0.01 mmol, 33%) as a green solid.

TLC: R_f = 0.50 (1:9 MeOH/DCM); UV.

^{1}H-NMR (400 MHz, CDCl$_3$): δ (ppm) = 8.86 (s, 1H), 8.56 (s, 1H), 7.88 (t, 1H, J = 7.9 Hz), 7.76 (d, 1H, J = 7.9 Hz), 7.57-7.44 (m, 3H), 7.37 (d, 1H, J = 7.6 Hz), 7.27 (d, 1H, J = 7.0 Hz), 7.00-6.85 (m, 3H), 5.78-5.65 (m, 1H), 5.09-5.02 (m, 1H), 5.02-4.99 (m, 2H), 4.75 (d, 2H, J = 6.1 Hz), 3.98 (s, 1H), 3.94-3.72 (m, 3H), 3.71-3.49 (m, 2H), 3.40-2.64 (m, 11H), 2.38-2.28 (m, 1H), 2.18-2.11 (m, 1H), 1.61 (s, 6H).

IR (ATR): ν (cm^{-1}) = 3377, 2968, 1682, 1617, 1405, 1120.

HRMS (ESI): m/z calculated for: C$_{43}$H$_{45}$N$_{11}$O$_6$ [M+H]$^+$, 812.3627, found: 812.3623.

2-(2,6-Dioxopiperidin-3-yl)-4-[(3R)-3-{4-[4-({1-[6-(2-hydroxypropan-2-yl)pyridin-2-yl]-

3-oxo-2-(prop-2-en-1-yl)-1H,2H,3H-pyrazolo[3,4-d]pyrimidin-6-

yl}amino)phenyl]piperazin-1-yl}pyrrolidin-1-yl]-2,3-dihydro-1H-isoindole-1,3-dione

(42d – MA159)

The crude product was purified by column chromatography on silica gel using 5% MeOH in DCM to afford the product **42d** (5.9 mg, 0.01 mmol, 45%) as a green solid.

TLC: R_f = 0.60 (1:9 MeOH/DCM); UV.

^{1}H-NMR (400 MHz, CDCl$_3$): δ (ppm) = 8.93-8.81 (m, 1H), 8.59-8.34 (m, 1H), 7.96-7.83 (m, 1H), 7.81-7.61 (m, 2H), 7.58-7.44 (m, 3H), 7.28-7.20 (m, 1H), 7.08-6.85 (m, 3H), 5.78-5.64 (m, 1H), 5.09-5.04 (m, 1H), 5.02-4.90 (m, 2H), 4.75 (d, 2H, *J* = 6.0 Hz), 4.04-3.83 (m, 2H), 3.85-3.32 (m, 7H), 3.26-3.02 (m, 3H), 2.94-2.66 (m, 3H), 2.33-2.23 (m, 1H), 2.19-2.10 (m, 1H), 1.62-1.53 (m, 8H).

IR (ATR): ν (cm^{-1}) = 3403, 2972, 1682, 1619, 1407, 1120.

2-(2,6-Dioxopiperidin-3-yl)-4-iodo-2,3-dihydro-1H-isoindole-1,3-dione (44)
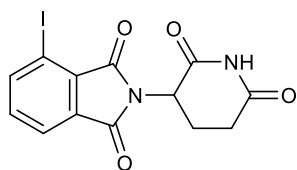
3-iodophtalic anhydride **43** (200 mg, 0.74 mmol, 1.0 eq.) and 3-aminopiperidine-2,6-dione HBr salt **22** (154 mg, 0.74 mmol, 1.0 eq.) were resuspended in AcOH (4 mL). KOAc (240 mg, 2.40 mmol, 3.0 eq.) was added to the flask and the reaction mixture was stirred overnight at r.t.. The reaction mixture was then concentrated, and the black solid was purified by column chromatography on silica gel and eluted with 10% MeOH in DCM to afford the product **44** (210 mg, 0.41 mmol, 55%) as a white solid.

TLC: R_f = 0.50 (1:9 MeOH/DCM); UV.

^{1}H-NMR (400 MHz, CDCl$_3$): δ (ppm) = 8.18 (dd, 1H, J = 8.0, 0.8 Hz), 8.01 (br s, 1H), 7.90 (dd, 1H, J = 7.4, 0.8 Hz), 7.46 (dd, 1H, J = 8.0, 7.4 Hz), 5.03 (dd, 1H, J = 12.4, 5.2 Hz), 3.00-2.72 (m, 3H), 2.22-2.15 (m, 1H).

1-[6-(2-Hydroxypropan-2-yl)pyridin-2-yl]-2-(prop-2-en-1-yl)-6-({4-[4-(prop-2-yn-1-yl)piperazin-1-yl]phenyl}amino)-1H,2H,3H-pyrazolo[3,4-d]pyrimidin-3-one (45)
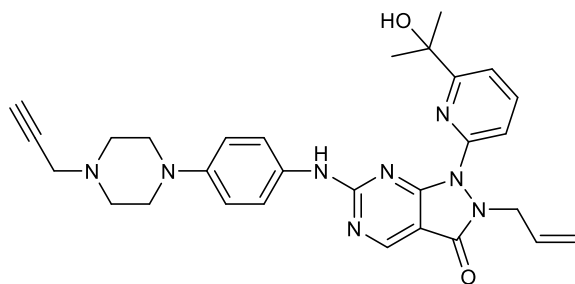
44 was Boc deprotected using general procedure **D** and was then attached to propargyl bromide following general procedure for nucleophilic substitution **C**. The crude product was purified by column chromatography on silica gel using 0.5% MeOH in DCM to afford the product **45** (25 mg, 0.05 mmol, 48%) as a yellow solid.

TLC: R_f = 0.70 (5:95 MeOH/DCM); UV.

^{1}H-NMR (400 MHz, CDCl$_3$): δ (ppm) = 8.73 (s, 1H), 7.96 (t, 1H, J = 7.9 Hz), 7.67-7.52 (m, 4H), 6.94 (d, 2H, J = 9.0 Hz), 5.75-5.63 (m, 1H), 5.12-5.07 (m, 1H), 4.96-4.88 (m, 1H), 4.76 (d, 2H, J = 6.3 Hz), 4.04 (d, 2H, J = 2.4 Hz), 3.67-3.34 (m, 8H), 2.74 (t, 1H, J = 2.4 Hz), 1.63 (s, 6H).

^{13}C-NMR (101 MHz, CDCl$_3$): δ (ppm) = 167.0, 166.8, 159.1, 155.5, 146.6, 139.4, 131.4, 130.6, 122.6, 120.3, 120.1, 118.1, 117.9, 117.2, 117.0, 100.8, 80.3, 73.0, 70.8, 50.4, 47.4, 46.7, 45.7, 30.5.

5.4.3 Synthesis of the second generation of VHL-PROTACs

(2S,4R)-1-[(2S)-2-(11-Bromoundecanamido)-3,3-dimethylbutanoyl]-4-hydroxy-N-{[4-(4-methyl-1,3-thiazol-5-yl)phenyl]methyl}pyrrolidine-2-carboxamide (47a)
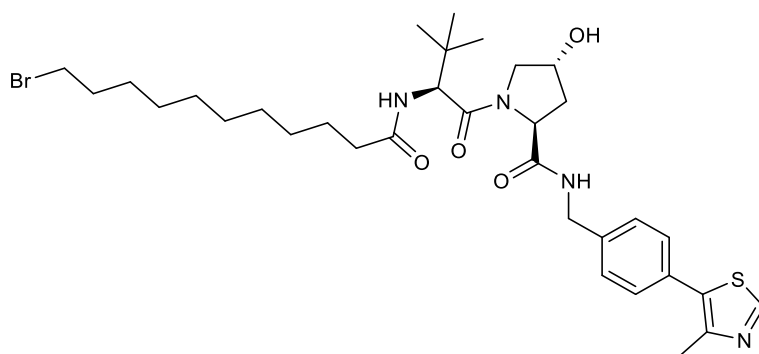
VH032 **18** was attached to the linker following general procedure **A** for HATU-mediated amide coupling. The crude product was purified by column chromatography on silica gel using 5% MeOH in DCM to afford the product **47a** (23 mg, 0.03 mmol, 37%) as a yellow solid.

TLC: R_f = 0.45 (1:9 MeOH/DCM); UV and KMnO$_4$.

^{1}H-NMR (400 MHz, CDCl$_3$): δ (ppm) = 8.70 (s, 1H), 7.42-7.31 (m, 5H), 6.13 (d, 1H, J = 8.7 Hz), 4.72(t, 1H, J = 7.9 Hz), 4.64-4.49 (m, 3H), 4.35 (dd, 1H, J = 15.0, 5.3 Hz), 4.10 (d, 1H, J = 11.5 Hz), 3.62 (dd, 1H, J = 11.5, 3.7 Hz), 3.41 (t, 2H, J = 6.9 Hz), 2.58-2.49 (m, 4H), 2.19

(t, 2H, *J* = 7.2 Hz), 2.17-2.08 (m, 1H), 1.86 (p, 2H, *J* =), 1.67-1.53 (m, 2H), 1.48-1.36 (m, 2H), 1.36-1.23 (m, 10H), 1.01-0.91 (m, 9H).

^{13}C-NMR (101 MHz, CDCl$_3$): δ (ppm) = 173.8, 171.9, 170.7, 150.3, 138.0, 131.0, 129.5, 128.1, 70.0, 58.5, 57.5, 56.7, 43.3, 36.5, 35.8, 34.9, 34.0, 32.8, 29.3, 29.3, 29.2, 29.2, 28.7, 28.1, 26.4, 25.6, 16.1, 14.1.

IR (ATR): v (cm^{-1}) = 3313, 2927, 2855, 1628, 1436, 1235, 849.

(2*S*,4*R*)-1-[(2*S*)-2-(15-Bromopentadecanamido)-3,3-dimethylbutanoyl]-4-hydroxy-N-{[4-(4-methyl-1,3-thiazol-5-yl)phenyl]methyl}pyrrolidine-2-carboxamide (47b)
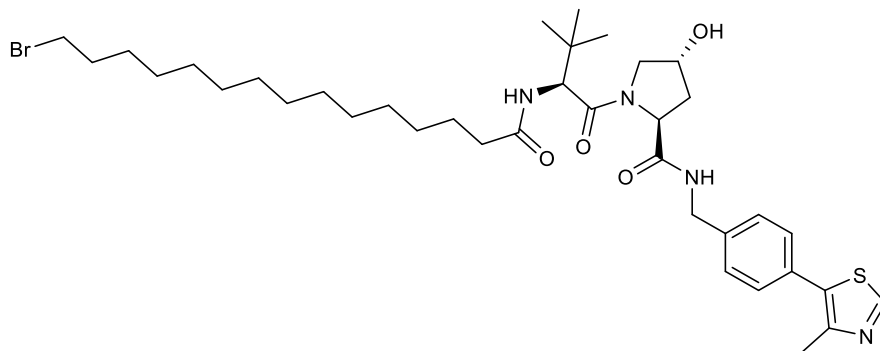
VH032 **18** was attached to the linker following general procedure **A** for HATU-mediated amide coupling. The crude product was purified by column chromatography on silica gel using 5% MeOH in DCM to afford the product **47b** (17 mg, 0.02 mmol, 42%) as a yellow solid.

TLC: *R*$_f$ = 0.55 (1:9 MeOH/DCM); UV and KMnO$_4$.

^{1}H-NMR (400 MHz, CDCl$_3$): δ (ppm) = 8.70 (s, 1H), 7.41-7.31 (m, 5H), 6.12 (dd, 1H, *J* = 8.6, 3.5 Hz), 4.73 (t, 1H, *J* = 7.9 Hz), 4.65 (t, 1H, *J* = 6.8 Hz), 4.62-4.48 (m, 3H), 4.35 (dd, 1H, *J* = 15.0, 5.3 Hz), 4.12 (d, 1H, *J* = 11.5 Hz), 3.78-3.68 (m, 1H), 3.62 (dd, 1H, *J* = 11.5, 3.5 Hz), 3.42 (t, 1H, *J* = 6.9 Hz), 3.26-3.16 (m, 1H), 2.60-2.54 (m, 1H), 2.53 (s, 3H), 2.24-2.11 (m, 3H), 1.97-1.82 (m, 2H), 1.65-1.53 (m, 2H), 1.34-1.23 (m, 18H), 0.95 (s, 9H).

^{13}C-NMR (101 MHz, CDCl$_3$): δ (ppm) = 173.9, 171.9, 170.6, 151.2, 150.3, 148.5, 138.1, 129.5, 129.2, 128.1, 120.6, 70.1, 58.5, 57.5, 56.6, 43.8, 43.3, 36.5, 35.8, 34.8, 34.1, 32.8, 29.6, 29.5, 29.5, 29.3, 29.2, 28.8, 28.2, 28.0, 26.4, 25.6, 25.4, 16.1, 12.6.

IR (ATR): ν (cm^{-1}) = 3311, 2924, 2853, 1627, 1435, 840.

(2*S*,4*R*)-4-Hydroxy-1-[(2*S*)-2-(11-{4-[4-({1-[6-(2-hydroxypropan-2-yl)pyridin-2-yl]-3-oxo-2-(prop-2-en-1-yl)-1H,2H,3H-pyrazolo[3,4-d]pyrimidin-6-yl}amino)phenyl]piperazin-1-yl}undecanamido)-3,3-dimethylbutanoyl]-N-{[4-(4-methyl-1,3-thiazol-5-yl)phenyl]methyl}pyrrolidine-2-carboxamide (48a – MA199)
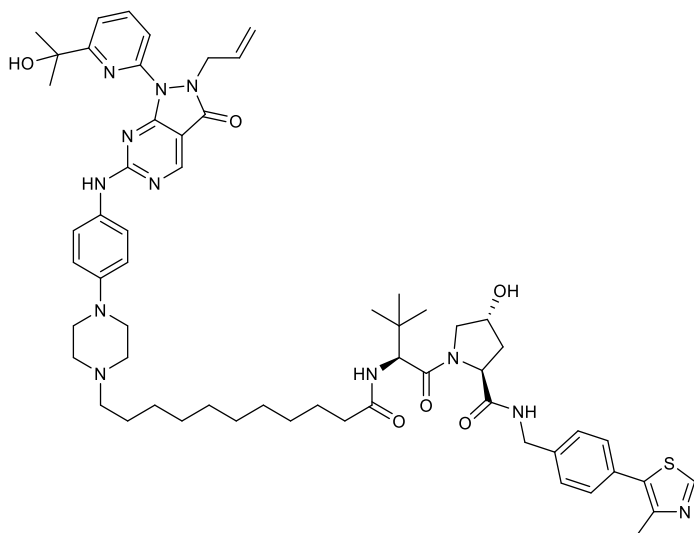
New AZD1775 building block **40** was Boc deprotected following general procedure **D** and attached to VH032 and linker **47a** using general procedure **C** for nucleophilic substitution. The crude product was purified by column chromatography on silica gel using 8% MeOH in DCM to afford the product **48a** (15 mg, 0.01 mmol, 41%) as a yellow solid.

TLC: *R*$_f$ = 0.40 (1:9 MeOH/DCM); UV, KMnO$_4$.

^{1}H-NMR (400 MHz, CDCl$_3$): δ (ppm) = 8.84 (s, 1H), 8.64 (s, 1H), 7.86 (t, 1H, *J* = 7.9 Hz), 7.76 (d, 1H, *J* = 8.3 Hz), 7.48 (d, 2H, *J* = 8.6 Hz), 7.41-7.32 (m, 6H), 6.94 (d, 2H, *J* = 8.6 Hz), 6.16 (d, 1H, *J* = 8.6 Hz), 5.77-5.65 (m, 1H), 5.05 (dq, 1H, *J* = 10.3, 1.2 Hz), 4.95 (dq, 1H, *J* = 17.0, 1.2 Hz), 4.80-4.71 (m, 3H), 4.64-4.50 (m, 3H), 4.34 (dd, 1H, *J* = 14.9, 5.1 Hz), 4.12 (d, 1H, *J*

= 11.4 Hz), 3.62 (dd, 1H, *J* = 11.4, 3.7 Hz), 3.26-3.19 (m, 4H), 2.70-2.62 (m, 4H), 2.60-2.50 (m, 4H), 2.46-2.40 (m, 2H), 2.23-2.08 (m, 4H), 1.39-1.21 (m, 14H), 0.95 (s, 9H).

^{13}C-NMR (101 MHz, CDCl$_3$): δ (ppm) = 173.8, 172.0, 170.6, 165.8, 162.3, 161.2, 156.3, 150.3, 148.5, 147.5, 138.8, 138.0, 131.6, 131.0, 129.5, 128.2, 122.1, 119.0, 116.4, 116.2, 116.0, 72.5, 70.0, 58.7, 58.5, 57.4, 56.7, 53.2, 49.4, 47.7, 43.3, 36.5, 35.8, 34.9, 30.6, 29.4, 29.4, 29.3, 29.2, 29.2, 27.5, 26.7, 26.4, 25.6, 16.1.

IR (ATR): ν (cm^{-1}) = 3285, 2929, 2853, 1675, 1619, 1418, 1235, 732.

HRMS (ESI): *m/z* calculated for: C$_{59}$H$_{78}$N$_{12}$O$_6$S [M+H]$^+$, 1083.5961, found: 1083.5907.

HPLC: 95.0% purity, 9.58 min.

(2*S*,4*R*)-4-Hydroxy-1-[(2*S*)-2-(15-{4-[4-({1-[6-(2-hydroxypropan-2-yl)pyridin-2-yl]-3-oxo-2-(prop-2-en-1-yl)-1H,2H,3H-pyrazolo[3,4-d]pyrimidin-6-yl}amino)phenyl]piperazin-1-yl}pentadecanamido)-3,3-dimethylbutanoyl]-N-{[4-(4-methyl-1,3-thiazol-5-yl)phenyl]methyl}pyrrolidine-2-carboxamide (48b – MA198)
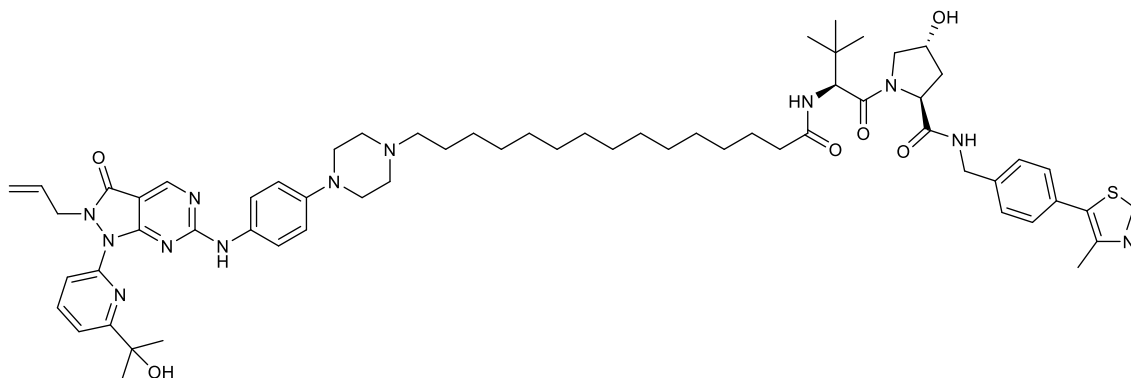
New AZD1775 building block **40** was Boc deprotected following general procedure **D** and attached to VH032 and linker **47b** using general procedure *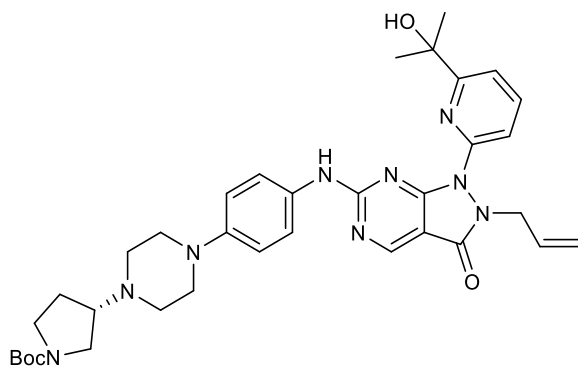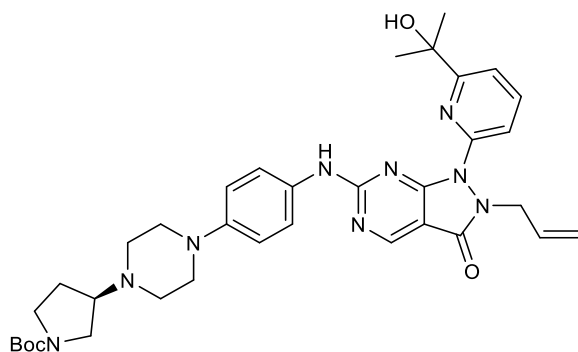*C** for nucleophilic substitution. The crude product was purified by column chromatography on silica gel using 8% MeOH in DCM to afford the product **48b** (2.5 mg, 0.002 mmol, 10%) as a yellow solid.

TLC: *R*$_f$ = 0.40 (1:9 MeOH/DCM); UV, KMnO$_4$.

^{1}H-NMR (400 MHz, CDCl$_3$): δ (ppm) = 8.89 (s, 1H), 8.82 (s, 1H), 8.00 (t, 1H, *J* = 7.9 Hz), 7.83-7.74 (m, 1H), 7.65 (dd, 1H, *J* = 7.9, 0.7 Hz), 7.59 (d, 2H, *J* = 8.9 Hz), 7.48 (d, 2H, *J* = 8.7 Hz), 7.42 (d, 2H, *J* = 8.7 Hz), 7.00 (d, 2H, *J* = 8.9 Hz), 5.79-5.67 (m, 1H), 5.08-5.02 (m, 1H), 4.96-4.89 (m, 1H), 4.82 (d, 2H, 6.1 Hz), 4.67-4.65 (m, 1H), 4.65-4.62 (m, 2H), 4.54-4.49 (m, 1H), 4.39-4.31 (m, 1H), 3.92 (d, 1H, *J* = 11.1 Hz), 3.82 (dd, 1H, *J* = 11.1, 4.0 Hz), 3.06-2.93 (m, 4H), 2.80-2.71 (m, 2H), 2.49 (s, 3H), 2.32-2.19 (m, 2H), 1.74-1.60 (m, 4H), 1.59 (s, 6H), 1.44-1.25 (m, 22H), 1.05 (s, 9H).

IR (ATR): v (cm^{-1}) = 3391, 2924, 2853, 1619, 1420, 834.

HRMS (ESI): *m/z* calculated for: C$_{63}$H$_{86}$N$_{12}$O$_6$S [M+2H]$^{2+}$, 570.3330, found: 570.3330.

HPLC: >99% purity, 10.53 min.

Methyl 2-{4-[4-({1-[6-(2-hydroxypropan-2-yl)pyridin-2-yl]-3-oxo-2-(prop-2-en-1-yl)-1H,2H,3H-pyrazolo[3,4-d]pyrimidin-6-yl}amino)phenyl]piperazin-1-yl}acetate (50)
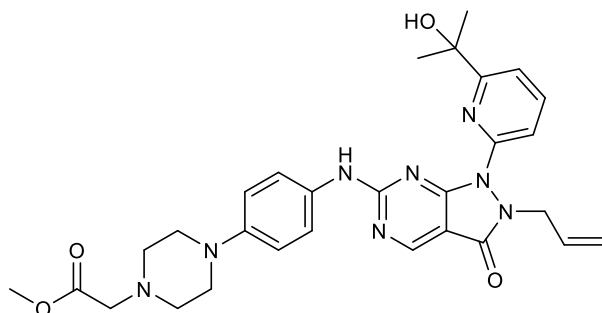
10 (175 mg, 0.56 mmol, 1.00 eq.) was resuspended in toluene (8 mL) and mCPBA (207 mg, 0.67 mmol, 1.20 eq.) was added (Matheson, Backos, *et al.*, 2016). The reaction mixture was stirred at r.t. for 1 h. Then, DIPEA (0.18 mL, 2.24 mmol, 4.00 eq.) was added, followed by aniline **49** (139.5 mg, 1.01 mmol, 1.00 eq.). The mixture was stirred overnight. In the morning, saturated NaHCO$_3$ (30 mL) was added and the mixture was extracted with EtOAc (3 × 30 mL), washed with brine (20 mL), dried over MgSO$_4$ and concentrated under reduced pressure to give the crude. The crude product was purified by column chromatography on silica gel with 3% MeOH in DCM to give the product **50** (30 mg, 0.04

mmol, 7%) as a yellow solid. The low yield was due to the aniline **49** not dissolving when added to the reaction mixture, the aniline was very sticky.

TLC: R_f = 0.25 (5:95 MeOH/DCM); UV.

^{1}H-NMR (400 MHz, CDCl$_3$): δ (ppm) = 8.82 (s, 1H), 7.87 (t, 1H, J = 7.8 Hz), 7.76 (d, 1H, J = 8.0 Hz), 7.57-7.50 (m, 2H), 7.37 (d, 1H, J = 7.8 Hz), 6.94 (d, 2H, J = 8.7 Hz), 5.78-5.65 (m, 1H), 5.05 (d, 1H, J = 10.4 Hz), 4.95 (d, 1H, J = 17.2 Hz), 4.76 (d, 2H, J = 6.0 Hz), 3.77 (m, 1H), 3.36 (s, 2H), 3.31-3.22 (m, 4H), 2.89-2.77 (m, 4H), 1.60 (s, 6H).

^{13}C-NMR (101 MHz, CDCl$_3$): δ (ppm) = 170.4, 165.8, 162.1, 161.0, 155.7, 148.0, 147.3, 138.9, 131.5, 130.8, 130.1, 128.1, 122.0, 119.1, 116.7, 116.3, 116.2, 72.5, 59.1, 52.9, 51.8, 49.4, 47.8, 30.5.

IR (ATR): v (cm^{-1}) = 3280, 2978, 1725, 1682, 1612, 1420, 1237, 732.

HRMS (ESI): m/z calculated for: C$_{29}$H$_{34}$N$_8$O$_4$ [M+H]$^+$, 529.2776, found: 529.2769.

2-{4-[4-({1-[6-(2-Hydroxypropan-2-yl)pyridin-2-yl]-3-oxo-2-(prop-2-en-1-yl)-1H,2H,3H-pyrazolo[3,4-d]pyrimidin-6-yl}amino)phenyl]piperazin-1-yl}acetic acid (51)
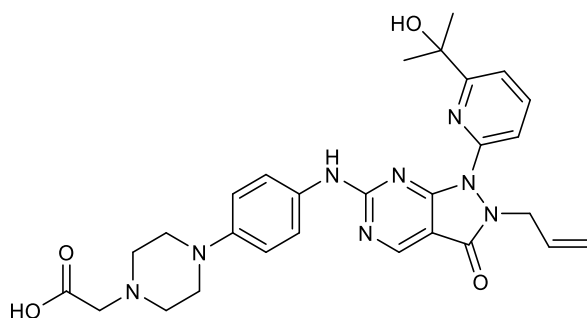
50 (25 mg, 0.04 mmol, 1.0 eq.) was resuspended in MeOH (0.5 mL) and water (0.5 mL) was added. LiOH (1.2 mg, 0.05 mmol, 1.2 eq.) was then added to the flask and the reaction mixture was stirred overnight at 60 °C. In the morning, **51** was concentrated (in quantitative yield) in vacuo to remove the solvent and was used in the next step without further purification.

(2S,4R)-4-Hydroxy-1-[(2S)-2-(2-{4-[4-({1-[6-(2-hydroxypropan-2-yl)pyridin-2-yl]-3-oxo-2-(prop-2-en-1-yl)-1H,2H,3H-pyrazolo[3,4-d]pyrimidin-6-yl}amino)phenyl]piperazin-1-yl}acetamido)-3,3-dimethylbutanoyl]-N-{[4-(4-methyl-1,3-thiazol-5-yl)phenyl]methyl}pyrrolidine-2-carboxamide (52 – MA204)
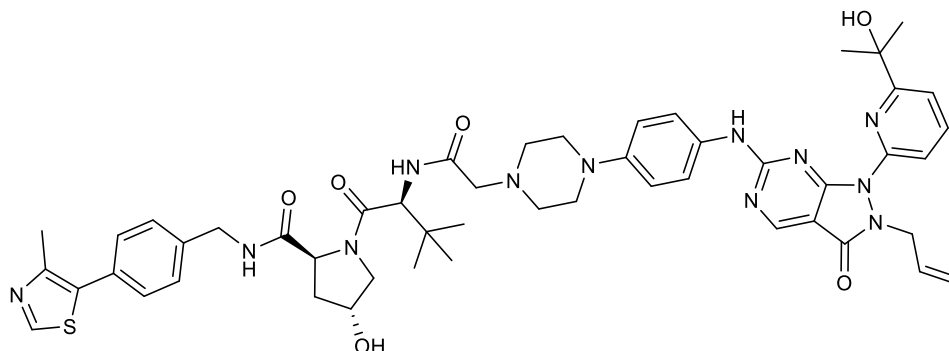
51 was coupled to VH032 building block **18** following general procedure **A** for HATU-mediated amide coupling. The crude product was purified by column chromatography on silica gel using 7% MeOH in DCM to give the product **52** (15 mg, 0.02 mmol, 34%) as a yellow solid.
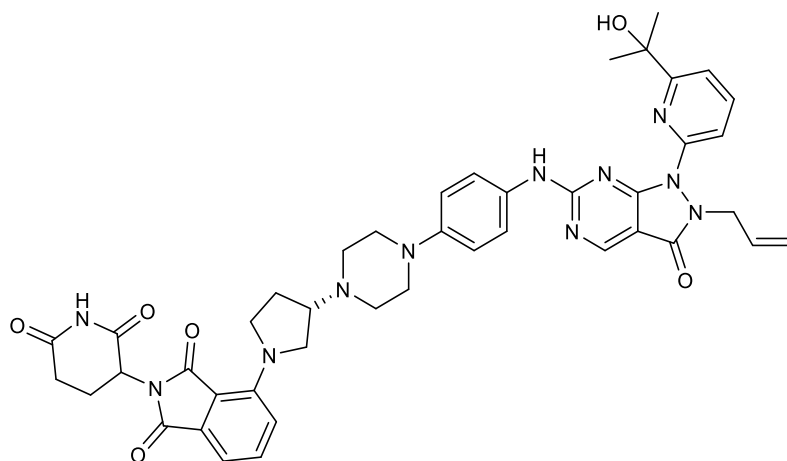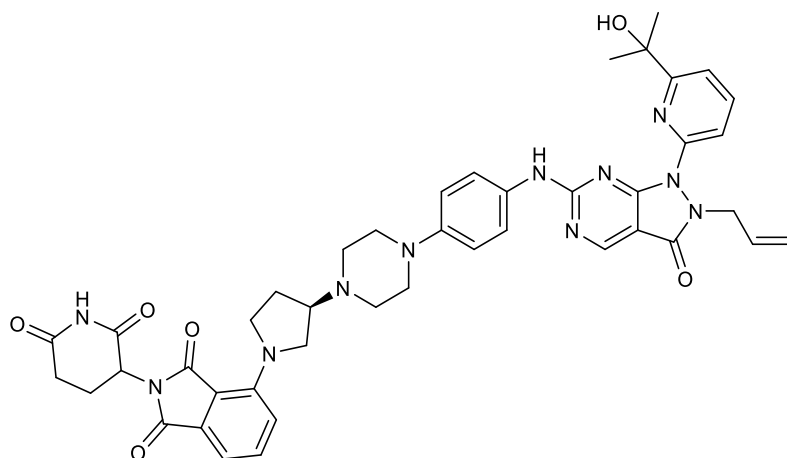
TLC: R_f = 0.20 (1:9 MeOH/DCM); UV.

^{1}H-NMR (400 MHz, CDCl$_3$): δ (ppm) = 8.85 (s, 1H), 8.68 (s, 1H), 7.89 (t, 1H, *J* = 7.9 Hz), 7.74 (d, 1H, *J* = 7.9 Hz), 7.49 (d, 2H, *J* = 8.7 Hz), 7.43-7.32 (m, 6H), 6.92 (d, 2H, *J* = 8.7 Hz), 5.79-5.66 (m, 1H), 5.09-5.04 (m, 1H), 4.99-4.92 (m, 1H), 4.83-4.72 (m, 3H), 4.61-4.51 (m, 3H), 4.46 (d, 1H, *J* = 8.7 Hz), 4.36 (dd, 1H, *J* = 15.0, 5.3 Hz), 4.19 (d, 1H, *J* = 10.6 Hz), 3.63 (dd, 1H, *J* = 11.3, 3.5 Hz), 3.28 (br s, 4H), 2.82 (br s, 4H), 2.61-2.48 (m, 4H), 2.26-2.15 (m, 1H), 1.61 (s, 6H), 1.55 (d, 1H, *J* = 6.6 Hz), 1.47 (d, 1H, *J* = 6.6 Hz), 1.00 (s, 9H).

IR (ATR): ν (cm^{-1}) = 3293, 2968, 1671, 1619, 1418, 1235, 1032.

HRMS (ESI): *m/z* calculated for: C$_{50}$H$_{60}$N$_{12}$O$_6$S [M+H]$^+$, 957.4552, found: 957.4507.

HPLC: 96.0% purity, 8.77 min.

5.4.4 Synthesis of a negative control PROTAC for the CRBN-series

4-[(3-{4-[4-({1-[6-(2-Hydroxypropan-2-yl)pyridin-2-yl]-3-oxo-2-(prop-2-en-1-yl)-1H,2H,3H-pyrazolo[3,4-d]pyrimidin-6-yl}amino)phenyl]piperazin-1-yl}propyl)amino]-2-(1-methyl-2,6-dioxopiperidin-3-yl)-2,3-dihydro-1H-isoindole-1,3-dione (53 – negMA144)
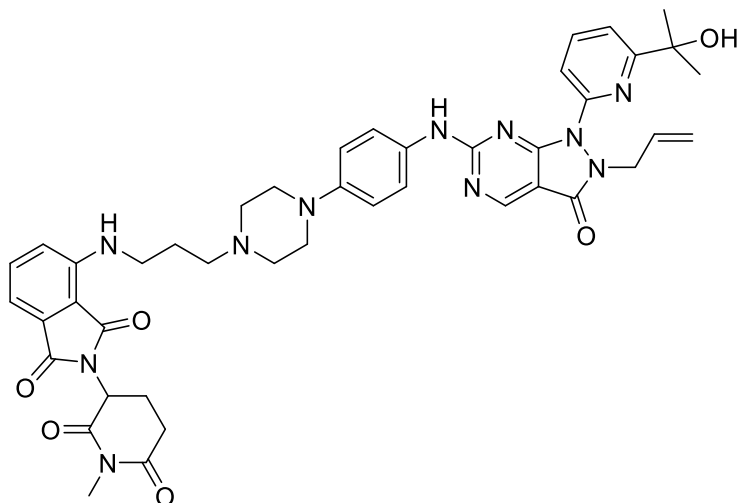
**41a** was Boc deprotected using general procedure **D** and was attached to Me-pomalidomide **34** by nucleophilic aromatic substitution following general procedure **B**. The crude product was purified by column chromatography on silica gel using 4.5% MeOH in DCM to afford the product **53** (10 mg, 0.01 mmol, 36%) as a green solid.

TLC: R_f = 0.55 (1:9 MeOH/DCM); UV.

^{1}H-NMR (400 MHz, CDCl$_3$): δ (ppm) = 8.86 (s, 1H), 7.87 (t, 1H, J = 7.9 Hz), 7.77 (dd, 1H, J = 8.1, 0.7 Hz), 7.55-7.44 (m, 3H), 7.41-7.34 (m, 1H), 7.11 (dd, 1H, J = 7.2, 0.7 Hz), 6.98-6.92 (m, 3H), 6.72 (br t, 1H), 5.78-5.68 (m, 1H), 5.09-5.04 (m, 1H), 5.00-4.93 (m, 1H), 4.92-4.86 (m, 1H), 4.76 (d, 2H, J = 6.2 Hz), 3.97(s, 1H), 3.76 (s, 1H), 3.45-3.39 (m, 2H), 3.30-3.24 (m, 4H), 3.18 (s, 3H), 2.96-2.89 (m, 1H), 2.76-2.63 (m, 6H), 2.57 (t, 2H, J = 6.5 Hz), 2.09-2.02 (m, 1H), 1.91 (p, 2H, J = 6.5 Hz), 1.61 (s, 6H).

IR (ATR): ν (cm^{-1}) = 3373, 2935, 1677, 1617, 1403, 1118.

HRMS (ESI): *m/z* calculated for: C$_{43}$H$_{47}$N$_{11}$O$_6$ [M+H]$^+$, 814.3784, found: 814.3769.

HPLC: 98.6% purity, 8.71 min.

5.5   Conclusion

A second generation of Wee1 PROTACs was designed and synthesised by using the observations from the first generation. The first generation of Wee1 PROTACs had shown successful, fast and maintained Wee1 degradation from 100 nM to 10 µM overall for the best PROTACs of each series recruiting the CRBN and the VHL E3 ligases. For both series, short and long linkers seemed to yield the most potent PROTACs. Thus, new PROTACs were synthesised with very short and rigid linkers for the CRBN-series, and short and long linkers for the VHL series. They were made from a new AZD1775 building block in order to remove one amide bond in the molecule to hopefully improve cell penetration, and thus potency. Four PROTACs recruiting CRBN were synthesised with very short linkers such as propyl and pyrrolidine (MA144, MA162, MA165, MA159), and three new PROTACs recruiting VHL were synthesised with two long alkyl linkers (MA198, MA199) and a very short linker (MA204).

All the second generation Wee1 PROTACs recruiting CRBN induced successful Wee1 degradation with MA144 being the most potent. MA144 reached maximal degradation at 100-300 nM, induced strong reduced pCDK1(Y15) for concentrations as low as 30 nM and showed strong hook effect at higher concentrations.

For the second generation of Wee1 PROTACs recruiting VHL, the long ten-carbon linker MA199 and the very short acetyl-linker MA204 induced successful Wee1 degradation whereas, MA198 with fourteen-carbon linker did not degrade Wee1. MA199 was the most potent and induced a comparable Wee1 degradation as well as downstream effect as MA144.

Both best PROTACs MA199 and MA144 were selected to conduct more experiments, and they induced strong Wee1 degradation at 300 nM after 24 h and 48 h treatment. Their IC_{50} values in BT549 were decreased compared to the best PROTACs of the first

generation and were similar to that of AZD1775, which confirmed improvements in the potency with the new generation. They were also confirmed to maintain selectivity towards Wee1. Investigation of their ternary complexes by ITC suggested that the MA199 ternary complex was a bit stronger than the ternary complex of MA055 of the first generation and MA204 of the second generation. More ternary complex binding constants for non-degrading PROTACs would be beneficial to understand the role of ternary complex in the Wee1 PROTACs system. Due to Covid and the restricted access to the ITC instrument, it was unfortunately not possible.

The potency reached by MA144 and MA199 is however very good and optimisation was definitely useful. Another group published similar PROTACs to ours in the middle of my PhD confirming the potency of MA144 and its selectivity by proteomics analysis (Z. Li *et al.*, 2020). By generating PROTACs recruiting VHL E3 ligase and not only CRBN, we showed that the PROTAC degradation profiles depend on the linker's nature but also the E3 ligase, and it is specific to every target as already shown in the literature with different examples of SAR for different systems. Both series of compounds are useful to develop further and could be profitable in the future as both E3 ligases (VHL and CRBN) are expressed at different levels depending on the tissues, which could be specific to certain cancers. The accessibility of two different E3 ligases for Wee1 degradation could also help with drug resistance.

6 Cubanes and interest in bioactive molecules

6.1 Introduction

6.1.1 Access to cubanes

6.1.1.1 Synthesis of 1,4-disubstituted cubanes

So far, only the 1,4-disubstituted cubane **61** can be made on large scale. The 1,4-cubane was first synthesised in 1964 by Eaton and Cole (Scheme 6.1) (Eaton *et al.*, 1964), and optimised later on by Chapman and colleagues (Chapman *et al.*, 1970), and then the Tsanaktsidis group (Falkiner *et al.*, 2013) improved the approach to work on multigram scale. In Eaton and Cole's synthesis (Scheme 6.1) (Eaton *et al.*, 1964), 2-cyclopentenone **54** reacts with *N*-bromosuccinimide to give the brominated ketone **55**. Further bromination then gave 2,3,4-cyclopentenone **56**, which underwent a dehydrobromination to give bromocyclopentadienone **57**. **58** directly underwent a spontaneous Diels-Alder to give **58**. **58** was heated at reflux in 50% potassium hydroxide to accomplish a double Favorskii-type rearrangement and give 1,4-cubanedicarboxylic acid **60**, which can be converted into the corresponding diester **61** by heating in methanol in the presence of an acid catalyst.
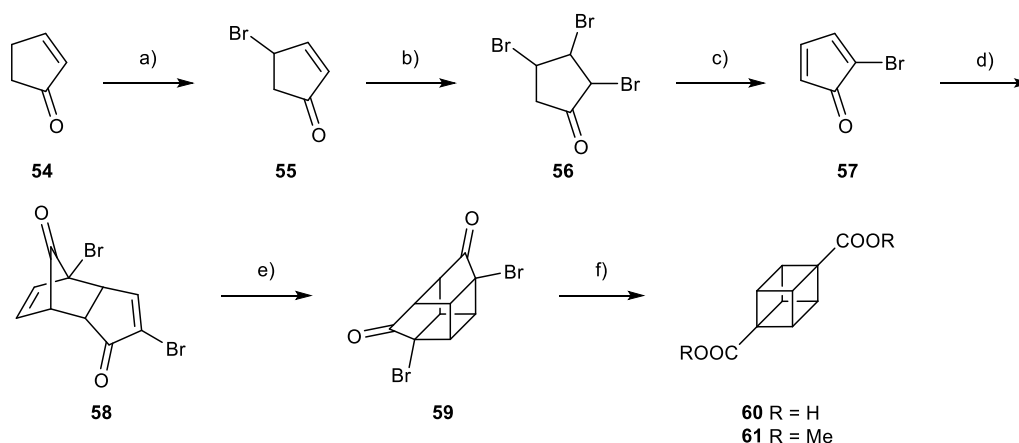
Scheme 6.1: Original synthesis of 1,4-disubstitued cubane. Reagents and conditions: a) NBS, $C(Cl)_4$, AIBN; b) Br_2, pentane/DCM, 0 °C; c) Et_2NH, ether, −20 °C; d) spontaneous Diels-Alder dimerisation; e) hv, HCl, MeOH (H_2O); f) i) 50% KOH, reflux; ii) HCl aq.; iii) MeOH, H_2SO_4 (cat.).

Chapman and colleagues (Chapman *et al.*, 1970) modified the Eaton/Cole synthesis to avoid the instability of various compounds from the original synthesis (Scheme 6.2). The synthesis started with cyclopentadienone ethylene ketal **62**, and this synthetic route was further optimised for larger scale (Falkiner *et al.*, 2013). Cyclopentadienone ethylene ketal **62** was tribrominated using bromine/1,4-dioxane to give **63**, and then reacted with sodium hydroxide to give the bisethylene ketal dimer **64**, through Diels-Alder reaction of the corresponding diene. Both ketal groups were then deprotected using concentrated sulfuric acid to obtain **58**. The ketal at the bottom is less constrained, so easier to deprotect, but the one at the bottom of the molecule required harsher conditions as previously proposed by Chapman *et al*. because of the strain of the bridged ketone. Falkiner *et al*. explained that the deprotection of the second ketal is facilitated by the destruction in situ of the ethylene glycol released during the reaction. **58** was then irradiated for about seven days in methanol with a catalytic amount of sulfuric acid to obtain **59**, containing two α-bromoketones that can undergo a double Favorskii-type ring contraction to form the cubane **60**. The diacid **60** can then be esterified by heating in methanol in the presence of an acidic resin to afford **61** (Scheme 6.2).
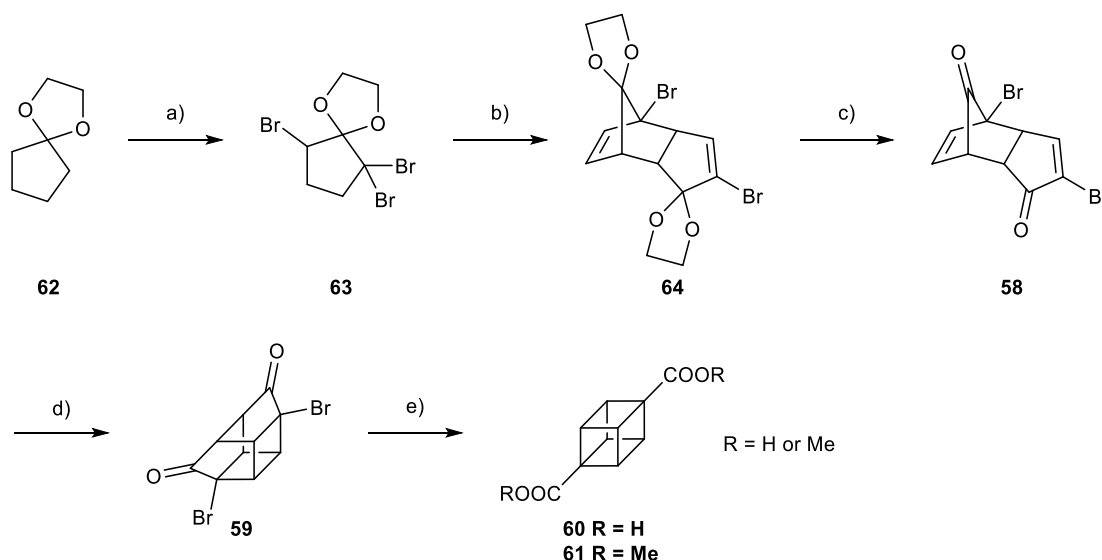
Scheme 6.2: Improved 1,4-disubstituted cubane by Chapman and co-workers followed by Tsanaktsidis group. Reagents and conditions: a) Br$_2$, 1,4-dioxane, 10 °C to r.t., 1 day; b) NaOH, MeOH, 5 °C to reflux, 20 h; c) H$_2$SO$_4$, 25 °C, 30 h; d) i) hv (Hg, Pyrex), MeOH, H$_2$SO$_4$, 40–45 °C, 7 days; ii) H$_2$O, reflux, 3 h; e) i) NaOH (30% aq), reflux, 3 h; ii) HCl (32%), <5 °C, 18 h; iii) Dowex 50WX8-100, MeOH, reflux, 18 h.

The 1,4-disubstituted cubane **61** is now a well-established system that has been developed and optimised by different groups as developed above. This is a reliable synthesis that can be done in the multigram scale (Falkiner *et al.*, 2013) but is composed of many steps: seven-step synthesis from commercially available cyclopentanone ethylene ketal **62** with the photoreaction step being very long. The sequence is not atom-efficient due to the number of intermediates and rearrangement that need to be done. Strong base and acids are required and are very toxic and corrosive. Nevertheless, 1,4-disubstituted cubanes **61** can be accessed in reasonable scale.

6.1.1.2 Synthesis of 1,3-disubstituted cubanes

Otherwise, the isomeric 1,3-disubstituted cubane **68** can only be made on small scale (Barborak *et al.*, 1966; Nigo *et al.*, 1993). The 1,3-cubane was first synthesised in 1966 by degrading cyclobutadieneiron tricarbonyl **65** in the presence of 2,5-dibromo-1,4-benzoquinone giving **66** through a Diels Alder reaction involving free cyclobutadiene (Scheme 6.3). **66** was then irradiated in benzene to give **67**, which was then heated in

aqueous potassium hydroxide to afford the 1,3-cubane dicarboxylic acid **68** (Barborak *et al.*, 1966). However, little experimental detail was given, and scale-up of this reaction sequence seems unfeasible, as cyclobutadiene iron tricarbonyl **65** is not commercially available, and must be prepared from expensive precursors in low yield.
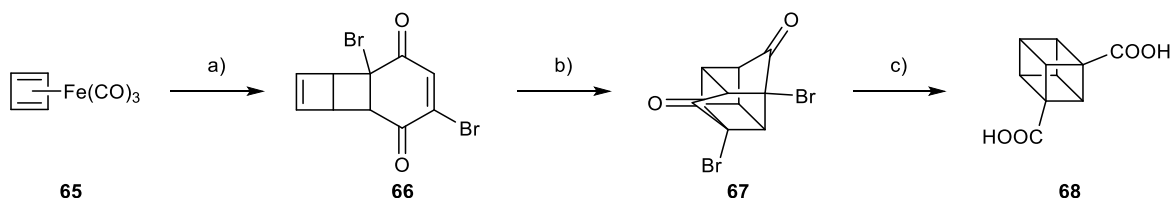
Scheme 6.3: Original synthesis of the 1,3-disubstituted cubane framework. Reagents and conditions: a) 2,5-dibromobenzoquinone; b) benzene, Hg lamps; c) aq. KOH, reflux.

More recently, Nigo *et al*. (Nigo *et al.*, 1993) proposed a synthesis for the 1,3-disubstituted cubane **68** that was similar to that of the 1,4-disubstituted cubane **61** from Chapman *et al*. (Chapman *et al.*, 1970). The authors reported that step a (Scheme 6.4) led to two enone regioisomers, the bromine substituent being placed either side of the bridgehead (i.e. adjacent to the ketal, or on the opposite side to the ketal). As such, one form was used as precursor for the 1,4-disubstituted cubane **61** as described before (Scheme 6.2), but the authors thought to use the other isomer as a precursor for the 1,3-disubstituted cubane **75** (Scheme 6.5). However, the transition state to make **70** (X = Br and Y = H) is very unfavourable (Eaton *et al.*, 1964) and led only to 4.5% yield of **70** compared to 95.5% for **64** (Scheme 6.4) (Nigo *et al.*, 1993).
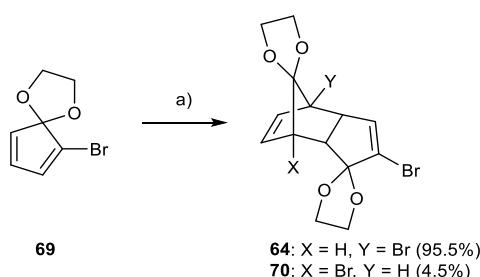
Scheme 6.4: Diels-Alder reaction giving two products. Reagents and conditions: a) KOH, MeOH, reflux, 4 h.

The next steps mirror the synthesis of the 1,4-cubane isomer, and led to very good yields (Scheme 6.5) (Nigo *et al.*, 1993). Thus, selective ketal deprotection (due the strength of the ketal bridging at the top) gave **71**, followed by intramolecular [2+2] photocycloaddition to give **72**. The subsequent Favorskii-type reaction giving **73** was followed by a second ketal deprotection to afford **74**, and a second Favorksii-type ring contraction to give **68** and **75** after methylation of the acids. The synthetic route offers a robust approach to 1,3-disubstituted cubanes **75**, but again comprises a number of steps and is not particularly atom-efficient. Nevertheless, this route currently constitutes the most promising approach to multi-gram quantities of **75**, and could be improved in a more efficient way to synthesise **70**. The 1,3-disubstituted cubane **75** could then be functionalised in the one and three positions to allow introduction of the cubane motif into other molecules, such as drugs. This idea will be developed in section 6.3.1.2.2.
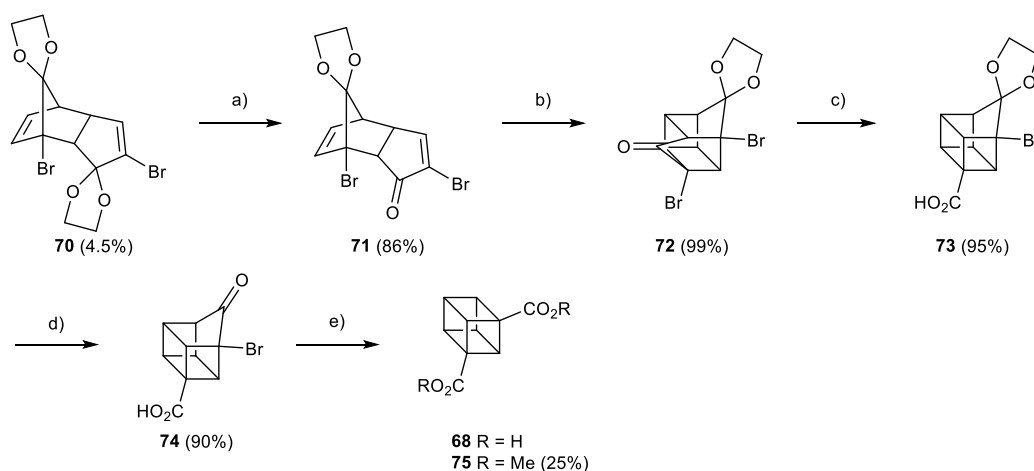
Scheme 6.5: Alternative 1,3-cubane synthesis. Reagents and conditions: a) HCl, THF, reflux, 86%; b) 4.6 M, DCM, 500 W Hg lamp, 4 h, 99%; c) 10% KOH, reflux, 2.5 h, 95%; d) 75% H_2SO_4, 24 h, 90%; e) i) 25% KOH, reflux, 3.5 h, ii) CH_2N_2, MeOH, reflux, overnight, 25%.

6.1.1.3 Synthesis of 1,2-disubstituted cubanes

The use of 1,2-disubstituted cubanes could be interesting in medicinal chemistry as well. However, accessing the 1,2-cubane framework is even more challenging than for 1,3-disubstituted cubanes **75**. The only approach available is very long and not efficient, using *ortho*-lithiation (Scheme 6.6) (Eaton *et al.*, 1985), starting from cubane

diisopropylcarboxamide **76** (which itself already requires a significant number of synthetic steps). Thus, the 1,2-cubane derivatives are attractive molecules for investigation, but require a lot of optimisation to be synthesised before being used in drugs and PROTACs, for instance.
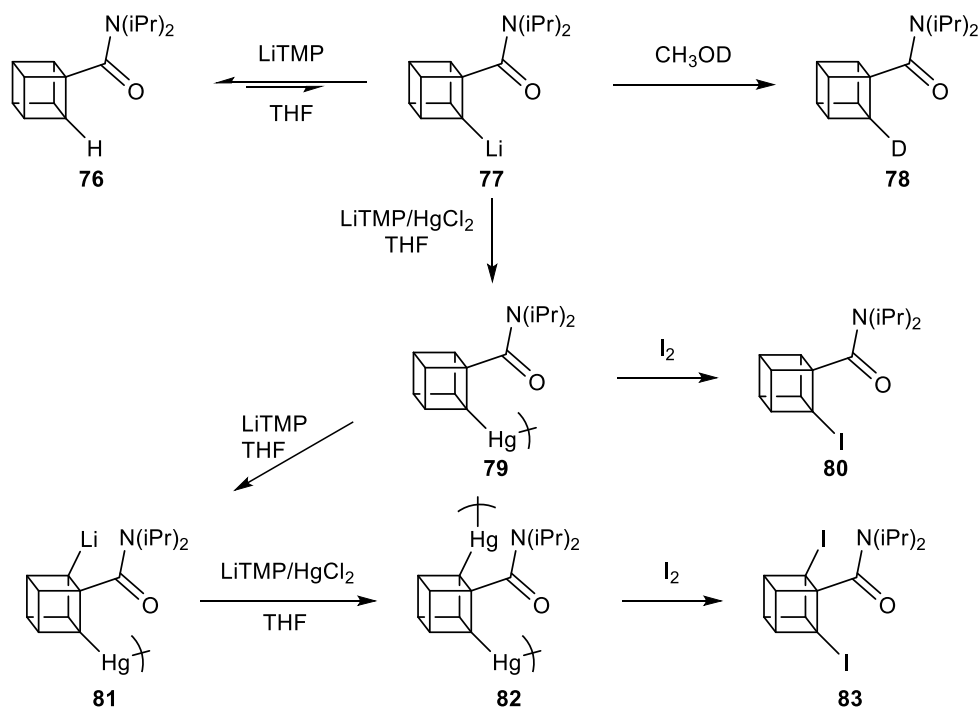
Scheme 6.6: Scheme of *ortho*-lithiation to access the 1,2-disubstituted cubane.

6.1.2 Interest and use in bioactive molecules

The 1,4-cubane **61** is the most easily accessible of the disubstituted cubanes and can be functionalised in different ways (Scheme 6.7) (Reekie *et al.*, 2019). **61** can be selectively hydrolysed to give the monoester **84**, which can then be decarboxylated (Barton) into the monosubstituted cubane, **85**. **85** can then be functionalised in many ways. A few examples are shown in Scheme 6.7, such as the hydrolysis of **85** to give **87**, which can then be transformed into the alcohol **89**, the bromo analogue **90** or the amine **88**. The ester **85** can also be converted to the Weinreb amide **86** for further functionalisation. The list is not exhaustive and a variety of reactions are possible to offer a wide range of compounds to use/attach the cubane moiety to other molecules.
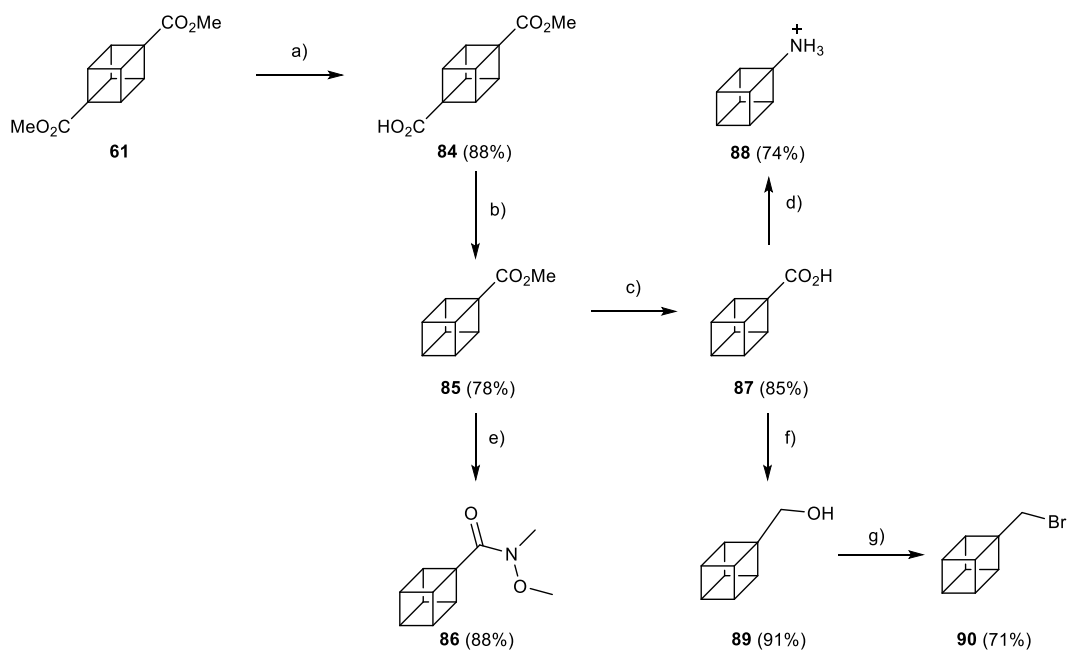
Scheme 6.7 Examples of possible substitutions and functional group interconversions on the cubane core. Reagents and conditions: a) NaOH, THF/MeOH, r.t., 18 h, 88%; b) (COCl)$_2$, DMF, CH$_2$Cl$_2$, 1 h and mercaptopyridine *N*-oxide sodium salt, 2,6-lutidine, hv (500 W tungsten), CHCl$_3$, reflux, 1 h, 78%; c) NaOH, MeOH, r.t., 2 h, 85%; d) i) DPPA, Et$_3$N, tBuOH, reflux, 5 h, 77%; ii) HCl (gas), MeOH, −60 °C to r.t., 20 h, 96%; e) MeNHOMe·HCl, iPrMgCl, THF, −40 °C to −30 °C, 2 h, 88%; f) BH$_3$·SMe$_2$, THF, 0 °C to r.t., 4 h, 95% and LiBH$_4$, THF, 0 °C to r.t., 12 h, 96%; g) PPh$_3$, CBr$_4$, CH$_2$Cl$_2$, r.t., 5 h, 71% (Reekie *et al.*, 2019).

Monosubstituted cubanes have been introduced in SAR studies as an isostere of the benzene ring, or as a comparison with polycycles such as adamantane as the cubane is smaller, less lipophilic and more metabolically stable (Wilkinson *et al.*, 2017). These cubanes also appear in patents such as compound **91** (US20150133428A1) and **92** (WO2017079641A1), a casein kinase 1 inhibitor and a metalloprotease inhibitor, respectively (Figure 6.1).
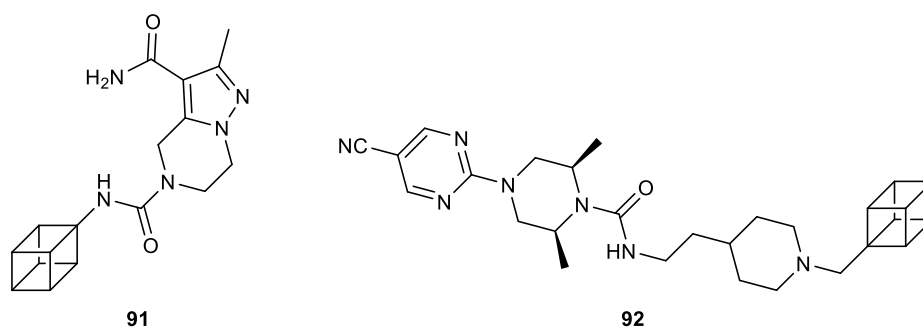
Figure 6.1: Molecules from the patent literature containing monosubstituted cubane.

The 1,4-disubstituted cubanes can also be functionalised and introduced in bioactive molecules (Reekie *et al.*, 2019). Cubanes can be kept symmetrical by hydrolysing ester **61** into the diacid **60** or changed into amines to be introduced into symmetrical molecules such as **96** (Targeting ATF4 luciferase, WO2017193034A1) (Figure 6.2) (Reekie *et al.*, 2019). The carboxylic acid of monoester cubane **84** can be changed to Cl, Br or I in **93** or to an amine **94/95** (Figure 6.2). The asymmetric cubanes are very interesting as they can then be introduced in asymmetric bioactive molecules such as **97** (Targeting Janus kinase 3, WO2011068881) (Figure 6.2).
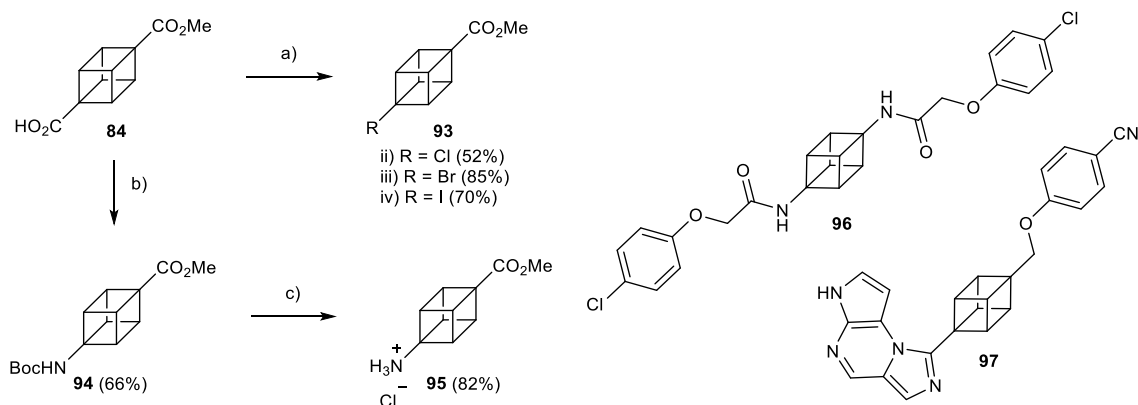
Figure 6.2: Examples of 1,4-disubsituted cubane substitutions and molecules containing disubstituted cubanes. Reagents and conditions: a) i) (COCl)$_2$, CH$_2$Cl$_2$, r.t., 1 h; ii) mercaptopyridine N-oxide sodium salt, DMAP, CCl$_4$, hv (500 W tungsten), heat, 2 h, 52%; iii) HgO, Br$_2$, CH$_2$Br$_2$, 80 °C, 2 h, 85%; iv) PhI(OAc)$_2$, I$_2$, toluene, 80 °C, 8 h, 70%; b) DPPA, Et$_3$N, ^{t}BuOH, reflux, 2 days, 66%; c) AcCl, MeOH, −15 °C to r.t., 1.25 h, 82%.

Overall, from what is available in the literature, cubanes have sometimes been used in SAR studies and show similar potency to similar other analogues. However, they could still present interesting properties in the future as they are very much underrepresented in medicinal chemistry. The synthesis of cubanes presents limitations, thus, generally only 1,4-disubstituted cubanes have been studied in this regard.

6.1.3 Potential use of cubanes in PROTACs

Following the study of Wee1 PROTACs recruiting both CRBN and VHL E3 ligases (Chapters 3,4 and 5), it was noted that the PROTACs with the shorter linkers were among the most potent for the target. This could come from the fact that a PROTAC with a small linker could be locked in a certain conformation that would favour ternary complex formation (determining step of degradation by PROTACs molecules) and thus lead to better degradation of the target. For this reason, using cubanes as a short, rigid and 3D linker could be a very interesting input in PROTAC technology as shown in Figure 6.3 with PROTACs **98a-d**. The biological properties of cubanes, as well as the different possible attachment points, are an appealing strategic avenue to explore.

Using the 1,3- or 1,2-disubstituted cubanes could allow even closer proximity when recruiting the E3 ligase protein and the target protein with PROTACs (Figure 6.3). The use of 1,4-disubsituted cubane could also be considered as it is already accessible in the gram scale. However, due to the challenge to synthesise the 1,2- and 1,3-cubanes, it will be more interesting for me to work on their methodology to apply to PROTAC design and useful for the cubane field. Different substituents could be used such as carboxylic acids or amines to facilitate the binding to other building blocks. As a matter of fact, most of the previous PROTAC building blocks discussed in Chapters 3, 4 and 5 were built this way, finishing with a carboxylic acid or amine to allow easier amide coupling. However, other substituents on the cubanes could be useful, to perform direct coupling to protein-recruiting ligands. Nevertheless, no work on incorporating the cubane framework into PROTACs has previously been reported, and this project sought to generate the first results in this area.
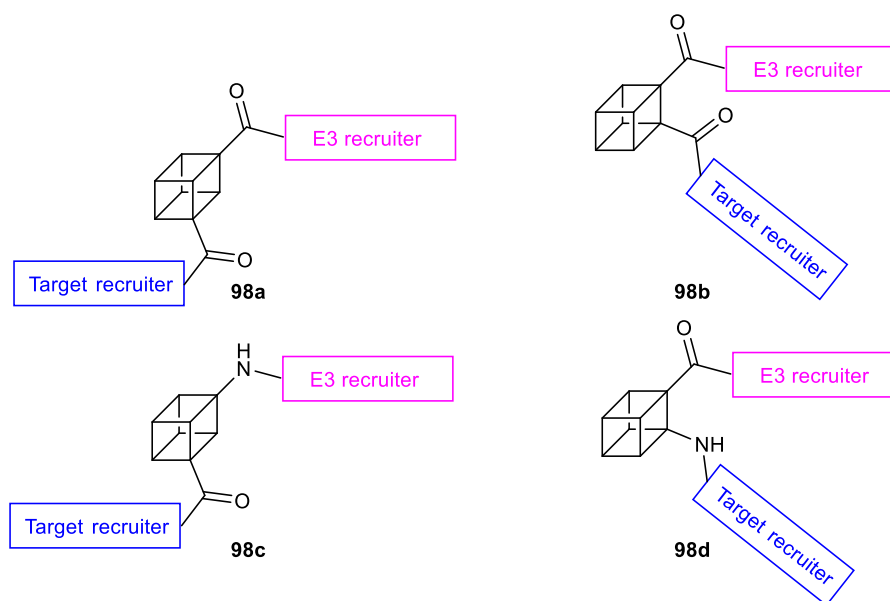
Figure 6.3: Examples of possible PROTACs made using 1,3- or 1,2-disubstituted cubanes **98a-d**.

6.2   Aims and objectives

The first aim is to optimise the synthesis of the 1,3-disubstituted cubane **75**, and to selectively transform one of the substituents to obtain two different functional groups (in order to allow selective attachment of one side of the cubane at a time) to generate asymmetric molecules (Figure 6.4).
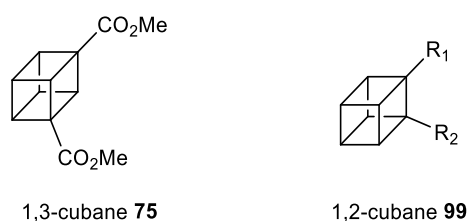
Figure 6.4: Structures of the 1,3-disubstituted ester cubane **75** and 1,2-disubstituted cubane **98**.

The second aim is to develop a new synthetic route to produce 1,2-disubstituted cubanes **98**. Since current approaches to 1,2-disubstituted cubanes require very long synthetic sequences starting from 1,4-disubstituted cubanes, a novel approach will be pursued, which – if successful – will allow rapid access to 1,2-disubstituted cubanes and facilitate the exploration of their potential applications in medicinal chemistry.

6.3   Results and discussion

6.3.1 1,3-Disubstituted cubane

6.3.1.1 First synthetic route

As discussed previously, Pettit and co-workers (Barborak *et al.*, 1966) proposed a synthetic route for the 1,3-diacid cubane **68** in 1966. This synthesis was inconvenient due to the instability of some compounds, as explained in the introduction, and was later improved upon (Chapman *et al.*, 1970; Nigo *et al.*, 1993). However, the first few steps remain impractical (use of cyclobutadiene, particularly for larger scale), and there is a need to optimise this synthesis to allow production on a larger scale, and ultimately to allow the study of a wider range of cubane derivatives in medicinal chemistry. Recently, a group in the US has been working on improving the synthesis by using bicyclic diazetidine **100**, access to which was published by the Coote group (Britten, Kemmitt, *et al.*, 2019) instead of the cyclobutadiene (personal communication). Their paper has not been published yet, but they provided outline reaction conditions in order to synthesise the cyclobutadiene from the bicycle (Scheme 6.8). From there, the rest of the proposed synthesis mirrors the original synthesis of 1,3-cubane dicarboxylic acid **68** that was published by Barborak *et al*. (Barborak *et al.*, 1966).
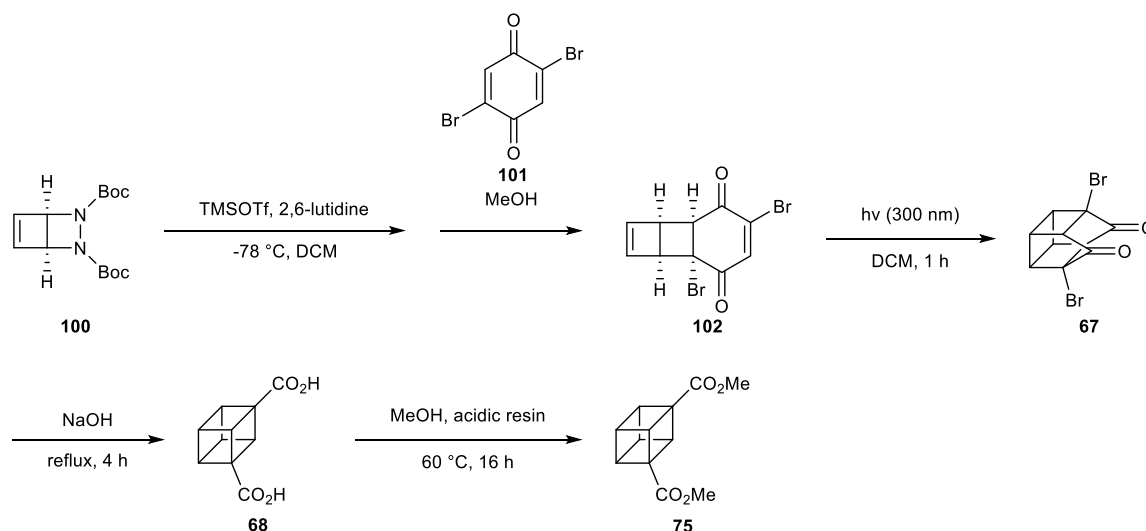
Scheme 6.8: Proposed synthetic route to access the 1,3-disubstituted cubane **75** by converting the bicyclic diazetidine **100** into cubane.

The bicyclic azetidine **100** was synthesised following the literature (Scheme 6.9) (Britten, Akien, *et al.*, 2019; Britten, Kemmitt, *et al.*, 2019). Crotonaldehyde was acetylated using acetic anhydride to obtain diene **104** after stirring for four days in 31% yield (Dolomanov *et al.*, 2009; Britten, Akien, *et al.*, 2019). **104** was then used in a Diels-Alder reaction with di-*tert*-butyl azodicarboxylate at 40 °C for 48 h to give cycloadduct **106** in quantitative yield. **106** was then involved in a palladium-catalysed elimination using palladium(II) acetate and triphenylphosphine to give 1,2-dihydropyridazine **107** in 65% yield. Finally, bicyclic 1,2-diazetidine **100** was obtained from a 4-π-photocyclization of 1,2-dihydropyridazine **107** in acetonitrile after irradiation at 350 nm for 48 h in 77% yield on a 5 g scale showing its suitable use in generation of libraries (Britten, Kemmitt, *et al.*, 2019).
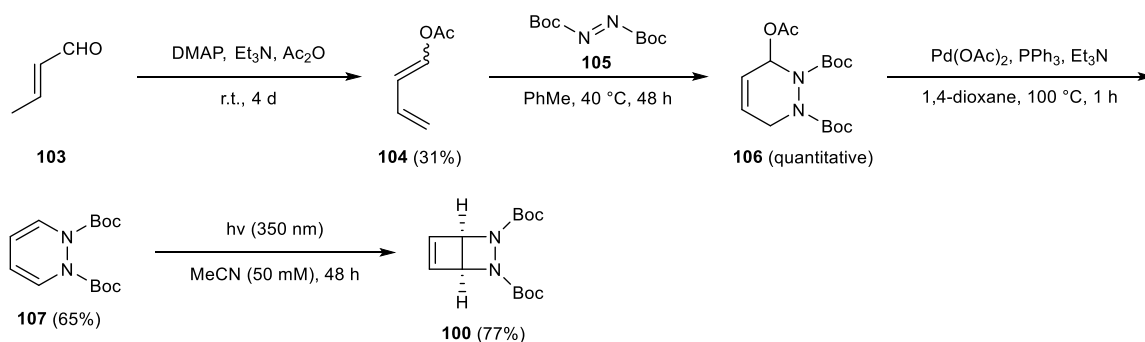
Scheme 6.9: Synthesis of the bicyclic 1,2-diazetidine **100**.

2,5-dibromobenzoquinone **101** was also prepared following the literature (Scheme 6.10) (López-Alvarado *et al.*, 2002). 2,5-dibromo-1,4-dimethoxybenzene **109** was synthesised from 1,4-dimethoxybenzene **108** in 76% yield, which was dibrominated and then oxidised using cerium ammonium nitrate to give 2,5-dibromobenzoquinone **101** after 1 h of reflux in 82% yield.
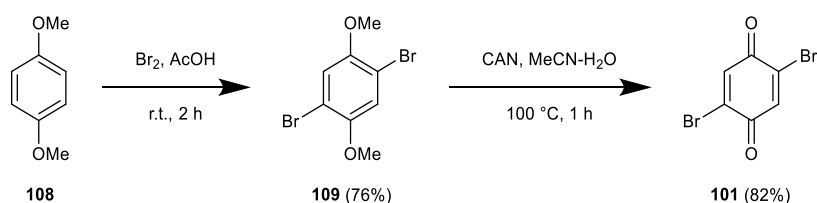
Scheme 6.10: Synthesis of 2,5-dibromobenzoquinone **101**.

The bicycle **100** (acting as a cyclobutadiene precursor) and dibromobenzoquinone **101** (acting as a dienophile) were then reacted together. By using TMSOTf, the Boc groups of bicycle **100** were first replaced by silyl carbamate to give **110** to then be deprotected to carbamic acids **111** using methanol. The carbamic acids **111** are not stable, and can undergo decarboxylation to obtain the bicyclic hydrazine **112**. **112** was then oxidised by the dibromoquione **101** to give azo compound **113**. The cyclobutadiene **114** was obtained from a *retro*-Diels-Alder of azo compound **113**, with the loss of nitrogen. The second equivalent of the dibromoquinone **101** then reacted with the cyclobutadiene **114** through a Diels-Alder reaction to give cycloadduct **102** (Scheme 6.11).
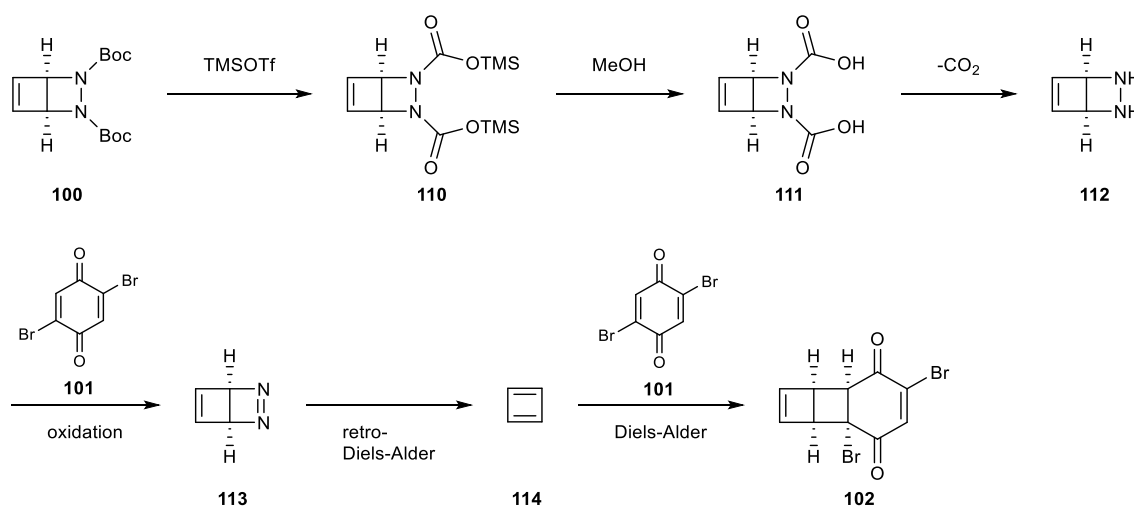
Scheme 6.11: Details of the first step.

Dichloromethane, 2,6-lutidine and trimethylsilyl trifluoromethanesulfonate (TMSOTf) needed to be freshly distilled before starting the reaction to avoid the presence of water or TMSOH (trimethylsilanol), both of which could lower the yield of the cyclobutadiene. Two solutions were prepared separately; the first was the rapid reaction of the bicycle **100** with 2,6-lutidine and TMSOTf to form the bicyclic hydrazine **112** as described previously. This solution was then added to a tube containing the second solution of dibromobenzoquinone **101** in dichloromethane and methanol. The reaction was analysed directly by ^{1}H NMR spectroscopy (with solvent suppression). New peaks appeared that did not correspond to the starting material **100**, and that integrated for the correct number of protons (denoted by arrows in Figure 6.5). The reaction seemed to have worked, however, the product **102** was not isolated. Purification by flash column chromatography was attempted but the product was not recovered, presumably due to its instability on silica. Thus, the yield was not determined.
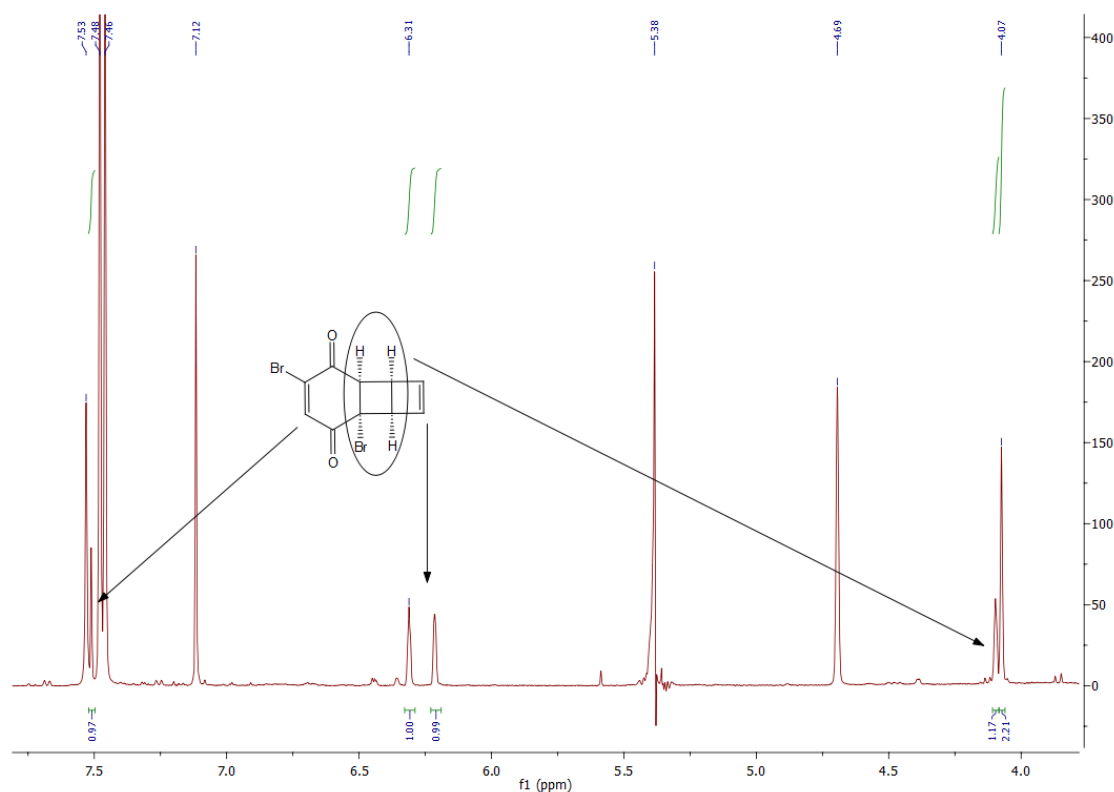
Figure 6.5: Zoom on the new peaks appearing for the cycloadduct **102**. (1H at 7.51 ppm for the akene of the dibromobenzoquinone, two peaks at 6.31 and 6.21 ppm integrate for 1H each for the protons of the diene of the bicycle, two peaks at 4.09 and 4.07 ppm integrate for one and two protons respectively for the three aliphatic protons of the molecule). The NMR was done directly in the reaction solvent (non-deuterated dichloromethane, peak at 5.38 ppm) using solvent suppression. The other peaks on the NMR spectrum come from the other reagents and biproducts that were not removed in the previous steps.

Assuming that the cycloadduct **102** (chemical shifts seem similar to the ones in the literature (Barborak *et al.*, 1966)), **102** should then be able to undergo an intramolecular [2+2] photocycloaddition. Due to its instability, **102** was taken directly to the next step in the same tube and placed into the photoreactor to avoid degradation. The photoreaction was irradiated directly at 300 nm for 1 h. The reaction was followed by ¹H NMR (with solvent suppression) and the starting material peaks disappeared after around 1 h (denoted by arrows in Figure 6.6). The new peaks appearing (denoted by arrows in Figure 6.7) around 3.5-3.9 and at 2.5 ppm could correspond to **67**, as the shifts correspond to the expected shifts in the literature from Falkiner *et al.* paper (Falkiner *et al.*, 2013).
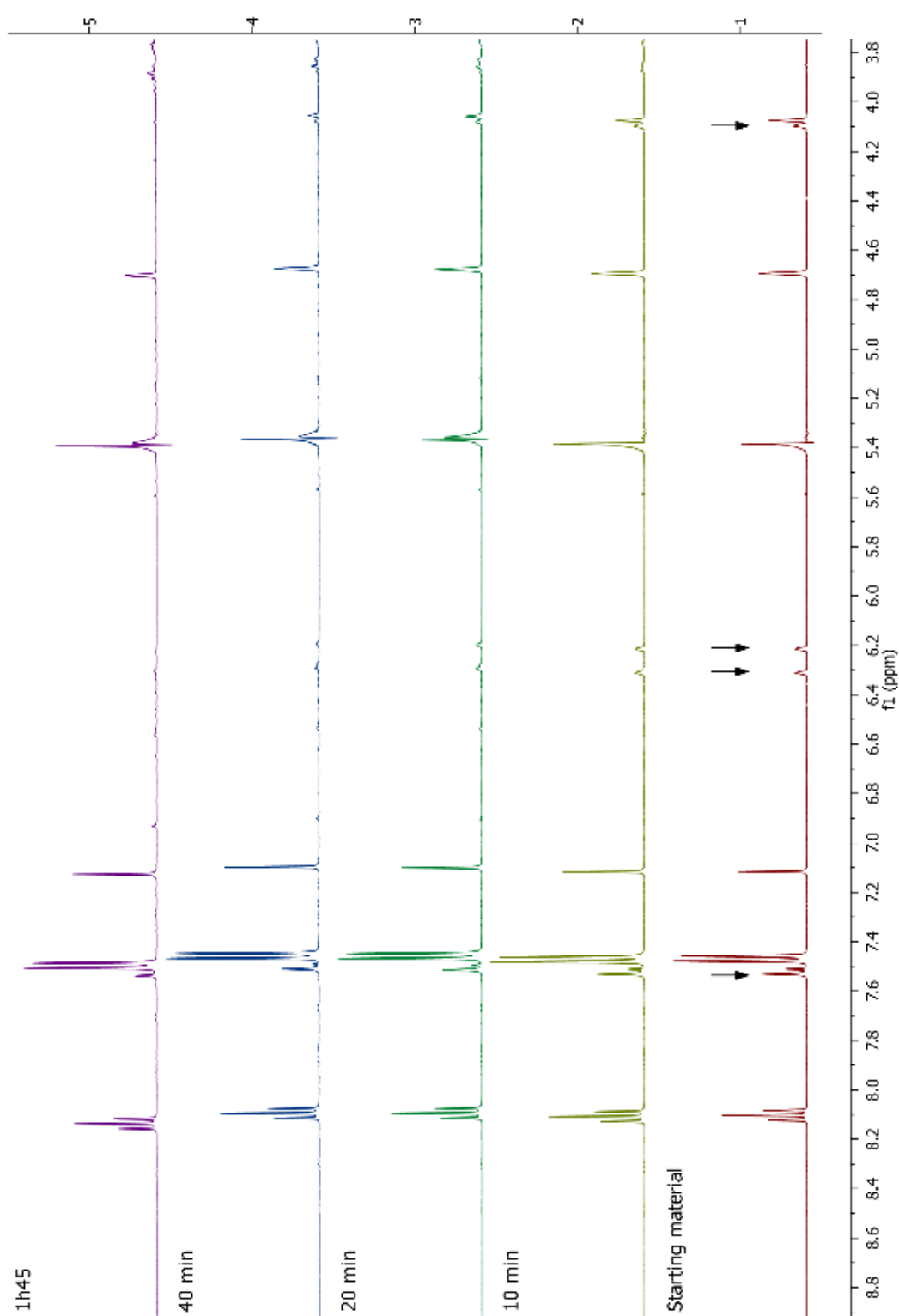
Figure 6.6: Zoom on the peaks of the starting material **102** disappearing. NMR spectra where the disappearing peaks are denoted by arrows for the photocycloaddition reaction over time (Starting material = 0 min, 10, 20, 40 min and 1h45).
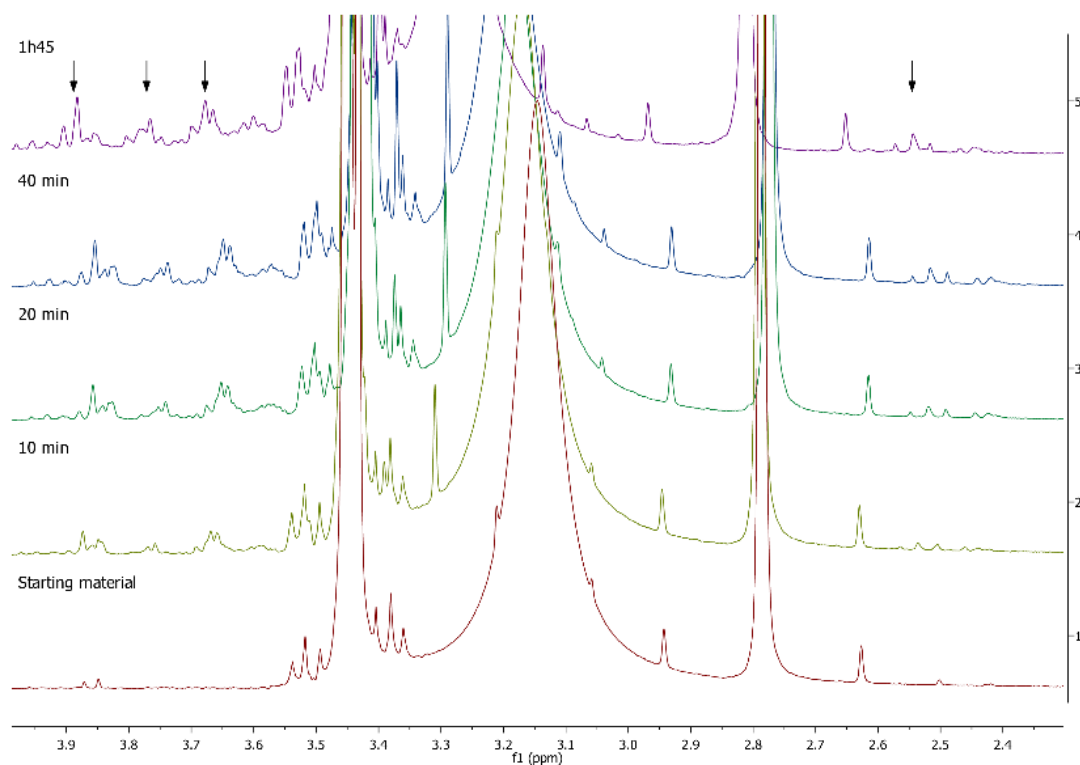
Figure 6.7: Zoom on the peaks appearing possibly for **67** on the NMR spectra for the photocycloaddition reaction over time. Peaks are denoted by arrows.

However, **67** was again not stable, so the compound was taken directly into the double Favorskii-type rearrangement using refluxing sodium hydroxide to make the 1,3-cubane diacid **68**. After acidic workup and extraction, characteristic peaks of the cubane were observed by ^{1}H NMR at 4.43, 4.22 and 4.01 ppm (Figure 6.8) (Falkiner *et al*., 2013). However, it was not possible to purify the diacid **68** due to its polarity with its two carboxylic acids. In addition, the presence of many impurities and the small amount of product made it impossible to fully characterise it.
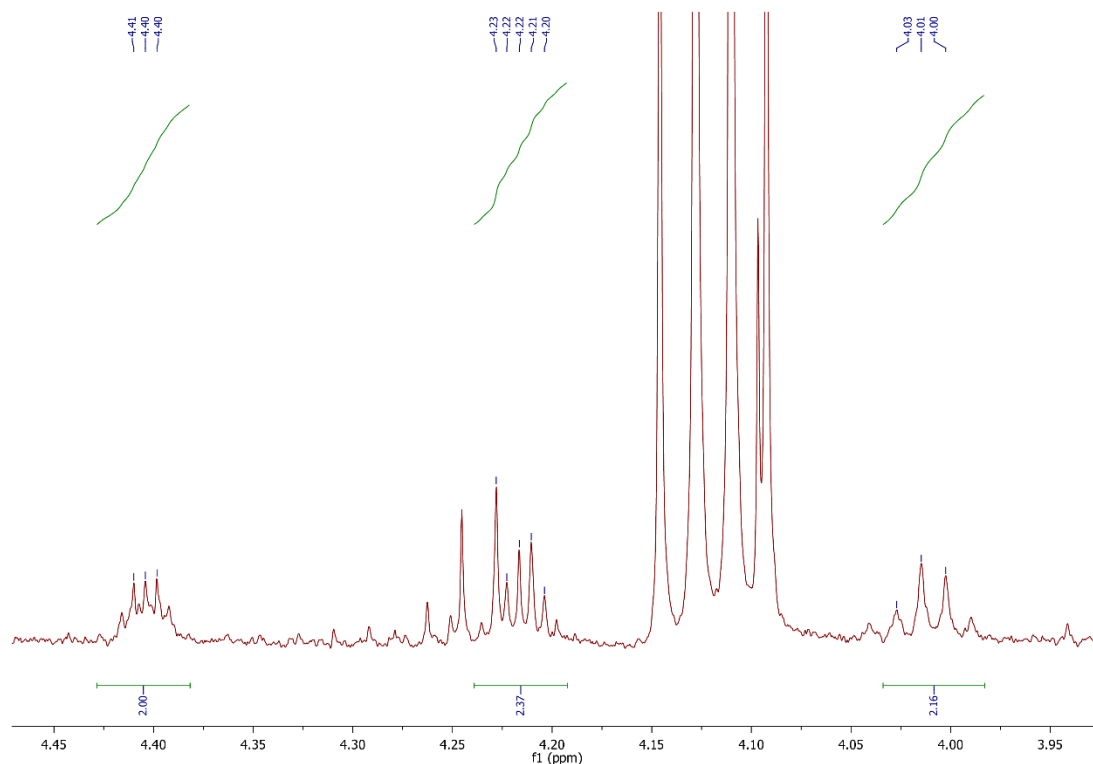
Figure 6.8: Zoom of the NMR spectrum showing the possible peaks for the 1,3-cubane diacid **68**.

Finally, to allow purification and isolation for full characterisation, the diacid **68** was esterified to give **75**. **68** was stirred overnight in methanol and acidic resin. After filtration and concentration, the characteristic peaks of the 1,3-diester cubane **75** were present by ^{1}H NMR (Figure 6.9). However, there were a large amount of impurities accumulating through the synthesis, with the instability of the previous intermediates not allowing purification at an earlier stage. Purification of the 1,3-diester cubane **75** was attempted, but with the yield being low through the multiple steps without purifications, it was impossible to recover material that was pure enough for full characterisation.
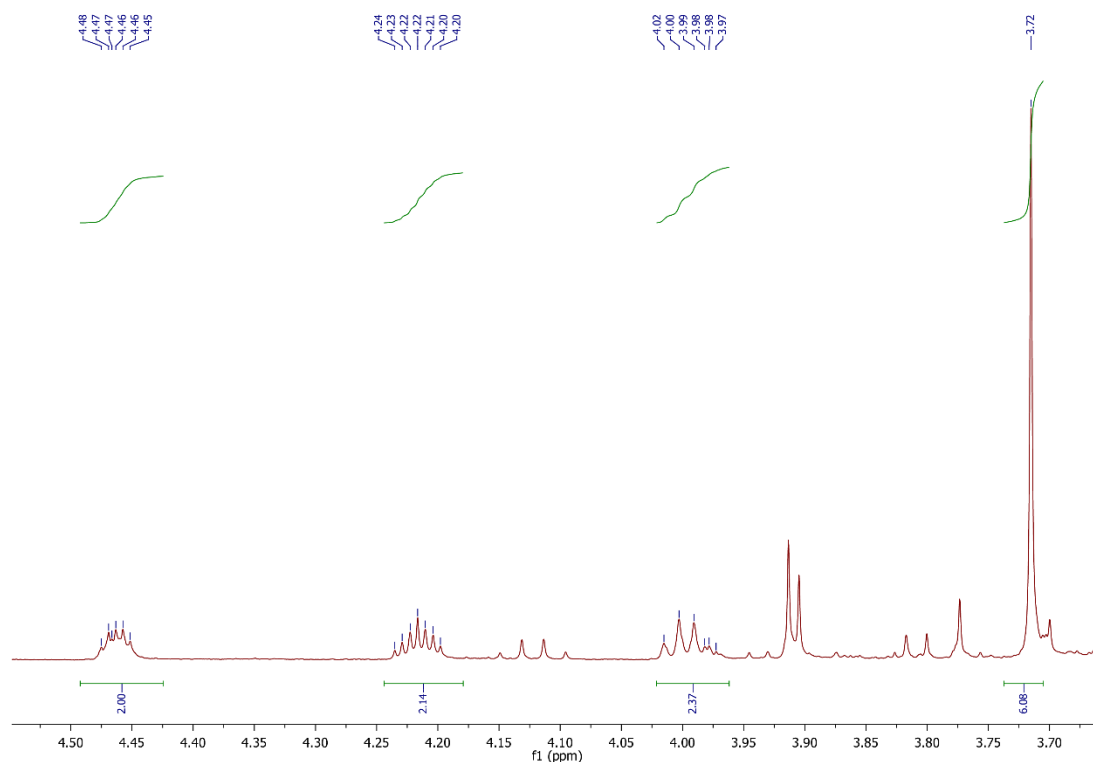
Figure 6.9: Zoom of the NMR spectrum showing the possible peaks for the 1,3-cubane diester **75**.

In conclusion, the cubane peaks were possibly observed by NMR, but the synthesis was deemed not useful due to low yields and impurities carried through the process. Whilst modifications to the process may allow convenient synthesis of **114**, it was decided that a different synthetic route should be pursued to provide more rapid access to cubane **75**. In particular, the US group working on this chemistry have not yet published their work (expected publication in summer 2021), suggesting that they also probably encountered some issues during the synthesis to either isolate intermediates or to obtain them in good yields.

6.3.1.2 Second synthetic route

6.3.1.2.1   Synthesis of the 1,3-diester cubane 75

After the first (unsuccessful) attempt to prepare the 1,3-disubstituted cubane **75**, another synthetic route was pursued based on a paper from Nigo *et al*. (Nigo *et al.*, 1993) (Scheme 6.12). In particular, a new transposition sequence to convert enone **115** (precursor to 1,4-

cubanes) into the isomeric enone **118** was envisaged, to allow the preparation of 1,3-disubstituted cubanes **75** on larger scale.
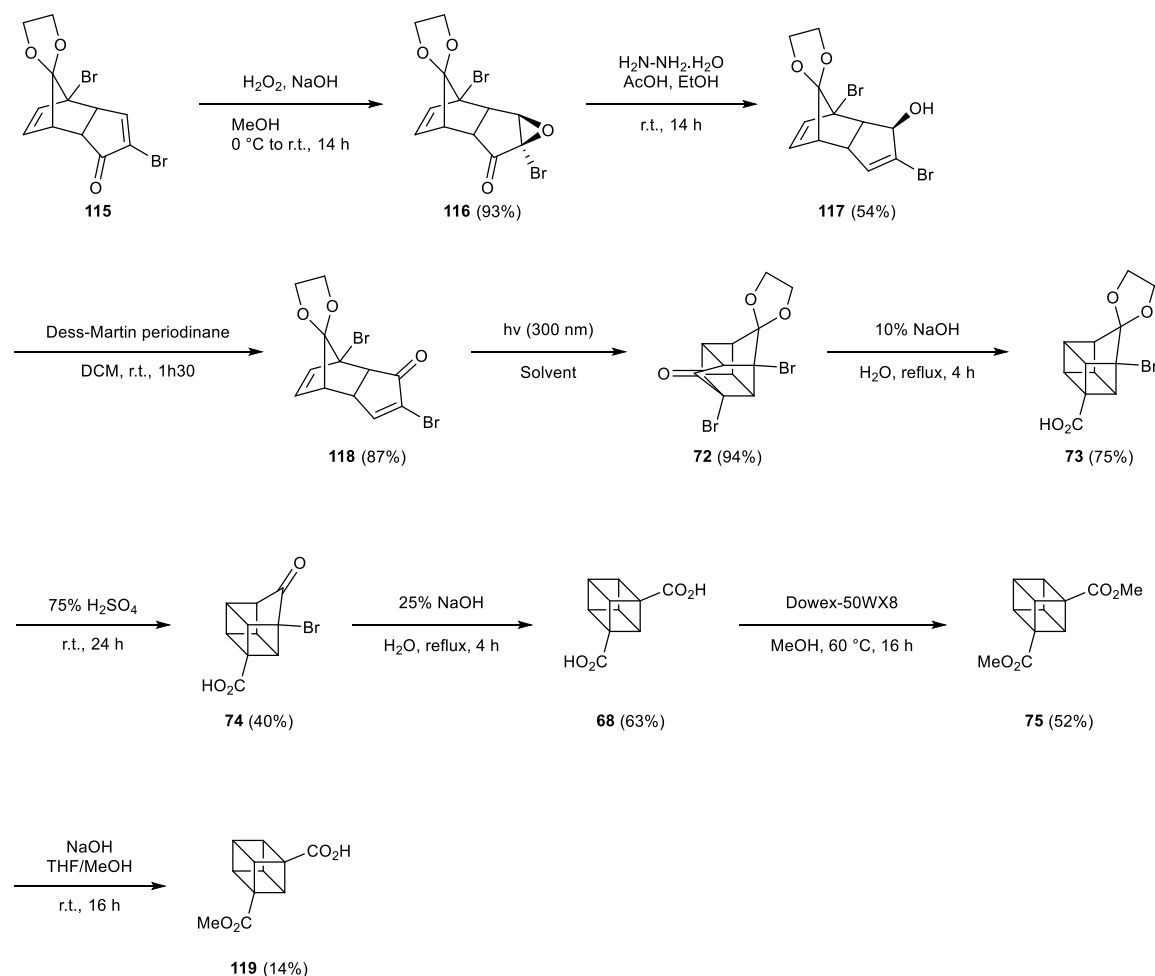
Scheme 6.12: Second synthetic route to access the 1,3-disubstituted cubane **119**.

Enone **118** was synthesised in three steps from the isomeric enone **115**, which is available on multi-gram scale as previously described. First, the enone of **115** was reacted with hydrogen peroxide and sodium hydroxide to give stereoselectively epoxide **116** in 93% yield (Suzuki *et al.*, 1988). Epoxy ketone **116** was then used in a Wharton reaction to obtain allylic alcohol **117** in 54% yield (Wharton *et al.*, 1961). Alcohol **117** was then oxidised with Dess-Martin periodinane to give enone **118** in 87% yield (Dess *et al.*, 1983). Overall, this three-step sequence allows the 1,3-transposition of the enone, to give a precursor for the synthesis of 1,3-disubstituted cubanes. The yield over the 3-step synthesis was good compared to the 4.5% yield to produce **70** in the literature (Eaton *et*

al., 1964). Enone **118** is then ready for the [2+2] photocycloaddition. Which was originally performed by Nigo *et al.* in dichloromethane (Nigo *et al.*, 1993). The reaction was attempted in different solvents and took 24 h to obtain full conversion in dichloromethane (Entry 1-Table 6.1), compared to 7 h in acetone (Entry 2-Table 6.1), a greener solvent, at the same concentration. Another attempt to run the photocycloaddition in acetone by decreasing the concentration from 50 to 25 mM led to full conversion in 4 h (Entry 3-Table 6.1). Thus, the reaction was faster in acetone (likely due to triplet sensitisation) and also faster when decreasing the concentration. However, 50 mM was selected because it was already relatively quick, and leads to less solvent waste to give isolated **72** in 94% yield.

Table 6.1: Conditions for the [2+2] photocycloaddition to give **72**.

	Concentration (mM)	Solvent	Conversion (%)	Time (h)
1	50	CH$_2$Cl$_2$	100	24
2	50	Acetone	100	7
3	25	Acetone	100	4

The photocycloaddition was followed by a Favorskii-type rearrangement to close one side of the cubane using refluxing NaOH to give **73** in 75% yield (Scheme 6.12). The acetal **73** was then deprotected with sulfuric acid for 24 h in a disappointing 40% yield. The low yield could be explained by the long workup, and in addition, some starting material was recovered, meaning the reaction was not going to completion. The Wharton reaction and the acetal **73** deprotection will be optimised by another PhD student in the lab, Nahin Kazi. **74** was then used in a second Favorskii-type reaction to give the 1,3-cubanediacid **68** in 63% yield. After heating the diacid **68** in methanol in the presence of acidic resin, the 1,3-cubanediester **75** was obtained and isolated by purification on silica in 52% yield,

sufficient to carry out a full characterisation. The moderate yield was probably due to the small scale of the reaction, leading to more loss during the filtration and the purification.

6.3.1.2.2   Functionalisation of cubane substituents

With the 1,3-cubanediester **75** in hand, work was next focused on functional group interconversions of the substituents, to allow attachment to other molecules. Various different approaches were investigated for the synthesis of a 1,3-disubstituted cubane bearing two different functional groups, and this work is summarised in the following sections.

6.3.1.2.2.1   Selective ester deprotection of 1,3-cubanediester 75

The first idea was to selectively deprotect one ester of **75** using sodium hydroxide in methanol, which would produce acid-ester **119** (Scheme 6.13) (Reekie *et al.*, 2019). In practice, although only one equivalent of NaOH was employed, the monoester **119**, the diester **75** and the diacid **68** were all recovered from this reaction in similar amounts. A small amount (14%) of the monoester was isolated using column chromatography to collect NMR data. A good ^{1}H NMR spectrum was obtained, but too little material was obtained to get good ^{13}C NMR data. The reaction was attempted at a more diluted concentration, at 0 °C, or with dropwise addition of NaOH, but the three products were always recovered in about the same ratio. It is assumed that the monoester might be more reactive than the diester, although it is interesting to note that a selective mono-deprotection of the corresponding 1,4-cubanediester **61** is possible in very high yield (Reekie *et al.*, 2019). Thus, although it is possible to make **119** this way on a 50 mg scale, the procedure is not very efficient, and will not be suitable for scale-up.
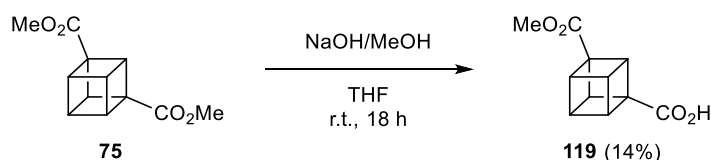
Scheme 6.13: Attempted selective deprotection of one ester of **75**, using reaction conditions developed for the corresponding 1,4-cubanediester **61**.

6.3.1.2.2.2 Conversion of the carboxylic acid group of 73 or 74 into an amine

The next attempts focused on changing the carboxylic acid group of **73** or **74** to a Boc protected amine, to then do a Favorskii-type rearrangement to obtain a carboxylic acid and a protected amine **123** as the two different substituents. The Curtius rearrangement using diphenylphosphoryl azide and triethylamine in dry *tert*-butanol heated to reflux (Nicolaou *et al.*, 2016) was successful on **73** and **74**, affording the corresponding Boc-protected amines (Scheme 6.14). During the first attempt with **73**, two products were isolated by column chromatography: the desired product **120** and the urea **121**. X-ray crystallography was used to determine the structure of this side product, as 1D and 2D NMR were not sufficient and MS analysis was not available. The urea was probably forming during the rearrangement in the presence of a small amount of water in the reaction. Drier conditions (fresh solvent) for the Curtius rearrangement were then used to successfully prevent the urea formation and obtain the product in good yield (50%).
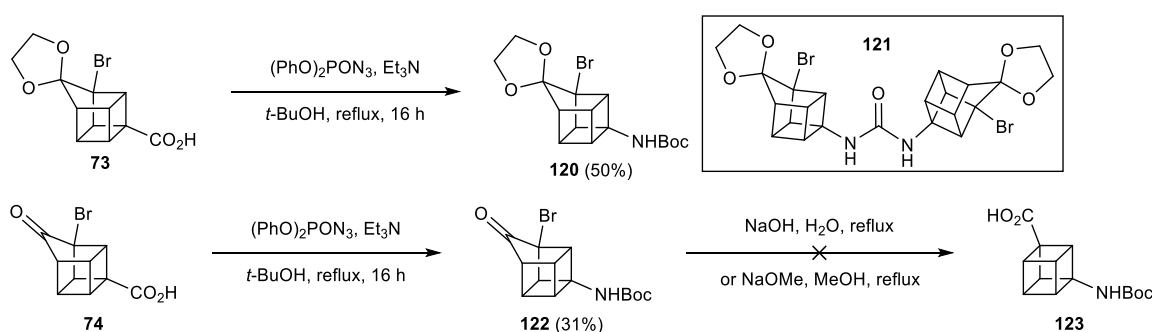
Scheme 6.14: Curtius reaction on **73** and **74**.

The same Curtius rearrangement conditions were then used for **74** to avoid taking **120** through very acidic conditions used to deprotect the acetal (75% sulfuric acid) which would probably deprotect the carbamate, making the product hard to isolate and purify. **122** was made successfully in low yield (31%) (Nicolaou *et al.*, 2016). Full characterisation using 1D and 2D NMR as well as X-ray crystallography were used to confirm the structure. The Curtius reaction on **74** could likely be further optimised and performed on larger scale

to obtain a higher yield, but enough material was recovered in the first test to attempt the next step and see if it was a viable synthetic route.

Afterwards, the Favorskii-type rearrangement was attempted on the Boc protected **122** (Scheme 6.14). However, using the same conditions as those to make the diacid (reflux in 25% NaOH in H_2O) led to a messy ^{1}H NMR with degradation products. It was impossible to determine if the cubane was present or to isolate the cubane. Less harsh conditions were also tried to avoid degradation: 10% NaOH instead of 25%, and lower temperatures. The temperature was increased slowly: 70 to 80 to 90 to 100°C and the reaction was followed by ^{1}H NMR (with solvent suppression). Only starting material **122** was observed from 70 to 90 °C (after 2 h at each temperature) and degradation products started to appear at 100 °C after 1 h and no more starting material was visible after 2 h. Again, the ^{1}H NMR was too messy to determine if the cubane was present. The pair NaOMe/MeOH was also tried for a Favorskii-type rearrangement but was also unsuccessful, as only starting material **122** was recovered.

Therefore, Boc-protected amine versions of **73** and **74** were synthesised successfully, but the Favorskii-type rearrangement to obtain **123** was not successful. Potentially, the high-temperature required for the Favorskii-type reaction could have removed the Boc protecting group, leading to an amine and a carboxylic acid on the same molecule, which might be very hard to isolate if the product is water-soluble. Very concentrated sodium hydroxide might also be too strong for this compound, however it requires a lot of energy to close the cubane, as the cubane is not a favourable structure to make.

6.3.1.2.2.3 Favorskii-type rearrangement to form an ester

As another way to obtain a disubstituted cubane with two different substituents, a second Favorskii-type rearrangement on **74** was attempted to lead directly to the monoester **119** or **124** (Scheme 6.15). Conditions such as NaOMe in MeOH, NaOEt in EtOH, [i]PrONa in [i]PrOH, or benzyl alcohol, as described in Table 6.2 were investigated. However, only starting material was recovered from each attempt. Only the reactions with [t]BuOK used as the nucleophile, in THF or [t]BuOH, led to something of interest: entries 7-9 of Tale 6.2. Solvent-suppressed ^{1}H NMR spectra were recorded in methanol after concentrating an aliquot of the reaction to follow the reaction,

and very small peaks characteristic of the cubane were detected. After work up, these peaks could still be observed by ^{1}H NMR in MeOD (Figure 6.10) (4-27-4.22, 4.07-4.04, 3.85-3.81, three multiplets integrating for two protons each with the expected shape and shift). A singlet at 1.22 ppm is integrating for nine protons and could correspond to the ^{t}Bu group.
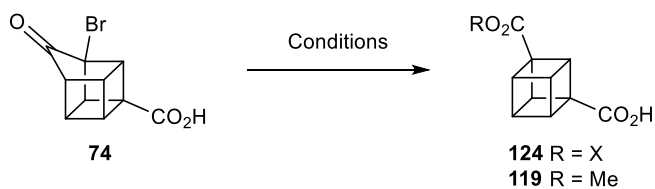
Scheme 6.15: Second Favorskii-type rearrangement. Attempt to synthesise an ester directly instead of the diacid **68**. X corresponds to any possible ester of Table 6.2.

Table 6.2: Conditions for Favorskii-type rearrangement on molecule **74**.

	Base	Eq. of base	Solvent	R	Temperature (°C)	Time (h)	Observations
1	NaOMe	3	MeOH	Me	r.t. to 40 to 60	24	SM **74**
2		3	Dioxane	Me	r.t. to 100	24	SM **74**
3		3	THF	Me	r.t. to 80	24	SM **74**
4	NaOEt	3	EtOH	Et	r.t. to 80	24	SM **74**
5	NaOiPr	5	iPrOH	iPr	r.t. to 80	24	SM **74**
6	tBuOK	3	THF	tBu	80	16	Cubane peaks?
7		3	THF	tBu	r.t.	16	Cubane peaks?
8		10	THF	tBu	r.t.	3-22	Cubane peaks?
9		3	tBuOH	tBu	80	16	Cubane peaks?
10	-	-	Benzyl alcohol	Benzyl	200	24	SM **74**
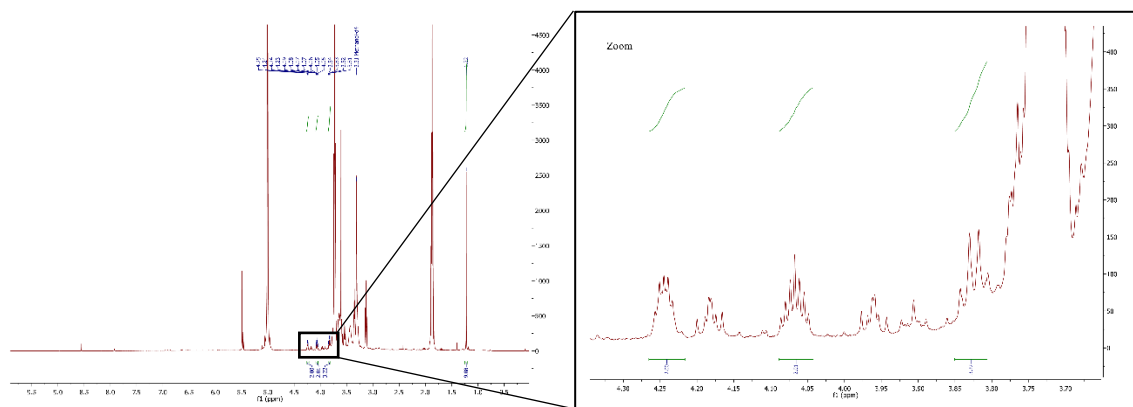
Figure 6.10: ^{1}H NMR spectrum of the possible cubane product's relevant peaks (zoom).

Unfortunately, after purification with a gradient of 0 to 10% MeOH in DCM, the product **124** (X = ^{t}Bu) was not isolated due to a very low yield. Thus, **124** structure could not be confirmed. Conditions for Favorskii-type rearrangements other than NaOH in water may be too mild to close the very high energy cubane, and thus not a viable way to proceed.

6.3.1.2.2.4 Selective protection of one carboxylic acid from the 1,3-cubanediacid 68

In another attempt to access 1,3-disubstituted cubanes **119** bearing two different substituents, the selective esterification of one of the carboxylic acids in **68** was attempted using two different reaction conditions with N,N'-Dicyclohexylcarbodiimide (DCC) or the Meerwein's salt (Scheme 6.16, Table 6.3).
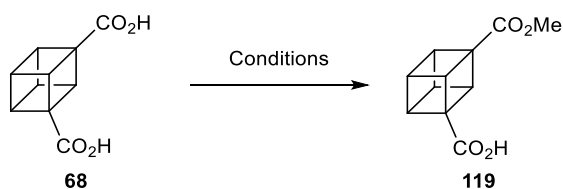
Scheme 6.16: Selective esterification of one carboxylic acid of 1,3-cubanediacid **68**.

6.3.1.2.2.4.1 The Meerwein's salt

In the first instance, the esterification was attempted with the Meerwein's salt Me_3OBF_4 (Raber *et al.*, 1979). The starting material **68** was resuspended in dichloromethane before adding the Meerwein's salt, followed by the N,N-Diisopropylethylamine (DIPEA) (Condition 1a-Table 6.3). However, the starting material was not soluble in dichloromethane and became soluble following DIPEA addition. Only the diester **75** was recovered from this first attempt, likely due to the insolubility of the starting material **68** in dichloromethane, the small scale and the fact that the starting material was the crude product from the previous reaction. Thus, more equivalents of Meerwein's salt than intended might have been added, leading to the double esterification. Another attempt on a larger scale and with a purer starting material led to the successful isolation of the mono ester **119** after workup and purification (Condition 1b-Table 6.3) in low yield (12%). Thus, although the Meerwein's salt reaction allowed the synthesis of the ester/acid cubane **119**, this requires optimisation to improve the yield. Working in using another solvent could help with solubility and controlling the formation of the monoester instead of the diester, as well as running the reaction on a larger scale to enable more accurate equivalents of reagents to be employed.

Table 6.3: Conditions for the selective esterification of the 1,3-cubanediacid **68**.

Entry	Reaction	Conditions	Observations
1a	Meerwein's salt	Me₃OBF₄, DIPEA, CH₂Cl₂, r.t., 18 h (20 mg scale)	Diester **75** and diacid **68** recovered. Starting material **68** not soluble in CH₂Cl₂; only soluble after addition of DIPEA. Crude starting material used.
1b		Me₃OBF₄, DIPEA, CH₂Cl₂, r.t., 18 h (200 mg scale)	Product **119** isolated in 12% yield.
2a	DCC coupling	MeOH, DCC, DMAP, MeCN, 0 °C to r.t., 18 h	Diester **75** recovered likely due to low solubility of the starting material **68** and the small scale.
2b		MeOH, DCC, DMAP, DMF, 0 °C to r.t., 18 h	Product **119** isolated in 25% yield. Improved solubility of the starting material.

6.3.1.2.2.4.2   DCC coupling

Another selective esterification of the diacid **68** was also attempted by DCC coupling. A first attempt using MeOH, DCC, DMAP in acetonitrile (Condition 2a-Table 6.3) (Neises *et al.*, 1978) only gave the diester **75**. This result could be explained by the small scale of the reaction and by the fact that the starting material was not soluble in acetonitrile. To avoid the solubility issue, the solvent was switched to DMF as a test reaction (Condition 2b-Table 6.3). The diacid was soluble in DMF, and the monoester **119** was isolated from the

reaction and purified successfully. A low yield of **119** (25%) was obtained due to the solvent not solubilising the starting material and the simultaneous formation of diester **75** (30%), but the amount of **119** recovered allowed full characterisation by NMR to confirm the product's structure. The DCC coupling is thus a reaction that could be further optimised and used to make the ester/acid cubane **119**. Performing the reaction on a larger scale, as well as finding a better solvent than DMF, could both be beneficial to the reaction in order to obtain a better yield.

Multiple conditions (selective ester deprotection with NaOH, or selective methylation using DCC or the Meerwein's salt) were investigated to synthesise the monoester cubane **119** and were successful. However, only low yields were obtained. Comparing to the 1,4-cubane, for the 1,3-cubane it is more difficult to selectively protect the 1,3-diacid cubane **68** or deprotect the 1,3-diester cubane **75**. More work is needed to optimise the conditions, especially using DCC or the Meerwein's salt. Changing the solvent to improve solubility of the diacid **68,** as well as working on a bigger scale should be useful, and will be investigated to pursue the synthesis of the ester/acid **119** for further use in drug molecules. Changing the coupling agent could also be an interesting approach as well as trying to use chloroformate at low temperature if **68** is soluble enough.

6.3.2   1,2-Disubstituted cubane

As previously explained in the introduction (Section 6.1.1.3), 1,2-cubanes **99** are even less accessible than 1,3-cubanes **75**. However, they would also be very interesting motifs to introduce in PROTACs to obtain short and constrained linkers to potentially impose a strict conformation in the molecule. Therefore, an ambitious new synthetic approach was designed and tested, and this work will be described in the following sections.

6.3.2.1 First synthetic route

Working towards a more consise and efficient way to synthesise the 1,2-disubstituted cubane **99**, the following synthetic route was designed (Scheme 6.17).
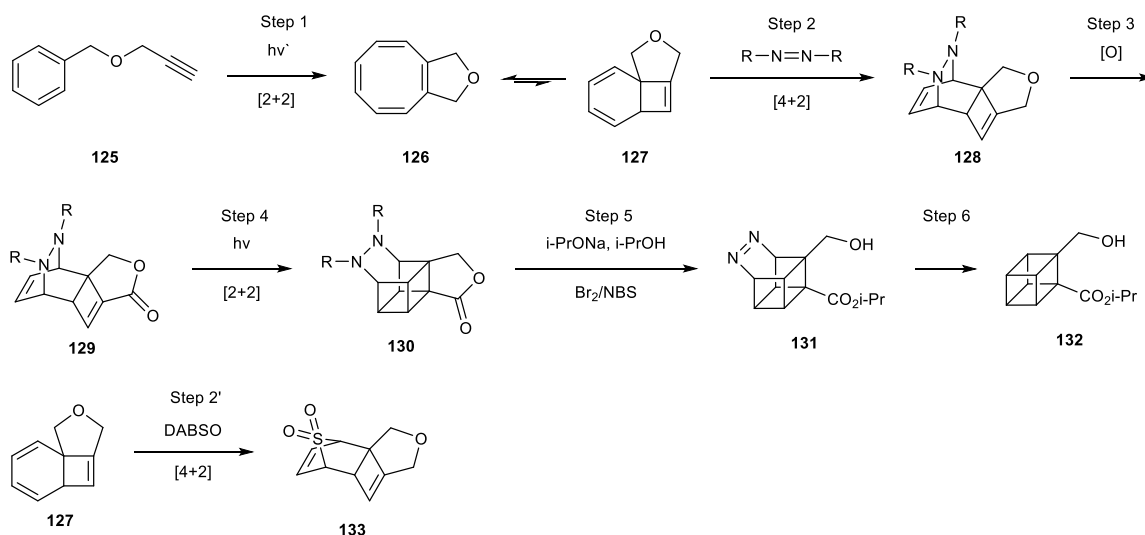
Scheme 6.17: Proposed synthetic route to access the 1,2-disubstituted cubane **132**.

This new route is advantageous, as it involves photochemical cycloadditions without requirement for extra reagents apart from light, and the starting material is cheap and accessible. Step 1 consists of an intramolecular photocycloaddition with the alkyne **125** to generate the tricycle **127** in equilibrium with its cyclooctatetraene version **126**. It is followed by a Diels-Alder reaction in step 2 with an azo compound as the dienophile and tricycle **127** as the diene. A few different azo compounds such as diethyl azodicaboxylate, diphenyl azodicarboxylate, dibenzyl azodicarboxylate, PTAD can be used. Only a few examples are present in the literature with other cyclooctatetraenes (Grange *et al.*, 2010). Potentially, SO_2 can also be used as the dienophile (Step 2') instead of the azo compound by reacting with crystalline DABSO as an SO_2 source, to avoid the use of toxic SO_2 gas to give **133**. Step 3 is an oxidation of **128** to generate a lactone **129**, which could then be cleaved to give two different substituents in **131** (Step 5), which could then be further functionalised to give a range of 1,2-disubstituted cubanes. Step 4 is an intramolecular [2+2] photocycloaddition, which closes the molecule into a shape close to the desired cubane motif. Step 5 with ^{i}PrOH/^{i}PrONa not only opens the lactone ring, but also replaces the R of **130** with ^{i}PrO, which could then be deprotected using NaOH. The resulting hydrazine could be oxidised using bromine or NBS to afford **131**, then the cubane can be closed in Step 6 by way of photochemical reactions or flash vacuum pyrolysis (FVP) (Hedaya *et al.*, 1971).

The starting material **125** for Step 1 was prepared in high yield (95%) following the literature from **124** and **135** (Scheme 6.18) (Chandankar *et al.*, 2020).
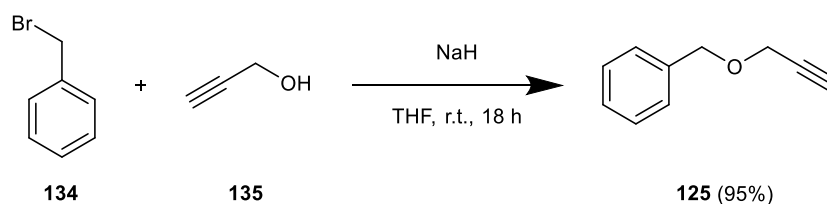
Scheme 6.18: Synthesis of starting material **125**.

Different conditions were investigated to synthesise cyclooctatetraene **126** (Scheme 6.19; Table 6.4). **125** was irradiated at 254 nm in hexane at different concentrations as indicated in Table 6.4 below. The reaction was followed by ^{1}H NMR (with solvent suppression) to determine the conversion of the starting material (conversion from starting material **125** to product **126** is calculated, but no internal standard was used and so any degradation is not taken into account).
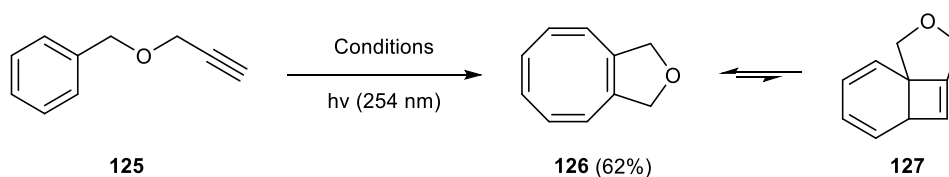
Scheme 6.19: Intramolecular *ortho*-PCA of **125**.

Table 6.4: Conditions for the intramolecular *ortho*-PCA of **125**.

	Concentration (mM)	Solvent	Conversion (%)	Time (h)
1	50	Hexane	<5	1-24
2	10	Hexane	80	7-24

At 50 mM, only small new peaks were observed after 1 h, which remained the same after 24 h irradiation (<5% conversion). The new peaks could correspond to the desired

product **126**, so another the reaction was attempted at a lower concentration, 10 mM, where 80% conversion was observed after 7 h of irradiation and then remained the same after 24 h irradiation (Table 6.4, Figure 6.11). A lower concentration was better for this intramolecular process and an even lower concentration might be required to reach completion. However, this would increase the volume of solvent used. So, in the first instance, the concentration was kept at 10 mM to see if the next steps were working before optimising the photocycloaddition. The product was not stable on silica, and was also not stable in air. NMR spectra were recorded at different times, and new peaks were observed, which showed degradation. Thus, the product had to be kept under argon and in the freezer, or to be used directly in the next step.
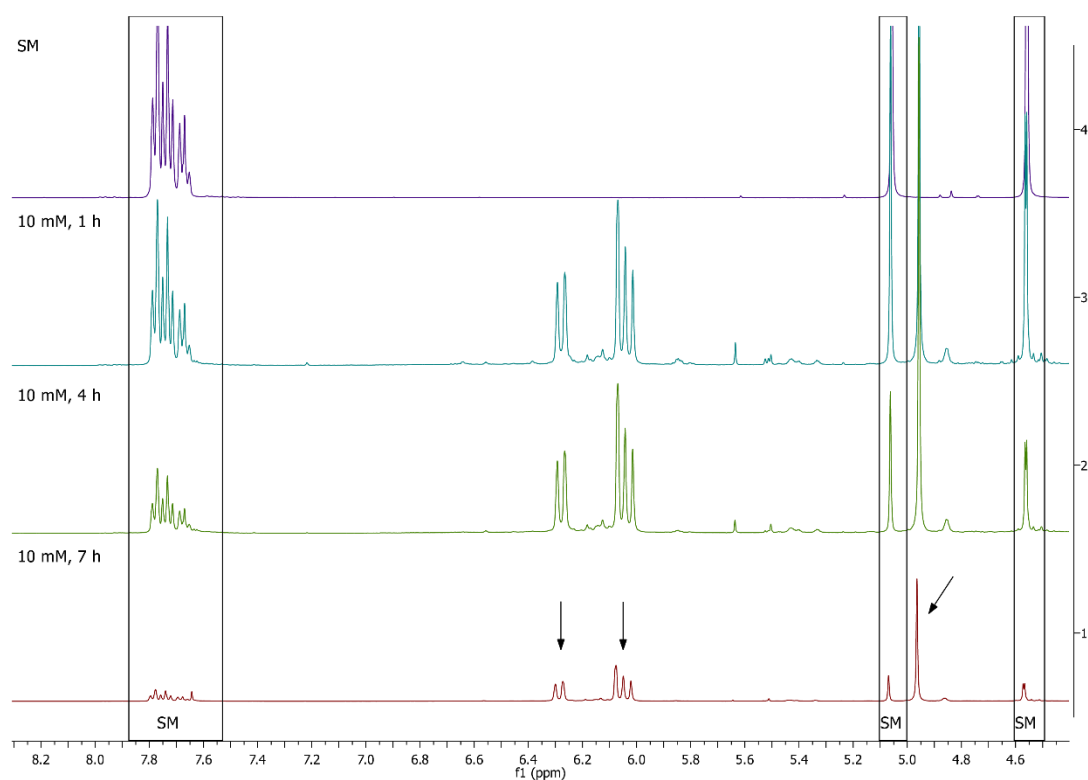
Figure 6.11: Spectra of the reaction progression depending on the time (indicated on the left). The starting material peaks are decreasing and new peaks for the products appear (denoted with the arrows).

Similar cyclooctatetraenes have been previously used in Diels-Alder reactions with azo compounds (Grange *et al.*, 2010), and similar reaction conditions were applied to

cyclooctatetraene **126** to attempt a Diels-Alder reaction for a [4+2] cycloaddition. **126** was reacted with azo compound **136** and with PTAD **139** in toluene or EtOAc respectively, at 80 °C under argon (Scheme 6.20). However, reaction monitoring by NMR spectroscopy only showed degradation products. Attempts to purify and isolate the potential product **137** were unsuccessful. In addition, a test reaction of [2+2] photocycloaddition in acetone irradiated at 300 nM was carried out using the crude product (potentially containing **137**), as the peaks of **138** should be easier to recognise, but product **138** was not observed. Thus, this synthetic approach was not a viable way to proceed for the synthesis of 1,2-disubsituted cubanes **99**.
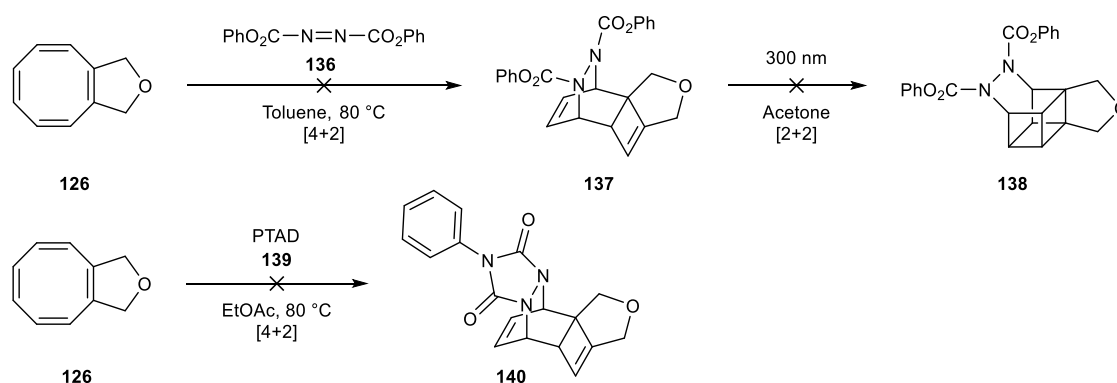
Scheme 6.20: Attempt of Diels-Alder reaction on **126**.

6.3.2.2 Second synthetic route

Due to the failure of the initial synthetic approach, an alternative approach to the desired 1,2-disubsituted cubane was pursued. It was postulated that cyclooctatetraenes bearing more electron-rich substituents are less stable than those bearing electron-withdrawing groups (Wagner *et al.*, 1987; Wagner, 2001), so a new cyclooctatetraene substrate (**146**) was designed, bearing a ketone adjacent to the cyclooctatetraene ring. It was proposed that **144** could be reached by initial intramolecular *ortho*-photocycloaddition of alkyne **143**, followed by immediate oxidation to **146**.

5-Phenylpent-1-yn-3-ol **143** was prepared through a Grignard reaction following the literature using **141** and **142** in very good yield (84%) (Scheme 6.21) (Ye *et al.*, 2010; Hilpert *et al.*, 2019).

Scheme 6.21: Synthesis of starting material **143**.

This new starting material was then used to attempt an intramolecular *ortho*-PCA reaction to form the cyclootatetraene **144** (Scheme 6.22; Table 6.5). The first attempt of the *ortho*-photocycloaddition reaction at 50 mM in hexane was unsuccessful. ^{1}H NMR spectroscopy was used to monitor the reaction after 1, 2, 7 and 24 h, but only very small new peaks appeared on the baseline (Figure 6.12; Figure 6.13). Lower concentrations were then attempted, starting with 10 mM, and 50% conversion was observed after 7 h of irradiation. As the conversion was rather low, lower concentrations were tested: 7.5 and 5 mM. Unfortunately, these attempts gave the same ratio of conversion as at 10 mM, and were therefore no better to work with.
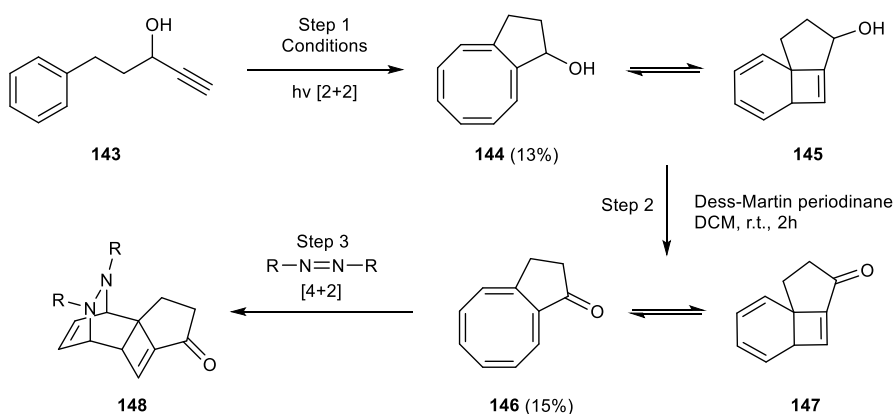
Scheme 6.22: Proposed second route to access the 1,2-disubstituted cubane.

Table 6.5: Conditions for the intramolecular *ortho*-photocycloaddition reaction of **143**.

	Concentration (mM)	Solvent	Time (h)	Observations
1	50	Hexane	24	Mostly SM
2	10	Hexane	24	Almost 50% conversion after 7 h and stayed the same after 24 h
3	7.5	Hexane	15	About 50% conversion
4	5	Hexane	15	About 50% conversion
5	5	CH$_2$Cl$_2$	24	Degradation products
6	5	Acetonitrile	24	Degradation products
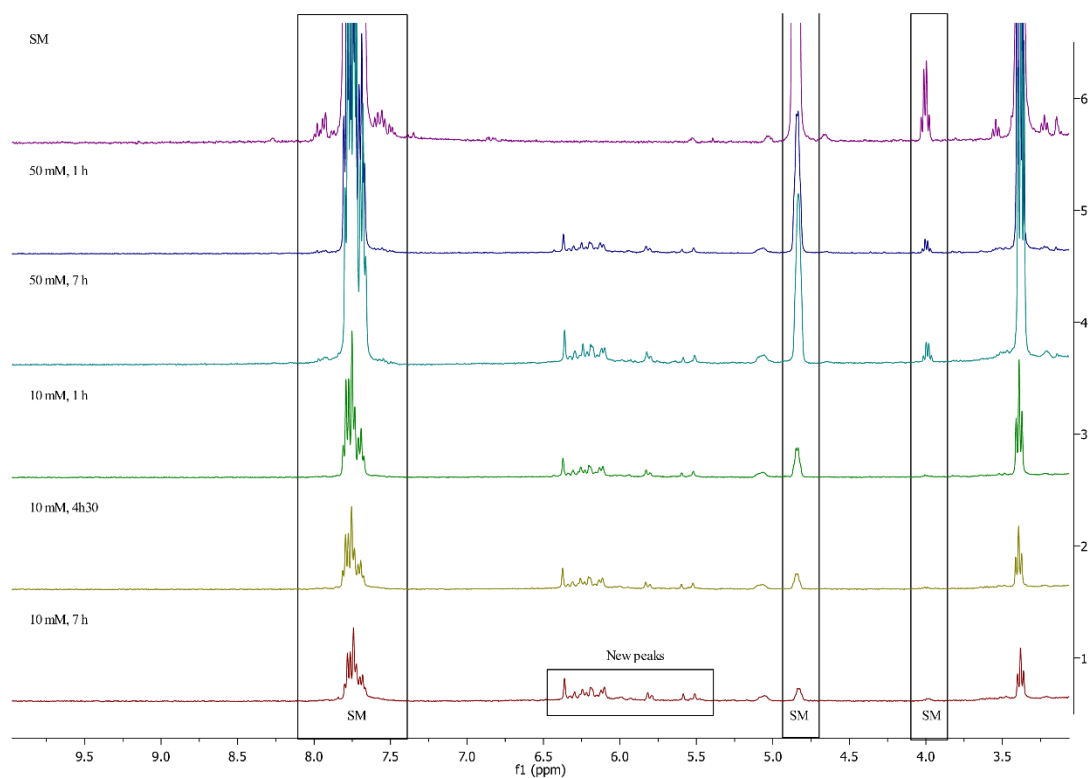
Figure 6.12: Spectra of the conversion of **143** to possible product **144** depending on the concentration and time (Indicated on the left).
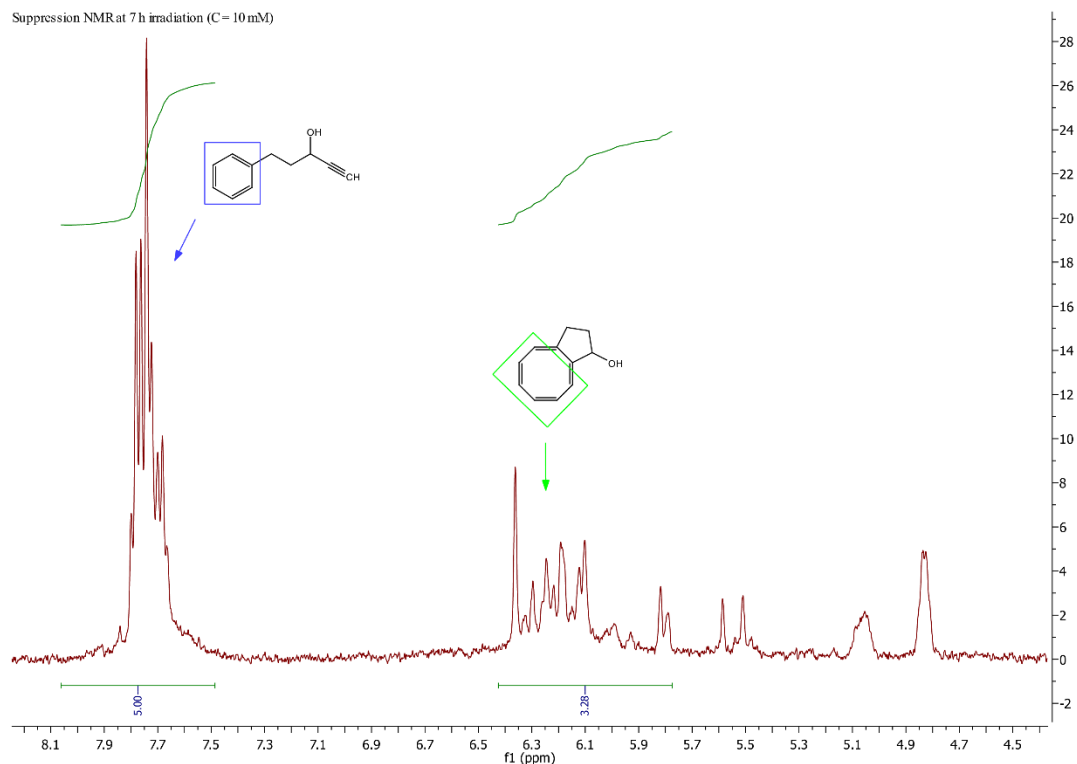
Figure 6.13: Zoom on the characteristic peaks of the starting material **143** and (putative) product **144** to calculate the approximate conversion with the new peaks appearing.

In addition to the low conversion into cyclooctatetraene **144**, the product **144** appeared to degrade quickly when removing the solvent of the photoreaction. **144** was hard to recover and impossible to purify by column chromatography on silica gel. Very little material was recovered after column purification due to the degradation, but it was enough for a ^{1}H NMR, in which the observed peaks were consistent with the desired product. In an attempt to make the product from the photoreaction more stable, the reaction was also tested in other solvents: dichloromethane and acetonitrile, intending to take **144** directly into the next step of oxidation without having to remove the photoreaction solvent. DCM and acetonitrile were chosen because the Dess-Martin oxidation can be run in both solvents. Nevertheless, only degradation products were observed upon irradiation (Table 6.5).

Even though **144** was not very stable after removing the hexane, it was concentrated quickly, kept under argon, and taken directly into the next oxidation step to see if the

ketone version **146** was more stable than the alcohol **144**, and if it was possible to purify it at this stage. A small amount of **146** was isolated upon reaction with Dess-Martin periodinane in dichloromethane and subsequent purification. However, the very low yield after the two steps did not make this synthetic route feasible.

In another attempt to synthesise an alternative starting material, an isomeric alkyne was prepared: 1-phenylpent-4-yn-1-ol (**153**), with the hydroxyl group next to the benzene ring instead of the alkyne. The three-step synthesis from the literature (Queignec *et al.*, 1988; Chaisan *et al.*, 2021) gave **151** in 55% yield, which was deprotected into **152** in 29% yield and reduced into **153** in 83% yield (Scheme 6.23).
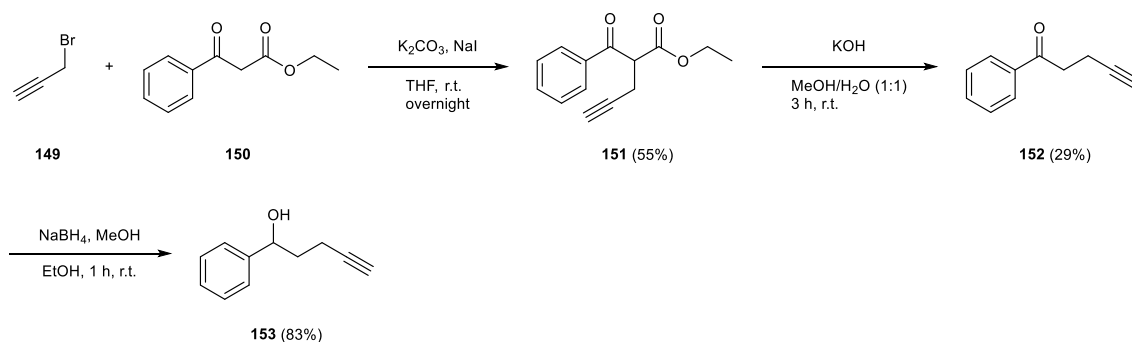
Scheme 6.23: Synthesis of starting material **153**.

153 was then used in an *ortho*-photocycloaddition reaction at different concentrations and solvents to form cyclooctatetraene **154** (Scheme 6.24; Table 6.6). The attempts to run the reaction at 10 and 5 mM in hexanes were not successful. Only very small new peaks were visible after 24 h irradiation at 254 nm. These new peaks seemed to correspond to the product **154** when compared with the NMR data from the *ortho*-photocycloaddition of the previous route. However, the conversion was very low for already low concentrations of the reaction, so it was considered unsuccessful. Another reaction at 5 mM in dichloromethane was tested, but only degradation products were observed by NMR spectroscopy after irradiation. Thus, changing the position of the alcohol group of the starting material did not have the desired effect, and the *ortho*-photocycloaddition was unsuccessful.
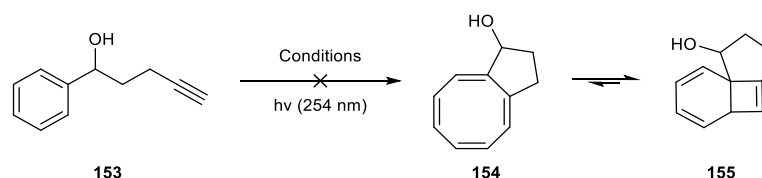
Scheme 6.24: Attempt of intramolecular *ortho*-PCA of **153**.

Table 6.6: Conditions attempted for intramolecular *ortho*-photocycloaddition of **153**.

	Concentration (mM)	Solvent	Time (h)	Observations
1	5	Hexane	24	Mostly SM **153**, very small peaks for the product **154** by NMR and light spot by TLC.
2	10	Hexane	24	Mostly SM **153**, very small peaks for the product **154** by NMR and light spot by TLC.
3	5	CH$_2$Cl$_2$	24	Degradation products.

6.3.2.3 Third synthetic route

After a few unsuccessful attempts at intramolecular *ortho*-photocycloadditions, it was proposed to use a new synthetic route, starting with a photoreaction (step 1), found in the literature (Grovenstein *et al.*, 1961; Bryce-Smith *et al.*, 1963), to give the dimethyl cyclooctateraene **159** from benzene **156** (Scheme 6.25). The methyl esters are then reduced to alcohols in step 2 to give **160** and protected again with an acetyl group in step 3 to afford **161,** for reasons explained below, to access a more electron-rich cyclooctatetraene. Different dienophiles can then be used in step 4 to attempt a Diels-Alder reaction and obtain **162** before performing a [2+2] photocycloaddition in step 5 to give **163**. The amines are further deprotected in **164** in step 6 and oxidised for **165** in step 7 to then close the 1,2-disubstituted cubane **166** in step 8 by losing N$_2$.
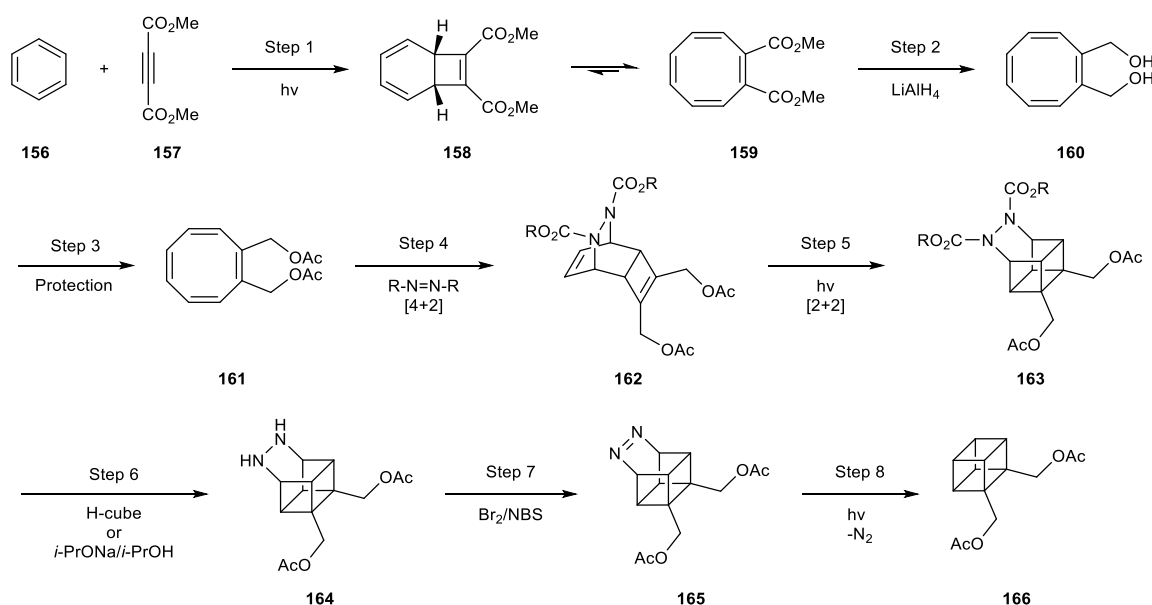
Scheme 6.25: Proposed new synthetic route to access the 1,2-disubstituted cubane **166** starting with benzene **156**.

The substituents on the cyclooctatetraene can play an important role in the reactivity and the Diels-Alder product formation in step 4. It was shown previously (Grange *et al.*, 2010) that the dimethyl cyclooctatetraenedicarboxylate **159** (which is more electron poor) reacting with 4-phenyl-1,2,4-triazole-3,5-dione (PTAD) formed only the 2,3-disubstituted adduct, whereas using a more electron-rich disubstituted cyclooctatetraene increased the ratio of 3,4-disubstituted adduct to 2,3-disubstituted adduct. Using diisopropyl azodicarboxylate (DIAD) instead of PTAD was shown to form selectively the 3,4-disubstituted adducts when using electron-rich starting materials. Thus, a more electron-rich disubstituted cyclooctatetraene could be interesting to use in order to form selectively one of the adducts, to facilitate the isolation and purification of the product in our case.

Thus, the acetyl protected cyclooctatetraene **161** was synthesised, a more electron rich compound to use as a starting material in the 1,2-disubstituted cubane synthesis, in a three-step synthesis. Dimethylcyclooctatetraene **159** was synthesized following the literature procedure using benzene **156** and irradiated for two days at 254 nm in 45% yield (Grovenstein *et al.*, 1961; Bryce-Smith *et al.*, 1963). Spectral data showed that **158** was present in the monocyclic tautomer **159** and not the bicyclic **158** (Scheme 6.26),

251

which needs to be formed to undergo the Diels-Alder. **158** is formed first but undergoes isomerisation to give **159** which is more thermodynamically stable (Grovenstein *et al.*, 1961).
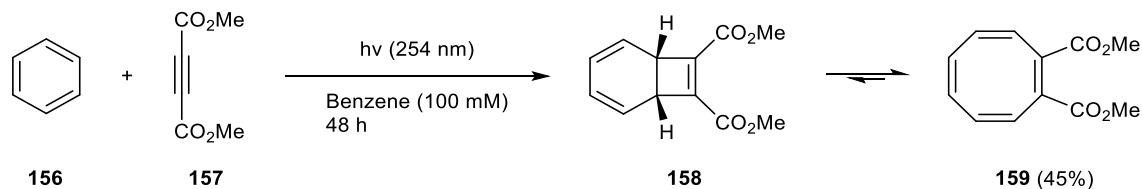
Scheme 6.26: Synthesis of cyclooctatetraene **159**.

6.3.2.3.1   Deprotection of dimethyl cyclooctatetraene 159

Conditions to deprotect and protect the dimethyl cyclooctatetraene-1,8-dicarboxylate **159** were found in the literature, but only for the corresponding monoester. **159** was reduced using lithium aluminium hydride in tetrahydrofuran (Grange *et al.*, 2010) (Scheme 6.27). After stirring overnight at room temperature, two new spots were observed by TLC, and the starting material was not present. The two reaction products were isolated using column chromatography. The lower spot was the desired deprotected alcohol **160**, obtained as a light-yellow oil in low yield (27%). The product is not stable on silica but it was isolated once in a low yield to collect analytical data. The other spot was a side product **167** recovered in 64% yield, as colourless crystals. 1D and 2D NMR as well as X-ray crystallography were used to determine the structure to develop strategies that might prevent its formation.
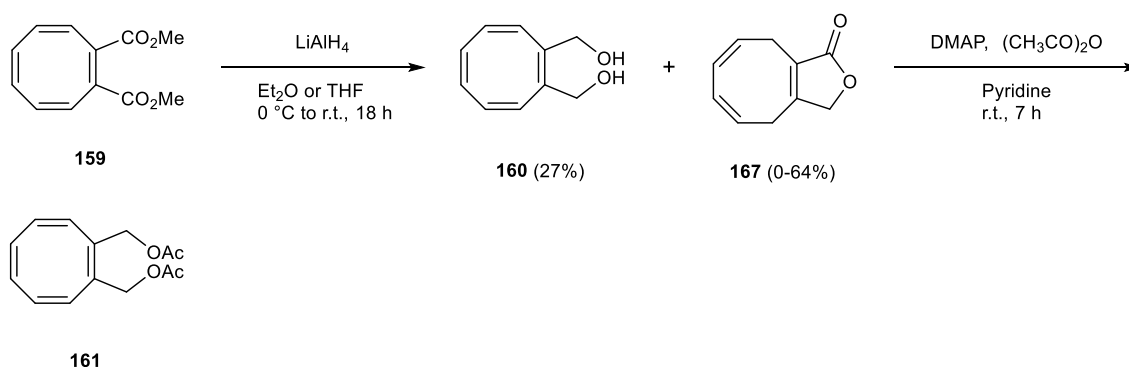
Scheme 6.27: Deprotection of methyl esters and acetyl protection of the alcohols to obtain an electron-rich disubstituted cyclooctatetraene.

The conditions of the reduction were investigated further in order to prevent the formation of lactone **167** (Entries 1-4, Table 6.7). An attempt to change the solvent from THF to Et$_2$O gave the same mixture of two products. One hypothesis to explain the side product formation is that one alcohol on one side reacts with the aldehyde on the other side before it is fully reduced. Thus, it was thought that reducing **159** more quickly could help avoid the formation of **167**. To improve this, the order of addition was changed. LiAlH$_4$ was resuspended in THF and then **159** in THF was added dropwise. The side product **167** formation was prevented on small scale but not when working on a bigger scale. Adding more equivalents of the reducing agent LiAlH$_4$ was also attempted (4.2 eq. instead of 2.2 eq.) as well as diluting the reaction, however the side product formation was not prevented.

Table 6.7: Conditions attempted to optimise the reduction of **159**.

Entry	Reducing agent	Eq.	Reaction details	Observations
1	LiAlH$_4$	2.2	LiAlH$_4$ added portionwise	Equal amount of **160** and lactone **167**
2	LiAlH$_4$	4.2	LiAlH$_4$ added portionwise	Equal amount of **160** and lactone **167**
3	LiAlH$_4$	2.2	More diluted	Equal amount of **160** and lactone **167**
4	LiAlH$_4$	2.2	SM **159** added to LiAlH$_4$ already in solution	Worked in small scale but not bigger scale
5	DIBAL-H	4.2		Maximum conversion of ~80% at 1h30
6	DIBAL-H	5		Maximum conversion of ~80% at 1h30
7	DIBAL-H	4.2 + 1	1 eq. added after 1h30 of reaction	Full conversion

After a few unsuccessful attempts, the mixture of the two products from Step 2 was taken into the next step to protect the alcohols with an acetyl group using acetic anhydride (Grange *et al.*, 2010). Thin layer chromatography (TLC) analysis showed completion of the reaction, however **161** appeared to have almost the same polarity as the side product **167** from the previous step, so it was difficult to purify, making this route inefficient and time consuming.

Another reducing agent was then tried. DIBAL-H was used to reduce the two esters into alcohols (Scheme 6.28). The reaction was fast (maximum conversion at 1.5 h) but did not

go to completion: ~ 80% calculated using ^{1}H NMR spectroscopy (Entry 5-Table 6.7). Thus, more DIBAL-H (5 eq. instead of 4.2 eq.) was used (Entry 6-Table 6.7), but this led to the same conversion. In a final attempt (Entry 7-Table 6.7), another equivalent of DIBAL-H was added after 1.5 h reaction time and the spot for **159** disappeared by TLC analysis after 30 min. The starting material **159** was successfully reduced. The crude NMR after work up was clean, so the crude product was taken directly to the next step to avoid decomposition on silica. **160** was acetylated in 66% yield using DMAP to give **161**.
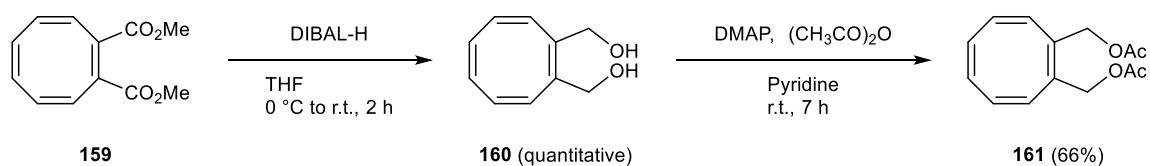
Scheme 6.28: Reduction reaction of **159** with DIBAL-H to avoid biproduct **167** formation.

6.3.2.3.2   Diels-Alder reactions

The new cyclooctatetraene **161** was reacted with different dienophiles to undergo a Diels-Alder reaction and generate two alkenes in **162**, which then can be used for intramolecular photocycloaddition to give **163** (Scheme 6.29). Azodicarboxylate compounds were selected to react with **161**. As explained above, very few examples of Diels-Alder reactions on the dimethyl cyclooctatetraene **159** are present in the literature (Grange *et al.*, 2010) and are using a limited number of dienophiles: PTAD and DIAD. However, the removal of the PTAD in the subsequent step of the synthesis is considered complicated, with the imide opening into a urea and a carbamic acid. Nucleophilic substitution on the urea is difficult due to the presence of an unreactive C=O. In order to facilitate the deprotection of the amines, the use of azodicarboxylate compounds is more promising. Diels-Alder reactions using diphenyl azodicarboxylate were attempted by a previous master student on the dimethyl cyclooctatetraene **159** and were unsuccessful. Diphenyl azodicarboxylate appeared to be less reactive than PTAD but remains a promising dienophile to use for further deprotection of the phenyl carbamate into a stable phenolate that would be easier to remove.
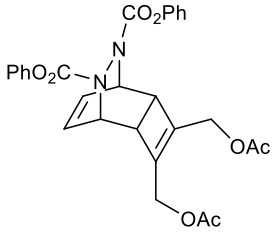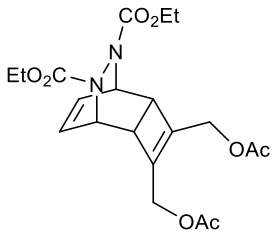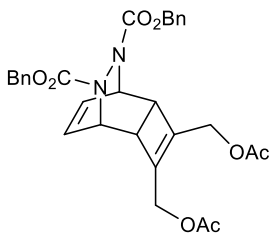
Diethyl and diphenyl azodicarboxylate were used first to test the Diels-Alder reaction as they should be deprotectable using a nucleophile. Dibenzyl azodicarboxylate was then used, as it should be possible to deprotect it via hydrogenolysis, so it might be easier to deprotect.

^{1}H NMR spectroscopy and TLC analysis were used to follow the reactions. The Diels-Alder reaction using diphenyl azodicarboxylate (Entry 1-Table 6.8) seemed to be more favourable towards product **162a** formation than the two others: diethyl azodicarboxylate for **162b** (Entry 2-Table 6.8), dibenzyl azodicarboxylate for **162c** (Entry 3-Table 6.8). For **162a**, small peaks for the product were observed at room temperature and it was heated to 80 °C to obtain maximum conversion (~60%). Whereas for **162b** and **162c**, small peaks for the product only appeared at 80 °C and it required heating to 110 °C to obtain maximum conversion ~50-65%. A spot below the starting material was observed by TLC for the three reactions and was isolated using column chromatography. None of the three reactions went to completion, probably due to an equilibrium with the starting material. Only one regioisomer - the 3,4-disubstituted adduct - was observed and isolated for the three attempts in moderate yields: 45%, 54% and 59% for **162a**, **162b** and **162c**, respectively.
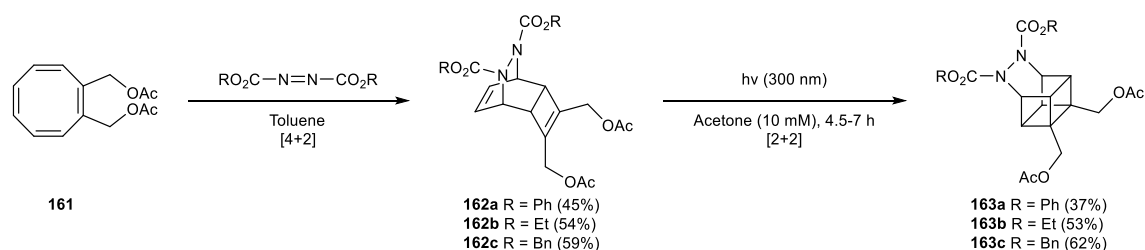
Scheme 6.29: Attempted Diels-Alder and PCA on cyclooctatetraene **161**.

Table 6.8: Diels-Alder reactions of **161** with different dienophiles.

	Dienophile	Temperature (°C)	Time (d)	Product	Observations
1	PhO$_2$C≡CO$_2$Ph	r.t. to 80	2.5		Small peaks for the product **162a** at r.t.. 60% conversion at 80 °C after 2.5 days.
2	EtO$_2$C≡CO$_2$Et	r.t. to 80 to 110	2.5		Only SM **161** at r.t.. Very small peaks for the product **162b** at 80 °C. ~60% conversion at 110 °C after 2.5 days.
3	BnO$_2$C≡CO$_2$Bn	80 to 110	2.5		Small peaks at 80°C for **162c**. ~65% conversion at 110 °C after 2.5 days.

The intramolecular [2+2] photocycloaddition after the Diels-Alder reaction was then attempted, using acetone as a triplet sensitizer. All three reactions (using compounds **162a**, **162b** and **162c**) went to completion at 10 mM after irradiation at 300 nm; after 4h30 for **163a** and **163b**, and 7 h for **163c**, and gave 35%, 63% and 52% yields, respectively, after purification. The crude products were reasonably pure by ^{1}H NMR

spectroscopy, so it should be possible to use them without further purification when scaling up the reaction.

6.3.2.3.3 Deprotection attempted

An attempt to deprotect the -CO_2Ph from **163a** with sodium hydroxide only led to the acetyl deprotection of the alcohols (Scheme 6.30).
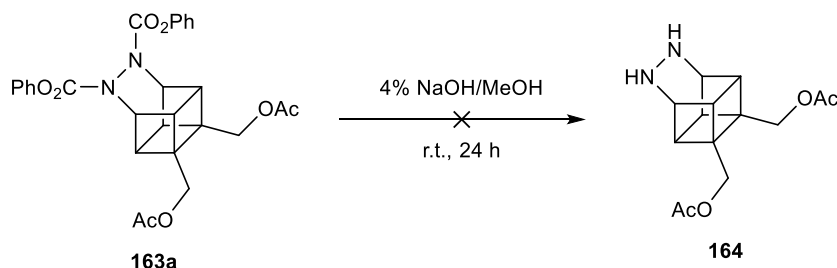
Scheme 6.30: Attempt of **163a** deprotection with sodium hydroxide.

In another attempt to obtain **164**, the H-Cube Mini+ from ThalesNano (a flow reactor for hydrogenation) was used, starting from compound **163c** (Scheme 6.31). Hydrogen is a hazardous gas so the H-Cube allows to limit the hazard by generating hydrogen in situ. A 10% Pd/C cartridge was used to run the reaction at room temperature in ethanol at 1 mL/min. TLC analysis showed leftover starting material and a new spot on the baseline. It was concentrated and analysed by ^1H NMR spectroscopy, but the spectrum was very messy. A column purification was attempted, but no product was recovered. The benzyl group would have likely been removed under these conditions but the N-N might have been too. Thus, it was not successful but the technique is potentially promising, and will be worth attempting again on a bigger scale.
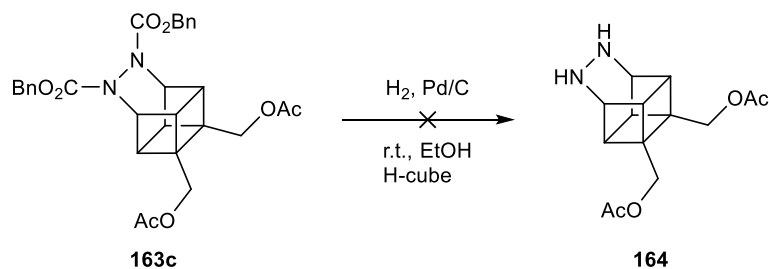
Scheme 6.31: Attempt to deprotect **163c** using the H-cube.

6.3.2.3.4   Diels-Alder reaction with SO₂

Expected to react in a similar way, a cheletropic reaction of **161** with SO₂ (using the crystalline SO₂ precursor DABSO) was also attempted (Scheme 6.32) (Woolven *et al.*, 2011), in the hope that the SO₂ group would be easier to remove and close the cubane after the [2+2] cycloaddition.
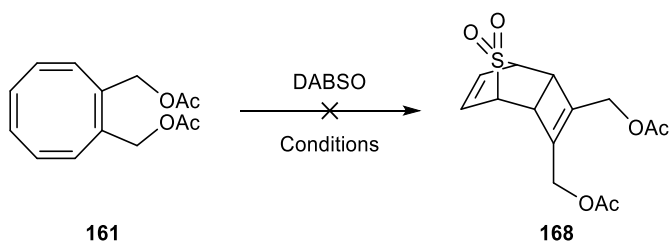
Scheme 6.32: [4+2] cycloaddition attempt of cyclooctatetraene **161** with DABSO.

Unfortunately, **168** was not obtained after testing the reaction in dioxane and tetrahydrofuran at reflux for three days (Table 6.9), with monitoring by ^{1}H NMR spectroscopy. The reaction was performed in a sealed microwave vial in order to keep the pressure and SO₂ inside, but only the starting material **161** was recovered.

Table 6.9: Conditions tried for the reaction of **161** with DABSO.

	Solvent	Temperature (°C)	Time (h)	Observations
1	Dioxane	100	96	Only SM **161** recovered after 96 h. Solubility issue.
2	THF	85	96	Only SM **161** recovered after 96 h.

6.4 Experimental

General procedures are detailed in the Materials and methods Chapter 2 Section 2.22.2.

6.4.1 1,3-Disubstituted cubane: first synthetic route

1-Acetoxy-1,3-butadiene (104) (Dolomanov *et al.*, 2009; Britten, Akien, *et al.*, 2019)
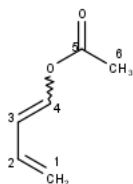
4-Dimethylaminopyridine (4.43 g, 0.04 mol, 0.1 eq.), triethylamine (106 mL, 0.76 mol, 2.1 eq.) and acetic anhydride (103 mL, 1.09 mol, 3.0 eq.) were added to crotonaldehyde **103** (30 mL, 0.36 mol, 1.0 eq.) at room temperature under argon. The solution was stirred for 4 days at room temperature, then diluted with Et$_2$O (200 mL), poured onto ice water (1.0 L) and stirred for 2 hours. The organic layer was washed with a saturated aqueous solution of NaHCO$_3$ (5 x 200 mL), filtered through Celite, dried (MgSO$_4$) and evaporated under reduced pressure to give the crude product. Purification by distillation (60-70 °C, 10 mm Hg) gave diene **104** (14.1 g, 0.13 mol, 31%; *E/Z* 8.0:1.0) as a colourless liquid.

TLC: R_f = 0.30 (7:3 petroleum ether/EtOAc); KMnO$_4$.

^{1}H NMR (400 MHz, CDCl$_3$): δ (ppm) = 7.41 (d, 1H, *J* = 12.4 Hz, H4), 6.35-6.22 (m, 1H, H2), 6.10-6.02 (m, 1H, H3), 5.26-5.20 (m, 1H, H1A or H1B), 5.13-5.08 (m, 1H, H1A or H1B), 2.16 (s, 3H, H6) (data for the major isomer).

^{13}C NMR (101 MHz, CDCl$_3$): δ (ppm) = 167.8 (C5), 138.7 (C4), 131.7 (C2), 117.3 (C1), 116.0 (C3), 20.7 (C6) (data for the major isomer).

IR (ATR): ν (cm^{-1}) = 1750 (s, C=O), 1665, 1420.

Spectral data matched those reported in the literature.

1,2-Di-*tert*-butyl 3-(acetyloxy)-1,2,3,6-tetrahydropyridazine-1,2-dicarboxylate (106)

(Britten, Akien, *et al.*, 2019)
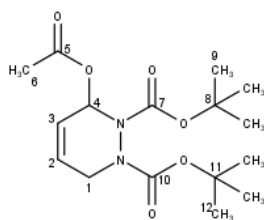
1-Acetoxy-1,3-butadiene **104** (7.7 mL, 65.1 mmol, 1.5 eq.) was added in one portion to a solution of di-*tert*-butyl azodicarboxylate **105** (10.0 g, 43.4 mmol, 1.0 eq.) in toluene (20 mL) and stirred at 40 °C for 48 hours. The reaction mixture was evaporated under reduced pressure and dried under high vacuum for 24 hours (until all traces of 1-acetoxy-1,3-butadiene had been removed). The resulting white product **106** was dried in a desiccator for 2 weeks over Drierite, and used directly in the next step. Quantitative yield.

TLC: R_f = 0.20 and 0.40 (7:3 petroleum ether/EtOAc – two spots, because it degrades on the TLC plate); UV.

^{1}H NMR (400 MHz, CDCl$_3$): δ (ppm) = 6.95-6.75 (m, 1H, H4), 6.14-6.01 (m, 1H, H2), 5.95-5.76 (m, 1H, H3), 4.53-4.44 (m, 1H, H1A), 3.83-3.56 (m, 1H, H1B), 2.08 (s, 3H, H6), 1.51 (s, 9H, H9 or H12), 1.48 (s, 9H, H9 or H12).

^{13}C NMR (101 MHz, CDCl$_3$): δ (ppm) = 169.3 (C5), 154.4 (C7 or C10), 153.1 (C7 or C10), 129.1 (C2), 122.3 (C3), 80.9 (C8 and C11), 74.0 (C4), 42.0 (C1), 28.2 (C9 or C12), 28.1 (C9 or C12), 21.0 (C6).

IR (ATR): ν (cm^{-1}) = 3000, 1750 (s, C=O), 1700 (s, C=O).

Spectral data matched those reported in the literature.

1,2-Di-*tert*-butyl 1,2-dihydropyridazine-1,2-dicarboxylate (107) (Britten, Akien, *et al.*, 2019)
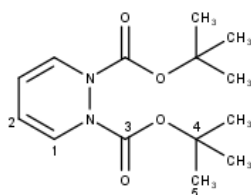
Ten microwave vials were used in parallel. To each vial was added cycloadduct **106** (2.0 g, 5.7 mmol, 1.0 eq.), 1,4-dioxane (11 mL), Pd(OAc)₂ (12 mg, 0.04 mmol, 0.01 eq.), triphenylphosphine (44 mg, 0.17 mmol, 0.03 eq.) and triethylamine (1.2 mL, 8.5 mmol, 1.5 eq.) under argon. The vials were sealed, heated at reflux (100 ˚C) for 1 hour, and allowed to cool to room temperature. The contents of the vials were then combined and concentrated under reduced pressure to give the crude product. The crude product was purified by flash column chromatography on silica gel starting with 100% petroleum ether, then 95:5 petroleum ether/EtOAc, then 9:1 petroleum ether/EtOAc to afford the product **107** (10.5 g, 37.2 mmol, 65%) as a white solid.

TLC: R_f = 0.50 (7:3 petroleum ether/EtOAc); UV.

^{1}H NMR (400 MHz, CDCl₃): δ (ppm) = 6.92-6.50 (m, 2H, H1), 5.83-5.46 (m, 2H, H2), 1.51 (s, 18H, H5).

^{13}C NMR (101 MHz, CDCl₃): δ (ppm) = 151.9 (C3), 127.9 (C1), 111.4 (C2), 82.3 (C4), 28.4 (C5).

IR (ATR): ν (cm⁻¹) = 2974, 2938, 1719 (s, C=O), 1572, 1475.

Spectral data matched those reported in the literature.

rac-2,3-Di-*tert*-butyl (1*R*,4*S*)-2,3-diazabicyclo[2.2.0]hex-5-ene-2,3-dicarboxylate (100)

(Britten, Kemmitt, *et al.*, 2019)
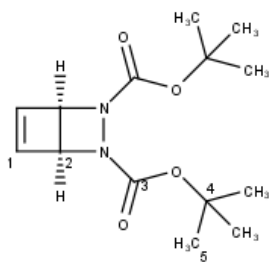
1,2-Dihydropyridazine **107** (5.0 g, 30.0 mmol) was dissolved in acetonitrile (354 mL). The mixture was distributed between 6 × 60 mL phototubes, and each tube was purged with argon for 15 minutes, then irradiated at room temperature (*h*ν = 350 nm) until consumption of the starting material: 48 h. The contents of the tubes were combined, and the solvent was evaporated under reduced pressure to give the crude product. The crude product was purified by flash column chromatography on silica gel (eluent: 100% hexane then 9:1 hexane/EtOAc) to afford the bicycle **100** (3.9 g, 13.7 mmol, 77%) as a white solid.

TLC: R_f = 0.40 (7:3 petroleum ether/EtOAc); UV.

^{1}H NMR (400 MHz, CDCl$_3$): δ (ppm) = 6.74-6.70 (m, 2H, H1), 5.13-5.09 (m, 2H, H2), 1.51 (s, 18H, H5).

^{13}C NMR (101 MHz, CDCl$_3$): δ (ppm) = 158.9 (C3), 143.3 (C1), 82.0 (C4), 66.6 (C2), 28.13 (C5).

IR (ATR): ν (cm^{-1}) = 2980, 2920, 1690 (s, C=O).

Spectral data matched those reported in the literature.

1,4-Dibromo-2,5-dimethoxybenzene (109) (López-Alvarado *et al.*, 2002)
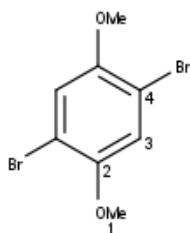
To a solution of 1,4-dimethoxybenzene **108** (10.0 g, 72.5 mmol, 1.0 eq.) in acetic acid (20 mL) was added dropwise Br$_2$ (7.4 mL, 145.0 mmol, 2.0 eq.) in CH$_3$CO$_2$H (7 mL), at room temperature. After stirring for 2 h at room temperature, the solution was cooled in an ice bath and filtered to give 2,5-dibromo-1,4-dimethoxybenzene **109** (16.3 g, 55.0 mmol, 76%) as a white solid. The filtrate was diluted with water (15 mL) and extracted with chloroform (2 × 40 mL), the organic layer was washed with sat. NaHCO$_3$ (20 mL), dried over Na$_2$SO$_4$ and evaporated to give some more 2,5-dibromo-1,4-dimethoxybenzene **109** (0.9 g, 3.0 mmol). The crude product was used in the next step without further purification.

^{1}H NMR (400 MHz, CDCl$_3$): δ (ppm) = 7.10 (s, 2H, H3), 3.84 (s, 6H, H1).

^{13}C NMR (101 MHz, CDCl$_3$): δ (ppm) = 150.5 (C2), 117.1 (C3), 110.5 (C4), 57.0 (C1).

IR (ATR): v (cm^{-1}) = 3400, 2980, 2900, 2750, 1490, 1420.

Spectral data matched those reported in the literature.

2,5-Dibromocyclohexa-2,5-diene-1,4-dione (101) (López-Alvarado *et al.*, 2002)
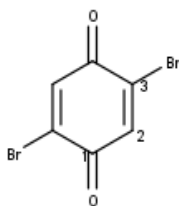
2,5-Dibromo-1,4-dimethoxybenzene **109** (4.4 g, 14.9 mmol) was dissolved in acetonitrile (44 mL) and heated at 100 °C. A solution of cerium ammonium nitrate (22.5 g, 41.6 mmol) in water (90 mL) was added to the boiling CH_3CN solution slowly over 5 min. After completion of the addition, the mixture was stirred whilst cooling to room temperature for 30 min. The yellow precipitate that formed was filtered and washed with water (15 mL) to give 2,5-dibromobenzoquinone **101** (3.2 g, 12.0 mmol, 82%) as a yellow solid. The crude product was used in the next step without further purification.

^{1}H NMR (400 MHz, CDCl$_3$): δ (ppm) = 7.48 (s, 2H, H2).

^{13}C NMR (101 MHz, CDCl$_3$): δ (ppm) = 176.9 (C1), 137.8 (C3), 137.1 (C2).

IR (ATR): ν (cm^{-1}) = 3080, 1690 (s, C=O), 1580, 1520.

Spectral data matched those reported in the literature.

rac-(1*R*,2*S*,5*R*,6*S*)-1,8-Dibromotricyclo[4.4.0.0^{2,5}]deca-3,8-diene-7,10-dione (102)
(personal communication)
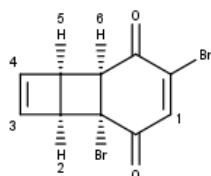
Dichloromethane, 2,6-lutidine and TMSOTf were freshly distilled before starting the reaction.

Solution A: To a solution of bicycle **100** (112 mg, 0.4 mmol, 1.0 eq.) in dry DCM (18 mL) under argon (in a 50 mL round-bottomed flask) was added 2,6-lutidine (186 µL, 1.6 mmol, 4.0 eq.). The reaction mixture was then cooled to −78 °C and TMSOTf (180 µL, 1.0 mmol, 2.4 eq.) was added dropwise over 30 seconds at −78 °C. The reaction mixture was then allowed to warm to r.t. over 30 min.

Solution B: In a 30 mL photoreaction tube, 2,5-dibromoquinone **101** (319 mg, 1.2 mmol, 3.0 eq.) was dissolved in dry DCM (8 mL) under argon, then MeOH (810 µL, ~50 eq.) was added.

Solution A was then added to solution B in the photoreaction tube. An aliquot was taken for NMR after addition to verify the presence of **102** and the tube was directly used in the next reaction (because the product was not stable).

Proposed proton NMR attribution for **102**: ^{1}H NMR (400 MHz, solvent suppression, CH_2Cl_2): δ (ppm) = 7.51 (br s, 1H, H1), 6.31 (br s, 1H, H3 or H4), 6.21 (br s, 1H, H3 or H4), 4.09 (br s, 1H, H2 or H5 or H6), 4.07 (br s, 1H, H2 or H5 or H6).

1,8-Dibromopentacyclo[4.4.0.0^{2,5}.0^{3,9}.0^{4,8}]decane-7,10-dione (67) (Personal communication, (Barborak *et al.*, 1966))
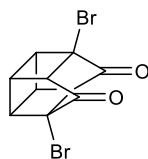
The phototube with **102** was placed in the photoreactor and it was irradiated (*hv* = 300 nm) for 1 h. After 50 min of irradiation, analysis of an aliquot by ^{1}H NMR spectroscopy (400 MHz, solvent suppression, CH_2Cl_2) showed that the peaks from the starting material disappeared. New peaks between 3.5 and 3.9 and at 2.5 ppm appeared, which could correspond to the product **67**.

The solvent was evaporated under reduced pressure and it was used directly in the next step (because the product was not stable, so it was not possible to isolate it). The next step was a double Favorskii-type rearrangement in 10% NaOH in water at 120 °C. An NMR of the crude **68** was run in MeOD. Very small peaks for the cubane were seen on the baseline but it was not isolated. The carboxylic acids were esterified using ion-exchange resin (Dowex-50WX8) in MeOH at 60 °C overnight directly from the crude. In the morning it was allowed to cool down to r.t., filtered to remove the resin and concentrated under

reduced pressure to give the crude as a black solid. It was purified by column chromatography on silica gel using 20-30% EtOAc in petroleum ether to afford the product **75** mixed with some impurities that were not removable even after two columns. Enough material was recovered for a proton NMR but not for a carbon. Data for **75** are detailed in the appropriate section bellow.

6.4.2 1,3-Disubstituted cubane: second synthetic route

rac-(3'*R*,5'*S*)-1',5'-Dibromo-4'-oxaspiro[1,3-dioxolane-2,11'-
tetracyclo[6.2.1.0^{2,7}.0^{3,5}]undecan]-9'-en-6'-one (116) (Suzuki *et al.*, 1988)
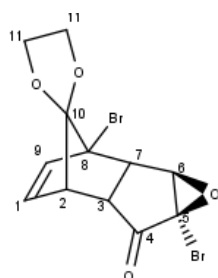
Enone **115** (10.0 g, 27.6 mmol, 1.0 eq.; already available in the lab) was suspended in methanol (150 mL) at 0 °C, open to air. NaOH (5.5 mL, 2.8 mmol, 0.1 eq., 0.5 M) was added dropwise to the suspension at 0 °C, followed by H$_2$O$_2$ (5.5 mL, >30% aq.) at 0 °C. The reaction mixture was allowed to warm slowly to room temperature (the ice bath was not removed) and was stirred at r.t. for 14 h. After full consumption of the starting material (by TLC analysis), a saturated aqueous solution of sodium bisulfite (500 mL) was added, and the mixture was extracted with EtOAc (4 × 100 mL), dried over MgSO$_4$ and concentrated under reduced pressure to afford the crude product **116** (9.7 g, 25.6 mmol, 93%) as a white solid. The crude product was used in the next step without further purification.

m.p.: 150–151 °C

TLC: *R*$_f$ = 0.50 (DCM); KMnO$_4$.

^{1}H NMR (400 MHz, CDCl$_3$): δ (ppm) = 6.23 (dd, 1H, *J* = 6.5, 1.5 Hz, H9), 6.15 (dd, 1H, *J* = 6.5, 3.6 Hz, H1), 4.26-4.19 (m, 2H, H11 or H12), 4.07-3.92 (m, 3H, H11 or H12 and H7 or

H3), 3.46 (d, 1H, J = 7.1 Hz, H6), 3.17 (ddd, 1H, J = 7.1, 5.6, 1.5 Hz, H7 or H3), 3.02 (ddd, 1H, J = 5.2, 3.6, 1.5 Hz, H2).

^{13}C NMR (101 MHz, CDCl$_3$): δ (ppm) = 199.4 (C4), 135.9 (C9), 132.8 (C1), 126.0 (C10), 69.7 (C5), 66.6 (C11 or C12), 65.9 (C11 or C12), 64.4 (C8), 64.3 (C7), 48.5 (C2 or C6), 48.1 (C2 or C6), 47.3 (C3).

IR (ATR): ν (cm^{-1}) = 2980, 2880, 1750 (C=O).

rac-(5'R)-4',7'-Dibromospiro[1,3-dioxolane-2,10'-tricyclo[5.2.1.0^{2,6}]decane]-3',8'-dien-5'-ol (117)
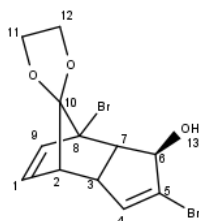
Epoxy enone **116** (9.7 g, 25.6 mmol, 1.0 eq.) was suspended in EtOH (200 mL). AcOH (7.4 mL, 130.0 mmol, 5.0 eq.) was added dropwise at r.t., then hydrazine (6.3 mL, 130 mmol, 5.0 eq.) was then added dropwise at r.t.. The resulting suspension was stirred for 14 h, during which time complete dissolution occurred. After full consumption of the starting material (by TLC analysis), the resulting solution was poured in of a sat. aq. solution of NaHCO$_3$ (500 mL) and extracted with EtOAc (4 × 100 mL). The organic layer was washed with sat. aq. NaHCO$_3$ (200 mL), and brine (200 mL), dried over MgSO$_4$ and concentrated under reduced pressure to give the crude product. The crude product was purified using flash column chromatography on silica gel with 100% DCM to give the product **117** (5.0 g, 13.7 mmol, 54%) as a white solid.

m.p.: 126–127 °C

TLC: R_f = 0.15 (DCM); KMnO$_4$.

^{1}H NMR (400 MHz, CDCl$_3$): δ (ppm) = 6.11 (ddd, 1H, J = 6.5, 1.6, 0.5 Hz, H1), 6.07 (dd, 1H, J = 6.5, 3.7 Hz, H9), 5.83 (dd, 1H, J = 2.3, 1.0 Hz, H4), 4.30-4.15 (m, 3H, H11 or H12 and H6), 4.07-3.98 (m, 1H, H11 or H12), 3.98-3.88 (m, 1H, H11 or H12), 3.59 (ddd, 1H, J = 10.1, 4.7, 2.3 Hz, H3), 3.12 (dd, 1H, J = 7.8, 2.3 Hz, H7), 2.66 (ddd, 1H, J = 4.7, 3.7, 1.6 Hz, H2), 2.18 (d, 1H, J = 5.5 Hz, H13).

^{13}C NMR (101 MHz, CDCl$_3$): δ (ppm) = 134.5 (C1), 134.1 (C4), 133.3 (C9), 126.4 (C5), 79.4 (C6), 67.9 (C8), 66.3 (C11 or C12), 65.5 (C11 or C12), 56.9 (C7), 52.5 (C2), 47.0 (C3).

IR (ATR): ν (cm^{-1}) = 3434 (w, OH), 2983, 2892.

4',7'-Dibromospiro[1,3-dioxolane-2,10'-tricyclo[5.2.1.0^{2,6}]decane]-3',8'-dien-5'-one (118) (Dess *et al*., 1983)
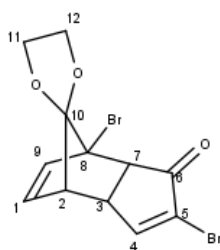
Allylic alcohol **117** (5 g, 13.2 mmol, 1.0 eq.) was dissolved in dry DCM (95 mL) under argon and Dess-Martin periodinane (6.72 g, 15.8 mmol, 1.2 eq.) was added portionwise at r.t.. After full consumption of the starting material (by TLC analysis) after 1h30, sat. aq. NaHCO$_3$ (45 mL) and sat. aq. Na$_2$S$_2$O$_3$ (45 mL) were added sequentially to the reaction and the resulting mixture was stirred at r.t. for 2 h. The layers were then separated and the aqueous layer was extracted with DCM (3 × 30 mL). The combined organic layers were washed with sat. aq. NaHCO$_3$ (2 × 50 mL), dried over MgSO$_4$ and concentrated under reduce pressure to afford the crude product. The crude product was purified by flash column chromatography on silica gel using 100% DCM to afford the product **118** (4.2 g, 11.5 mmol, 87%) as a white semi-solid.

m.p.: 127–128 °C

TLC: R_f = 0.30 (DCM); KMnO$_4$.

^{1}H NMR (400 MHz, CDCl$_3$): δ (ppm) = 7.42 (d, 1H, J = 2.9 Hz, H4), 6.05 (dd, 1H, J = 6.5, 1.3 Hz, H9), 5.96 (dd, 1H, J = 6.5, 3.7 Hz, H1), 4.35-4.28 (m, 1H, H11 or H12), 4.28-4.21 (m, 1H, H11 or H12), 4.10-4.04 (m, 1H, H11 or H12), 4.01-3.95 (m, 1H, H11 or H12), 3.67 (ddd, 1H, J = 5.6, 4.5, 2.9 Hz, H3), 3.24 (d, 1H, J = 5.6 Hz, H7), 2.87 (ddd, 1H, J = 4.5, 3.7, 1.3 Hz, H2).

^{13}C NMR (101 MHz, CDCl$_3$): δ (ppm) = 197.8 (C6), 158.7 (C4), 134.7 (C9), 130.5 (C1), 130.0 (C5), 127.1 (C10), 66.5 (C11 or C12), 66.0 (C8), 65.9 (C11 or C12), 51.8 (C7), 47.3 (C2), 45.4 (C3).

IR (ATR): ν (cm^{-1}) = 2987, 2894, 1716 (s, C=O).

7',9'-Dibromospiro[1,3-dioxolane-2,6'-pentacyclo[5.3.0.0^{2,5}.0^{3,9}.0^{4,8}]decan]-10'-one (72) (Nigo *et al.*, 1993)
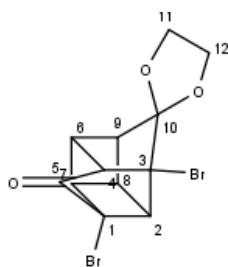
118 (2.0 g, 5.5 mmol, 1.0 eq.) was dissolved in dry acetone (110 mL) and split between four phototubes. Each tube was purged with argon for 15 min, then the tubes were irradiated at 300 nm. The reaction was followed by NMR, and completion of the reaction was reached at 7 h. The contents of the tubes were combined and evaporated under reduce pressure to afford the crude product **72** (1.9 g, 5.2 mmol, 94%) as a white/brown solid. The crude product was used in the next step without further purification.

m.p.: 169–171 °C

TLC: R_f = 0.40 (1:9 MeOH/DCM); ammonium molybdate.

^{1}H NMR (400 MHz, CDCl$_3$): δ (ppm) = 4.37-4.25 (m, 2H, H11 or H12), 4.09-3.96 (m, 2H, H11 or H12), 3.60-3.52 (m, 1H, H2 or H4 or H5 or H6 or H8 or H9), 3.47-3.41 (m, 1H, H2 or H4 or H5 or H6 or H8 or H9), 3.42-3.36 (m, 1H, H2 or H4 or H5 or H6 or H8 or H9), 3.17-3.09 (m, 1H, H2 or H4 or H5 or H6 or H8 or H9), 3.01 (dd, 1H, J = 6.2, 2.3 Hz, H2 or H4 or H5 or H6 or H8 or H9), 2.79-2.71 (m, 1H, H2 or H4 or H5 or H6 or H8 or H9).

^{13}C NMR (101 MHz, CDCl$_3$): δ (ppm) = 204.2 (C5), 121.5 (C10), 66.5 (C11 or C12), 66.1 (C11 or C12), 63.5 (C3), 55.2 (C1), 55.1 (C2 or C4 or C5 or C6 or C8 or C9), 50.8 (C2 or C4 or C5 or C6 or C8 or C9), 41.5 (C2 or C4 or C5 or C6 or C8 or C9), 41.4 (C2 or C4 or C5 or C6 or C8 or C9), 40.2 (C2 or C4 or C5 or C6 or C8 or C9), 38.4 (C2 or C4 or C5 or C6 or C8 or C9).

IR (ATR): ν (cm^{-1}) = 2994, 2894, 1770, 1787.

1'-Bromospiro[1,3-dioxolane-2,9'-pentacyclo[4.3.0.0^{2,5}.0^{3,8}.0^{4,7}]nonane]-5'-carboxylic acid (73) (Nigo *et al.*, 1993)
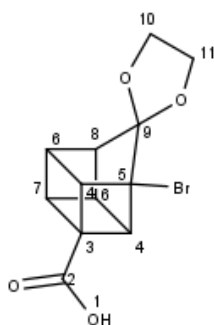
72 (1.9 g, 5.2 mmol, 1.0 eq.) was suspended in 10% NaOH in H$_2$O and the resulting mixture was heated to reflux for 4 h at 120 °C. TLC (eluent TBME) showed that there was no starting material left. The reaction mixture was cooled to r.t. then in an ice bath, then acidified to pH 1 with concentrated HCl, and extracted with CHCl$_3$ (5 × 30 mL). The combined organic layers were washed with H$_2$O (50 mL), brine (50 mL), dried over MgSO$_4$ and concentrated under reduced pressure to afford the crude product **73** (1.2 g, 4.4 mmol, 75%) as a light brown solid, which was used in the next step without further purification.

m.p.: 175–176 °C

TLC: R_f = 0.20 (5:95 MeOH/DCM); ammonium molybdate.

^{1}H NMR (400 MHz, CDCl$_3$): δ (ppm) = 4.32-4.27 (m, 2H, H10 or H11), 4.05-3.99 (m, 2H, H10 or H11), 3.92-3.88 (m, 2H, H4), 3.66-3.58 (m, 3H, H6 and H8), 2.98-2.93 (m, 1H, H7).

^{13}C NMR (101 MHz, CDCl$_3$): δ (ppm) = 175.4 (C2), 124.5 (C9), 66.2 (C10 and C11), 62.6 (C3 or C5), 52.2 (C4), 50.8 (C3 or C5), 43.4 (C7), 42.5 (C8), 40.0 (C6).

IR (ATR): ν (cm^{-1}) = 2998, 2890, 1727, 1690.

HRMS (ESI): m/z calculated for: C$_{12}$H$_{11}$O$_4$^{79}Br [M-H]$^-$, 296.9768, found: 296.9760.

8-Bromo-9-oxopentacyclo[4.3.0.0^{2,5}.0^{3,8}.0^{4,7}]nonane-4-carboxylic acid (74) (Nigo *et al.*, 1993)
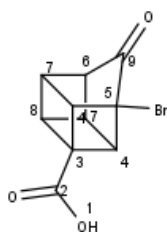
73 (1.8 g, 6.0 mmol, 1.0 eq.) was dissolved in 75% H$_2$SO$_4$ and stirred at r.t. for 24 h. The resulting mixture was then poured into ice-water (400 mL), saturated with (NH$_4$)$_2$SO$_4$ and extracted with EtOAc (4 x 70 mL). The organic layer was concentrated under reduced pressure to give a beige solid. The solid was dissolved in sat. aq. NaHCO$_3$ (30 mL) and extracted with DCM, acidified with concentrated HCl to pH 1, and extracted again with DCM (20 mL). The aqueous layer was then saturated with (NH$_4$)$_2$SO$_4$ and extracted with EtOAc (4 × 40 mL), dried over MgSO$_4$ and concentrated under reduced pressure to give the crude product **74** (606 mg, 2.4 mmol, 40 %) as a beige solid. The crude product was used in the next step without further purification.

TLC: R_f = 0.05 (5:95 MeOH/DCM); ammonium molybdate.

^{1}H NMR (400 MHz, d_6-DMSO): δ (ppm) = 12.43 (br s, 1H, H1), 3.92-3.87 (m, 2H, H4), 3.82-3.77 (m, 1H, H6), 3.77-3.69 (m, 2H, H7), 3.18 (t, 1H, J = 5.3 Hz, H8).

^{13}C NMR (101 MHz, d_6-DMSO): δ (ppm) = 210.7 (C9), 171.2 (C2), 58.0 (C3 or C5), 54.7 (C3 or C5), 49.9 (C4), 46.0 (C6), 39.3 (C8), 37.7 (C7).

IR (ATR): ν (cm^{-1}) = 2990, 2890, 1730 (s, C=O).

HRMS (ESI): m/z calculated for: $C_{10}H_7O_3{}^{79}Br$ [M-H]$^-$, 252.9506, found: 252.9496.

Cubane-1,3-dicarboxylic acid (68) (Nigo *et al.*, 1993)
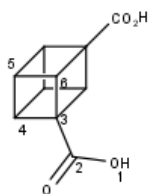
74 (950 mg, 3.7 mmol, 1.0 eq.) was suspended in 25% (w/v) NaOH (aq.) (5 mL) and the resulting mixture was stirred at reflux for 4 h, then cooled to r.t., then in an ice bath, and acidified to pH 1 with concentrated HCl. The resulting mixture was saturated with $(NH_4)_2SO_4$ and extracted with EtOAc (3 × 20 mL). The organic phase layer was then dried over MgSO$_4$ and concentrated under reduced pressure to afford the crude product **68** (450 mg, 2.3 mmol, 63%) as a white solid. The crude product was used in the next step without further purification.

m.p.: 184–186 °C

TLC: R_f = 0 (5:95 MeOH/DCM); bromocresol green.

^{1}H NMR (400 MHz, d_6-DMSO): δ (ppm) = 4.42-4.38 (m, 2H, C6 or C4), 4.22 (sept, 2H, J = 2.5 Hz, C5), 4.05-3.97 (m, 2H, C6 or C4).

^{13}C NMR (101 MHz, d_6-DMSO): δ (ppm) = 172.6 (C2), 53.2 (C3), 50.7 (C4 or C6), 49.4 (C4 or C6), 42.1 (C5).

IR (ATR): ν (cm^{-1}) = 3450 (w, OH), 2998, 2926, 1692 (s, C=O).

HRMS (ESI): *m/z* calculated for: $C_{10}H_8O_4$ [M-H]$^-$, 191.0350, found: 191.0356.

1,3-Dimethyl cubane-1,3-dicarboxylate (75) (Nigo *et al.*, 1993)
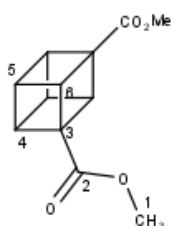
68 (500 mg, 2.6 mmol, 1.0 eq.) was suspended in MeOH and a spatula of ion exchange resin (Dowex-50WX8) was added. The resulting suspension was stirred at reflux overnight, then cooled to r.t., filtered and concentrated under reduced pressure to afford the crude product. The crude product was purified by flash column chromatography on silica gel using 0-1.5% MeOH in DCM as the eluent to afford the product **75** (295 mg, 1.4 mmol, 52%) as a white solid. The low yield was due to the approximate mass of the starting material **68**, because it was a crude product from the previous reaction.

m.p.: 120–122 °C

TLC: R_f = 0.80 (1:9 MeOH/DCM); ammonium molybdate.

^{1}H NMR (400 MHz, CDCl$_3$): δ (ppm) = 4.51-4.47 (m, 2H, H4 or H5 or H6), 4.24 (sept, 2H, *J* = 2.5 Hz, H4 or H5 or H6), 4.05-4.00 (m, 2H, H4 or H5 or H6), 3.74 (s, 6H, H1).

^{13}C NMR (101 MHz, CDCl$_3$): δ (ppm) = 171.6 (C2), 53.3 (C1), 51.7 (C4 or C5 or C6), 51.1 (C4 or C5 or C6), 49.9 (C4 or C5 or C6), 42.9 (C3).

IR (ATR): ν (cm^{-1}) = 2996, 2953, 1722 (s, C=O).

HRMS (ESI): *m/z* calculated for: C$_{11}$H$_{10}$O$_4$ [M-H]$^-$, 205.0506, found: 205.0503.

6.4.3 1,3-Disubstituted cubane: functionalisation

3-(Methoxycarbonyl)cubane-1-carboxylic acid (119)
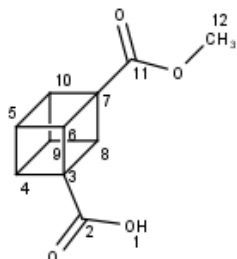
a) **Selective deprotection of the diester 75 with NaOH** (Reekie *et al.*, 2019)

Diester **75** (50 mg, 0.2 mmol, 1.0 eq.) was resuspended in THF (5 mL) and a solution of NaOH in MeOH (113 µL of 2M NaOH in MeOH, 0.2 mmol, 1.0 eq.) was added dropwise. The resulting mixture was stirred for 16 h at room temperature, then concentrated to remove the solvent, resuspended in H$_2$O (5 mL) and extracted with DCM (5 mL). It was then acidified to pH 1 with HCl and extracted with DCM (2 × 5 mL), and finally extracted with EtOAc (3 × 5 mL). The crude product was purified by flash column chromatography on silica gel using 100% DCM to elute the diester **75** (9 mg, 0.04 mmol, 18%) and 1% MeOH in DCM for the product. The fractions containing **119** were concentrated under reduced pressure to afford the product (7 mg, 0.04 mmol, 14%) a white oil/solid. Enough material was recovered under these conditions for a proton NMR, but not a carbon NMR.

b) **Selective esterification of the diacid 68 with Meerwein's salt** (Raber *et al.*, 1979)

Diacid **68** (215 mg, 1.1 mmol, 1.0 eq.) and Me$_3$OBF$_4$ (212 mg, 1.1 mmol, 1.0 eq.) were placed in an oven dried flask under N$_2$ with dry DCM (2 mL). DIPEA (145 µL, 1.1 mmol, 1.0 eq.) was then added at r.t. and the reaction was stirred at r.t. for 18 h. The reaction mixture was then washed with 1M HCl (10 mL). The aqueous layer was extracted with EtOAc (2 × 10 mL). The combined organic layer was washed with brine (10 mL) and dried over MgSO$_4$. The solvent was removed under reduced pressure and the crude product

was purified by column chromatography on silica gel twice using 1.5% MeOH in DCM to afford the product **119** (28 mg, 0.14 mmol, 12%) as a white solid.

c) **Selective esterification of the diacid 68 by DCC coupling reaction** (Neises *et al.*, 1978)

Diacid **68** (80 mg, 0.39 mmol, 1.0 eq.) was dissolved in anhydrous DMF (1 mL) under nitrogen. DMAP (5 mol%) was added followed by MeOH (15 μL, 0.39 mmol, 1.0 eq.). The reaction mixture was cooled to 0 °C and DCC (80 mg, 0.39 mmol, 1.0 eq.) was added portion-wise. The reaction was slowly warmed to room temperature (the ice bath was left to melt slowly overnight) and stirred overnight. The precipitated urea was filtered off and the filtrate was concentrated under reduced pressure. The crude product was purified by column chromatography on silica gel twice using 1.5% MeOH in DCM to afford the product **119** (20 mg, 0.10 mmol, 25%) as a white solid.

TLC: R_f = 0.20 (1:9 MeOH/DCM); ammonium molybdate.

^{1}H NMR (400 MHz, CDCl$_3$): δ (ppm) = 4.55-4.50 (m, 2H, H5 or H9), 4.32-4.22 (m, 2H, H6 or H8), 4.08-4.02 (m, 2H, H10 or H4), 3.72 (s, 3H, H12).

^{13}C NMR (101 MHz, CDCl$_3$): δ (ppm) = 176.2 (C2), 171.6 (C11), 53.3 (C3 or C7), 51.8 (C12), 51.1 (C5 or C9), 49.9 (C3 or C7), 49.9 (C6 or C8), 42.9 (C10 or C14).

IR (ATR): ν (cm^{-1}) = 2994, 2954, 1716 (s, C=O).

Tert-Butyl N-{1'-bromospiro[1,3-dioxolane-2,9'-pentacyclo[4.3.0.0^{2,5}.0^{3,8}.0^{4,7}]nonan]-5'-yl}carbamate (120) and 1,3-Bis({1'-bromospiro[1,3-dioxolane-2,9'-pentacyclo[4.3.0.0^{2,5}.0^{3,8}.0^{4,7}]nonan]-5'-yl})urea (121) (Nicolaou *et al.*, 2016)
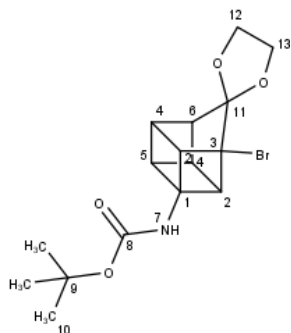
120 and **121** were synthesised following general procedure **E** for the Curtius rearrangement from **73** (200 mg, 0.7 mmol, 1.0 eq.). Purification by flash column chromatography on silica gel using 2% MeOH in DCM gave the product **120** (125 mg, 0.3 mmol, 50%) as a white solid and urea **121** (37 mg, 0.1 mmol, 10%) as a white solid.

Data for carbamate **120**:

m.p.: 120–121 °C

TLC: R_f = 0.60 (5:95 MeOH/DCM); KMnO$_4$.

^{1}H NMR (400 MHz, CDCl$_3$): δ (ppm) = 5.19 (br s, 1H, H7), 4.29-4.22 (m, 2H, H12 or H13), 4.04-3.96 (m, 2H, H12 or H13), 3.76-3.36 (m, 5H, H2, H4, and H6), 2.89 (t, 1H, *J* = 5.4 Hz, H5), 1.47 (s, 9H, H10).

^{13}C NMR (101 MHz, CDCl$_3$): δ (ppm) = 125.6 (C8), 80.1 (C9 or C11), 80.2 (C9 or C11), 66.1 (C12 and C13), 61.1 (C3), 59.2 (C1), 54.8 (C2 or C4 or C6), 42.3 (C5), 37.6 (C2 or C4 or C6), 28.3 (C10).

IR (ATR): ν (cm^{-1}) = 3336, 2980, 2892, 1703 (s, C=O).

HRMS (APCI): *m/z* calculated for: C$_{16}$H$_{20}$NO$_3$^{79}Br [M-Boc-H]$^-$, 224.9800, found: 224.0319.

Data for urea **121**:
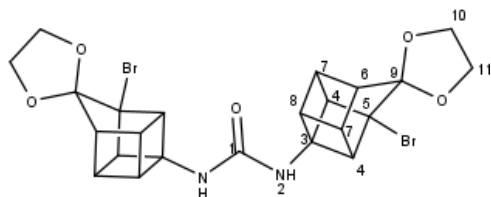
m.p.: 220–222 °C (decomposed)

TLC: R_f = 0.30 (5:95 MeOH/DCM); KMnO$_4$.

^{1}H NMR (400 MHz, CDCl$_3$): δ (ppm) = 5.30-5.19 (br m, 2H, H2), 4.31-4.22 (m, 4H, H12 or H13), 4.06-3.96 (m, 4H, H12 or H13), 3.78-3.73 (m, 4H, H2), 3.66-3.61 (m, 2H, H6), 3.55-3.48 (m, 4H, H4), 2.88 (t, 2H, J = 4.2 Hz, H8).

^{13}C NMR (101 MHz, CDCl$_3$): δ (ppm) = 154.8 (C1), 125.5 (C9), 66.1 (C12, C13), 62.5 (C3 or C6), 61.5 (C6), 55.0 (C4), 47.4 (C3 or C5), 42.1 (C8), 37.8 (C7).

IR (ATR): ν (cm^{-1}) = 3345, 2993, 2890, 1627 (s, C=O), 1546.

HRMS (APCI): m/z calculated for: C$_{23}$H$_{22}$N$_2$O$_5$^{79}Br$_2$ [M+H]$^+$, 564.9968, found: 564.9976.

Tert-Butyl N-{8-bromo-9-oxopentacyclo[4.3.0.0^{2,5}.0^{3,8}.0^{4,7}]nonan-4-yl}carbamate (122)
(Nicolaou _et al._, 2016)
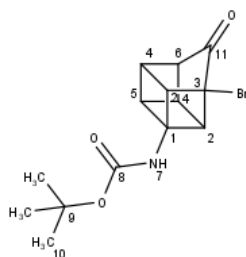
122 was synthesised following general procedure **E** for the Curtius reaction from **74** (50 mg, 0.2 mmol, 1.0 eq.). The crude was purified by column chromatography on silica gel using 2% MeOH in DCM and gave the product **122** (20 mg, 0.06 mmol, 31%) as a white/beige wet solid. The low yield was due to the impurities in the **74** and the collection of only very pure fractions.

TLC: R_f = 0.45 (5:95 MeOH/DCM); KMnO$_4$.

^{1}H NMR (400 MHz, d_6-DMSO): δ (ppm) = 3.81-3.66 (m, 3H, H2 or H4 or H6), 3.63-3.50 (m, 2H, H2 or H4 or H6), 3.09-3.07 (m, 1H, H5), 1.39 (s, 9H, H10).

^{13}C NMR (101 MHz, d_6-DMSO): δ (ppm) = 211.0 (C11), 155.1 (C8), 80.6 (C9), 64.2 (C1 or C3), 59.9 (C1 or C3), 51.9 (C2 or C4), 50.8 (C6), 38.4 (C2 or C4), 35.1 (C5), 28.3 (C10)

IR (ATR): ν (cm^{-1}) = 3821, 2980, 1761 (s, C=O), 1699 (s, C=O).

HRMS (APCI): m/z calculated for: $C_{14}H_{16}NO_3{}^{79}Br$ [M-Boc+H]$^+$, 270.0104, found: 270.0107.

6.4.4 1,2-Disubsituted cubane: first synthetic route

[(Prop-2-yn-1-yloxy)methyl]benzene (125) (Chandankar *et al.*, 2020)
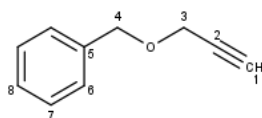
A solution of NaH (1.5 mg, 36.0 mmol, 1.2 eq., 60% w/w dispersion in mineral oil) in THF was prepared in a dry flask under argon and a solution of propargyl alcohol **135** (1.7 g, 30.0 mmol, 1.0 eq.) in THF was added dropwise at 0 °C. It was stirred at 0 °C for 1 h. Then, benzyl bromide **134** (3.9 mL, 33.0 mmol, 1.1 eq.) was added dropwise and the reaction mixture was stirred at room temperature overnight. The reaction was quenched with NH$_4$Cl (50 mL). The aqueous layer was extracted with EtOAc (3 × 80 mL). The combined organic phase was washed with water (80 mL) and brine (80 mL), dried over Na$_2$SO$_4$ and concentrated under reduced pressure. The crude was purified by column

chromatography on silica gel using 5% EtOAc in hexane to afford the product **125** (4.2 g, 28.4 mmol, 95%) as a colourless oil.

TLC: R_f = 0.35 (5:95 EtOAc/Hexane); KMnO$_4$.

^{1}H NMR (400 MHz, CDCl$_3$): δ (ppm) = 7.41-7.30 (m, 5H, H6 or H7 or H8), 4.65 (s, 2H, H4), 4.21 (d, 2H, J = 2.4 Hz, H3), 2.50 (t, 1H, J = 2.4 Hz, H1).

^{13}C NMR (101 MHz, CDCl$_3$): δ (ppm) = 137.3 (C5), 128.5 (C6 or C7), 128.2 (C6 or C7), 127.9 (C8), 79.7 (C2), 74.6 (C1), 71.6 (C3), 57.1 (C4).

IR (ATR): ν (cm^{-1}) = 3289, 3030, 2855, 2120 (w, C≡C).

Spectral data matched those reported in the literature.

1H,3H-Cycloocta[c]furan (126)
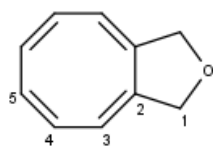
A solution of benzyl propargyl ether **125** (C = 10 mM, 87.7 mg, 0.6 mmol, 1.0 eq.) was prepared in dry hexane (60 mL) in a quartz tube under argon. Argon was bubbled for 10 min and it was irradiated at 254 nm. The reaction was followed by ^{1}H NMR with solvent suppression. The reaction reached 80% conversion at 7 h and did not progress thereafter, so it was stopped and concentrated under reduced pressure and purified by column chromatography on silica gel and eluted with a gradient of 0-10% petroleum ether in chloroform. The fractions containing the products were combined and concentrated under reduced pressure to give the product **126** (55 mg, 0.4 mmol, 62%) as a yellow oil.

TLC: R_f = 0.30 (2:8 petroleum ether/chloroform); KMnO$_4$.

^{1}H NMR (400 MHz, CDCl$_3$): δ (ppm) = 5.93-5.87 (m, 2H, H3 or H4 or H5), 5.68-5.59 (m, 4H, H3 or H4 or H5), 4.58 (s, 4H, H1).

^{13}C NMR (101 MHz, CDCl$_3$): δ 136.9 (ppm) = (C2), 134.4 (C3 or C4 or C5), 132.6 (C3 or C4 or C5), 126.0 (C3 or C4 or C5), 78.0 (C1).

IR (ATR): ν (cm^{-1}) = 3030, 2855.

HRMS: product not stable.

6.4.5 1,2-Disubsituted cubane: second synthetic route

5-Phenylpent-1-yn-3-ol (143) (Ye *et al.*, 2010; Hilpert *et al.*, 2019)
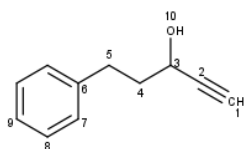
Ethynylmagnesium bromide **142** (24.2 mL of 0.37 M solution in THF, 8.9 mmol, 1.2 eq.) was added to a microwave vial under argon and cooled to 0 °C. 3-Phenylpropanal **141** (1.0 mL, 7.5 mmol, 1 eq.) was then added dropwise to the solution. The resulting mixture was allowed to warm to room temperature and stirred for 2 h. After full consumption of the starting material (by TLC analysis), H$_2$O (10 mL) was added, and the mixture was extracted with Et$_2$O (2 × 10 mL). The organic phase was washed twice with brine (2 × 10 mL), dried over Na$_2$SO$_4$ and concentrated to afford the crude product as a yellow oil. The crude product was purified by column chromatography on silica gel using a 4:1 mixture of hexane and Et$_2$O. The fractions with the product were combined and concentrated to afford the product **143** (1.0 g, 6.2 mmol, 84%) as a very light-yellow oil.

TLC: R_f = 0.20 (4:1 hexane/Et$_2$O); UV, *p*-anisaldehyde.

^{1}H NMR CDCl$_3$ (400 MHz): δ (ppm) = 7.35-7.28 (m, 2H, H9), 7.27-7.8 (m, 3H, H7 or H8), 4-4.36 (dd, 1H, J = 6.6, 2.1 Hz, H3), 2.82 (t, 2H, *J* = 7.9 Hz, H5), 7.52 (d, 1H, *J* = 2.1 Hz, H10), 2.11-2.02 (m, 2H, H4), 1.98-1.90 (m, 1H, H1).

^{13}C NMR CDCl$_3$ (101 MHz): δ (ppm) = 141.1 (C6), 128.5 (C7 or C8), 128.5 (C7 or C8), 126.1 (C9), 84.7 (C2), 73.4 (C1), 61.6 (3), 39.1 (C4), 31.3 (C5).

IR (ATR): ν (cm^{-1}) = 3532 (w, OH), 3358, 3288, 2928, 2863, 2100 (w, C≡C).

Spectral data matched those reported in the literature.

1H,2H,3H-Cyclopenta[8]annulen-1-ol (144)
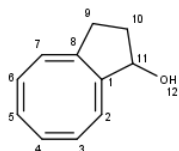
5-Phenylpent-1-yn-3-ol **143** (16 mg, 0.1 mmol, 1.0 eq.) was dissolved in hexane (10 mL) at a concentration of 10 mM in a photoreaction vial under argon and the solution was purged with argon for 15 minutes and then irradiated at 254 nm at room temperature for 7 h. The reaction was followed by ^{1}H NMR spectroscopy with solvent suppression and the maximum conversion was of 50% at 7 h irradiation. The photoproduct was hard to isolate as it degraded upon concentrating the solution from the photoreaction. Only a small amount was recovered after purification by column chromatography on silica gel eluting with 5% EtOAc in hexane. A small amount of product **144** (2.0 mg, 0.1 mmol, 13%) was recovered which was only enough for a proton NMR.

TLC: R_f = 0.20 (4:1 hexane/EtOAc); UV, KMnO$_4$.

^{1}H NMR CDCl$_3$ (400 MHz): δ (ppm) = 5.91-5.78 (m, 1H, H2 or H3 or H4 or H5 or H6 or H7), 5.86-5.81 (m, 2H, H2 or H3 or H4 or H5 or H6 or H7), 5.76-5.66 (m, 3H, H2 or H3 or H4 or H5 or H6 or H7), 4.67-4.59 (m, 1H, H11), 2.50-2.36 (m, 2H, H9 or H10), 2.29-2.20 (m, 1H, H9 or H10), 1.88-1.78 (m, 1H, H9 or H10), 1.50 (d, 1H, J = 7.4 Hz, H12).

^{13}C NMR (101 MHz, CDCl$_3$): δ (ppm) = it was not possible to isolate enough material to obtain ^{13}C NMR data.

IR (ATR): ν (cm^{-1}) = 3450 (w, OH), 2960.

HRMS: Product not stable

1H,2H,3H-Cyclopenta[8]annulen-1-on (146)
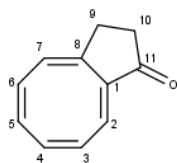
144 was used directly from the previous step to avoid decomposition. **144** (70 mg, 0.4 mmol, 1.0 eq.) was resuspended in dry DCM (4 mL) under argon. Dess-Martin periodinane (222 mg, 0.5 mmol, 1.2 eq.) was then added. After full consumption of the starting material (by TLC analysis) after 2 h, sat. NaHCO$_3$ (5 mL) and sat. Na$_2$S$_2$O$_3$ (5 mL) were added to the reaction and the mixture was stirred for 2 h. It was then extracted with DCM (3 × 5 mL) and washed once with NaHCO$_3$ (5 mL), dried over Na$_2$SO$_4$ and concentrated to afford a crude mixture of degradation product, desired product **146** and the ynone product resulting from oxidation of left-over **143** from the previous step. The crude product was purified by column chromatography on silica gel using 2% EtOAc in hexane to remove the ynone product and 7% EtOAc in hexane to give the product **146** (10 mg, 0.06 mmol, 15%) as a light-yellow oil.

TLC: R_f = 0.25, (3:2 hexane/EtOAc); UV, KMnO$_4$.

^{1}H NMR (400 MHz, CDCl$_3$): δ (ppm) = 6.14-6.09 (m, 1H, H2 or H3 or H4 or H5 or H6 or H7), 5.70-5.60 (m, 4H, H2 or H3 or H4 or H5 or H6 or H7), 5.25 (dd, 1H, J = 10.8, 1.0 Hz, H2 or H3 or H4 or H5 or H6 or H7), 2.45 (t, 2H, J = 8.0 Hz, H10), 1.97-1.91 (m, 2H, H9).

^{13}C NMR (101 MHz, CDCl$_3$): δ (ppm) = not enough material isolated.

IR (ATR): ν (cm^{-1}) = 3009, 2924, 1798 (s, C=O).

HRMS: Product not stable

Ethyl 2-benzoylpent-4-ynoate (151) (Queignec *et al.*, 1988; Chaisan *et al.*, 2021)
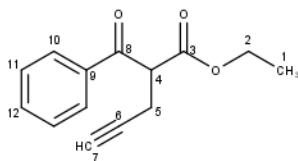
To a solution of ethyl benzoylacetate **150** (471 µL, 2.73 mmol, 1.03 eq.) in tetrahydrofuran (15 mL) was added propargyl bromide **149** (200 µL, 2.66, 1.00 eq.), K_2CO_3 (566 mg, 4.10 mmol, 1.50 eq.) and NaI (102 mg, 0.68 mmol, 0.25 eq.) under argon. The resulting mixture was stirred overnight at r.t.. After full consumption of the starting material (by TLC analysis), the suspension was then diluted with water (5 mL). The aqueous phase was extracted three times with EtOAc (3 × 5 mL), and the combined organic phases were washed with brine (5 mL), dried over Na_2SO_4 and concentrated under reduced pressure. The crude product was purified by column chromatography on silica gel using 5% EtOAc in hexane to afford the product **151** (400 mg, 1.8 mmol, 65%) as a colourless oil.

TLC: R_f = 0.50 (2:3 EtOAc/Hexane); UV, *p*-anisaldehyde, $KMnO_4$.

^{1}H NMR (400 MHz, CDCl$_3$): δ (ppm) = 8.08-8.03 (m, 2H, H11), 7.65-7.59 (m, 1H, H12), 7.54-7.49 (m, 2H, H10), 4.57 (t, 1H, *J* = 7.4 Hz, H4), 4.22-4.15 (m, 2H, H2), 3.00-2.84 (m, 2H, H5), 1.95 (t, 1H, *J* = 2.6 Hz, H7), 1.17 (t, 3H, *J* = 7.1 Hz).

^{13}C NMR (101 MHz, CDCl$_3$): δ (ppm) = 193.3 (C8), 168.3 (C3), 135.9 (9), 133.8 (C12), 128.9 (C10 or C11), 128.8 (C10 or C11), 87.4 (C6), 70.4 (C7), 61.5 (C2), 53.2 (C4), 18.4 (C5), 13.9 (C1).

IR (ATR): ν (cm^{-1}) = 3293, 2984, 1737 (s, C=O), 1685 (s, C=O).

Spectral data matched those reported in the literature.

1-Phenylpent-4-yn-1-one (152)
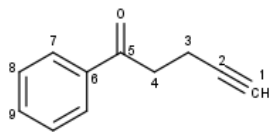
Ethyl 2-benzoylpent-4-ynoate **151** (400 mg, 1.7 mmol, 1 eq.) was resuspended in MeOH and water (1:1 solution, 10 mL). KOH (263 mg, 4.7 mmol, 2.8 eq.) was added and the resulting mixture was stirred at r.t.. After full consumption of the starting material (by TLC analysis) after 3 h, the reaction was then diluted with water (5 mL). The aqueous phase was extracted three times with EtOAc (3 × 5 mL), and the combined organic phases were washed with brine, dried over Na_2SO_4 and concentrated under reduced pressure. The crude product was purified by column chromatography on silica gel using 3% EtOAc in hexane to afford the product **152** (79.3 mg, 0.5 mmol, 29%) as a white solid.

TLC: R_f = 0.55 (2:3 EtOAc/Hexane); UV, *p*-anisaldehyde (purple spot), KMnO₄.

^{1}H NMR (400 MHz, CDCl₃): δ (ppm) = 8.03-7.98 (m, 2H, H7 or H8), 7.63-7.58 (m, 1H, H9), 7.53-7.47 (m, 2H, H7 or H8), 3.28-3.23 (m, 2H, H4), 2.67-2.63 (m, 2H, H3), 1.98 (t, 1H, *J* = 2.6 Hz, H1).

^{13}C NMR (101 MHz, CDCl₃): δ (ppm) = 197.7 (C5), 136.5 (C6), 133.3 (C9), 128.7 (C7 or C8), 128.0 (C7 or C8), 83.3 (C2), 68.8 (C1), 37.6 (C4), 13.2 (C3).

IR (ATR): ν (cm^{-1}) = 3293, 1687 (s, C=O), 1206, 744, 690.

Spectral data matched those reported in the literature.

1-Phenylpent-4-yn-1-ol (153)
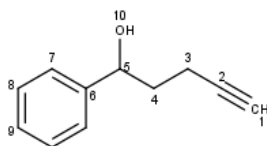
1-phenylpent-4-yn-1-one **152** (69 mg, 0.4 mmol, 1 eq.) was suspended in EtOH (1.5 mL)

in a flask under argon. Dry MeOH (5 drops) was added, followed by NaBH$_4$ (19 mg, 0.5 mml, 1.1 eq.) and the resulting mixture was stirred at room temperature. After full consumption of the starting material (by TLC analysis) after 1 h, the reaction was diluted with water (5 mL). The aqueous phase was extracted with EtOAc (3 × 5 mL), and the combined organic phases were washed with brine (5 mL), dried over Na$_2$SO$_4$ and concentrated under reduced pressure. The crude product was purified by column chromatography on silica gel using 10% EtOAc in hexane to afford the product **153** (58.5 mg, 0.37 mmol, 83%) as a colourless oil.

TLC: R_f = 0.50 (2:3 EtOAc/Hexane); UV, *p*-anisaldehyde (dark purple spot), KMnO$_4$.

^{1}H NMR (400 MHz, CDCl$_3$): δ (ppm) = 7.39-7.33 (m, 4H, H7 and H8), 7.33-7.27 (m, 1H, H9), 4.90-4.84 (m, 1H, H5), 2.42-2.32 (m, 1H, H3), 2.30-2.21 (m, 1H, H3), 2.06-1.96 (m, 3H, H4, H1 and H10), 1.95-1.86 (m, 1H, H4).

^{13}C NMR (101 MHz, CDCl$_3$): δ (ppm) = 144.0 (C6), 128.6 (C7 or C8), 127.8 (C9), 125.8 (C7 or C8), 83.9 (C2), 73.2 (C5), 69.0 (C1), 37.4 (C3), 15.2 (C4).

IR (ATR): ν (cm^{-1}) = 3367, 3294, 2924, 2117 (w, C≡C).

Spectral data matched those reported in the literature.

6.4.6 1,2-Disubsituted cubane: third synthetic route

Dimethyl cyclooctatetraene-1,8-dicarboxylate (159) (Grovenstein *et al.*, 1961; Bryce-Smith *et al.*, 1963)
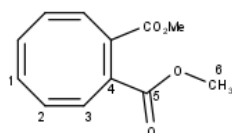
Dimethyl acetylenedicarboxylate **157** (2.5 mL, 20.0 mmol, 1 eq.) was dissolved in benzene **156** (200 mL, C = 100 mM). The resulting solution was transferred into four oven-dried quartz phototubes, purged with argon for 15 min and irradiated at 254 nm for 48 h. The

solvent was removed under reduced pressure to afford a yellow crude product and excess dimethyl acetylenedicarboxylate **157**. The crude product was purified by column chromatography on silica gel using 10% ethyl acetate in hexane to give the product **159** (2.0 g, 9.1 mmol, 45%) as a yellow solid.

m.p.: 95–97 °C (lit. (Bryce-Smith *et al.*, 1963), 109.5–110.5 °C).

TLC: R_f = 0.35 (7:3 hexane/EtOAc); UV and KMnO$_4$.

^{1}H-NMR (400 MHz, CDCl$_3$): δ (ppm) = 7.21 (d, 2H, *J* = 3.4 Hz, H3), 6.10-6.03 (m, 2H, H2), 5.99-5.94 (m, 2H, H1), 3.73 (s, 6H, H3).

^{13}C-NMR (101 MHz, CDCl$_3$): δ (ppm) = 165.9 (C5), 143.1 (C3), 132.7 (C1), 132.0 (C4), 130.1 (C2), 52.1 (C6).

IR (ATR): ν(cm^{-1}) = 3009, 2952, 1712 (s, C=O).

HRMS (APCI): *m/z* calculated for: C$_{12}$H$_{12}$O$_4$ [M+H]$^+$, 221.0808, found: 221.0815.

[(1Z,3Z,5Z,7Z)-2-(Hydroxymethyl)cycloocta-1,3,5,7-tetraen-1-yl]methanol (160) and 1H,3H,4H,9H-cycloocta[c]furan-1-one (167)

Data for **160**:
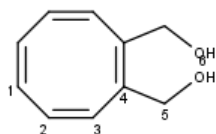
Reduction of **159** with LiAlH$_4$ (Grange *et al.*, 2010)

Dimethyl cyclooctatetraene-1,8-dicarboxylate **159** (40 mg, 0.2 mmol, 1.0 eq.) was dissolved in dry THF (1 mL) in a vial under argon and cooled to 0 °C. LiAlH$_4$ (15.9 mg, 0.42 mmol, 2.2 eq.) was added. The mixture was allowed to warm to r.t. and it was stirred overnight. A few drops of water were added, and the mixture was diluted with EtOAc (5 mL). The precipitate was filtered and the filtrate was dried over MgSO$_4$ and concentrated

under reduced pressure to afford the crude product. The crude product was purified by column chromatography on silica with 20% EtOAc in hexane to isolate some product **160** (8 mg, 0.05 mmol, 27%) for characterisation as a light-yellow oil, however it was not stable on silica. The presence of a side product **167** (19 mg, 0.1 mmol, 64%) was observed. The formation of **167** was not prevented after trying different conditions: changing the order of addition, the temperature, the equivalents of reducing agents. The side product **167** (25-64% depending on the conditions as detailed in the results and discussion) was obtain as a white solid.

Data for **167**:
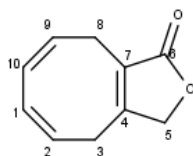
TLC: R_f = 0.30 (1:1 heptane/EtOAc); KMnO$_4$.

^{1}H-NMR (400 MHz, CDCl$_3$): δ (ppm) = 6.32 (ddd, 1H, J = 10.5, 2.7, 1.0 Hz, H1 or H10), 6.24 (ddd, 1H, J = 10.5, 2.7, 1.0 Hz, H1 or H10), 5.70-5.52 (m, 2H, H2 and H9), 4.66 (sept, 2H, J = 1.0 Hz, H5), 3.00-2.96 (m, 4H, H3, H8).

^{13}C-NMR (101 MHz, CDCl$_3$): δ (ppm) = 174.3 (C6), 158.8 (C4), 131.8 (C10 or C1), 130.2 (C10 or C1), 125.0 (C9 or C2), 124.9 (C7), 121.8 (C9 or C2), 71.8 (C5), 26.3 (C3 or C8), 22.4 (C3 or C8).

IR (ATR): ν(cm^{-1}) = 3015, 2927, 1742 (s, C=O lactone).

HRMS (APCI): m/z calculated for: C$_{10}$H$_{10}$O$_2$ [M+H]$^+$, 163.0754, found: 163.0746.

a) Reduction of **159** with DIBAL-H

The starting material **159** (100 mg, 0.5 mmol, 1.0 eq.) was suspended in dry THF (5 mL). The solution was cooled to 0 °C, and DIBAL-H (2.05 mL of a 1 M solution in THF, 2.3 mmol, 4.5 eq.) was added dropwise over 15 min. The reaction was stirred for 1h30, then one more equivalent of DIBAL-H was added, and the reaction was stirred for another 30 min.

After full consumption of the starting material (by TLC analysis), the reaction was quenched with sat. aq. NH_4Cl and diluted with H_2O (5 mL). The mixture was extracted with EtOAc (3 × 30 mL), dried over $MgSO_4$ and concentrated to afford the crude product **160** as a yellow oil (quantitative).

Data for **160**:

TLC: R_f = 0.80 (1:1 heptane/EtOAc); $KMnO_4$.

^{1}H-NMR (400 MHz, $CDCl_3$): δ (ppm) = 6.00-5.95 (m, 2H, H3), 5.90-5.83 (m, 4H, H2 and H1), 4.28 (d, 2H, J = 12.5 Hz, H5), 4.16 (d, 2H, J = 12.5 Hz, H5).

^{13}C-NMR (101 MHz, $CDCl_3$): δ (ppm) = 143.4 (C4), 131.4 (C1), 130.9 (C3), 130.5 (C2), 65.8 (C5).

IR (ATR): $v(cm^{-1})$ = 3380 (w, OH), 2972, 2920, 2868.

HRMS: product not stable.

[(1Z,3Z,5Z,7Z)-2-[(Acetyloxy)methyl]cycloocta-1,3,5,7-tetraen-1-yl]methyl acetate (161) (Grange *et al.*, 2010)
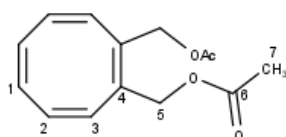
160 (174 mg, 1.1 mmol, 1.0 eq.) was suspended in dry pyridine (2.5 mL) under argon. Dimethylaminopyridine (DMAP) (5.9 mg, 0.05 mmol, 0.06 eq.) and acetic anhydride (242 µL, 2.5 mmol, 2.4 eq.) were added and the mixture was stirred at r.t. for 7 h. After full consumption of the starting material (by TLC analysis), the reaction mixture was poured into ice, and extracted with petroleum ether (3 × 15 mL). The organic layer was washed with 1M HCl (15 mL), water (15 mL) and $NaHCO_3$ (15 mL), then dried over $MgSO_4$ and concentrated under reduced pressure to give the crude product. The crude product was

purified by column chromatography on silica gel using 10% EtOAc in hexane to afford the product **161** (160 mg, 0.6 mmol, 66%) as a light-yellow oil.

TLC: R_f = 0.40 (7:3 heptane/EtOAc); UV, KMnO$_4$, *p*-anisaldehyde.

^{1}H-NMR (400 MHz, CDCl$_3$): δ (ppm) = 6.01 (br s, 2H, H3), 5.87 (br s, 4H, H1, H2), 4.71 (d, 2H, *J* = 12.9 Hz, H5), 4.55 (d, 2H, *J* = 12.9 Hz, H5), 2.07 (s, 6H, H7).

^{13}C-NMR (101 MHz, CDCl$_3$): δ (ppm) = 170.6 (C6), 137.8 (C4), 132.3 (C3), 131.7 (C2), 130.4 (C1), 65.7 (C5), 21.0 (C7).

IR (ATR): ν(cm^{-1}) = 3006, 2946, 1738 (C=O).

7,8-Diphenyl 3,4-bis[(acetyloxy)methyl]-7,8-diazatricyclo[4.2.2.0^{2,5}]deca-3,9-diene-7,8-dicarboxylate (162a)
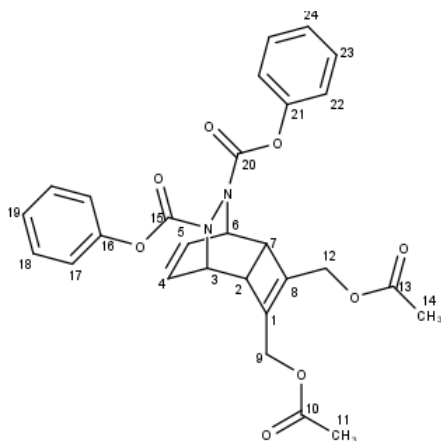
162a was prepared following general procedure **F** from **161** (42 mg, 0.17 mmol, 1.0 eq.) and diphenyl azodicarboxylate (54 mg, 0.2 mmol, 1.2 eq.). The crude product was purified by column chromatography on silica gel using a ratio of 8:2 hexane in EtOAc to afford **162a** (40 mg, 0.08 mmol, 45%) as a colourless oil.

TLC: R_f = 0.35 (1:1 heptane/EtOAc); UV + KMnO$_4$.

^{1}H-NMR (400 MHz, CDCl$_3$): δ (ppm) = 7.42-7.30 (m, 4H, H17, H18, H19, H22, H23 or H24), 7.27-7.21 (m, 2H, H17, H18, H19, H22, H23 or H24), 7.19-7.07 (m, 4H, H17, H18, H19, H22,

H23 or H24), 6.57-6.49 (m, 1H, H4 or H5), 6.27 (td, 1H, H4 or H5), 5.33-5.23 (m, 1H, H3 or H6), 5.22-5.17 (m, 1H, H3 or H6), 4.67-4.47 (m, 4H, H9, H12), 3.40-3.28 (m, 1H, H2 or H7), 3.28-3.17 (m, 1H, H2 or H7), 2.15-2.10 (m, 6H, H11, H14).

^{13}C-NMR (101 MHz, CDCl$_3$): δ (ppm) = broad peaks 170.4 (C10, C13), 151.0 (C15, C20), 142.4 (C16, C21), 129.4 (C17, C18, C19, C22, C23 or C24, C1, C8), 125.9 (C4, C5), 125.9 (C17, C18, C19, C22, C23 or C24), 125.8 (C17, C18, C19, C22, C23 or C24), 121.5 (C17, C18, C19, C22, C23 or C24), 121.3 (C17, C18, C19, C22, C23 or C24), 59.0 (C9 or C12), 58.8 (C9 or C12), 55.2 (H3 or H6), 54.0 (H3 or H6), 37.2 (C2 or C7), 36.3 (C2 or C7), 20.8 (C11 or C14), 20.7 (C11 or C14).

^{1}H and ^{13}C NMR have broad peaks due to rotamers. Due to time constraints, other solvents such as DMSO or other temperatures to run the NMR analysis have not been tried yet.

IR (ATR): v(cm^{-1}) = 3065, 2935, 1735 (s, C=O), 1716 (s, C=O).

HRMS (ESI): *m/z* calculated for: C$_{28}$H$_{26}$N$_2$O$_8$Na [M+Na]$^+$, 541.1581, found: 541.1562.

7,8-Diethyl 3,4-bis[(acetyloxy)methyl]-7,8-diazatricyclo[4.2.2.0^{2,5}]deca-3,9-diene-7,8-dicarboxylate (162b)
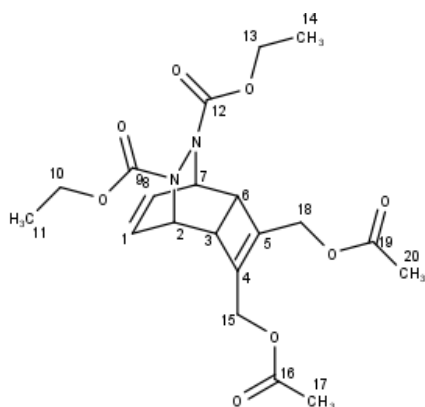
162b was prepared following general procedure **F** from **161** (42 mg, 0.17 mmol, 1.0 eq.) and diethyl azodicarboxylate (35 mg, 0.2 mmol, 1.2 eq.). The crude product was purified

by column chromatography on silica gel using a ratio of 7:3 hexane in EtOAc to afford **162b** (39 mg, 0.1 mmol, 54%) as a colourless oil.

TLC: R_f = 0.25 (1:1 heptane/EtOAc); UV, KMnO$_4$.

^{1}H-NMR (400 MHz, CDCl$_3$): δ (ppm) = 6.36-6.28 (m, 1H, H1 or H8), 6.14-6.05 (m, 1H, H1 or H8), 5.14-4.90 (m, 2H, H2, H7), 4.60-4.41 (m, 4H, H15, H18), 4.33-4.08 (m, 4H, H10, H13), 3.23-2.85 (m, 2H, H3, H5), 2.11-2.06 (m, 6H, H17, H20), 1.34-1.20 (m, 6H, H11, H14).

^{13}C-NMR (101 MHz, CDCl$_3$): δ (ppm) = broad peaks 170.4 (C16 or C19), 170.3 (C16 or C19), 158.9 (C9 or C12), 157.2 (C9 or C12), 142.2 (C4 or C5), 141.1 (C4 or C5), 131.7 (C1 or C8), 125.5 (C1 or C8), 62.6 (C10 or C13), 62.4 (C10 or C13), 59.1 (C15 or C18), 58.8 (C15 or C18), 54.5 (C2 or C7), 53.5 (C2 or C7), 37.2 (C3 or C6), 36.4 (C3 or C6), 20.7 (C17, C20), 14.6 (C11 or C14), 14.4 (C11 or C14).

^{1}H and ^{13}C NMR have broad peaks due to rotamers. Due to time constraints, other solvents such as DMSO or other temperature to run the NMR analysis have not been tried yet.

IR (ATR): v(cm^{-1}) = 2981, 2937, 1735 (s, C=O), 1695 (s, C=O).

HRMS (ESI): *m/z* calculated for: C$_{20}$H$_{26}$N$_2$O$_8$Na [M+Na]$^+$, 445.1581, found: 445.1566.

7,8-Dibenzyl 3,4-bis[(acetyloxy)methyl]-7,8-diazatricyclo[4.2.2.0²,⁵]deca-3,9-diene-7,8-dicarboxylate (162c)
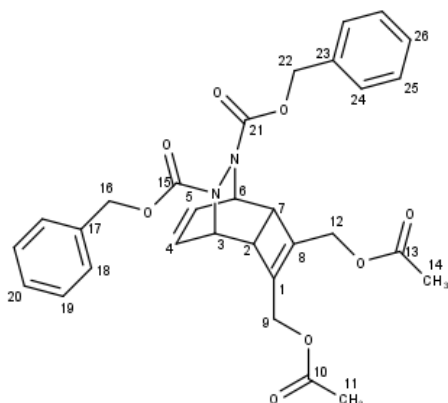
162c was prepared following general procedure **F** from **161** (45 mg, 0.18 mmol, 1.00 eq.) and dibenzyl azodicarboxylate (65 mg, 0.22 mmol, 1.20 eq.). The crude product was purified by column chromatography on silica gel using a ratio of 7:3 hexane in EtOAc to afford **162c** (58.8 mg, 0.1 mmol, 59%) as a colourless oil.

TLC: R_f = 0.25 (1:1 heptane/EtOAc); UV, KMnO₄.

^{1}H-NMR (400 MHz, CDCl₃): δ (ppm) = 7.48-7.20 (m, 10H, H18, H19, H20, H24, H25, H26), 6.30 (br s, 1H, H4 or H5), 6.11 (br s, 1H, H4 or H5), 4.37-4.82 (m, 6H, H16, H22, H3, H6), 4.63-4.38 (m, 4H, H9, H12), 2.79-2.66 (m, 1H, H2 or H7), 3.06-2.89 (m, 1H, H2 or H7), 2.08-1.93 (m, 6H, H11, H14).

^{13}C-NMR (101 MHz, CDCl₃): δ (ppm) = 170.3 (C10, C13), 157.3 (C15 or C21), 156.1 (C15 or C21), 142.3, 141.0, 136.1 (C1 or C8), 135.9 (C1 or C8), 131.8, 128.5 (C17, C18, C19, H20, C23, C24, C25, C26), 128.2 (C17, C18, C19, H20, C23, C24, C25, C26), 127.8 (C17, C18, C19, H20, C23, C24, C25, C26), 127.5 (C17, C18, C19, C20, C23, C24, C25, C26), 125.5 (C4, C4), 68.2 (C16 or C22), 67.9 (C16 or C22), 59.0 (C9 or C12), 58.9 (C9 or C12), 54.8 (C3 or C6), 54.3 (C3 or C6), 53.7 (C3 or C6), 38.1 (C2 or C7), 37.2 (C2 or C7), 36.3 (C2 or C7), 20.7 (C11, C14).

^{1}H and ^{13}C NMR have broad peaks due to rotamers. Due to time constraints, other solvents such as DMSO or other temperature to run the NMR analysis have not been tried yet.

IR (ATR): v(cm^{-1}) = 2981, 2937, 1736 (s, C=O), 1697 (s, C=O).

HRMS (ESI): *m/z* calculated for: C$_{30}$H$_{30}$N$_2$O$_8$Na [M+Na]$^+$, 547.2075, found: 547.2059.

9,10-Diphenyl 4,5-bis[(acetyloxy)methyl]-9,10-diazapentacyclo[4.4.0.0^{2,5}.0^{3,8}.0^{4,7}]decane-9,10-dicarboxylate (163a)
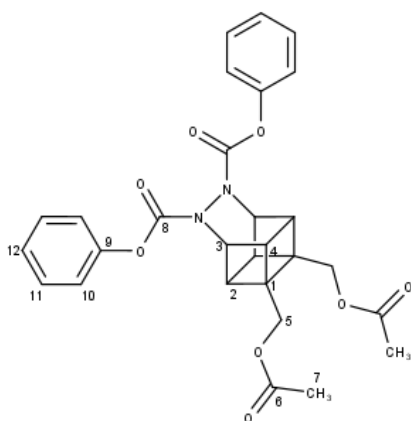
163a was prepared following general procedure **G** from **162a** (40 mg, 0.08 mmol, 1.0 eq.). Full conversion was obtained after 4h30 and the crude product was purified by column chromatography on silica gel using a ratio of 3:1 hexane in EtOAc to afford **163a** (14.1 mg, 0.03 mmol, 35%) as a thick colourless oil.

TLC: R_f = 0.25 (1:1 heptane/EtOAc); KMnO$_4$.

^{1}H-NMR (400 MHz, CDCl$_3$): δ (ppm) = 7.42-7.35 (m, 4H, H10 or H11), 7.27-7.21 (m, 2H, H12), 7.19-7.13 (m, 4H, H10 or H11), 5.11 (td, 2H, *J* = 6.5, 1.0 Hz, H3), 4.26 (br s, 4H, H5), 3.63 (dd, 2H, *J* = 13.2, 6.5 Hz, H2 or H4), 3.47 (dd, 2H, *J* = 12.5, 6.5 Hz, H2 or H4), 2.11 (s, 6H, H7).

^{13}C-NMR (101 MHz, CDCl$_3$): δ (ppm) = 170.8 (C6), 151.0 (C8), 129.4 (C9, C10 or C11), 125.2 (C12), 121.4 (C10 or C11), 61.1 (C5), 48.6 (C1), 47.5 (C3), 40.0 (C2 or C4), 37.0 (C2 or C4), 20.9 (C7).

IR (ATR): v(cm^{-1}) = 3065, 2935, 1735 (s, C=O), 1697 (s, C=O).

HRMS (ESI): *m/z* calculated for: $C_{28}H_{26}N_2O_8Na$ [M+Na]$^+$, 541.1581, found: 541.1580.

9,10-Diethyl 4,5-bis[(acetyloxy)methyl]-9,10-

diazapentacyclo[4.4.0.0^{2,5}.0^{3,8}.0^{4,7}]decane-9,10-dicarboxylate (163b)
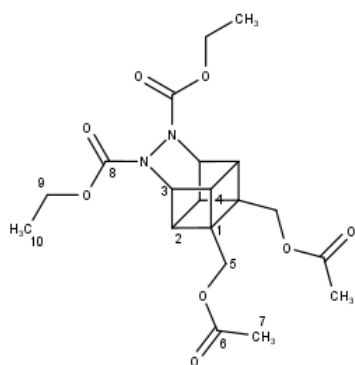
163b was prepared following general procedure **G** from **162b** (939 mg, 0.1 mmol, 1.0 eq.). Full conversion was obtained after 4h30 and the crude product was purified by column chromatography on silica gel using a ratio of 7:3 hexane in EtOAc to afford **163b** (24.4 mg, 0.06 mmol, 63%) as a white solid.

m.p.: 96–97 °C

TLC: R_f = 0.15 (1:1 heptane/EtOAc); KMnO$_4$.

^{1}H-NMR (400 MHz, CDCl$_3$): δ (ppm) = 4.87 (td, 2H, *J* = 6.5, 1.0 Hz, H3), 4.33-4.15 (m, 8H, H5, H9), 3.44 (dd, 2H, *J* = 13.2, 6.5 Hz, H2 or H4), 3.26 (dd, 2H, *J* = 12.8, 6.5 Hz, H2 or H4), 2.08 (s, 6H, H7), 1.29 (t, 6H, *J* = 7.0 Hz, H10).

^{13}C-NMR (101 MHz, CDCl$_3$): δ (ppm) = 170.8 (C6), 156.7 (C8), 62.5 (C9), 61.2 (C5), 48.3 (C1), 47.0 (C3), 39.9 (C2 or C4), 36.7 (C2 or C4), 20.8 (C7), 14.5 (C10).

IR (ATR): ν(cm^{-1}) = 3032, 2935, 1735 (s, C=O), 1698 (s, C=O).

HRMS (ESI): *m/z* calculated for: $C_{20}H_{26}N_2O_8Na$ [M+Na]$^+$, 445.1581, found: 445.1567.

9,10-Dibenzyl 4,5-bis[(acetyloxy)methyl]-9,10-

diazapentacyclo[4.4.0.0^{2,5}.0^{3,8}.0^{4,7}]decane-9,10-dicarboxylate (163c)
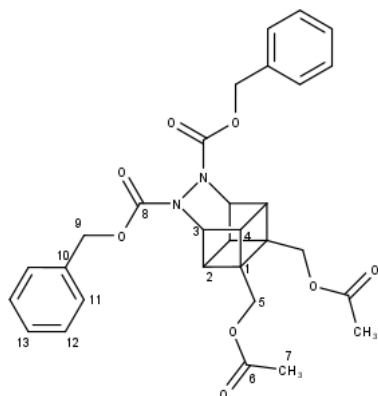
163c was prepared following general procedure **G** from **162b** (58 mg, 0.1 mmol, 1.0 eq.). Full conversion was obtained after 7 h and the crude product was purified by column chromatography on silica gel using a ratio of 7:3 hexane in EtOAc to afford **163c** (30 mg, 0.06 mmol, 52%) as a thick colourless oil.

TLC: R_f = 0.25 (1:1 heptane/EtOAc); KMnO$_4$.

^{1}H-NMR (400 MHz, CDCl$_3$): δ (ppm) = 7.38-7.30 (m, 10H, H11, H12, H13), 5.16-5.23 (m, 4H, H9), 4.90 (t, 2H, J = 6.3 Hz, H3), 4.22-4.10 (m, 4H, H5), 3.44 (dd, 2H, J = 13.4, 6.3 Hz, H2 or H4), 3.25 (dd, 2H, J = 12.9, 6.3 Hz, H2 or H4), 2.08-2.03 (m, 6H, H7).

^{13}C-NMR (101 MHz, CDCl$_3$): δ (ppm) = 170.8 (C6), 156.6 (C8), 136.0 C10), 128.5 (C11, C12 or C13), 128.2 (C11, C12 or C13), 127.8 (C11, C12 or C13), 68.0 (C9), 61.2 (C5), 48.3 (C1), 47.2 (C3), 39.9 (C2 or C4), 36.7 (C2 or C4), 20.8 (C7).

IR (ATR): ν(cm^{-1}) = 2974, 1735 (s, C=O), 1699 (s, C=O).

HRMS (ESI): *m/z* calculated for: C$_{30}$H$_{30}$N$_2$O$_8$Na [M+Na]$^+$, 547.2075, found: 547.2094.

6.4.7 X-ray diffraction data and refinement

X-Ray Crystal Structure for Carbamate **120**:
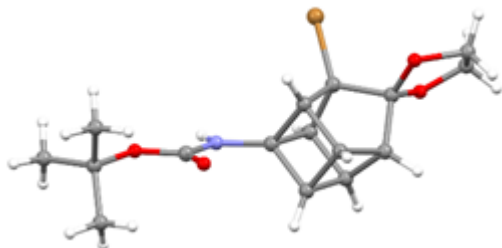
Table 6.10: Crystal data and structure refinement for **120**.

Identification code	120_auto
Empirical formula	$C_{16}H_{20}BrNO_4$
Formula weight	370.24
Temperature/K	100.00(10)
Crystal system	orthorhombic
Space group	Pbca
a/Å	13.3671(2)
b/Å	11.6951(2)
c/Å	20.1767(2)
α/°	90
β/°	90
γ/°	90
Volume/Å^3	3154.22(8)
Z	8
ρ_{calc}g/cm^3	1.559
μ/mm^{-1}	3.713
F(000)	1520.0
Crystal size/mm^3	$0.1 \times 0.08 \times 0.02$
Radiation	Cu Kα (λ = 1.54184)
2Θ range for data collection/°	8.766 to 154.12
Index ranges	$-16 \leq h \leq 16$, $-13 \leq k \leq 14$, $-25 \leq l \leq 16$
Reflections collected	16879
Independent reflections	3298 [R_{int} = 0.0476, R_{sigma} = 0.0266]
Data/restraints/parameters	3298/0/202
Goodness-of-fit on F^2	1.052
Final R indexes [I>=2σ (I)]	R_1 = 0.0551, wR_2 = 0.1400
Final R indexes [all data]	R_1 = 0.0560, wR_2 = 0.1407
Largest diff. peak/hole / e Å^{-3}	0.70/-1.35

X-Ray Crystal Structure for Urea **121**:
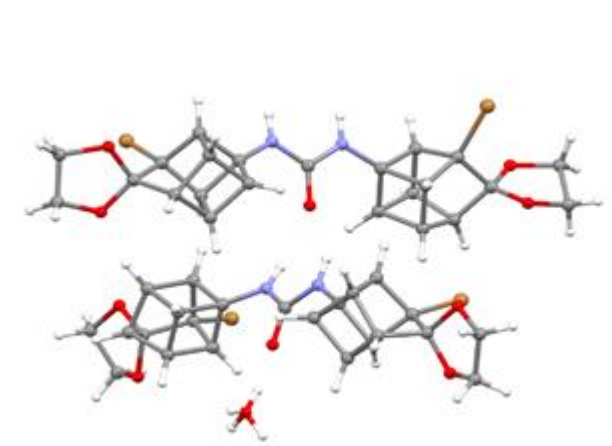
Table 6.11: Crystal data and structure refinement for **121**.

Identification code	121_auto
Empirical formula	$C_{23}H_{22.5}Br_2N_2O_{5.25}$
Formula weight	570.75
Temperature/K	99.99(10)
Crystal system	monoclinic
Space group	C2/c
a/Å	18.1229(5)
b/Å	16.1213(4)
c/Å	29.8237(8)
α/°	90
β/°	99.954(2)
γ/°	90
Volume/Å^3	8582.3(4)
Z	16
ρ_{calc}g/cm^3	1.767
μ/mm^{-1}	5.150
F(000)	4584.0
Crystal size/mm^3	$0.16 \times 0.05 \times 0.02$
Radiation	Cu Kα (λ = 1.54184)
2Θ range for data collection/°	7.388 to 148.802
Index ranges	$-22 \le h \le 21, -13 \le k \le 19, -35 \le l \le 37$
Reflections collected	20784
Independent reflections	8500 [R_{int} = 0.0702, R_{sigma} = 0.0677]
Data/restraints/parameters	8500/0/585
Goodness-of-fit on F^2	1.026
Final R indexes [I>=2σ (I)]	R_1 = 0.0748, wR_2 = 0.1919
Final R indexes [all data]	R_1 = 0.0883, wR_2 = 0.2032
Largest diff. peak/hole / e Å^{-3}	2.19/-2.57

X-Ray Crystal Structure for Carbamate **123**:
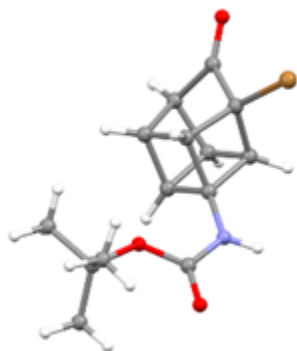
Table 6.12: Crystal data and structure refinement for **123**.

Identification code	123_auto
Empirical formula	$C_{14}H_{16}BrNO_3$
Formula weight	326.19
Temperature/K	220.00(10)
Crystal system	triclinic
Space group	P-1
a/Å	6.6870(2)
b/Å	10.3869(4)
c/Å	11.6869(4)
α/°	71.740(4)
β/°	75.633(3)
γ/°	74.499(3)
Volume/Å^3	730.74(5)
Z	2
ρ_{calc}g/cm^3	1.482
μ/mm^{-1}	3.874
F(000)	332.0
Crystal size/mm^3	$0.16 \times 0.09 \times 0.03$
Radiation	Cu Kα (λ = 1.54184)
2Θ range for data collection/°	8.098 to 153.19
Index ranges	$-8 \leq h \leq 8$, $-13 \leq k \leq 13$, $-14 \leq l \leq 14$
Reflections collected	14846
Independent reflections	3043 [R_{int} = 0.0581, R_{sigma} = 0.0356]
Data/restraints/parameters	3043/0/175
Goodness-of-fit on F^2	1.057
Final R indexes [I>=2σ (I)]	R_1 = 0.0505, wR_2 = 0.1287
Final R indexes [all data]	R_1 = 0.0518, wR_2 = 0.1301
Largest diff. peak/hole / e Å^{-3}	1.77/-0.97

X-Ray Crystal Structure for Lactone **167**:
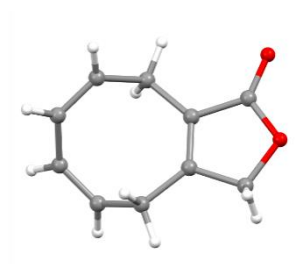
Table 6.13: Crystal data and structure refinement for **167**.

Identification code	167_auto
Empirical formula	$C_{10}H_{10}O_2$
Formula weight	162.18
Temperature/K	120.00(10)
Crystal system	orthorhombic
Space group	Pbca
a/Å	8.4795(3)
b/Å	12.0703(4)
c/Å	15.2334(5)
α/°	90
β/°	90
γ/°	90
Volume/Å^3	1559.14(9)
Z	8
ρ_{calc}g/cm^3	1.382
μ/mm^{-1}	0.777
F(000)	688.0
Crystal size/mm^3	$0.12 \times 0.09 \times 0.06$
Radiation	Cu Kα ($\lambda = 1.54184$)
2Θ range for data collection/°	11.618 to 148.804
Index ranges	$-10 \leq h \leq 9, -9 \leq k \leq 14, -18 \leq l \leq 18$
Reflections collected	3381
Independent reflections	1541 [$R_{int} = 0.0145$, $R_{sigma} = 0.0181$]
Data/restraints/parameters	1541/0/109
Goodness-of-fit on F^2	1.087
Final R indexes [I>=2σ (I)]	$R_1 = 0.0337$, wR$_2 = 0.0830$
Final R indexes [all data]	$R_1 = 0.0356$, wR$_2 = 0.0847$
Largest diff. peak/hole / e Å^{-3}	0.18/-0.22

6.5 Conclusion

The first attempt to synthesise the 1,3-cubane **75** was overall unsuccessful. The generation of bicyclic diazetidine **100** instead of cyclobutadiene in order to react it with 2,5-dibromobenzoquinone **101** lead to the synthesis of very unstable intermediates which did not allow any purification through the multi-step synthesis, and gave low yield. The possible peaks of the diester cubane **75** were observed in a crude NMR, but it was not possible to isolate it. As such, this was considered unsuccessful. The second attempt consisted of generating the isomeric enone **118** and then using the protocol from Nigo *et al.* (Nigo *et al.*, 1993), which led to the successful synthesis and isolation of the 1,3-disubstituted cubane diacid **68** and diester **75**. The Coote group is currently working on optimising a few steps in order to improve the yields further. Unfortunately, obtaining the 1,3-disubstituted cubane with two different substituents was very challenging.

Compared to the 1,4-cubane, the selective deprotection of one ester of cubane **75** was not efficient. Other attempts to substitute a carboxylic acid by an amide did not lead to a successful second-Favorskii-type rearrangement to close the cubane. Finally, the selective protection of one acid of the cubane was investigated (using DCC or the Meerwein's salt) and seems to be a viable way to obtain the ester/acid cubane **119** with two different substituents. However, this requires more optimisation to improve the yield of the reactions. The 1,3-ester/acid cubane **119** could then be attached to another molecule using the carboxylic acid. Amide coupling to a recruiting ligand finishing with an amine could be possible. It could be linked to the other recruiting ligand and the other position after deprotection of the ester. The carboxylic acid could also be functionalised and transformed into an amine using the Curtius reaction, in order to allow attachment to other type of functional groups such as carboxylic acids, for the PROTAC building blocks made for the Wee1 project for instance.

As expected, the 1,2-cubane synthesis was very ambitious. Different starting materials were used to generate cyclooctatetraenes **126**, **144**, **154** by intramolecular *ortho*-photocycloaddition with an alkyne. The synthetic route was promising on paper, however, the cyclooctatetraene synthesised for this first proposed synthetic route were

not stable and thus non-usable in the reaction, making this synthetic route unviable. A third synthetic route using another approach of [2+2] photocycloaddition from benzene and an alkyne seems very promising. As a matter of fact, after optimisation of the first few steps, the acetyl protected cyclooctatetraene **161** was synthesised and allows successful Diels-Alder reactions with different dienophiles to give **162a-c**. [2+2] cycloaddition with these products then lead successfully to the "almost cubane" molecules **163a-c**. Further work now needs to be performed to close the last bond of the cubane. The hydrogenation using H-Cube Mini+ from ThalesNano seems to be a potentially useful technique to deprotect the benzyl group from the amines in order to allow reduction and then closure of the cubane by losing N_2. Other conditions could also be investigated to deprotect other types of protecting groups.

To go even further with the linker engineering in a PROTAC molecule, trisubstituted cubanes could also be used in the field. It would allow the attachment of two E3 ligase recruiters and one target recruiter, for instance, or a single PROTAC could recruit both E3 ligases at the same time by attaching the CRBN and the VHL recruiters as well as the target ligand on the same cubane to make the ubiquitination more efficient. Recruiting one E3 ligase and two different proteins of interest could also be relevant for targeted pharmacology. In the last couple years, trivalent PROTACs have started to appear following the hypothesis that increasing the binding valence could improve degradation. For instance, the Ciulli's group published SIM1, a trivalent PROTACs with two target warheads recruiting BRD4[BD2] and one recruiting VHL. It showed more sustained and higher degradation compared to the bivalent PROTAC MZ1 (Imaide *et al.*, 2021). Shortly after, Huang et al. (Huang *et al.*, 2022) developed trivalent PROTACs for BRD4[BD2] with a functionalised site that can control the orientation (benzene ring with a *tert*-butyl ester). This followed the same idea of controlling the PROTACs conformation to improve degradation that we have we the use of cubane molecules and is proof of concept that could be applied to other targets.

7 Design, synthesis and assessment of KIFC1 PROTACs

7.1 Introduction

7.1.1 Kinesins and centrosomes

Kinesin motor proteins were discovered almost 40 years ago (Vale *et al.*, 1985) and play an important role in cytoskeletal rearrangement. They use the energy from ATP hydrolysis to work on cellular processes, such as spindle and chromosome movement, as well as working along microtubules (MTs). The kinesin family contains 14 groups, some of which are mitotic kinesins that function only during mitosis (Rath *et al.*, 2012). They allow chromosomes to attach spindle fibres for metaphase, and they also have an impact on microtubules which generate spindle dynamics. Thus, kinesins play an important role in cell division. In order to transmit accurate genetic information, DNA replication and chromosome separation must happen perfectly. In most cancer cells, centrosome amplification is correlated with disruption of the poles of the mitotic spindle, leading to problems in the separation of chromosomes during cell division (Mahoney *et al.*, 2006; Tillement *et al.*, 2009) and further genetic instability.

Centrosomes are organelles composed of two centrioles (MT-based structures) and pericentriolar material (PCM) (Fry *et al.*, 2017; Loncarek *et al.*, 2017). Two centrosomes organise the poles of the mitotic spindle during mitosis through interactions with the MTs. Many cancers display more than two centrosomes, which is related to a change in centriole length (Marteil *et al.*, 2018) and PCM size (Patel *et al.*, 2018). Many of these cancer cells exhibiting centrosome amplification manage it by clustering the centrosomes into two groups to allow successful cell division and proliferation (Kwon *et al.*, 2008). Disrupting this process can lead to multipolar mitotic cells, which would lead to cell death, and is a potential therapeutic avenue used to target cancer.

The role of kinesins in division during mitosis has brought a lot of interest to the kinesin family as drug targets. As a matter of fact, inhibiting them could block uncontrolled division caused by cancers, and as a consequence be used as new targets for cancer treatments. One kinesin, KIFC1, is of particular interest due to the role it plays in centrosome clustering in cancer cells.

7.1.2 KIFC1 and its role in cancer

Kinesin-like protein KIFC1 or HSET (KIFC1) is part of the mitotic kinesin-14 family and has recently emerged as an anti-cancer drug target. KIFC1 contains three domains: an MT-binding domain, a stalk domain, and a motor domain located on the C-terminus (Yang *et al.*, 2014). Its role during mitosis is the opposite of KSP, a member of the kinesin-5 family. KSP has been a cancer target of many inhibitors (Heald, 2000) and its inhibition induces cell arrest during mitosis by preventing normal bipolar spindle formation, which leads to apoptosis/cell death (Mayer *et al.*, 1999).

KIFC1 motor protein slides and cross-links MTs from the minus-end of spindles during mitosis to facilitate chromosome segregation (Fink *et al.*, 2009) whereas KSP slides them from the plus-end (Yang *et al.*, 2014). KIFC1 is a centrosome clustering protein playing an important role in cancer cells where it is often overexpressed and allows multiple centrosomes to cluster leading to successful cell division and proliferation (Godinho *et al.*, 2009) (Figure 7.1). Many cancer cells become dependent on KIFC1 to cluster their centrosomes, which is not required in healthy cells. Such kinesins function only during mitosis, so they have more impact on proliferating cells (Sarli *et al.*, 2006). Thus, KIFC1 is an interesting motor protein to target and design a small molecule inhibitor for (Xiao *et al.*, 2016) (Figure 7.1). The recent progress in kinesin motor protein inhibition is promising as some inhibitors are now in clinical trials (Lee *et al.*, 2008; Woessner *et al.*, 2009; Holen *et al.*, 2012; Gerecitano *et al.*, 2013). However, the number of KIFC1 inhibitors is still low and they are not very potent. Kinesins have very similar sequences, and thus are hard to target selectively, adding another challenge to design inhibitors. For instance, KIFC1 and KSP have 80% similarity in their sequence (Watts *et al.*, 2013) in their motor domain and 56% in their binding loop 5.
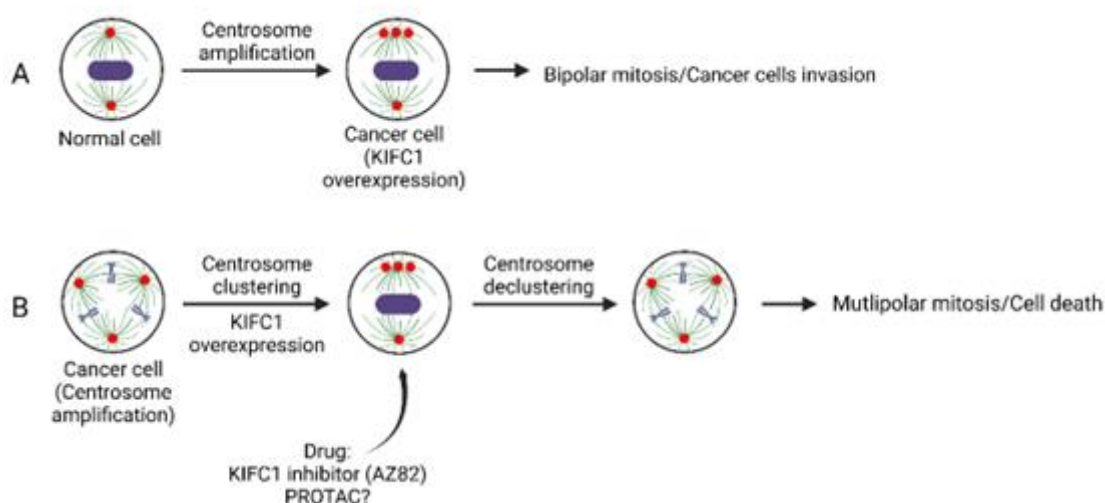
Figure 7.1: Targeting centrosome clustering as a therapeutic approach to target cancer. **A)** Centrosome amplification and clustering for successful mitosis. **B)** Target KIFC1 to induce centrosome declustering and further cell death (Using BioRender).

KIFC1 is degraded during mitosis by anaphase-promoting complex/cyclosome (APC/C) E3 ligase (Singh *et al.*, 2014). Singh *et al.* demonstrated that KIFC1 degradation depends on APC/C which regulates the bipolar spindle formation for cell division. Using proteomics experiments, they also highlighted that a stabilising CDK1-dependent phosphorylation site modulates KIFC1 degradation. Thus, modulating and regulating KIFC1 level has a critical role in the cell cycle.

KIFC1 was shown to play a more important role in cancer cells than in healthy cells (Kwon *et al.*, 2008) as the MT architecture appeared not to change upon KIFC1 ablation in normal cells, whereas cell lines such as BT549 and MDA-MB-231 (two breast cancer cell lines with KIFC1 overexpression) are very sensitive to KIFC1 siRNA knockdown. Thus, they are interesting cells to use to look at the dependency on KIFC1 levels to treatments. KIFC1 overexpression was reported in aggressive breast cancers (Pannu *et al.*, 2015). This could suggest the possibility to target centrosome-amplified cancer cells selectively making it even more interesting to work on, and that certain cell lines are better to use than others. Moreover, in cancers, KIFC1 overexpression was correlated with accelerated cell cycle kinetics, specifically at the G_2/M checkpoint (Pannu *et al.*, 2015).

Therefore, KIFC1 is an interesting target that would be interesting to degrade. Previous work in the Gadd and Fielding labs has shown that KIFC1 is degradable using a HaloPROTAC approach (Amanda Thomaz, unpublished results). Following this, we decided to design and synthesise PROTACs to target and degrade endogenous KIFC1.

7.1.3 KIFC1 inhibitors

In order to generate PROTACs targeting KIFC1, I first had to select an inhibitor binding to KIFC1. In the last 10 years, a few KIFC1 inhibitors were discovered. The first two papers were published in 2013, proposing two small molecule inhibitors CW069 (Watts *et al.*, 2013) and AZ82 (Wu *et al.*, 2013; Yang *et al.*, 2014) targeting KIFC1 motor protein in cancer cells with centrosome amplification (Figure 7.2). SR31527 was discovered a few years later, also inhibiting the ATPase activity of MT-stimulated KIFC1 (Zhang *et al.*, 2016) (Figure 7.2). However, these inhibitors are not very potent, and there are no existing crystal structures of the inhibitors bound to KIFC1 to understand their mode of binding. For PROTAC design, the choice of the attachment point of the E3 ligase to the target ligand is most often studied by looking at the target inhibitor binding into the protein's pocket, verifying which part is pointing out of the pocket, and thus would be available to attach the E3 ligase recruiting ligand part of the PROTAC. I looked at the published KIFC1 inhibitors synthesis and studies in order to verify what is known and which one could be the best candidate to use to make PROTACs.
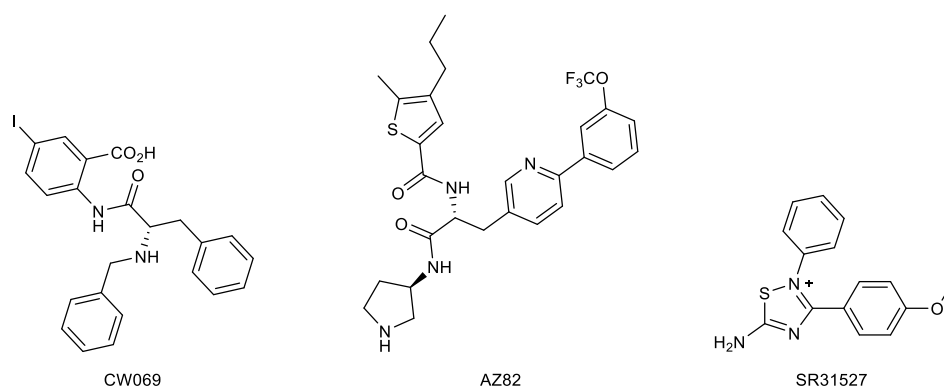
Figure 7.2: Structure of KIFC1 inhibitors: CW069, AZ82 and SR31527.

7.1.3.1 SR31527

SR31527 was discovered by high-throughput screening using an ATPase assay looking at KIFC1 enzymatic activity (Zhang *et al.*, 2016). SR31527 was selected as the more potent compound among 30 molecules and was shown to inhibit KIFC1 without involving the microtubules. However, this inhibitor is a very small molecule. No SAR has been done on this compound. Some molecular simulations and docking suggested that the aromatic rings are interacting in the KIFC1 pocket, whereas the amine could be solvent exposed, and the methyl group does not seem to have critical interactions with the protein. This model is not convincing enough to choose an attachment point, and is thus not a very good candidate to use to make PROTACs to target KIFC1.

7.1.3.2 CW069

CW069 was designed and discovered by Watts *et al.*, who applied chemogenomic principles to screen 500 KSP inhibitors and looked at the scoring in their bioactivity models to select fifty ligands (Watts *et al.*, 2013). Two structures were then selected after enzymatic assays. From this, they made analogues and studied by an SAR to find CW069 with an IC_{50} value of 75 ± 20 µM, which was statistically selective towards KIFC1 over another kinesin, KSP. Their synthetic route seems short and straightforward to access this KIFC1 inhibitor (Scheme 7.1). Another compound showed the three-fold greater potency towards KIFC1, but this was not selective over KSP. The other molecules were not inhibiting KIFC1, highlighting a narrow SAR and binding pocket.

The authors were able to show reduction in cell growth and centrosome clustering in cancer cells such as BT549 and MDA-MB-231 with CW069 (Watts *et al.*, 2013). Inhibition of KIFC1 with CW069 lead to cell apoptosis through catastrophic aneuploidy caused by multipolar mitosis in cancer cells with extra centrosomes. Watts *et al*. also observed that CW069 increased multipolar spindles in cancer cells with centrosome amplification. Therefore, CW069 could be a good candidate to make a PROTAC. The amide bonds could be useful to attach an E3 ligase to a strategic place in CW069 molecule and the iodine could also allow a coupling.
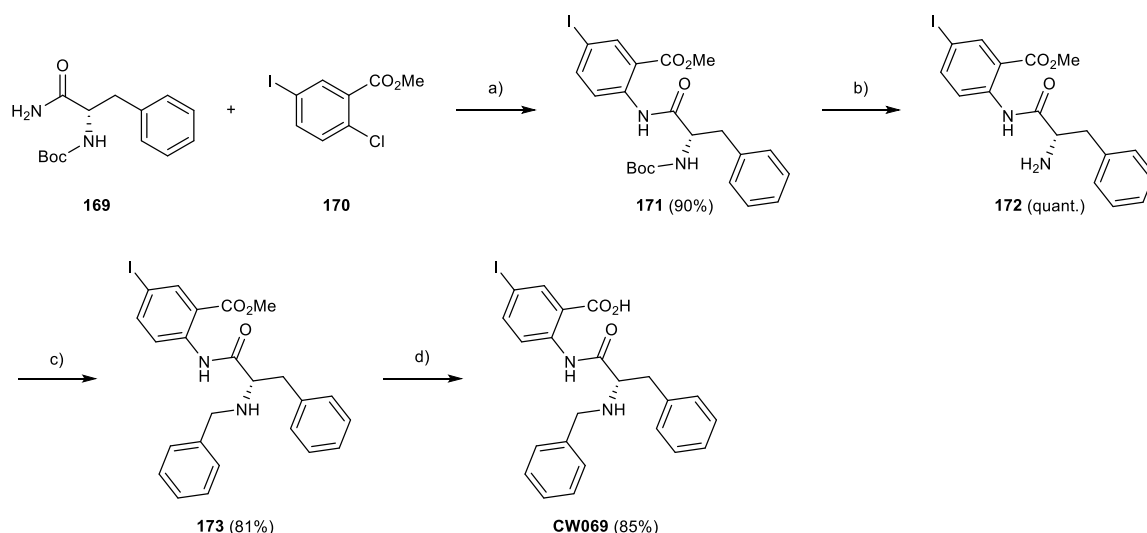
Scheme 7.1: Synthesis of CW069. Reagents and conditions: a) $Pd_2(dba)_3$, Xantphos, Cs_2CO_3, dioxane, 110 °C, 20 h; b) TFA, DCM, r.t., 1 h; c) i) Et_3N, THF, ii) benzaldehyde, THF, iii) $NaBH_3CN$, THF, r.t., 16 h; d) LiOH, THF, water, 60 °C, 16 h.

To find a possible attachment point in the CW069 molecule, I looked at the binding-model hypothesis proposed by Watts *et al.* into loop 5 of KIFC1 (Watts *et al.*, 2013). The compound seemed overall buried in the binding pocket, creating interactions with its carboxylic acid and amines, which thus seem important functional groups of the molecule. However, the overall illustration of the model was of poor quality and provided little information on which atoms might be solvent exposed. The computational model using KIFC1 loop5 seemed to explain the selectivity of CW069 over KIC1 due to the dynamic selectivity of loop 5 that cannot be achieved by KSP as well as electrostatic interactions. Given the lack of binding information of the inhibitor into the pocket, as well as the low affinity of CW069, it may be possible candidate to make PROTAC, but only in the event there are no better candidates. As a matter of fact, this is a computational model presenting overlapping of loop 5 of KIFC1 with the inhibitor for some energy poses to try and predict interactions but cannot be yet verified yet.

7.1.3.3 AZ82

AZ82 was first published in 2013 (Wu *et al.*, 2013) showing its mechanism of action and inhibition potency. The first publication was followed by another paper detailing AZ82

discovery, synthesis and optimisation (Yang *et al.*, 2014). AZ82 inhibits KIFC1 MT-stimulated enzymatic activity in an ATP-competitive manner, and binds to KIFC1/MT binary complex. KIFC1 was shown to enable centrosome declustering in centrosome-amplified cancer cells, underlining that it could have a potential therapeutic purpose in cancer treatments.

To design this KIFC1 inhibitor, the authors used an ATPase assay applied to a library of compounds for high-throughput screening. Compounds with a phenylalanine moiety showed some KIFC1 inhibition and were taken into SAR exploration. A number of rounds of SAR led to the discovery of AZ82. SAR was done on R_1 and R_2 groups, keeping the phenylalanine scaffold **174** (Yang *et al.*, 2014) (Scheme 7.2). Starting with R_1, the group was shown to induce a binding pocket in the motor protein, similar to some KSP inhibitors (Yan *et al.*, 2004). For this reason, it was hypothesised that it could act similarly for KIFC1. SAR around R_1 revealed a broad range of possible patterns, with more polar substituents decreasing the overall potency of the inhibitor. After further optimisation, they discovered that a thiophene (5-membered heteroaryl ring) with methyl and propyl groups, in compound **175,** most effectively improved the inhibitor potency. Then, exploration of the R_2 group revealed more freedom, suggesting that it could maybe be solvent exposed due to the possible lack of interactions (Scheme 7.2). A pattern of N-C-C-N seemed to come out of investigations of R_2 modifications, with ethylene diamine and pyrrolidine particularly effective. Changes in the m-CF$_3$-Ph were only tolerated when replacing it by m-CF$_3$O-Ph, which may show the importance of this group in the inhibitor binding mode, and especially of the trifluoromethyl moiety.
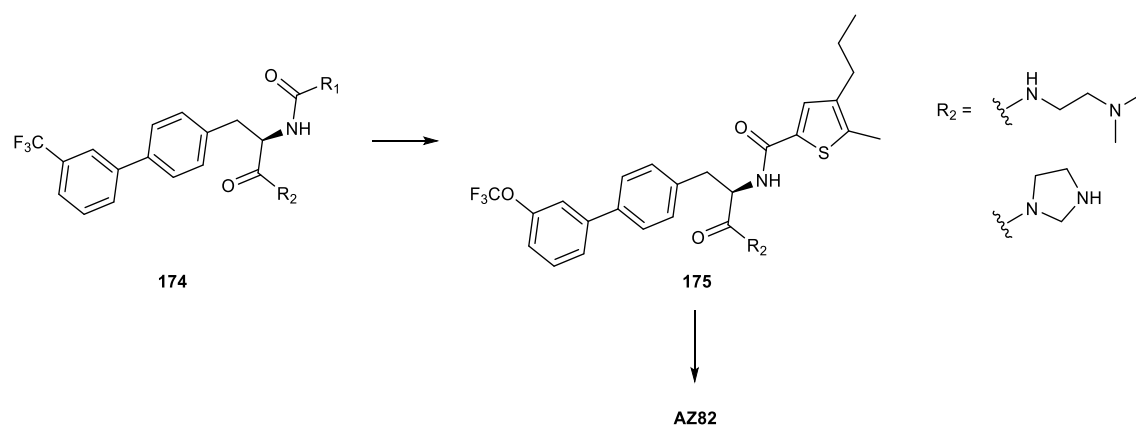
Scheme 7.2: SAR around R_1 and R_2 leading to AZ82 synthesis.

Wu *et al*. developed a seven-step synthesis to make AZ82 inhibitor (Wu *et al*., 2013; Yang *et al*., 2014) (Scheme 7.3). The inhibitor is composed of different type of couplings such as Suzuki in step a to give **178** and amide in step d and f, to give **183** and **186**, as well as deprotections, such as Boc in step e and ester in step c, to give **184** and **181**, respectively. Due to the E3 ligase ligand building blocks for CRBN and VHL made previously (developed in Chapter 3 Sections 3.3.2.2 and 3.3.3.2), the presence of carboxylic acids and amines in AZ82 molecule, make it a good candidate to work with in order to facilitate the linking to build PROTAC molecules.
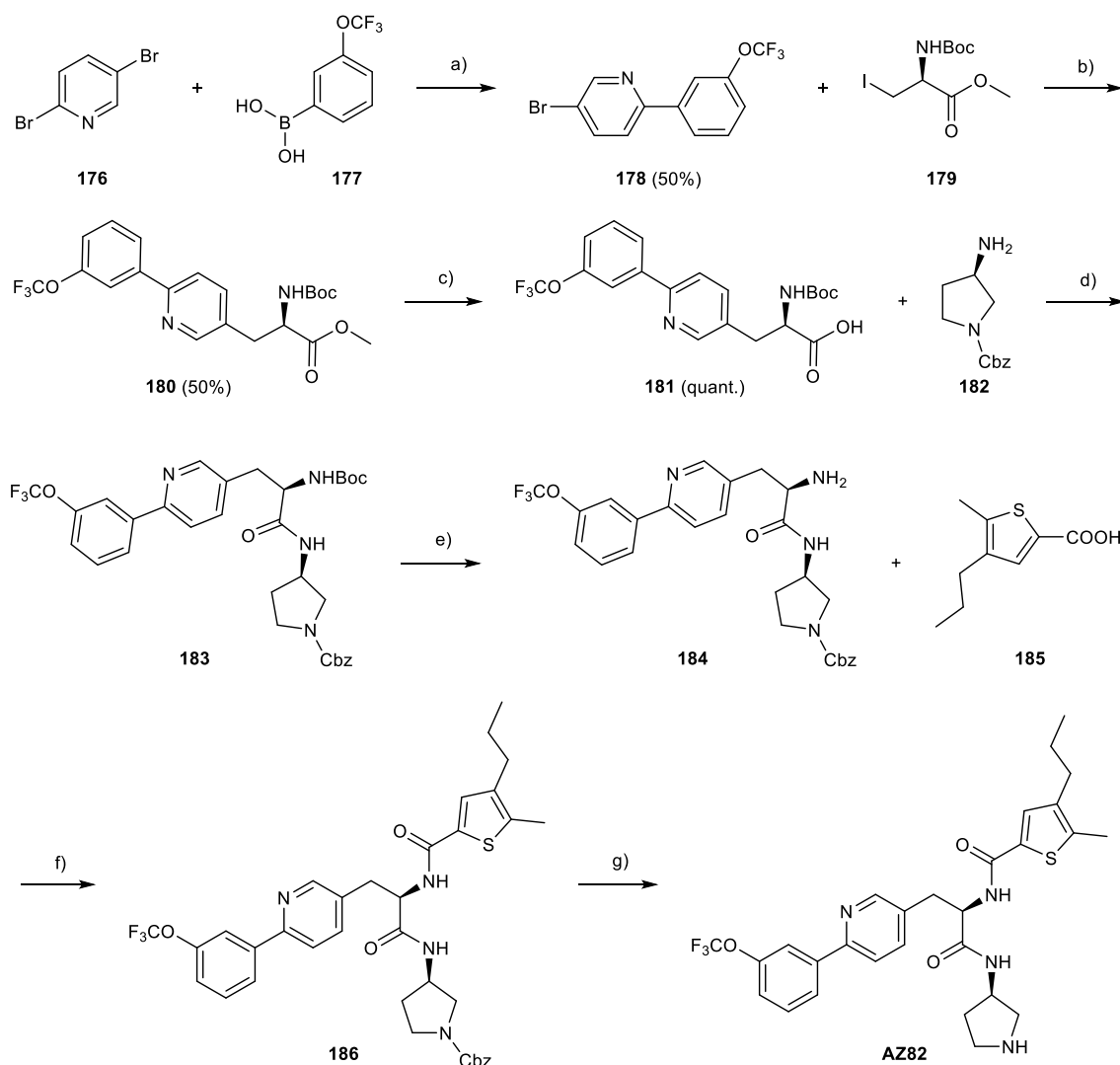
Scheme 7.3: AZ82 synthesis. Reagents and conditions: a) Pd(Ph₃P)₄, Na₂CO₃, dioxane, H₂O, 100 °C, 3 h; b) I₂, Zn, PdCl₂(PPh₃)₂, DMF, 0 to 50 °C, 5 h; c) LiOH, MeOH, H₂O, 60 °C, 12 h; d) HATU, DIPEA, DMF, r.t., 2 h; e) 4N HCl (dioxane), DCM, r.t., 2 h; f) HATU, DIPEA, DMF, r.t., 0.5 h; g) H₂, Pd/C, MeOH, r.t., overnight. Published data (Wu *et al.*, 2013; Yang *et al.*, 2014).

Park *et al*. published a model of AZ82 bound in their KIFC1 structure proposing a binding site for AZ82 (Park *et al.*, 2017). They compared KIFC1 to Ncd (a kinesin-related microtubule motor protein) and KIFC3 in order to see which part of KIFC1 was involved in the binding as AZ82 does not bind Ncd and KIFC3. Docking calculations were also used. It was shown that movement of residues Y409, L599 and F656 of KIFC1 are likely to form the binding site due to their highest predicted free energy changes when they move. The trifluoromethoxy group of AZ82 has contacts with Y409 and the pyridine is stacked

against F656. The movement of F656 seems to stabilise AZ82 binding by allowing the trifluoro group to become buried deep in the KIFC1 α4/α6 pocket. This model suggested that this part of the molecule should be kept.

Overall, AZ82 seemed a better candidate (IC$_{50}$ = 0.3 μM) to make PROTACs than CW069, as it is more potent, has been investigated by SAR, and possible details of the binding site were proposed by Park *et al.*. The models and SAR helped hypothesise how AZ82 might be binding. Looking at the SAR published by Yang *et al.*, as well as their proposed binding model of AZ82 into KIFC1 and the crystal structure from Park *et al.*, led us to decide to make PROTACs by attaching the E3 ligase ligand in the R$_2$ position of AZ82. However, making PROTACs for a new target is challenging, especially when the attachment point is only a hypothesis. The design and synthesise a small library of KIFC1 PROTACs was proposed using an analogue of AZ82 identified as a good binder by SAR, and recruiting the VHL or CRBN E3 ligases, to determine if it is possible to degrade KIFC1 using PROTAC technology (Figure 7.3).
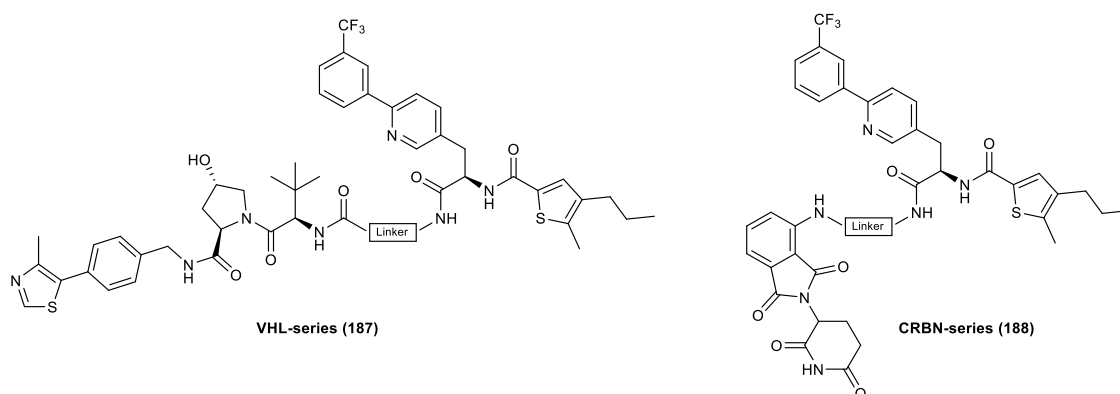
Figure 7.3: Proposed structures of the VHL- and CRBN-series of KIFC1 PROTACs. With the 'linker' possibly including the 'N-C-C-N' pattern.

7.2 Aims and objectives

The first aim is to design and synthesise KIFC1 PROTACs using a KIFC1 inhibitor AZ82 analogue by attaching it through a linker to CRBN and VHL ligands to degrade KIFC1.

The second aim is to assess KIFC1 PROTACs degradation activity profiles in cells and investigate cell survival in cancer cells if degradation is successful.

7.3 Results and discussion

7.3.1 Design and synthesis of KIFC1 PROTACs

7.3.1.1 Design and synthesis of the KIFC1 ligand

KIFC1 PROTACs were synthesised using AZ82 analogue as the KIFC1 recruiter, that could then be attached to the E3 ligase ligands already linked to a linker (Scheme 7.4). Due to the cost vs efficiency of the synthesis, some changes were made to the proposed synthesis from Wu *et al*. (Wu *et al.*, 2013). Even though 5-Methyl-4-propylthiophene-2-carboxylic acid **185** is expensive, it was attached first to **189** and then to the E3 ligase with the linker due to its multiple step synthesis which also makes it valuable (Scheme 7.4).
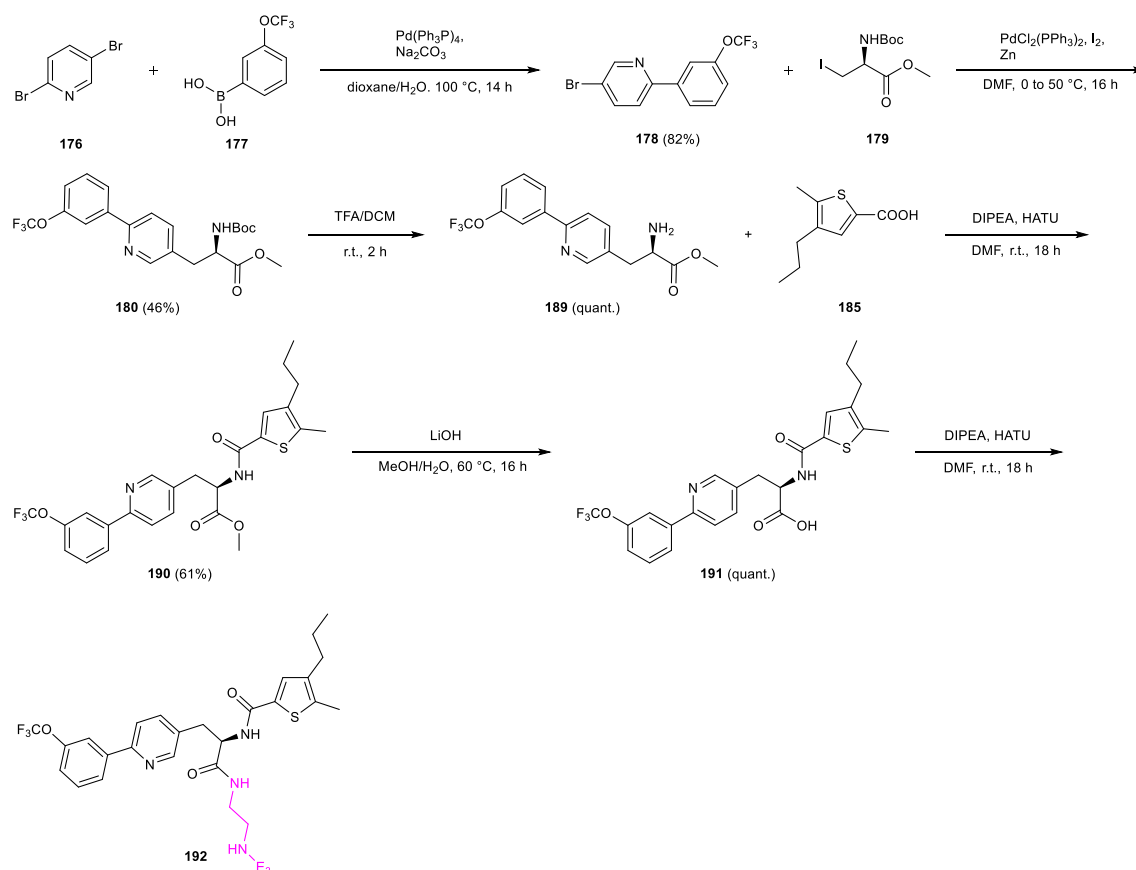
Scheme 7.4: Proposed KIFC1 PROTAC synthetic route.

Thus, **178** was obtained from a Suzuki coupling between **176** and **177** stirred at 100 °C overnight in Step 1, in 82% yield (Scheme 7.4). **178** was next used in a Sonogashira

coupling in step 2 with **179**, to obtain **180** after stirring overnight at 50 °C in 46% yield. Then, **180** was Boc deprotected to give **189** in quantitative yield, which could then be attached to thiophene **185** by HATU-mediated amide coupling to afford **190** in 61% yield. **191** was obtained by refluxing **190**, in a 40-500 mg scale, with lithium hydroxide overnight in step 5 to deprotect the methyl ester into a carboxylic acid in quantitative yield to allow its attachment to the E3 ligase ligand and linker amine by HATU-mediated amide coupling in step 6.

To keep the N-C-C-N pattern that seemed to be important when looking at AZ82 SAR, the attachment of a N-C-C-N pattern to the E3 ligase building blocks previously made for CRBN and VHL (Chapter 3) was attempted (Scheme 7.5). **25a** for CRBN and **20b** for VHL were selected to attempt a reductive amination on the amine end of the E3 ligase building block with *tert*-butyl N-(2-oxoethyl)carbamate **194** (Scheme 7.6). This has the objective of avoiding an additional amide bond that would be introduced if attempting an amide coupling directly, and could help with compound cell penetration.
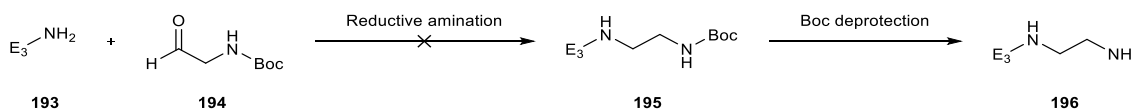
Scheme 7.5: Proposed access to E3 ligase with "N-C-C-N" pattern **196**.

Sodium triacetoxyborohydride was used first as a reductive agent in the reductive amination of **25a**. The pomalidomide molecule contains a glutarimide ring, as a consequence, it seemed a good idea to start with Na(AcO)$_3$BH as it should not reduce it and thus not open the glutarimide ring as a side reaction. However, the reaction gave a lot of by-products (8 spots by TLC analysis) that were hard to isolate. Thus, it was not possible to conclude if the product was present in the reaction. Using the same reducing agent with **20b**, the reductive amination gave a lot of reaction products and it was not possible to isolate the wanted product. Sodium cyanoborohydride (NaBH$_3$CN), another stronger reducing agent, was then tried on **25a**. But it led to the same problem. Unfortunately, the reductive amination to obtain the N-C-C-N pattern was not successful after trying different reaction conditions. Due to time constrains no other conditions were attempted.
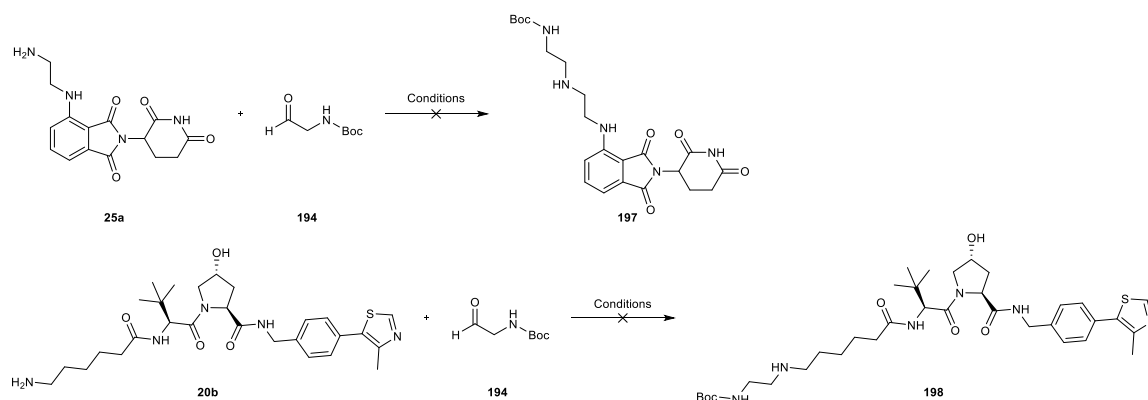
Scheme 7.6: Attempts of reductive amination. Reagents and conditions: reductive agent (2 eq.), AcOH (2 eq.), THF, r.t..

7.3.1.2 Synthesis of the KIFC1 PROTACs

Therefore, it was decided to proceed and choose E3 ligase building blocks linked to different linkers already made for the Wee1 project: **20a**, **20c** and **20d** for the VHL-series and **25a**, **25b** for the CRBN-series (Chapter 3). These finished with an amine that was used to attach them directly to the carboxylic acid of AZ82 analogue building block **191** by HATU-mediated amide coupling. After a series of purifications by column chromatography on silica gel using different solvent systems: EtOAc/Hexane and MeOH/DCM, and also by preparative TLC (100% EtOAc or 5% MeOH in DCM), five KIFC1 PROTACs were obtained in low yields. Three PROTACs were isolated after the signle amide coupling step, recruiting VHL: **187a (MA186)**, **187b (MA187)** and **187c (MA191)** in 10-155 yield (Scheme 7.7); and two recruiting CRBN: **188a (MA182)** and **188b (MA185)** in 11 and 14% yield, respectively (Scheme 7.8).
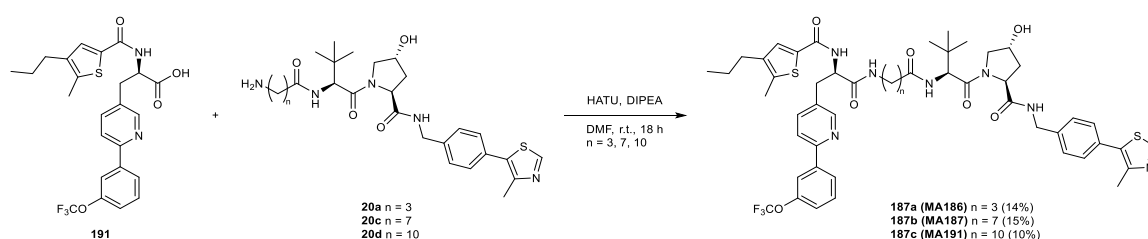
Scheme 7.7: Synthesis of KIFC1 PROTACs recruiting the VHL E3 ligase.
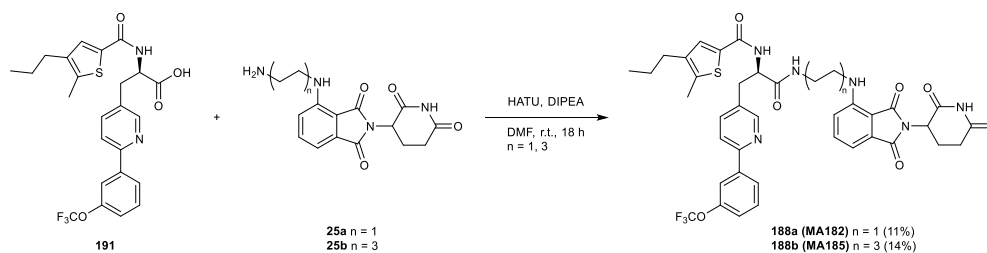
Scheme 7.8: Synthesis of KIFC1 PROTACs recruiting the CRBN E3 ligase.

Only five PROTACs were synthesised to make a small library using the two E3 ligases VHL and CRBN, and assess if it was possible to degrade KIFC1 (Table 7.1). This could then lead to optimisation if successful. For the VHL-series, to also study the influence of the linker's length, three PROTACs were synthesised with three-, seven- and ten-carbon linkers for MA186, MA187 and MA191 respectively (Scheme 7.7). For the CRBN-series, MA182 features a two-carbon linker, and MA185 has a longer linker of six carbons to study the influence of two different linker lengths on KIFC1 degradation (Scheme 7.8).

Table 7.1: SAR of KIFC1 PROTACs. Table showing the linker's length of the KIFC1 PROTACs and their E3 ligase.

PROTAC	E3 ligase	Linker length
MA186		5
MA187	VHL	9
MA191		12
MA182	CRBN	3
MA185		7

7.3.2 Assessment of KIFC1 PROTACs

7.3.2.1 Assessment of the CRBN-series

After designing and synthesising five KIFC1 PROTACs, they were tested in different cancer cell lines to investigate the target degradation. The two KIFC1 PROTACs recruiting CRBN, MA182 and MA185, were obtained first. After 4 h incubation in HeLa S3 cell treated with decreasing dose of PROTACs from 10 µM to 1 nM (Figure 7.4 A and D), they did not show KIFC1 degradation. As explained before, BT549 and MDA-MB-231 cells seemed more promising for looking at the effect of drugs on KIFC1 levels due to their reliance on the protein. So, the PROTACs were then tested for 24 h in BT549 (Figure 7.4 B and E) and MDA-MB-231 (Figure 7.4 C and F) cells with the same doses. The cells were treated for 24 h instead of 4 h as KIFC1 is normally degraded during mitosis, so it could be more relevant to leave the PROTAC for a full division cycle.
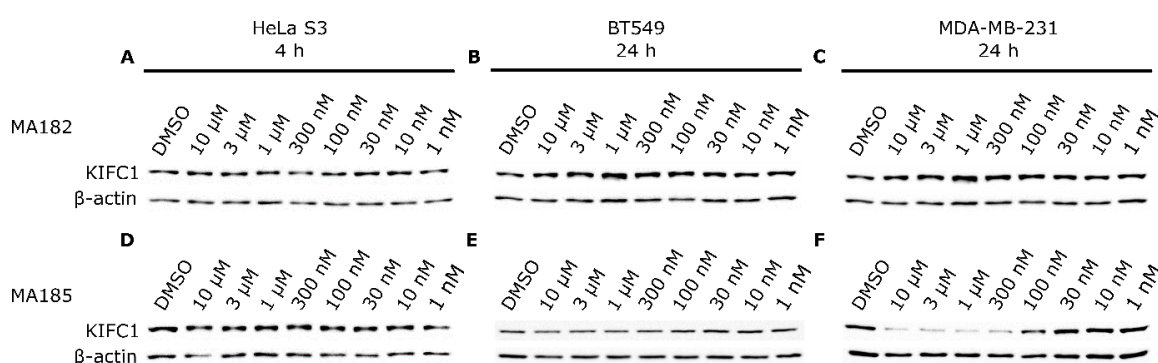
Figure 7.4: Dose response of the KIFC1 PROTACs recruiting the CRBN E3 ligase. Western blots of the dose response of MA182 in **A**) HeLa S3, **B**) BT549, **C**) MDA-MB-231 cells and MA185 in **D**) HeLa S3, **E**) BT549 and **F**) MDA-MB-231 cells treated for the indicated time (n = 2). The membrane was blotted for KIFC1, and β-actin as the loading control.

MA185, containing the six-carbon linker, induced a decrease in KIFC1 levels from 100 nM to 10 µM in MDA-MB-231 cells (Figure 7.4 F), after 24 h treatment, as well as a small decrease in BT549 cells (Figure 7.4 E), from 300 nM to 10 µM. However, MA182, with a two-carbon linker, did not decrease KIFC1 levels in BT549 nor MDA-MB-231 cells (Figure 7.4 B and C). In order to quantify KIFC1 degradation by MA185 in BT549 and MDA-MB-231 cells more precisely, the same 24 h dose response experiments were blotted and

imaged using near infrared fluorescent imaging (LICOR). GAPDH was used as the loading control as our usual β-actin showed inconsistency (Figure 7.5). Tubulin was also blotted for to verify that levels were similar. KIFC1 bands were quantified and normalised with GAPDH and the DMSO control to obtain the dose response curves in Figure 7.5 C and D.
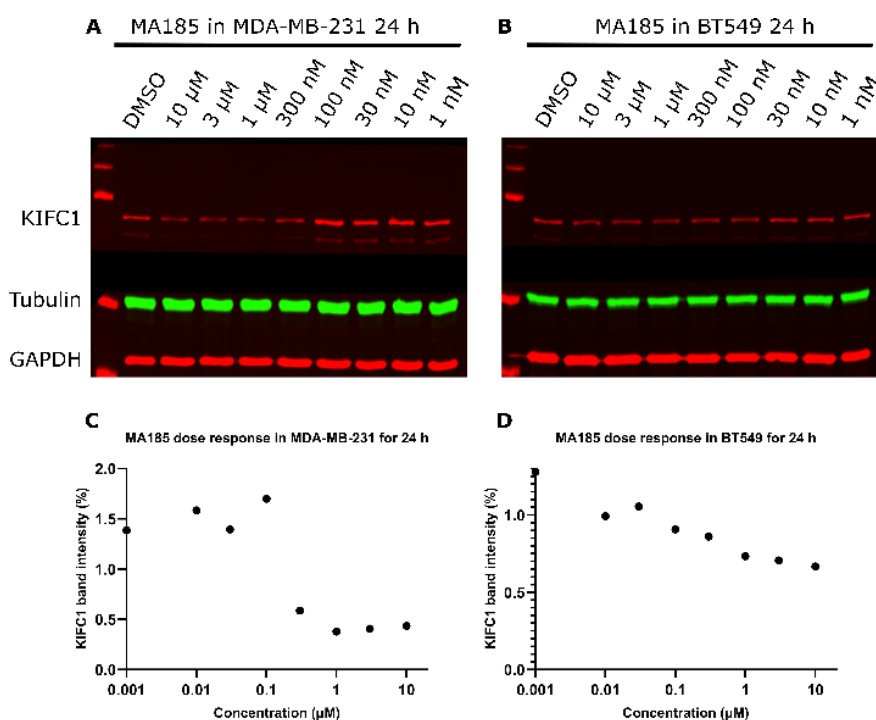
Figure 7.5: Dose response of PROTAC MA185. Western blot analysis of MA185 dose response for 24 h in **A**) BT549 and **B**) MDA-MB-231 cells imaged using the near infrared fluorescent imaging (LICOR). The membrane was blotted for KIFC1 and other control proteins (GAPDH and tubulin). **C**) and **D**) The KIFC1 band was blotted and normalised using GAPDH and the DMSO control for both cell lines.

The quantification of KIFC1 after MA185 treatment, for 24 h in MDA-MB-231 and BT549 cells, confirmed the degradation observations made from the normal Western blots (Figure 7.5). MA185 degraded KIFC1 much more strongly in MDA-MB-231 cells compared to BT549 cells. Maximal degradation seemed to be reached between 300 nM and 1 µM with around 45% of KIFC1 remaining in MDA-MB-231 and 70% in BT549. No hook effect was observed at higher concentrations for MA185 in MDA-MB-231 and BT549 cells after 24 h. This could indicate that the PROTAC does not have a strong affinity with both

partners, or that there is a significant cooperativity, or that there is a relatively low concentration of PROTAC inside the cells.

7.3.2.2 Assessment of the VHL-series

The three VHL-PROTACs were then obtained and tested in HeLa S3 and MDA-MB-231 cells for 24 h with a dose response of PROTAC from 10 µM to 1 nM (Figure 7.6). After analysis by Western blot, MA186, MA187 and MA191 did not show KIFC1 degradation in either cell line. KIFC1 levels remained the same for the three PROTACs at all concentrations tested.
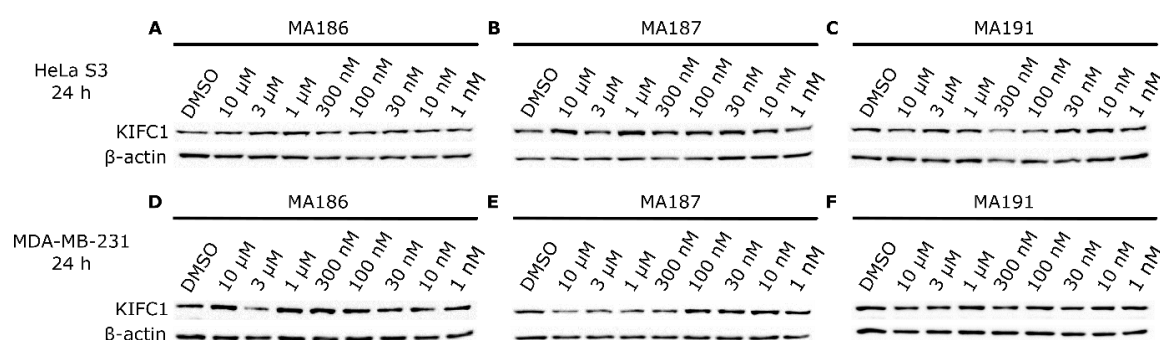
Figure 7.6: Dose response of the KIFC1 PROTACs recruiting the VHL E3 ligase. Western blots of the dose response of **A**) MA186, **B**) MA187, **C**) MA191 in HeLa S3 and **D**) MA186, **E**) MA187, **F**) MA191 in MDA-MB-231 cells treated for 24 h (n = 2).

Therefore, after the first tests of KIFC1 PROTACs following a dose response for 24 h, we were able to see degradation for one PROTAC of the CRBN-series: MA185 featuring a six-carbon linker, whereas none of the PROTACs of the VHL-series nor the other PROTAC of the CRBN-series induced KIFC1 degradation.

HaloTAGs (reacting with hexyl chloride tags) have been used in the literature for the VHL E3 ligase with HaloPROTAC1 for example (Buckley *et al.*, 2015), and cIAP E3 ligase (Tomoshige *et al.*, 2015, 2016). The target protein is fused with a HaloTag. Then, HaloPROTAC1 is designed to recognise it, and recognises the E3 ligase on the other side. Work in our group has previously shown that it is possible to target and degrade KIFC1 using HaloPROTAC-e (Tovell *et al.*, 2019), recruiting the VHL E3 ligase to HaloTag7-fused KIFC1 (Amanda Thomaz, unpublished results). This suggests that KIFC1 is a degradable

target when recruiting VHL, however, there may be restrictions in the right attachment point in the PROTAC, as well as the linker's length, when targeting endogenous KIFC1.

7.3.2.3 Comparison of all the KIFC1 PROTACs

In order to confirm KIFC1 degradation and to compare the PROTACs together, the five PROTACs were tested at a single concentration (1 µM) in HeLa S3 and MDA-MB-231 cells for 24 h for consistency in the data (Figure 7.7 A and B). Using Western blotting and the LICOR, KIFC1 bands were quantified (Figure 7.7 C; Table 7.2). Only MA185 (CRBN-series) reduced KIFC1 levels in MDA-MB-231 cells with 53% of KIFC1 remaining. The other PROTACs, MA182 of the CRBN-series, and MA186, MA187 and MA191 of the VHL-series, did not reduce KIFC1 levels which stayed around 100% after 24 h treatment. KIFC1 levels stayed the same as the DMSO control in HeLa S3 cells for all the PROTACs. This correlates with the dose response investigations presented earlier for each PROTAC (Figure 7.4; Figure 7.5; Figure 7.6).
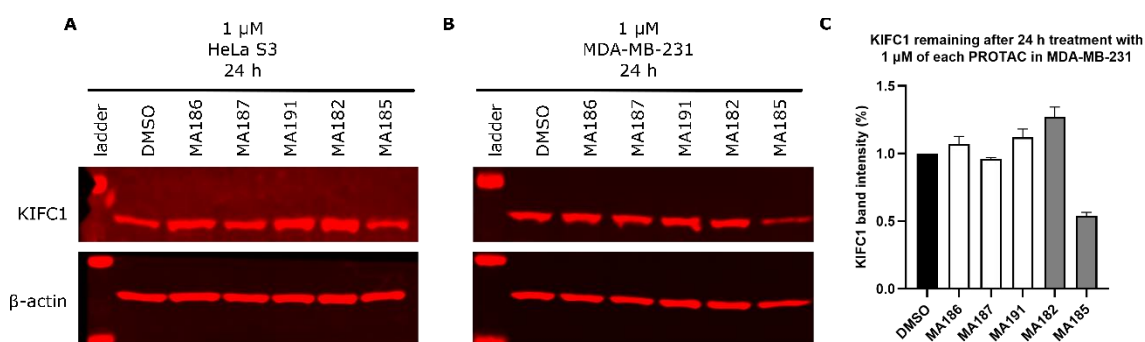
Figure 7.7: SAR of KIFC1 PROTACs recruiting either the VHL or the CRBN E3 ligases. LICOR images of the Western blots of **A**) HeLa S3 and **B**) MDA-MB-231 cells treated for 24 h with 1 µM of each PROTACs. **C**) Level of KIFC1 remaining in MDA-MB-231 after 24 h treatment with 1 µM of PROTAC, reported as a percentage of KIFC1 protein normalised with the DMSO control. Data are presented as the mean ± s.d. of n = 2 biological independent experiments.

Table 7.2: Table of KIFC1 remaining after 24 h treatment in MDA-MB-231 cells. Comparison of KIFC1 levels of all the PROTACs in MDA-MB-231 cells treated with 1 µM of each PROTAC (Related to Figure 7.7).

PROTAC	KIFC1 remaining (%)
MA186	107 ± 6
MA187	96 ± 1
MA191	112 ± 6
MA182	127 ± 7
MA185	54 ± 3

7.3.2.4 Target engagement

To validate the mechanistic activity of MA185 PROTAC, I next verified that it was a degrader dependent on the proteasome and E3 ligase activity (Figure 7.8). MDA-MB-231 cells were pre-treated with MG132 proteasome inhibitor (40 µM) for 3 h before adding the PROTAC for 21 h. MG132 abrogated KIFC1 degradation, showing that the degradation we observed is proteasome dependent. Likewise, cells were pre-treated with MLN4924 (3 µM), a neddylation inhibitor of CRLs, for 3 h. KIFC1 degradation was also prevented which confirmed the PROTAC activity dependence on the neddylation and activation of CRL4^{CRBN}.

MA185 (1 µM)	-	+	-	+	-	+	-	+	-	+	21 h
AZ82 (10 µM)	-	-	+	+	-	-	-	-	-	-	
MG132 (40 µM)	-	-	-	-	+	+	-	-	-	-	
MLN4924 (3 µM)	-	-	-	-	-	-	+	+	-	-	3 h
POM (10 µM)	-	-	-	-	-	-	-	-	+	+	
KIFC1											
GAPDH											
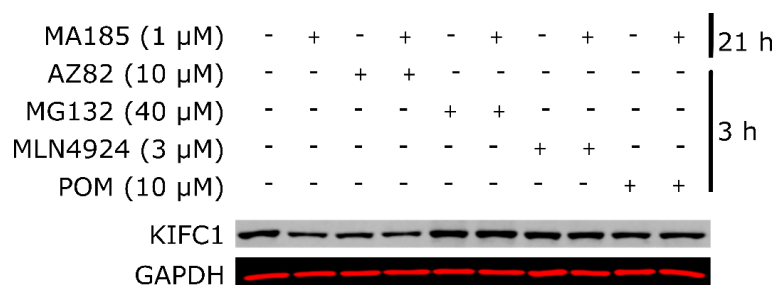
Figure 7.8: Target engagement for KIFC1 degradation. Competition experiment of PROTAC MA185 with pre-treatments with AZ82 (10 µM), MG132 (40 µM), MLN4924 (3 µM), POM (10 µM) for 3 h prior to 21 h PROTAC treatment.

To show the importance of ternary complex formation and the recruitment of both binding partners (target protein and E3 ligase), MDA-MB-231 cells were pre-treated with the corresponding target inhibitors. Pre-treatment with AZ82 (10 µM) for 3 h, KIFC1 inhibitor, and subsequent treatment with and without MA185 gave the same levels of KIFC1. Similarly, pre-treatment with pomalidomide (10 µM), also prevented KIFC1 degradation. This showed that the recruitment of both target protein and E3 ligase were essential for KIFC1 degradation.

7.3.2.5 Centrosome clustering/declustering analysis

In order to look at KIFC1 degradation and centrosome clustering/declustering upon treatment with PROTAC MA185, immunofluorescence (IF) assays in MDA-MB-231 cells, cancer cells exhibiting centrosome amplification, were performed (Section 2.9). KIFC1 expression is known to result in centrosome clustering for cells with dependent on KIFC1 for cluster centrosomes, leading to cell survival. By degrading KIFC1, we hoped to induce centrosome declustering to lead to multipolar mitosis and thus failed mitosis. MDA-MB-231 cells were treated with 1 µM of PROTAC MA185, or DMSO as a control, for 24 h. Cells were then fixed and stained with centrin/pericentin/tubulin as developed in the Section 2.9. Using the confocal microscope, cells were investigated to look at centrosomes in mitotic cells (Figure 7.9). Nevertheless, the PROTAC appears to be toxic to the cells, which only grow slowly after treatment, and explains the low number of mitotic cells in the sample.
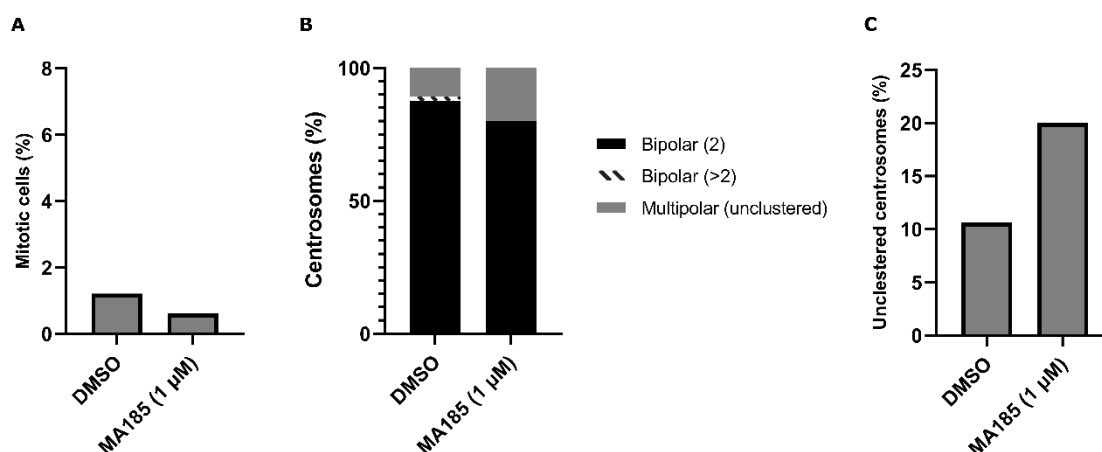
Figure 7.9: Centrosome declustering upon treatment with PROTAC MA185. Confocal analysis of mitotic cells from MDA-MB-231 cells treatment with either DMSO as a control or with PROTAC MA185 (1 μM). **A**) Graph of the percentage of mitotic cells. **B**) Quantification of centrosomes in mitotic cells that are either bipolar with two centrosomes, bipolar with more than two centrosomes (Clustered) or multipolar with more than two unclustered centrosomes. **C**) Percentage of centrosome declustering. Quantifications of this figure are the result of one experiment and the average of five confocal pictures for each condition (with an average of ten mitotic cells per image for the control and three mitotic cells for the treatment).

A decrease in the number of mitotic cells upon treatment with PROTAC MA185 was observed (Figure 7.9 A) suggesting that MDA-MB-231 cells are sensitive to the PROTAC treatment. To verify if the MA185 was affecting centrosome clustering, centrosomes were quantified in mitotic cells and cells were classified in three categories: bipolar with two centrosomes, bipolar with more than two centrosomes (clustered) or multipolar with more than two unclustered centrosomes (Figure 7.9 B and C). Centrosome amplification was observed as expected in MDA-MB-231 cells. In cells treated with DMSO as a control, bipolar mitotic cells were present with either a normal number of centrosomes or with more than two centrosomes, which were clustered in the normal two poles of the mitotic cells. More multipolar mitotic cells were observed in cells treated with the PROTAC suggesting that MA185 caused centrosome declustering. This experiment represents only preliminary data as it is one repeat of the experiment, but it suggests that MA185 treatment acts as expected on centrosome declustering, which could further lead to mitotic defects compared to the control with multiple clustered centrosomes. To confirm

the preliminary observations, other repeats in MDA-MB-231 cells as well as BT549 cells are required and are currently being undertaken in the group.

7.3.2.6 Cell cycle analysis – Flow cytometry

In order to see if PROTAC MA185 has an effect on the cell cycle, cell cycle analysis by flow cytometry was undertaken using MDA-MB-231 and BT549 cells (Section 2.8). Cells were treated with MA185, AZ82 or the DMSO control for 24 h before being harvested and stained with PI to be analysed. Two concentrations of AZ82 inhibitor (1 or 5 µM) were used in a first instance, but showed the same effect in the cell cycle, so experiments will be focused on the 1 µM treatment for greater clarity.

In BT549 cells, the cells treated with either AZ82 or MA185 showed an increase in the G_2 phase grouped with M (mitosis) with 30-33% comparing to the DMSO control with only 25% (Figure 7.10; Table 7.3). This change suggests that treatments by either the PROTAC or the inhibitor could lead to multipolar cells by either degrading or inhibiting KIFC1 and delaying the G_2 phase or blocking the cells during mitosis. It has been shown previously that KIFC1 knockdown could delay the G_2 phase (Li *et al.*, 2018). This could be a consequence of delayed cell growth, as shown in the literature after treatments with AZ82 or CW069 (Wei *et al.*, 2019), or maybe preventing entry into or exit from mitosis due to abnormalities. Both cases are possible and need further investigation. Very few mitotic cells upon PROTAC treatment for the IF experiments were observed (Section 7.3.2.5).
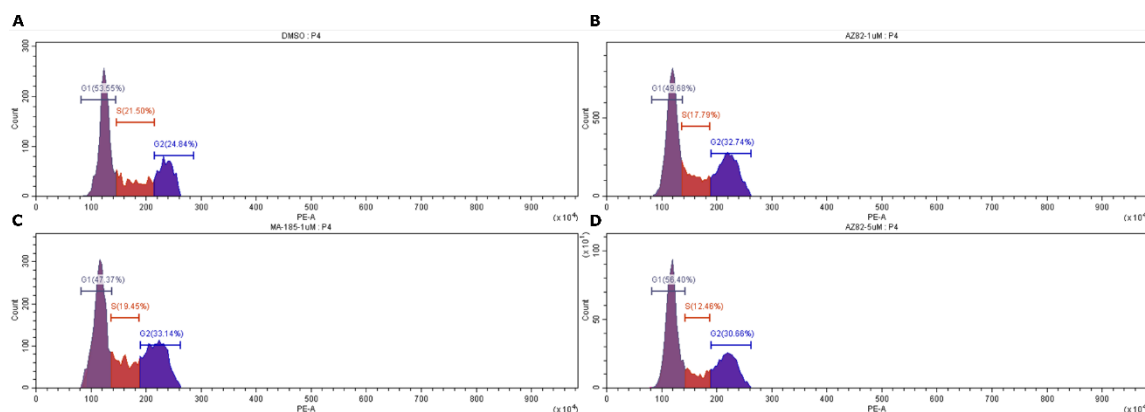
Figure 7.10: Cell cycle analysis in BT549 cells. Flow cytometry experiment of BT549 cells stained with Propidium Iodide (PI) after treatment with **A**) DMSO, **B**) AZ82 (1 µM), **C**) MA185 (1 µM) and **D**) AZ82 (5 µM) for 24 h (n = 1, preliminary data).

Table 7.3: Cell cycle analysis in BT549 cells related to Figure 7.10. Table showing the percentage of cells at the indicated stage of the cell cycle (G_1, S or G_2/M) depending on the treatment conditions (n = 1, preliminary data).

BT549	G_1	S	G_2/M
DMSO	53.55	20.50	24.84
MA185 (1 µM)	47.37	19.45	33.14
AZ82 (1 µM)	48.68	17.79	32.74
AZ82 (5 µM)	56.40	12.46	30.66

In MDA-MB-231 cells, the cells treated with either AZ82 or MA185 also showed a difference in the percentage of cells in G_2. It was increased upon treatment with MA185 (~25%) and decreased upon treatment with AZ82 (~17%) compared to the DMSO control (~21%) (Figure 7.11; Table 7.4). This was similar to BT549 cells with the PROTAC treatment but not for the inhibitor. Due to the preliminary nature of the data, this disparity could be due to the difficulties to separate the fractions from S or G_2 phase in the graph, rather than a real biological effect.
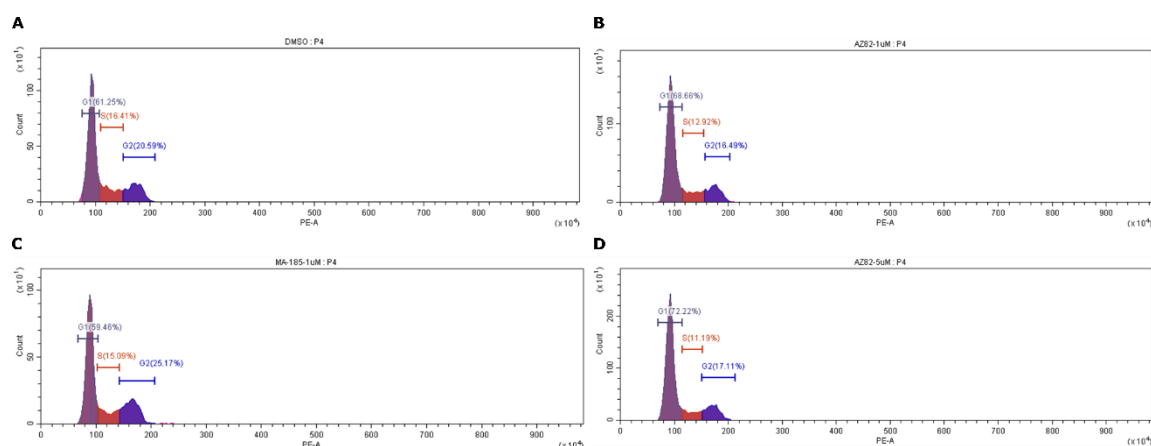
Figure 7.11: Cell cycle analysis in MDA-MB-231 cells. Flow cytometry experiment of BT549 cells stained with Propidium Iodide (PI) after treatment with **A**) DMSO, **B**) AZ82 (1 µM), **C**) MA185 (1 µM) and **D**) AZ82 (5 µM) for 24 h (n = 1, preliminary data).

Table 7.4: Cell cycle analysis in MDA-MB-231 cells related to Figure 7.11. Table showing the percentage of cells at the indicated stage of the cell cycle (G_1, S, G_2/M) depending on the treatment conditions (n = 1, preliminary data).

MDA-MB-231	G_1	S	G_2/M
DMSO	61.25	16.41	20.59
MA185 (1 µM)	59.46	15.09	25.17
AZ82 (1 µM)	68.66	12.92	16.49
AZ82 (5 µM)	72.22	11.19	17.11

Thus, MA185 may influence the cell cycle but it needs to be confirmed with more repeats of the experiment. With these preliminary data, it suggests that KIFC1 degradation using MA185 would arrest cells in the G_2 phase to at the G_2/M checkpoint or at the spindle checkpoint due to the possible formation of multipolar spindle. Very recently, Khan *et al*. published a virtual screening, docking and molecular dynamic simulation to understand how inhibitors affect KIFC1 (Khan *et al*., 2022). They highlighted that upon inhibition, KIFC1 would be unable to interact with proteins such as CDC20, CDK1 and PLK1 that play

an important role in the cell cycle. This would lead to possible cell cycle arrest, preventing bipolar mitosis, and slowing down cell proliferation and thus would facilitate cell apoptosis. KIFC1 and CDK1 were shown to be related in the APC/C complex. Singh *et al*. proposed that KIFC1 degradation is modulated by a stabilizing CDK1-dependent phosphorylation using quantitative proteomics (Singh *et al.*, 2014). This correlates with the preliminary data we have so far with the PROTAC for the observations we have made around the accumulation of cell in G_2 as well as the fact that MA185 slows down cell proliferation and possibly entry into mitosis. Further study of this would help understand the effect of MA185 on KIFC1 degradation and the cell cycle. Furthermore, experiments with different time points and GFP-KIFC1 cell lines could also be used to investigate KIFC1 degradation over time using flow cytometry. These experiments will be performed by Amanda Thomaz using MA185 to further pursue the project.

7.3.2.7 Cell proliferation

7.3.2.7.1   MTS assay

After looking at the disruption of the cell cycle and centrosome clustering, the cytotoxicity of KIFC1 PROTAC MA185 was evaluated. Cell proliferation assays were performed in MDA-MB-231 and BT549 cells treated for 72 h with a dose response of 1 nM to 20 μM of MA185 and AZ82. The plates were analysed using the MTS assay. After reading the plates, the dose response curves were obtained as shown in Figure 7.12.

IC50 (MA185) = 0.13 ± 0.01
IC50 (AZ82) = 8.70 ± 0.05

IC50 (MA185) = 0.52 ± 0.03
IC50 (AZ82) = 11.90 ± 0.75
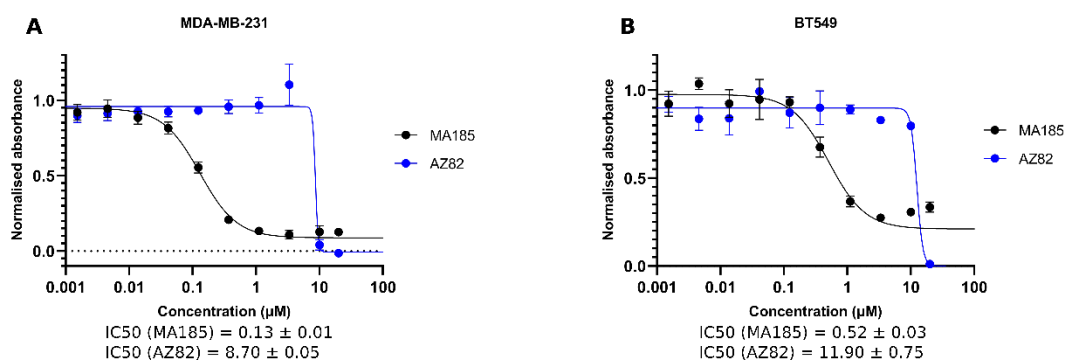
Figure 7.12: Cell proliferation inhibition of cancer cells by PROTAC MA185 and KIFC1 inhibitor AZ82. Superimposition of cell proliferation assays normalised with the DMSO control for MA185 and AZ85 in **A**) MDA-MB-231 and **B**) BT549 cells treated for 72 h, and their IC_{50}. Data are presented as the mean ± s.d. of n = 3 biological independent experiments (GraphPad Prism).

MA185 has an IC_{50} of 0.12 µM in MDA-MB-231 cells compared to 8.70 µM for AZ82, and 0.52 and 11.90 µM in BT549 for MA185 and AZ82, respectively. MA185 is thus considerably more cytotoxic than KIFC1 inhibitor AZ82, with a 20-fold improvement in BT549, and a 60-fold difference in MDA-MB-231 cells. These results suggest that PROTAC MA185 potency was significantly greater compared to the inhibitor AZ82 that it was based upon. MA185 and AZ82 were tested for significance by Mann–Whitney T-test in both BT549 and MDA-MB-231 cell lines, and were shown significantly different (*$p < 0.05$) in both.

7.3.2.7.2　Clonogenic assay

Cell viability assays were done in MDA-MB-231 and BT549 cells to look at the ability of the cells to form colonies after treatment with PROTAC MA185 or AZ82 inhibitor (Figure 7.13; Section 2.10). Two concentrations of AZ82 were used in a first instance to verify the working concentration of the inhibitor. Treatments with either 1 or 5 µM of the inhibitor had the same effect on the cells so 1 µM was chosen for the next experiments. 1 µM of MA185 reduced considerably the colony formation compared to AZ82 (Figure 7.13; Figure 7.14). Colonies were quantified using the plugin ColonieArea in ImageJ (Guzmán *et al.*, 2014), and results are presented as the ratio of colonies for the compound treatment over the colonies from the DMSO control, in three different areas (Section 2.10). Only

20% of colonies are forming for the treatment of BT549 cells with MA185 and 30% in MDA-MB-231. Around 100% of colonies are formed with the inhibitor AZ82 in both cell lines. This indicates that the PROTAC affects the cell proliferation in both cell lines whereas the inhibitor does not at these concentrations.
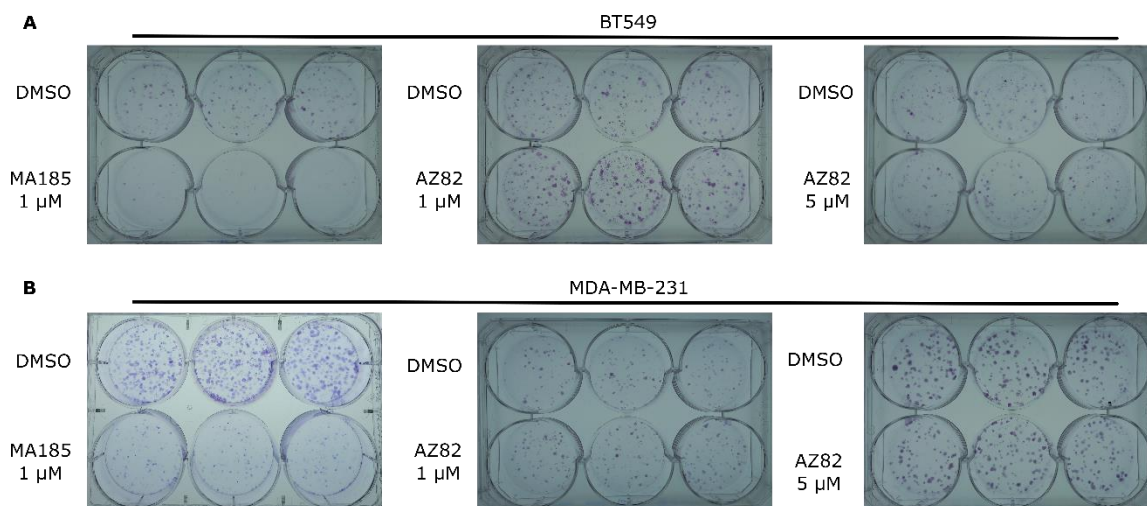
Figure 7.13: Investigation of cell viability and colony formation. Images of the clonogenic assays plates of PROTAC MA185 (1 µM), inhibitor AZ82 (1 or 5 µM) and DMSO control treatments in **A)** BT549 and **B)** MDA-MB-231 cells, treated for 24 h followed by 7-10 days incubation.
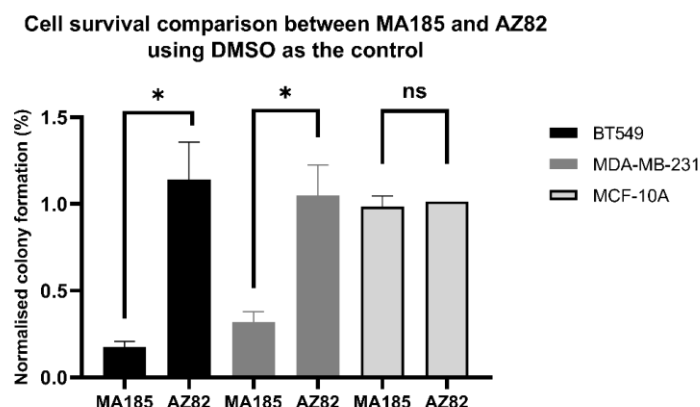
Figure 7.14: Investigation of cell viability and colony formation in BT549, MDA-MB-231 and MCF-10A cells related to Figure 7.13 and Figure 7.15. Clonogenic assays of cell survival after treatment with 1 µM PROTAC MA185 or inhibitor AZ82 for 24 h, and 10 days of colony growth for BT549 and MDA-MB-231 cells, and 7 days for MFC-10A cells. Data are presented as the mean ± s.d. of n = 2 biological independent experiments, tested by Mann–Whitney T-test for significance, *p < 0.05, **p < 0.01, ***p < 0.001, ****p < 0.0001. Some repeats were conducted by Amanda Thomaz due to time constraints.

After completing my efforts in the lab, Amanda Thomaz took over the work with PROTAC MA185. We decided to look at cells lines which do not overexpress KIFC1 or do not exhibit centrosome amplification, in order to see if the PROTAC is acting specifically against KIFC1 overexpression and role in centrosome clustering. Thus, Amanda tested PROTAC MA185 in MCF-10A cells, a breast epithelial cell line, which are not cancerous and therefore do not show KIFC1 overexpression or a dependency on centrosome clustering, compared to MDA-MB-231 and BT549 cells (Figure 7.15) (Pannu *et al.*, 2015). A clonogenic assay after 24 h treatment and 7 days growth, showed the same number of colonies from either MA185 or AZ82 treatments, and the DMSO control (Figure 7.15 A). This suggests that PROTAC MA185 is selectively cytotoxic in cells dependent on KIFC1 to cluster their centrosomes (Figure 7.13). Amanda also performed an MTS assay using MA185 to confirm the effect on the cell proliferation and viability in MCF-10A (Figure 7.15 B) compared to those I did in MDA-MB-231 and BT549 cells (Figure 7.12). MA185 IC_{50} in MCF-10A cells is 11.19 µM which is roughly 100-fold greater than that in BT549, and 50-fold different compared to MDA-MB-231 cells (Figure 7.12; Figure 7.15 B). This correlates with the observations from the clonogenic assays. The dose response of MA185 in MCF-

10A cells showed only degradation at 10 µM after 24 h. Levels of KIFC1 at 2.5 and 1 µM were also investigated for AZ82 after 24 h treatment and were the same as the DMSO control. As expected, the inhibitor AZ82 does not affect KIFC1 levels in this time frame unlike the degrader MA185. Moreover, MCF-10A cells seemed less sensitive to KIFC1 degradation than MDA-MB-231 and BT549 cells, which could be explained by the dependency of the cells on KIFC1 to cluster centrosomes in the later.
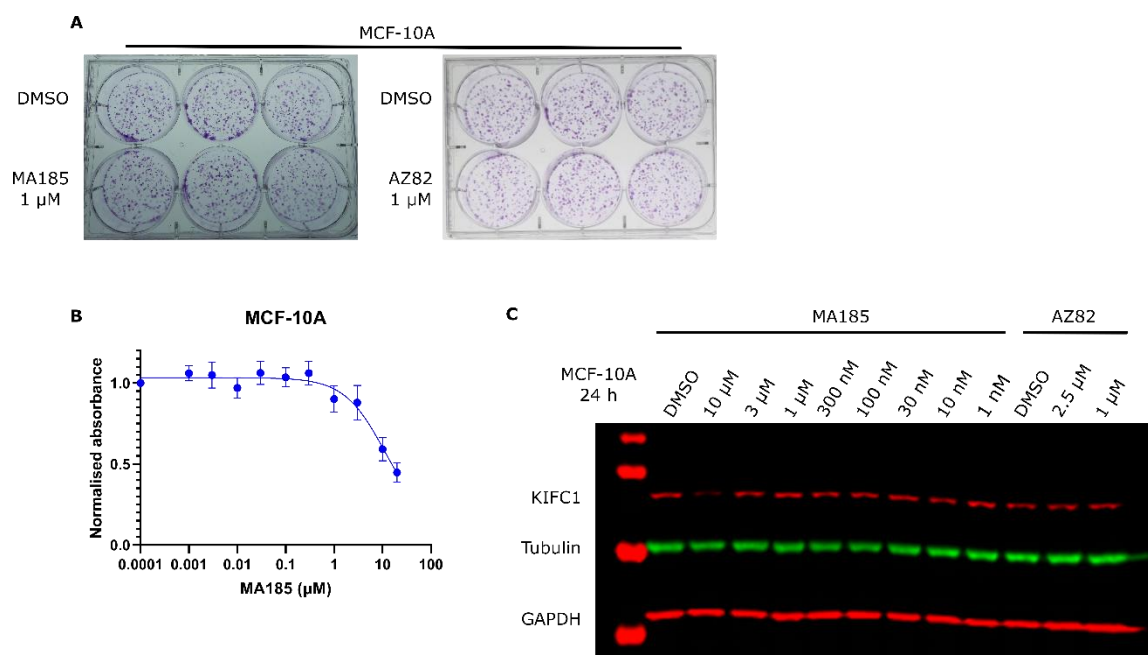
Figure 7.15: Assessment of PROTAC MA185 and inhibitor AZ82 in MCF-10A. **A**) Clonogenic assays of MCF-10A cells treated for 24 h with MA185 (1 µM) or AZ82 (1 µM). Cells were seeded at 1000 cells/well and left to grow colonies for 5 days. **B**) MTS assay of MCF-10A cells treated with a dose response of PROTAC MA185 for 72 h (n = 3). **C**) Western blot of the indicated dose response of MA185 and AZ82 in MCF-10A cells for 24 h. The membrane was blotted for KIFC1 and GAPDH as a control. The data of this figure were generated by Amanda Thomaz.

7.4   Experimental

General procedures are detailed in the Material and methods Chapter 2 Section 2.22.2.

7.4.1   KIFC1 ligand synthesis

5-Bromo-2-(3-(trifluoromethoxy)phenyl)pyridine (178) (Wu *et al.*, 2013)
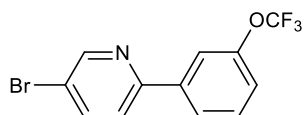
A 25-mL round-bottomed flask was loaded with the four solids under argon: sodium carbonate (1.1 g, 5.2 mmol, 1.5 eq.), tetrakis(triphenylphosphine)palladium(0) (347 mg, 0.3 mmol, 0.1 eq.), 2,5-dibromopyridine **176** (800 mg, 3.4 mmol, 1.0 eq.) and 3-(trifluoromethoxy)phenylboronic acid **177** (692 mg, 3.4 mmol, 1.0 eq.). The flask was purged with nitrogen and then H_2O (1.2 mL) and dioxane (8 mL) were added to the flask. The resulting solution was degassed for 3 minutes with nitrogen and heated at 100°C for 14 h. The reaction mixture was then cooled to room temperature and was concentrated under reduced pressure. The crude product was purified by column chromatography on silica gel and eluted with EtOAc in hexane (0 to 20 %) to give the product **178** (880 mg, 2.8 mmol, 82%) as a yellow solid/oil, with a little leftover of triphenylphosphine that could not be removed by column chromatography.

TLC: R_f = 0.30 (1:9 EtOAc/Hexane); UV.

^{1}H-NMR (400 MHz, CDCl$_3$): δ (ppm) = 8.78 (dd, 1H, *J* = 2.4, 0.6 Hz), 7.94-7.90 (m, 2H), 7.90-7.88 (m, 1H), 7.65 (dd, 1H, *J* = 8.4, 0.6 Hz), 7.52 (t, 1H, *J* = 8.0 Hz), 7.34-7.37 (m, 1H).

^{19}F-NMR (400 MHz, CDCl$_3$): δ (ppm) = -50.66.

^{13}C-NMR (101 MHz, CDCl$_3$): δ (ppm) = 154.2, 150.9, 149.9, 140.3, 139.5, 130.2, 124.9, 123.5, 121.6, 120.4 (split), 120.1, 119.4.

IR (ATR): ν (cm^{-1}) = 1254 (s, C-O), 1217 (s, C-F).

Methyl (2*R*)-2-{[(*tert*-butoxy)carbonyl]amino}-3-{6-[3-(trifluoromethoxy)phenyl]pyridin-3-yl}propanoate (180) (Wu *et al.*, 2013)
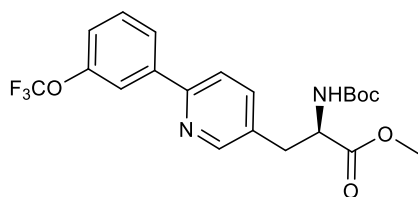
A flask was charged with zinc (302 mg, 4.6 mmol, 1.4 eq.) and iodine (42 mg, 0.17 mmol, 0.05 eq.) before being flushed three times with nitrogen. DMF (2.5 mL) was then added and it was cooled to 0 °C in an ice bath. A solution of (*S*)-methyl 2-(*tert*-butoxycarbonylamino)-3-iodopropanoate **179** (1.2 g, 3.6 mmol, 1.1 eq.) in 2.5 ml of DMF was added dropwise to the stirred suspension of zinc under nitrogen in an ice/water bath. The reaction mixture was stirred at 0 °C for 30 min under nitrogen and the ice bath was then removed. 5-bromo-2-(3-(trifluoromethoxy)phenyl)pyridine **178** (1.1 g, 3.3 mmol, 1.0 eq.) and dichlorobis(triphenylphosphine)-palladium (II) (116 mg, 0.2 mmol, 0.05 eq.) were added to the flask. The reaction mixture was then heated at 50 °C overnight. The mixture was cooled to room temperature, the zinc was filtered and the mixture was concentrated in vacuo to remove the solvent. H_2O (100 mL) was added to the residue and the solution was extracted with EtOAc (3 × 100 mL), dried over $MgSO_4$ and concentrated under reduced pressure. The crude product was purified by column chromatography on silica gel with a gradient of 0 to 50% EtOAc in Hexane to afford the product **180** (670 mg, 1.5 mmol, 46 %) as a yellow solid.

TLC: R_f = 0.50 (3:7 EtOAc/Hexane); UV.

^{1}H-NMR (400 MHz, CDCl₃): δ (ppm) = 8.48 (s, 1H), 7.94-7.89 (m, 1H), 7.68 (dd, 1H, *J* = 8.0, 0.7 Hz), 7.63-7.56 (m, 1H), 7.50 (t, 1H, *J* = 8.0 Hz), 7.28-7.25 (m, 1H), 5.18-5.04 (m, 1H), 4.72-5.61 (m, 1H), 3.78 (s, 3H), 3.24 (dd, 1H, *J* = 13.9, 5.5 Hz), 3.10 (dd, 1H, *J* = 13.9, 5.9 Hz), 1.44 (s, 9H).

^{13}C-NMR (101 MHz, CDCl₃): δ (ppm) = 171.7, 154.6, 150.5, 149.8, 141.2, 137.8, 134.9, 130.9, 130.1, 128.0, 125.0, 121.2, 120.2, 119.5, 80.2, 54.1, 52.5, 35.4, 28.3.

IR (ATR): ν (cm^{-1}) = 2978, 1742, 1707, 1153.

Methyl (2*R*)-2-[(5-methyl-4-propylthiophen-2-yl)formamido]-3-{6-[3-(trifluoromethoxy)phenyl] pyridin-3-yl}propanoate (190) (Wu *et al.*, 2013)
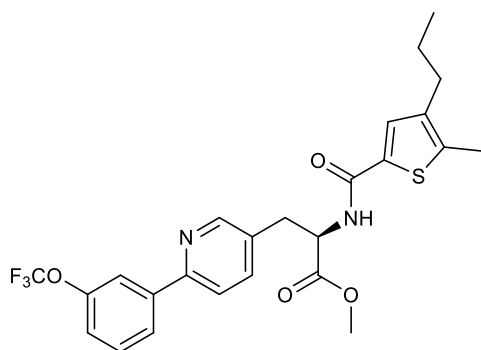
180 was Boc deprotected following general procedure **D** to give **189** and was used without further purification. **189** (108 mg, 0.3 mmol, 1.0 eq.) and 5-Methyl-4-propylthiophene-2-carboxylic acid **185** (59 mg, 0.3 mmol, 1.0 eq.) were reacted through HATU-mediated amide coupling following general procedure **A**. The crude product was purified by column chromatography on silica gel using 1% MeOH in DCM to afford the product **190** (99 mg, 0.2 mmol, 61%) as a yellow pale solid.

TLC: R_f = 0.80 (5:95 MeOH/DCM); UV.

^{1}H-NMR (400 MHz, CDCl$_3$): δ (ppm) = 8.47 (dd, 1H, *J* = 2.3, 0.7 Hz), 7.93-7.83 (m, 2H), 7.67 (dd, 1H, *J* = 8.0, 0.7 Hz), 7.59 (dd, 1H, *J* = 8.0, 2.3 Hz), 7.50 (t, 1H, *J* = 8.0 Hz), 7.28-7.25 (m, 2H), 6.44 (d, 1H, *J* = 7.1 Hz), 5.12-5.06 (m, 1H), 3.82 (s, 3H), 3.38 (dd, 1H, *J* = 14.0, 5.1 Hz), 3.26 (dd, 1H, *J* = 14.0, 5.1 Hz), 2.51-2.44 (m, 2H), 2.39 (s, 3H), 1.69-1.54 (m, 2H), 0.94 (t, 3H, *J* = 7.3 Hz).

^{13}C-NMR (101 MHz, CDCl$_3$): δ (ppm) = 171.6, 161.6, 154.6, 150.5, 149.8, 141.1, 139.6, 139.6, 137.9, 132.3, 131.0, 130.9, 130.6, 130.1, 125.0, 121.2, 120.3, 119.5, 53.2, 52.7, 35.0, 30.2, 23.5, 13.8, 13.5.

IR (ATR): ν (cm^{-1}) = 2927, 2857, 1640, 1619, 1531.

HRMS (ESI): *m/z* calculated for: $C_{25}H_{25}F_3N_2O_4SNa$ [M+Na]$^+$, 507.1511, found: 507.1511.

(2*R*)-2-[(5-Methyl-4-propylthiophen-2-yl)formamido]-3-{6-[3-(trifluoromethoxy)phenyl]pyridin-3-yl}propanoic acid (191) (Wu *et al.*, 2013)
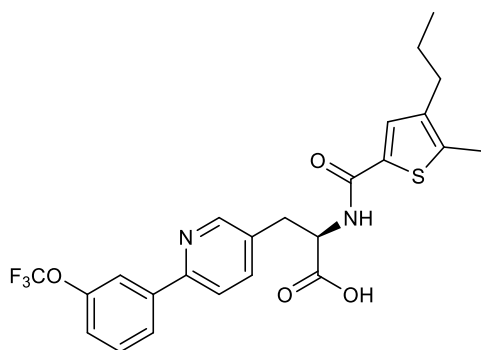
190 (40 mg, 0.08 mmol, 1.00 eq.) was resuspended in MeOH (0.5 mL) and the same amount of water (0.5 mL) was added. LiOH (2.28 mg, 0.09 mmol, 1.20 eq.) was then added to the flask and it was stirred overnight at 60 °C. In the morning, the solution was concentrated under vacuo to remove the solvent and **191** was used in the next step without further purification. Proton NMR was run on the crude to verify that the methyl group was gone. Quantitative yield.

HRMS (ESI): *m/z* calculated for: $C_{24}H_{23}F_3N_2O_4S_2$ [M+H]$^+$, 493.1403, found: 493.1392.

7.4.2 Synthesis of the VHL-series of KIFC1 PROTACs

The KIFC1 VHL-PROTACs: **187a**, **187b**, **187c** (MA186, MA187 and MA191, respectively), were synthesised following general procedure **A** for HATU-mediated amide coupling between **191**, and **20a**, **20c** and **20d**, respectively. The building blocks of the VHL ligand attached to the linker were synthesised before and details are in Chapter 3.

(2S,4R)-1-[(2S)-3,3-Dimethyl-2-{4-[(2R)-2-[(5-methyl-4-propylthiophen-2-yl)formamido]-3-{6-[3-(trifluoromethoxy)phenyl]pyridin-3-yl}propanamido]butanamido}butanoyl]-4-hydroxy-N-{[4-(4-methyl-1,3-thiazol-5-yl)phenyl]methyl}pyrrolidine-2-carboxamide (187a – MA186)
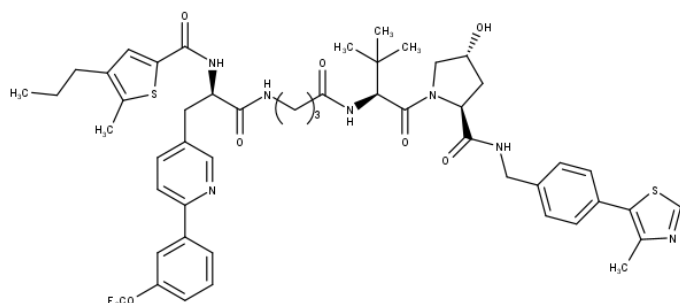
The crude product was purified by column chromatography on silica gel using 4% MeOH in DCM to give the product **187a** (9 mg, 0.01 mmol, 14%) as a white solid.

TLC: R_f = 0.45 (1:9 MeOH/DCM); UV.

^{1}H-NMR (400 MHz, CDCl$_3$): δ (ppm) = 8.70-8.65 (m, 2H), 7.88-7.83 (m, 2H), 7.82-7.77 (m, 1H), 7.65-7.60 (m, 2H), 7.47 (t, 1H, J = 8.2 Hz), 7.39-7.31 (m, 5H), 7.28-7.24 (m, 1H), 6.88 (d, 1H, J = 7.9 Hz), 6.44 (d, 1H, J = 8.2 Hz), 4.95 (q, 1H, J = 7.6 Hz), 4.78 (t, 1H, J = 8.3 Hz), 4.60 (dd, 1H, J = 15.1, 6.7 Hz), 4.36 (dd, 1H, J = 15.1, 5.2 Hz), 4.09 (d, 1H, J = 11.1 Hz), 3.67 (dd, 1H, J = 11.1, 3.2 Hz), 3.27-2.96 (m, 4H), 2.49 (s, 3H), 2.47-2.41 (m, 2H), 2.37 (s, 3H), 2.29-2.22 (m, 1H), 2.17 -2.08 (m, 1H), 1.79-1.72 (m, 4H), 1.59-1.52 (m, 2H), 1.00 (s, 9H), 0.92 (t, 3H, J = 7.3 Hz).

IR (ATR): v (cm^{-1}) = 3289, 2957, 2931, 1619, 1218.

HRMS (ESI): *m/z* calculated for: C$_{50}$H$_{58}$F$_3$N$_7$O$_7$S$_2$ [M+H]$^+$, 990.3864, found: 990.3829.

HPLC: 86.7% purity, t_R = 14.24 min.

(2*S*,4*R*)-1-[(2*S*)-3,3-Dimethyl-2-{8-[(2*R*)-2-[(5-methyl-4-propylthiophen-2-yl)formamido]-3-{6-[3-(trifluoromethoxy)phenyl]pyridin-3-yl}propanamido]octanamido}butanoyl]-4-hydroxy-N-{[4-(4-methyl-1,3-thiazol-5-yl)phenyl]methyl}pyrrolidine-2-carboxamide (187b – MA187)
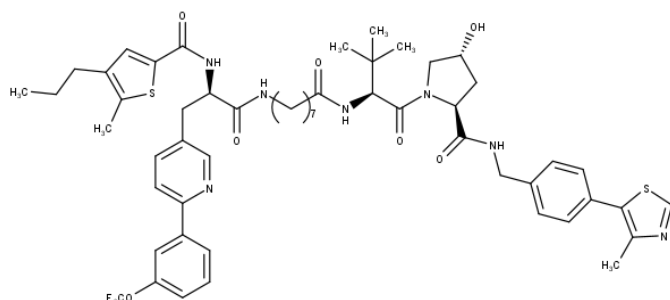
The crude product was purified by column chromatography on silica gel using 4% MeOH in DCM to give **187b** (10 mg, 0.01 mmol, 15%) as a white solid.

TLC: R_f = 0.40 (1:9 MeOH/DCM); UV.

^{1}H-NMR (400 MHz, CDCl$_3$): δ (ppm) = 8.69 (s, 1H), 8.63 (s, 1H), 7.89-7.83 (m, 2H), 7.69-7.62 (m, 2H), 7.48 (t, 1H, J = 8.0 Hz), 7.39-7.31 (m, 5H), 7.28-7.24 (m, 2H), 7.05-6.95 (m, 2H), 6.30 (d, 1H, J = 9.4 Hz), 4.90 (q, 1H, J = 7.4 Hz), 4.77 (t, 1H, J = 8.0 Hz), 4.68 (d, 1H, J = 9.1 Hz), 4.62-4.49 (m, 3H), 4.38 (dd, 1H, J = 15.1, 4.2 Hz), 4.09 (d, 1H, J = 11.5 Hz), 3.63 (dd, 1H, J = 11.2, 3.3 Hz), 3.27-3.12 (m, 4H), 2.52 (s, 3H), 2.50-2.44 (m, 2H), 2.40-2.35 (m, 4H), 2.16-2.07 (m, 2H), 1.59-1.55 (m, 2H), 1.52-1.45 (m, 2H), 1.24-1.13 (m, 6H), 1.00-0.90 (m, 14H).

IR (ATR): ν (cm^{-1}) = 3291, 2957, 2927, 1623, 1218.

HRMS (ESI): *m/z* calculated for: C$_{54}$H$_{66}$F$_3$N$_7$O$_7$S$_2$ [M+H]$^+$, 1046.4490, found: 1046.4497

HPLC: 95.4% purity, t_R = 15.17 min.

(2S,4R)-1-[(2S)-3,3-Dimethyl-2-{11-[(2R)-2-[(5-methyl-4-propylthiophen-2-yl)formamido]-3-{6-[3-(trifluoromethoxy)phenyl]pyridin-3-yl}propanamido]undecanamido}butanoyl]-4-hydroxy-N-{[4-(4-methyl-1,3-thiazol-5-yl)phenyl]methyl}pyrrolidine-2-carboxamide (187c – MA191)
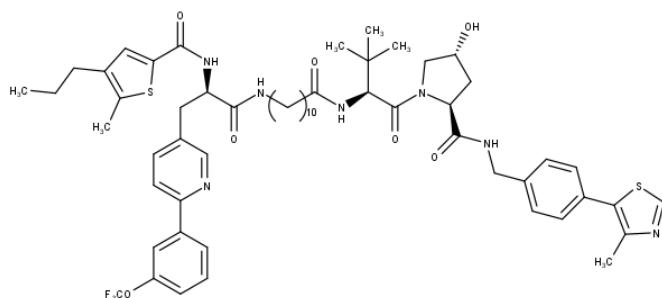
The crude product was purified by column chromatography on silica gel using 4% MeOH in DCM to give **187c** (7 mg, 0.01 mmol, 10%) as a white solid.

TLC: R_f = 0.45 (1:9 MeOH/DCM); UV.

^{1}H-NMR (400 MHz, CDCl$_3$): δ (ppm) = 8.70 (s, 1H), 8.61 (s, 1H), 7.88-7.81- (m , 2H), 7.69-7.60 (m, 2H), 7.46 (t, 1H J = 8.0 Hz), 7.40-7.31 (m, 5H), 7.27-7.21 (m, 1H), 7.10 (d, 1H), J = 8.0 Hz), 6.95 (t, 1H, J = 5.7 Hz), 6.41 (d, 1H, J = 8.9 Hz), 4.91 (q, 1H, J = 7.4 Hz), 4.75 (t, 1H, J = 8.0 Hz), 4.63-4.48 (m, 3H), 4.42-4.33 (m, 1H), 4.11 (d, 1H, J = 11.2 Hz), 3.68-3.60 (m, 1H), 3.31-3.11 (m, 4H), 2.57-2.41 (m, 7H), 2.40-2.32 (m, 3H), 2.20-2.12 (m, 3H), 1.61-1.51 (m, 4H), 1.31-1.12 (m, 12H), 0.96 (s, 9H), 0.92 (t, 3H, J = 7.4 Hz).

IR (ATR): ν (cm^{-1}) = 3293, 2927, 1619, 1218.

HRMS (ESI): m/z calculated for: C$_{57}$H$_{72}$F$_3$N$_7$O$_7$S$_2$ [M+H]$^+$, 1110.4779, found: 1110.4766.

HPLC: 94.0% purity, t_R = 16.55 min.

7.4.3 Synthesis of the CRBN-series of KIFC1 PROTACs

The KIFC1 CRBN-PROTACs: **188a (MA182)** and **188b (MA185)**, were synthesised following general procedure **A** for HATU-mediated amide coupling of **191** to **85a** and **85c**, respectively. The building blocks of the CRBN ligand attached to the linker were synthesised before and details are in Chapter 3.

(2*R*)-N-(2-{[2-(2,6-Dioxopiperidin-3-yl)-1,3-dioxo-2,3-dihydro-1H-isoindol-4-yl]amino}ethyl)-2-[(5-methyl-4-propylthiophen-2-yl)formamido]-3-{6-[3-(trifluoromethoxy)phenyl]pyridin-3-yl}propenamide (188a – MA182)
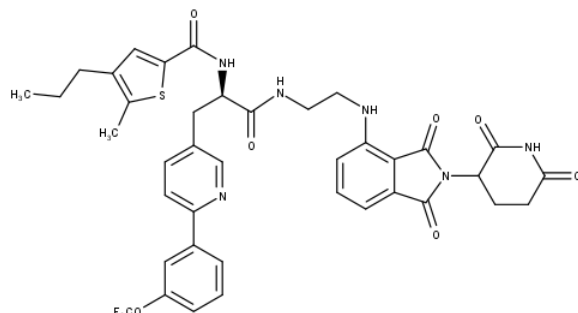
188a was purified twice by column chromatography on silica gel, the first time using 2% MeOH in DCM and the second time using 80% EtOAc in Hexanes. It was then purified by preparative TLC using 100% EtOAc to afford **188a** (8 mg, 0.01 mmol, 11%) as a green solid.

TLC: R_f = 0.25 (5:95 MeOH/DCM); UV.

^{1}H-NMR (400 MHz, CDCl$_3$): δ (ppm) = 8.57 (d, 1H, *J* = 1.7 Hz), 7.75-7.67 (m, 2H), 7.59 (dd, 1H, *J* = 8.2, 2.1 Hz), 7.56-7.50 (m, 1H), 7.46-7.41 (m, 1H), 7.37-7.30 (m, 2H), 7.20-7.14 (m, 1H), 6.85-6.71 (m, 3H), 5.57-5.40 (m, 1H), 5.28-5.18 (m, 1H), 3.77-3.59 (m, 2H), 3.33-3.09 (m, 3H), 2.92-2.61 (m, 3H), 2.32-2.22 (m, 2H), 2.11 (s, 3H), 2.05-1.96 (m, 1H), 1.51-1.40 (m, 2H), 0.94-0.87 (m, 2H), 0.87-0.79 (m, 3H).

IR (ATR): ν (cm^{-1}) = 1697, 1623, 1256.

HRMS (ESI): *m/z* calculated for: C$_{39}$H$_{37}$F$_3$N$_6$O$_7$S [M+H]$^+$, 791.2469, found: 791.2439.

HPLC: 98.8% purity, t_R =14.64 min.

(2*R*)-N-(6-{[2-(2,6-Dioxopiperidin-3-yl)-1,3-dioxo-2,3-dihydro-1H-isoindol-4-yl]amino}hexyl)-2-[(5-methyl-4-propylthiophen-2-yl)formamido]-3-{6-[3-(trifluoromethoxy)phenyl]pyridin-3-yl}propenamide (188b – MA185)
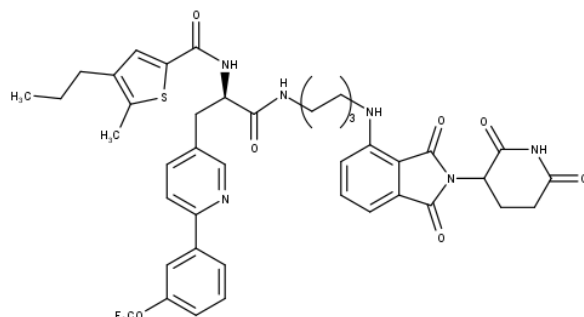
188b was purified twice by column chromatography on silica gel, the first time using 2% MeOH in DCM and the second time using 80% EtOAc in Hexanes. It was followed by two preparative TLC purifications using 5% MeOH in DCM for the first one and then with 100% EtOAc, to afford **188b** (7.5 mg, 0.01 mmol, 14%) as a green solid.

TLC: R_f = 0.50 (1:9 MeOH/DCM); UV.

^{1}H-NMR (400 MHz, CDCl$_3$): δ (ppm) = 8.59-8.55 (m, 1H), 7.89-7.83 (m, 2H), 7.71 (dd, 1H, *J* = 8.2, 1.2 Hz), 7.65-7.53 (m, 1H), 7.52-7.44 (m, 2H), 7.28-7.24 (m, 1H), 7.13-7.09 (m, 1H), 6.84-6.74 (m, 2H), 6.45-6.33 (m, 1H), 6.18-6.05 (m, 1H), 5.15-4.95 (m, 1H), 4.94-4.79 (m, 1H), 3.23-2.99 (m, 4H), 2.93-2.74 (m, 3H), 2.45 (t, 2H, *J* = 7.5 Hz), 2.37 (s, 3H), 2.18-2.09 (m, 1H), 1.63-1.50 (m, 4H), 1.45-1.38 (m, 2H), 1.38-1.29 (m, 4H), 1.24-1.16 (m, 2H), 0.96-0.86 (m, 5H).

IR (ATR): ν (cm^{-1}) = 3386, 2959, 1697, 1254.

HRMS (ESI): *m/z* calculated for: C$_{43}$H$_{45}$F$_3$N$_6$O$_7$S [M+H]$^+$, 847.3095, found: 847.3063.

HPLC: 97.5% purity, t_R = 15.99 min.

7.5   Conclusion

The first KIFC1 degrader to our knowledge was successfully designed and synthesised. PROTAC MA185 was shown to degrade KIFC1 by recruiting the CRBN E3 ligase on one side and KIFC1 on the other side using AZ82 inhibitor analogue as a building block linked with a six-carbon linker to pomalidomide. MA185 degraded almost 50% of KIFC1 after 24 h in MDA-MB-231 cells. Another shorter linker of two carbons, also recruiting CRBN, did not induce degradation. This suggests that the linker needs to be longer than two carbons. Out of the three PROTACs made for the VHL-series with different linkers length: three, seven and ten carbons, none of them degraded KIFC1. This showed that either the length/nature of the linker is not adapted to this target and cannot form a ternary complex for ubiquitination and further degradation, or that VHL may not be a good choice of E3 ligase for this specific target. The VHL-PROTACs may also not have the right properties such as solubility and cell penetration for example.

With no available crystal structure of the inhibitor into the protein, the hypothesis we made on the attachment point seemed to be correct as the molecule MA185 was able to bind to KIFC1 and to recruit the CRBN E3 ligase for degradation of the target. However, it would be interesting to have a crystal structure of AZ82 inhibitor in KIFC1 and the PROTAC bound to KIFC1 and CRBN to confirm this hypothesis, and to help improve the attachment point in order to discover even more potent KIFC1 PROTACs.

Out of the five PROTACs synthesised, only one induced degradation, showing that the linker's length and the E3 ligase used have a significant impact on KIFC1 degradation. Only a small library of two compounds recruiting CRBN and three compounds recruiting VHL was made, but the successful degradation of KIFC1 showed proof of concept and offers a scope of optimisation to improve the PROTAC molecule to further obtain better KIFC1 degradation. Thus, the project could be taken forward and more PROTACs could be synthesised to explore KIFC1 degradation with a larger SAR. The study of different linkers for the CRBN-series could be helpful to investigate if it is possible to obtain an even more potent PROTAC. The alkyl and PEG linkers have been the most used in the PROTAC field until now, but more sophisticated linkers are now being investigated, designed and used

to work on this very influential part of the PROTAC molecule (Troup *et al.*, 2020). The lack of rules and rationality in the field still make PROTAC design and synthesis time consuming and intensive. A deeper understanding of the ternary complex will be very useful for the next milestone of PROTACs as it will hopefully help to link computational modelling and X-ray structure to in vitro bioassays, to help rationalise the role of the linker (Troup *et al.*, 2020).

Even though PROTAC MA185 does not seem to induce impressive degradation at 24h, it successfully degrades 50% of KIFC1 protein. Further experiments should explore the time dependency of degradation, in particular longer incubation times would be useful such as at 48 and 72 h. MA185 exhibited a greater effect in cells than KIFC1 inhibitor AZ82 as shown with different type of cell proliferation experiments (MTS, clonogenic). This is an exciting invention, and the project is ongoing with Amanda Thomaz doing further biological experiments to investigate our PROTAC mechanism of action against KIFC1. Furthermore, our preliminary results suggest that the effect on cells without KIFC1 overexpression (MCF-10A) is minimal. It remains to be determined if it is dependent on this cell line, or applicable to other cells lines without KIFC1 overexpression and dependency. Further tests in cells with less centrosome amplification, such as MCF7, could also bring some insight. This will help understand if KIFC1 PROTAC could be effective selectively in centrosome-amplified tumor cells (Kwon *et al.*, 2008).

This project is very promising, and a patent is under preparation. One of the main objectives to take this project forward would be to understand when KIFC1 is being degraded by the PROTAC. Thus, we are planning to set up live cell imaging using IF to investigate if KIFC1 is being degraded by the PROTAC during mitosis or at another point in the cell cycle. More cell cycle analysis using flow cytometry will also be performed to understand the effect of KIFC1 in the cell cycle, and to verify if our hypotheses about cell cycle arrest at the G_2/M checkpoint can be confirmed (Figure 7.16). As a matter of fact, KIFC1 overexpression was shown to enhanced cell-cycle kinetics through G_2/M checkpoint (Pannu *et al.*, 2015), and our observations so far suggest some cell-cycle arrest in G_2 or mitosis phases upon treatment with MA185. In order to verify the PROTAC activity and selectivity over other proteins, proteomic analysis will also be undertaken.
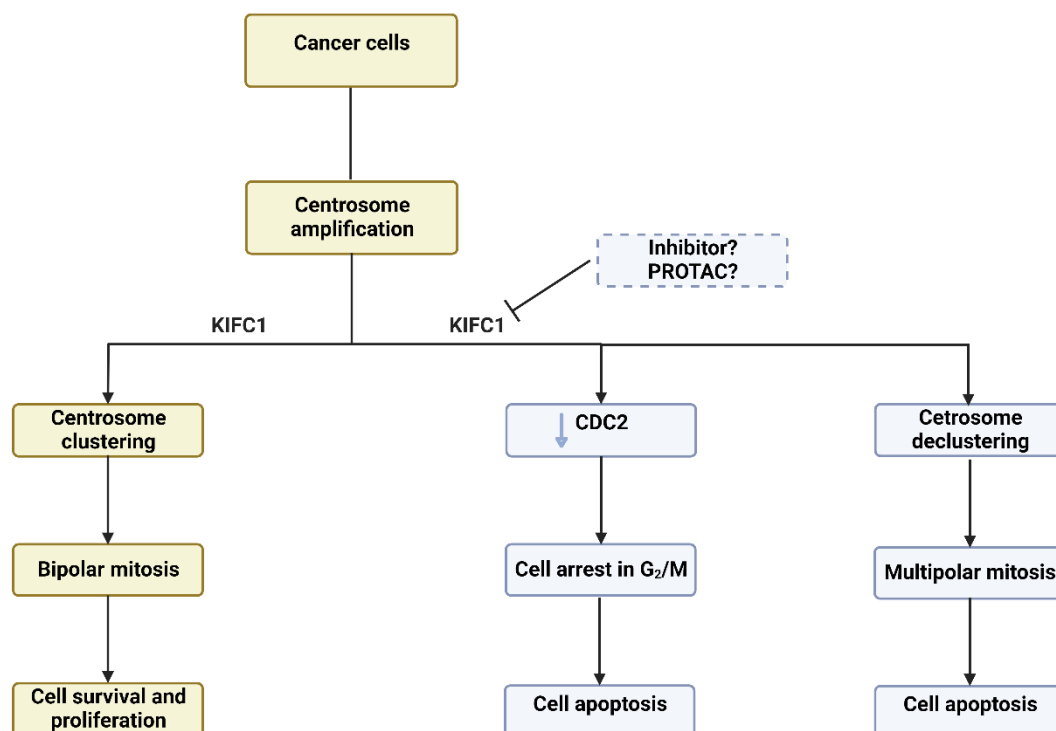
Figure 7.16: KIFC1 mechanism with or without inhibitor in cancers. Known KIFC1 mechanism of action in cancer cells in yellow. Proposed mechanism of action of KIFC1 inhibited by an inhibitor or degraded by a PROTAC molecule in blue (Inspired form Khan *et al*. study (Khan *et al.*, 2022) and made using BioRender).

8 General discussion

Cancer is a devastating disease caused by uncontrolled cell division. Commonly it is due to mutations and overexpression of regulatory proteins, which affect the cell cycle kinetics (Hanahan, 2022). Thus, the cell cycle has appeared as an interesting target for cancer therapy (Suski *et al.*, 2021). Current therapies for cancers such as chemotherapy (Kanzawa *et al.*, 2004; Amaravadi *et al.*, 2007) and radiotherapy (Paglin *et al.*, 2001; Yao *et al.*, 2003), can be very harmful to the healthy tissues of the individual (Stone *et al.*, 2003; Gao *et al.*, 2019). Thus, it is important to find better and more selective treatments.

Over the last 20 years, targeted protein degradation using PROTACs has appeared as an interesting tool to target undruggable parts of the proteome (Sakamoto *et al.*, 2001). PROTACs are bifunctional molecules recruiting the target on one side and an E3 ligase on the other to form a ternary complex between the two proteins by creating new protein-protein interactions to allow polyubiquitination and degradation of the target by the proteasome (Sakamoto *et al.*, 2001, 2003). PROTACs usually use an existing target inhibitor as the target recruiting ligand, and can significantly improve on its potency and selectivity in their action. Moreover, PROTACs degrade the target instead of just inhibiting it, compared with traditional small molecule inhibitors, which offers a very different perspective for questions of targeting aberrant protein activity, as well as issues related to drug resistance in the future (Burslem *et al.*, 2018). Since the discovery of PROTACs, the field has dramatically improved and continues to expand (Deshaies, 2015).

In this thesis, I designed and synthesised PROTACs against Wee1 protein, a kinase overexpressed in many cancers and involved in the G_2/M checkpoint (Do *et al.*, 2013) in Chapter 3. By using AZD1775 inhibitor (Hirai *et al.*, 2009), a potent but not fully selective inhibitor of Wee1 (Zhu *et al.*, 2017), PROTACs were made recruiting either the VHL or CRBN E3 ligases, the two most used E3 ligases in the field (An *et al.*, 2018). The PROTACs were assessed in Chapter 4 to look at their degradation profiles depending on the linker nature and length. These PROTACs successfully and selectively degrade Wee1 depending on the type and length of linker used (Aublette *et al.*, 2022). For the CRBN-PROTACs, short

alkyl linkers seemed the more potent, and for the VHL-PROTACs, short and long linkers seemed better than intermediate length linker. Thus, the identity of the linker appeared to play an important role in ternary complex formation and target degradation (Troup *et al.*, 2020). Ternary complex formation experiments such as ITC, SEC and native PAGE experiments were performed to help further understand the PROTACs' mechanism. These revealed successful ternary complex formation as expected, but require further optimisation to fully characterise the ternary complex between Wee1:PROTAC:VHL. More work could also be done to express CRBN protein in order to use it for ternary complex experiments. Recombinant baculovirus CRBN expression was attempted for this project, but the baculovirus particles were unfortunately not successfully generated after transfection (Fischer *et al.*, 2014; Petzold *et al.*, 2016). Understanding the ternary complex has often been proven key to help with PROTAC optimisation (Nowak *et al.*, 2018; Rodriguez-Rivera *et al.*, 2021). For instance, the first X-ray structure of the ternary complex of MZ1 bound to VHL and BRD4 lead to the synthesis to a more selective PROTAC AT1, thanks to the observations made on the folding of the linker creating new PPIs (Gadd *et al.*, 2017).

Due to the pattern in the degradation profiles of the Wee1 PROTACs, I designed, synthesised and assessed a second generation of degraders in Chapter 5, aiming to improve the potency. Better degraders MA199 (long alkyl linker) for the VHL-series and MA144 (short alkyl linker) for the CRBN-series of the second generation of Wee1 PROTACs were successfully obtained. MA144 was published in another study during the course of this project (Z. Li *et al.*, 2020). Both compounds were found to be of around the same potency as each other in the cancer cells, and are more potent than the best PROTACs of the first generation from Chapter 3 and 4. To take the Wee1 project forward, it would be useful to assess complex formation in solution or in cells using approaches such as AlphaScreen (amplified luminescent proximity homogeneous assays) or time-resolved fluorescence energy transfer (TR-FRET) (Milroy *et al.*, 2014; Wurz *et al.*, 2018; Zorba *et al.*, 2018; X. Liu *et al.*, 2020; Lin *et al.*, 2021). For example, AlphaScreen (PerkinElmer), an amplified luminescent proximity-based assay, was used to rapidly quantify ternary complex formation to select candidate molecules, and link it to the

degradation observations (Wurz *et al.*, 2018). Additionally, TR-FRET, where proteins are labelled with donor and acceptor fluorophores that emit fluorescence when in close proximity/interacting, was successfully used to study the linker influence in the ternary complex formation (Zorba *et al.*, 2018). Assessing the PROTACs cell permeability would also be profitable. Assays are being developed such as the NanoBRET technology from Promega, a proximity-based method using a live-cell assay with a NanoLuc fused E3 ligase and a fluorescent E3 ligase tracer competing with the PROTAC (Vasta *et al.*, 2021). By measuring proximity in live-cells combined with permeabilised-cells, it allows one to measure the actual intracellular availability and therefore effective concentration of the degrader.

This project generated potent and selective Wee1 degraders. The two best PROTACs of the second generation are now being investigated further in other cancer cell lines (lung, renal) with different levels of VHL and CRBN E3 ligases. This work aims to find similarities or differences between the two PROTACs in their mechanism of actions depending on which E3 ligase they recruit. It could bring some insight in the PROTAC field on how specifically E3 ligases can be recruited to become tissue specific or even cancer-type specific (Liu *et al.*, 2019).

Further work can also be done to understand Wee1 PROTAC mechanism of action at the G_2/M checkpoint, and to investigate how it can enhance DNA damaging therapies to be more efficient than current inhibitors (Yang *et al.*, 2020). This part of the work on the cell cycle is currently undergoing by another PhD student, Lauryn Buckley-Benbow. The influence of the cell lines p53 status in the PROTAC degradation is also being investigated.

By dictating our Wee1 PROTACs degradation, the linkers appeared to be a key part of the molecule (Cyrus *et al.*, 2010, 2011; Gadd *et al.*, 2017; Troup *et al.*, 2020). Therefore, generating new innovative linkers would be very useful for the field, and for medicinal chemistry in general. In this instance, part of my work was focused on the methodology around substitutable cubanes to enable a new class of short and rigid 3D linker in Chapter 6 (Reekie *et al.*, 2019). The 1,3-disubstituted cubane was generated successfully for the first time in the gram scale. The final step to obtain two different substituents in the one

and three positions was successful after a long optimisation to allow selective attachment on each side. More work is ongoing in the Coote lab in order to do this final step in a bigger scale. The 1,2-disubstituted cubane required a lot of work, and the intermediate prior to the formation of the cubane was successfully obtained. Further work needs to be done in closing the final bond, but it is very promising. These hard to make molecules that rely extensively on green photochemistry would be of wide interest in the medicinal chemistry community, and in particular in the PROTAC field where they could allow one to lock the PROTAC in a specific conformation to improve degradation.

Finally, I designed and synthesised PROTACs for a more challenging target, KIFC1, as discussed in Chapter 7. Without a crystal structure of the selected inhibitor AZ82 into the protein, studying the published SAR and models allowed the selection of the attachment point on the molecule (Yang *et al.*, 2014; Park *et al.*, 2017). KIFC1 was degraded successfully by one PROTAC recruiting the CRBN E3 ligase: MA185. Once again, the linker's length was important, as a shorter linker did not induce degradation. The E3 ligase recruited was also key as the VHL-PROTACs were not successful degraders. The project is now being developed by Amanda Thomaz to investigate the PROTAC mechanism of action and its role in the cell cycle, as well as in cancer cells with different levels of KIFC1 and centrosome amplification. The project could be taken forward by optimising the PROTAC design, as only a small library was synthesised.

Overall, successful PROTACs were designed and synthesised for two targets: Wee1 and KIFC1. The E3 ligase and the linker used in the PROTACs molecules had a determining influence on the degradation profiles of the PROTACs. This shows how useful it would be to predict which E3 ligase is best to use by looking at the E3 ligase's expression in specific tissues of the target for instance, as well as being able to predict the best protein-protein interactions between the E3 ligase and the target protein computationally (Skrabanek *et al.*, 2008; Liu *et al.*, 2019). Expanding the E3 ligase toolbox would also be useful, as emphasised by Schapira *et al.* (Schapira *et al.*, 2019). By classifying human E3 ligases, ubiquitination mechanism, expression in specific tissues and cancers, greater progress could be made in this area for the effectiveness of the PROTAC field, and for the treatment choice (Gonçalves *et al.*, 2022).

Computational modelling has already been utilised to predict ternary complex formation by simply docking the PROTAC into one protein, and then superimposing the second protein for instance (Zorba *et al.*, 2018). More developed computational modelling would bring a better insight into the PROTAC system. A group in Canada recently tried to generate in silico ensembles of PROTAC-mediated ternary complexes (Drummond *et al.*, 2019, 2020) to discriminate the PROTAC-mediated degradation. Even though this ternary complex formation algorithm presents limitations, the approach they use is very interesting and provides insights that correlated strongly with observed experimental data. Such modelling tools show much promise for further development in the future. The new protein structure database AlphaFold could also be used and help the PROTAC field (Evans *et al.*, 2021; Jumper *et al.*, 2021; Varadi *et al.*, 2022). AlphaFold can be used as a highly accurate predicator of protein structures and an extension AlphaFold-Multimer (in bioRxiv, (Evans *et al.*, 2021)) could be useful for multimeric interfaces.

Two different ways to make PROTACs were explored in this thesis, for Wee1, with a potent inhibitor and X-ray bound structure, or for KIFC1, with a less potent inhibitor and no structures that might indicate actual binding modes, and were both successful. Donovan *et al*. highlighted that a selective inhibitor towards a target does not necessarily lead to a selective degrader, as exemplified with a selective PROTAC for CDK17 that use a selective inhibitor for another target: BRAF (Donovan *et al.*, 2020). PROTACs design and selectivity is still very complex. Tools such as assessment of degradability or computational models need development, and an understanding of cooperativity and ternary complex kinetics (Rodriguez-Rivera *et al.*, 2021) will help rationalise PROTAC design by making the process faster and less empirical (Burslem *et al.*, 2020). Furthermore, the next effort in the PROTAC field will be to face complex drug metabolism and pharmacokinetics (DMPK) challenges compared with traditional small molecule inhibitors to make then orally bioavailable (Cantrill *et al.*, 2020; Poongavanam *et al.*, 2021).

Final summary

The work presented here shows the successful use of the PROTAC technology to target two different cancer targets: Wee1 and KIFC1. The work on Wee1 can now be used as a comparison of the use of the two E3 ligases to make potent molecules. The structure activity relationship and optimisation of Wee1 PROTACs lead to a useful understanding of the Wee1:PROTAC:E3 ligase system, which is different to every target and appeared to be dependent strongly on the linker. PROTAC effectiveness at the G_2/M checkpoint can now be compared to AZD1775, Wee1 inhibitor, against DNA damaging therapies for cancer treatments. The discovery of the first KIFC1 PROTAC: MA185, has established an exciting solid foundation for further research on the PROTAC degradation of KIFC1 as a selective treatment for targeting cancer cells over healthy cells. This functional KIFC1 PROTAC, capable of declustering amplified centrosomes and generating cytotoxicity in affected cells, can now be used as a starting point and model for further optimisation of the molecule and to better understand its mechanism of action.

9 References

Adams, J. (2003) 'The proteasome: structure, function, and role in the cell', *Cancer Treatment Reviews*, 29, pp. 3–9. Available at: https://doi.org/10.1016/S0305-7372(03)00081-1.

Ahn, G. *et al.* (2021) 'LYTACs that engage the asialoglycoprotein receptor for targeted protein degradation', *Nature Chemical Biology*, 17, pp. 937-946. Available at: https://doi.org/10.1038/s41589-021-00770-1.

Akutsu, M. *et al.* (2016) 'Ubiquitin chain diversity at a glance', *Journal of Cell Science*, 129(5), pp. 875–880. Available at: https://doi.org/10.1242/jcs.183954.

Amaravadi, R.K. *et al.* (2007) 'Autophagy inhibition enhances therapy-induced apoptosis in a Myc-induced model of lymphoma.', *The Journal of clinical investigation*, 117(2), pp. 326–336. Available at: https://doi.org/10.1172/JCI28833.

An, S. *et al.* (2018) 'Small-molecule PROTACs: An emerging and promising approach for the development of targeted therapy drugs', *EBioMedicine*, 36, pp. 553–562. Available at: https://doi.org/10.1016/j.ebiom.2018.09.005.

Anderhub, S.J. *et al.* (2012) 'Centrosome amplification in tumorigenesis.', *Cancer letters*, 322 1, pp. 8–17. Available at: https://doi.org/10.1016/j.canlet.2012.02.006.

Ardito, F. *et al.* (2017) 'The crucial role of protein phosphorylation in cell signaling and its use as targeted therapy.', *International Journal of Molecular Medicine,* 40, pp. 271-280. Available at: https://doi.org/10.3892/ijmm.2017.3036.

Au - Lindner, S. *et al.* (2019) 'Chemical Inactivation of the E3 Ubiquitin Ligase Cereblon by Pomalidomide-based Homo-PROTACs', *JoVE*, (147), p. e59472. Available at: https://doi.org/doi:10.3791/59472.

Aublette, M.C. *et al.* (2022) 'Selective Wee1 degradation by PROTAC degraders recruiting VHL and CRBN E3 ubiquitin ligases', *Bioorganic & Medicinal Chemistry Letters*,

64, p. 128636. Available at: https://doi.org/10.1016/j.bmcl.2022.128636.

Banik, S.M. *et al.* (2020) 'Lysosome-targeting chimaeras for degradation of extracellular proteins', *Nature*, 584(7820), pp. 291–297. Available at: https://doi.org/10.1038/s41586-020-2545-9.

Barborak, J.C. *et al.* (1966) 'A Convenient Synthesis of the Cubane System', *Journal of the American Chemical Society*, 88(6), pp. 1328–1329. Available at: https://doi.org/10.1021/ja00958a050.

Barnieh, F.M. *et al.* (2021) 'Progress towards a clinically-successful ATR inhibitor for cancer therapy', *Current Research in Pharmacology and Drug Discovery*, 2, p. 100017. Available at: https://doi.org/10.1016/j.crphar.2021.100017.

Bartlett, J.B. *et al.* (2004) 'The evolution of thalidomide and its IMiD derivatives as anticancer agents', *Nature Reviews Cancer*, 4(4), pp. 314–322. Available at: https://doi.org/10.1038/nrc1323.

Bemis, T.A. *et al.* (2021) 'Unraveling the Role of Linker Design in Proteolysis Targeting Chimeras', *Journal of Medicinal Chemistry*, 64(12), pp. 8042–8052. Available at: https://doi.org/10.1021/acs.jmedchem.1c00482.

Berndsen, C.E. *et al.* (2014) 'New insights into ubiquitin E3 ligase mechanism', *Nature Structural and Molecular Biology*, 21, pp. 301–307. Available at: https://doi.org/10.1038/nsmb.2780.

Bondeson, D.P. *et al.* (2015) 'Catalytic in vivo protein knockdown by small-molecule PROTACs', *Nature Chemical Biology*, 11(8), pp. 611–617. Available at: https://doi.org/10.1038/nchembio.1858.

Bondeson, D.P. *et al.* (2018) 'Lessons in PROTAC Design from Selective Degradation with a Promiscuous Warhead', *Cell Chemical Biology*, 25(1), pp. 78-87.e5. Available at: https://doi.org/10.1016/j.chembiol.2017.09.010.

Britten, T.K. *et al.* (2019) '4-π-Photocyclization of 1,2-Dihydropyridazines: An Approach

to Bicyclic 1,2-Diazetidines with Rich Synthetic Potential', *Organic Letters*, 21(22), pp. 9232–9235. Available at: https://doi.org/10.1021/acs.orglett.9b03613.

Britten, T.K., *et al.* (2019) 'An efficient preparation of 1,2-dihydropyridazines through a Diels-Alder/palladium-catalysed elimination sequence', *Tetrahedron Letters*, 60(22), pp. 1498–1500. Available at: https://doi.org/10.1016/j.tetlet.2019.04.054.

Bryce-Smith, D. *et al.* (1963) 'Liquid-phase photolysis. Part VI. Preparation of cyclo-octatetraenes by the photoaddition of acetylenes to benzene: dimerisation of phenylacetylene to 1-phenylazulene and 1-phenylnaphthalene', *Journal of the Chemical Society*, pp. 695–701. Available at: https://doi.org/10.1039/JR9630000695.

Buckley, D.L. *et al.* (2012) 'Targeting the von Hippel-Lindau E3 ubiquitin ligase using small molecules to disrupt the VHL/HIF-1α interaction', *Journal of the American Chemical Society*, 134(10), pp. 4465-8. Available at: https://doi.org/10.1021/ja209924v.

Buckley, D.L. *et al.* (2015) 'HaloPROTACS: Use of Small Molecule PROTACs to Induce Degradation of HaloTag Fusion Proteins', *ACS Chemical Biology*, 10(8), pp. 1831–1837. Available at: https://doi.org/10.1021/acschembio.5b00442.

Burotto, M. *et al.* (2014) 'The MAPK pathway across different malignancies: A new perspective', *Cancer*, 120(22), pp. 3446–3456. Available at: https://doi.org/10.1002/cncr.28864.

Burslem, G.M. *et al.* (2018) 'The Advantages of Targeted Protein Degradation Over Inhibition: An RTK Case Study', *Cell Chemical Biology*, 25(1), pp. 67-77.e3. Available at: https://doi.org/10.1016/j.chembiol.2017.09.009.

Burslem, G.M. *et al.* (2020) 'Proteolysis-Targeting Chimeras as Therapeutics and Tools for Biological Discovery', *Cell*, 181(1), pp. 102–114. Available at: https://doi.org/10.1016/j.cell.2019.11.031.

Cai, S. *et al.* (2010) 'Proper organization of microtubule minus ends is needed for midzone stability and cytokinesis.', *Current biology : CB*, 20(9), pp. 880–885. Available at: https://doi.org/10.1016/j.cub.2010.03.067.

Cantrill, C. *et al.* (2020) 'Fundamental aspects of DMPK optimization of targeted protein degraders', *Drug Discovery Today*, 25(6), pp. 969–982. Available at: https://doi.org/10.1016/j.drudis.2020.03.012.

Cao, S. *et al.* (2021) 'Proteolysis-Targeting Chimera (PROTAC) Modification of Dovitinib Enhances the Antiproliferative Effect against FLT3-ITD-Positive Acute Myeloid Leukemia Cells', *Journal of Medicinal Chemistry*, 64(22), pp. 16497–16511. Available at: https://doi.org/10.1021/acs.jmedchem.1c00996.

Ceccarelli, D.F. *et al.* (2011) 'An allosteric inhibitor of the human Cdc34 ubiquitin-conjugating enzyme', *Cell*, 145(7), pp. 1075–1087. Available at: https://doi.org/10.1016/j.cell.2011.05.039.

Chaisan, N. *et al.* (2021) 'Dibrominative Spirocyclization of 2-Butynolyl Anilides: Synthesis of gem-Dibromospirocyclic Benzo[d][1,3]oxazines and Their Application in the Synthesis of 4H-Furo[3,2-b]indoles', *The Journal of Organic Chemistry*, 86(6), pp. 4671–4698. Available at: https://doi.org/10.1021/acs.joc.1c00086.

Chalmers, B.A. *et al.* (2016) 'Validating Eaton's Hypothesis: Cubane as a Benzene Bioisostere', *Angewandte Chemie International Edition*, 55(11), pp. 3580–3585. Available at: https://doi.org/10.1002/anie.201510675.

Chamberlain, P.P. (2018) 'Linkers for protein degradation', *Nature Chemical Biology*, 14(7), pp. 639–640. Available at: https://doi.org/10.1038/s41589-018-0057-9.

Chan, K.-H. *et al.* (2018) 'Impact of Target Warhead and Linkage Vector on Inducing Protein Degradation: Comparison of Bromodomain and Extra-Terminal (BET) Degraders Derived from Triazolodiazepine (JQ1) and Tetrahydroquinoline (I-BET726) BET Inhibitor Scaffolds', *Journal of Medicinal Chemistry*, 61(2), pp. 504–513. Available at: https://doi.org/10.1021/acs.jmedchem.6b01912.

Chandankar, S.S. *et al.* (2020) 'Stereoselective Synthesis of Dysoxylactam A', *Organic Letters*, 22(2), pp. 653–655. Available at: https://doi.org/10.1021/acs.orglett.9b04426.

Chapman, N.B. *et al.* (1970) 'Preparations and properties of caged polycyclic systems. 1.

Pentacyclo[5.3.0.02,5.03,9.04,8]decane and pentacyclo[4.3.0.02,5.03,8.04,7]nonane derivatives', *The Journal of Organic Chemistry*, 35(11), pp. 3860–3867. Available at: https://doi.org/10.1021/jo00836a062.

Chen, T. *et al.* (2012) 'Targeting the S and G2 checkpoint to treat cancer', *Drug Discovery Today*, 17(5), pp. 194–202. Available at: https://doi.org/10.1016/j.drudis.2011.12.009.

Ciechanover, A. (1994) 'The ubiquitin-proteasome proteolytic pathway', *Cell*, 79(1), pp. 13–21. Available at: https://doi.org/10.1016/0092-8674(94)90396-4.

Clague, M.J. *et al.* (2010) 'Ubiquitin: Same Molecule, Different Degradation Pathways', *Cell*, 143(5), pp. 682–685. Available at: https://doi.org/10.1016/j.cell.2010.11.012.

Cockman, M.E. *et al.* (2000) 'Hypoxia Inducible Factor-α Binding and Ubiquitylation by the von Hippel-Lindau Tumor Suppressor Protein', *Journal of Biological Chemistry*, 275(33), pp. 25733–25741. Available at: https://doi.org/10.1074/jbc.M002740200.

Cole, K.A. *et al.* (2020) 'Phase I clinical trial of the Wee1 inhibitor adavosertib (AZD1775) with irinotecan in children with relapsed solid tumors: A COG phase I consortium report (ADVL1312)', *Clinical Cancer Research*, 26(6), pp. 1213–1219. Available at: https://doi.org/10.1158/1078-0432.CCR-19-3470.

Conway, S.J. (2020) 'Bifunctional Molecules beyond PROTACs', *Journal of Medicinal Chemistry*, 63(6), pp. 2802–2806. Available at: https://doi.org/10.1021/acs.jmedchem.0c00293.

Cyrus, K. *et al.* (2010) 'Jostling for position: optimizing linker location in the design of estrogen receptor-targeting PROTACs', *ChemMedChem*, 5(7), pp. 979–985. Available at: https://doi.org/10.1002/cmdc.201000146.

Cyrus, K. *et al.* (2011) 'Impact of linker length on the activity of PROTACs.', *Molecular BioSystems*, 7(2), pp. 359–364. Available at: https://doi.org/10.1039/C0MB00074D.

D'Amato, R.J. *et al.* (1994) 'Thalidomide is an Inhibitor of Angiogenesis', *Proceedings of the National Academy of Sciences of the United States of America*, 91(9), pp. 4082–

4085. Available at: http://www.jstor.org/stable/2364596.

Deshaies, R.J. (1999) 'SCF and Cullin/RING H2-Based Ubiquitin Ligases', *Annual Review of Cell and Developmental Biology*, 15(1), pp. 435–467. Available at: https://doi.org/10.1146/annurev.cellbio.15.1.435.

Deshaies, R.J. (2015) 'Prime time for PROTACs', *Nature Chemical Biology*, 11, p. 634. Available at: https://doi.org/10.1038/nchembio.1887.

Dess, D.B. et al. (1983) 'Readily accessible 12-I-5 oxidant for the conversion of primary and secondary alcohols to aldehydes and ketones.' *The Journal of Organic Chemistry*, 48(22), pp. 4155-4156. Available at: https://doi.org/10.1021/jo00170a070

Dhillon, A.S. *et al.* (2007) 'MAP kinase signalling pathways in cancer', *Oncogene*, 26, p. 3279. Available at: https://doi.org/10.1038/sj.onc.1210421.

Do, K. *et al.* (2015) 'Phase I Study of Single-Agent AZD1775 (MK-1775), a Wee1 Kinase Inhibitor, in Patients With Refractory Solid Tumors', *Journal of clinical oncology : official journal of the American Society of Clinical Oncology*, 33(30), pp. 3409–3415. Available at: https://doi.org/10.1200/JCO.2014.60.4009.

Do, K. *et al.* (2013) 'Wee1 kinase as a target for cancer therapy', *Cell Cycle*, 12(19), pp. 3159–3164. Available at: https://doi.org/10.4161/cc.26062.

Dolomanov, O. V *et al.* (2009) 'OLEX2: a complete structure solution, refinement and analysis program', *Journal of Applied Crystallography*, 42(2), pp. 339–341. Available at: https://doi.org/10.1107/S0021889808042726.

Donovan, K.A. *et al.* (2020) 'Mapping the Degradable Kinome Provides a Resource for Expedited Degrader Development', *Cell*, 183(6), pp. 1741–1731. Available at: https://doi.org/10.1016/j.cell.2020.10.038.

Douglass Jr, E.F. *et al.* (2013) 'A comprehensive mathematical model for three-body binding equilibria', *Journal of the American Chemical Society*, 135(16), pp. 6092–6099. Available at: https://doi.org/10.1021/ja311795d.

Drummond, M.L. *et al.* (2020) 'Improved Accuracy for Modeling PROTAC-Mediated Ternary Complex Formation and Targeted Protein Degradation via New In Silico Methodologies', *bioRxiv*. Available at: https://doi.org/10.1101/2020.07.10.197186.

Drummond, M.L. *et al.* (2019) 'In Silico Modeling of PROTAC-Mediated Ternary Complexes: Validation and Application', *Journal of Chemical Information and Modeling*, 59(4), pp. 1634–1644. Available at: https://doi.org/10.1021/acs.jcim.8b00872.

Duncan, L.M. *et al.* (2006) 'Lysine-63-linked ubiquitination is required for endolysosomal degradation of class I molecules', *The EMBO Journal*, 25(8), pp. 1635–1645. Available at: https://doi.org/10.1038/sj.emboj.7601056.

de Duve, C. *et al.* (1966) 'Functions of Lysosomes', *Annual Review of Physiology*, 28(1), pp. 435–492. Available at: https://doi.org/10.1146/annurev.ph.28.030166.002251.

Eaton, P.E. (1992) 'Cubanes: Starting Materials for the Chemistry of the 1990s and the New Century', *Angewandte Chemie International Edition in English*, 31(11), pp. 1421–1436. Available at: https://doi.org/10.1002/anie.199214211.

Eaton, P.E. *et al.* (1985) 'Systematic substitution on the cubane nucleus. Amide activation for metalation of "saturated" systems', *Journal of the American Chemical Society*, 107(3), pp. 724–726. Available at: https://doi.org/10.1021/ja00289a046.

Eaton, P.E. *et al.* (1964) 'The Cubane System', *Journal of the American Chemical Society*, 86(5), pp. 962–964. Available at: https://doi.org/10.1021/ja01059a072.

Evans, R. *et al.* (2021) 'Protein complex prediction with AlphaFold-Multimer', *bioRxiv*. Available at: https://doi.org/10.1101/2021.10.04.463034.

Falkiner, M.J. *et al.* (2013) 'Pilot-Scale Production of Dimethyl 1,4-Cubanedicarboxylate', *Organic Process Research & Development*, 17(12), pp. 1503–1509. Available at: https://doi.org/10.1021/op400181g.

Farnaby, W. *et al.* (2019) 'BAF complex vulnerabilities in cancer demonstrated via structure-based PROTAC design', *Nature chemical biology*, 15(7), pp. 672–680. Available

at: https://doi.org/10.1038/s41589-019-0294-6.

Ferguson, F. et al. (2018) 'Kinase inhibitors: the road ahead.', *Nature Reviews Drug Discovery*, 17, pp. 353–377. Available at: https://doi.org/10.1038/nrd.2018.21.

Fink, G. *et al.* (2009) 'The mitotic kinesin-14 Ncd drives directional microtubule–microtubule sliding', *Nature Cell Biology*, 11(6), pp. 717–723. Available at: https://doi.org/10.1038/ncb1877.

Finley, D. *et al.* (2012) 'The ubiquitin-proteasome system of Saccharomyces cerevisiae', *Genetics*, 192(2), pp. 319–360. Available at: https://doi.org/10.1534/genetics.112.140467.

Fischer, E.S. *et al.* (2014) 'Structure of the DDB1–CRBN E3 ubiquitin ligase in complex with thalidomide', *Nature*, 512(7512), pp. 49–53. Available at: https://doi.org/10.1038/nature13527.

Forster, M. *et al.* (2016) 'Selective JAK3 Inhibitors with a Covalent Reversible Binding Mode Targeting a New Induced Fit Binding Pocket', *Cell Chemical Biology*, 23(11), pp. 1335–1340. Available at: https://doi.org/10.1016/j.chembiol.2016.10.008.

Frost, J. *et al.* (2016) 'Potent and selective chemical probe of hypoxic signalling downstream of HIF-α hydroxylation via VHL inhibition', *Nature Communications*, 7, p. 13312. Available at: https://doi.org/10.1038/ncomms13312.

Fry, A.M. *et al.* (2017) 'Recent advances in pericentriolar material organization: ordered layers and scaffolding gels', *F1000Research*, 6, p. 1622. Available at: https://doi.org/10.12688/f1000research.11652.1.

Gadd, M.S. *et al.* (2017) 'Structural basis of PROTAC cooperative recognition for selective protein degradation', *Nature Chemical Biology*, 13(5), pp. 514-521. Available at: https://doi.org/10.1038/nchembio.2329.

Galan, J.-M. *et al.* (1997) 'Ubiquitin Lys63 is involved in ubiquitination of a yeast plasma membrane protein', *The EMBO Journal*, 16(19), pp. 5847–5854. Available at:

https://doi.org/10.1093/emboj/16.19.5847.

Galdeano, C. *et al.* (2014) 'Structure-guided design and optimization of small molecules targeting the protein-protein interaction between the von Hippel-Lindau (VHL) E3 ubiquitin ligase and the hypoxia inducible factor (HIF) alpha subunit with in vitro nanomolar affinities', *Journal of Medicinal Chemistry*, 57(20), pp. 8657–8663. Available at: https://doi.org/10.1021/jm5011258.

Gao, Q. *et al.* (2019) 'How chemotherapy and radiotherapy damage the tissue: Comparative biology lessons from feather and hair models', *Experimental Dermatology*, 28(4), pp. 413–418. Available at: https://doi.org/10.1111/exd.13846.

Gao, X. *et al.* (2022) 'Phase 1/2 study of ARV-110, an androgen receptor (AR) PROTAC degrader, in metastatic castration-resistant prostate cancer (mCRPC).', *Journal of Clinical Oncology*, 40(6_suppl), p. 17. Available at: https://doi.org/10.1200/JCO.2022.40.6_suppl.017.

Geetha, T. *et al.* (2005) 'Lysine 63 Polyubiquitination of the Nerve Growth Factor Receptor TrkA Directs Internalization and Signaling', *Molecular Cell*, 20(2), pp. 301–312. Available at: https://doi.org/10.1016/j.molcel.2005.09.014.

Gerecitano, J.F. *et al.* (2013) 'A Phase I trial of the kinesin spindle protein (Eg5) inhibitor AZD4877 in patients with solid and lymphoid malignancies.', *Investigational new drugs*, 31(2), pp. 355–362. Available at: https://doi.org/10.1007/s10637-012-9821-y.

Ghoreschi, K. *et al.* (2011) 'Modulation of Innate and Adaptive Immune Responses by Tofacitinib (CP-690,550)', *The Journal of Immunology*, 186(7), pp. 4234–4243. Available at: https://doi.org/10.4049/jimmunol.1003668.

Godinho, S.A. *et al.* (2009) 'Centrosomes and cancer: how cancer cells divide with too many centrosomes', *Cancer and Metastasis Reviews*, 28(1), pp. 85–98. Available at: https://doi.org/10.1007/s10555-008-9163-6.

Gonçalves, E. *et al.* (2022) 'Pan-cancer proteomic map of 949 human cell lines.', *Cancer cell*, 40(8), pp. 835-849.e8. Available at: https://doi.org/10.1016/j.ccell.2022.06.010.

Grange, R.L. *et al.* (2010) '[4+2] Cycloaddition Reactions Between 1,8-Disubstituted Cyclooctatetraenes and Diazo Dienophiles: Stereoelectronic Effects, Anticancer Properties and Application to the Synthesis of 7,8-Substituted Bicyclo[4.2.0]octa-2,4-dienes', *Chemistry – A European Journal*, 16(29), pp. 8894–8903. Available at: https://doi.org/10.1002/chem.200903454.

Gray, J.E. *et al.* (2017) 'Phase II trial of AZD1775 in combination with carboplatin and paclitaxel in stage IV squamous cell lung cancer (sqNSCLC): Preliminary results.', *Journal of Clinical Oncology*, 35(15), p. e20672. Available at: https://doi.org/10.1200/jco.2017.35.15_suppl.e20672.

Grovenstein, E. *et al.* (1961) 'Photochemical reaction of benzene with dimethyl acetylenedicarboxylate', *Tetrahedron Letters*, 2(4), pp. 148–150. Available at: https://doi.org/10.1016/S0040-4039(01)99227-5.

Guzmán, C. *et al.* (2014) 'ColonyArea: An ImageJ Plugin to Automatically Quantify Colony Formation in Clonogenic Assays', *PLOS ONE*, 9(3), p. e92444. Available at: https://doi.org/10.1371/journal.pone.0092444.

Hall, A.B. *et al.* (2014) 'Potentiation of tumor responses to DNA damaging therapy by the selective ATR inhibitor VX-970.', *Oncotarget*, 5(14), pp. 5674–5685. Available at: https://doi.org/10.18632/oncotarget.2158.

Hamerla, C. *et al.* (2020) 'Photochemical mechanism of DEACM uncaging: a combined time-resolved spectroscopic and computational study', *Phys. Chem. Chem. Phys.*, 22(24), pp. 13418–13430. Available at: https://doi.org/10.1039/C9CP07032J.

Hamilton, E.P. *et al.* (2022) 'ARV-471, an estrogen receptor (ER) PROTAC degrader, combined with palbociclib in advanced ER+/human epidermal growth factor receptor 2–negative (HER2-) breast cancer: Phase 1b cohort (part C) of a phase 1/2 study.', *Journal of Clinical Oncology*, 40(16_suppl), pp. TPS1120–TPS1120. Available at: https://doi.org/10.1200/JCO.2022.40.16_suppl.TPS1120.

Han, T. *et al.* (2017) 'Anticancer sulfonamides target splicing by inducing RBM39

degradation via recruitment to DCAF15', *Science*, 356(6336), p. eaal3755. Available at: https://doi.org/10.1126/science.aal3755.

Han, X. *et al.* (2019) 'Discovery of Highly Potent and Efficient PROTAC Degraders of Androgen Receptor (AR) by Employing Weak Binding Affinity VHL E3 Ligase Ligands', *Journal of Medicinal Chemistry*, 62(24), pp. 11218-11231. Available at: https://doi.org/10.1021/acs.jmedchem.9b01393.

Hanahan, D. (2022) 'Hallmarks of Cancer: New Dimensions', *Cancer Discovery*, 12(1), pp. 31–46. Available at: https://doi.org/10.1158/2159-8290.CD-21-1059.

Hartwell, L.H. *et al.* (1989) 'Checkpoints: Controls That Ensure the Order of Cell Cycle Events', *Science*, 246(4930), pp. 629–634. Available at: https://doi.org/10.1126/science.2683079.

Haslett, P.A. *et al.* (1998) 'Thalidomide costimulates primary human T lymphocytes, preferentially inducing proliferation, cytokine production, and cytotoxic responses in the CD8+ subset.', *The Journal of experimental medicine*, 187(11), pp. 1885–1892. Available at: https://doi.org/10.1084/jem.187.11.1885.

Heald, R. (2000) 'Motor function in the mitotic spindle', *Cell*, 102(4), pp. 399–402. Available at: https://doi.org/10.1016/s0092-8674(00)00044-1.

Hedaya, E. *et al.* (1971) 'Flash vacuum pyrolysis. X. Azocine. Flash vacuum pyrolysis of 7,8-diazapentacyclo[4.2.2.02,5.03,9.04,10]dec-7-ene (diazabasketene)', *Journal of American Chemical Society*, 93(15), pp. 3817–3818. Available at: https://doi.org/10.1021/ja00744a071

Hendrick, C.E. *et al.* (2022) 'Direct-to-Biology Accelerates PROTAC Synthesis and the Evaluation of Linker Effects on Permeability and Degradation', *ACS Medicinal Chemistry Letters*, 13(7), pp. 1182–1190. Available at: https://doi.org/10.1021/acsmedchemlett.2c00124.

Henning, N.J. *et al.* (2021) 'Deubiquitinase-Targeting Chimeras for Targeted Protein Stabilization', *bioRxiv*, p. 2021.04.30.441959. Available at:

https://doi.org/10.1101/2021.04.30.441959.

Hershko, A. *et al.* (1992) 'The ubiquitin system for protein degradation.', *Annual review of biochemistry*, 61, pp. 761–807. Available at: https://doi.org/10.1146/annurev.bi.61.070192.003553.

Hershko, A. *et al.* (1998) 'THE UBIQUITIN SYSTEM', *Annual Review of Biochemistry*, 67(1), pp. 425–479. Available at: https://doi.org/10.1146/annurev.biochem.67.1.425.

Hidaka, H. *et al.* (1984) 'Isoquinolinesulfonamides, novel and potent inhibitors of cyclic nucleotide-dependent protein kinase and protein kinase C', *Biochemistry*, 23(21), pp. 5036–5041. Available at: https://doi.org/10.1021/bi00316a032.

Hilpert, L.J. *et al.* (2019) 'Rhodium-Catalyzed Parallel Kinetic Resolution of Racemic Internal Allenes Towards Enantiopure Allylic 1,3-Diketones', *Angewandte Chemie - International Edition*, 58(29), pp. 9939–9943. Available at: https://doi.org/10.1002/anie.201903365.

Hines, J. *et al.* (2019) 'MDM2-Recruiting PROTAC Offers Superior, Synergistic Antiproliferative Activity via Simultaneous Degradation of BRD4 and Stabilization of p53', *Cancer research*, 79(1), pp. 251–262. Available at: https://doi.org/10.1158/0008-5472.CAN-18-2918.

Hirai, H. *et al.* (2009) 'Small-molecule inhibition of Wee1 kinase by MK-1775 selectively sensitizes p53-deficient tumor cells to DNA-damaging agents', *Molecular cancer therapeutics*, 8(11), p. 2992. Available at: https://doi.org/10.1158/1535-7163.MCT-09-0463.

Hochstrasser, M. (2009) 'Origin and function of ubiquitin-like proteins.', *Nature*, 458(7237), pp. 422–429. Available at: https://doi.org/10.1038/nature07958.

Holen, K. *et al.* (2012) 'A phase I trial of MK-0731, a kinesin spindle protein (KSP) inhibitor, in patients with solid tumors.', *Investigational new drugs*, 30(3), pp. 1088–1095. Available at: https://doi.org/10.1007/s10637-011-9653-1.

Huang, H.T. *et al.* (2018) 'A Chemoproteomic Approach to Query the Degradable Kinome Using a Multi-kinase Degrader', *Cell Chemical Biology*, 25(1), 88-99.e6. Available at: https://doi.org/10.1016/j.chembiol.2017.10.005.

Huang, P.Q. *et al.* (2021) 'Discovery of ZN-c3, a Highly Potent and Selective Wee1 Inhibitor Undergoing Evaluation in Clinical Trials for the Treatment of Cancer', *Journal of Medicinal Chemistry*, 64(17), pp. 13004–13024. Available at: https://doi.org/10.1021/acs.jmedchem.1c01121.

Huang, Y. *et al.* (2022) 'Design, Synthesis, and Evaluation of Trivalent PROTACs Having a Functionalization Site with Controlled Orientation', *Bioconjugate Chemistry*, 33(1), pp. 142–151. Available at: https://doi.org/10.1021/acs.bioconjchem.1c00490.

Imaide, S. *et al.* (2021) 'Trivalent PROTACs enhance protein degradation via combined avidity and cooperativity', *Nature Chemical Biology*, 17(11), pp. 1157–1167. Available at: https://doi.org/10.1038/s41589-021-00878-4.

Ito, T. *et al.* (2010) 'Identification of a primary target of thalidomide teratogenicity', *Science*, 327(5971), pp. 1345–1350. Available at: https://doi.org/10.1126/science.1177319.

Itoh, Y. *et al.* (2010) 'Protein Knockdown Using Methyl Bestatin−Ligand Hybrid Molecules: Design and Synthesis of Inducers of Ubiquitination-Mediated Degradation of Cellular Retinoic Acid-Binding Proteins', *Journal of the American Chemical Society*, 132(16), pp. 5820–5826. Available at: https://doi.org/10.1021/ja100691p.

Jackson, S.P. *et al.* (2009) 'The DNA-damage response in human biology and disease', *Nature*, 461(7267), pp. 1071–1078. Available at: https://doi.org/10.1038/nature08467.

Jiang, B. *et al.* (2019) 'Development of Dual and Selective Degraders of Cyclin-Dependent Kinases 4 and 6', *Angewandte Chemie - International Edition*, 58(19), pp. 6321–6326. Available at: https://doi.org/10.1002/anie.201901336.

Jones, C.D. *et al.* (2013) 'Abstract 2348: Discovery of AZD6738, a potent and selective inhibitor with the potential to test the clinical efficacy of ATR kinase inhibition in cancer

patients.', *Cancer Research*, 73, p. 2348. Available at: https://doi.org/10.1158/1538-7445.AM2013-2348.

Jumper, J. *et al.* (2021) 'Highly accurate protein structure prediction with AlphaFold', *Nature*, 596(7873), pp. 583–589. Available at: https://doi.org/10.1038/s41586-021-03819-2.

Kanzawa, T. *et al.* (2004) 'Role of autophagy in temozolomide-induced cytotoxicity for malignant glioma cells.', *Cell death and differentiation*, 11(4), pp. 448–457. Available at: https://doi.org/10.1038/sj.cdd.4401359.

Karnitz, L.M. *et al.* (2015) 'Molecular Pathways: Targeting ATR in Cancer Therapy', *Clinical Cancer Research*, 21(21), pp. 4780–4785. Available at: https://doi.org/10.1158/1078-0432.CCR-15-0479.

Kato, H. *et al.* (2020) 'Safety, Pharmacokinetics, and Clinical Activity of Adavosertib in Combination with Chemotherapy in Asian Patients with Advanced Solid Tumors: Phase Ib Study', *Targeted Oncology*, 15(1), pp. 75–83. Available at: https://doi.org/10.1007/s11523-020-00701-5.

Kawadler, H. *et al.* (2006) 'Lys63-linked polyubiquitin chains: Linking more than just ubiquitin', *Cancer Biology & Therapy*, 5(10), pp. 1273–1274. Available at: https://doi.org/10.4161/cbt.5.10.3289.

Khan, M.K.A. *et al.* (2022) 'Target-based virtual screening, computational multiscoring docking and molecular dynamics simulation of small molecules as promising drug candidate affecting kinesin-like protein KIFC1', *Cell Biochemistry and Function*, 40(5), pp. 451–472. Available at: https://doi.org/10.1002/cbf.3707.

Kibel, A. *et al.* (1995) 'Binding of the von Hippel-Lindau Tumor Suppressor Protein to Elongin B and C', *Science*, 269(5229), pp. 1444–1446. Available at: https://doi.org/10.1126/science.7660130.

Kim, J.H. *et al.* (2015) 'Structural analysis of the polo-box domain of human Polo-like kinase 2', *Proteins: Structure, Function, and Bioinformatics*, 83(7), pp. 1201–1208.

Available at: https://doi.org/10.1002/prot.24804.

Kong, A. *et al.* (2020) 'Phase I trial of WEE1 inhibition with chemotherapy and radiotherapy as adjuvant treatment, and a window of opportunity trial with cisplatin in patients with head and neck cancer: The WISTERIA trial protocol', *BMJ Open*, 10(3), p. e033009. Available at: https://doi.org/10.1136/bmjopen-2019-033009.

Kostic, M. *et al.* (2020) 'Critical Assessment of Targeted Protein Degradation as a Research Tool and Pharmacological Modality', *Trends in Pharmacological Sciences*, 41(5), 305-317. Available at: https://doi.org/10.1016/j.tips.2020.02.006.

Kreahling, J.M. *et al.* (2012) 'MK1775, a selective Wee1 inhibitor, shows single-agent antitumor activity against sarcoma cells', *Molecular cancer therapeutics*, 11(1), pp. 174–182. Available at: https://doi.org/10.1158/1535-7163.MCT-11-0529.

Kwon, M. *et al.* (2008) 'Mechanisms to suppress multipolar divisions in cancer cells with extra centrosomes', *Genes & development*, 22(16), pp. 2189–2203. Available at: https://doi.org/10.1101/gad.1700908.

Lai, A.C., Toure, M., *et al.* (2016) 'Modular PROTAC Design for the Degradation of Oncogenic BCR-ABL', *Angewandte Chemie*, 55(2), pp. 807–810. Available at: https://doi.org/10.1002/anie.201507634.

Lai, A.C. and Crews, C.M. (2016) 'Induced protein degradation: an emerging drug discovery paradigm', *Nature Reviews Drug Discovery*, 16, p. 101. Available at: https://doi.org/10.1038/nrd.2016.211.

Lai, A.C. *et al.* (2017) 'Induced protein degradation: an emerging drug discovery paradigm', *Nature reviews. Drug discovery*, 16(2), pp. 101–114. Available at: https://doi.org/10.1038/nrd.2016.211.

Law, R.P. *et al.* (2021) 'Discovery and Characterisation of Highly Cooperative FAK-Degrading PROTACs', *Angewandte Chemie International Edition*, 60(43), pp. 23327–23334. Available at: https://doi.org/10.1002/anie.202109237.

LeBlanc, R. *et al.* (2004) 'Immunomodulatory drug costimulates T cells via the B7-CD28 pathway', *Blood*, 103(5), pp. 1787–1790. Available at: https://doi.org/10.1182/blood-2003-02-0361.

Lebraud, H. *et al.* (2016) 'Protein degradation by in-cell self-assembly of proteolysis targeting chimeras', *ACS Central Science*, 2(12), pp. 927–934. Available at: https://doi.org/10.1021/acscentsci.6b00280.

Lee, R.T. *et al.* (2008) 'A University of Chicago consortium phase II trial of SB-715992 in advanced renal cell cancer.', *Clinical genitourinary cancer*, 6(1), pp. 21–24. Available at: https://doi.org/10.3816/CGC.2008.n.003.

Leijen, S. *et al.* (2016) 'Phase II Study of WEE1 Inhibitor AZD1775 Plus Carboplatin in Patients With TP53-Mutated Ovarian Cancer Refractory or Resistant to First-Line Therapy Within 3 Months', *Journal of Clinical Oncology*, 34(36), pp. 4354–4361. Available at: https://doi.org/10.1200/JCO.2016.67.5942.

Lentzsch, S. *et al.* (2002) 'S-3-Amino-phthalimido-glutarimide Inhibits Angiogenesis and Growth of B-Cell Neoplasias in Mice', *Cancer Research*, 62(8), p. 2300. Available at: http://cancerres.aacrjournals.org/content/62/8/2300.abstract

Li, G. *et al.* (2018) 'Kinesin Motor Protein KIFC1 Is a Target Protein of miR-338-3p and Is Associated With Poor Prognosis and Progression of Renal Cell Carcinoma.', *Oncology research*, 27(1), pp. 125–137. Available at: https://doi.org/10.3727/096504018X15213115046567.

Li, L.-Y. *et al.* (2020) 'DNA Repair Pathways in Cancer Therapy and Resistance.', *Frontiers in pharmacology*, 11, p. 629266. Available at: https://doi.org/10.3389/fphar.2020.629266.

Li, L. *et al.* (2020) 'In vivo target protein degradation induced by PROTACs based on E3 ligase DCAF15', *Signal transduction and targeted therapy*, 5(1), p. 129. Available at: https://doi.org/10.1038/s41392-020-00245-0.

Li, M. *et al.* (2015) 'Ubiquitin-Dependent Lysosomal Membrane Protein Sorting and

Degradation', *Molecular Cell*, 57(3), pp. 467–478. Available at: https://doi.org/10.1016/j.molcel.2014.12.012.

Li, X. *et al.* (2012) 'Abnormal MDMX degradation in tumor cells due to ARF deficiency', *Oncogene*, 31(32), pp. 3721–3732. Available at: https://doi.org/10.1038/onc.2011.534.

Li, Z. *et al.* (2020) 'Development and Characterization of a Wee1 Kinase Degrader', *Cell Chemical Biology*, 27(1), pp. 57-65.e9. Available at: https://doi.org/10.1016/j.chembiol.2019.10.013.

Lin, W. *et al.* (2021) 'General Stepwise Approach to Optimize a TR-FRET Assay for Characterizing the BRD/PROTAC/CRBN Ternary Complex.', *ACS pharmacology & translational science*, 4(2), pp. 941–952. Available at: https://doi.org/10.1021/acsptsci.1c00032.

Liu, J. *et al.* (2020) 'Light-induced control of protein destruction by opto-PROTAC', *Science Advances*, 6(8), pp. eaay5154–eaay5154. Available at: https://doi.org/10.1126/sciadv.aay5154.

Liu, L. *et al.* (2019) 'UbiHub: a data hub for the explorers of ubiquitination pathways', *Bioinformatics*, 35(16), pp. 2882–2884. Available at: https://doi.org/10.1093/bioinformatics/bty1067.

Liu, X. *et al.* (2020) 'Assays and technologies for developing proteolysis targeting chimera degraders', *Future Medicinal Chemistry*, 12(12), pp. 1155-1179. Available at: https://doi.org/10.4155/fmc-2020-0073.

Loncarek, J. *et al.* (2017) 'Building the right centriole for each cell type', *Journal of Cell Biology*, 217(3), pp. 823–835. Available at: https://doi.org/10.1083/jcb.201704093.

López-Alvarado, P. *et al.* (2002) 'EFFICIENT, MULTIGRAM-SCALE SYNTHESIS OF THREE 2,5-DIHALOBENZOQUINONES', *Synthetic Communications*, 32(20), pp. 3233–3239. Available at: https://doi.org/10.1081/SCC-120013751.

Lu, G. *et al.* (2014) 'The myeloma drug lenalidomide promotes the cereblon-dependent

destruction of Ikaros proteins', *Science*, 343(6168), pp. 305–309. Available at: https://doi.org/10.1126/science.1244917.

Lu, J. *et al.* (2015) 'Hijacking the E3 Ubiquitin Ligase Cereblon to Efficiently Target BRD4', *Chemistry and Biology*, 22(6), pp. 755–763. Available at: https://doi.org/10.1016/j.chembiol.2015.05.009.

Mahoney, N.M. *et al.* (2006) 'Making microtubules and mitotic spindles in cells without functional centrosomes.', *Current biology : CB*, 16(6), pp. 564–569. Available at: https://doi.org/10.1016/j.cub.2006.01.053.

Manasanch, E.E. *et al.* (2017) 'Proteasome inhibitors in cancer therapy', *Nature Reviews Clinical Oncology*, 14, p. 417. Available at: https://doi.org/10.1038/nrclinonc.2016.206.

Maniaci, C. *et al.* (2017) 'Homo-PROTACs: Bivalent small-molecule dimerizers of the VHL E3 ubiquitin ligase to induce self-degradation', *Nature Communications,* 8(830). Available at: https://doi.org/10.1038/s41467-017-00954-1.

Marteil, G. *et al.* (2018) 'Over-elongation of centrioles in cancer promotes centriole amplification and chromosome missegregation', *Nature communications*, 9(1), p. 1258. Available at: https://doi.org/10.1038/s41467-018-03641-x.

Matheson, C.J. *et al.* (2016) 'A WEE1 Inhibitor Analog of AZD1775 Maintains Synergy with Cisplatin and Demonstrates Reduced Single-Agent Cytotoxicity in Medulloblastoma Cells', *ACS Chemical Biology*, 11(4), pp. 921–930. Available at: https://doi.org/10.1021/acschembio.5b00725.

Matheson, C.J., Backos, D.S., *et al.* (2016) 'Targeting WEE1 Kinase in Cancer', *Trends in Pharmacological Sciences*, 37(10), pp. 872–881. Available at: https://doi.org/10.1016/j.tips.2016.06.006.

Mayer, T.U. *et al.* (1999) 'Small Molecule Inhibitor of Mitotic Spindle Bipolarity Identified in a Phenotype-Based Screen', *Science*, 286(5441), pp. 971–974. Available at: https://doi.org/10.1126/science.286.5441.971.

Mendez, E. *et al.* (2018) 'A phase I clinical trial of AZD1775 in combination with neoadjuvant weekly docetaxel and cisplatin before definitive therapy in head and neck squamous cell carcinoma', *Clinical Cancer Research*, 24(12), pp. 2740–2748. Available at: https://doi.org/10.1158/1078-0432.CCR-17-3796.

Milroy, L.-G. *et al.* (2014) 'Modulators of Protein–Protein Interactions', *Chemical Reviews*, 114(9), pp. 4695–4748. Available at: https://doi.org/10.1021/cr400698c.

Mizuno, T. *et al.* (2011) 'Ubiquitination is associated with lysosomal degradation of cell surface-resident ATP-binding cassette transporter A1 (ABCA1) through the endosomal sorting complex required for transport (ESCRT) pathway', *Hepatology*, 54(2), pp. 631–643. Available at: https://doi.org/10.1002/hep.24387.

Moore, K.N. *et al.* (2015) 'Multicenter randomized Phase II study of AZD1775 plus chemotherapy versus chemotherapy alone in patients with platinum-resistant TP53-mutated epithelial ovarian, fallopian tube, or primary peritoneal cancer.', *Journal of Clinical Oncology*, 33(15). Available at: https://doi.org/10.1200/jco.2015.33.15_suppl.tps5608.

Mou, J. *et al.* (2015) 'Structure–activity relationship study of E6 as a novel necroptosis inducer', *Bioorganic & Medicinal Chemistry Letters*, 25(15), pp. 3057–3061. Available at: https://doi.org/10.1016/j.bmcl.2015.04.038.

Naro, Y. *et al.* (2020) 'Optical Control of Small Molecule-Induced Protein Degradation', *Journal of the American Chemical Society*, 142(5), pp. 2193–2197. Available at: https://doi.org/10.1021/jacs.9b12718.

Neises, B. *et al.* (1978) 'Simple Method for the Esterification of Carboxylic Acids', *Angewandte Chemie International Edition in English*, 17(7), pp. 522–524. Available at: https://doi.org/10.1002/anie.197805221.

Neklesa, T.K. *et al.* (2017) 'Targeted protein degradation by PROTACs', *Pharmacology & Therapeutics*, 174, pp. 138–144. Available at: https://doi.org/10.1016/j.pharmthera.2017.02.027.

Nguyen, H.C. *et al.* (2015) 'Insights into Cullin-RING E3 ubiquitin ligase recruitment: structure of the VHL-EloBC-Cul2 complex', *Structure*, 23(3), pp. 441–449. Available at: https://doi.org/10.1016/j.str.2014.12.014.

Nicolaou, K.C. *et al.* (2016) 'Total Synthesis and Biological Evaluation of Natural and Designed Tubulysins', *Journal of the American Chemical Society*, 138(5), pp. 1698–1708. Available at: https://doi.org/10.1021/jacs.5b12557.

Nigo, T. *et al.* (1993) 'Base-Promoted Rearrangement of 1,5-Dibromopentacyclo[5.3.0.02,5.03,9.04,8]decane-6,10-dione: Easy Entry of a Novel Cage System, 10-Oxa-9-oxopentacyclo[5.3.0.02,4.03,6.05,8]decane', *Bulletin of the Chemical Society of Japan*, 66(7), pp. 2068–2072. Available at: https://doi.org/10.1246/bcsj.66.2068.

Nolen, B. *et al.* (2004) 'Regulation of protein kinases; controlling activity through activation segment conformation.', *Molecular cell*, 15(5), pp. 661–675. Available at: https://doi.org/10.1016/j.molcel.2004.08.024.

Nowak, R.P. *et al.* (2018) 'Plasticity in binding confers selectivity in ligand-induced protein degradation article', *Nature Chemical Biology*, 14(7), pp. 706–714. Available at: https://doi.org/10.1038/s41589-018-0055-y.

Ohoka, N. *et al.* (2019) 'Different Degradation Mechanisms of Inhibitor of Apoptosis Proteins (IAPs) by the Specific and Nongenetic IAP-Dependent Protein Eraser (SNIPER)', *Chemical and Pharmaceutical Bulletin*, 67(3), pp. 203–209. Available at: https://doi.org/10.1248/cpb.c18-00567.

Paglin, S. *et al.* (2001) 'A novel response of cancer cells to radiation involves autophagy and formation of acidic vesicles.', *Cancer research*, 61(2), pp. 439–444. Available at: https://pubmed.ncbi.nlm.nih.gov/11212227/.

Palmer, B.D. *et al.* (2006) '4-Phenylpyrrolo[3,4-c]carbazole-1,3(2H,6H)-dione Inhibitors of the Checkpoint Kinase Wee1. Structure–Activity Relationships for Chromophore Modification and Phenyl Ring Substitution', *Journal of Medicinal Chemistry*, 49(16), pp.

4896–4911. Available at: https://doi.org/10.1021/jm0512591.

Pannu, V. *et al.* (2015) 'HSET overexpression fuels tumor progression via centrosome clustering-independent mechanisms in breast cancer patients.', *Oncotarget*, 6(8), pp. 6076–6091. Available at: https://doi.org/10.18632/oncotarget.3475.

Park, H.W. *et al.* (2017) 'Structural basis of small molecule ATPase inhibition of a human mitotic kinesin motor protein', *Scientific Reports,* 7(15121). Available at: https://doi.org/10.1038/s41598-017-14754-6.

Patel, N. *et al.* (2018) 'Integrated genomics and functional validation identifies malignant cell specific dependencies in triple negative breast cancer', *Nature communications*, 9(1), p. 1044. Available at: https://doi.org/10.1038/s41467-018-03283-z.

Petzold, G. *et al.* (2016) 'Structural basis of lenalidomide-induced CK1α degradation by the CRL4CRBN ubiquitin ligase', *Nature*, 532(7597), pp. 127–130. Available at: https://doi.org/10.1038/nature16979.

Pfaff, P. *et al.* (2019) 'Reversible Spatiotemporal Control of Induced Protein Degradation by Bistable PhotoPROTACs', *ACS Central Science*. 2019/09/17, 5(10), pp. 1682–1690. Available at: https://doi.org/10.1021/acscentsci.9b00713.

Poongavanam, V. *et al.* (2021) 'PROTAC cell permeability and oral bioavailability: a journey into uncharted territory', *Future Medicinal Chemistry*, 14(3), pp. 123–126. Available at: https://doi.org/10.4155/fmc-2021-0208.

Queignec, R. *et al.* (1988) 'High yield synthesis of α propargylic acrylic ester : A general access to α substituted acrylic esters', *Synthetic Communications*, 18(11), pp. 1213–1223. Available at: https://doi.org/10.1080/00397918808060913.

Raber, D.J. *et al.* (1979) 'Esterification of carboxylic acids with trialkyloxonium salts', *The Journal of Organic Chemistry*, 44(7), pp. 1149–1154. Available at: https://doi.org/10.1021/jo01321a027.

Rath, O. *et al.* (2012) 'Kinesins and cancer.', *Nature reviews. Cancer*, 12(8), pp. 527–539. Available at: https://doi.org/10.1038/nrc3310.

Reekie, T.A. *et al.* (2019) 'Cubanes in medicinal chemistry', *Journal of Medicinal Chemistry*, 62(3), pp. 1078–1095. Available at: https://doi.org/10.1021/acs.jmedchem.8b00888.

Reynders, M. *et al.* (2020) 'PHOTACs enable optical control of protein degradation', *Science Advances*, 6(8), p. eaay5064. Available at: https://doi.org/10.1126/sciadv.aay5064.

Rodriguez-Rivera, F.P. *et al.* (2021) 'Unifying Catalysis Framework to Dissect Proteasomal Degradation Paradigms', *ACS Central Science*, 7(7), pp. 1117–1125. Available at: https://doi.org/10.1021/acscentsci.1c00389.

Roger, J. *et al.* (2009) 'Ligand-free palladium-catalyzed direct arylation of thiazoles at low catalyst loadings', *Journal of Organic Chemistry,* 74(3), pp. 1179–1186. Available at: https://doi.org/10.1021/jo802360d.

Roy, M.J. *et al.* (2019) 'SPR-Measured Dissociation Kinetics of PROTAC Ternary Complexes Influence Target Degradation Rate', *Acs Chemical Biology*, 14(3), pp. 361–368. Available at: https://doi.org/10.1021/acschembio.9b00092.

Roy, R.D. *et al.* (2017) 'Cooperative binding mitigates the high-dose hook effect', *BMC systems biology*, 11(1), p. 74. Available at: https://doi.org/10.1186/s12918-017-0447-8.

Sakamoto, K.M. *et al.* (2001) 'Protacs: Chimeric molecules that target proteins to the Skp1-Cullin-F box complex for ubiquitination and degradation', *Proceedings of the National Academy of Sciences of the United States of America*, 98(15), pp. 8554–9. Available at: https://doi.org/10.1073/pnas.141230798.

Sakamoto, K.M. *et al.* (2003) 'Development of Protacs to target cancer-promoting proteins for ubiquitination and degradation.', *Molecular & cellular proteomics : MCP*, 2(12), pp. 1350–1358. Available at: https://doi.org/10.1074/mcp.T300009-MCP200.

Santos, R. *et al.* (2016) 'A comprehensive map of molecular drug targets', *Nature Reviews Drug Discovery*, 16, p. 19. Available at: https://doi.org/10.1038/nrd.2016.230

Sarikas, A. *et al.* (2011) 'The cullin protein family.', *Genome biology*, 12(4), p. 220. Available at: https://doi.org/10.1186/gb-2011-12-4-220.

Sarli, V. *et al.* (2006) 'Inhibitors of mitotic kinesins: next-generation antimitotics.', *ChemMedChem*, 1(3), pp. 293–298. Available at: https://doi.org/10.1002/cmdc.200500045.

Schapira, M. *et al.* (2019) 'Targeted protein degradation: expanding the toolbox', *Nature Reviews Drug Discovery*, 18(12), pp. 949–963. Available at: https://doi.org/10.1038/s41573-019-0047-y.

Schiemer, J. *et al.* (2021) 'Snapshots and ensembles of BTK and cIAP1 protein degrader ternary complexes', *Nature Chemical Biology*, 17(2), pp. 152–160. Available at: https://doi.org/10.1038/s41589-020-00686-2.

Schneekloth, A.R. *et al.* (2008) 'Targeted intracellular protein degradation induced by a small molecule: En route to chemical proteomics', *Bioorganic and Medicinal Chemistry Letters,* 18(22), pp. 5904-5908. Available at: https://doi.org/10.1016/j.bmcl.2008.07.114.

Schneekloth, J.S. *et al.* (2004) 'Chemical Genetic Control of Protein Levels: Selective in Vivo Targeted Degradation', *Journal of the American Chemical Society*, 126(12), pp. 3748–3754. Available at: https://doi.org/10.1021/ja039025z.

Shan, H.-M. *et al.* (2015) 'Crystal structure of the polo-box domain of polo-like kinase 2', *Biochemical and Biophysical Research Communications*, 456(3), pp. 780–784. Available at: https://doi.org/10.1016/j.bbrc.2014.11.125.

Singh, S.A. *et al.* (2014) 'Co-regulation proteomics reveals substrates and mechanisms of APC/C-dependent degradation', *The EMBO Journal*, 33(4), pp. 385–399. Available at: https://doi.org/10.1002/embj.201385876.

Siriwardena, S.U. *et al.* (2020) 'Phosphorylation-Inducing Chimeric Small Molecules', *Journal of the American Chemical Society*, 142(33), pp. 14052–14057. Available at: https://doi.org/10.1021/jacs.0c05537.

Skrabanek, L. *et al.* (2008) 'Computational Prediction of Protein-Protein Interactions', *Molecular biotechnology*, 38, pp. 1–17. Available at: https://doi.org/10.1007/s12033-007-0069-2.

Smith, B.E. *et al.* (2019) 'Differential PROTAC substrate specificity dictated by orientation of recruited E3 ligase', *Nature communications*, 10(1), p. 131. Available at: https://doi.org/10.1038/s41467-018-08027-7.

Spradlin, J.N. *et al.* (2019) 'Harnessing the anti-cancer natural product nimbolide for targeted protein degradation', *Nature Chemical Biology*, 15(7), pp. 747–755. Available at: https://doi.org/10.1038/s41589-019-0304-8.

Stone, H.B. *et al.* (2003) 'Effects of radiation on normal tissue: consequences and mechanisms.', *The Lancet. Oncology*, 4(9), pp. 529–536. Available at: https://doi.org/10.1016/s1470-2045(03)01191-4.

Suski, J.M. *et al.* (2021) 'Targeting cell-cycle machinery in cancer', *Cancer Cell*, 39(6), pp. 759–778. Available at: https://doi.org/10.1016/j.ccell.2021.03.010.

Suzuki, M. *et al.* (1988) 'Palladium(0)-catalyzed isomerization of α,β-epoxy ketones to β-diketones.', *Recl. Trav. Chim.*, 107, pp. 230-236. Available at: https://doi.org/10.1002/recl.19881070324

Szmyd, R. *et al.* (2019) 'Premature activation of Cdk1 leads to mitotic events in S phase and embryonic lethality', *Oncogene*, 38(7), pp. 998–1018. Available at: https://doi.org/10.1038/s41388-018-0464-0.

Takahashi, D. *et al.* (2019) 'AUTACs: Cargo-Specific Degraders Using Selective Autophagy', *Molecular Cell*, 76(5), pp. 797-810.e10. Available at: https://doi.org/10.1016/j.molcel.2019.09.009.

Tanaka, K. (2009) 'The proteasome: Overview of structure and functions', *Proceedings of the Japan Academy Series B: Physical and Biological Sciences*, 81(5), pp. 12–36. Available at: https://doi.org/10.2183/pjab.85.12.

Tillement, V. *et al.* (2009) 'Spindle assembly defects leading to the formation of a monopolar mitotic apparatus.', *Biology of the cell*, 101(1), pp. 1–11. Available at: https://doi.org/10.1042/BC20070162.

Tomoshige, S. *et al.* (2015) 'Degradation of HaloTag-fused nuclear proteins using bestatin-HaloTag ligand hybrid molecules', *Organic & Biomolecular Chemistry*, 13(38), pp. 9746–9750. Available at: https://doi.org/10.1039/C5OB01395J.

Tomoshige, S. *et al.* (2016) 'Efficient protein knockdown of HaloTag-fused proteins using hybrid molecules consisting of IAP antagonist and HaloTag ligand', *Bioorganic & Medicinal Chemistry*, 24(14), pp. 3144–3148. Available at: https://doi.org/10.1016/j.bmc.2016.05.035.

Tong, B. *et al.* (2020) 'Bardoxolone conjugation enables targeted protein degradation of BRD4', *Scientific Reports*, 10(1), p. 15543. Available at: https://doi.org/10.1038/s41598-020-72491-9.

Tovell, H. *et al.* (2019) 'Design and Characterization of SGK3-PROTAC1, an Isoform Specific SGK3 Kinase PROTAC Degrader', *ACS Chemical Biology,* 14(9), pp. 2024-2034. Available at: https://doi.org/10.1021/acschembio.9b00505.

Towers, C.G. *et al.* (2016) 'Therapeutic Targeting of Autophagy.', *EBioMedicine*, 14, pp. 15–23. Available at: https://doi.org/10.1016/j.ebiom.2016.10.034.

Troup, R.I. *et al.* (2020) 'Current strategies for the design of PROTAC linkers: a critical review', *Exploration of Targeted Anti-tumor Therapy*, 1(5), pp. 273–312. Available at: https://doi.org/10.37349/etat.2020.00018.

Uehara, T. *et al.* (2017) 'Selective degradation of splicing factor CAPERα by anticancer sulfonamides', *Nature Chemical Biology*, 13(6), pp. 675–680. Available at: https://doi.org/10.1038/nchembio.2363.

Umezawa, H. *et al.* (1976) 'Bestatin, an inhibitor of aminopeptidase B, produced by actinomycetes', *The Journal of Antibiotics*, 29(1), pp. 97–99. Available at: https://doi.org/10.7164/antibiotics.29.97.

Vale, R.D. *et al.* (1985) 'Identification of a novel force-generating protein, kinesin, involved in microtubule-based motility.', *Cell*, 42(1), pp. 39–50. Available at: https://doi.org/10.1016/s0092-8674(85)80099-4.

Varadi, M. *et al.* (2022) 'AlphaFold Protein Structure Database: massively expanding the structural coverage of protein-sequence space with high-accuracy models', *Nucleic Acids Research*, 50(D1), pp. D439–D444. Available at: https://doi.org/10.1093/nar/gkab1061.

Vasquez-Limeta, A. *et al.* (2021) 'Human centrosome organization and function in interphase and mitosis', *Seminars in Cell & Developmental Biology*, 117, pp. 30–41. Available at: https://doi.org/10.1016/j.semcdb.2021.03.020.

Vassilev, L.T. *et al.* (2004) 'In Vivo Activation of the p53 Pathway by Small-Molecule Antagonists of MDM2', *Science*, 603(5659), pp. 844–848. Available at: https://doi.org/10.1126/science.1092472.

Vassiliou, S. *et al.* (2007) 'A synthetic method for diversification of the P1' substituent in phosphinic dipeptides as a tool for exploration of the specificity of the S1' binding pockets of leucine aminopeptidases', *Bioorganic & Medicinal Chemistry*, 15(9), pp. 3187–3200. Available at: https://doi.org/10.1016/j.bmc.2007.02.042.

Vasta, J.D. *et al.* (2021) *'A High-Throughput Method to Prioritize PROTAC Intracellular Target engagement and Cell Permeability Using NanoBRET'*. In: Cacace, A.M., Hickey, C.M., Békés, M. (eds) Targeted Protein Degradation. Methods in Molecular Biology, vol 2365. Humana, New York, NY. Available at: https://doi.org/10.1007/978-1-0716-1665-9_14.

Wagner, P.J. (2001) 'Photoinduced Ortho [2 + 2] Cycloaddition of Double Bonds to Triplet Benzenes', *Accounts of Chemical Research*, 34(1), pp. 1–8. Available at:

https://doi.org/10.1021/ar000113n.

Wagner, P.J. *et al.* (1987) 'Regiospecific intramolecular reaction of an alkene group with the benzene ring of a triplet ketone', *Journal of the American Chemical Society*, 109, pp. 4404–4405.Available at: https://doi.org/10.1021/ja00248a051.

Wang, Y. *et al.* (2001) 'Radiosensitization of p53 Mutant Cells by PD0166285, a Novel G_2 Checkpoint Abrogator', *Cancer Research*, 61(22), p. 8211. Available at: http://cancerres.aacrjournals.org/content/61/22/8211.abstract.

Ward, C.C. *et al.* (2019) 'Covalent Ligand Screening Uncovers a RNF4 E3 Ligase Recruiter for Targeted Protein Degradation Applications', *ACS Chemical Biology*, 14(11), pp. 2430–2440. Available at: https://doi.org/10.1021/acschembio.8b01083.

Ward, C.L. *et al.* (1995) 'Degradation of CFTR by the ubiquitin-proteasome pathway', *Cell*, 83(1), pp. 121–127. Available at: https://doi.org/10.1016/0092-8674(95)90240-6.

Ward, S.P. (1962) 'Thalidomide and congenital abnormalities', *British medical journal*, 2(5305), pp. 646–647. Available at: https://doi.org/10.1136/bmj.2.5305.646.

Watts, C.A. *et al.* (2013) 'Design, synthesis, and biological evaluation of an allosteric inhibitor of HSET that targets cancer cells with supernumerary centrosomes', *Chemistry and Biology*, 20(11), pp. 1399-1410. Available at: https://doi.org/10.1016/j.chembiol.2013.09.012.

Weber, A.M. *et al.* (2015) 'ATM and ATR as therapeutic targets in cancer', *Pharmacology & Therapeutics*, 149, pp. 124–138. Available at: https://doi.org/10.1016/j.pharmthera.2014.12.001.

Wei, Y.-L. *et al.* (2019) 'Kinesin-14 motor protein KIFC1 participates in DNA synthesis and chromatin maintenance', *Cell Death & Disease*, 10(6), p. 402. Available at: https://doi.org/10.1038/s41419-019-1619-9.

Wharton, P.S. *et al.* (1961) 'Communications- Hydrazine Reduction of α,β-Epoxy Ketones to Allylic Alcohols', *Journal of Organic Chemistry*, 26, pp. 3615–3616. Available at:

https://doi.org/10.1021/jo01067a117.

Wilkinson, S.M. *et al.* (2017) 'Pharmacological Evaluation of Novel Bioisosteres of an Adamantanyl Benzamide P2X7 Receptor Antagonist', *ACS Chemical Neuroscience*, 8(11), pp. 2374–2380. Available at: https://doi.org/10.1021/acschemneuro.7b00272.

Willam, C. *et al.* (2002) 'Peptide blockade of HIFα degradation modulates cellular metabolism and angiogenesis', *Proceedings of the National Academy of Sciences*, 99(16), p. 10423. Available at: https://doi.org/10.1073/pnas.162119399.

Winter, G.E. *et al.* (2015) 'Phthalimide conjugation as a strategy for in vivo target protein degradation', *Science*, 348(6241), pp. 1376–1381. Available at: https://doi.org/10.1126/science.aab1433.

Wittig, I. *et al.* (2005) 'Advantages and limitations of clear-native PAGE', *PROTEOMICS*, 5(17), pp. 4338–4346. Available at: https://doi.org/10.1002/pmic.200500081.

Woessner, R. *et al.* (2009) 'ARRY-520, a novel KSP inhibitor with potent activity in hematological and taxane-resistant tumor models.', *Anticancer research*, 29(11), pp. 4373–4380. Available at: https://doi.org/10.1186/1479-5876-7-63.

Woolven, H. *et al.* (2011) 'DABCO-Bis(sulfur dioxide), DABSO, as a Convenient Source of Sulfur Dioxide for Organic Synthesis: Utility in Sulfonamide and Sulfamide Preparation', *Organic Letters*, 13(18), pp. 4876–4878. Available at: https://doi.org/10.1021/ol201957n.

Wright, G. *et al.* (2017) 'Dual Targeting of WEE1 and PLK1 by AZD1775 Elicits Single Agent Cellular Anticancer Activity', *ACS Chemical Biology*, 12(7), pp. 1883–1892. Available at: https://doi.org/10.1021/acschembio.7b00147.

Wu, G. S. (2004) 'The functional Interactions Between the MAPK and p53 Signaling Pathways', *Cancer Biology & Therapy*, 3(2), pp. 156-161. Available at: https://doi.org/10.4161/cbt.3.2.614.

Wu, J. *et al.* (2013) 'Discovery and mechanistic study of a small molecule inhibitor for

motor protein KIFC1', *ACS Chemical Biology*, 8(10), pp. 2201-2208. Available at: https://doi.org/10.1021/cb400186w.

Wurz, R.P. *et al.* (2018) 'A "click Chemistry Platform" for the Rapid Synthesis of Bispecific Molecules for Inducing Protein Degradation', *Journal of Medicinal Chemistry*, 61(2), pp. 453–461. Available at: https://doi.org/10.1021/acs.jmedchem.6b01781.

Xiao, Y.-X. *et al.* (2016) 'KIFC1: a promising chemotherapy target for cancer treatment?', *Oncotarget*, 7(30), pp. 48656–48670. Available at: https://doi.org/10.18632/oncotarget.8799.

Xue, G. *et al.* (2019) 'Light-Induced Protein Degradation with Photocaged PROTACs', *Journal of the American Chemical Society*, 141(46), pp. 18370–18374. Available at: https://doi.org/10.1021/jacs.9b06422.

Yamazoe, S. *et al.* (2020) 'Heterobifunctional Molecules Induce Dephosphorylation of Kinases–A Proof of Concept Study', *Journal of Medicinal Chemistry*, 63(6), pp. 2807–2813. Available at: https://doi.org/10.1021/acs.jmedchem.9b01167.

Yan, Y. *et al.* (2004) 'Inhibition of a Mitotic Motor Protein: Where, How, and Conformational Consequences', *Journal of Molecular Biology*, 335(2), pp. 547–554. Available at: https://doi.org/10.1016/j.jmb.2003.10.074.

Yang, B. *et al.* (2014) 'Discovery of potent KIFC1 inhibitors using a method of integrated high-throughput synthesis and screening', *Journal of Medicinal Chemistry*, 57(23), pp. 9958-70. Available at: https://doi.org/10.1021/jm501179r.

Yang, L. *et al.* (2020) 'Wee1 Kinase Inhibitor AZD1775 Effectively Sensitizes Esophageal Cancer to Radiotherapy.', *Clinical cancer research : an official journal of the American Association for Cancer Research*, 26(14), pp. 3740–3750. Available at: https://doi.org/10.1158/1078-0432.CCR-19-3373.

Yao, K.C. *et al.* (2003) 'Molecular response of human glioblastoma multiforme cells to ionizing radiation: cell cycle arrest, modulation of the expression of cyclin-dependent kinase inhibitors, and autophagy.', *Journal of neurosurgery*, 98(2), pp. 378–384.

Available at: https://doi.org/10.3171/jns.2003.98.2.0378.

Ye, L. *et al.* (2010) 'Gold-Catalyzed One-Step Practical Synthesis of Oxetan-3-ones from Readily Available Propargylic Alcohols', *Journal of the American Chemical Society*, 132(25), pp. 8550–8551. Available at: https://doi.org/10.1021/ja1033952.

Yildirim, T. *et al.* (1998) 'Solid cubane: A brief review', *Carbon*, 36(5), pp. 809–815. Available at: https://doi.org/10.1016/S0008-6223(98)00009-8.

Yuan, M.-L. *et al.* (2018) 'Inhibition of WEE1 Suppresses the Tumor Growth in Laryngeal Squamous Cell Carcinoma', *Frontiers in Pharmacology*, 9(1041). Available at: https://doi.org/10.3389/fphar.2018.01041.

Zagidullin, A. *et al.* (2020) 'Novel approaches for the rational design of PROTAC linkers', *Exploration of Targeted Anti-tumor Therapy*, pp. 381–390. Available at: https://doi.org/10.37349/etat.2020.00023.

Zengerle, M. *et al.* (2015) 'Selective Small Molecule Induced Degradation of the BET Bromodomain Protein BRD4', *ACS Chemical Biology*, 10(8), pp. 1770–1777. Available at: https://doi.org/10.1021/acschembio.5b00216.

Zhang, M. *et al.* (2017) 'WEE1 inhibition by MK1775 as a single-agent therapy inhibits ovarian cancer viability', *Oncology letters*, 14(3), pp. 3580–3586. Available at: https://doi.org/10.3892/ol.2017.6584.

Zhang, P. *et al.* (2021) 'Reprogramming of Protein-Targeted Small-Molecule Medicines to RNA by Ribonuclease Recruitment', *Journal of the American Chemical Society*, 143(33), pp. 13044–13055. Available at: https://doi.org/10.1021/jacs.1c02248.

Zhang, W. *et al.* (2016) 'Discovery of a novel inhibitor of kinesin-like protein KIFC1', *Biochemical Journal*, 473(8), pp. 1027–35. Available at: https://doi.org/10.1042/BJ20150992.

ZHANG, W. *et al.* (2002) 'MAPK signal pathways in the regulation of cell proliferation in mammalian cells', *Cell Research*, 12(1), pp. 9–18. Available at:

https://doi.org/10.1038/sj.cr.7290105.

Zhang, X. *et al.* (2019) 'Electrophilic PROTACs that degrade nuclear proteins by engaging DCAF16', *Nature Chemical Biology*, 15(7), pp. 737–746. Available at: https://doi.org/10.1038/s41589-019-0279-5.

Zhang, Y. *et al.* (2019) 'Targeted protein degradation mechanisms', *Drug Discovery Today: Technologies*, 31, pp. 53–60. Available at: https://doi.org/10.1016/j.ddtec.2019.01.001.

Zheng, N. *et al.* (2017) 'Ubiquitin Ligases: Structure, Function, and Regulation', *Annual Review of Biochemistry*, 86, pp. 129–157. Available at: https://doi.org/10.1146/annurev-biochem-060815-014922.

Zhu, J.-Y. *et al.* (2017) 'Structural Basis of Wee Kinases Functionality and Inactivation by Diverse Small Molecule Inhibitors', *Journal of Medicinal Chemistry*, 60(18), pp. 7863–7875. Available at: https://doi.org/10.1021/acs.jmedchem.7b00996.

Zhu, K. *et al.* (2016) 'Phospho-Pon Binding-Mediated Fine-Tuning of Plk1 Activity', *Structure*, 24(7), pp. 1110–1119. Available at: https://doi.org/10.1016/j.str.2016.04.012.

Zoppi, V. *et al.* (2019) 'Iterative Design and Optimization of Initially Inactive Proteolysis Targeting Chimeras (PROTACs) Identify VZ185 as a Potent, Fast, and Selective von Hippel-Lindau (VHL) Based Dual Degrader Probe of BRD9 and BRD7', *Journal of Medicinal Chemistry*, 62(2), pp. 699-726. Available at: https://doi.org/10.1021/acs.jmedchem.8b01413.

Zorba, A. *et al.* (2018) 'Delineating the role of cooperativity in the design of potent PROTACs for BTK', *Proceedings of the National Academy of Sciences of the United States of America*, 115(31), pp. E7285–E7292. Available at: https://doi.org/10.1073/pnas.1803662115.
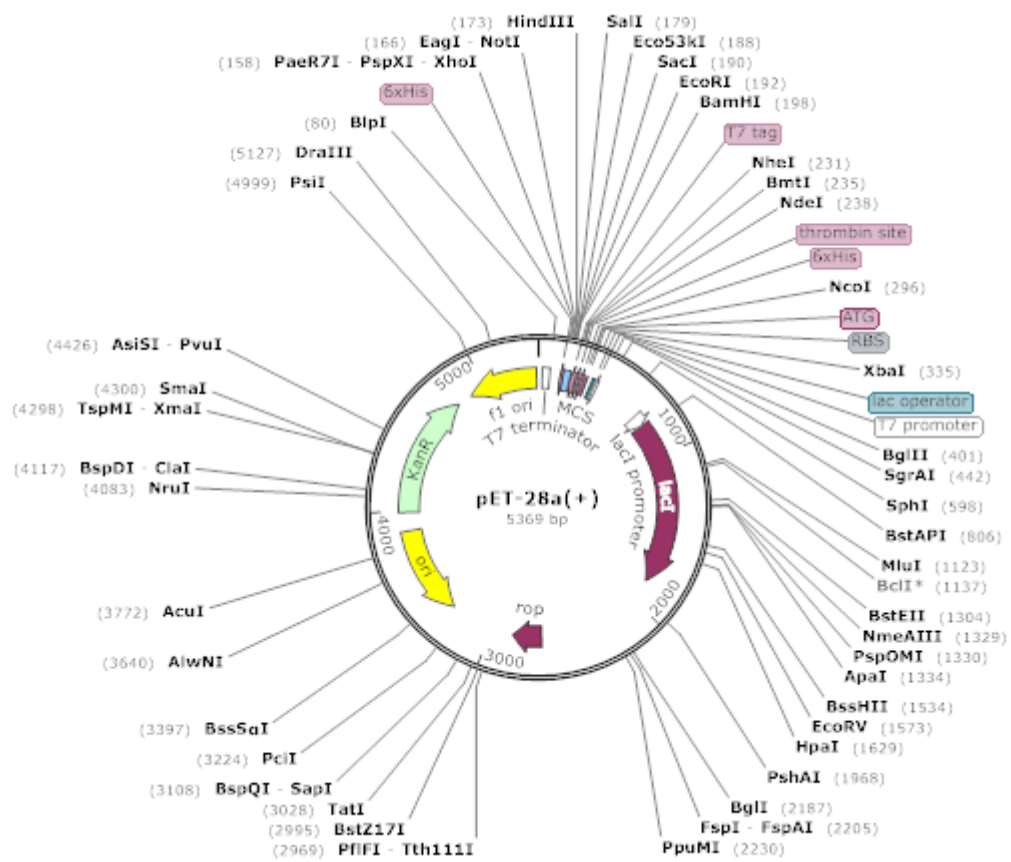
Appendix 1

Figure 9.1: pET28a vector map (SnapGene by Dotmatics).

Appendix 2 - Wee1 sequence details (Using Expasy – ProtParam)

Wee1 (with tag) sequence:

MGSSHHHHHHSSGLVPR/GSHMKSRYTTEFHELEKIGSGEFGSVFKCVKRLDGCIYAIKRSKKPLAGS
VDEQNALREVYAHAVLGQHSHVVRYFSAWAEDDHMLIQNEYCNGGSLADAISENYRIMSYFKEAE
LKDLLLQVGRGLRYIHSMSLVHMDIKPSNIFISRTSIPNAASEEGDEDDWASNKVMFKIGDLGHVTRI
SSPQVEEGDSRFLANEVLQENYTHLPKADIFALALTVVCAAGAEPLPRNGDQWHEIRQGRLPRIPQ
VLSQEFTELLKVMIHPDPERRPSAMALVKHSVLLSASRK

Number of amino acids: 305

Molecular weight: 34234.31 Da

Theoretical pI: 6.63

Extinction coefficient: extinction coefficients are in units of M^{-1} cm^{-1}, at 280 nm measured in water

- 30160, 0.880
- 29910 (all Cys are reduced), 0.872

Wee1 thrombin cleaved (LVPR/GS) sequence:

GSHMKSRYTTEFHELEKIGSGEFGSVFKCVKRLDGCIYAIKRSKKPLAGSVDEQNALREVYAHAVLGQ
HSHVVRYFSAWAEDDHMLIQNEYCNGGSLADAISENYRIMSYFKEAELKDLLLQVGRGLRYIHSMS
LVHMDIKPSNIFISRTSIPNAASEEGDEDDWASNKVMFKIGDLGHVTRISSPQVEEGDSRFLANEVL
QENYTHLPKADIFALALTVVCAAGAEPLPRNGDQWHEIRQGRLPRIPQVLSQEFTELLKVMIHPDPE
RRPSAMALVKHSVLLSASRK

Number of amino acids: 288

Molecular weight: 32403 Da

Theoretical pI: 6.37

Extinction coefficient: extinction coefficients are in units of M^{-1} cm^{-1}, at 280 nm measured in water

- 30160, 0.931
- 29910 (all Cys are reduced), 0.923

Appendix 3 - VBC sequence details (Using Expasy – ProtParam)

VBC (with tag) sequence:

MNTIHHHHHHNTSGSGGGGGRLVPRGSMSENLYFQ/GSMEAGRPRPVLRSVNSREPSQVIFCNR
SPRVVLPVWLNFDGEPQPYPTLPPGTGRRIHSYRGHLWLFRDAGTHDGLLVNQTELFVPSLNVDG
QPIFANITLPVYTLKERCLQVVRSLVKPENYRRLDIVRSLYEDLEDHPNVQKDLERLTQERIAHQRMG
DMDVFLMIRRHKTTIFTDAKESSTVFELKRIVEGILKRPPDEQRLYKDDQLLDDGKTLGECGFTSQTA
RPQAPATVGLAFRADDTFEALCIEPFSSPPELPDVMKMMYVKLISSDGHEFIVKREHALTSGTIKAML
SGPGQFAENETNEVNFREIPSHVLSKVCMYFTYKVRYTNSSTEIPEFPIAPEIALELLMAANFLDC

Number of amino acids: 398

Molecular weight: 45130.46

Theoretical pI: 6.32

Extinction coefficient: extinction coefficients are in units of M^{-1} cm^{-1}, at 280 nm measured in water

- 27765, 0.615
- 27390 (all Cys are reduced), 0.607

VBC TEV cleavage (LYFQ/GS) sequence:

GSMEAGRPRPVLRSVNSREPSQVIFCNRSPRVVLPVWLNFDGEPQPYPTLPPGTGRRIHSYRGHLW
LFRDAGTHDGLLVNQTELFVPSLNVDGQPIFANITLPVYTLKERCLQVVRSLVKPENYRRLDIVRSLYE
DLEDHPNVQKDLERLTQERIAHQRMGDMDVFLMIRRHKTTIFTDAKESSTVFELKRIVEGILKRPPD
EQRLYKDDQLLDDGKTLGECGFTSQTARPQAPATVGLAFRADDTFEALCIEPFSSPPELPDVMKMM
YVKLISSDGHEFIVKREHALTSGTIKAMLSGPGQFAENETNEVNFREIPSHVLSKVCMYFTYKVRYTN
SSTEIPEFPIAPEIALELLMAANFLDC

Number of amino acids: 363

Molecular weight: 41337.33

Theoretical pI: 5.92

Extinction coefficient: extinction coefficients are in units of M^{-1} cm^{-1}, at 280 nm measured in water

- 26275, 0.636
- 25900 (all Cys are reduced), 0.627

Appendix 4

Publication: Selective Wee1 degradation by PROTAC degraders recruiting VHL and CRBN E3 ubiquitin ligases.

Selective Wee1 degradation by PROTAC degraders recruiting VHL and CRBN E3 ubiquitin ligases

Marine C. Aublette, Tom A. Harrison, Elizabeth J. Thorpe, Morgan S. Gadd [*]

Division of Biomedical and Life Sciences, Faculty of Health and Medicine, Lancaster University, Lancaster LA1 4YG, United Kingdom

ABSTRACT

The Ser/Thr protein kinase Wee1 plays a regulatory role at the G_2/M checkpoint by phosphorylating CDK1 when DNA is damaged to allow time for DNA to repair, disruption of which is a key approach to sensitise cancer cells to DNA-damaging therapies. The main selective inhibitor for Wee1 undergoing development in clinical trials, AZD1775, however, has been shown to have off target effects towards other protein kinases with similar potency. Here we describe the synthesis and assessment of a series of Wee1-degrading PROTACs using AZD1775 linked to either the VHL ligand VH032 or to the CRBN ligand pomalidomide using different types and lengths of linkers. The conversion of AZD1775 into a PROTAC induces selective Wee1 degradation for compounds of both series depending on the nature of the linker.

Introduction

Cells are dependent on cell-cycle checkpoints to repair DNA and maintain genome integrity.[1] In cancer cells, p53 is often mutated, leading to a deficient G_1/S checkpoint that means these cells are reliant on the G_2/M checkpoint to repair their DNA prior to cell division in order to produce viable daughter cells.[2] Wee1 is a serine/threonine kinase-family member that plays an important role in regulating the G_2/M checkpoint. When DNA is damaged, a CHK1-driven signalling cascade results in Wee1 phosphorylating CDK1 (CDC2) at tyrosine 15 (Tyr15) to inactivate the CDK-Cyclin B complex and thus arrest entry into mitosis, which allows time for DNA repair.[3] Wee1 is overexpressed in many cancers, and has been correlated with poor disease-free survival for cancer patients.[4] Thus, inhibition of Wee1 is likely to be an effective strategy for therapeutic intervention as it results in abrogation of the G_2/M DNA repair checkpoint and could lead to mitotic lethality in cancer cells.[4]

AZD1775/adavosertib is the first selective inhibitor towards Wee1. It acts as an ATP competitor and inhibits the phosphorylation of CDK1 at Tyr15 by Wee1,[5] leading to the abrogation of the G_2/M checkpoint. AZD1775 is the most selective inhibitor to date towards Wee1, leading to apoptosis when used in combination with DNA-damaging agents to treat p53-inactive cells. AZD1775 is currently undergoing Phase I and Phase II clinical trials in combination with several other treatments, including chemotherapies and radiotherapies.[6] However, due to the

highly conserved nature of ATP-binding sites, additional AZD1775 targets have been identified, with some, such as PLK1, inhibited to a similar potency as Wee1.[7,8] PLK1 has an important role in negatively regulating Wee1 activity.[9] As such, the activity of AZD1775 may not solely be a result of selectivity against Wee1.

Targeted protein degradation is a powerful new modality for targeting specific proteins and treating disease.[10] Proteolysis targeting chimeras (PROTACs) are bifunctional molecules composed of a target protein-recruiting moiety on one side and an E3 ligase-recruiting moiety on the other,[11] joined by a flexible linker. The role of a PROTAC is to bring the target protein into a ternary complex with the E3 ubiquitin ligase, resulting in polyubiquitination of the target and its degradation by the ubiquitin-proteasome system.[12,13] As PROTACs require the interaction of multiple partner proteins to form ternary complexes that productively ubiquitinate and degrade the target, these novel contacts can result in enhanced potency, efficacy and selectivity in targeted protein degradation.[13-15] AZD1775 is an ideal candidate to use as a target-binding moiety in the design of PROTAC molecules to selectively degrade Wee1 over other targets.

Here, we present a library of Wee1 PROTACs generated by coupling the AZD1775 inhibitor to two different E3 ubiquitin ligase recruiters: VH032[16] binding the VHL E3 ligase and pomalidomide[17] binding the CRBN E3 ligase. We found that these Wee1 PROTACs recruiting either E3 ubiquitin ligase are able to induce selective degradation of Wee1 in different cell lines. While we were characterising our compounds, Li *et*

al. published their discovery of ZNL-02‑096, a potent and selective Wee1 degrader that recruits CRBN as the E3 ligase.[18] As such, we turned our focus to evaluating the structure‑activity relationship (SAR) of our PROTACs and comparing one from each of the VHL and CRBN series that were among the most potent. We find that the composition and length of the linker has a direct influence on the degradation of Wee1, likely due to ternary complex formation, and is a critical variable in determining the potency of the PROTACs.

The strength and efficacy of PROTAC degradation can be influenced by the length and type of the linker, as well as the approach to E3 ligase and target recruitment.[19] To investigate if it was possible to convert AZD1775 into a selective degrader, we analysed the available co-crystal structure of AZD1775 with Wee1 (RCSB PDB: 5V5Y[7]). We selected the 4-methylpiperazinyl region of the Wee1 inhibitor, which is solvent exposed and had been successfully modified previously for covalent linkage[8] (Fig. S1). We then developed Wee1 degraders based on AZD1775 that we linked to the von Hippel‑Lindau (VHL) ligand VH032[16] or the Cereblon (CRBN) ligand pomalidomide[17] (Fig. 1).

Guided by previously published conditions,[8,20] we used the commercially available compound **26** and, following its sulfur oxidation using m-chloroperoxybenzoic acid, coupled it with aniline **25** synthesised from 4-nitrophenylpiperazine (**24**) (Scheme S1). This yielded **1**, an analogue of AZD1775 with a 3-carboxypropyl group instead of the methyl of the original inhibitor to allow amide coupling with linkers and E3 ligase ligands. The amine of VH032 (**22**) (Scheme S2) was synthesized,[16] starting with the Suzuki coupling between the commercially available 4-bromobenzonitrile[27] and 4-methylthiazole[28] to yield.[29] This was followed by amide coupling with Boc-*trans*-hydroxyproline, deprotection under acidic conditions and another amide coupling with Boc-L-*tert*-leucine to yield **22**. A 4-fluoro substituted analogue of thalidomide/pomalidomide (**23**) was prepared from commercially available 3-fluorophthalic anhydride (**33**) reacted by dehydrative condensation with 3-aminopiperidine-2,6-dione HBr salt (**32**) (Scheme S4).

We added linker moieties to **22** by HATU-mediated amide coupling (compounds **31a-f**) and to **23** by nucleophilic aromatic substitution (compounds **34g-m** and **35a-f**). After Boc-deprotection, we coupled each resulting compound to **1** by HATU-mediated amide coupling in order to construct a series of Wee1 PROTACs **2‑21** (Table 1 and Schemes S3 and S5). In total we synthesised seven different compounds for the VHL series and thirteen for the CRBN series. By using two different E3 ligases, as well as different types and lengths of linkers, we hoped to compare the efficacy of the recruited E3 ligase and the influence of the

linker nature on Wee1 degradation activity. Both components have been shown to have an important impact on PROTAC activity.[21,22] We compared the ability of our PROTACs to degrade Wee1 and reduce levels of Tyr15 phosphorylation of CDK1 (pCDK1(Y15)), the key target of Wee1′s kinase activity, using Western blot to establish a SAR for different types and lengths of linkers using each of the E3 ligase binders (Table 1).

After 24 h treatment with 1 µM of PROTAC in HeLa S3 cells, we observed a wide range of Wee1 levels across compounds using both E3 ligase binders, suggesting that while both E3 ligases can form productive complexes with Wee1, different linkers resulted in different extents of degradation for Wee1. We also observed closely matched decreases in pCDK1(Y15) levels, indicating that this closely correlates with Wee1 degradation activity. To establish the optimal treatment time in which to analyse Wee1 degradation, we treated HeLa S3 cells for a range of timeframes using 1 µM of PROTACs selected for exhibiting the strongest and weakest degradation (Fig. S3). We found that the compounds generally reach the greatest reduction in Wee1, or maximal degradation, following approximately 4 h of treatment. To evaluate the Wee1 degradation profiles of the PROTACs, we treated HeLa S3 cells with each degrader from 10 µM to 1 nM for 4 h; Wee1, pCDK1(Y15), CDK1 and β-actin, were probed by Western blot using the corresponding specific antibodies (Fig. 2, S4 and S5).

After 24 h treatment with 1 µM of PROTAC in HeLa S3 cells, the five PROTACs of the VHL series featuring an alkyl linker (**2‑6**) resulted in effective Wee1 degradation (Table 1), with **2** (MA055) (three-atom linker) and **6** (15-atom linker) being the most efficient, removing about 65% and 50% of Wee1 protein, respectively. They consequently induced a decrease in pCDK1(Y15) levels, with only 50% remaining after 24 h. PROTACs **3**, **4** and **5**, with intermediate linker lengths of 8‑12 atoms, appeared to be less efficient, with ~ 70% of Wee1 remaining. The compounds with polyethylene glycol linkers (**7**, **8**) had even less effect on Wee1 degradation (0‑6%) after 24 h treatment.

Compound **MA055** of the VHL series successfully induced Wee1 degradation from 30 nM to 3 µM after 4 h incubation in HeLa S3 cells (Fig. 2). Levels of Wee1 were largely restored at 10 µM of **MA055**, a consequence of self-inhibition of the compound due to the hook effect generating unproductive binary over productive ternary complexes. Treatment with **MA055** from 30 nM to 10 µM also resulted in decreased levels of pCDK1(Y15) as a consequence of modulation of Wee1 activity. Degradation by the other VHL-based PROTACs of this series did not result in substantial Wee1 degradation after 4 h treatment, however, pCDK1(Y15) levels were reduced at higher concentrations of alkyl-
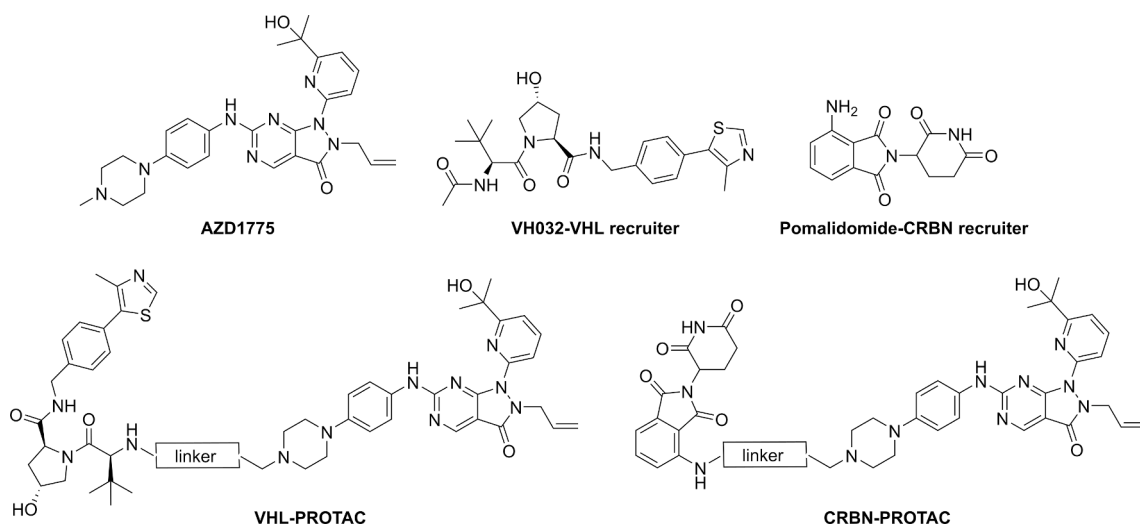
Fig. 1. AZD1775 Wee1 inhibitor, and the two E3 ligase ligands, VH032 (VHL) and pomalidomide (CRBN). The two PROTAC series: VHL-PROTAC and CRBN-PROTAC, using AZD1775 inhibitor linked to either E3 ligase ligand (VHL or CRBN).

2

Table 1

SAR of PROTACs recruiting two E3 ubiquitin ligases (VHL and CRBN) by changing the linker composition and length. Levels of Wee1 and pCDK1(Y15), reported as the percentage of protein observed by Western blot following treatment of HeLa S3 cells with 1 μM of PROTAC for 24 h (Fig. S2; n = 4).

PROTAC	Linker	E3 ligase	# of O and N atoms	Linker length	Wee1 24 h (%)	pCDK1(Y15) 24 h (%)
2 (MA055)	*(structure)*		1	3	34	49
3	*(structure)*		3	8	68	55
4	*(structure)*		3	10	71	64
5	*(structure)*		3	12	68	53
6	*(structure)*	VHL	3	15	50	47
7	*(structure)*		6	15	94	72
8	*(structure)*		7	19	108	80
9	*(structure)*		2	6	21	38
10	*(structure)*		2	10	23	39
11	*(structure)*		3	9	38	41
12 (MA071)	*(structure)*		4	12	27	51
13	*(structure)*		5	15	59	66
14	*(structure)*		6	18	45	65
15	*(structure)*	CRBN	7	21	51	78
16	*(structure)*		6	15	81	80
17	*(structure)*		7	18	96	84
18	*(structure)*		4	11	47	60
19	*(structure)*		4	13	75	54
20	*(structure)*		4	15	83	88
21	*(structure)*		4	18	41	41

linked compounds **2**‑**6**, but not PEG-linked compounds **7** and **8** (Fig. S4).

Multiple PROTACs of the CRBN series induced strong Wee1 degradation following 24 h treatment in HeLa S3 cells with 1 μM of compound (Table 1). 21‑38% of Wee1 and 38‑51% of pCDK1(Y15) remains following treatment with **9**, **10**, **11** and **12** (MA071), each featuring shorter linkers of 6‑12 atoms. **14** and **21**, each featuring longer linkers of 18 atoms, also showed strong degradation at 24 h with 40‑45% of Wee1 and 40‑65% of pCDK1(Y15) remaining in each case. Overall, medium-length linker PROTACs with thirteen to fifteen atoms (**13**, **19**, **20**) seemed less potent for Wee1 degradation compared to PROTACs with similar linkers with a shorter or longer length. Additionally, PROTACs with a PEG linker and one more amide bond (**16**, **17**) are poor degraders of Wee1.

The PROTACs **9**, **10**, **11** and **12** (MA071) exhibited the most comprehensive Wee1 reduction over a range of concentrations, with Wee1 degradation observed from 30 nM to 10 μM of compound after 4 h treatment in HeLa S3 cells (Fig. 2 and S5). A less prominent hook effect on Wee1 degradation is observed for these CRBN-PROTACs compared to the VHL-PROTACs. pCDK1(Y15) levels are also decreased at treatment concentrations of 100 nM to 10 μM. The relative range of concentrations at which degradation takes places roughly correlates with the level of degradation at 1 μM, with the most potent degradation seen for shorter linker compounds **10** and **11**, and **21** with a longer linker.

AZD1775 has been the most potent and selective Wee1 inhibitor in clinical development,[5] however, it has been found to inhibit PLK1 with a similar potency.[8] PLK1 is a negative regulator of Wee1 activity and thus inhibition of both Wee1 and PLK1 at the same time may be counter-productive. Furthermore, kinome profiling of AZD1775 revealed off-target activity against many kinases, including PLK1, PLK2, PLK3, JAK2 and MAP3K4.[7] In designing our PROTAC molecules, we hoped to target Wee1 more selectively and avoid modulation of off-target kinases. Previous studies have shown how selective degraders can be made starting from a non-selective inhibitor as the target ligand.[13,23] Thus we assessed whether PROTACs derived from AZD1775 exhibited similarly increased selectivity.

We analysed the selectivity of our PROTACs using Western blot and
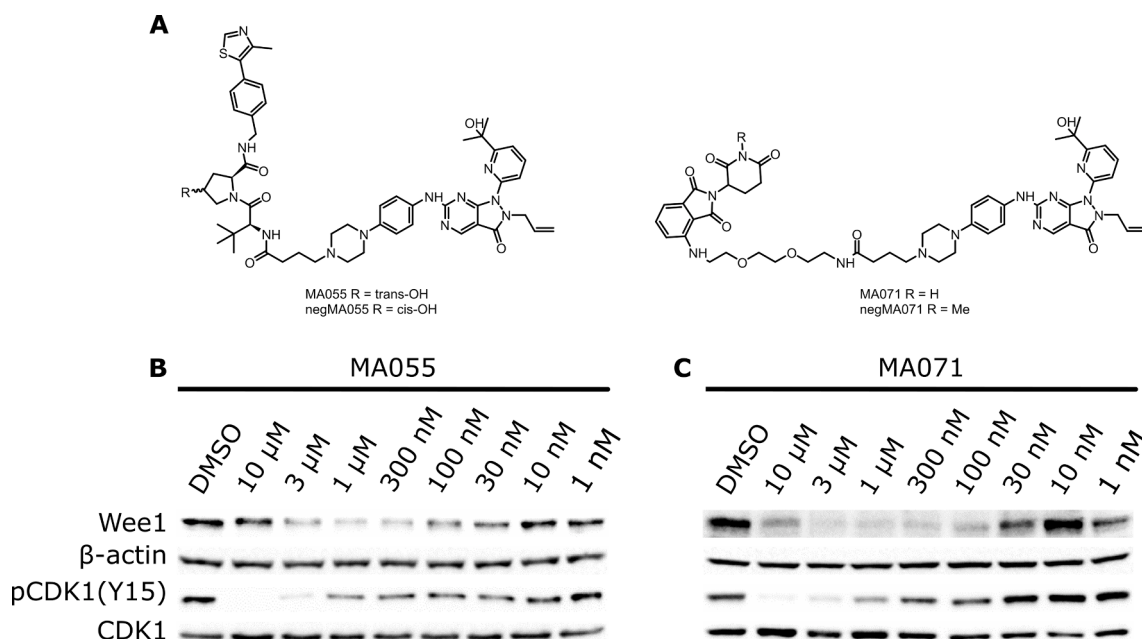
Fig. 2. Characterisation of Wee1 degraders for each series recruiting either the VHL or the CRBN E3 ligases.
(**A**) Chemical structures of the selective degraders **MA055** and **MA071**, and their respective negative control molecules. Western blot of HeLa S3 cells treated for 4 h with decreasing concentrations of PROTACs (**B**) **MA055** recruiting VHL and (**C**) **MA071** recruiting CRBN. The membrane was probed for Wee1, pCDK1(Y15), CDK1 and β-actin as the loading control.

antibodies for a number of off-target proteins of AZD1775, including PLK1, PLK2, PLK3, MAP3K4 and JAK2.[7] To assess this, we focused on one PROTAC targeting each E3 ligase, **MA055** for VHL and **MA071** for CRBN, which were amongst the best degraders of Wee1 in their respective series, although each of these had slightly less of an effect on pCDK1(Y15) levels compared to AZD1775 (Fig. S6). PROTACs **MA055** and **MA071** did not degrade PLK1 following treatment in HeLa S3 after 4 h (Fig. 3A and B). No decrease was observed in levels of PLK2, PLK3, MAP3K4 and JAK2 over the range of concentrations when HeLa cells were treated with these PROTACs under the same conditions. Furthermore, **MA055** and **MA071** significantly degraded Wee1 at 1 μM in HeLa S3 cells for 24 h and 48 h, while the other kinases remained unaffected (Fig. 3C and D). Together these data indicate that our PROTACs, using the non-selective Wee1 inhibitor AZD1775, have the desired selectivity for the degradation of Wee1 over other AZD1775 targets across multiple time points.

To validate the mechanistic activities of our PROTACs, we synthesised corresponding negative control compounds for our PROTACs, including **negMA055** (**MA055** containing *cis*-hydroxyproline) and **negMA071** (**MA071** containing an *N*-methylated glutarimide). These modifications to the E3 ligase-binding ligands prevent their respective E3 ligases from being recruited by the PROTAC, enabling assessment of the activities of the compounds in the absence of E3 ligase.[13,24] Negative control compounds for both VHL- and CRBN-based PROTACs were synthesised following the same methods as the corresponding active PROTACs (Schemes S6 and S7).

Neither **negMA055** or **negMA071** exhibited degradation of Wee1 in HeLa S3 cells at 24 h and up to 48 h (Fig. 3C and D), whereas the active PROTACs showed loss of Wee1 at these timepoints. However, both **negMA055** and **negMA071** were found to inhibit Wee1 by showing some reduction in pCDK1(Y15) levels when treated with 1 μM and above (Fig. 3C, D and S6). As these compounds cannot recruit the E3 ligase, they must form a binary complex with Wee1 and act as inhibitors rather than degraders in this instance. This demonstrated that while productive recruitment of VHL or CRBN is mandatory for the degradation of Wee1, at higher concentrations of PROTAC a combination of inhibition and degradation modulates Wee1 activity. Critically, for **MA071** there is a

greater reduction in pCDK1(Y15) than for **negMA071**, whereas for **MA055** this is similar to **negMA055**, indicating the degradation activity of our CRBN-based Wee1 PROTAC modulates Wee1 activity more effectively than the VHL-based Wee1 PROTAC. The observed inhibitory effect of the negative control compounds is lower than that of AZD1775 itself (Fig. S6), likely due to the reduced cell penetration of the PROTACs (and their negative controls) compared to the inhibitor.

To verify that the PROTACs are degraders dependent on the E3 ligase and proteasome activity, we compared their efficiency in the presence and absence of proteasome and E3 ligase inhibitors. Pre-treating HeLa S3 cells with proteasome inhibitor MG132 (20 μM) for 2 h before adding the PROTAC for 5 h abrogated Wee1 degradation by **MA055** and **MA071**, indicating that the observed degradation is proteasome dependent (Fig. 3E and F). Similarly, we pre-treated cells with MLN4924, which inhibits neddylation of CRLs,[25] at 1 μM for 2 h and observed that Wee1 degradation by **MA055** and **MA071** was similarly blocked, confirming the dependence of our PROTAC activity on the neddylation and activation of CRLs (CRL2VHL and CRL4CRBN, respectively).

To confirm the essentiality of engaging the partner proteins, we pre-treated the cells with inhibitors engaging the PROTAC-binding sites. Pre-treatment with Wee1 inhibitor AZD1775 (1 μM) for 2 h and subsequent treatment with **MA055** and **MA071** failed to degrade Wee1 (Fig. 3E and F). Pre-treatment with AZD1775 decreased pCDK1(Y15) levels, in keeping with its inhibitory effect on Wee1 activity, which does not depend on degradation. In contrast, pre-treatment with VHL inhibitor VH298[26] (100 μM), prevented very little Wee1 degradation by **MA055** (Fig. 3E). Similarly, pre-treatment with pomalidomide (10 μM), only prevented some Wee1 degradation by **MA071** (Fig. 3F). The abrogation of Wee1 degradation by AZD1775 was more profound than that of VH298 or pomalidomide for the PROTACs engaging their respective E3 ligases (VHL or CRBN), neither of which completely recovered Wee1 levels. While we were unable to competitively inhibit our PROTACs with their conjugate E3 ligase binders, the lack of activity in our negative control PROTACs (**negMA055** and **negMA071**) confirmed the essentiality of E3 ligase recruitment for their activity.

We next verified that the Wee1 degradation observed in HeLa S3
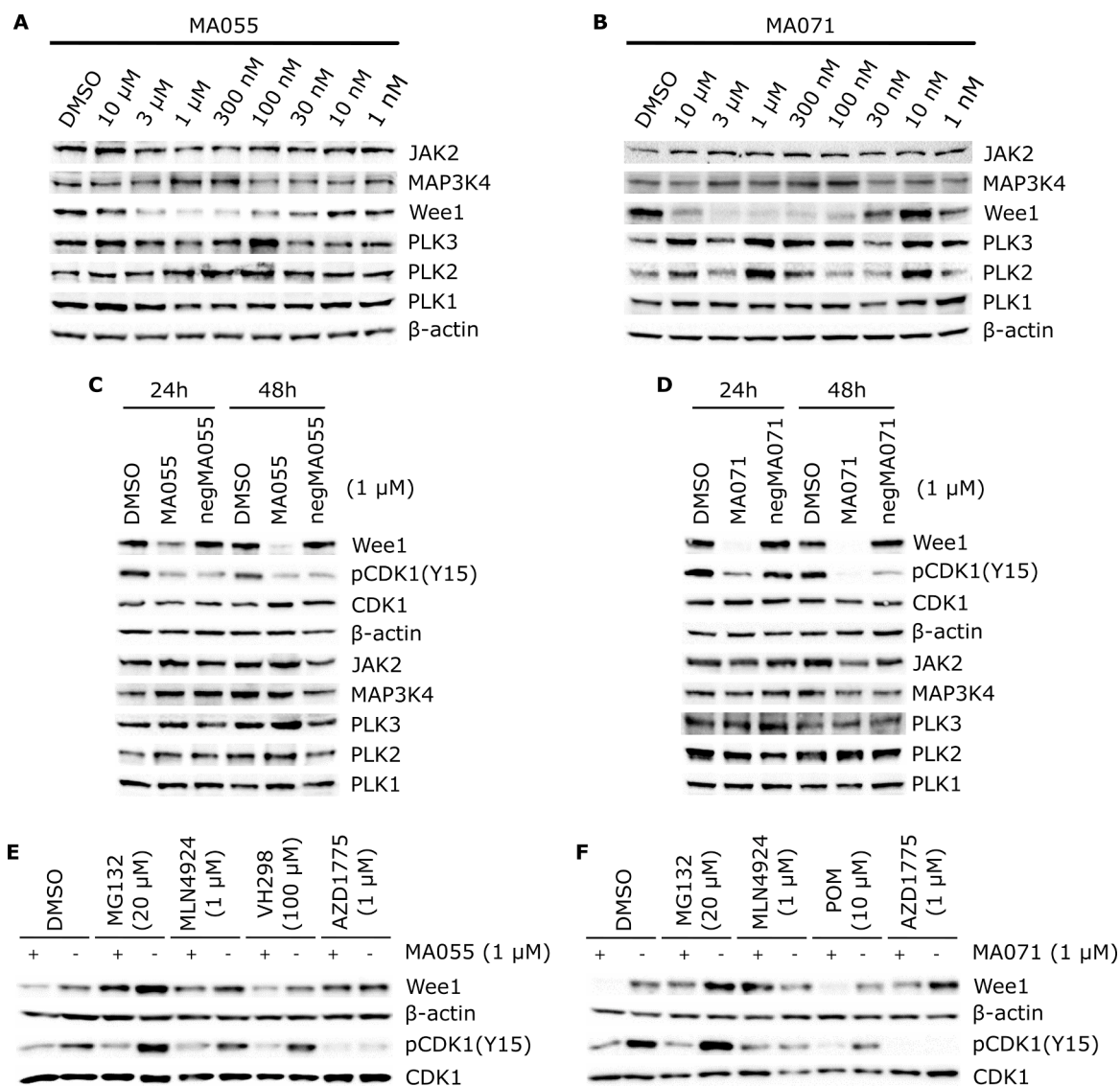
Fig. 3. Assessment of PROTAC selectivity for AZD1775 targets with the PROTACs **MA055** and **MA071**, and target engagement.
Western blot of HeLa S3 cells treated for 4 h with decreasing concentrations of PROTACs (**A**) **MA055** and (**B**) **MA071**. The membrane was probed for JAK2, MAP3K4, Wee1, PLK3, PLK2, PLK1 and β-actin as the loading control. Western blot of HeLa S3 cells treated with 0.1% DMSO, 1 μM of (**C**) **MA055** and **negMA055** or (**D**) **MA071** and **negMA071**, for 24 and 48 h. The membrane was probed for Wee1, pCDK1(Y15), CDK1, JAK2, MAP3K4, PLK3, PLK2, PLK1, and β-actin as the loading control. Inhibition of PROTAC mechanism for (**E**) **MA055** recruiting VHL and (**F**) **MA071** recruiting CRBN. HeLa S3 cells were pre-treated with DMSO, MG132 (20 μM), MLN4924 (1 μM), VH298 (100 μM) or pomalidomide (10 μM), and AZD1775 (1 μM) for 2 h prior to the addition of the indicated PROTAC (1 μM) for a further 5 h. The membrane was probed for Wee1, pCDK1(Y15), CDK1 and β-actin as the loading control.

cells was reproducible in other cancer cell lines. Prostate cancer cell lines PC3 and LNCaP, and breast cancer cell lines BT549 and MCF7, are p53 mutant and p53 wild type, respectively, for each tissue. Following treatment with either **MA055** or **MA071**, both Wee1 degradation and reduced pCDK1(Y15) levels were observed in all four cell lines (Fig. S7). For both PROTACs, the Wee1 band largely disappears at 100 nM and above in PC3 and BT549 cells, and at 300 nM or higher in MCF7 and LNCaP cells. On the other hand, degradation in MCF7 and LNCaP was less affected by the hook effect, which is more prominent in the treatments of HeLa, PC3 and BT549 cells. Variations in the expression or activity of Wee1 or the E3 ligases could explain these differences, but overall Wee1 degradation by our PROTACs is largely similar between the cancer cell lines for PROTACs utilising either of the E3 ligases.

As we observed Wee1 degradation and reduction of pCDK1(Y15) levels in a number of different cancer cell lines (Fig. S7), we sought to establish the half-maximum response (IC$_{50}$) of the best PROTACs as agents of cell growth inhibition or cytotoxicity compared to their

negative controls and the inhibitor AZD1775 using the MTS cell viability assay (Fig. 4).

MCF7, BT549, LNCaP and PC3 were treated with varying concentrations of PROTACs **MA055** and **MA071**, their negative controls (**negMA055** and **negMA071**, respectively), or the inhibitor AZD1775, for 72 h (Fig. 4 and Table 2). BT549 cells were more sensitive to all tested compounds than MCF7 for the breast cancer cell lines, and LNCaP cells were more sensitive to all tested compounds than PC3 for the prostate cancer cell lines. **MA055** exhibits similar IC$_{50}$ values to its negative control **negMA055** and **MA071** also exhibits similar IC$_{50}$ values to its negative control **negMA071**, however, these are higher than those for **MA055**. Given this, we confirmed that **MA055** does not generate a more profound reduction in Wee1 or pCDK1(Y15) levels than **MA071** after 72 h treatment (Fig. S8), consistent with earlier timepoints. Both PROTACs were found to be roughly an order of magnitude less potent than equivalent treatment with AZD1775.

We describe the synthesis and evaluation of a new series of PROTACs
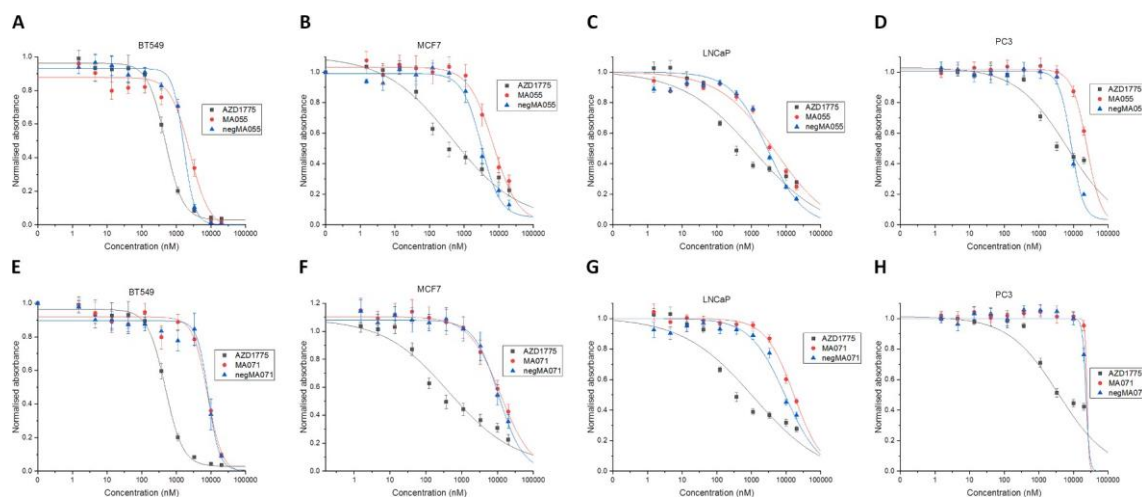
Fig. 4. Cell proliferation inhibition of cancer cell lines by the PROTACs and control compounds.
Superimpostion of cell proliferation assays normalised with DMSO for a PROTAC and its negative control for the VHL series (**A**, **B**, **C** and **D**) and CRBN series (**E**, **F**, **G** and **H**) in BT549, MCF7, LNCaP and PC3 cells treated for 72 h: **MA055**, **negMA055**, **MA071**, **negMA071** and inhibitor AZD1775. Data are presented as mean ± s.d. of n = 4 biologically independent experiments.

Table 2
Table of IC_{50} values of the MTS antiproliferation assay in four different cell lines BT549, MCF7, PC3 and LNCaP, treated with AZD1775, **MA071**, **negMA071**, **MA055** and **negMA055** for 72 h (n = 4).

Compound	IC_{50} (µM)			
	BT549	MCF7	PC3	LNCaP
AZD1775	0.49 ± 0.10	1.1 ± 1.0	8 ± 4	0.5 ± 0.3
MA071	7.9 ± 1.0	14 ± 7	>20	16.6 ± 1.8
negMA071	9 ± 3	11 ± 5	>20	11 ± 2
MA055	2.4 ± 0.6	7 ± 3	>20	5.2 ± 0.8
negMA055	1.7 ± 0.3	3.3 ± 1.2	8.7 ± 0.8	3.46 ± 0.19

targeting Wee1, using the most selective Wee1 inhibitor to date, AZD1775, and E3 ligase binders for VHL and CRBN. These PROTAC molecules successfully and rapidly degrade Wee1 protein and elicit a decrease in pCDK1(Y15) levels as a downstream effect. By recruiting the two different E3 ubiquitin ligases and by investigating linkers of different length and composition, we have obtained a number of Wee1 degraders that are selective for it over other AZD1775 targets.

The extent of Wee1 degradation was found to be dependent on both the length and the nature (alkyl or polyethylene glycol) of the linker. Using either E3 ligase binder, PROTACs with shorter linkers: **2** (MA055) for VHL and **9**, **10**, **11** and **12** (MA071) for CRBN, and the PROTACs with longer linkers: **6** for VHL and **15** and **21** for CRBN, showed the best degradation profiles. Meanwhile intermediate length linkers, such as **4** or **5** for VHL and **19** or **20** for CRBN, resulted in less effective degraders. This suggests that molecules with either shorter or longer linkers can adopt a better conformation for the recruitment of VHL or CRBN and Wee1 to form productive ternary complexes that result in target ubiquitination and degradation. Analysis by Bemis *et al.* suggested that PROTAC design can be rationalised by identifying the optimal "zone" for linker length that leads to compounds with the greatest degradation activity, with linker lengths outside of this zone resulting in increasingly less active PROTAC molecules.[27] Our work characterising Wee1 PROTACs illustrates that the "linker landscape" can be more complex than this, where different linker lengths can facilitate target degradation but with intermediate linker lengths yielding unproductive degraders. The recent discovery of highly cooperative FAK-degrading PROTACs identified a series of FAK:PROTAC:E3 complexes with both longer and shorter linkers yielding stronger FAK degradation than intermediate ones, owing to their higher cooperativities.[28] Previous work has shown

that cooperative stabilisation of PROTAC ternary complexes can result in both more[15,29] and less[30,31] effective targeted protein degradation, and that the nature and length of the linker greatly influences this. A perspective by Rodriguez-Rivera and Levi illustrates how, depending on the nature of the ternary complex formed, cooperativity may either promote or inhibit the formation of productive complexes that results in effective target degradation.[32]

The use of non-selective inhibitors as target-binding moieties in PROTAC molecules can result in target selectivity beyond that of the original inhibitor.[13-15] The Wee1 inhibitor AZD1775, while relatively selective for a kinase binder, exhibits off-target inhibition of a number of other kinases.[7,8] Treatment of HeLa S3 cells with our Wee1-targeting PROTACs resulted in selective Wee1 degradation over that of known AZD1775 targets (PLK1, PLK2, PLK3, MAP3K4 and JAK2) for the best PROTACs of both series, within a range of treatment timeframes. Assessment and characterisation of the degradable kinome using a diverse set of kinase binding moieties identified Wee1 as a readily degradable kinase,[33] suggesting our observations of selectivity may be more a result of the inherent degradability of Wee1 compared to other kinases, as opposed to selectivity induced by the ternary complexes formed by the PROTACs. Donovan *et al.* largely utilised PROTACs (in particular those identified as degrading Wee1) with similar design strategies to our own, i.e. C4-linked on pomalidomide, *N*-linked amides of the *tert*-Leucine of VH032, and *N*-linked alkylation of piperazine (or similar) linkages of kinase binders. Whether Wee1 is an intrinsically readily degradable kinase, or simply happens to be selected as a favourable conjugate pair for PROTACs with these specific E3 ligase and linker design strategies remains to be determined.

For both series there was a reduction in pCDK1(Y15) levels, a key signifier that Wee1 activity had been modulated. However, in both cases the negative control PROTACs also decreased pCDK1(Y15) levels. Despite being effective degraders of Wee1, the degradation activity of the VHL-recruiting PROTACs did not significantly enhance the disruption of Wee1 activity, whereas degradation by the CRBN-recruiting PROTACs did have an additional impact beyond that of inhibition alone. This strong inhibition by negative control compounds (roughly 10-fold less than AZD1775) also highlights that these Wee1-targeting PROTACs are relatively cell penetrant, bolstering previous observations[34] and suggesting that only some PROTAC systems are much less cell penetrant than their parent target binder, such as MZ1, which is more than five orders of magnitude less cell penetrant than JQ1.[35]

Cell growth experiments revealed that even though the CRBN-

PROTACs are better degraders of Wee1 than the VHL-PROTACs, our VHL-PROTACs were more cytotoxic, although these differences were only significant (p < 0.05) in BT549 and LNCaP cell lines. Given each of the negative controls exhibited similar effects on cell proliferation as their equivalent PROTACs, this may suggest that one or both of the E3 ligase-binding moieties has some non-specific activity mediated by another portion of the binder that has had an impact on cell growth. Ultimately the lack of substantial efficacy of our PROTAC compounds for influencing cell proliferation suggests the need to further optimise Wee1 degraders around either shorter or longer linker options, as was pursued for shorter linkers by Li *et al.*[18]

In summary, we reveal a SAR in the design of Wee1 PROTAC degraders, which could be further investigated to optimise Wee1 PROTACs and improve degradation activity. Using the Wee1-VHL or Wee1-CRBN pairs, we show both E3 ligases can be hijacked to induce productive and selective Wee1 ubiquitination and degradation, provided the right length and nature of linker.

Declaration of Competing Interest

The authors declare that they have no known competing financial interests or personal relationships that could have appeared to influence the work reported in this paper.

Acknowledgements

Appendix A. Supplementary data

Supplementary data to this article can be found online at https://doi.org/10.1016/j.bmcl.2022.128636.

References

1 Chen T, Stephens PA, Middleton FK, Curtin NJ. Targeting the S and G2 checkpoint to treat cancer. Drug Discov Today [Internet]. 2012;17(5):194‑202. Available from: 10.1016/j.drudis.2011.12.009.

2 Do K, Doroshow JH, Kummar S. Wee1 kinase as a target for cancer therapy. Cell Cycle [Internet]. 2013/08/26. 2013;12(19):3159‑64. Available from: 10.4161/cc.26062.

3 Matheson CJ, Backos DS, Reigan P. Targeting WEE1 Kinase in Cancer. Trends Pharmacol Sci [Internet]. 2016;37(10):872‑81. Available from: 10.1016/j.tips.2016.06.006.

4 Szmyd R, Niska-Blakie J, Diril MK, Renck Nunes P, Tzelepis K, Lacroix A, et al. Premature activation of Cdk1 leads to mitotic events in S phase and embryonic lethality. Oncogene [Internet]. 2019;38(7):998‑1018. Available from: 10.1038/s41388-018-0464-0.

5 Hirai H, Iwasawa Y, Okada M, Arai T, Nishibata T, Kobayashi M, et al. Small-molecule inhibition of Wee1 kinase by MK-1775 selectively sensitizes p53-deficient tumor cells to DNA-damaging agents. Mol Cancer Ther [Internet]. 2009;8(11):2992. Available from: 10.1158/1535-7163.MCT-09-0463.

6 Kong A, Mehanna H. WEE1 Inhibitor: Clinical Development. Curr Oncol Rep [Internet]. 2021 Jul 16;23(9):107. Available from: 10.1007/s11912-021-01098-8.

7 Zhu J-Y, Cuellar RA, Berndt N, Lee HE, Olesen SH, Martin MP, et al. Structural Basis of Wee Kinases Functionality and Inactivation by Diverse Small Molecule Inhibitors. J Med Chem [Internet]. 2017;60(18):7863‑75. Available from: 10.1021/acs.jmedchem.7b00996.

8 Wright G, Golubeva V, Remsing Rix LL, Berndt N, Luo Y, Ward GA, et al. Dual Targeting of WEE1 and PLK1 by AZD1775 Elicits Single Agent Cellular Anticancer Activity. ACS Chem Biol [Internet]. 2017;12(7):1883‑92. Available from: 10.1021/ acschembio.7b00147.

9 Liu Z, Sun Q, Wang X. PLK1, A Potential Target for Cancer Therapy. Transl Oncol [Internet]. 2017;10(1):22‑32. Available from: 10.1016/j.tranon.2016.10.003.

10 Lai AC, Crews CM. Induced protein degradation: an emerging drug discovery paradigm. Nat Rev Drug Discov [Internet]. 2016/11/25. 2017;16(2):101‑14. Available from: 10.1038/nrd.2016.211.

11 Sakamoto KM, Kim KB, Verma R, Ransick A, Stein B, Crews CM, et al. Development of Protacs to target cancer-promoting proteins for ubiquitination and degradation. Mol Cell Proteomics [Internet]. 2003;2(12):1350‑8. Available from: 10.1074/mcp. T300009-MCP200.

12 Bondeson DP, Mares A, Smith IED, et al. Catalytic in vivo protein knockdown by small-molecule PROTACs. Available from: *Nat Chem Biol [Internet]*. 2015/06/10. 2015,;11(8):611‑617. https://www.ncbi.nlm.nih.gov/pubmed/26075522.

13 Zengerle M, Chan KH, Ciulli A. Selective Small Molecule Induced Degradation of the BET Bromodomain Protein BRD4. ACS Chem Biol [Internet]. 2015;10(8):1770‑7. Available from: 10.1021/acschembio.5b00216.

14 Jiang B, Wang ES, Donovan KA, Liang Y, Fischer ES, Zhang T, et al. Development of Dual and Selective Degraders of Cyclin-Dependent Kinases 4 and 6. Angew Chemie - Int Ed [Internet]. 2019;58(19):6321‑6. Available from: 10.1002/anie.201901336.

15 Smith BE, Wang SL, Jaime-Figueroa S, Harbin A, Wang J, Hamman BD, et al. Differential PROTAC substrate specificity dictated by orientation of recruited E3 ligase. Nat Commun [Internet]. 2019;10(1):131. Available from: 10.1038/s41467-018-08027-7.

16 Galdeano C, Gadd MS, Soares P, et al. Structure-guided design and optimization of small molecules targeting the protein-protein interaction between the von Hippel-Lindau (VHL) E3 ubiquitin ligase and the hypoxia inducible factor (HIF) alpha subunit with in vitro nanomolar affinities. Available from: *J Med Chem [Internet]*. 2014/08/28. 2014,;57(20):8657‑8663. https://pubs.acs.org/doi/pdfplus/10.1021/jm5011258.

17 Ito T, Ando H, Suzuki T, et al. Identification of a primary target of thalidomide teratogenicity. Available from: *Science (80-) [Internet]*. 2010;327(5971):1345‑1350. https://www.science.org/doi/pdf/10.1126/science.1177319.

18 Li Z, Pinch BJ, Olson CM, Donovan KA, Nowak RP, Mills CE, et al. Development and Characterization of a Wee1 Kinase Degrader. Cell Chem Biol [Internet]. 2020;27(1): 57-65.e9. Available from: 10.1016/j.chembiol.2019.10.013.

19 Troup RI, Fallan C, Baud MGJ. Current strategies for the design of PROTAC linkers: a critical review. Explor Target Anti-tumor Ther [Internet]. 2020;1(5):273‑312. Available from: 10.37349/etat.2020.00018.

20 Matheson CJ, Venkataraman S, Amani V, Harris PS, Backos DS, Donson AM, et al. A WEE1 Inhibitor Analog of AZD1775 Maintains Synergy with Cisplatin and Demonstrates Reduced Single-Agent Cytotoxicity in Medulloblastoma Cells. ACS Chem Biol [Internet]. 2016 Jul 15;11(7):2066‑7. Available from: 10.1021/acschembio.6b00466.

21 Cyrus K, Wehenkel M, Choi E-Y, Han H-J, Lee H, Swanson H, et al. Impact of linker length on the activity of PROTACs. Mol Biosyst [Internet]. 2011;7(2):359‑64. Available from: https://doi.org/10.1039/C0MB00074D.

22 Lai AC, Toure M, Hellerschmied D, et al. Modular PROTAC Design for the Degradation of Oncogenic BCR-ABL. Available from: *Angew Chem Int Ed Engl [Internet]*. 2015/11/23. 2016,;55(2):807‑810. https://www.ncbi.nlm.nih.gov/pubmed/26593377.

23 Bondeson DP, Smith BE, Burslem GM, Buhimschi AD, Hines J, Jaime-Figueroa S, et al. Lessons in PROTAC Design from Selective Degradation with a Promiscuous Warhead. Cell Chem Biol [Internet]. 2018;25(1):78-87.e5. Available from: 10.1016/j.chembiol.2017.09.010.

24 Lebraud H, Wright DJ, Johnson CN, Heightman TD. Protein degradation by in-cell self-assembly of proteolysis targeting chimeras. ACS Cent Sci [Internet]. 2016;2(12): 927‑34. Available from: 10.1021/acscentsci.6b00280.

25 Ceccarelli DF, Tang X, Pelletier B, Orlicky S, Xie W, Plantevin V, et al. An allosteric inhibitor of the human Cdc34 ubiquitin-conjugating enzyme. Cell [Internet]. 2011; 145(7):1075‑87. Available from: 10.1021/acscentsci.6b00280.

26 Frost J, Galdeano C, Soares P, Gadd MS, Grzes KM, Ellis L, et al. Potent and selective chemical probe of hypoxic signalling downstream of HIF-α hydroxylation via VHL inhibition. Nat Commun [Internet]. 2016;7:13312. Available from: 10.1038/ncomms13312%0D.

27 Bemis TA, La Clair JJ, Burkart MD. Unraveling the Role of Linker Design in Proteolysis Targeting Chimeras. J Med Chem [Internet]. 2021 Jun 24;64(12): 8042‑52. Available from: 10.1021/acs.jmedchem.1c00482.

28 Law RP, Nunes J, Chung C, Bantscheff M, Buda K, Dai H, et al. Discovery and Characterisation of Highly Cooperative FAK-Degrading PROTACs. Angew Chemie Int Ed [Internet]. 2021 Aug 20;60(43):23327‑34. Available from: 10.1002/anie.202109237.

29 Farnaby W, Koegl M, Roy MJ, Whitworth C, Diers E, Trainor N, et al. BAF complex vulnerabilities in cancer demonstrated via structure-based PROTAC design. Nat

Chem Biol [Internet]. 2019/06/10. 2019 Jul;15(7):672‑80. Available from: 10.1038/s41589-019-0294-6.

30 Schiemer J, Horst R, Meng Y, Montgomery JI, Xu Y, Feng X, et al. Snapshots and ensembles of BTK and cIAP1 protein degrader ternary complexes. Nat Chem Biol [Internet]. 2021;17(2):152‑60. Available from: 10.1038/s41589-020-00686-2.

31 Zorba A, Nguyen C, Xu Y, Starr J, Borzilleri K, Smith J, et al. Delineating the role of cooperativity in the design of potent PROTACs for BTK. Proc Natl Acad Sci U S A [Internet]. 2018;115(31):E7285‑92. Available from: 10.1073/pnas.1803662115.

32 Rodriguez-Rivera FP, Levi SM. Unifying Catalysis Framework to Dissect Proteasomal Degradation Paradigms. ACS Cent Sci [Internet]. 2021 Jun 16;7(7):1117‑25. Available from: 10.1021/acscentsci.1c00389.

33 Donovan KA, Ferguson FM, Bushman JW, Eleuteri NA, Bhunia D, Ryu S, et al. Mapping the Degradable Kinome Provides a Resource for Expedited Degrader Development. Cell [Internet]. 2020;183(6):1741‑1731. Available from: 10.1016/j. cell.2020.10.038.

34 Maple HJ, Clayden N, Baron A, Stacey C, Felix R. Developing degraders: Principles and perspectives on design and chemical space. Medchemcomm [Internet]. 2019;10: 1755‑64. Available from: 10.1039/C9MD00272C.

35 Foley CA, Potjewyd F, Lamb KN, James LI, Frye S V. Assessing the cell permeability of bivalent chemical degraders using the chloroalkane penetration assay. ACS Chem Biol [Internet]. 2020;15(1):290‑5. Available from: 10.1021/acschembio.9b00972.